Activation and Maintenance of Intestinal Intraepithelial Lymphocytes (IELs)

Ulrika Cecilia Frising

The Babraham Institute

University of Cambridge

This dissertation is submitted for the degree of

Doctor of Philosophy

Homerton College March 2018

i. Declaration

I hereby declare that my thesis entitled *Activation and Maintenance of Intestinal Intraepithelial Lymphocytes (IELs)* is the result of my own work and includes nothing which is the outcome of work done in collaboration except as declared in the Acknowledgements and specified in the text. It is not substantially the same as any that I have submitted, or, is being concurrently submitted for a degree or diploma or other qualification at the University of Cambridge or any other University or similar institution except as declared in the preface and specified in the text. I further state that no substantial part of my dissertation has already been submitted, or, is being concurrently submitted for any such degree diploma or other qualification at the University of Cambridge or any other University or similar institution except as declared in the preface and specified in the text. It does not excess the prescribed word limit for the relevant Degree committee. The research in this thesis was carried out at the Babraham Institute, Cambridge, between October 2014 and March 2018.

Ulrika Cecilia Frising

March 2018

ii. Acknowledgements

I would like to thank many people for their generous support during my Ph.D.:

Dr. Jörg Stange. Many thanks for the input and support I received as your mentee between 2014-2016. I really appreciated the continuous support and interest I received from you, as well as our weekly meetings we had together with Dr. Joana Guedes, your other mentee.

Dr. Geoff Butcher. Many thanks for all your support, particularly during the last part of my Ph.D., as well as all the time you spent reading and providing feedback on my thesis. I would also like to thank Dr. John Pascall for reading parts of my thesis. I am very grateful for the insightful comments about my Ph.D. thesis.

Dr. Silvia Innocentin that supported my Ph.D. research with genotyping of transgenic mice, as well as providing a helpful hand for the initial step of IEL isolation for many of the big experiments presented in this thesis.

Dr. Joana Guedes. I still remember this day in 2014 that we for the first time observed IELs associated to organoids. Many thanks for all your support, particularly with the *Eimeria vermiformis* work and your support while I was writing my thesis.

I would like to thank the many people that have provided assistance and support for my research. I have received support from the Babraham Institute Imaging, Flow, Lipidomics and Biological support unit (BSU) facilities.

I would like to thank Dr. Simon Walker and Dr. Hanneke Okkenhaug, from the imaging facility, for all assistance and inputs with imaging acquisition and analysis.

From the flow facility, I would like to thank Dr. Rachel Walker, Arthur Davis, Dr. Rebecca Roberts, Lynzi Waugh, Dr. Winston Vetharoy and Nathan Richoz. They have provided

excellent support with cell sorting of IELs, as well as support to keep all cytometers in excellent condition to ensure smooth run on analysers.

I would like to thank all past and present members of BSU breeding, BSU transgenic, BSU experimental and BSU import teams for excellent care and monitoring of the mice used for the experiments, as well as all assistance with the experimental procedures.

I would also like to thank the security team for the company during my out-of-hours working. I clearly remember the moments I explained the science I spent so many hours on by showing the organoids, “the jelly-fishes” as well as the many “colour-full plots” at the flow facility.

I would also like to give special thanks to Dr. Melanie Keene, my College tutor. You have provided lots of support, particularly during the last part of my Ph.D., which has been valuable for finishing this thesis.

I would also like to give particular thanks to the National Centre of the 3Rs (NC3R) for founding of my studentship, as well as Funds for Women Graduates (FfWG) for support for my Ph.D. research. My research has also received support from the strategic funding the Babraham Institute received by Biotechnology and Biological Sciences Research Council (BBRSC).

Finally, I would like to give special thanks to fellow student Shan-Zheng Chong for the friendly support during our Ph.D.s and for reading parts of my thesis. I would also thank Amy Niklasson and Gustaf Olsson, two great friends that also have read parts of my thesis and provided feedback. I would also like to thank some special friends for support during this journey, namely Dr. Alejandro López Tóbon, Dr. Caroline Weight, Christina Thuresson, Cassandra Göransson, Josefin Olsson, Maria Jernsax, Emelie Persson and Victoria Ptastinski.

Many thanks to you all.

---

iii. Table of acknowledgement of assistance received during course of Ph.D. thesis

1) Initial training in techniques and laboratory practice and subsequent mentoring: -Dr. Jörg Stange, Dr. Silvia Innocentin, Dr. Joana Guedes and Marc Veldhoen.
2) Data obtained from a technical service provider (e.g. DNA sequencing, illustrations, simple bioinformatics information etc.) -Dr. Silvia Innocentin: Genotyping of mice. -Miss Marta Baptista: Genotyping of mice.
3) Data produced jointly (e.g. where it was necessary or desirable to have two pairs of hands) -Dr. Jörg Stange and Dr. Joana Guedes: *Eimeria vermiformis* infection model. Bringing the parasite model to the Babraham Institute (Dr. Stange), assistance with infections of mice (Dr. Stange and Dr. Guedes), oocyst counts (Dr. Guedes) and inputs about experimental planning (Dr. Stange and Dr. Guedes). -Osama Eisa, Dr. Barbara Blacklaws and Prof. Jonathan Heeney (The Department of Veterinary Medicine at University of Cambridge): Murine norovirus work (MNV-O7, MNV-CW3, MNV-3) and *Salmonella* infection models: providing viruses for *in vitro* experiments used in Chapter 4, providing infected small intestines for me to assess the IEL activation status and for Osama to quantify the pathogen load in mice and organoids. - Dr. Spela Konjar: The Seahorse experiment presented in Chapter 5.
4) Data/materials provided by someone else (e.g. one-off analysis, bioinformatics analysis, where parallel data or technical provision in a very different area is needed to provide a connected account in the thesis) -The Babraham Institute Biological Services Unit (BSU): Mouse housekeeping and experimental procedures such as i.v. and i.p. injections -The Babraham Institute Flow cytometry Team: Flow service, particularly sorting of IELs. -The Babraham Institute Imaging Facility: Training and support with imaging and analysis -The Babraham Institute Lipidomic Facility: Lipid extraction and acquisition used for cardiolipin data presented in Chapter 6.

iv. Abstract

The intestinal tissue is charged with a delicate immunological task. The intestinal immune system needs to be tolerant towards nutrients and microbiota present in the intestinal lumen, while simultaneously detecting and responding to dangers such as pathogens. A single-cell layer of intestinal epithelial cells (IECs) acts as a first line of defence. There is a T cell population located between the IECs that have been named intraepithelial lymphocytes (IELs). As the main lymphoid population within the intestinal barrier, IELs are thought to have an important role in intestinal homeostasis maintenance, as well as a role in intestinal inflammatory and autoimmune diseases such as inflammatory bowel disease and celiac disease. Despite extensive research on IEL biology, there are still questions remaining in terms of the development, maintenance and activation of IELs. Furthermore, IELs survive poorly *in vitro,* which hinders mechanistic insights. In this thesis, a co-culture system between IELs and intestinal organoids, "mini-guts", provides an *in vitro* model for IELs. With this IEL-organoid co-culture system, IELs associated with the organoids survive for at least 4 days. Additional findings suggest that IELs are kept in a poised state of activation due to differences in their mitochondria compared to other T cells found in spleen, lung and skin. Upon activation or intestinal inflammation, the mitochondrial mass in IELs increases. This increase correlates with effector functions such as cytokine production and proliferation. In addition, the composition of the mitochondria-specific lipid, cardiolipins, alters drastically in IELs after activation. These data support a model of mitochondria-dependent activation of IELs. The mitochondria-dependent activation in IELs appears to have at least two pathways: one T cell receptor-dependent and one microbiota-dependent. The latter pathway suggests a model in which IELs can become activated regardless of the cause of intestinal epithelial barrier damage.

v. List of Figures

Figure 1.1. The intestinal epithelial barrier organisation in the small and large intestine 57

Figure 1.2. IEL development and homing to the small intestine 62

Figure 4.1. The intestinal stem cell niche and the organoid model 99

Figure 4.2. Schematic overview of published co-cultures of IEC and IEL cell lines 102

Figure 4.3. Association of IELs with organoids is independent of IL-2, -3, -7 and IL-15 ...107

Figure 4.4. Association of IELs with organoids is dependent on the seeding density of IELs 111

Figure 4.5. Selectivity of lymphocyte migration into organoids 113

Figure 4.6. Altered DAPI staining protocol discriminates live organoids and lymphocytes from dead cells 116

Figure 4.7. Automatic quantification of subsets in organoids enables rapid analysis 119

Figure 4.8. IL-15 signalling is important for IEC proliferation, goblet cell differentiation and AMP production.....121

Figure 4.9. Organoids mediate IEL-specific survival independently of IL-15 trans-presentation 124

Figure 4.10. Organoid proliferation is reduced in the presence of MNV-O7 infection.....129

Figure 4.11. Addition of IELs prevents the MNV-O7-mediated decrease in IEC proliferation 132

Figure 4.12. Addition of *E. coli* reduces the proliferation in organoids 134

Supplemental Figure to 4.5: Naïve and Memory splenic CD8α^+ T cell sorting strategy ...135

Supplemental Figure to 4.7-1: Organoid proliferation data. 136

v. List of Figures

Supplemental Figure to 4.7-2: Image quantification of IEL-organoid cultures.....138

Supplemental Figure to 4.7-3: Image quantification of intestinal tissue-sections.....139

Figure 5.1. Schematic illustration of the gut-associated lymphoid tissue (GALT) 148

Figure 5.2. Schematic overview of the structure of mitochondria.....152

Figure 5.3. Schematic overview of the main metabolic pathways in cells. 156

Figure 5.4. IELs have more accumulation of lipid droplets than splenic CD8α^+ T cells 160

Figure 5.5. IELs have no spare respiratory capacity (SRC) while splenic CD8α^+ T cells do 162

Figure 5.6. IELs have lower mitochondrial mass than splenic CD8α^+ T cells 164

Figure 5.7. IELs are set apart from other TCR$\gamma\delta^+$ cells and epithelial-resident lymphocytes by their MTG staining.....167

Figure 5.8. IELs have higher cardiolipin (CL) content than splenic CD8α^+ T cells.....169

Figure 5.9. Mitochondrial membrane potential is lower in IELs than in splenic CD8α^+ T cells 171

Figure 5.10. IELs have a similar level of mitochondrial ROS production to splenic CD8α^+ T cells 173

Figure 5.11. Despite low mitochondrial mass, IELs are equipped with granzyme B.....175

Supplemental Figure to 5.6: MitoTracker Deep Red (MTDR) staining show a similar difference as MTG staining between splenic CD8α^+ T cells and IELs 177

Figure 6.1. TCR stimulation increases mitochondrial mass and CD44 expression in IELs… 187

Figure 6.2. TCR stimulation led to transient increase of the activation marker CD69.....188

v. List of Figures

Figure 6.3. TCR stimulation led to increased IEL proliferation, but no cytokine production 191

Figure 6.4. TCR-activated IELs have a higher level of mitochondrial ROS production.....193

Figure 6.5. TCR-activated IELs have unchanged membrane potential and CL content 195

Figure 6.6. IEL transfer into IL-2Rγ-/-Rag2-/- mice generated a more representative IEL population compared to Rag2-/- mice.....199

Figure 6.7. IELs respond directly to αCD3 activation 201

Figure 6.8. Co-stimulatory CD28 does not lead to cytokine production in IELs. 203

Figure 6.9. Co-stimulatory CD28 does not alter TCR-mediated IEL activation. 205

Figure 6.10. T-bet-deficient IELs may have a higher threshold to enable increase in mitochondrial mass during activation.....209

Figure 6.11. Eomes is dispensable to enable increase in mitochondrial mass and Ki-67 expression during activation 213

Figure 6.12. AhR may be involved in the threshold to enable MTG increase in IELs.....217

Figure 6.13. AhRR is dispensable for MTG increase and Ki-67 response.....219

Figure 6.14. Cyp1a enzymes have a role in the αCD3-mediated Ki-67 response in IELs. ..221

Figure 6.15. Activation of IELs leads to drastic changes in CL composition. 225

Supplemental Figure to 6.5. Quantification of the amount of CLs per 10^7 cells. 228

Supplemental Figure to 6.15. PCA analysis of CL species in activated and non-activated IELs.....229

Figure 7.1. Overview of the taxonomic classification of murine microbiota 247

v. List of Figures

Figure 7.2. IEC stress in Villin-Cre-XBP1$^{fl/fl}$ mice is not sufficient to fully activate IELs.. 251

Figure 7.3. Ileum-sourced IELs are in a more activated state than other small intestinal IELs 255

Figure 7.4. IELs increase their mitochondrial mass during *E. vermiformis* infection. 259

Figure 7.5. IELs produce cytokines during *E. vermiformis* infection.....263

Figure 7.6. IELs increase their expression of Ki-67 during *E. vermiformis* infection.....265

Figure 7.7. During *E. vermiformis* infection, TCRαβ^{+} CD8αβ^{+} IELs responded most strongly in regards to Ki-67 expression and cytokine production 266

Figure 7.8. *E. vermiformis*-activated IELs have a higher level of mitochondrial ROS production. 269

Figure 7.9. *E. vermiformis*-activated IELs show no increase in mitochondrial membrane potential.....270

Figure 7.10. MNV infection-induced IEL activation is dependent on the MNV-strain.....273

Figure 7.11. *Salmonella* infection fails to activate IELs.....276

Figure 7.12. IELs in IL-22-/- mice are activated in a microbiota-dependent manner 281

Figure 7.13. Commensal microbiota are activating IELs in MNV-CW3 infection 285

Figure 7.14. IEL activation by MNV-CW3 infection does not lead to cytokine production. 287

Figure 7.15. Commensal microbiota are activating IELs in *E. vermiformis* infection. 291

Figure 7.16. Commensal microbiota are mediating the cytokine production in activated IELs 293

Figure 7.17. Broad-spectrum antibiotic treatment does not lead to a more severe *E. vermiformis* infection 295

Figure 7.18. IELs are selectively activated by Gram-positive bacteria during intestinal parasite infection 299

Figure 7.19. The cytokine production in activated IELs is mediated by Gram-positive bacteria 301

Figure 7.20. Gram-positive and Gram-negative antibiotic treatments do not lead to a more severe *E. vermiformis* infection 303

Figure 7.21. The increase of *E. vermiformis* parasite load in Rag2-/- mice is dependent on commensal microbiota 307

Figure 7.22. αCD3-mediated IEL activation is not reduced by antibiotic treatment 311

Figure 7.23. DSS-induced colitis model used for IEL activation assessment 315

Figure 7.24. DSS-induced colitis model does not fully activate small intestinal IELs 317

Figure 7.25. IELs transferred into IL-2Rγ-/-Rag2-/- mice have more mitochondrial mass in a microbiota-independent manner 321

Figure 7.26. IELs transferred into IL-2Rγ-/-Rag2-/- mice are more activated due to IL-15R-dependent and/or IL-22 producing cells. 324

Supplemental Figure to 7.10. Adaptive immune system is used for MNV-O7 replication.. 325

Figure 9.1. Summary of IEL maintenance 355

Figure 9.2. Graphical summary of findings related to IEL activation 356

vi. List of Tables

Table 3.1. Medium used for cell and tissue isolation and culture procedures 69

Table 3.2. Antibodies and probes used for image acquisition and analysis.....70

Table 3.3. Antibodies and probes used for flow cytometric analysis 71

Table 3.4. Primers used for qPCR analysis.....72

Table 3.5. Antibiotics used for antibiotic depletion experiments 76

Supplemental Table to 6.15. Table of CL species measured between non-infected IELs, infection-mediated activation of IELs, naïve, effector and effector splenic CD8α^{+} T cells…

.....226

vii. List of Abbreviations

2-DG	2-Deoxy-D-glucose
3D	Three-dimensional (3D)
ABx	Antibiotic
ACK-buffer	Ammonium-chlorine-potassium buffer
αCD28	anti-CD28
αCD3	anti-CD3
ADCC	Antibody-dependent cell cytotoxicty
ADH	Alcohol dehydrogenase
ADP	Adenosine diphosphate
AF	Alexa fluorochromes
AhR	Aryl hydrocarbon receptor
AhRR	Aryl hydrocarbon receptor repressor
AID	Activation-induced cytidine deaminase
AIP	Aryl hydrocarbon receptor interacting protein
AMP	Adenosine monophosphate
AMPs	Antimicrobial peptides
ANOVA	Analysis of variance
APCs	Antigen presenting cells
Arnt	Aryl hydrocarbon receptor nuclear translocator
ASPA	Animals Scientific Procedures Act
ATP	Adenosine triphosphate
BAC	Bacterial artificial chromosome
BAFF	B cell-activating factor
BALT	Bronchus-associated lymphoid tissues
BCR	B cell receptor
BM	Bone Marrow
BMP	Bone morphogenesis protein
BSA	Bovine serum albumin
C. rodentium	*Citrobacter rodentium*
CAR	Chimeric antigen receptor
CBCs	Crypt-base columnar cells
CCCP	Carbonyl cyanide m-chlorophenyl hydrazone

vii. List of Abbreviations

CCL	Chemokine ligand
CCR	Chemokine receptor
CD	Cluster of differentiation
CD	Celiac disease
Cfu	Colony-forming unit
CL	Cardiolipin
CLP	Common lymphoid progenitor
CLS	CL synthase
CMPs	Common myeloid progenitors
CoA	Coenzyme A
CPs	Cryptopatches
CR	Complement receptor
CRAC	Ca2+ release-activated Ca2+
CTLA-4	Cytotoxic T lymphocyte-associated protein 4
CTLs	Cytotoxic T Lymphocytes
Cyp	Cytochrome P450
Cyp1aT-/-	Cyp1A1, 1A2 and 1B triple-/- mice
DAI	Disease activity index
DAMPs	Damage-associated molecular patterns
DAPI	4',6-diamidino-2-phenylindole
DCLK-1	Doublecortin-like kinase 1
DCs	Dendritic cells
DeSEQ	Differential sequence analysis
DETCs	Dendritic epidermal T cells
Dll	Delta-like ligands
DMEM	Dulbecco's modified Eagle medium
dnRARα	Dominant negative form of the retinoic acid receptor alpha
dnTGFβRII	Dominant negative form of the TGFβRII
DRE	Dioxin response element
Drp1	Dynamin-related protein 1
DSS	Dextran sulphate sodium
E. coli	*Escherichia coli*
E. vermiformis	*Eimeria vermiformis*

vii. List of Abbreviations

EAE	Experimental autoimmune encephalomyelitis
ECAR	Extracellular acid rate
ECM	Extracellular matrix
EDN	Eosinophil-derived neurotoxin
EDTA	Ethylenediaminetetraaacetic acid
EdU	5-ethynyl-2'-deoxyuridine
EGF	Epidermal growth factor
EHS	Engelbreth-Holm-Swarm
Eomes	Eomesodermin
EpCAM	Epithelial cell adhesion molecule
EPO	Eosinophil peroxidase
ER	Endoplasmic reticulum
ERK	Extracellular signal-regulated kinase
ETC	Electron transport chain
FAB	fatty acid binding protein
FACS	Fluorescence activated cell sorting
FAE	Follicle-associated epithelium
FAO	Fatty acid oxidation
FAS	Fatty acid synthesis
FBS, FCS	Fetal bovine serum, fetal calf serum
Fc receptor	Antibody receptor
FCCP	Carbonyl cyanide-p-trifluoromethoxyphenylhydrazone
FICZ	6-formylindolo[3,2-b]carbazole
FITC-Dextran	Fluorescein isothiocyanate–dextran
FMO	Fluorescent-Minus-One
Foxp3	Forkhead box P3
FSC	Forward scatter
FT-MS	Fourier-transform ion cyclotron resonance mass spectrometry
GALT	Gut associated lymphoid tissue
GAPDH	Glyceraldehyde 3-phosphate dehydrogenase
Gata3	Gata binding factor 3
GF	Germ-free
GFP	Green fluorescent protein

vii. List of Abbreviations

GI	Gastrointestinal
GLS	Glutaminase
GLUT	Glucose transporter
GPR	G-protein receptor
GSK3	Glycogen synthase kinase 3
HFD	High fat diet
HIF	Hypoxia-inducible factor
HSP90	Heat shock protein 90
HSPCs	Haematopoietic stem/progenitor cells
i.p.	Intraperitoneal injection
i.v.	Intravenous
iBALT	inducible BALT
IBD	Intestinal Bowel Disease
ICAM	Intracellular adhesion molecules
iCOS	Inducable T cell co-stimulator
Id2	Inhibitor of DNA binding 2
IECs	Intestinal epithelial cells
IELs	Intraepithelial lymphocytes
IESCs	Intestinal epithelial stem cells
IFNα	Interferon alpha
IFNβ	Interferon beta
IFNγ	Interferon gamma
IFNλ	Interferon lamba
Ig	Immunoglobulin
IgA	Immunoglobulin A
IH	Innate helper
IL	Interleukins
ILC1	Type 1 Innate lymphoid cells
ILC2	Type 2 Innate lymphoid cells
ILC3	Type 3 Innate lymphoid cells
ILCs	Innate lymphoid cells
ILF	Isolated lymphoid follicle
IMDM	Iscove’s modified Dulbecco’s medium

vii. List of Abbreviations

IMM	Inner mitochondrial membrane
Ims	Imaris file format
IRF4	Interferon regulatory factor 4
IRF8	Interferon regulatory factor 8
KLRG1	Killer-cell lectin like receptor G1
KO	Knock-out
L. monocytogenes	*Listeria monocytogenes*
L/D	Live/dead
LAG3	Lymphocyte-activation gene 3
LB medium	Lysogeny broth medium
LC-MS	Liquid chromatography–mass spectrometry
LCMV	Lymphocytic choriomeningitis virus
LCs	Langerhans cells
LD	Lipid droplets
Lgr5	Leucine-rich-repeat-containing G-protein-coupled receptor 5
LN	Lymph node
LP	Lamina propria
LPLs	Lamina propria lymphocytes
LPS	Lipopolysaccharide
LTA	Lipoteichoic acid
LTi	Lymphoid tissue inducer
LTα	Lymphotoxin alpha
LTβR	Lymphotoxin beta receptor
M cells	Microfold cells
MAC	Membrane attack complex
MACS	Magnetic cell separation
MAdCAM1	Mucosal addressin cell adhesion molecule 1
MAITs	Musocal-associated innate T cells
MALT	Mucosal associated lymphoid tissues
MAM	Mitochondrial associated ER-membrane
MAMPs	Microbe-associated molecular patterns
MAPK	Mitogen-activated protein kinase
MAVS	Mitochondrial antiviral signalling protein

vii. List of Abbreviations

MCP-1	Monocyte chemoattractant protein 1
MedLN	Mediastinal lymph nodes
MFI	Mean fluorescent intensity
Mfn1	Mitofusin 1
Mfn2	Mitofusin 2
MHC	Major histocompatibility complex
MICA	MHC class I polypeptide-related chain A
MICB	MHC class I polypeptide-related chain B
MLNs	Mesenteric lymph nodes
MMNs	Monomorphonuclear
MNV	Murine norovirus
MPs	Macrophages
mtDNA	Mitochondrial DNA
MTDR	MitoTracker Deep Red
MTG	MitoTracker Green
MTO	MitoTracker Orange
Muc-2	Mucin-2
MyD88	Myeloid differentiation primary response gene 88
N. brasiliensis	*Nippostrongylus brasiliensis*
NAO	Acridine Orange 10-nonyl bromide
NCR	Natural cytotoxicity receptor
NETs	Neutrophil extracellular traps
NFAT	Nuclear factor of activated T-cells
NHCs	Natural helper cells
NICD	Notch intracellular domain
NK cells	Natural killer cells
NKG2D	Natural killer Group 2D
NKT cells	Natural killer T Cells
NLRs	NOD-like receptors
NOD	Nucleotide-binding oligomerization domain
OCR	Oxygen consumption rate
OCT	Optimal cutting temperature
OD	Optical density

vii. List of Abbreviations

OMM	Outer mitochondrial membrane
Opa1	Optic atrophy 1
Opn	Osteopontin
OT-I cells	Ovalbumin-specific CD8α+ cells
OTU	Operational taxonic unit
OVA	Ovalbumin
OXPHOS	Oxidative phosphorylation
PA	Phosphatidic acid
PAMPs	Pathogen associated molecular patterns
PC	Principal component
PCA	Principal component analysis
PCR	Polymerase chain reaction
PD-1	Programmed cell death 1
PEG	Polyethylene glycol
PFA	Paraformaldehyde
PHA	Phosphatidylhydroxy acetyl
PhAM	photo-activatable mitochondria
PMN	Polymorphonuclear
Pou2f3	POU class 2 homeobox 3
PPs	Peyer's patches
PRRs	Pattern recognition receptors
RA	Retinoic acid
Rag	Recombination activating gene
RALDH	Retinal dehydrogenase
RANK	Receptor activator of nuclear factor-kappa B
RegIIIβ	Regenerating islet-derived protein III beta
RegIIIγ	Regenerating islet-derived protein III gamma
RELMβ	Resistin-like molecule β
RET	Reverse electron transfer
RIG	Retinoic acid-inducible gene
RLRs	RIG-I-like receptors
RORα	Retinoic acid receptor-related orphan receptor alpha
RORγ	Retinoic acid receptor-related orphan receptor gamma

vii. List of Abbreviations

ROS	Reactive oxygen species
Rpm	Rotations per minute
RT	Room temperature
RT qPCR	Real time quantitative polymerase chain reaction
Runx	Runt-related transcription factor
S. pneumonia	*Streptococcus pneumonia*
SALT	Skin-associated lymphoid tissues
SCFA	Short chain fatty acid
SD	Standard deviation
SEM	Structural equation modeling
SFB	Segmented filamentous bacteria
SILT	Solitary Isolated lymphoid follicle
SIM	Selected-ion monitoring chromatogram
SLO	Secondary lymphoid organ
Sox9	SRY-Box 9
SPF	Specific pathogen-free
SRC	Spare respiratory capacity
SSC	Side scatter
STAT	Signal transducer and transcrition protein
T. gondii	*Toxoplasma gondii*
T. muris	*Trichuris muris*
TA cells	Transit-amplifying cells
TAK1	TGFβ-activated kinase 1 (TAK1)
T-bet	Gene encoded by T-box transcription factor TBX21
TCA cycle	Tricarboxylic acid cycle
TCDD	2,3,7,8-Tetrachlorodibenzo-p-dioxin
TCF-1	T cell factor 1
TCID	Tissue culture infective dose
Tcm	Central memory T cells
TCR	T cell receptor
TCRδ-eGFP	Enhanced GFP reporter coupled to TCRδ-chain
Teff	Effector T cells
TF	Transcription factor

vii. List of Abbreviations

TFAM	Mitochondrial transcription factor A
Tfh	T follicular helper
TGFβ	Transforming growth factor beta
Th	T helper
ThPOK	Th Inducing POZ-Kruppel Factor
TiPARP	TCDD-inducible poly(ADP-ribose) polymerase
TJ	Tight junction
TL	Thymus leukemia antigen
TLRs	Toll like receptors
Tmem	Memory T cells
Tn	Naïve T cells
TNBS	Trinitrobenzenesulfonic acid
TNF	Tumor necrosis factor
TRAF	TNF receptor associated factor
Tregs	Regulatory T cells
TRIF	TIR-domain-containing adapter inducing interferon β
Trm	Tissue resident memory T cells
TSLP	Thymic stromal lymphopoietin
UEA	Ulex Europaeus Agglutinin
UPR	Unfolded protein response
VEGF	Vascular endothelial growth factor
Wnt	Wingless
WT	Wild Type
XBP1	X-box binding protein 1
YFP	Yellow fluorescent protein

Table of Content

i. Declaration....1

ii.Acknowledgements....2

iii.Table of acknowledgement of assistance received during course of Ph.D. thesis 4

iv.Abstract....5

v.List of Figures....6

vi.List of Tables 11

vii.List of Abbreviations 12

Table of Content 21

Chapter 1: Thesis Introduction....30

1. Introduction....30

1.1. Cellular Immune System....30

1.2. Innate Immunity....30

1.2.1. Granulocytes: neutrophils, eosinophils and basophils....31

1.2.2. Mast cells 33

1.2.3. Dendritic cells (DCs) 33

1.2.4. Monocytes....35

1.2.5. Macrophages....35

1.2.6. Natural Killer (NK) cells 36

1.2.7. Innate lymphoid cells (ILCs): ILC1, ILC2 and ILC3....36

1.3. Adaptive Immunity....37

1.3.1. B cells: B1, B2 and plasma cells....37

1.3.2. $CD4^+$ T cells....38

1.3.2.1. T helper (Th) cells....39

1.3.2.2. IFNγ-secreting Th1 cells....39

1.3.2.3. IL-4-secreting Th2 cells....40

1.3.2.4. IL-9-secreting Th9 cells....41

1.3.2.5. IL-17-secreting Th17 cells....41

1.3.2.6. IL-22-secreting Th22 cells....42

1.3.2.7. T regulatory (Treg) cells....43

1.3.3. $CD8\alpha^+$ T cells....43

1.3.3.1. Effector $CD8\alpha^+$ T (Teff) cells....44

1.3.3.2. Memory T (Tmem) cells....45

1.3.3.3. Tissue Resident T (Trm) cells....47

1.3.4. $TCR\gamma\delta^+$ T cells....47

1.3.5. Natural Killer T cells (NK T cells)....48

1.3.6. Mucosal-associated invariant T cells (MAITs)....49

1.4. Humoral immune system....49

1.5. Mucosal-associated lymphoid tissues (MALTs)....50

1.6.1. Intestinal epithelial cells (IECs) organisation....51

1.6.1.1. Intestinal epithelial stem cells (IESCs)....53

1.6.1.2. Absorptive enterocytes....54

1.6.1.3. Goblet cells 54

1.6.1.4. Paneth cells 55

1.6.1.5. Enteroendocrine cells 55

1.6.1.6. Microfold (M) cells 56

1.6.1.7. Tuft and cup cells 56

1.6.2. Lamina propria lymphocytes (LPLs) 58

1.6.3. Intestinal intraepithelial lymphocytes (IELs) – the main immune cell population within the intestinal epithelium 59

Chapter 2: Ph.D. Thesis specific aims 67

Chapter 3: Materials and Methods 69

3.1. Reagents 69

3.2. Mice 72

3.3. *In vivo* experimental procedures 73

3.3.1. T and B cell transfer model 73

3.3.2. Isolation of IELs from small and large intestine 73

3.3.3. IEL sort 74

3.3.4. IEL transfer model 74

3.3.5. Bone marrow (BM) transfer model 75

3.3.6. 5-ethynyl-2'-deoxyuridine (EdU) incorporation 75

3.3.7. αCD3 and αCD28 T cell activation model 76

3.3.8. Dextran sulphate sodium (DSS) model of intestinal inflammation 76

3.3.9. Antibiotic depletion model 76

3.3.10. Murine norovirus (MNV)-O7 and MNV-CW3 infection models 77

3.3.11. *Eimeria vermiformis (E. vermiformis)* infection model 77

3.3.12. *Salmonella* infection model 78

3.4. *Ex vivo* experimental procedures 78

3.4.1. Isolation of lamina propria lymphocytes (LPLs) 78

3.4.2. Isolation of splenic lymphocytes 79

3.4.3. Splenic $CD8\alpha^+$ lymphocyte sort 79

3.4.4. Isolation of liver lymphocytes 80

3.4.5. Isolation of lung lymphocytes 80

3.4.6. Isolation of skin lymphocytes 80

3.4.7. $CD8\alpha^+$ T cell culture 81

3.4.8. Intestinal organoid set-up 81

3.4.9. Organoid maintenance 82

3.4.10. IEL-organoid-co-culture system 82

3.4.11. MNV-organoid-co-culture system 83

3.4.12. IEL-MNV-organoid tri-culture system 84

3.4.13.*Escherichia coli (E. coli)*-organoid co-culture system 84

3.4.14. Immunofluorescence 84

3.4.15. Immunofluorescence of intestinal tissue staining 85

3.4.16. Image acquisition and analysis 86

3.4.17. qPCR analysis of organoids 88

3.4.18. Flow cytometric analysis 89

3.4.19. Cardiolipin (CL) analysis 90

3.4.20. Mitochondrial capacity assay 90

3.5. Statistical analysis 91

Chapter 4: Establishing an IEL-Organoid Co-Culture System to study IEL function, maintenance and activation 92

4.1. Modelling IECs: From cell lines to organoid cultures 92

4.1.1. Two-dimensional cell culture models 92

4.1.2. Intestinal stem cell niche 92

4.1.3. Requirement for Wnt/EGF/BMP signalling for IESCs 93

4.1.4. The role of extracellular matrix (ECM) for IEC cultures 96

4.1.5. Intestinal spheroids 97

4.1.6. Intestinal organoids 99

4.1.7. Organoid expansion: more tissues, tools and applications 99

4.2. Modelling intestinal intraepithelial lymphocytes *in vitro* 101

4.3. It is possible to incorporate IELs into intestinal organoids 103

4.4. Adding IELs in the Matrigel significantly increases the number of IEL-associated organoids 104

4.5. The seeding density of IELs is important for a high level of IEL-incorporation 108

4.6. Organoids enable IELs specifically to migrate into them 112

4.7. IELs survive for at least 4 days in co-culture with organoids 114

4.8. IECs have their own requirement for IL-15 signalling.....120

4.9. Organoid-mediated IEL survival is independent of IL-15 trans-presentation.....122

4.10. Specific murine norovirus strains replicate in organoids and reduce their proliferation – the latter being reversed by adding IELs. 125

4.11. Combining organoids with *E. coli* led to reduction of proliferation.....133

4.12. Supplemental chapter figures.....135

4.13. Chapter Discussion 140

Chapter 5: IELs have a different activation and metabolic status to other CD8α+ T cells ...145

5.1. BALT: bronchus-associated lymphoid tissues.....145

5.2. SALT: skin-associated lymphoid tissues.....146

5.3. GALT: gut-associated lymphoid tissues.....147

5.4. Overview of mitochondrial structure and function.....149

5.4.1. Cardiolipins (CLs) – almost exclusively found in mitochondria……..150

5.4.2. Electron transport chain (ETC) for generation of ATP and ROS…….151

5.4.3. Metabolic pathways: ATP, metabolite and signalling molecules generation…….....153

5.4.4. The currently known role of mitochondria for innate and adaptive immunity…….157

5.5. IELs accumulate lipid droplets – a sign of their semi-activated status.....159

5.6. IELs lack mitochondrial spare respiratory capacity (SRC) 161

5.7. IELs have lower mitochondrial mass compared to splenic CD8α^+ T cells.....162

5.8. Other epithelial-resident and TCR$\gamma\delta^+$ lymphocytes have more mitochondrial mass than IELs….. 165

5.9. Additional differences in IEL mitochondria: higher cardiolipin (CL) content and lower mitochondrial potential than splenic CD8α$^+$ T cells 168

5.10. IELs have similar mitochondrial ROS production to splenic CD8α$^+$ T cells 172

5.11. Low mitochondrial mass may not prevent cytolytic capacity in IELs 174

5.12. Supplemental chapter figure 177

5.13. Chapter discussion 178

Chapter 6: IELs show mitochondrial plasticity during activation 184

6.1. TCR stimulation is sufficient to activate IELs, resulting in increased mitochondrial mass and Ki-67 expression 184

6.2. TCR-activated CD8αβ$^+$ IELs have higher production of mitochondrial ROS 192

6.3. TCR-activated IELs have unchanged CL content and mitochondrial membrane potential…..... 194

6.4. IELs become activated by αCD3 independently of other T cells 196

6.5. Co-stimulatory CD28 is not sufficient to trigger cytokine production in IELs 201

6.6. Mechanistic insights behind the mitochondrial changes in IELs during TCR-stimulated activation 206

6.7. T-bet-deficient IELs may have a higher threshold to enable increase in mitochondrial mass…..... 207

6.8. Eomes is dispensable for mitochondrial remodeling and Ki-67 response in IELs 210

6.9. AhR may be involved in the threshold to enable MTG increase in IELs 214

6.10. AhRR is dispensable for the TCR-mediated activation response in IELs 218

6.11. Cyp1a enzymes are involved in the αCD3-mediated Ki-67 response 220

6.12. IEL activation leads to drastic CL composition alternations 222

6.13. Supplemental chapter figures.....228

6.14. Chapter Discussion 230

Chapter 7: Full IEL activation depends on lumenal/bacterial compound(s) 240

7. Enteric microbiota and pathogens.....240

7.1. Enteric viral pathogens: Murine norovirus (MNV) 241

7.2.Bacterial pathogens: *Salmonella*.....242

7.3. Eukaryotic pathogens: *Eimeria vermiformis (E. vermiformis)*.....243

7.4. Gut microbiota 244

7.4.1. Gram-positive bacteria.....245

7.4.2. Gram-negative bacteria.....246

7.5. IEC stress in Villin-Cre- $XBP1^{fl/fl}$ mice is not sufficient to fully activate IELs.....248

7.6. IELs become fully activated during *E. vermiformis* infection 252

7.7. *E. vermiformis*-activated IELs have higher mitochondrial ROS production, but show no increase in mitochondrial membrane potential.....267

7.8. MNV-CW3, but not MNV-O7, infection led to IEL activation. 271

7.9. *Salmonella* infection does not activate IELs.....274

7.10. IELs are activated in IL-22-/- mice in a microbiota-dependent manner.....277

7.11. Commensal microbiota are activating IELs in MNV-CW3 infection 283

7.12. Commensal microbiota are activating IELs in *E. vermiformis* infection.....288

7.13. Gram-positive microbiota are activating IELs in *E. vermiformis* infection.....296

7.14. IELs are not essential for coping with load of *E. vermiformis* 304

7.15. Anti-CD3-medaited IEL activation is not reduced by antibiotics 308

7.16. DSS-induced colitis does not fully activate small intestinal IELs.....312

7.17. Common gamma chain signalling is involved in determining IEL activation state……318

7.18. Supplemental chapter figure 325

7.19. Chapter Discussion 326

Chapter 8: Discussion 336

8.1. IEL-organoid system provides an *in vitro* option for IELs.....336

8.2. IELs have compromised mitochondrial status.....340

8.3. IELs have mitochondrial plasticity induced by TCR-stimulation 341

8.4. Gram-positive commensal bacteria can fully activate IELs 344

Chapter 9. Conclusions.....350

Chapter 10. References.....358

Chapter 1: Introduction

1. Introduction

The immune system needs to respond appropriately towards infections caused by bacteria, viruses or parasites threatening the homeostasis of the host. The immune system consists of both cellular and humoral components that can respond to both non-specific and specific antigens. Here, I am going to introduce the immune system, with the focus on the intestinal immune system.

1.1. Cellular Immune System

All immune cells originate from hematopoietic stem/progenitor cells (HSPCs). These cells are located in the bone marrow (BM). HSPCs can further differentiate into common lymphoid progenitors (CLPs) and common myeloid progenitors (CMPs). CLPs can differentiate into T cells, B cells and natural killer (NK) cells, while CMPs generate e.g. dendritic cells (DCs) and macrophages (MPs) (Seita and Weissman, 2010). Below, I am going describe the different immune cells. Particular focus will be on T cells, intestinal epithelial cells (IECs) and intraepithelial lymphocytes (IELs).

1.2. Innate Immunity

The system of innate immunity consists of a range of different immune cells and the complement system. Innate immunity generates rapid immune responses towards non-specific antigens. They are able to do so by using a limited number of receptors such as pattern recognition receptors (PRRs) that recognize common patterns of pathogens. Examples of PRRs are toll-like-receptors (TLRs), nucleotide-binding oligomerization domain (NOD)-like receptors (NLRs) and retinoic acid-inducible gene-(RIG)-like receptors (RLRs).

1.2.1. Granulocytes: neutrophils, eosinophils and basophils

Granulocytes are immune cells classified by the presence of granules in their cytoplasm and the morphology of their nucleus. Hence, another name for granulocytes is polymorphonuclear (PMN) cells.

Neutrophils are usually the first type of immune cells recruited to inflammatory sites. In mice, it has been reported that circulating neutrophils have a half-life of 1.5 hours (Kolaczkowska and Kubes, 2013). Like other PMN cells, they phagocytose pathogens. For intestinal sites, it has been suggested that interleukin (IL)-18 alters the tight junction (TJ) proteins between IECs, to enable neutrophils to transmigrate between IECs (Lapointe and Buret, 2012). One of the characteristics of neutrophils is their ability to form neutrophil extracellular traps (NETs). NETs consist of intracellular content, such as DNA elements and proteins, which can immobilize and subsequently kill pathogens. It has recently been discovered that mitochondrial reactive oxygen species (ROS) play a role for NET formation: inhibition of mitochondrial ROS production leads to reduced release of NETs (Lood et al., 2016). In addition to their anti-inflammatory properties, neutrophils appear to have tissue healing properties. A role of neutrophil-mediated interactions with IECs, via intracellular adhesion molecules (ICAM), have been shown to promote IEC proliferation. Lack of this ICAM-mediated interaction led to fewer wounds being healed *in vivo* (Sumagin et al., 2016).

Another type of PMN cells are eosinophils. Eosinophils have granules containing antimicrobial proteins (AMPs), cytokines, chemokines and cationic proteins such as eosinophil peroxidase (EPO) and eosinophil-derived neurotoxin (EDN) (Strandmark et al., 2016; Forman et al., 2016). Eosinophils are characterized by their expression of the cell surface protein Siglec-F. Mice lacking the transcription factor Gata1 lack eosinophils. Using

Gata1-deficient mice and a *Trichuris muris (T. muris)* infection model as an inducer of eosinophil immunity, it has been shown that there are fewer IgA^+ plasma cells in the small intestine, while the number of IgA^+ plasma cells in the large intestine is unaffected (Forman et al., 2016). These observations highlight differences in the small and large intestinal compartments. Unlike neutrophils and basophils, it has been shown that eosinophils require the transcription factor (TF) X-box binding factor 1 (XBP1) for eosinophil differentiation. XBP1 is a key factor for the stress response of the organelle endoplasmic reticulum (ER) (Shen and Malter, 2015). Eosinophils also differ from the other PMN cells in their recruitment to the intestinal compartment. Using a dextran sulphate sodium (DSS)-induced model of colitis combined with antibiotic depletion, it has been shown that Gram-positive bacteria are required for the recruitment of macrophages (MPs), monocytes and neutrophils to the intestinal compartment. However, the recruitment of eosinophils is unaffected by the different antibiotic treatments (Nakanishi et al., 2014). These data suggest a role for commensal microbiota in the recruitment process of macrophages, monocytes and neutrophils, but other factor(s) to induce eosinophil recruitment during intestinal inflammation.

The rarest granulocytes are basophils. They have similarities with mast cells (see section 1.2.2), sharing the expression of the antibody receptor Fc epsilon receptor. However, while mast cells undergo their final differentiation in the homing tissue, basophils are fully differentiated already in the blood circulation. It has been suggested that basophils secrete IL-4 and hence have a role in Th2-mediated immunity (Sullivan and Locksley, 2009).

1.2.2. Mast cells

In addition to PMN cells, there are monomorphonuclear (MMNs) immune cells such as T cells, B cells and mast cells. Like PMN cells, mast cells contain granules. The granules in mast cells contain for example proteases, prostaglandins and tumour necrosis factor alpha (TNFα) (Lee and Lee, 2016). Anti-TNFα antibodies are currently the main therapy to treat inflammatory bowel disease (IBD). However, TNFα therapy is only successful in approximately 40% of the treated patients (West et al., 2017). Intestinal mast cells are mainly found in the lamina propria (LP) compartment. Mast cells can become activated via IgE-dependent and IgE-independent mechanisms. In IgE-mediated activation, the allergen binds the FC epsilon receptor. The binding of IgE to FC epsilon receptors on mast cells results in the release of a range of intracellular mediators, such as the vasoactive substances histamine, prostaglandins and vascular endothelial growth factor (VEGF),which contribute to type I hypersensitivity responses (Abraham and St. John, 2010; Galli and Tsai, 2013; Lee and Lee, 2016) Mast cells have also been associated with celiac disease (CD) (Frossi et al., 2016), in which another important intestinal immune cell subset are also implicated: IELs. (Cukrowska et al., 2017).

1.2.3. Dendritic cells (DCs)

Dendritic cells (DCs) are a heterogeneous group of antigen presenting cells (APCs) that were first discovered by Ralph Steinman and colleagues based on their morphological features. DCs were initially described as large stellate cells (Steinman and Cohn, 1973). Studies performed after the discovery of DCs demonstrated that DCs stimulated T cell proliferation (Steinman and Witmer, 1978). Further studies have revealed the heterogeneity of DCs: they can be further categorised based on their developmental pathways, tissue of residence, circulatory capacities and a range of surface markers such as CD11b, CD11c, CD103 and

major histocompatibility complex (MHC)-II (Steinman and Idoyaga, 2010). For example, some DCs are derived from monocytes and are hence named monocyte-derived DCs (Guilliams et al., 2014). Intestinal DCs act as sentinels and sensors, monitoring the luminal content by sampling bacteria and food antigens, before migrating to the draining mesenteric lymph nodes (MLNs), where they activate adaptive immune responses (Persson et al., 2010). As such, DCs are important players for intestinal immunity and homeostasis. Further investigations of the DC sampling processing have suggested a role of the commensal microbiota: antibiotic treatment reduces the number of DC extrusions through the IEC barrier. Furthermore, using toll-like receptor (TLR) ligands for TLR2, TLR4 and TLR9, an increase in the number of DC extrusions through the IEC barrier was observed, while TLR3 and TLR5 ligands had no significant effect on the number of DC extrusions. Bone marrow chimeras deficient in Myd88, TLR2 or TLR4 had fewer DC extrusions through the IEC barrier (Chieppa et al., 2006). These data suggest that interactions between commensal microbiota, IECs and other immune cells may be able to affect the number of DC extrusions used for sampling the intestinal lumen, and thus may be able to alter the downstream immune responses.

It has been demonstrated that mice, that have depletion of the TF interferon regulatory factor 4 (IRF4) by CD11c promoter-driven Cre-expression, have fewer intestinal $CD103^+$ $CD11b^+$ DCs. The fewer $CD103^+$ $CD11b^+$ DCs in CD11c-Cre-$IRF4^{fl/fl}$ mice had a reduced DC-mediated Th17 response, while the Th1 and Treg responses were unaffected (Persson et al., 2013). Another TF, interferon regulatory factor 8 (IRF8), was later shown to be important for $CD103^+$ $CD11b^-$ DCs. Depleting $CD103^+$ $CD11b^-$ DCs led to a reduction in the number of all IEL subsets (see section 1.6.3). Furthermore, the reduction of $CD103^+$ $CD11b^-$ DCs led to a

reduced intestinal Th1 response (Luda et al., 2016). These data indicate that different subsets of DCs have different roles and capacities to induce T cell responses.

1.2.4. Monocytes

Monocytes, formed in the bone marrow, are precursors to macrophages (MPs). Via the activation of the chemokine receptor CCR2, monocytes egress from the bone marrow to the blood circulation (Boring et al., 1997). Once the monocytes are in the blood circulation, they migrate to peripheral tissues, where they differentiate into DCs and MPs. *In vitro* and *ex vivo* data suggest a model in which monocytes differentiate into anti-inflammatory MPs when recruited to a steady state intestinal compartment. In contrast during intestinal inflammation, monocytes generate pro-inflammatory DCs (Rivollier et al., 2012; Tamoutounour et al., 2012; Bain et al., 2013). These data suggest that local factors determine monocyte differentiation. In contrast, one report suggested that monocytes could become primed whilst still in the bone marrow via IFNγ production sourced from natural killer (NK) cells (Askenase et al., 2015). In addition, it has also been suggested that monocytes can interact with IECs, specifically the intestinal epithelial stem cells (IESCs), and can induce proliferation in those cells (Skoczek et al., 2014).

1.2.5. Macrophages (MPs)

Macrophages (MPs) are phagocytic and antigen presenting immune cells. They are commonly divided into two categories: M1 and M2 MPs. This categorization mirrors that of Th1 and Th2 cells (see section 1.3.2.1): M1 MPs are induced by classical Th1 cytokines such as IFNγ, while M2 MPs are induced by Th2 cytokines such as IL-4. M1 and M2 MPs also differ in their cytokine production: M1 MPs produce high amounts of IL-12 and IL-23 and low amounts of IL-10, while the reverse cytokine production applies to M2 MPs (Mantovani

et al., 2005). However, some MPs, such as those found in the intestine, show a mixture of M1 and M2 phenotypes. Intestinal-resident MPs usually have inflammatory anergic properties, but retain high phagocytic and bactericidal activities and are thought to play important roles in tissue homeostasis via the clearance of apoptotic cells (Smith et al., 2005), such as of stressed and shed IECs (Cummings et al., 2016). It has been shown that TLR2 and TLR4 stimulation is required for mitochondrial ROS-mediated bactericidal activity in MPs (West et al., 2011).

1.2.6. Natural Killer (NK) cells

Natural killer cells (NK cells) are classified as innate immune cells. However, unlike other innate immune cells, NK cells are derived from CLPs that also generate T and B cells (Yokoyama et al., 2004). Unlike T and B cells, NK cells do not express any antigen receptor. NK cells can be divided into conventional NK and NK-like cells. Conventional NK cells express the markers NK1.1 and NKp46 and are able to lyse infected cells by secreting granzymes and perforin, which forces the target cells into apoptosis (Vivier et al., 2008). NK cells are dependent on signalling via IL-2Rγ (Cao et al., 1995) and IL-15Rα (Kennedy et al., 2000). In addition, NK cells are a source of IFNγ which affect other immune cells such as Th1 cells, monocytes and M1 MPs. NK-like cells on the other hand, are less cytotoxic and rather secrete IL-22, which promotes proliferation of IECs, hence NK-like cells are sometimes named NK-22 cells (Fuchs and Colonna, 2011).

1.2.7. Innate Lymphoid cells (ILCs): ILC1, ILC2 and ILC3

Sometimes, NK cells are classified as one of the innate lymphoid cell (ILC) subsets. ILCs were discovered in recombination activating gene 2 (Rag2)-/- mice that lack both T and B cells (Shinkai et al., 1992). Injecting IL-25 into Rag2-/- mice led surprisingly to secretion of

Th2-associated cytokines - despite the lack of T cells (Fallon et al., 2006). Early literature about ILCs refer to these cells as natural helper cells (NHCs) and innate helper (IH) cells (Walker et al., 2013). ILCs are thought to be innate versions of the T cells, for which NK cells mirror cytotoxic $CD8\alpha^+$ T cells (CTLs), while ILC1, ILC2 and ILC3 mirror $CD4^+$ T helper (Th) cells Th1, Th2 and Th17 cells, respectively. This mirroring is thought to apply to both the master transcription factor and the cytokines secreted: like Th1 cells, ILC1 express Tbx21 and secrete IFNγ, ILC2 express Gata3 and secrete IL-4, -5 and IL-13 and ILC3 express RORγt and secrete IL-22 and IL-17. Lymphoid tissue inducer (LTi) cells are usually classified as part of ILC3 subset. Unlike their adaptive counterparts, ILCs do not require to undergo clonal selection and expansion but can instead respond immediately with cytokine secretion (Eberl et al., 2015). Further characterization of ILCs, using single-cell RNA sequencing analysis, has suggested that the grouping of ILC1, ILC2 and ILC3 cells can each be split into additional 4-5 subsets (Gury-BenAri et al., 2016).

1.3. Adaptive Immunity

To complement innate immunity, there is an adaptive immune system that can respond to specific antigens. Adaptive immune cells can be classified into B and T cells, which can be further divided based on their cell surface protein expression and their tissue location. Both T and B lymphocytes are dependent on the Rag enzymes for arrangement of their respective antigen receptor, as Rag2-/- mice lack both T and B cells (Shinkai et al., 1992).

1.3.1. B cells: B1, B2 and plasma cells

B cells are an important part of the adaptive immune system. Two lineages of B cells are found in mice: B1 and B2 cells. They differ in the expression of surface markers, such as CD5 and CD23 (Bao et al., 1998). B cells are important for the secretion of antibodies such

as IgA, IgD, IgE, IgG and IgM originating from heavy chains α, δ, ε, γ and μ, respectively. B cells, which each produce one class of Ig at any given time, are called plasma cells (Angelin-Duclos et al., 2000). The kind of Ig that is produced by the plasma cells depends on the class switch that has taken place. Activation-induced cytidine deaminase (AID) is essential for class switching and only IgM-producing B cells are present in AID-deficient mice (Fagarasan et al., 2002). In the mucosal site, B cells can be found in secondary lymphoid organs (SLOs) such as Peyer's Patches (PPs) and MLNs (Roy et al., 2013). In the intestinal compartment, there is a preference for plasma cells secreting IgA. The majority of IgA^+ plasma cells originate from B2 cells from PPs, although B1 cells also contribute to IgA production (Bao et al., 1998). The intestinal compartment has conditions favouring IgA class switching. One such factor that promotes IgA class switching is transforming growth factor beta (TGFβ) that is present in the intestinal compartment (Brandtzaeg and Johansen, 2005). Combination of TGFβ and the vitamin A derivative retinoic acid (RA) have been shown to have additive effects in increasing IgA class switching (Watanabe et al., 2010).

1.3.2. $CD4^+$ T cells

The other important part of the adaptive immune system is T cells. These cells are named T cells as they develop in the thymus. In the thymus, T cells undergo both positive and negative selection processes to eliminate any potential T cells that are reactive to host antigens. T cells can be classified depending on which co-receptor they express: CD4 or CD8α. $CD4^+$ T cells can receive antigens from MHC-II^+ APCs, while $CD8\alpha^+$ T cells receive antigens from MHC-I^+ APCs. During the thymus development, there is a trend towards generation of higher numbers of $CD4^+$ T cells than $CD8\alpha^+$ T cells (Van Laethem et al., 2012). This is thought to be because more $CD8\alpha^+$ T cells die during the selection processes (Sinclair et al., 2013). During the thymus selection process, the T cell receptor (TCR) is arranged. This arrangement is

strictly dependent on Rag enzymes, as Rag2-/- mice lack T cells (Shinkai et al., 1992). $CD4^+$ T cells are found in many organs such as spleen, lymph nodes (LNs), IEC and LP compartments.

1.3.2.1. T helper (Th) cells

In the past, T helper (Th) cells were thought to consist of two different Th subsets based on their cytokine secretion profile, namely Th1 and Th2 cells (Mosmann et al., 1986; Cherwinski et al., 1987). In 2006, a third Th subset, Th17 cells able to secrete IL-17, was discovered (Mangan et al., 2006; Zhou et al., 2007). In addition, there are reports suggesting additional Th subsets such as Th9 and Th22 cells. Interestingly, there are reports suggesting plasticity between the different Th subsets (Magombedze et al., 2013; Lee et al., 2009), suggesting that Th cell differentiation may be adjustable to changes in their microenvironment.

1.3.2.2. IFNγ-secreting Th1 cells

Th1 cells were initially defined by their secretion of IFNγ (Mosmann et al., 1986). It was later discovered that the TF T-bet functions as a master transcription factor for Th1 differentiation. T-bet is also important for IFNγ secretion. If T cells are deficient in T-bet expression, then these cells cultured under Th1 differentiation conditions have lower IFNγ production (Lazarevic et al., 2011; Yang et al., 2008). In addition, T-bet together with another transcription factor named Runx3, is important for Th1 differentiation. T cells cultured under Th1 conditions do not secrete the Th2-associated cytokine IL-4, but when T cells lack Runx3, there is a small proportion of cells that secrete IL-4 (Djuretic et al., 2007).

There are studies that have shown a role of the vitamin A derivative RA for Th1 and Th17 cytokine production. Mice on diets that lack vitamin A during *Toxoplasma gondii (T. gondii)* infection showed a lower production of both IFNγ and IL-17 in the spleen and LP compartment (Hall et al., 2011a). The processing of vitamin A to RA involves the enzymes alcohol dehydrogenases (ADH) and retinal dehydrogenase (RALDH). Fewer cells express RALDH compared to ADH. RALDH have been found expressed in cells such as intestinal DCs and IECs (Hall et al., 2011b). The evidence for the importance of RA for Th1 cells was strengthened by using a dominant negative form of the retinoic acid receptor alpha (dnRARα). DnRARα $CD4^+$ T cells generated less IFNγ and expressed lower levels of T-bet, while production of IL-17 and RORγ expression was increased (Brown et al., 2015), suggesting an important role of RA for Th1 cell stability.

Th1 cells and IFNγ has been showed to be important for immune responses against intracellular pathogens such as *Listeria monocytogenes (L. monocytogenes)* (Romagnoli et al., 2016), vaccinia virus (Huang et al., 1993), *Mycobacterium tuberculosis* (Cooper et al., 1993), *Leishmania major* (Reiner and Locksley, 1995) and *Eimeria vermiformis* (Smith and Hayday, 2000).

1.3.2.3. IL-4-secreting Th2 cells

The second Th subset, Th2 cells, was initially characterized by the lack of secretion of IFNγ, but secretion of IL-4 and IL-5 (the names MCGF2 and TCGF2 were used in the 1986 paper for IL-4 and IL-5, respectively) (Mosmann et al., 1986; Ziegler, 2016). Since the discovery of Th2 cells, it has been shown that their master transcription factor is Gata3. Th2 cells are important for type 2 responses against helminth infections. In barrier tissues such as the intestinal barrier, the Th2-associated cytokines IL-4 and IL-13 can aid IECs to expel

helminths (Paul and Zhu, 2010) such as *Heligmosomoides polygyrus* (Urban et al., 1991) and *T. muris* (Allison Bancroft et al., 1998). Previous reports suggest that basophils and specific subsets of DCs are important to prime Th2 cytokine responses (Perrigoue et al., 2009; Mayer et al., 2017), while eosinophils have a role in supressing Th2 responses (Strandmark et al., 2016).

1.3.2.4. IL-9-secreting Th9 cells

Another proposed Th subset is Th9 cells that secret IL-9. Th9 cells have been reported to be induced by IL-4 and TGFβ. TGFβ, in combination with other cytokines, has been reported to induce other Th cells: Th17 cells when combined with IL-6 and Treg cells when combined with IL-2 (Schmitt and Bopp, 2017). The IL-9 secretion from Th9 cells is reduced in the absence of the transcription factor IRF8 (Humblin et al., 2017). Using oxazolone treatment as a model to induce colitis, it has been shown that mice deficient in IL-9, or on anti-IL-9 treatment, showed less weight loss compared to controls (Gerlach et al., 2014), suggesting a role of Th9 in colitis pathology. In contrast, has been suggested that Th9 cells and IL-9 also have anti-tumour properties. IL-9R-/- mice and WT mice receiving anti-IL-9 antibodies showed increased tumour volume, while rIL-9 treatment of mice led to decreased tumour volume in the B16F10 cancer model (Purwar et al., 2012).

1.3.2.5. IL-17-secreting Th17 cells

Th17 cells were discovered in 2006, by observing IL-17 production in the presence of TGFβ and either the absence of IFNγ, using anti-IFNγ or IFNγ-/- mice (Mangan et al., 2006), or the presence of IL-6 (Zhou et al., 2007). Further studies demonstrated that retinoic acid related orphan receptor gamma thymus (RORγt) is the master transcription factor for Th17 differentiation (Muranski and Restifo, 2013). IECs are one source of TGFβ secretion (Artis,

2008; Jiang et al., 2016). It has also been shown that Th17 cells from the small intestinal LP compartment lack IL-17 production in germ-free (GF) mice (Atarashi et al., 2015). Interestingly, it has been shown that Th17 differentiation is reversible: Th17 differentiation can be reversed, and instead converted to Th1 cells, by removing TGFβ and adding IL-12 (Muranski and Restifo, 2013). Induction of T-bet during Th17 differentiation leads to shift from IL-17 to IFNγ production (Lazarevic et al., 2011). In addition to secrete IL-17, Th17 cells have also been reported to be able to secrete IL-22 (Liang et al., 2006; Zheng et al., 2007). Other cells that are able to secrete IL-22 are ILCs (Sonnenberg et al., 2011), IELs (Ahlfors et al., 2014), NK-like cells (Fuchs and Colonna, 2011) and Th22 cells (Basu et al., 2012). Th17 cells have been showed to be important to generate protective immunity against a range of fungi and bacterial infections such as *Candida albica* (Huang et al., 2004), *Staphylococcus aureus* (Lin et al., 2009) and *Citrobacter rodentium (C. rodentium)* (Reis et al., 2015).

1.3.2.6. IL-22-secreting Th22 cells

In addition to IL-22-secreting Th17 cells, there are several reports about a Th22 subset. Unlike Th17 cells, these Th22 cells do not secrete IL-17. Th22 cells can be generated *in vitro* under culture conditions with IL-6, with enhanced differentiation in combination with IL-23, but reversed in the presence of TGFβ – an important factor for Th17 differentiation. In addition, Th22 cells differ from Th17 by lacking expression of the TF aryl hydrocarbon receptor (AhR) and instead have expression of the TF T-bet. The majority of IL-22-/- mice succumb to *C. rodentium* infection. However, transfer of Th22 cells, but not Th17 cells, into IL-22-/- mice significantly increases the survival rate of IL-22-/- mice (Basu et al., 2012). Another laboratory confirmed the involvement of Th22 cells in *C. rodentium* infection (Backert et al., 2014), supporting the notion of an important role of Th22 cells in bacterial

infections. The research on Th22 cells is still limited and not as extensive as the other Th cells.

1.3.2.7. T regulatory (Treg) cells

Treg cells are the immune regulatory subset of $CD4^+$ T cells. They are classified by expression of the TF forkhead box P3 (Foxp3) and suppress effector functions. Later studies have suggested that the Treg cell population is heterogeneous. Some studies are suggesting that there are Treg cells that co-express Foxp3 and one of the Th master transcription factor T-bet, Gata3 and RORγt and form Th1-, Th2- and Th17- like Treg cells (Zhu and Paul, 2010). The principle that Treg cells are important for intestinal health is used in the Powrie model of colitis, in which colitis is induced by transferring naïve $CD4^+$ T cells into Rag-deficient hosts. Transferring $CD4^+$ T cells, including Treg cells, prevents the induction of colitis (Powrie et al., 1994a; b). Treg cells are also affected by RA. Unlike Th1 and Th17 cells, the proportion of Treg cells is increased in the presence of RA. In addition, culturing conditions including RA, TGFβ and IL-6, turn Th17 cells into Treg cells (Mucida et al., 2007).

1.3.3. $CD8\alpha^+$ T cells

$CD8\alpha^+$ T cells are the cytotoxic arm of T cell immunity. It has been reported that CD8α expression is required for T cell cytotoxicity. Using *in vitro* cytotoxic assays, CD8a-/- splenocytes showed low cytotoxic capacity (Fung-Leung et al., 1991). Yet, CD8β-/- mice can still generate a response towards lymphocytic choriomeningitis virus (LCMV) (Angelov et al., 2009). Activated $CD8\alpha^+$ T cells produce effector proteins such as IFNγ, perforin and granzyme B, making them an essential component for coping with intracellular pathogens,

viral infections and tumours (Cruz-Guilloty et al., 2009). As mentioned in section 1.3.2, $CD8\alpha^+$ T cells can become activated by antigen presentation from MHC-I^+ APCs.

1.3.3.1. Effector $CD8\alpha^+$ T (Teff) cells

Another name for activated $CD8\alpha^+$ T cells is cytotoxic T lymphocytes (CTLs). Studies of CTLs' proteome have shown that CTLs mainly express proteins related to e.g. cell metabolism, such as GLUT1, and cytotoxic proteins such as granzyme B. Granzyme B was among the top 10 most abundant proteins in CTLs (Hukelmann et al., 2015). Another proteomic study has suggested that IL-2 is involved in promoting a range of protein interactions in CTLs, such as gene expression and proteins associated to cytoskeleton and their regulation (Ross et al., 2016).

Like $CD4^+$ effector cells, it has been shown that $CD8\alpha^+$ Teff cells require glycolysis for effector functions. Addition of the glycolysis inhibitor 2-Deoxy-D-glucose (2-DG) led to a reduction in proliferation and IFNγ secretion (Cham et al., 2008). In addition to $CD8\alpha^+$ CTLs, there are reports suggesting the presence of $CD4^+$ CTLs. These cells have been formed by the loss of the expression of the TF Th-Inducing POZ-Kruppel Factor (ThPOK) and instead express the TF Runx3 (Cheroutre and Husain, 2013). Runx3 has been showed to be important for $CD8\alpha^+$ T cell maintenance, as Runx3-/- mice have a reduced number of $CD8\alpha^+$ thymocytes and splenocytes (Woolf et al., 2003).

In addition to the requirement of glycolysis for $CD8\alpha^+$ Teff cell functions, it has been reported that an interplay between the T-box factors T-bet and Eomesdermin (Eomes) are essential for IFNγ production from $CD8\alpha^+$ Teff cells. Absence of one of these T-box factors still led to IFNγ production from activated $CD8\alpha^+$ T cells. However, absence of both T-box

factors led to low IFNγ production and instead significant production of IL-17. This shift in immune response also led to more weight loss and an increased pathogen load in mice infected with LCMV (Intlekofer et al., 2008).

1.3.3.2. Memory T (Tmem) cells

Memory $CD8\alpha^+$ T (Tmem) cells are antigen experienced T cells defined by a high expression in the lymphocyte activation marker CD44 and a low expression in CD62L. The exact kinetics of Tmem cell formation is still being debated. One hypothesis suggests that upon activation, naïve $CD8\alpha^+$ T cells undergo clonal expansion and form $CD8\alpha^+$ Teff cells. Once the inflammatory stimuli are cleared, the majority of these $CD8\alpha^+$ Teff cells die. The remaining cells form a Tmem cell population. A second hypothesis is that Tmem cells are formed directly from naïve $CD8\alpha^+$ T cells and then generate Teff cells. A third hypothesis suggests that both Teff and Tmem cells can be generated from naïve $CD8\alpha^+$ T cells. Indeed, single-cell barcoding experiments have shown that naïve $CD8\alpha^+$ T cells can generate both Tmem and Teff cells (Gerritsen and Pandit, 2015), supporting the third hypothesis of Tmem cell formation.

Tmem cells are characterised by a fast response upon re-encounter with their antigen. One example of the speed of the re-call response was demonstrated using *L. monocytogenes* as a model. Using this model, it was demonstrated that Tmem cells could respond within hours of re-infection (Bajénoff et al., 2010). However, Tmem cells appear to be a heterogeneous group of T cells. There are some hypo-responsive T cells named exhausted T cells. They express several inhibitory molecules such as PD-1, CTLA-4 and LAG3 (Programmed death 1, cytotoxic T lymphocyte-associated protein 4 and lymphocyte-activation gene 3, respectively) (Scott-Browne et al., 2016). Another marker used for Tmem cells is killer cell lectin-like

receptor G1 (KLRG1), which is proposed to assist in distinguishing between long-lived ($KLRG1^{lo}$) and short-lived ($KLRG1^{Hi}$) Tmem cells (Omilusik et al., 2015).

Bacterial infections such as *L. monocytogenes* and *Salmonella* lead to increased level of acetate in the serum. For Tmem cells, this increase of acetate resulted in increased acetylation and thereby activation of glyceraldehyde 3-phosphate dehydrogenase (GAPDH) and thus increased glycolysis and subsequently resulted in an increase in IFNγ-production as part of the re-call Tmem cell response (Balmer et al., 2016). To sustain this response, it was also shown that both TCR stimulation, demonstrated using αCD3, as well as co-stimulatory CD28 stimulation were required (Gubser et al., 2013). Further investigations into the metabolic requirements for memory and effector $CD8\alpha^+$ T cells have revealed metabolic differences between these subsets: $CD8\alpha^+$ Teff cells store more lipids and are dependent on fatty acid oxidation (FAO) for full functionality, while Tmem cells do not store lipids and instead use glycolysis for their functions (O'Sullivan et al., 2014). In addition, there are some evidence that the cytokine IL-15, which is important for maintenance of memory $CD8\alpha^+$ T cells, NK cells and IELs (Lodolce et al., 1998), also could be linked to the metabolic properties of Tmem cells. Tmem cells have increased mitochondrial spare respiratory capacity (SRC) compared to naïve T cells. This increase in SRC is thought to be due to the increased mitochondrial biogenesis, which was demonstrated when culturing antigen experienced ovalbumin-specific $CD8\alpha^+$ T cells (OT-I cells) with IL-15 (van der Windt et al., 2012). It has also been suggested that DCs and MPs can support Tmem cells via IL-15 trans-presentation (Mortier et al., 2009).

1.3.3.3. Tissue resident T (Trm) cells

Recent studies have split Tmem cells into those cells that are able to re-circulate and those cells that are tissue resident (Trm) cells. Trm cells are characterized by expression of CD69 and CD103, for which TGFβ has been shown to be important for the CD103 expression of skin and intestinal Trm cells. In addition, it has been showed that tissue resident IL-15 is required for skin Trm cell maintenance (Mackay et al., 2013). It seems that skin Trm require lipid uptake for their maintenance (Pan et al., 2017).

It has been reported that the TFs Hobit and Blimp1 are expressed in Trm cells found in the liver and skin. Mice deficient in both TFs Hobit and Blimp1 had reduced CD69 and CD103 expression (K.Mackay et al., 2016), supporting the involvement of Hobit and Blimp1 for Trm cells. There are also evidence that T-bet and Eomes are involved in Trm cell maintenance, as forced expression of either of those TFs reduced CD103 expression (Mackay et al., 2015).

It has recently been shown *ex vivo* that pro-inflammatory cytokines such as IL-12, IL-18 and IFNβ, in combination with TGFβ can downregulate the CD103 expression on intestinal Trm cells (Bergsbaken et al., 2017). The authors did not present any quantification of the number of Trm cells remaining in the different conditions. It would be interesting to know whether the downregulation of the Trm marker CD103 correlates with reduction in the number of Trm cells due to cell death or due to the Trm cells re-gaining their ability to re-circulate. λ

1.3.4. TCRγδ$^+$ T cells

Most systemic T cells express TCRs consisting of α and β chains. However, there are T cells that express non-classical γ and δ chains. These cells are found in tissues such as spleen, liver, kidney and epithelial sites such as intestine, skin, lung and uterus (Muñoz-Ruiz et al.,

2017). The ratio of TCRγδ$^+$ cells among T cells is small in most tissues, except for the skin and the intestinal compartment. Unlike TCRγδ$^+$ IELs from the small intestine, TCRγδ$^+$ cells sourced from spleen and LNs can be cultured *in vitro* (Ribot et al., 2009). Figure 5.6 A-E in Chapter 5 illustrates the distribution of TCRγδ$^+$ and TCRαβ$^+$ T cells in lung, spleen, liver and intestinal compartments.

Despite the observation that most non-intestinal TCRγδ$^+$ cells do not express CD8α, they seem not to require interactions with MHC-II, as MHC-II-/- mice have a similar number of TCRγδ$^+$ cells as control mice (Bigby et al., 1993). There seem to be interactions between the different T cells, as it has been demonstrated that TCRγδ$^+$ T cells sourced from spleen are prevented from proliferation by splenic TCRαβ$^+$ T cells (French et al., 2005).

Both IL-17- and IFNγ-secreting versions of TCRγδ$^+$ T cells have been identified. It has been reported that the marker CD27 can distinguish between IL-17- and IFNγ-producing TCRγδ$^+$ cells. Most CD27-expressing TCRγδ$^+$ cells produce IFNγ (Ribot et al., 2009). In addition, strong TCR signalling and expression of CD45RB also promotes IFNγ-producing TCRγδ$^+$ cells (Sumaria et al., 2017).

1.3.5. Natural killer T cells (NK T cells)

There is a group of T cells that also express the typical NK marker NK1.1 and are hence named natural killer (NK) T cells. These are found in tissues such as spleen, liver and thymus (Kronenberg and Gapin, 2002). Unlike other T cells that become activated by peptides presented from MHC molecules, NK T cells have been reported to become activated by glycolipids presented on CD1d$^+$ cells (Tupin and Kronenberg, 2006). CD1d appears to be essential for IFNγ production, as NK T cells from CD1d-/- mice produce very little IFNγ

compared to controls (Mattner et al., 2005). There are no NK T cells in GF mice, suggesting that commensal microbiota is important for maintenance of these cells. In addition, there are data suggesting that NK T cell may have subsets analogous to $CD4^+$ T helper cell subsets (Lee et al., 2013).

1.3.6. Mucosal-associated invariant T cells (MAITs)

Mucosal-associated invariant T cells (MAITs) are a rare T cell population in mice. MAITs are found in various tissues such as liver, lung and LP compartment (Rahimpour et al., 2015). These cells have semi-invariant T cells that recognise antigens from cells expressing MHC related protein 1 (MR1). A report suggests that MAIT may be able to recognize microbial- and vitamin B2-derived antigens. MAITs are absent in GF mice, suggesting an essential role of commensal microbiota for the maintenance of MAITs (Ussher et al., 2014).

1.4. Humoral immune system

As previously described, there are numerous types of different specialised immune cells. In common, these cells secrete various cytokines and interleukins as a response towards non-specific and specific antigens. The secreted proteins include TNFα, interferons (IFN), chemoattractant cytokines named chemokines and pro- and anti-inflammatory interleukins (ILs). Interferons can be classified into type I, II and III, which correspond to IFNα and IFNβ, IFNγ and IFNλ, respectively (Pott and Stockinger, 2017). IFNγ is secreted from e.g. Th1 cells and has been shown to be important for managing infection by the intestinal parasite *Eimeria vermiformis* (Smith and Hayday, 2000). IFNλ has received attention as being important for clearance of enteric viruses such as rotavirus (Pott et al., 2011) and murine norovirus (MNV) (Nice et al., 2015).

As previously described, plasma cells in the intestinal immune system produce IgA molecules. IgA is abundant in the mucus layer, topping the intestinal epithelial barrier. IgA both coats and contains the commensal microbiota. Interestingly, these IgA molecules have been suggested to be polyreactive towards commensal microbiota (Bunker et al., 2017). The importance of IgA has been shown by using AID-/- mice. These mice fail to undergo antibody class switching and hence cannot produce IgA. These mice had altered and increased microbiota abundance (Wei et al., 2011; Fagarasan et al., 2002). IgA production is almost absent in GF mice (Wu et al., 2016). The role of the microbiota for the immune system will be discussed further in Chapter 7 and Chapter 8.

Finally, within the humoral immune system there is the complement system. This system can become activated by three different pathways: classical, lectin and alternative pathways. In common, all three pathways lead to the activation of the enzyme C3 convertase, leading to the cleavage of the protein C3 into C3b and C3a. C3a is released and together with C5a recruit other immune cells such as phagocytes to eliminate the target, while C3b is opsonizing targets which enables phagocytic uptake (Ricklin et al., 2010). In addition, other factors form a membrane attack complex (MAC) that can destroy the target cell (Bohlson et al., 2007).

1.5. Mucosal-associated lymphoid tissues (MALTs)

The composition of different immune cells, as described above, varies depending on which tissue is examined. Each tissue has its own challenges and requirements. Therefore, tissue-resident immunity has gained particular interest, especially at the mucosal sites such as skin, lung and the intestinal compartment (Belkaid and Naik, 2013; Rosato et al., 2017). The immune system at those sites does not only consist of immune cells, but also secondary and

tertiary lymphoid clusters and other arrangements. The collective names for those have been named after each sites: bronchus-associated lymphoid tissues (BALT), skin-associated lymphoid tissues (SALT) and gut-associated lymphoid tissues (GALT). These sites vary in terms of size, immune cell composition, exposure to microbiota and the challenges they face. All these lymphoid tissues, particularly GALT, will be described in more details in Chapter 5. The rest of this chapter will focus on describing the intestinal immune system, particularly intestinal epithelial cells (IECs) and intraepithelial lymphocytes (IELs).

1.6.1. Intestinal epithelial cells (IECs) organisation

The gastrointestinal (GI) tract is one of the largest mucosal areas exposed to the external environment. It is exposed to dietary components, beneficial and pathogenic microorganisms (Artis, 2008). The intestinal immune system needs to be tolerant towards nutrients and microbiota present in the intestinal lumen, while simultaneously detecting and responding to dangers such as pathogens. In addition, even beneficial microorganisms present in the intestinal lumen can become opportunistic pathogens. Failure to maintain the delicate balance between tolerance and immune responses can lead to a hypo- or hyper-responsive immune system. The latter could lead to intestinal inflammatory or autoimmune diseases such as inflammatory bowel disease (IBD) and celiac diseases (CD). Therefore, a properly regulated intestinal immune system is critical.

The first line of defence in the GI tract consists of a single-cell layer of intestinal epithelial cells (IECs) that forms a physical barrier, which separates the intestinal lumenal content from the intestinal compartments. A specialized IEC subset, namely goblet cells, secrete mucus. This mucus, in addition to secreted IgA from intestinal plasma cells, forms a protective layer that spatially separates the IEC barrier from commensal microbiota.

The organisation of the IEC barrier varies along the intestinal tract. The small intestine can be divided into three segments. Starting from the junction with the stomach is duodenum, followed by jejunum and ileum. There are reported differences between the different small intestinal segments such as different amount of microbial colonization, the number of PPs (Ramanan and Cadwell, 2016), gene expression (Lickwar et al., 2017), alternation in the number and subset composition of IELs (Suzuki et al., 2000; Chennupati et al., 2010; Hoytema van Konijnenburg et al., 2017) and IEC subsets (Cheng and Leblond, 1974; Haber et al., 2017). In the small intestine, IECs are organised into finger-like epithelial projections called villi domains and epithelial invaginations called crypt domains (Peterson and Artis, 2014) (Fig 1.1 A). In contrast, the IEC barrier in the colon and caecum lack villi structures and contain crypt domains only (Barker, 2014) (Fig 1.1 B). The IEC barrier is not a mere physical barrier. IECs are actively interacting with dietary residues, commensal microorganisms and potential pathogens at the apical side. On the basal and basolateral sides, IECs are interacting with the immune cells localized beneath and between IECs, as well as other supporting cells present closely to the IEC barrier.

There is a symbiotic relationship between IECs and commensal microbiota. The commensal microbiota are using the large IEC barrier area as their habitat, while IECs benefit from commensal microbiota. For example, in antibiotic treated mice, IECs showed down-regulation of genes involved in cell proliferation (Reikvam et al., 2011). IECs make use of pattern recognition receptors (PRRs), such as Toll-like-receptors (TLRs), to recognize various molecular patterns from microorganisms. Most of the TLRs present on IECs are found on their basolateral side (Lavelle et al., 2010). It has been suggested that IECs' expression of TLRs may be spatially and functionally different to organize and cope with stimuli from commensal microorganisms, pathogens and immune cells. Moreover, it has been

shown that mice having deficiency in the TLR signalling molecule MyD88, specifically in the IECs, secreted less of the antimicrobial proteins (AMPs) RegIIIγ, and are more susceptible to *L. monocytogenes* infection (Brandl et al., 2007).

Furthermore, it has been suggested that IECs may have the ability to function as antigen presenting cells (APCs) to the underlying immune cells: IECs express MHC-II, CD1d and other molecules involved in the antigen presentation machinery (Hershberg and Mayer, 2000). The molecular mechanisms behind the IEC interactions with their environment are still poorly understood. In this thesis, the focus will be on the interactions between the IECs and cells from the hematopoietic immune system, but first I will describe the different IEC subsets that have been identified.

1.6.1.1. Intestinal epithelial stem cells (IESCs)

Intestinal epithelial stem cells (IESCs) reside in the crypt domains of the small and large intestine. In each crypt domain, there are approximately 15 multipotent IESCs. Two distinct IESC populations have been identified. One IESC population is long-lived and characterized by the expression of leucine-rich-repeat-containing G-protein-coupled receptor 5 (Lgr5). Lgr5 has been identified as a gene targeted by Wnt signalling (see section 4.1.3.). With the use of Lgr5-lacZ reporter mice, Lrg5 expression in the crypt structures has been confirmed, as well as the ability of $Lrg5^+$ cells to renew the whole IEC barrier (Barker et al., 2007). $Lgr5^+$ IESCs are responsible for the continuous renewal of IECs. The second identified IESC population is located four cells from the crypt base, and these cells are named +4 IESCs. They are thought to be quiescent until any kind of epithelial injury or stress occurs (Horita et al., 2014; Gracz and Magness, 2014). IESCs divide every 24 hours generating between 16 to 32 daughter cells per day (Sato and Clevers, 2013). Thus, the whole mouse intestinal

epithelial barrier is renewed every 3-5 days (Clevers, 2013). This makes the IEC barrier the fastest self- renewing tissue in the body (Snippert et al., 2010).

IESCs generate all epithelial cell subsets via their daughter cells, named transit-amplifying cells (TA cells). The main epithelial subsets are enterocytes, Paneth cells, goblet cells and enteroendocrine cells, with the three cell subsets latter being called secretory IECs (Sato and Clevers, 2013). Recent single-cell RNA sequencing study of the intestinal epithelium suggests that additional subsets of e.g. Paneth cells, Tuft cells and enteroendocrine cells are present (Haber et al., 2017).

1.6.1.2. Absorptive enterocytes

The vast majority of IECs are enterocytes, which are responsible for the absorption of fluid and nutrients from the intestinal lumen. Therefore, enterocytes are also called the absorptive IEC subset. On their apical side, Enterocytes have mini-villi structures called microvilli, to maximize the absorption area. In addition to their absorptive capacities, enterocytes express AMPs such as the C-type lectin RegIIIγ (Vaishnava et al., 2008).

1.6.1.3. Goblet cells

The second major IEC subset are goblet cells that secrete mucus, which forms a protective layer on top of the intestinal epithelial barrier (Sato and Clevers, 2012). In the small intestine, the secreted mucus from goblet cells fills the space from the crypt domains up beyond to the villi tips (Ermund et al., 2013). This layer forms spatial segregation between IECs and commensal microbiota. The Th2 cytokines IL-4 and IL-13 can both lead to goblet cell hyperplasia with mucus release (Gerbe et al., 2016). In addition, goblet cells have been

reported to be capable of transferring low molecular antigens through the epithelial barrier to $CD103^+$ intestinal DCs (McDole et al., 2012).

1.6.1.4. Paneth cells

Paneth cells are characterised by secretion of various AMPs such as cryptdins and RegIIIγ (Cash et al., 2006). Cryptidin kills bacteria by disrupting their membrane, while the mechanism of actions of the other AMPs remain to be fully characterized (Mukherjee et al., 2008). Paneth cells can de-granulate rapidly if exposed to pro-inflammatory cytokines such as IFNγ (Farin et al., 2014). In addition, Paneth cells secrete epidermal growth factor (EGF) and Wnt, two essential factors to support IESCs in the crypt domains (Sato et al., 2011). It has been shown that the TF Sox9 is essential for Paneth cell formation, as Villin-Cre-$Sox9^{fl/fl}$ mice lack Paneth cells. Interestingly, these mice have normal numbers of the remaining IEC subsets (Mori-Akiyama et al., 2007). Paneth cells remain in the crypt domains, supporting IESCs, while the other IEC subsets migrate upwards along the crypt-villus axis (Cheng, 1974). Paneth cells are also the longest lived IEC subset with reports suggesting that Paneth cells can be maintained for up to two months (Gerbe et al., 2012).

1.6.1.5. Enteroendocrine cells

Up to one percent of the epithelial barrier consists of enteroendocrine cells (Cheng and Leblond, 1974; Worthington et al., 2017) These cells secrete various hormones necessary for intestinal homeostasis such as serotonin, cholecystokinin, vasoactive intestinal peptide and enteroglucagon. Studies have demonstrated that there are at least 10 different enteroendocrine subsets. These are identified by the hormone the cells secrete (Schonhoff et al., 2004). Studies have shown that enteroendrocrine cells express TLRs and can respond to TLR

stimulation by releasing the hormone characteristic of that particular subset of enteroendocrine cells (Abreu, 2010).

1.6.1.6. Microfold (M) cells

Microfold (M) cells are located just above the secondary lymphoid organ Payers' Patches (PPs). M cells are able to transfer luminal antigens to underlying secondary lymphoid organs such as PPs, and thereby provide the main entry of antigens to PPs (Reboldi and Cyster, 2016). It has been reported that receptor activator of nuclear factor-kappa B (RANK) and its ligand RANKL are essential for M cell formation. M cells are characterized by staining for the lectin ulex europaeus agglutinin-1 (UEA-1) and the number of UEA-1^{+} cells is significantly reduced in RANKL-/- mice. In addition to the reduction in the number of M cells, the faecal level of IgA is significantly reduced in RANKL-/- mice (Knoop et al., 2009). These data suggest that PPs are the main source of IgA, an essential component of the intestinal humoral immune system. The source of RANKL is suggested to be from intestinal stromal cells located underneath PPs (Mabbott et al., 2013).

1.6.1.7. Tuft and cup cells

In addition to the above IEC subsets, there are additional epithelial subsets found at low frequency, namely tuft cells and cup cells. The exact functions of tuft cells and cup cells remain unknown. Particularly cup cells are poorly studied (Mabbott et al., 2013; Gerbe et al., 2012).

To date, the best identification of tuft cells are based on their morphological structures as well as expression of doublecortin-like kinase 1 (DCLK-1) (Gerbe et al., 2012). It has been estimated that between 0.4-1.0% of murine IECs are tuft cells. Although their exact functions

remain to be determined, it has been shown that the number of tuft cells increases during *T. muris* infection (Howitt et al., 2016). An increase in the number of tuft cells is also observed during *Nippostrongylus brasiliensis (N. brasiliensis)* infection. This study also identified POU class 2 homeobox 3 (Pou2f3) as an additional factor specific for tuft cells. Mice deficient in this protein showed a higher *N. brasiliensis* infection burden than control mice (Gerbe et al., 2016).

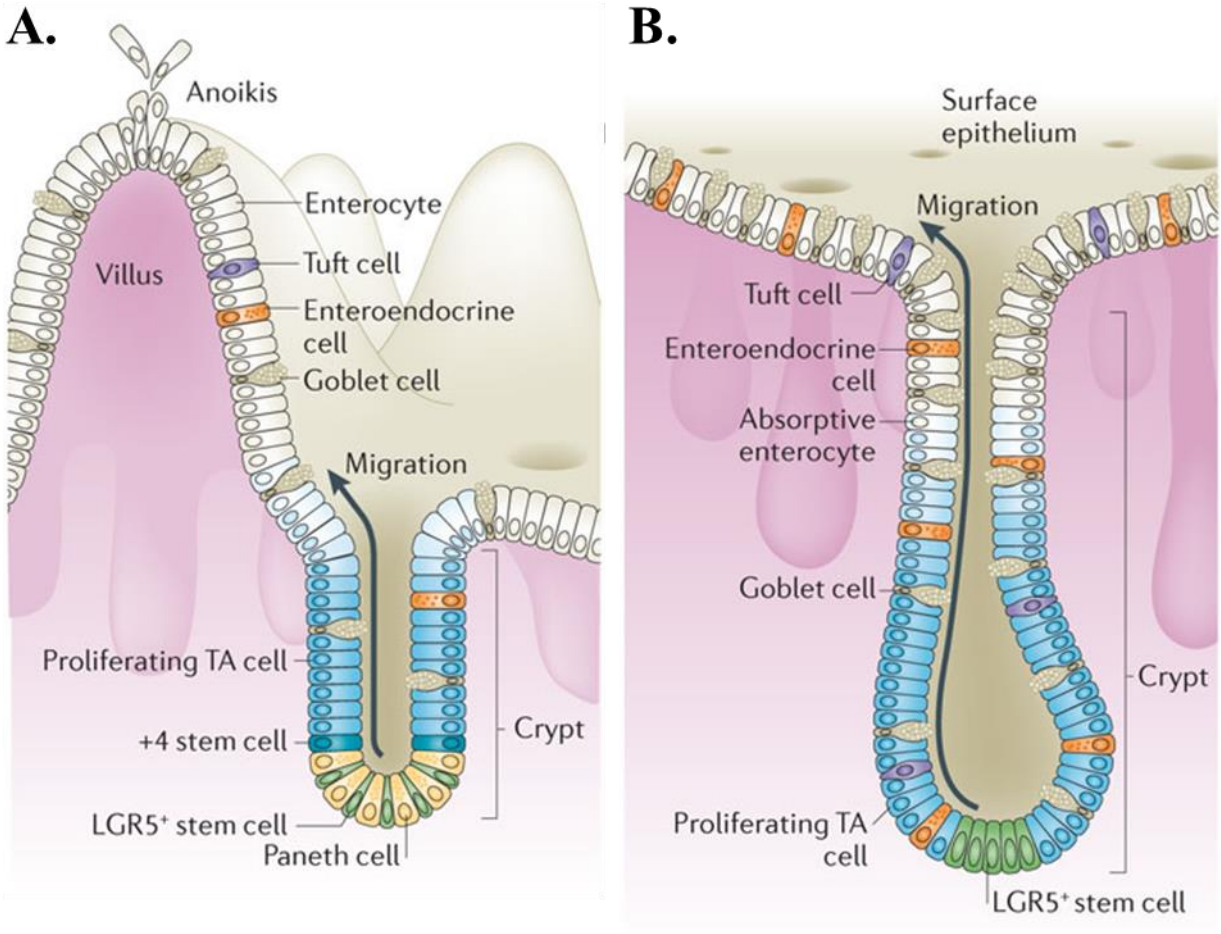

Figure 1.1. The intestinal epithelial barrier organisation in the small and large intestine. The distrubution of the different IEC subsets varies between A) small intestine and B) large intestine; there are no Paneth cells and more goblet cells in the large intestine compared to the small intestine. IELs are found in the beige areas, while lamina propria lymphocytes (LPLs) are found in the pink areas in the illustrations. Modified from Barker N, Nat Rev Mol Cell Biol, Vol:15(1):19-33.

1.6.2. Lamina propria lymphocytes (LPLs)

In the lamina propria compartment, beneath the IEC barrier, there is a network of connective tissue, SLOs such as MLNs and PPs, and immune cells such as intestinal DCs, MPs, and T cells. Intestinal DCs and MPs were briefly described in section 1.2.3. and 1.2.5., respectively.

The majority of the T cells found in the LP, named lamina propria lymphocytes (LPLs) are $CD4^+$ T cells. In addition, there are barely any $CD8\alpha\alpha^+$ LPLs (Romagnani et al., 2017). The number of $CD8\alpha^+$ LPLs are reduced in the absence of the chemokine ligand 25 (CCL25) and chemokine receptor 9 (CCR9) (Wurbel et al., 2007). All the different subsets of $CD4^+$ cells, Th1, Th2, Th17 and Treg cells are found in the LP compartment (van Wijk and Cheroutre, 2009; Wurbel et al., 2007). These $CD4^+$ cell subsets were introduced in section 1.3.2.2.-1.3.2.7.

The number of intestinal Th17 cells are reduced in germ-free (GF) mice, but not in MyD88-/-TRIF-/- mice. Interestingly, the authors showed that addition of ATP increased the number of Th17 cells, and luminal ATP is reduced in GF mice (Atarashi et al., 2008). Another group demonstrated that addition of the Gram-positive segmented filamentous bacteria (SFB) to GF mice is sufficient to induce intestinal Th17 cells (Ivanov et al., 2009).

In contrast to intestinal Th17 cells, the number of intestinal Treg cells are not reduced in GF mice (Min et al., 2007). It has been reported that TGFβ is essential for intestinal Treg cell functions. This was shown using a dominant negative form of the TGFβRII (dnTGFβRII) and the Powrie colitis model. Addition of WT Treg cells in this model rescue the mice from the induced intestinal inflammation, but that was not the case with dnTGFβRII Treg cells. These Tregs also failed to suppress IFNγ production from Th1 cells (Fahlén et al., 2005).

1.6.3. Intestinal intraepithelial lymphocytes (IELs) – the main immune cell population within the intestinal epithelium

Most immune cells within the intestinal epithelium are IELs (Fig 4.3. A-B). They reside in close proximity to IECs, particularly in the small intestine. On average, there is one IEL for every 4-10 IECs in the small intestine (Edelblum et al., 2012), while in the colon there is one IEL for every 30-50 IECs (Kunisawa et al., 2007). IELs are a unique class of lymphocytes. They differ from naïve $CD8\alpha^+$ T cells, found in tissues such as spleen, in that IELs express some lymphocyte activation markers such as CD69 and CD44, but lack or express at low levels other common $CD8\alpha^+$ T cell activation markers such as CD25, Ly6C and OX40 (Wang et al., 2002). Like NK cells, IELs have high expression of cytotoxic proteins such as granzyme A, granzyme B and Fas ligands (Fahrer et al., 2001). It is worth noting that, in addition to its cytotoxic properties, granzyme B has recently been reported to affect bacterial protein synthesis (Dotiwala et al., 2017).

In the small intestine, most IELs do not express the classical TCRαβ (30-40%) but rather the non-classical TCRγδ (60-70%). In the colon, the opposite ratio between $TCR\gamma\delta^+$ and $TCR\alpha\beta^+$ IEL has been reported (Kunisawa et al., 2007). TCRs are associated with invariable CD3 membrane proteins consisting of γ-, δ-, ε- and ζ domains. In mice lacking the ζ domain, TCR^+ lymphocytes in the spleen are missing. In contrast, $TCR\alpha\beta^+$ IELs seem unaffected by the lack of the ζ domain and only $TCR\gamma\delta^+$ IELs are reduced in number (Liu et al., 1993).

Past studies have identified seven different γ-chain segments (Heiling and Tonegawa, 1986; Elliott et al., 1988) and seven different δ-chain segments that can be used for TCR recombination (Garman et al., 1986). Interestingly, the expression of a specific Vγ-chain correlates strongly with the tissue location. For example, all dendritic epidermal $TCR\gamma\delta^+$ T

cells (DETCs) express Vγ5 or Vγ3 (according to the Heilig & Tonegawa or Garman nomenclature)**.** In contrast, IELs express Vγ7 or Vγ5**.** The Vγ7 segment that IELs carry can be combined with several different Vδ segments, but most IELs express Vδ4 (Allison and Havran, 1991)**.** Thus, the potential antigen repertoire is more restricted in IELs compared to other T cells. What the TCRs of IELs recognise is still unknown.

The IEL population can be divided with respect to expression of the co-receptors CD8αα, CD8αβ and CD4. There are five major IEL subsets: TCRγδ$^+$ CD8αα$^+$, TCRαβ$^+$ CD8αα$^+$, TCRαβ$^+$ CD8αβ$^+$ and CD8αα$^+$ CD4$^+$IELs (Guy-Grand et al., 2013), with a fifth TCRγδ$^+$ CD8αβ$^+$ IEL population having been identified (Kadivar et al., 2016). In contrast to systemic T cells, which all express the co-stimulatory molecule CD28, only CD8αβ$^+$ IELs do so, while remaining IEL subsets lack this protein in IELs sourced from BALB/c mice (Ohteki and MacDonald, 1993).

There has been some evidence reported that there is a plasticity between peripheral CD4$^+$ T cells and IELs. One paper demonstrated that CD4$^+$ T cells can be re-programmed into IELs by co-expressing the TFs T-bet and Runx3 (Reis et al., 2014). As TCRγδ$^+$ CD8αα$^+$, TCRαβ$^+$ CD8αα$^+$ and TCRαβ$^+$ CD8αβ$^+$ IELs as well as Tmem and Tcm cells from spleen have been shown to express T-bet (Klose et al., 2014), induction of Runx3 seems to be the critical factor for IEL re-programming. Another group developed a transnuclear mouse colony, with mice carrying a monoclonal TCR sourced from a CD4$^+$ Treg cell. Using these mice, the authors demonstrated that these cells could become either Treg cells or CD8αα$^+$ CD4$^+$ IELs. This plasticity was shown to be dependent on the commensal microbiota, as mice on antibiotic treatment had fewer CD8αα$^+$ CD4$^+$ IELs which had less proliferative capacity (Bilate et al., 2016).

The origin of IELs is still under debate, with both thymic and extrathymic pathways having been suggested (Rocha et al., 1994; Cheroutre and Lambolez, 2008). Depletion of TCRδ genes does not affect the frequency of TCRαβ$^+$ and CD4$^+$ T cells (Itohara et al., 1993). TCRγδ$^+$ CD8αα$^+$ and TCRαβ$^+$ CD8αα$^+$ IELs are thought to be able to home to the intestinal compartment directly from the thymus and are named natural IELs or type b IELs. TCRαβ$^+$ CD8αβ$^+$ and CD8αα$^+$ CD4$^+$IELs are thought to be activated in SLOs such as MLNs and PPs, prior to homing to the intestinal compartment, and are called induced IELs or type a IELs (Guy-Grand et al., 1991; Cheroutre et al., 2011) (Fig 1.2). Indeed, fate-mapping experiments have suggested that all TCRαβ$^+$ IELs first become activated in MLNs and PPs before homing to the intestinal compartment (Eberl and Littman, 2004). In contrast, it has been reported that CD8$^+$ thymic emigrants can home to the small intestine in lymphotoxin-α-deficient mice – mice that lack SLOs (Staton et al., 2006). These data suggest that it is possible for IELs to home to the intestinal compartment without previous activation in SLOs. TCRγδ$^+$ IELs have been reported to be able to originate from emigrated T cell-committed progenitor cells (Lambolez et al., 2006), as well as being present in athymic mice (Emoto et al., 2004). Recent data suggest that TCRαβ$^+$ IELs have two types of precursors, one expressing PD-1 and the other T-bet, as both identified populations can generate IELs when transferred into Rag2-/- mice (Ruscher et al., 2017).

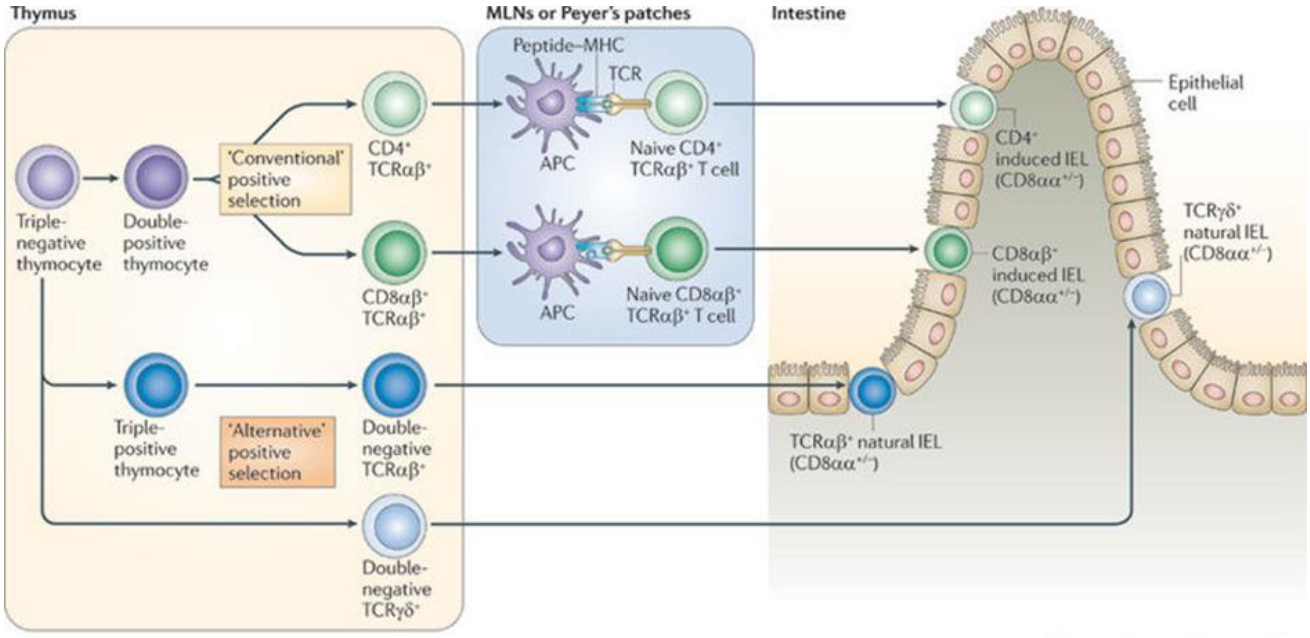

Figure 1.2. IEL development and homing to the small intestine. This schematic overview illustrates the model of a conventional and an alternative thymic selection process for induced and natural IELs, respectively. It also illustrates the suggested priming-dependent and priming-independent homing pathways for induced and natural IELs, respectively. Modified from Cheroutre et al. Nat Rev Immunol. (7):445-56.

In terms of immunopathology and immunoprotection, different roles have been suggested for TCRγδ$^+$ and TCRαβ$^+$ IELs. It has been reported that TCRα-/-, TCRβ-/- and TCRβ-/- TCRδ-/- mice develop spontaneous symptoms of intestinal inflammation, which are most severe in TCRα-/- mice. TCRβ-/- TCRδ-/- mice have higher frequency of spontaneous development of these than TCRβ-/- mice (Mombaerts et al., 1993). In the *Toxoplasma gondii (T. gondii)* infection model, the transfer of TCRαβ$^+$ IELs into Rag2-/- mice caused more tissue damage than the transfer of TCRγδ$^+$ IELs (Egan et al., 2011). The parasite load in TCRγδ-/-mice is higher than that in WT controls (Edelblum et al., 2015). In another infection model, i.e. that involving *Eimeria vermiformis (E. vermiformis)* (for further information about the *Eimeria* model, see Chapter 7) TCRαβ-/- mice have higher parasite production than control mice, while TCRγδ-/- mice have lower parasite production (Roberts et al., 1996). TCRγδ-/- mice

exhibit worse DSS-induced colitis symptoms, such as more severe weight loss, than control mice (Kober et al., 2014) (for further information about the DSS-induced colitis model, see Chapter 7). Overall, it seems that TCRγδ$^+$ IELs may have properties biased towards promoting intestinal tissue integrity, while TCRαβ$^+$ IELs may be biased towards immunoprotective properties.

Previous publications suggest that TCRγδ$^+$ and TCRαβ$^+$ IEL populations require different factors for their maintenance in the intestinal epithelium. It has been reported that in vitamin D receptor-deficient mice the number of TCRαβ$^+$ IELs is reduced, while the number of TCRγδ$^+$ IELs remain unchanged (Bruce and Cantorna, 2011). A similar trend was observed in mice deficient in TGFβ (Konkel et al., 2011). On the other hand, in G-protein receptor (GPR)18-deficient mice, the number of TCRγδ$^+$ IELs is reduced, while the number of TCRαβ$^+$ IELs remain at a similar numbers to control mice (Wang et al., 2014). It has been reported that the transcription factor T-bet is important for IEL development, with reduction in the numbers of all IEL subsets (Reis et al., 2014). Reduction in the number of TCRγδ$^+$ IELs is observed in mice deficient in the extracellular matrix protein osteopontin (Opn) (Ito et al., 2017). Using various knock-out mice, it has been reported that TCRγδ$^+$ IELs are reduced in the context of deficiency in MyD88 (Yu et al., 2006), TLR2 (particularly CD8αα$^+$ and TCRγδ$^+$ IELs, but not CD4$^+$ IELs) (Qiu et al., 2016), the TF aryl hydrocarbon receptor (AhR) (Li et al., 2011), CCL25, CCR9 (Wurbel et al., 2007), CD103 (Schön et al., 1999), common γ chain (Cao et al., 1995), IL-15Rα (Lodolce et al., 1998) and IL-7R (Maki et al., 1996).

The reduction in the number of IELs in MyD88-/- and TLR2-/- mice suggests that commensal organisms may be important for the maintenance of TCRγδ$^+$ IELs, as commensals are involved in generating products triggering toll-like-receptor (TLR)

signalling. Interestingly, in germ-free (GF) mice, only CD8αβ$^+$ TCRαβ$^+$ IELs have been reported to be reduced in numbers, while the other IEL populations remain at a similar number to control mice (Kawaguchi et al., 1993; Di Marco Barros et al., 2016; Klose et al., 2014). These observations suggest a smaller role for commensal microbiota for IEL maintenance and raising the possibility that another TLR stimulating factor such as viruses may be required for triggering MyD88 signalling.

As AhR is suggested to be an environmental sensor and has reported ligands derived from the diet (Gu et al., 2000), the reduction of TCRγδ$^+$ IELs observed in AhR-/- mice would suggests that TCRγδ$^+$ IELs require stimuli from the diet for their maintenance. In contrast, mice deficient in the AhR receptor nuclear translocator (ARNT) have reduced number of TCRαβ$^+$ CD8αα$^+$ IELs, while the number of TCRγδ$^+$ CD8αα$^+$, TCRαβ$^+$ CD8αβ$^+$ and TCRαβ$^+$ CD4$^+$ IELs remains at a similar level to controls (Nakajima et al., 2013).

The reduction of total IELs in CCL25-/- and CCR9-/- mice, indicates the importance of this chemokine combination for IEL homing, but at the same time suggest that these are not strictly required for IELs, as there are still IELs found in both these KO mice. The common γ chain is part of the IL-2, -4, -7, -9, -15 and -21 receptors and their signalling (Asao et al., 2001; Cao et al., 1995) suggesting an important role for one or more of these cytokines for IELs. Further studies are required to understand the role of the different IEL subsets in intestinal homeostasis.

One of these cytokines has received particular interest for IEL maintenance, namely IL-15. It has been reported that IECs can trans-present IL-15 to IELs (Ma et al., 2009). For the IL-15 trans-presentation, the presenting cells present the cytokine via IL-15Rα to the responding

cells that accept IL-15 via the IL-15Rβ-IL-2Rγ heterodimer. This suggests that IECs may be directly important for IEL survival. The reduction in the number of IELs in IL-15Rα-/- mice, and in Villin-cre-IL-15Rα mice (Mortier et al., 2009), could be restored in IL-15Rα-/- mice, that in addition had a villin-specific knock-in of IL-15Rα, hence making IL-15 trans-presentation possible in the IEC compartment only (Ma et al., 2009). However, the number of IELs in these knock-in mice was above the level found in WT control mice. This shows the complexity of the role of IL-15 and IL-15 trans-presentation for IEL-IEC interactions.

The above sections have described murine IELs, which will be the focus in this thesis. Murine IELs have some similarities to human IELs. Like murine IELs, the vast majority of human IELs are $CD8\alpha^+$ (Leon, 2011) and $CD103^+$ (Cerf-Bensussan et al., 1987). Furthermore, like murine IELs, human IELs exhibit a preference in terms of which TCR segments they express. Thus, while murine $TCR\gamma\delta^+$ IELs are reported to consist mainly of $V\gamma5^+ V\delta4/6^+$ cells (Allison and Havran, 1991), human $TCR\alpha\beta^+$ IELs and $TCR\gamma\delta^+$ IELs mainly consist of $V\beta6.7^+$ (Van Kerckhove et al., 1992) and $V\delta1^+$ cells (Groh et al., 1998), respectively. These data suggest that both murine and human IELs may have a restricted set of antigens to which they can respond. In addition, both murine and human IELs are frequent in the intestinal epithelial compartment. One report suggests that 5-15 % of the cells isolated from human intestinal epithelium are IELs (Camarero et al., 2007). Another report suggests that there is 1 human IEL per 4-50 IECs (Hayat et al., 2002), while other reports suggest that there is 1 murine IEL per 4-10 IECs (Beagley et al., 1995; Schön et al., 1999; Wurbel et al., 2007; Edelblum et al., 2012). Both human and murine IELs can exhibit type 1 responses such as IFNγ, TNFα and granzyme B production. However after re-stimulation with PMA and ionomycin, murine IELs contain more granzyme B relative to IFNγ while the opposite trend applies to human IELs (Mayassi and Jabri, 2018). Another difference between murine and human IELs is the

IEL subset composition. The largest murine IEL subset is TCR$\gamma\delta^+$ CD8$\alpha\alpha^+$ IELs, while the largest human IEL subset is TCR$\alpha\beta^+$ CD8$\alpha\beta^+$ IELs. In addition, murine IELs mainly express the co-receptor CD8αα, while human IELs expressing CD8αα are not detectable (Mayassi and Jabri, 2018). These data illustrate that murine and human IELs have different IEL subset composition. Changes to human IEL subset composition have been shown in an intestinal disorder: increased proportion of human TCR$\gamma\delta^+$ IELs is detected early in celiac disease patients (Leon, 2011; De Andrés et al., 2015). The similarities and differences between murine and human IELs are important to consider for translational research.

Despite extensive research on IEL biology there are still many questions remaining in terms of their development, maintenance and activation - with the two latter being particularly important for appropriate immune tolerance and protective responses that are essential for intestinal homeostasis. Therefore, these are the main areas of focus in my thesis.

Chapter 2: Ph.D. Thesis specific aims

The overall aim of this thesis is to investigate further the requirements for IEL activation and maintenance. One major hindrance for further understanding of IEL biology has been the lack of *in vitro* models for IELs. Developing an effective *in vitro* model for IELs would make it possible to gain and address mechanistic insights into IEL biology. Further understanding of IEL activation would have significance for deeper understanding and discovery of potential treatments of intestinal disorders, in which IELs are thought to play a role. I have investigated IEL biology by utilizing both *in vitro* and *in vivo* techniques.

In Chapter 4, I investigate further the issue of IEL maintenance through a series of experiments combining IELs with intestinal organoids, "mini-guts". The observation that IELs survive poorly *in vitro* suggests that factor(s) may be missing that are present in the *in vivo* intestinal compartment. Intestinal organoids could supply these missing factors, increasing IEL survivability *in vitro.*

In Chapter 5, I dissect further differences between IELs and other $CD8\alpha^+$ T cells, $TCR\gamma\delta^+$ T cells and epithelial-resident lymphocytes. The focus of this assessment has been on metabolic pathways, particularly those involving mitochondria, in the light of the recent recognition of the importance of cell metabolism for immune effector functions.

In Chapter 6, I demonstrate that IELs exhibit mitochondrial plasticity during their activation. Additionally, these experiments were performed to study the differences between IEL subsets. Among IEL subsets, there are significant differences in terms of kinetics and amplitude of activation responses. In addition, the data acquired suggest an IEL activation model, in which mitochondrial changes seem to be required for effector functions.

Finally, in Chapter 7, I use intestinal infection models to obtain IEL activation data from physiologically relevant settings. These data do not only a support mitochondria-dependent IEL activation mechanism but also suggest a role for commensal microbiota as one inducer of IEL activation.

Chapter 3: Materials and Methods

3.1. Reagents

Table 3.1 Medium used for cell and tissue isolation and culture procedures

Medium / Buffer	Compound	Concentration	Company
IEL buffer	Ca^{2+} and Mg^{2+}-free PBS		Sigma Aldrich
	Fetal bovine serum (FBS)	10 % (v/v)	Sigma Aldrich
	Sodium pyruvate	1 mM	Gibco
	HEPES	10 mM	Gibco
	EDTA	10 mM	Sigma Aldrich
	Penicillin	100 U/ml	Gibco
	Streptomycin	100 µg/ml	Gibco
	Polymyxin B	10 mg/ml	Sigma Aldrich
Percoll density gradient medium	MilliQ water	Base	Prepared at the Babraham Institute
	Percoll (15-30 nm colloidal silica particles coated with polyvinylpyrrolidone in 23% w/w water)	37.5 % (v/v)	Sigma Aldrich
	10x PBS	1x	Sigma Aldrich
MACS buffer	1x PBS	Base	Prepared at the Babraham Institute
	FBS	1 % (v/v)	Sigma Aldrich
	EDTA	1.25 mM	Sigma Aldrich
ACK buffer	MilliQ water	Base	Prepared at the Babraham Institute
	NH_4CL	8.024 mg/ml	Sigma Aldrich
	$KHCO_3$	1.001 mg/ml	Sigma Aldrich
	EDTA-Na_2-$2H_20$	3.722 mg/ml	Sigma Aldrich
Complete IMDM	IMDM	Base	Sigma Aldrich
	FBS	5 % (v/v)	Sigma Aldrich
	L-Glutamine	2 mM	Gibco
	Penicillin	100 U/ml	Gibco
	Streptomycin	100 µg/ml	Gibco
	β-mercaptoethanol	2.86 mM	Sigma Aldrich
Basal organoid medium	Advanced DMEM/F12	Base	Gibco
	Penicillin	100 U/ml	Gibco
	Streptomycin	100 µg/ml	Gibco
	HEPES	10 mM	Gibco
	GlutaMAX	2 mM	Gibco

Complete organoid medium	Advanced DMEM/F12	Base	Gibco
	Penicillin	100 U/ml	Gibco
	Streptomycin	100 µg/ml	Gibco
	HEPES	10 mM	Gibco
	GlutaMAX	2 mM	Gibco
	N2 supplement	1x	Life Technologies
	B27 supplement	1x	Life Technologies
	EGF	50 ng/mL	Life Technologies
	N-acetylcysteine	1 mM	Sigma Aldrich
	Noggin	100 ng/mL	eBioscience / Peprotech
	R-spondin	10 % (v/v)	293T-HA-RspoI-Fc cells (Provided by Calvin Kuo)

Table 3.2 Antibodies and probes used for image acquisition and analysis

Specificity	Clone	Reactivity	Company
CD45.2	104	Mouse	Biolegend
Click it Plus EdU			Thermo Scientific
DAPI			Thermo Scientific
E-Cadherin	36/E-Cadherin	Mouse and human	BD Biosciences
EpCAM	G8.8	Mouse	Biolegend
Ki-67	Rabbit polyclonal (ab15580)	E.g. mouse	Abcam
Lysozyme	Rabbit polyclonal (ab2408)	E.g. mouse	Abcam
MitoTracker Deep Red (MTDR)			Thermo Scientific
MitoTracker Orange (MTO)			Thermo Scientific
Mucin-2	Rabbit polyclonal (H-300)	E.g. mouse	Santa Cruz Biotechnology
Phalloidin			Thermo Scientific
Goat anti-rabbit IgG	Goat Polyclonal	Rabbit IgG	Life Technologies

Table 3.3 Antibodies and dyes used for flow cytometric analysis

Specificity	Clone	Reactivity	Company
CD4	GK1.5	Mouse	Biolegend
CD4	RM4-5	Mouse	Biolegend
CD8α	53-6.7	Mouse	Biolegend
CD8β	YTS156.7.7	Mouse	Biolegend
CD11b	M1/70	Mouse and human	Biolegend
CD11c	N418	Mouse	Biolegend
CD19	6D5	Mouse	Biolegend
CD24	M1/69	Mouse	Biolegend
CD25	PC61	Mouse	Biolegend
CD44	IM7	Mouse and human	Biolegend
CD45.1	A20	Mouse	Biolegend
CD45.2	104	Mouse	Biolegend
CD62L	MEL-14	Mouse	Biolegend
CD69	H1.2F3	Mouse	Biolegend
CD90.2	30-H12	Mouse	Biolegend
CD103	2EF	Mouse	Biolegend
F4/80	BM8	Mouse	Biolegend
Gr-1	RB6-8C5	Mouse	Biolegend
GranzymeB	16G6	Mouse and human	eBioscience
I-A/I-E (MHCII)	M5/114.15.2	Mouse	Biolegend
IFNγ	XMG1.2	Mouse	Biolegend
IL-10	JES5-16E3	Mouse	Biolegend
IL-13	13A	Mouse	Biolegend
Ki-67	B56	Mouse and human	BD Biosciences
MitoSOX			Thermo Scientific
MitoTracker Deep Red (MTDR)			Thermo Scientific
MitoTracker Green (MTG)			Thermo Scientific
MitoTracker Orange (MTO)			Thermo Scientific
Acridine Orange 10-nonyl bromide (NAO)			Sigma Aldrich
Near IR L/D			Thermo Scientific
Nile Red			Cayman Chemicals
NK1.1	PK136	Mouse	BD Biosciences
TCRβ	H57-597	Mouse	Biolegend
TCRγδ	UC7-13D5 / GL3	Mouse	Biolegend
TNFα	MP6-XT22	Mouse	Biolegend
Vγ3	536	Mouse	Biolegend

Table 3.4 Primers used for qPCR analysis

Gene	Primer AssayName	Detection system	Supplier
Hprt1	mm00446968 m1	TaqMan	Thermo Scientific
Muc2	mm0045299 m1	TaqMan	Thermo Scientific
RegIIIγ	mm 00441127 m1	TaqMan	Thermo Scientific
RegIIIβ	Mm00440616_g1	TaqMan	Thermo Scientific
Hprt	Mm_Hprt_1_SG	SybrGreen	Qiagen
Defa5	Mm_Defa5_1_SG	SybrGreen	Qiagen
IL15rα	Mm_Il15ra_1_SG	SybrGreen	Qiagen
IL15	Mm_15_1_SG	SybrGreen	Qiagen
Lyz	Mm_Lyz1_1_SG	SybrGreen	Qiagen
TJP1	Mm_Tjp1_1_SG	SybrGreen	Qiagen
Ocln	Mm_Ocln_1_SG	SybrGreen	Qiagen
CCL25	Mm_CCL25_1_SG	SybrGreen	Qiagen

3.2. Mice

All animal work was performed at the Babraham Institute, or at the Department of Veterinary Medicine at University of Cambridge, in accordance with the Animals Scientific Procedures Act (ASPA) 1986 under the Project Licences 80/2488 and 70/9073 and with the approval of the Babraham Institute Animal Welfare and Ethics Review Body (AWERB).

Female and male C57BL/6J mice (Jackson Laboratories), were maintained at the Babraham institute), as well the following transgenic mice: TCRδ-H2B-eGFP (Prinz et al., 2006), AhR-/- (Schmidt et al., 1996), Cyp1aT-/- (Dalton et al., 2000), Rag1-Cre (McCormack et al., 2003), $Tbx21^{fl/fl}$, $Eomes^{fl/fl}$ (Intlekofer et al., 2008), $AhR^{fl/fl}$ (Lahvis and Bradfield, 1998), $AhRR^{fl/fl}$ (generated at the Babrham Institute; from University of California, Davis targeting facility), $XBP1^{fl/fl}$ (Kaser et al., 2008), Villin-Cre (Madison et al., 2002), IL-22-/- (Kreymborg et al., 2007), IL-15Rα-/- (Lodolce et al., 1998), IL-7R-/- (Maki et al., 1996), IL-2Rγ-/- (Disanto et al., 1995), Rag2-/- (Hao and Rajewsky, 2001), and Rag2-/- and cytokine KO combinations knock-out mice generated by crosses at the Babraham Institute. These mice were used for

experiments between the age of 5-20 weeks. Standard cages were used, which allowed maximum of five mice per cage. Unless otherwise stated, the mice received standard diet and autoclaved drinking water *ab libitum.* Mice were maintained under a twelve hours light/dark cycle and under specific pathogen-free (SPF) conditions at the Babraham Institute in accordance with the Babraham Institute Animal Welfare, Experimentation & Ethics Committee and the UK Home Office.

3.3. *In vivo* experimental procedures

All procedures were carried out at room temperature (RT), except when specified.

3.3.1. T and B cell transfer model

T and B cells were isolated by processing spleens and MLNs through 70 µm mesh filters. The cell suspension obtain in this way were underlayered with Lympholyte (Cedarlane), centrifuged at 1250 g for 15 min, then stained on ice with anti-CD90.2 and anti-CD19 antibodies prior to FACS for T cells ($CD90.2^+$ $CD19^-$ cells) and B cells ($CD19^+$ $CD90.2^-$ cells), respectively. 1.0-2.5x10^6 cells re-suspended in sterile PBS were injected intravenously (i.v.) into each Rag2-/- recipient mice without anaesthesia. These mice were between 5-12 weeks of age at the time of i.v. transfer.

3.3.2. Isolation of IELs from small and large intestine

Small intestines were dissected, flushed with PBS, cut open longitudinally and subsequently cut transversely into 0.5 cm pieces. These fragments were transferred into IEL buffer and incubated in 37 °C at 200 rpm for 10 min in an Infors triple stack incubator shaker, followed by incubation in 37 °C at 100 rpm for 20 min. The resulting suspension was passed through a

100 µm filter and cells were collected at 500 g for 8 min. The cell pellet was resuspended in 37.5 % Percoll density gradient medium and centrifuged at 700 g at RT for 10 min. The top layer was gently removed followed by the remaining Percoll supernatant. The pellet was processed further for flow cytometric analysis or cell sorting.

3.3.3. IEL sort

The resulting pellet, as described in section 3.3.2., was stained with anti-CD8α-PE or APC antibody and incubated on ice for 5 min in MACS buffer, followed by washing (500 g, 8 min). Then anti-PE or APC beads (Miltenyi Biotec) were added and the cells were incubated at 4 °C in the dark for 15 min. The cells were washed in MACS buffer and the solution was passed through a 40 µm mesh filter prior to AutoMACS enrichment (Miltenyi Biotec) using the positive selection programme (POSSEL) on the sample and subsequently on the negative fraction. The cells were then sorted based on CD8α expression using a BD Influx cell sorter. For live/dead discrimination, 4',6-diamidino-2-phenylindole (DAPI) was added prior to the sort. The gating of $DAPI^-$ $CD8\alpha^+$ IELs confirmed successful MACS-enrichment with over 80 % of live cells being $CD8\alpha^+$. Afterwards the cells were collected (500 g, 8 min) and re-suspended in PBS. Live cells were quantified with a Countess Automated Cell Counter (Life Technologies) by diluting a small volume of the sorted cells with trypan blue according to the manufacturer's instructions.

3.3.4. IEL transfer model

$1.0x10^5$ IELs were injected i.v. into each recipient mice without anaesthesia. The recipient mice had the following genotypes: Rag2-/-, IL-2Rγ-/-Rag2-/- and IL-15Rα-/-Rag2-/-. Both female and male recipient mice were used with ages ranging from 5-12 weeks at the time of i.v.

injection. The recipient mice were left for 3 weeks before small intestines were harvested, processed and stained for flow analysis of the donor IELs.

3.3.5. Bone marrow (BM) transfer model

The femurs and tibias of donor mice (C57BL/6, Rag2-/-, IL-7R-/-Rag2-/-, IL-15Rα-/-Rag2-/- and IL-22-/-Rag2-/-) were used to isolate bone marrow (BM) cells. Tissues surrounding the bones were removed and femur and tibia carefully separated. Under sterile conditions, the bones were washed briefly in 70 % ethanol followed by sterile PBS. The ends of femur and tibia were cut off and the content of the bones flushed with sterile PBS using a 27 g needle. The cells were collected by centrifugation at 1200 rpm for 7 min at 4°C followed by red blood cell (RBC) lysis with ACK-buffer for 3 min on ice, followed by another centrifugation (at 1200 rpm for 7 min at 4°C). Rag2-sufficient bone marrow cell suspensions were stained with 2 µl of anti-CD90.2 microbeads per one femur and one tibia combination on ice for 10-15 min followed by AutoMACS depletion programme (DEPLETE) from which the negative fraction was collected. Resulting cell suspension was quantified using the Countess Automated Cell Counter as previously described. 2-5x10^6 BM cells were injected i.v. into each recipient mice, which had undergone sublethal irradiation (450 rads) prior to injection. Recipient mice were housed for 3-6 weeks after transfer after which the mice were used in subsequent experiments.

3.3.6. 5-ethynyl-2'-deoxyuridine (EdU) incorporation

5-ethynyl-2'-deoxyuridine EdU (Invitrogen) was dissolved in sterile PBS and 100 µg EdU per mouse was delivered by i.p. injection. Mice were killed 24 hours later and small intestines dissected for imaging analysis.

3.3.7. Anti-CD3 and anti-CD28 T cell activation model

Mice were injected with 25 µg anti-CD3 (αCD3) (clone: 145-2C11) and/or 25 µg αCD28 (clone: 37.51) i.p. Small intestines from treated mice were collected at 4, 24 and 48 hours post injection for flow analysis.

3.3.8. Dextran sulphate sodium (DSS) model of intestinal inflammation

C57BL/6 mice received 2.5 % (w/v) dextran sulphate sodium (DSS Mr 40 000, Sigma Aldrich) and 5 % (w/v) D-glucose, in their drinking water *ad libitum* for 5-7 days. Each day the mice were weighed, their general well-being monitored and their faeces were assessed for their consistency and the presence of blood. At the end of the treatment period the small intestine, caecum, colon and spleen of the mice were harvested and processed for flow analysis.

3.3.9. Antibiotic depletion model

C57BL/6, IL-22-/- and IL-2Rγ-/-Rag2-/- mice reconstituted with IELs received various antibiotic mixes in their drinking water for 10-14 days. All antibiotic mixes contained 5 % (w/v) D-glucose. Two versions of broad-spectrum antibiotic mixes were used: (I) 1 g/l ampicillin, 1 g/l colistin and 5 g/l streptomycin or (II) 1 g/l ampicillin and 5 g/l streptomycin. One g/l colistin or 1 g/l vancomycin were used to deplete Gram-negative or Gram-positive bacteria, respectively.

Table 3.5 Antibiotics used for antibiotic depletion experiments

Compound	Concentration	Depletion spectrum	Company
Ampicillin	1g/l	Broad	Melford
Streptomycin	5g/l	Broad	Sigma Aldrich
Colistin	1g/l	Gram-negative	Sigma Aldrich
Vancomycin	1g/l	Gram-positive	Sigma Aldrich

The antibiotic drinking water were exchanged every five days. At the end of the antibiotic treatment period, the small intestines of the mice were harvested and processed for flow analysis.

3.3.10. Murine Norovirus (MNV)-O7 and MNV-CW3 infection model

C57BL/6 mice were infected with 5 x 10^6 tissue culture infective dose (TCID) of either MNV-O7 or MNV-CW3 per mouse via oral gavage. The MNV strains were kindly provided by the Heeney laboratory at the University of Cambridge. Two, four and seven days post infection, a small portion of the ileums were collected to assay viral quantification, while the rest of the small intestines were harvested and processed for flow analysis. A combination of broad-spectrum antibiotic depletion model and MNV-CW3 infection experiments were also performed.

Rag2-/- mice and Rag2-/- mice which had received T, B or T and B cells (3-6 weeks post i.v. transfer) were infected with MNV-O7 in the same way as described above. The small intestinal samples were taken for analysis of the viral quantification.

3.3.11. *Eimeria vermiformis (E. vermiformis)* infection model

E. vermiformis oocysts were stored in 2.5 % (w/v) potassium bicarbonate prior to infection. The oocysts were washed in deionized water (1800 g, 8 min), which was repeated three times before flotation centrifugation (1100 g, 10 min) in which oocysts gets enriched in the top layer. The oocyst enriched fraction was sterilized by using sodium hypochloride solution, followed by three more deionized water washes prior to oocyst quantification using a Fuchs-Rosenthal chamber. The quantification was controlled by screening a 50 µl droplet on a McMaster

chamber. C57BL/6 mice, Rag2-/- mice and Rag2-/- mice reconstituted with CD8α$^+$ IELs were infected with 1000 oocysts via oral gavage. From day 6 onwards, mice were single-caged with sand bedding to enable the collection of faeces for oocyst quantification. Day 5 and 10 post infection, duodenum, jejunum and ileum were harvested from the mice, processed for flow analysis or for cell sorting to perform cardiolipin (CL) mass spectrometry analysis.

3.3.12. *Salmonella* infection model

Male C57BL/6 were infected with *Salmonella enterica typhimurium* strain SL1344 (4-6.2 x 10^8 colony-forming unit (Cfu) in 200 µl sterile PBS per mouse via oral gavage). Two, 5, 12 and 24 hours post infection, the faeces were collected for bacterial quantification and the small intestines of the mice were harvested and processed for flow analysis.

3.4. *Ex vivo* experimental procedures

All procedures were carried out at RT, except when specified.

3.4.1. Isolation of lamina propria lymphocytes (LPLs)

The remaining intestinal tissue after the protocol for IEL isolation, as described in section 3.3.2, were washed in PBS. This was performed by transferring the intestinal tissues into tubes with PBS and manual shaking to remove traces of EDTA. Afterwards, the content was filtered through a 100 µm mesh filter. The intestinal tissues were transferred into tubes with plain 37 °C pre-warmed IMDM (Sigma-Aldrich) supplemented with Collagenase D (1 mg/ml, enzyme activity >0.15 Wünsch units /mg, Roche) and DNase I (0.1 mg/ml, enzyme activity >2000 U/mg, Roche). This was shaken at 70 rpm, at 37 °C for 25 min. After the incubation, the content

was filtered through a 40 µm mesh filter and washed three times with plain IMDM prior to staining for flow cytometry.

3.4.2. Isolation of splenic lymphocytes

Spleens were pressed through a 70 µm mesh filter. The filters were washed with PBS prior to centrifugation (1350 rpm, 7 min). The supernatant was removed and 3 ml of ACK buffer (Table 3.1) was added and the cells were then incubated for 3 min on ice. The tube was topped up with PBS prior to cell washing by centrifugation (1350 rpm, 7 min). The pellet was re-suspended in PBS and either used for flow cytometric analysis or staining for FACS.

3.4.3. Splenic CD8α$^+$ lymphocyte sort

Splenic cells were stained with anti-CD8α-APC and anti-CD44-PE antibodies and incubated on ice for 5 min. The cells were washed (500 g, 8 min) prior to addition of anti-APC beads (Miltenyi Biotec) followed by 15 min incubation at 4°C in the dark, followed by another wash (500 g, 8 min). The cell suspension was filtered through a 40 µm mesh filter prior to AutoMACS enrichment (Miltenyi Biotec) using the positive selection programme (POSSEL) on both the sample and the subsequent negative fraction. The cells were then sorted based on CD8α and CD44 expression (memory: CD8α$^+$CD44^{Hi} cells and naïve: CD8α$^+$CD44^{Int} cells) using either the BD Influx or the Aria III sorter (see supplemental Figure to 4.5). For live/dead discrimination, DAPI was added prior to the sort and the sorting purity of the sort was checked. The gating of DAPI$^-$ CD8α$^+$ cells confirmed successful MACS-enrichment with over 80 % of live cells being CD8α$^+$. Afterwards the cells were centrifuged (500 g, 8 min) and the pelleted cells re-suspended in cold basal medium or PBS. A small fraction was mixed with Trypan Blue

to quantify the number of live cells using Countess Automated Cell counter (Life Technologies).

3.4.4. Isolation of liver lymphocytes

Liver tissue was pressed through a 70 µm mesh filter and the resultant cell suspension was washed with PBS and centrifuged (500 g, 8 min). The pellet was resuspended in 37.5 % Percoll and centrifuged for 700 g for 10 min. The pellet was then treated with ACK red cell lysing buffer for 3 min on ice prior to collection of the remaining cells (500 g, 8 min) which were used for flow cytometric analysis.

3.4.5. Isolation of lung lymphocytes

Lung tissue was cut into small pieces. The pieces were transferred into 15 ml tube containing 2.5 ml plain IMDM with 0.4 mg/ml Liberase TL (containing Collagenase I and II, enzyme activity >5.2 Wünsch units/mg, Roche) and 0.01 mg/ml Collagenase D (enzyme activity >0.15 Wünsch units/mg, Roche) and incubated at 37 °C, 200 rpm, for 30 min. This was followed by filtration through a 50 µm filters. The cells were collected by centrifugation (500 g, 8 min). Then 37.5 % Percoll density gradient was performed (700 g, 10 min) followed by ACK buffer lysis of red blood cells for 3 min on ice prior to centrifugation (500 g, 8 min). The cell pellet was re-suspended and used for flow analysis.

3.4.6. Isolation of skin lymphocytes

Ears of C57BL/6 mice were cut close to the skull. The ear sheets were peeled apart using forceps and were cut into very small pieces. These pieces were transferred into 15 ml tubes which were filled with plain IMDM containing 0.4 mg/ml Liberase TL (containing Collagenase

I and II, enzyme activity >5.2 Wünsch units/mg, Roche) and 0.02 mg/ml Collagenase D (enzyme activity >0.15 Wünsch units/mg, Roche) and incubated at 37 °C, 200 rpm for 90-120 min. This was followed by filtration through a 50 µm mesh filters. The cells were collected by centrifugation (500g, 8 min) and used for flow cytometric analysis.

3.4.7. CD8α$^+$ T cell culture

Spleens were pressed through a 70 µm mesh filter which were washed with PBS and topped up to 7 ml of cell suspension. It was underlayered with 5 ml Lympholyte (Cedarlane) and centrifuged at 1250 g for 15 min. The top layer was transferred to another tube and centrifuged in 500 g for 8 min. The suspension was stained with anti-CD8α-APC antibody and MACS-enriched and quantified, as previously described in section 3.4.3. The cells were re-suspended in complete IMDM supplemented with 5 ng/ml IL-2 (purity ≥ 98 %, activity ≥ 5x10^6 units/mg, Peprotech) and 250 000 cells per well were plated in pre-coated 24-well plates (made of polystyrene from Fisher Nunc). For the coating 1 µg/ml αCD3 and 3µg/ml αCD28 in sterile PBS were added to each well and the plate stored in 4 °C overnight. Afterwards, the solution was removed from the wells and cells added to the wells. The medium was exchanged every other day with 5 ng/ml IL-2 in complete IMDM.

3.4.8. Intestinal organoid set-up

The organoid set-up method is adapted from Clevers' protocol (Sato and Clevers, 2012). The proximal part of the small intestine was isolated, flushed with PBS, cut open and divided into 0.5 cm pieces. The intestinal fragments were washed in PBS by pipetting up and down, then the fragments were allowed to settle and the PBS was poured off. This was repeated 5-10 times until the PBS remained clear. Then the intestinal fragments were incubated in 2 mM EDTA at 50 rpm in 4 °C for 20 min. Afterwards the fragments were fractionated by adding PBS, shaken

forcefully for 15 seconds and the supernatant was poured into a new tube (the procedure repeated 7 times). All fractions were checked by inverted microscopy to select the crypt enriched fractions. Those were pooled, filtered through 70 µm mesh filters, washed twice (10 ml, 3 min 300 g, 4 °C) and then re-suspended into 100 % Matrigel (Corning). The resultant suspension was kept on ice and was plated in 50 µl hemi-spherical droplets on 37 °C pre-warmed 24-well plates. The droplets were polymerized for 15 min before addition of 500 µl complete organoid medium.

3.4.9. Organoid maintenance

The culture medium was exchanged every 2-3 days. The organoids were passaged every 6-8 days. For the passaging, the culture medium was removed and replaced with ice-cold basal organoid medium. The Matrigel droplets containing the organoids were gently disrupted using an Eppendorf p1000 pipette, then the suspension was passaged through a 25 g needle 5 times before washing (in final volume of 10 ml for 3 min at 300 g, 4 °C). The supernatant was removed and 1 ml basal organoid medium was added. Then the suspension was passaged through p1000 and p200 pipettes 10-15 times each, respectively, before another centrifugation (in final volume of 10 ml for 3 min at 300 g, 4 °C). The supernatant was removed and the organoids re-suspended into 50-70 % Matrigel and 30-50 % basal organoid medium mixture and plated as described above.

3.4.10. IEL-organoid-co-culture system

Three days old organoids were harvested by gently removing the culture medium and adding ice-cold basal medium. The Matrigel droplets were very gently scraped off by using an Eppendorf p1000 pipette. These were transferred into a 15 ml falcon tube and centrifuged (for

3 min at 300 g, 4 °C). The supernatant was discarded and 1 ml ice-cold basal medium added. The suspension was passaged through an Eppendorf p1000 pipette tip 10-15 times. The tube was topped up to 10 ml with basal organoid medium and another centrifugation performed (300 g, 4 min, 4 °C). Afterwards the organoids were re-suspended in basal organoid medium, followed by distribution into the different test conditions for each experiment. The IELs or splenic T-cells were added prior to resuspension in 50 % Matrigel. The suspension was plated in 25 µl hemi-spherical droplets on pre-warmed 8-well ibiTreat µ-slides from the vendor ibidi. The Matrigel was polymerized for 15 min before addition of 300 µl complete organoid medium.

3.4.11. MNV-organoid-co-culture system

The numbers of organoids were manually quantified using bright field microscopy. Using my estimation of the number of IECs per organoid three days after organoid passage (see Fig 4.7 for illustration of the method used for IEC quantification of organoids), the total number of IECs per well was estimated. Then 0.5-5 TCID of each strain of MNV (MNV-O7, MNV-CW3, MNV-3) per counted IEC was added either in the Matrigel or in the culture medium. For the latter the medium was mixed by pipetting up and down three times. After indicated time points after the MNV introduction to the organoids, they were either fixed and stained as described below or lysed with RNA lysis buffer (Sigma Aldrich) supplemented with β-mercaptoethanol at the concentration of 1 % (v/v), before the lysis.

In one experiment, 25 ng/ml IFNλ (PeproTech) was added to steady state and MNV-infected organoids for 24 hrs prior to image analysis as will be described in section 3.4.16.

3.4.12. IEL-MNV-organoid tri-culture system

To combine IELs, MNV and organoids, the IEL-organoid co-cultures were first set up as previously described (3.4.10.). Then the MNV was added in the medium as described above.

3.4.13. *Escherichia coli (E. coli)*-organoid co-culture system

The numbers of organoids were manually quantified under bright field microscopy. Using an estimation of the number of IECs per organoid at three days after passage, the total number of IECs was estimated. *E. coli* was prepared by taking a small sample from a culture and put into Lysogeny broth (LB) medium (prepared at the Babraham Institute) and put this on a shaker at 37 °C for 3 hours. Afterwards a small fraction was taken, spun and quantified using spectrophotometry for optical density (OD) values at wavelength 600. Then, the number of *E. coli* was quantified based on the assumption that OD600 measurement on 0.1 equals 10^8 bacteria/ml. Bacteria were added to the organoids either in the culture medium or the Matrigel followed by fixation and subsequent stainings.

3.4.14. Immunofluorescence

At indicated time points after the co- or tri-culture system set up, the culture medium was removed and the organoids washed with PBS. The organoids were fixed by adding 200 µl of 3.7 % formaldehyde (Sigma Aldrich) in RT for 20 min. The formaldehyde was gently removed, followed by another PBS wash. The organoids were permeabilised using 1 % (v/v) Triton X-100 in RT for 60 min, followed by blocking using 2 % (w/v) bovine serum albumin (BSA) and 1 % (v/v) Triton X-100 in RT for 60 min.

The organoids were then stained with an anti-CD45.2 antibody conjugated to either FITC, AF488, APC or AF647 and phalloidin conjugated to AF568 or AF555 (Life Technologies) in

RT for 45 min. Next, the organoids were washed and counter stained with DAPI in the mounting medium (Vectashield).

For live/dead staining, the culture medium was removed and the co-cultures were stained with DAPI for 10 min in RT. Afterwards the co-cultures were washed, fixed, permeabilised, blocked and stained as described above. For these samples, mounting medium without DAPI was used (Vectashield).

For EdU incorporation assays, Click-it EdU AF555 Plus kit (Life Technologies) was used. Ten nM EdU was added in the culture medium 2 hours prior to harvesting. After the fixation, permeabilization and blocking as described above, Click-it reaction mixture was freshly prepared and 110 µl of the mixture was added per well for 30 min staining in RT in the dark. Afterwards the wells were washed twice prior to further stainings.

For the IEC subset stainings, the organoids were permeabilised and blocked as described above. They were incubated at 4 °C overnight with primary antibody (see table 3.2) diluted in blocking buffer. Afterwards the cultures were allowed to return to room temperature before two washes with blocking buffer, followed by further staining, or mounted with Vectashield with DAPI.

3.4.15. Immunofluorescence of intestinal tissue staining

For staining including EdU, mice were injected with EdU i.p prior to small intestinal harvest. For whole tissue staining, the small intestine was flushed with PBS, cut open and rolled up like a “swiss roll” (Moolenbeek and Ruitenberg, 1981) which was placed in 4 % (v/v) PFA at 4 °C for 24 hours fixation. The tissue rolls were then dehydrated in 30% sucrose for 24 hours. Afterwards the tissue was stripped from the wooden stick and placed into plastic molds filled

with optimal cutting temperature (OCT) medium and frozen on dry ice before being cut into 10 µm slices. The cut slices were mounted on VWR Superfrost Plus slides. Under brightfield microscope, the quality of the cut section was observed and, if suitable, the tissues was then placed on dry ice while further sections from the same tissue sample were cut.

For the staining, the slides were allowed to dry at RT for 10-15 min before fixation with 4 % (v/v) PFA to ensure the tissue remained on the slide. Then the slides were permeabilised using 100 µl 1 % (v/v) Triton/PBS for 20 min with parafilm part on top of it to ensure all tissue is covered by the treatment. The slides were washed twice with PBS before being blocked for one hour in PBS, 1 % (v/v) Triton-X-100, 2 % (w/v) BSA, 5 % (v/v) FBS. For the EdU staining using the Click-it reaction, it was performed after the blocking step, followed staining with primary antibody diluted in blocking buffer and incubated overnight at 4 °C. Then, the slides were washed three times with PBS before staining with secondary or directly conjugated antibodies for 1 hour, followed by washing slides three times with PBS. The slides were mounted with Vectashiled with DAPI and allowed to dry before imaging.

3.4.16. Image acquisition and analysis

The co- and tri-cultures were analysed using either Zeiss LM780 or Nikon A1R confocal systems. For the Zeiss system, a 20x0.80 objective was used with the following lasers and filters: 405 (410-512), 488 (508-553), 561 (562-624) and 633 (629-751). For the Nikon system, a 20x0.75 objective was used with the following lasers and filters: 407.7 (450/50), 487.7 (525/50), 561.8 (595/50) and 639.7 (700/75).

Twenty-five organoids per well were selected using a channel showing the organoids only: for the IEL-organoid co-cultures, phalloidin-AF568/AF555 was used, while for EdU incorporation

panels DAPI or EpCAM was used for organoid detection instead. For the acquisition, an optical section between 120-155 µm with 2.0 µm steps was used. Most images were acquired using bi-directional mode. The images were processed and the number of IELs / EdU^+/ $Ki\text{-}67^+$ / $Muc\text{-}2^+$ / Lyz^+ IEC per organoid were automatically quantified using Imaris (v.8.1.2 Bitplane).

3.4.17. qPCR analysis of organoids

For mRNA analysis of organoids, the wells were lyzed with 250 µl of RLT buffer from Qiagen Rneasy Mini Kit. The mixture was vortexed prior to mixing with 350 µl of ethanol, followed by transfer into spin columns placed in two ml tubes. The tubes were centrifuged for 30 sec at 10 000 g. The flow through was discarded and 700 µl of RW1 buffer was added. The tubes were centrifuged for 30 sec at 10 000 g. The flow through was discarded and 500 µl of RPE buffer was added to each spin column. This procedure was repeated, and at the second time, tubes were centrifuged for two min at 10 000 g. The spin columns were placed in 1.5 ml eppendorf tubes and 30 µl of RNase-free water was added to each spin column centre. This was incubated in RT for three-five min before 13 000 g centrifugation for one min. The isolated RNA was quantified using NanoDrop to enable up to one µg of RNA to be converted into cDNA using Qiagen Quantitect reverse transcription kit. The RNA was diluted in RNase-free water prior elimination of genomic DNA by adding DNA wipeout mix from the kit and the samples were incubated at 42 °C for two min. For the transcription mastermix of Quantiscript rev Transcriptase, Quantiscript RT 5x buffer and RT Primer Mix was added to the samples. The samples were then run through cDNA protocol consisting of incubation at 42 °C for 15 min, followed by 95 °C incubation for three min. To ensure the same amount of cDNA was used for the RT-PCR, the cDNA was measured by Nanodrop to use 100 ng per reaction.

For the qPCR assessment, either SYBR green (Invitrogen's Platinum SYBR Green qPCR SuperMix-UDG) or Taqman system (TaqMan Universal PCR Master Mix, Applied Biosystems) were used on Biorad CFX96 qPCR machines. Hypoxanthine phosphoribosyltransferase (Hprt) was used as house keeping gene for $2^{(-\Delta\Delta CT)}$ method analysis.

3.4.18. Flow cytometric analysis

Samples for flow cytometric analysis were plated in round–bottom 96-well plates (made of polystyrene from Fisher Nunc). Ten µl counting beads (SpheroTech) were added to each well followed by surface staining on ice for 20 min. For intracellular staining, the Foxp3/transcription factor staining buffer set (eBioscience) was used after the surface staining. The samples were incubated in the fixation and permeabilisation buffer for 30 min on ice, followed by intracellular staining in the permeabilisation buffer for 45 min on ice.

For MitoTracker Green (MTG), MitoTracker Orange (MTO), MitoTracker Deep Red (MTDR), MitoSOX and NAO stainings, the samples were pre-incubated at 37 °C with their respective probe prior to surface staining according to the manufacturers' recommendations, followed by surface staining prior to flow analysis. For the dye titration experiments, Fluorescent-Minus-One (FMO) controls, for which samples were stained with all fluorochromes except for MTG / MTO/ MTDR/ MitoSOX/ NAO, were used to determine positive staining for each probe mentioned.

For Nile Red samples, the cells were surface-stained prior to fixation and Nile Red incubation according to the manufacturer's recommendations. Then the cells were washed with PBS and centrifuged for 2.5 min at 500 g twice, before being resuspended in 100 µl PBS.

The cells were acquired using either BD LSRFortessa or LSRII (BD) and analysed on FlowJo v.10.2 (FlowJo). The tSNE plugin was used with FlowJo to capture the heterogeneity of IEL populations.

3.4.19. Cardiolipin (CL) analysis

For the CL mass spectrometry analysis, liquid chromatography–mass spectrometry (LC-MS) graded solvents (Fischer Scientific) were used. The sample pellets were resuspended in 1.5 ml methanol. This was thoroughly mixed by vortexing with 1.5 ml water and 3 ml chloroform. To each sample, 200 ng of tetramyristoyl $(14:0)_4$-CL (Avanti Polar Lipids) was added as internal control for CL quantification. The lower phase from each solution were concentrated with Speedvac. The new pellet was dissolved in 100 µl chloroform, from which 17 µl of this chloroform solution were used for LC-MS analysis. Normal phase HPLC on MicroSolv Type C silica column with Shimadzu Prominence system were used to separate the different classes of lipids. CL analysis was performed on selected-ion monitoring chromatogram (SIM) mode with fourier-transform ion cyclotron resonance mass spectrometry (FT-MS) with the following settings: (mass range 560-880m/z, mass resolution 240k at m/z 400, mass accuracy ~3 ppm).

3.4.20. Mitochondrial capacity assay

The mitochondrial capacity in IELs, naïve and memory $CD8\alpha^+$ splenocytes were assessed using the Seahorse Mito stress assay on a Seahorse Extracellular flux 24e Analyser (Seahorse Bioscience). 24-well assay plates (special Seahorse plates made of polystyrene from Seahorse Bioscience) were incubated with Seahorse calibration medium and sample plates were coated with 50µl 0.01 % poly-lysine (Sigma Aldrich) and incubated overnight in a Seahorse incubator at 37 °C. 750 000 cells per well were plated in Seahorse medium and put in the Seahorse incubator for 45-60 min prior to assay. The following compounds in this order were injected to the plated cells: oligomycin (2.5 µM final), carbonyl cyanide-p-trifluoromethoxphenylhydrazone (FCCP) (0.5-5 µM final) and mixture of antimycin and

rotenone (both 1µM final), to assess the basal mitochondrial oxygen consumption, ATP production and spare mitochondrial respiratory capacity (SRC).

3.5. Statistical analysis

Unless otherwise stated in the figure legends, the data are presented as mean ± standard deviation (SD). Normality tests (D'Agostiro-Pearson omnibus, Shapiro-Wilk or Kolmogorov-Smirrov normality tests) were performed to determine whether to use parametric or non-parametric statistical tests. For one-way ANOVA analysis performed, the no matching option was selected together with the Bonferroni correction. The same selections were used for performing the two-way ANOVA analysis. For Mann-Whitney U and Spearman correlation analysis, the two-tailed option was selected with a 95 % confidence interval. For principal component analysis (PCA), RStudio (version 1.0.153 with R 3.3.1.) was used. Statistical significance was denoted as follows: *$p < 0.05$, **$p < 0.01$ and ***$p < 0.001$. Except for PCA analysis, the remaining statistical analyses were performed using GraphPad Prism version 7 for Windows.

Chapter 4: Establishing an IEL-Organoid co-culture system to study IEL function, maintenance and activation

4.1. Modelling IECs: From cell lines to organoid cultures

4.1.1. Two-dimensional cell culture models

The first *in vitro* model of IECs was established by the generation of the human colon carcinoma cell line (Caco-2) (Artursson, 1990). Having an *in vitro* model enabled mechanistic studies on both the basolateral and luminal sides of the IECs. There are numerous alternative cell lines originating from human, mouse and rat and derived from the different sections of the intestinal tract: duodenum, jejunum and ileum. However, these cell lines model enterocytes - which is the main epithelial subset - but only one of the many epithelial subsets identified *in vivo* (see sections 1.6.1.1-1.6.1.7). All cell lines have been immortalized, which differs from *in vivo* IECs that are one of the most rapidly renewing tissues (Clevers, 2013). In the renewal process of the IEC barrier, the shed IECs are undergoing a detachment-induced apoptosis called anoikis (Coll et al., 2002), a property not mimicked in cell lines. In addition, there have been reports of differences between Caco-2 cells and human duodenum samples in regards to gene expression. There are even differences observed during culture between day 4 and day 16 of Caco-2 culture (Sun et al., 2002). Long-term culture is also associated with differences in cell properties with increased passage of the cells (Hughes et al., 2007). Hence, there is a need to obtain a more accurate and stable *in vitro* model of IECs.

4.1.2. Intestinal stem cell niche

As previously mentioned (1.6.1), a single-cell layer of IECs that form finger-like villus domains and crypt domains lines the small intestine. The intestinal epithelial stem cells (IESCs) reside in the crypt domains. In each crypt domain, there are approximately 15 multipotent

IESCs. There are two distinct IESCs populations identified: $Lgr5^+$ and +4 IESCs, as described in section 1.6.1.1.

Around the intestinal crypt structures are various immune cells and supporting cells such as stromal cells. Stromal cells support IESCs by providing non-canonical Wnt. Canonical Wnt are provided from Paneth cells (Pinchuk et al., 2010). The different IEC subsets require different signalling: enterocyte differentiation requires Notch signalling to be active , while the secretory IECs require Notch signalling to be inactive and Wnt signaling to be active instead (Yin et al., 2014; VanDussen et al., 2012). Stromal cells also express BMP4 underneath villus domains (Gracz and Magness, 2014), supporting the villus-crypt organization. In addition, stromal cells can respond to pro-inflammatory cytokines such as TNFα (Armaka et al., 2008) and IL-1β and interact with other immune cells in the intestinal tissues (Owens and Simmons, 2013) providing both renewal and immunological support to IECs.

To summarize, there are multiple different IEC subsets that support each other for intestinal homeostasis. In addition, there are supporting stromal cells that provide relevant factors, all of which are required to be taken into account for generating *in vitro* models of IECs.

4.1.3. Requirement for Wnt/EGF/BMP signalling for IESCs

Wnt signalling is an essential process for the intestinal compartment. There are at least three known pathways: canonical, non-canonical and Ca^{2+}-dependent Wnt signalling pathways. These three pathways share the binding to the main receptor, Frizzled, but have different co-receptors bound to them, leading to different downstream signalling cascades. For the canonical pathway, Wnt binds to the receptor Frizzled that leads to inactivation of a complex consisting of proteins such as glycogen synthase kinase 3 (GSK3). The inactivation of this

complex leads to β-catenin stabilization. Stable β-catenin can then form complex with transcription factors, such as Tcf4, that leads to transcription of Wnt targeted genes (Niehrs, 2012; Clevers and Nusse, 2012). Tcf4 deficiency in mice is lethal and experiments on embryos show that these lack intestinal stem cell compartments (Korinek et al., 1998). R-spondin is a Wnt signalling amplifier that brings about increased proliferation (Kim, 2005) and increased numbers of Paneth cells in the crypts (Hayase et al., 2017). However, depleting Wnt specifically in the intestinal compartment using Villin-Cre-ERT2;$Wnt3^{fl/fl}$ mice brings about no obvious phenotype. When culturing IECs from these mice on their own in the form of organoids (see section 4.1.6) there are phenotypes observed such as reduced Lgr5 expression, fewer Paneth cells and less bud (crypt structure) formation (Farin et al., 2012). These findings highlight the importance of the intestinal niche that is present in the mice, which can compensate for the lack of Wnt3a and which organoids cultured without supporting intestinal cells cannot. Another approach that supports this finding is the use of the GSK3-inhibitor CHIR99021 that increases the number of Paneth cells in a dose-dependent manner (Sato et al., 2011). It has been reported that Wnt signalling decreases with age and, as a consequence, there are fewer IESCs observed in older individuals (Nalapareddy et al., 2017).

Another factor important for IEC renewal is epidermal growth factor (EGF). EGF binds to its receptor EGFR and activates extracellular signal-regulated kinase (ERK) signalling leading to proliferation (Frey et al., 2004; Sato and Clevers, 2013). EGFR is expressed in IECs located in the crypt structures and the lower part of the villous structures (Suzuki et al., 2010; Yang et al., 2017). EGF is expressed by Paneth cells to support IESCs (Sato et al., 2011).

Another factor that has been shown to promote IEC growth is the cytokine IL-22. Addition of IL-22 to organoids increases their surface area in a STAT3-dependent manner. Injection of IL-

22 into mice increased the transition amplifying (TA)- and crypt height (Lindemans et al., 2015).

In addition to factors such as Wnt, EGF and R-spondin, that promote IEC proliferation, there are factors suggested to be important for *in vivo* IEC organisation and IEC subset differentiation, and these include Notch and bone morphogenetic protein (BMP) signalling.

Notch signalling is taking place between two cells closely located to each other: one cell expressing the Notch receptor and the other cells expressing transmembrane Notch ligands such as delta-like ligands (Dll) and Jagged. Upon receptor-ligand binding, an enzyme called γ-secretase is cleaving the Notch ligand. The intracellular domain of the Notch ligand, called Notch intracellular domain (NICD), is then translocating to the nucleus, binding to transcription factors to induce transcription (Kopan and Ilagan, 2009). Paneth cells express the Notch ligand delta like ligand 4 (Dll4), to support IESCs (Sato et al., 2011). Notch signalling has been showed to be important for differentiation towards the enterocyte lineage. Using Notch inhibitors *in vivo*, the frequency of cells in the secretory epithelial lineages increases drastically (VanDussen et al., 2012; van Es et al., 2005). Similar observations were made using knock-out mice for the Notch ligands specifically in the intestinal compartment (Pellegrinet et al., 2011).

BMP signalling is part of the TGFβ signalling family. Upon ligand binding, there are two known pathways. One pathway includes phosphorylation of either Smad1, Smad5 or Smad8, which then forms a heterodimer with Smad4 and the heterodimer translocates to the nucleus. The other pathway is mediated via TGFβ-activated kinase 1 (TAK1) instead (Zhang and Li, 2005). BMP signalling restricts IESCs (Qi et al., 2017). Addition of Noggin inhibits BMP

pathway and as a consequence prevents formation of proper villus domains (Haramis et al., 2004).

4.1.4. The role of extracellular matrix (ECM) for IEC cultures

In the 1970s, a tumour that produced an abundant amount of extracellular matrix (ECM) proteins was discovered. The tumour was named the Engelbreth-Holm-Swarm (EHS) mouse sarcoma (Kleinman and Martin, 2005). Among the ECM proteins identified from this tumour were laminin, collagen and heparan sulfate proteoglycan (Kleinman et al., 1982). From this tumour, an ECM mixture was generated and named Matrigel. Growing both cell lines and primary cells in Matrigel was shown to have effect on cells' differentiation and/or three-dimensional (3D) formation (Orkin et al., 1977). Using Matrigel enabled the first intestinal organoid cultures: "mini-guts" in culture well plates (see section 4.1.6). However, the exact composition of the extracellular proteins in Matrigel is rather poorly defined. To overcome this hurdle but still grow 3D organoid cultures scientists have tried to develop alternatives to Matrigel.

A collagen I gel mixture has been showed to be able to support intestinal epithelial organoid growth. The gene expression of some typical markers for the different IEC subsets were not altered between collagen-I-grown and Matrigel-grown organoids. However, the growth rate of collagen I-grown organoids was lower compared to their Matrigel-grown equivalents (Jabaji et al., 2013). In addition to collagen I mixture, crosslinked polyethylene glycol (PEG) hydrogels have been tested for organoid cultures. On their own, the support for organoid formation is non-existent but addition of either fibronectin, laminin or collagen IV into the PEG hydrogel improved the organoid formation significantly (Gjorevski et al., 2016).

All organoid experiments presented in this thesis have been performed using Matrigel, but the potential effect alternative 3D matrices would have on the co-culture system will be discussed in the discussion section.

4.1.5. Intestinal spheroids

The first long-lived primary intestinal epithelial cell culture system was established in 2009. The system - intestinal spheroids - consisted of murine neonatal intestinal tissue placed on a collagen gel layer and grown in an air-liquid interface system. By immunohistochemistry the presence of all main IEC subsets was confirmed. The intestinal spheroid cultures survived for at least 30 days. These properties were already better than cell line models such as Caco-2. However, the intestinal spheroids failed to recapitulate the characteristic villus and crypt morphology observed *in vivo* (Ootani et al., 2009).

4.1.6. Intestinal organoids

The recapitulation of *in vivo* IEC organization was established with the organoid model: small intestinal crypts, containing both IESCs and Paneth cells, cultured in semi-spherical droplets of Matrigel. The 3D matrix formed by the Matrigel enabled crypts to grow and organize into 3D structures recapitulating the villus-crypt morphology observed *in vivo* (Fig 4.1 A and D) (Sato et al., 2009). Although organoids recapitulate *in vivo* crypt and villi organization, the organoid model are inside-out compared to the *in vivo* situation. In the organoids, the crypt domains form finger-like structures (Fig 4.1 C), while the villi domains form finger-like structures in the *in vivo* situation (Fig 4.1 A). This also means that organoids enclose their lumen. The organoids are cultured in the presence of the growth factors noggin, R-spondin and EGF. To recapitulate, EGF activates the ERK pathway to promote proliferation, while R-spondin amplifies the Wnt pathway and noggin inhibits BMP signaling. Both R-spondin and

noggin promote and sustain stemness (Fig 4.1 C). Immunofluorescence experiments have confirmed the presence of the main IEC subsets enterocytes, Paneth cells, goblet cells and enteroendocrine cells (Sato et al., 2009), as well as tuft cells (Howitt et al., 2016) in the organoids. After the initial two passages of intestinal organoids, the organoids grow in a repeatable pattern after each passage. The passage generates separated crypt domains that subsequently form new organoids. Time-imaging investigation, as illustrated in Figure 4.1 E, shows that crypt formation is observed after one-two days after passage, indicating the speed of IEC proliferation.

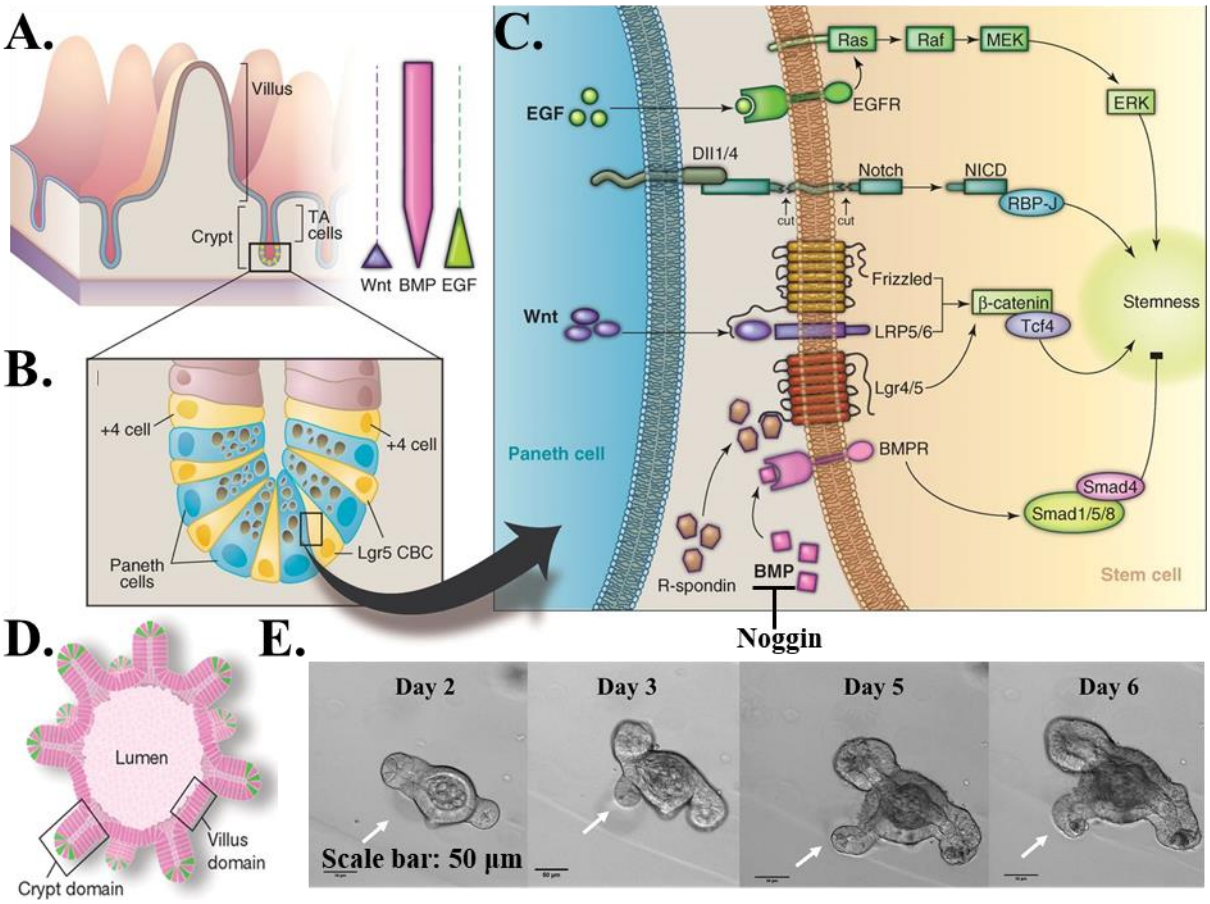

Figure 4.1. The intestinal stem cell niche and the organoid model. A) Schematic view of the IEC barrier in the small intestine *in vivo*, including which signaling pathways that are active in the crypt and villus domains. B) Zoom-in between Lgr5^{+} and +4 IESCs and Paneth cells. C) The EGF, BMP and Wnt signaling represented between stem cells and Paneth cells. Panel A, B and C are modified from Sato and Clevers, Science 340(6137):1190-4. D) Schematic view of the organoid model illustrating the presence of crypt and villus domains. Panel D is modified from Sato and Clevers Methods Mol Biol 945, 319–328. E) Kinetics of small intestinal organoid growth using brightfield time-lapse imaging. Scale bar: 50 µm.

4.1.7. Organoid Expansion: more tissues, tools and applications

The interest in the organoid technique and its applications have expanded rapidly: with the use of Lgr5 as a stem cell marker, organoid culturing protocols have now been established for other tissues, such as colon (Yui et al., 2012; Wang et al., 2013), pancreas (Huch et al., 2013a), stomach (Barker et al., 2010), liver (Huch et al., 2013b), uterus (Boretto et al., 2017) and

mammary tissue (Zhang et al., 2017). Another approach for generation of organoids involves stem cell isolation and differentiation from these into organoids. Organoids from lung (Dye et al., 2015; Barkauskas et al., 2017; Nikolić and Rawlins, 2017), inner ear (Koehler et al., 2017; DeJonge et al., 2016) and brain (Lancaster et al., 2013) have been generated with the induced stem cells approach. In addition, it has been shown that both kidney organoids (Takasato et al., 2015; Taguchi et al., 2014) and intestinal organoids are genetically stable for prolonged period of time (Huch et al., 2015). This is advancement compared to cell lines that alter after short period of culturing. These advances allow interesting science as methods used for intestinal organoids may be applied to organoids sourced from other tissues, just as the use of Lgr5, as stem cell marker, has been. It could also facilitate advances in understanding tissue-specific development, steady state and diseases, and tissue-resident immunity. *In vitro* cell culture techniques such as transfection (Wang et al., 2014; Koo et al., 2013), bacterial artificial chromosome (BAC) transfection (Schwank et al., 2013) and CRISPR/Cas9 gene editing (Driehuis and Clevers, 2017) have been optimized for organoid cultures.

The organoid models have great potential in various fields such as stem cell biology, drug candidate screening and transplantation medicine: from modelling organ development from stem-cell-induced organoids to assessing drug on patient-derived organoids (Astashkina and Grainger, 2014). This illustrates the potential organoid models have for the life sciences and health care in the longer term. To make the organoid models even more like the corresponding *in vivo* systems, one needs to add back layer by layer, more *in vivo* complexity. One of the most obvious missing factors is the immune system. Here, I will report on experiments in which I have added back IELs to intestinal organoids. Although different tissues have different requirements and challenges, the methods developed and applied in this chapter may be useful

for other tissue organoids to address tissue-specific questions about cell-cell interactions, tissue-specific pathogens, disease and remodelling.

4.2. Modelling intestinal intraepithelial lymphocytes *in vitro*

In the past, there have been some trials to model IEL-IEC interactions *in vitro*. This has been done using human cell lines for both IEC (T84) and IELs (032891). Human IELs differ significantly from murine IELs in terms of subset composition. For example, only a minor fraction of human IELs are TCR$\gamma\delta^+$ cells (Jabri and Ebert, 2007; Mayassi and Jabri, 2018) unlike murine IELs of which TCR$\gamma\delta^+$ cells form the majority of murine IELs. In addition, murine IELs survive poorly *in vitro*. For the human cell line cultures, transwells have been inserted into culture wells with IEC cell lines at the bottom of the transwell. Then IELs have been added either on top of the IEC cell line or added underneath the transwell into the well (Fig 4.2 A+C). The different culture techniques were shown to have different effect on IEC surface markers (Shibahara et al., 2005), indicating there are both contact interactions between IECs and IELs as well as soluble factor secretion from IELs that affect IECs. Another group (Shaw et al., 1998) used a similar approach but grew the IEC cell line either on the underside or the upperside of the transwell to mimic apical and basolateral sides of the IEC barrier to study IEL interactions (Fig 4.2). They showed that by 4 hours of co-culture, IELs had migrated more effectively when IEC were cultured on the underside, indicating that IEL approached them from the basolateral side (Shaw et al., 1998). With the discovery of Matrigel, more co-culture techniques have been explored (Pereira et al., 2015). However, murine studies describing IEL-IEC interactions are lacking. When culturing, *in vitro* antibiotics are commonly used in the cell culture medium to avoid contamination. Published data on the number of IELs in germ-free mice demonstrate that only specific IEL subsets are reduced in germ-free mice. Two papers demonstrated that only TCR$\alpha\beta^+$ CD8$\alpha\beta^+$ IELs are significantly reduced in numbers

compared to specific-pathogen-free (SPF) mice (Kawaguchi et al., 1993; Supplemental Information: The Transcription Factor T-bet Is Induced by IL-15 and Thymic Agonist Selection and Controls CD8αα+ Intraepithelial Lymphocyte Development, 2014), while another paper showed that there was only a reduction in TCRαβ^{+} CD8αα^{+} IELs (Hoytema van Konijnenburg et al., 2017).This indicates that the absence of the microbiota should not be a limiting factor for culturing a representative murine IEL population *in vitro.*

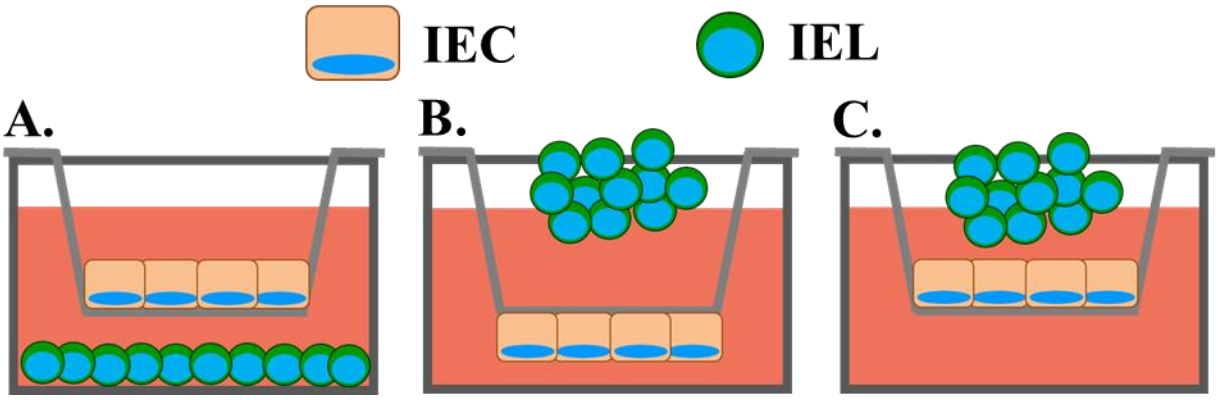

Figure 4.2. Schematic overview of published co-cultures of IEC and IEL cell lines. Human IEC and IEL cell lines have been used for co-culture experiments. To assess different aspects of their interactions, transwell inserts have been used. A) IEC cell line has been cultured on the transwell membrane and inserted on well with IEL cell line cultured underneath. B) IEC cell line cultured on the culture well side of the transwell, with IEL cell line added inside the transwell. Panel A-B are inspired from methods described by Shibahara et al., J. Gastroenterology (2005). C) IEC cell line cultured on the transwell and IELs added inside the transwell. Panel B-C are inspired from methods described by Shaw et al., Am. J. Physiol (1998).

The current knowledge about IEC-IEL interactions is derived from *in vivo* models and cell lines such as described above. Both approaches have their limitations. The intestinal immune system is complex – intestinal epithelium, hematopoietic immune cells, diet, commensals and pathogens, all interacting with each other – hence dissecting the molecular mechanisms behind IEC-IEL interactions *in vivo* is a difficult task. In addition, live cell analysis of IEC-IEL interactions by intravital imaging is a highly complex approach (Ritsma et al., 2013). Epithelial

cell lines are much more accessible for live cell imaging. However, due to immortalisation, frequent passaging and the lack of the structural organisation observed *in vivo*, cell lines do not represent the *in vivo* situation very well. A novel approach to overcome these issues and dissect the molecular mechanisms behind IEL-IEC interactions is to take advantage of intestinal organoids model and to explore if it is possible to co-culture these with IELs.

4.3. It is possible to incorporate IELs into intestinal organoids

In contrast to other T cells IELs survive poorly *in vitro* ((Lai et al., 2013) and own data not shown). Not having an *in vitro* model for IELs limits the available approaches for mechanistic investigation of IEL biology. These are particularly needed as the intestinal immune system consist of various kinds of immune cells, epithelial cells and microbiota which all can respond to administration of particular compounds, making it hard to dissect direct and indirect effects on the cells of interest and to define the sequence of events.

The poor *in vitro* survival of IELs indicates that there are factor(s) lacking from the *in vivo* intestinal compartment in the tested culture conditions. As there have been significant advancement with modeling IECs, in the form of intestinal organoids, the question is if intestinal organoids resemble the *in vivo* situation to the extent that the organoids can maintain IELs alive for a longer period of time. To test whether IELs and organoids can be co-cultured, live IELs were sorted based on their CD8α expression with DAPI staining as discriminator of live and dead cells. For the experiment, intestinal organoids were cultured for 3 days post passage, in order to use organoids in which the majority have clear villi and crypt structures. For the incorporation, IELs were added either in the Matrigel droplet together with the organoids or added in the medium after the Matrigel had been polymerized. As previous literature and experience indicated that IELs survive poorly *in vitro*, I analysed the co-cultures

as early as 12 hours post set up. The fixation and staining protocol is described in the Materials and Methods section. The CD45 staining was used to detect IELs specifically. The DAPI staining was used to detect nuclei in both IECs and IELs. Finally, phalloidin a probe that stains F-actin, provides a clearer inner and outer structure the organoids compared to what the DAPI staining alone provides. The first observation was that IELs were detected both inside and on the organoids by CD45 staining in both conditions (Fig 4.3 C). This observation was promising as it offered optimization possibilities for the system. However, the number of IELs found on the organoids ranged from 1 to 8 (data not shown). From *in vivo* and tissue sectioning data the expected number of IELs per IEC would be 1 IEL per 4-10 IEC (Edelblum et al., 2012; Beagley et al., 1995; Wurbel et al., 2007; Schön et al., 1999). Examining images from IEL-organoid co-cultures clearly indicates that there are fewer IELs per IEC on the organoids, suggesting that there are still factors missing from the *in vivo* situation.

4.4. Adding IELs in the Matrigel significantly increases the number of IEL-associated organoids

Having been able to show that IEL and organoids indeed can be co-cultured (Fig 4.3 C), I next need to optimize and validate the co-culture system. To further optimize the co-culture system, I tested whether adding IELs into the medium or Matrigel did have an impact of the IEL incorporation rate. A possible reason why few IELs are detected on the organoids (1-8 IELs per organoids) could be that they die and thus become undetectable with CD45 staining, so I tested whether the addition of cytokines suggested to be important for IEL survival, namely IL-2, -3, -7 and IL-15, would increase the number of IELs observed per organoid. To address this, I added IELs in the Matrigel or organoid culture medium with or without the cytokine cocktail (four conditions in total) (Fig 4.3 D-F) and fixed the co-cultures 12 hours post set-up. Interestingly, I observed that the number of organoids having IELs associated to them (both on

and inside organoids) increased significantly, when the IELs were added into the Matrigel compared to adding IELs in the medium (Fig 4.3 E). However, the addition of cytokines at 12 hours post culture set-up did not make a significant contribution, suggesting that the starting point with low number of IELs does not seem be mediated by death because of lack of IL-2-3,-7 and IL-15. I also quantified the number of IELs observed on each organoid and also there I observed a statistically significant increase of the number of IELs observed per organoids in the condition where IELs were added in the Matrigel. The additional cytokines did not make a significant impact on the number of IELs per organoid (Fig 4.3 F). Following this experiment, the subsequent experiments were all performed with IELs co-cultured in the Matrigel.

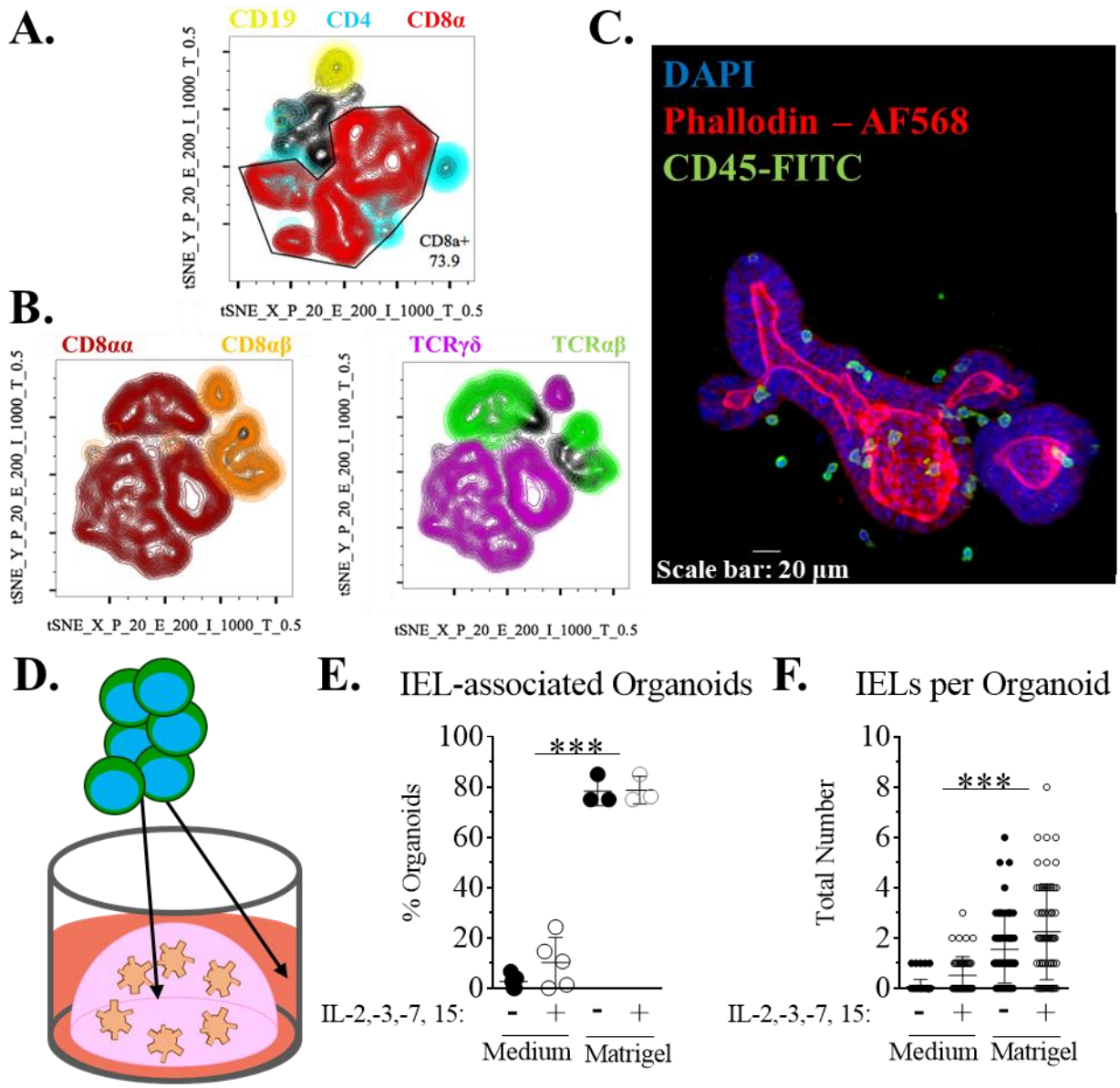

Figure 4.3. Association of IELs with organoids is independent of IL-2, -3, -7 and IL-15. 38 000 IELs and approximately 100 organoids per well were co-cultured at 37 °C for 12 hours either in medium or in Matrigel in the presence or absence of a cocktail of interleukins -2, -3, -7 and -15. A) IELs used for the co-culture experiments were sorted based on CD8α expression. The proportion of $CD8\alpha^+$ IELs in the small intestinal epithelium compartment was analysed by flow cytometry. The plots were gated on live $CD45^+$ cells and the cell staining patterns analysed by tSNE. The tSNE plot is overlaid with CD8α, CD19 and CD4 expression. These are representative plots from at least ten independent experiments. B) The same experiments as shown in panel A except this time the population was pre-gated on live $CD45^+CD8\alpha^+$ prior to tSNE analysis and the tSNE plots overlaid with stainings for either CD8αα and CD8αβ (left)

Figure 4.3. Association of IELs with organoids is independent of IL-2, -3, -7 and IL-15 (cont.) or TCRγδ and TCRαβ (right). C) After 12 hours of co-culture, IEL-organoid co-cultures were fixed and stained for DAPI, phalloidin conjugated to AF568 and CD45. The scale bar represents 20 µm. D) Schematic illustration of a well with intestinal organoids cultured in Matrigel and the two incorporation techniques used. E) Organoids containing at least one IEL were counted for each growth condition. The result is expressed as percentage of 25 organoids per well analysed and represented as mean ± SD. The experiment was performed twice. F) The number of IELs present in the organoids under the various conditions. Each point represents the number of IELs present in a single organoid as mean ± SD. The experiment was performed twice. Statistically significant changes were identified by one-way ANOVA for panel E and the Kruskal-Wallis test for panel F. ***: $p<0.001$.

4.5. The seeding density of IELs is important for a high level of IEL-incorporation

After testing different incorporation techniques, I next asked whether the missing factor(s) could be derived from IELs or IECs. It may be that intestinal organoids do not fully resemble the *in vivo* IEC surface protein expression, or that IELs may have lower homing capacity, as they have already homed to the intestinal compartment once in the donor mice. To address this, I carried out titrations using constant numbers of organoids, or converseley of IELs, and then I assessed the impact of different numbers of the partner in the co-culture system. When adding 40 000 IELs to varying numbers of organoids, as indicated on the figure, I observed no significant differences in terms of percentage of IELs associated with organoids (Fig 4.4 A). However, when I increased the number of IELs added to the same number of organoids, I observed an increase in the percentage of IEL associated organoids (Fig 4.4 C) suggesting that one or more IEL derived factors is missing from the *in vivo* situation. An alternative explanation could be that only a small percentage of the heterogeneous IEL population (Fig 4.3 A-B) is actually able to access and associate with the organoids and the more total IELs that are added

the larger this subpopulation will be in the culture well. In terms of number of IELs on the organoids, it seems that the number of organoids per well is not a critical factor as all organoid concentrations contain similar range of IELs per organoid (Fig 4.4 B). The same applies when titrating the number of IELs (Fig 4.4 D).

To understand further what these limiting IEL-derived factor(s) may be, I also compared TCR$\alpha\beta^+$ and TCR$\gamma\delta^+$ IELs co-cultured separately with WT organoids. By 12 hours post set-up, TCR$\gamma\delta^+$ IELs are more numerous per organoid compared to TCR$\alpha\beta^+$ IELs co-cultures and there is also a higher frequency of organoids carrying TCR$\gamma\delta^+$ IELs (Fig 4.4 E and F). This data is promising, as indeed there are more TCR$\gamma\delta^+$ IELs compared to TCR$\alpha\beta^+$ IEL in *in vivo* small intestine. However, over time in the CD8α^+ IEL co-cultures, the ratio of TCR$\gamma\delta^+$ IELs associated with organoid decreases (Fig 4.9 C), suggesting that current culture conditions favor TCR$\alpha\beta^+$ IEL maintenance.

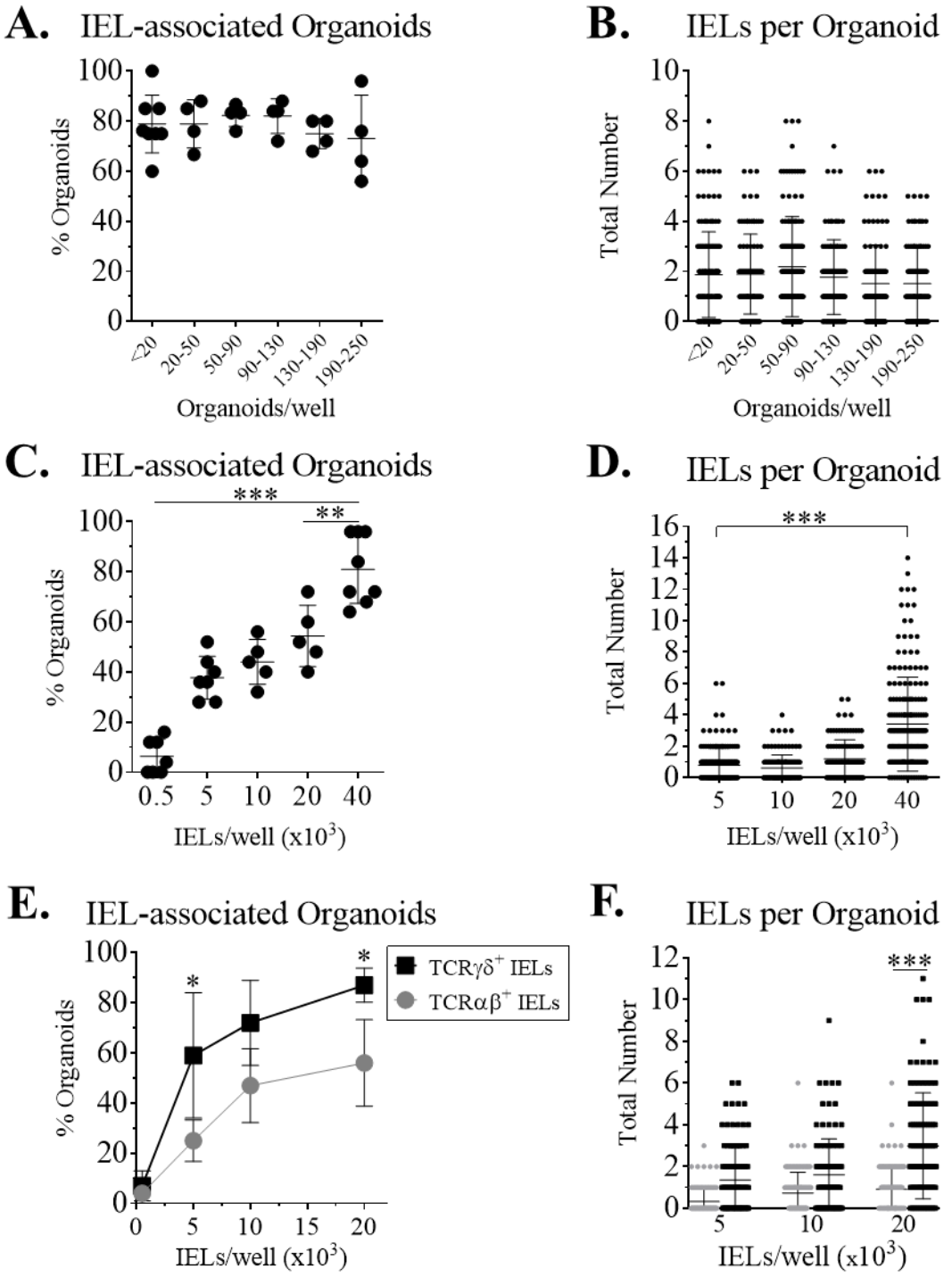

Figure 4.4. Association of IELs with organoids is dependent on the seeding density of IELs. IELs and organoids were co-cultured in Matrigel for 12 hours at 37°C with differing numbers of organoids (A-B) or IELs (C-D) seeded per well as indicated. A) The number of organoids per well was varied with 40 000 IELs per well seeded. Each point is presented as percentage of IEL-carrying organoids (at least one associated IEL) per well and represented as mean ± SD.

Figure 4.4. Association of IELs with organoids is dependent on the seeding density of IELs (cont.) 4-6 wells with 25 organoids per well were screened in 2 independent experiments. B) Using the same dataset as in panel A, the number of IELs associated with individual organoids was quantified. Data are presented as mean ± SD. C) The number of IELs per well was varied with estimated 100 organoids per well seeded. The percentage of organoids with IELs was determined in the same way as in panel A. D) Using the same dataset as in panel C, the number of IELs associated with individual organoids was determined in the same way as in panel B. E) Organoids were co-cultured with varying numbers of either TCR$\alpha\beta^+$ or TCR$\gamma\delta^+$ IELs and the percentage of IEL-associated organoids determined in each case, as in panel A. F) Using the same data as in panel E, the number of IELs associated with individual organoids was determined in the same way as panel in B. The experiments were performed twice with final 4-6 wells. Each data point presents the percentage of IEL-carrying-organoids per well or the number of IELs per organoid. Statistically significant changes were identified by one-way ANOVA for panel A, C and E and the Kruskal-Wallis test for panel B, D and F. *: $p<0.05$ **: $p<0.01$ ***: $p<0.001$.

4.6. Organoids enable IELs specifically to migrate into them

One important factor for model establishment is to test specificity. There is a need to address whether similar numbers of other T cells would be associated to organoids as IELs. To test co-culture specificity, I set up co-culture with organoids and either naïve ($CD8\alpha^+$ $CD44^{Int}$) or memory ($CD8\alpha^+$ $CD44^{Hi}$) T splenocytes (Supplemental figure to Fig 4.5) as comparative populations for IELs. IELs are usually described as semi-activated, and therefore the best comparative populations would be both naïve and memory T cells (non-activated and formerly activated T cells). I observed that IELs were superior in intraepithelial localisation compared to the splenocytes (Fig 4.5 E-F): the number of splenocytes in intraepithelial location increased with increase number (Fig 4.5 E-F) suggesting addition of more cells may be saturating the organoid system. It could also be that either IECs only allow IELs to migrate to intraepithelial sites, or that only IELs have the capacity to migrate between the IECs and occupy the niche as tissue resident cells.

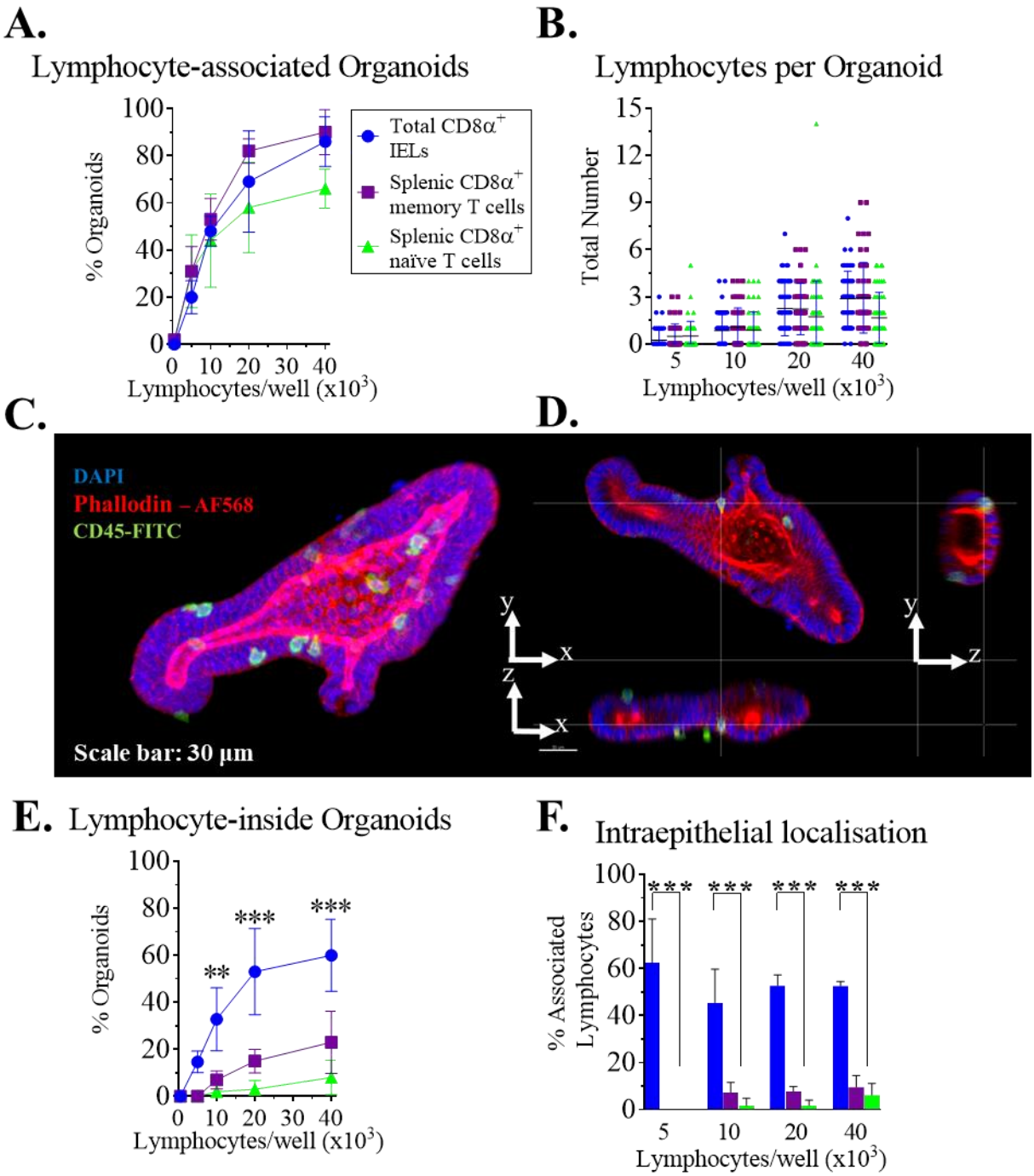

Figure 4.5. Selectivity of lymphocyte migration into organoids. Organoids were co-cultured separately with varying numbers of lymphocytes of IELs, naïve ($CD44^{int}$) and memory ($CD44^{Hi}$) $CD8\alpha^+$ T cells for 12 hours prior to analysis. Immunocytochemical analysis was then performed to determine the association with or entry into the organoids co-cultured with the lymphocytes. A) The percentage of the organoids per well associated with the three types of lymphocytes was determined.

Figure 4.5 Selectivity of lymphocyte migration into organoids (cont.) Each data point presents the percentage of lymphocyte-carrying-organoids per well represented as mean ± SD**.** 4 wells with 25 organoids per well were screened and performed in 2 independent experiments. B) Using the same dataset as in panel A, the number of IELs associated with individual organoids was counted. Each data point presents the number of IELs per organoid and is presented as mean ± SD. C) Representative image of IELs within an organoid - scale bar is 30 μm. D) Three-dimensional representation of the same image as in C). E) The percentage of organoids per well containing lymphocytes within them was determined for all three lymphocyte types. F) The same dataset as in panel E was used to determine the percentage of the total associated lymphocytes that has entered the organoids. The experiment was performed twice. Statistically significant changes were identified by one-way ANOVA for panel A and E and the Kruskal-Wallis test for panel B and F. **: $p<0.01$ ***: $p<0.001$.

4.7. IELs survive for at least 4 days in co-culture with organoids

Another important question to address is whether the IELs associated to organoids remain alive for a prolonged period of time. If IEL survive longer *in vitro* with the organoids than alone that would open up new possibilities with mechanistic studies of IEL biology and provide an *in vitro* option for IELs to complement the *in vivo* observations. To address whether IELs survive in the IEL-organoid co-culture system, I adapted a live dead imaging system for the co-culture system. I added DAPI to the co-culture before fixation instead of using it as a counter-stain. As positive control, I added splenocytes from another experiment in which they had been stored in sub-optimal conditions leading to generation of dead cells to ensure sufficient DAPI staining to be able to distinguish live and dead IELs, as well as live and dead organoids. By this method, I would be able to address whether the IELs observed on the organoids are alive or not and for how long they stay alive. The altered staining method worked as anticipated (Fig 4.6 A-B). I used this staining method on IEL-organoids co-cultures. In Figure 4.6 C, I show a representative of an organoid co-cultured with IELs for which the vast majority of the cells are alive 24 hours after set up. Using this method, I observed that the IELs on the organoids were

indeed alive for four days in culture, while both splenic naïve and memory CD8α^+ T cells died over time (Fig 4.9 B).

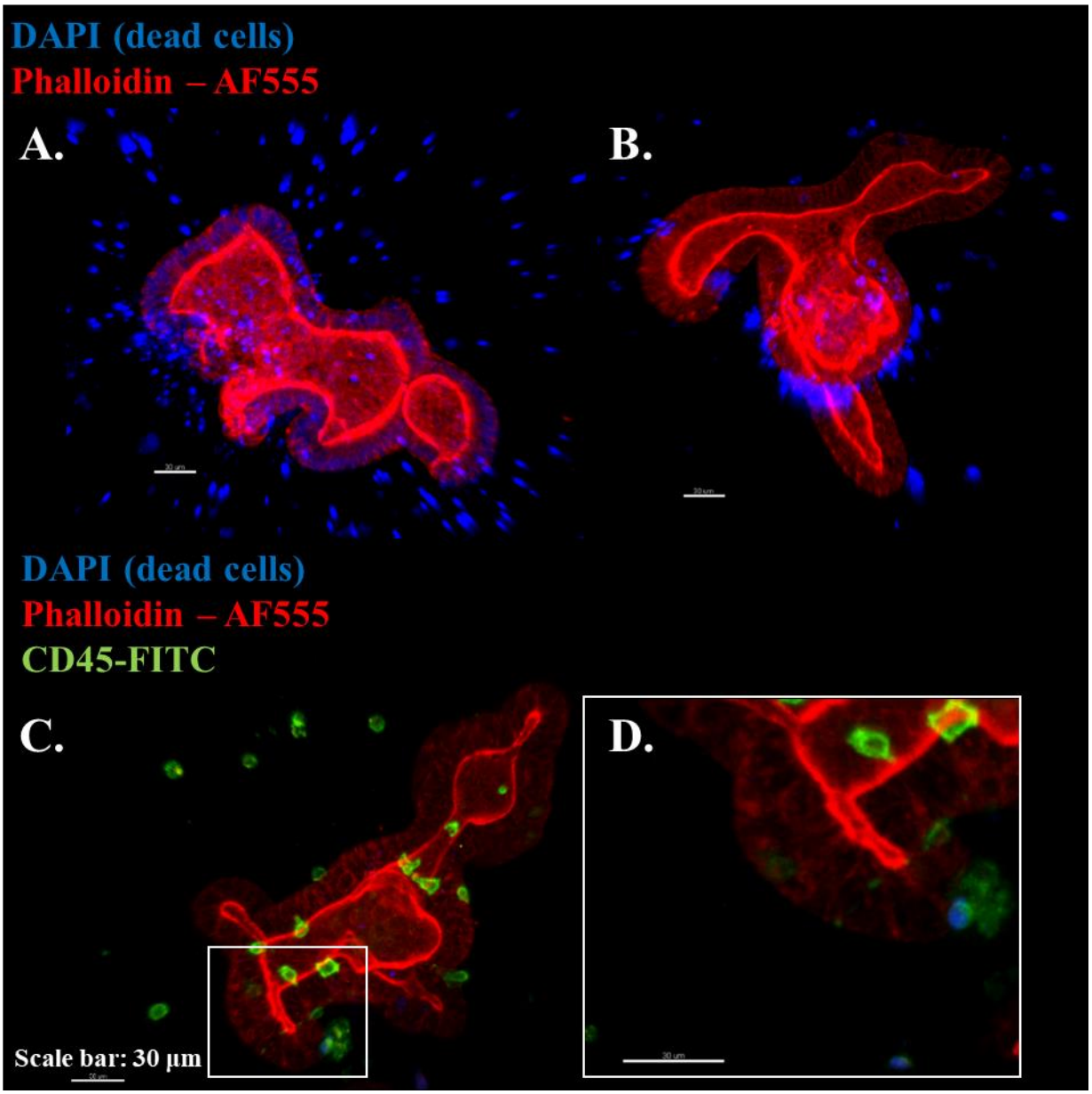

Figure 4.6. Altered DAPI staining protocol discriminates live organoids and lymphocytes from dead cells. DAPI was added to organoid cultures and lymphocyte-organoid co-cultures prior to fixation. A) As a positive control for this test, a splenic lymphocyte suspension that been stored at 4 °C for nine days was added to the organoids for co-culturing for 72 hours prior to DAPI staining followed by fixation. B) A representative image of an organoid cultured without lymphocytes and stained by this method. C) A representative image of an organoid co-cultured with IELs co-culturing for 24 hours prior to DAPI staining and fixation with this staining method. D) A higher magnification image of the same image as panel C. The scale bars on all images represents 30 µm.

In addition, as the co-culture system was up and running, it became interesting to address the role of IELs on the organoids in terms of proliferation. In the literature, quantification of proliferative IECs and IEC subset has been performed by manual counting on selected number of tissue sections. This is a very time-consuming method. Therefore, I wanted to test if I could speed up the process by using image data analysis software. Having this method would also enable me to obtain an estimation of the number of IELs per IEC in the IEL-organoid co-cultures.

To perform the experiment, I cultured WT organoids and harvested them every 24 hours after passage. Two hours prior to each harvest, I added EdU to be able to stain for EdU incorporation as a parameter of IEC proliferation. The organoids were stained for Ki-67, DAPI and EpCAM. Twenty-five organoids per well were acquired and analyzed using Imaris. Using Imaris, I could set parameters to enable the software to detect the different IECs: $DAPI^+$, $DAPI^+$ $Ki\text{-}67^+$ and $DAPI^+$ EdU^+ IECs. The EpCAM staining was useful in this regard to distinguish IECs on the organoids from shed IECs. Imaris is intuitive as it informs the user about cells that have been quantified by adding spots on top of the detected cells. Figure 4.7 B illustrates detection of $DAPI^+$, $DAPI^+$ $Ki\text{-}67^+$ and $DAPI^+$ EdU^+ IECs. After observing a large number of images, I concluded that the parameters are reliably detecting the requested IEC subsets and I started to use these parameters for further analyzing (Fig 4.7 C-D). These data demonstrate that organoids are most proliferative during the first days in culture and the organoid proliferation tends to increase after culture medium change. Similar analyzing strategy was successfully applied to organoids stained for different IEC subsets such as Paneth cells and goblet cells, by Lyzosome and Muc-2 staining, respectively.

I have also tried to design parameters for quantification of IELs (Supplemental Figure to 4.7-2). In this way, I can detect the total number of IELs associated with the organoids. However, some optimization is required to be able to distinguish intraepithelial localized IELs from IELs merely associated to an organoid.

The quantification of number of IEC per organoid provides an estimate of the number of IELs per IEC: one IEL per 20-200 IECs (data not shown). This data indicate that the size of the organoids does not seem to be the determining factor as the same number of IELs can be found on both small (few IECs) and on large (many IECs) organoids.

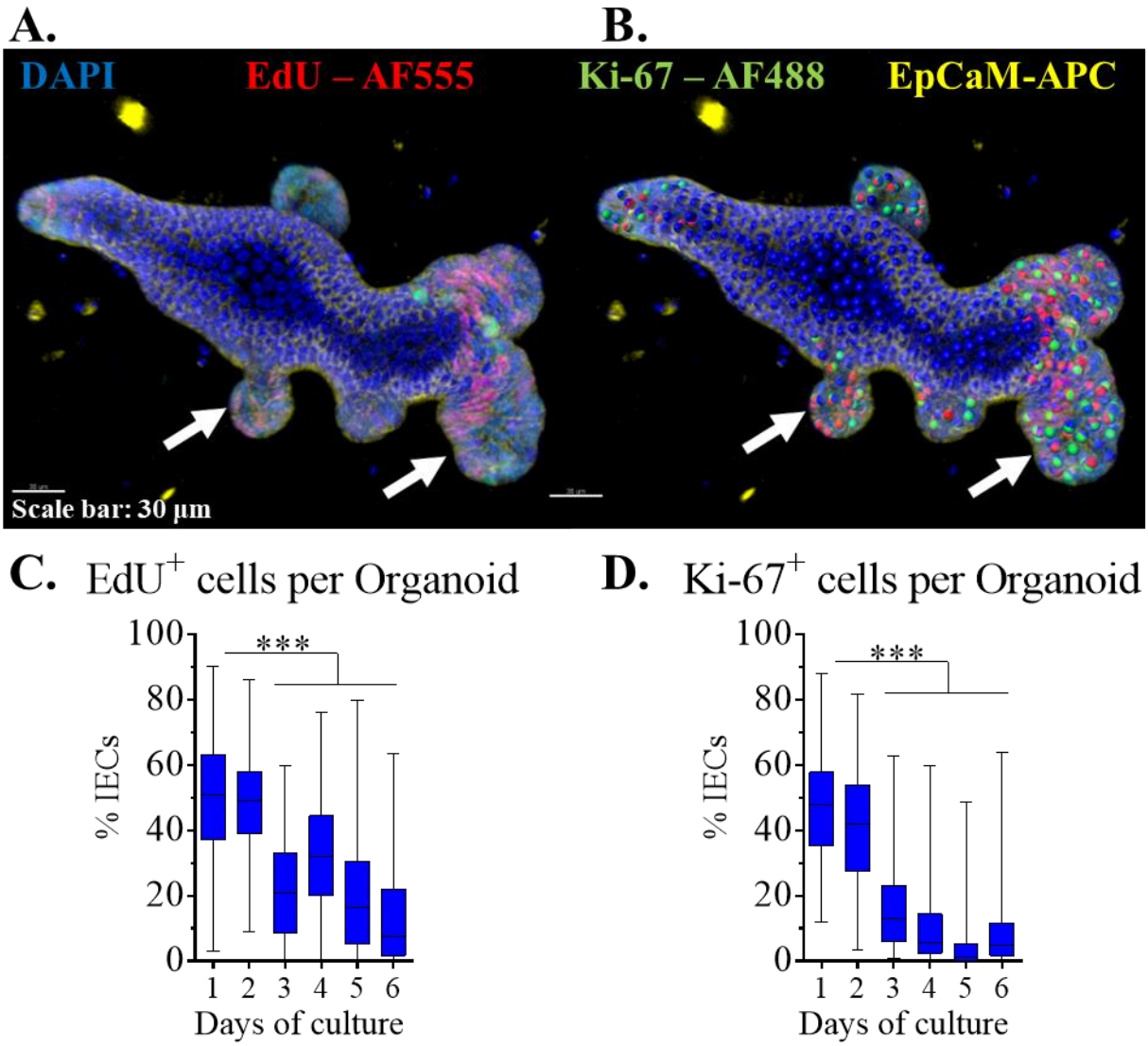

Figure 4.7. Automatic quantification of subsets in organoids enables rapid analysis. Organoids were cultured, fixed and stained for proliferation markers at the indicated time points. A) A representative image of an organoid 3 days after passage. B) The same image as panel A, with addition of colour-coded spots that Imaris detects as the different subsets ($DAPI^+$, EdU^+, $Ki\text{-}67^+$ IECs) present on the organoid. The white arrows points at the crypt domain to exemplify the colour-coded spots. C-D) Quantification of C) EdU^+ and D) $Ki\text{-}67^+$ subsets over the course of six days in culture with medium change at day three from three independent organoid cultures. The data are expressed with boxplots showing whiskers from minimum to maximum values. Statistically significant changes were identified by the Kruskal-Wallis test. ***: $p<0.001$.

4.8. IECs have their own requirement for IL-15 signalling

After discovering that IELs indeed can be found alive on the organoids, I next asked what factors or conditions might promote their survival. The literature has highlighted IL-15 as an important survival factor for IELs. IL-15Rα-/- mice lack IELs, memory CD8 and NK cells (Lodolce et al., 1998). However, the reason(s) for this lack of IELs could be several, such as a developmental requirements for IL-15 by IELs or that IL-15 is indeed required for the maintenance of the mature cells. With the organoid model, I have a cleaner approach to address this question. Hence, I next asked if IELs would stay alive on organoids lacking the IL-15R.

To ensure that the results of this experiment were dependent on the lack of IL-15R, I performed some characterization of IL-15Rα-/- organoids. Organoids set up from IL-15Rα-/- mice grow successfully, enabling the experiment to take place. To confirm that the organoids indeed lack IL-15R, I carried out qPCR analysis of the organoids compared to WT organoids. As expected, IL-15Rα-/- organoids lack IL-15Rα expression (Fig 4.8 E). Expression of IL-15 is unaffected by the lack of IL-15Rα (Fig 4.8 F), suggesting that IL-15 signaling between IECs and other cells may still occur in IL-15Rα-/- mice. Interestingly, the qPCR analysis showed statistically significant differences in several genes such as the antimicrobial proteins (AMPs) RegIIIγ and RegIIIβ (Fig 4.8 H-I), the gene for lysosome Lyz1 (Fig 4.8 L) and the chemokine CCL25 (Fig 4.8 G). Expression of Muc-2 and Cxcl-10 showed no differences (Fig 4.8 J-K). In further characterization, I also discovered that IL-15Rα-/- organoids contain a higher percentage of goblet cells than WT organoids (Fig 4.8 B), but similar percentage of Paneth cells (Fig 4.8 A). In addition, the organoids originating from IL-15Rα-/- intestine grow slower than WT as quantified by EdU incorporation and Ki-67 staining (Fig 4.8 C-D). These data indicate that IECs have their own requirement for IL-15 signaling.

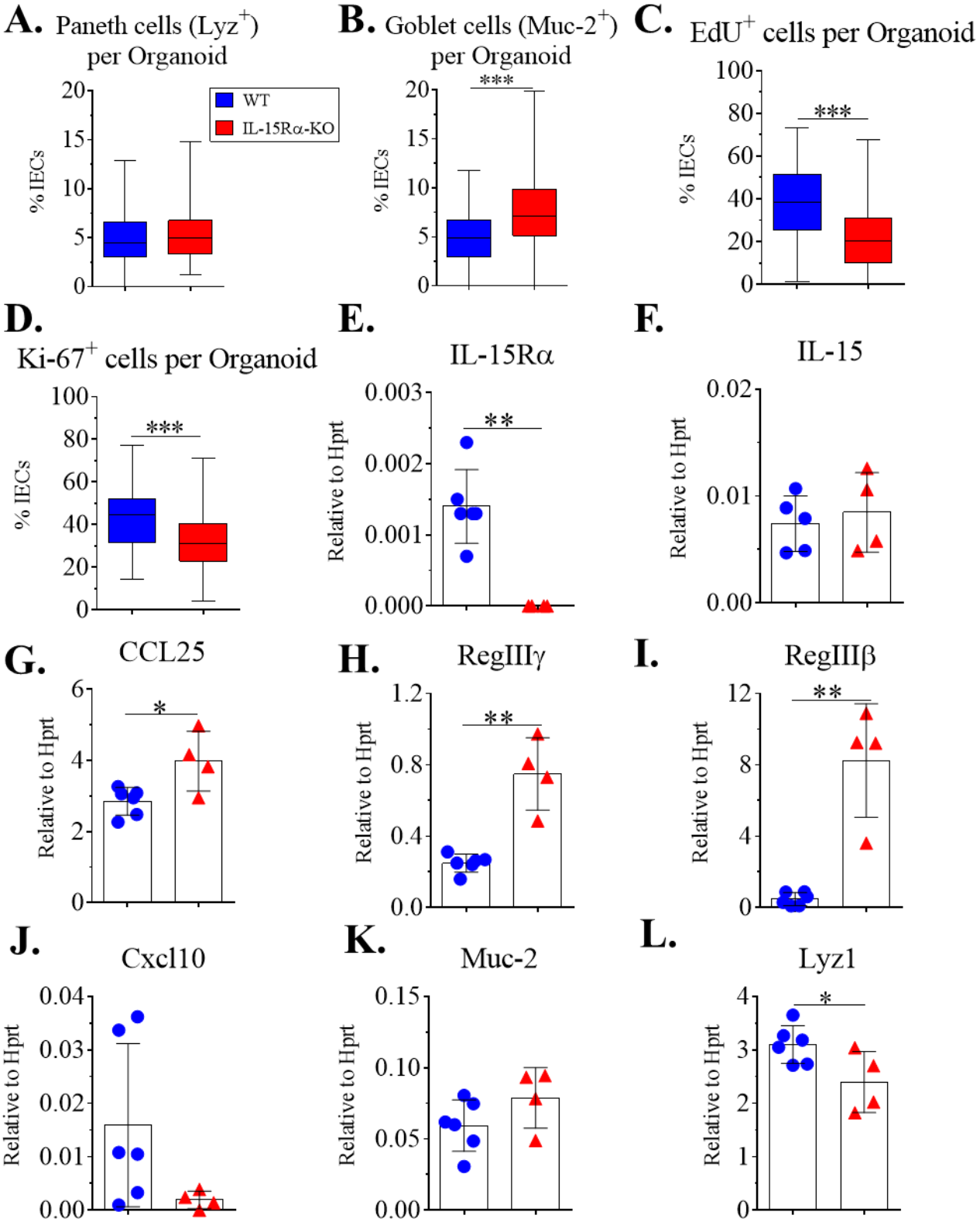

Figure 4.8. IL-15 signalling is important for IEC proliferation, goblet cell differentiation and AMP production. WT and IL-15Rα-/- organoids were harvested 3 days post passage for image and mRNA quantification of indicated parameters. A) Quantification of the percentage of Paneth cells amongst IECs in indicated organoids. The data are expressed with boxplots showing whiskers from minimum to maximum values. B) Quantification of the percentage of goblet cells amongst IECs expressed in same way as panel A. C) Quantification of the percentage of EdU^+ amongst IECs expressed in same way as panel A. D) Quantification of the percentage of Ki-67^+ amongst IECs expressed in same way as panel A. E-L) mRNA expression by WT and IL-15Rα-/- organoids for the following genes: E) IL-15Rα (confirming the IL-15Rα-/- genotype), F) IL-15, G) CCL25, H) RegIIIγ, I) RegIIIβ, J) CXCL10, K) Muc-2 and L) Lyz1. The mRNA expression data are presented as mean ± SD. Data are pooled from two independent experiments. Statistically significant changes were identified by Mann-Whitney U test. *: $p<0.05$., **: $p<0.01$., ***: $p<0.001$.

4.9. Organoid-mediated IEL survival is independent of IL-15 trans-presentation

To assess the role of IL-15 trans-presentation for organoid-mediated IEL survival, I sorted WT IELs, added them to WT and IL-15Rα-/- organoids and fixed them at 12, 24, 36, 72 and 96 hours post set-up. I found that both $TCR\alpha\beta^+$ and $TCR\gamma\delta^+$ IELs survived on both WT and IL-15Rα-/- organoids. The number of IELs associated to WT and IL-15Rα-/- organoids were similar at the assessed time points (Fig 4.9 A). Using the DAPI survival staining, as established in Figure 4.6, I observed that the majority of the IELs associated to both WT and IL-15Rα-/- organoids were alive at the tested time points (Fig 4.9 B). Interestingly, I observed that both naïve and memory splenic $CD8\alpha^+$ T cells co-cultured with organoids had poor survival: the majority of naïve and memory splenic $CD8\alpha^+$ T cells associated to organoids are dead after 72 hours of culture (Fig 4.9 B). In addition, I observed live IELs on WT organoids after organoid passage (data not shown), indicating that IELs may survive for even longer period of time in culture. These data indicate that organoids supply conditions for IELs to survive, but not all T cells.

Finally, I observed a decrease of the percentage of TCR$\gamma\delta^+$ IELs associated on WT organoids over time (Fig 4.9 C), suggesting that TCR$\alpha\beta^+$ IELs are favored for "long-term" maintenance. Collectively, these data suggest that organoids enable IELs specifically to survive on them. Moreover, the data suggests that IL-15 trans-presentation is not strictly required for IEL survival for these 4 days tested *in vitro* and that the role of IL-15 for IEL maintenance may be more complex than previously thought.

As validation of the *in vitro* experiment, I transferred WT IELs into IL-15Rα-/- Rag2-/- mice, Rag2-/- mice (as control) and IL-2Rγ-/- Rag2-/- mice and was able find the IELs back in the IEC compartment in all three groups of mice (Fig 4.9 D). However, the number of IELs in IL-15Rα-/- Rag2-/- was lower compared to control Rag2-/- mice. These data suggest that IL-15 trans-presentation may instead be important for long-term IEL maintenance. In addition, the *in vivo* data highlights the complexity of IL-15 signaling. This also nicely illustrates how the newly established IEL-organoid system can be used for probing IEL biology and combined with validation in the *in vivo* situation.

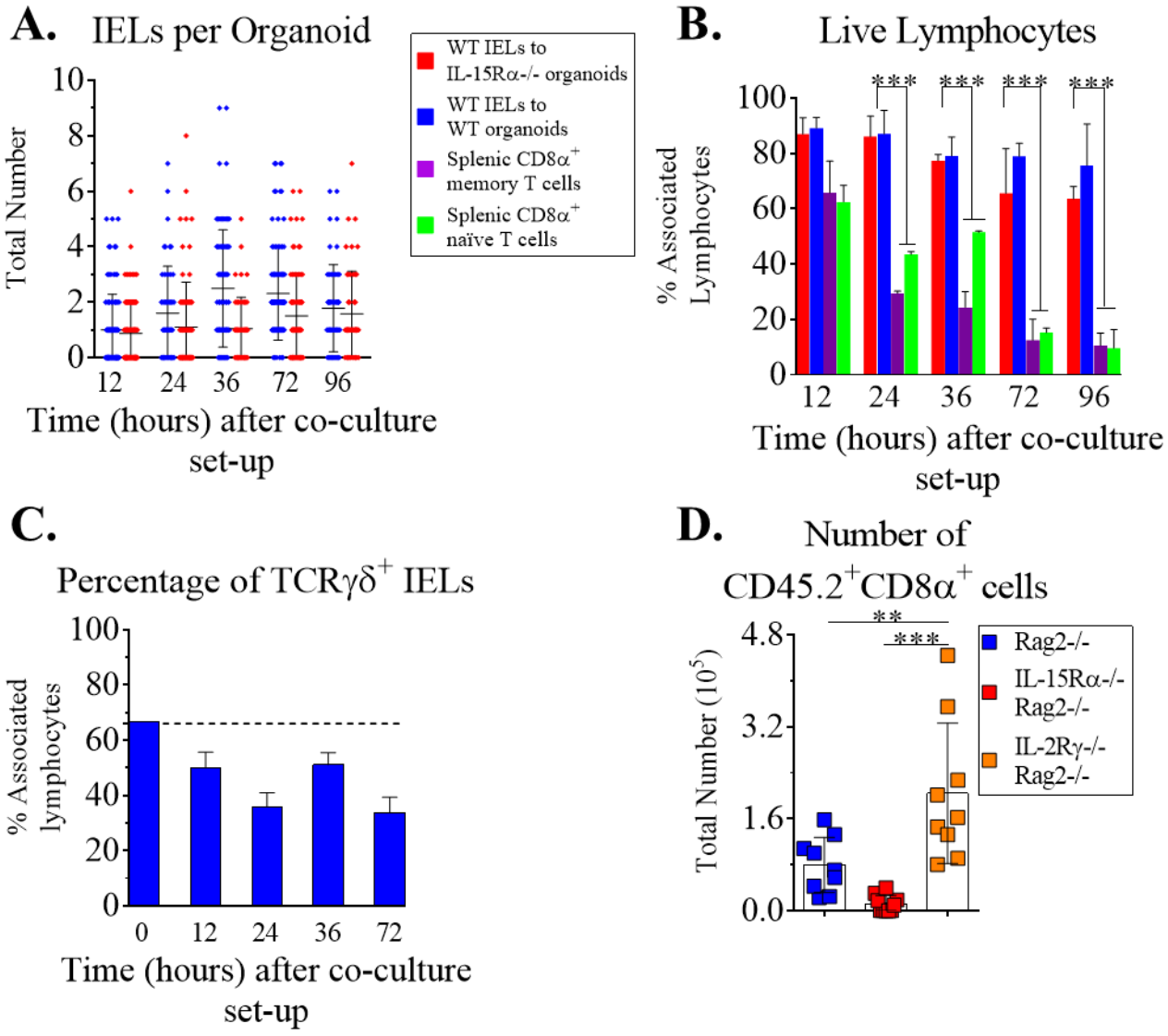

Figure 4.9. Organoids mediate IEL-specific survival independently of IL-15 trans-presentation. WT IELs were sorted and co-cultured with either WT or IL-15Rα-/- organoids for indicated time points. Co-cultures of WT memory and naïve CD8α$^+$ T cells with WT organoids were used as controls. A) Number of IELs per WT or IL-15Rα-/- organoid at the indicated time points. B) The DAPI survival staining, as described in Fig 4.6, was used to determine survival of associated IELs or splenocytes for indicated time points. C) The ratio of WT TCRγδ$^+$ IELs co-culture with WT organoids over time D). The number of CD8α$^+$ IEL quantified three weeks after IEL transfer. Data are presented as mean ± SD from two independent experiments. Statistically significant changes were identified by one-way ANOVA. **: p<0.01., ***: p<0.001.

4.10. Specific murine norovirus strains replicate in organoids and reduce their proliferation – the latter being reversed by adding IELs.

Now that I had established IEL-organoid co-cultures, I wanted to test what would happen if I stressed organoids with enteric microorganisms or pathogens, such as *Escherichia coli* (*E. coli)* and murine norovirus (MNV), and how this response might potentially be altered by addition of IELs.

MNV is a single-stranded RNA virus which is a common cause of gastroenteritis (Newman and Leon, 2015). There are many different MNV strains identified. MNV can be divided into acute and persistent strains, of which both have been used in this Chapter. The persistent strain I used, MNV-O7, was obtained from STAT1-/- mice from the Department of Veterinary Medicine at University of Cambridge (Shortland et al., 2014). As an acute MNV strain, I used MNV-CW3 that is cleared in WT mice but fails to be cleared in Rag1-/- mice (Tomov et al., 2013).

For *in vitro* work with MNV, the infection dose is determined as tissue culture infective dose (TCID) per cell (Shortland et al., 2014). I was kindly provided with stocks of MNV-O7 and MNV-CW3 from the laboratory of Jonathan Heeney. However, organoid cultures cannot be quantified as single cells without disruption of their 3D structure. To overcome this hurdle, I utilized a quantification parameter, as shown in Figure 4.7 B. The quantification of $DAPI^+$ cells, when using DAPI as a counterstain, determines the number of IEC present in each organoid. I have used the DAPI quantification from the experiments presented in Figure 4.7 C -D, which generates an average number of IEC per organoid 3 days after organoid passage. To estimate the number of IECs present in each well, I quantify the number of organoids present

in each well by bright field microscopy. Then, I multiply the number of organoids with the average number of IEC per organoid 3 days after passage.

To test if intestinal organoids can be infected by MNV, I treated organoids with 0.5 and 5 TCID MNV per IEC, added into the culture medium. Samples were harvested for qPCR viral quantification and imaging analysis. As controls for the qPCR analysis, I set up wells with Matrigel and medium spiked with 5 TCID of each MNV strain, but with no organoids. For the viral quantification analysis, the MNV-organoid wells were harvested 1, 12, 18, 24 and 45 hours post set up. Interestingly, I observed a difference in the basal level of virus strains already at one hour post infection (Fig 4.10 A-D). These data may suggest potential differences in the ability of each MNV strain to attach to organoids. Even more interestingly, the viral quantification of the MNV-O7 strain specifically increases over time. No increase over time was observed with MNW-CW3 or the UV-radiated strains (Fig 4.10 A and C). These observations with MNV-O7 and MNV-CW3 were reproducible. In addition, an additional persistent MNV strain, MNV-3 (Hsu et al., 2007), also had increased viral quantification in organoids (Fig 4.10 D). These increases suggest that IECs are potential target cells for MNV-O7 and MNV-3 infection, as both strains can replicate within them.

To validate that MNV-O7 specifically are located inside the organoids, I have tested various antibodies targeting different parts of the MNV virus particles. Being able to stain MNV would also be beneficial to determine the rate of organoid infection with MNV. There is the possibility that not all organoids are infected, which could potentially explain some of the variation in the response to MNV-O7 infection (Fig 4.10 and 4.11). However, none of the tested antibodies has given a strong signal (data not shown). A possible explanation for this is that the target epitopes

are too few to enable detection with my imaging protocol. Therefore, additional imaging optimization concerning signal amplification may be required.

In addition to the viral quantification analysis, I harvested MNV-infected organoids and stained them for the proliferation makers EdU and Ki-67, as previously shown (Fig 4.7 B). Interestingly, I observed a dose-dependent reduction in EdU and Ki-67 staining in MNV-O7-treated organoids (Fig 4.10 E-F). In contrast, I did not detect any changes in EdU or Ki-67 staining with MNV-CW3-treated organoids (Fig 4.10 G-H). These data support the interpretation that MNV-O7 specifically infects intestinal organoids, while MNV-CW3 cannot.

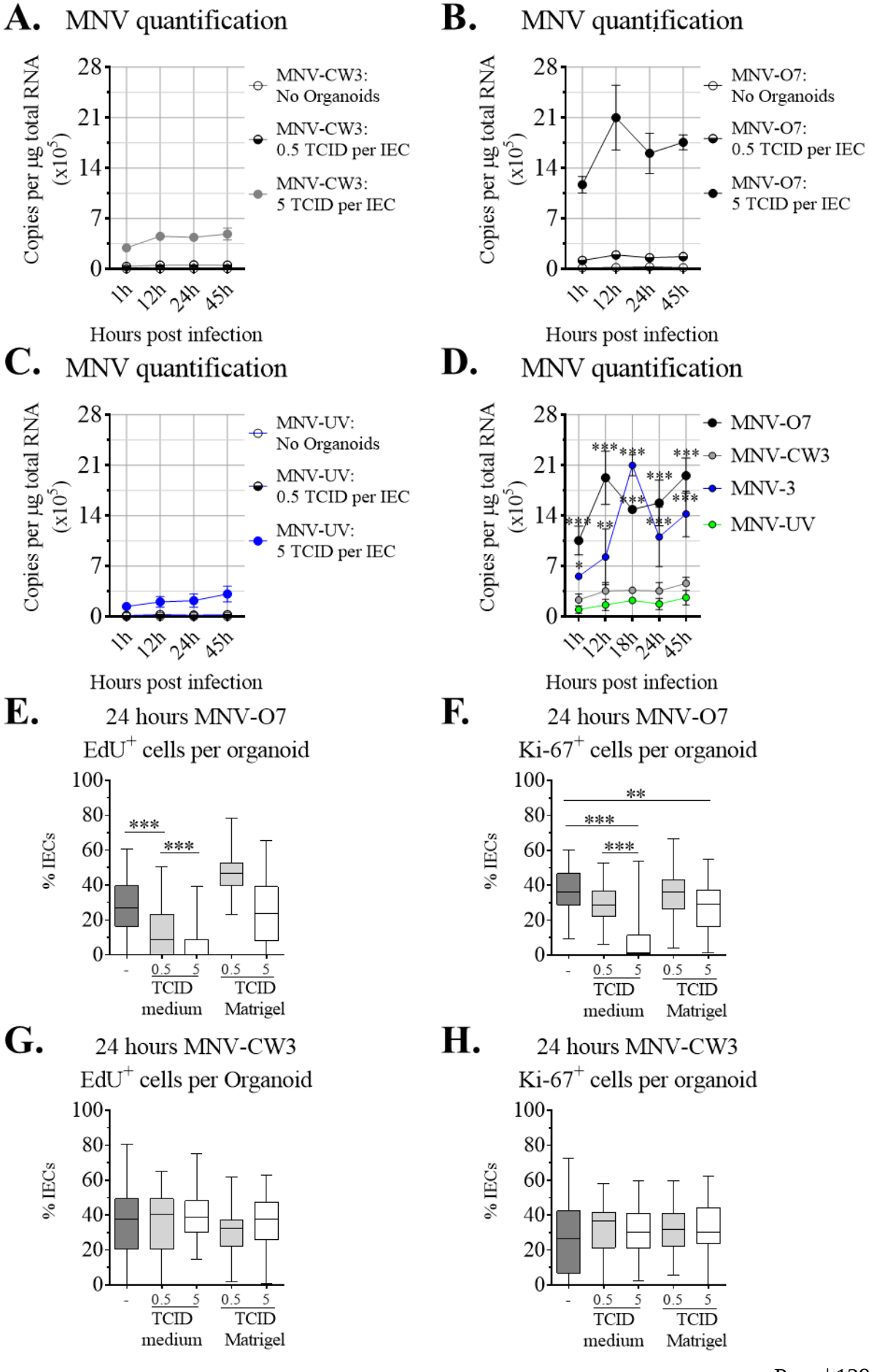

Figure 4.10. Organoid proliferation is reduced in the presence of MNV-O7 infection. To establish an MNV infection model, I added two doses of MNV-O7, MNV-CW3 and UV-radiated MNV in the culture medium of freshly plated organoids, or Matrigel droplets with no organoids as control. The organoids were harvested at indicated time points after treatment. The detected viral quantification of A) MNV-CW3 B) MNV-O7 and C) UV-radiated control. The experiment was performed once with two organoid wells per condition. D) A repeat experiment was performed with 5 TCID dose, including the MNV-3 strain. E-H) 0.5 or 5 TCID per IEC of MNV-O7 and MNV-CW3 were added either in the organoid culture medium or the Matrigel. After 24 hours, the organoids were harvested and stained for the proliferation markers EdU and Ki-67. E- F) MNV-O7-infected organoids stained for E) EdU or F) Ki-67. G-H) MNV-CW3 infected organoids stained for G) EdU or H) Ki-67. Statistically significant changes were identified by one-way ANOVA. **: $p<0.01$., ***: $p<0.001$.

Next, I next wanted to assess if any differences were observed after adding IELs to MNV-O7-infected organoids. For the experiments, IELs were added in the Matrigel together with the organoids. After the Matrigel polymerization, MNV-O7-spiked complete organoid medium was added and the cultures harvested after 24, 48 and 72 hours post set up. Adding IELs to steady state organoids did not lead to increased proliferation at these three time points (Fig 4.11 A-C), suggesting that addition of IEL does not increase proliferation in organoids. However, in conditions with MNV-O7-spiked medium, addition of IELs prevent the decrease in proliferation in the organoids at 24 and 48 hours after infection (Fig 4.11 A-B). At 72 hours post infection, the control organoids have lower proliferation, a trend already observed in Figure 4.7 C and D. This may be due to organoids exhausting the provided growth factors in the culture medium by this time. In these conditions, IELs fail to prevent the decrease in proliferation in organoids (Fig 4.11 C).

One factor that has been suggested to be important for MNV clearance *in vivo* is IFNλ (Nice et al., 2015). Therefore, I asked what would happen if I added IFNλ into the medium of MNV-

organoid co-cultures. For the experiment, 25 ng/ml IFNλ (PeproTech) were added to steady state and MNV-infected organoids for 24 hrs. Surprisingly, addition of IFNλ did not rescue the proliferation, but reduced it even further (Fig 4.11 D). Determining the viral quantifications under the different conditions would give further insights into the mechanisms behind these observations and whether maintenance of proliferation is beneficial for the IECs or the MNV-O7.

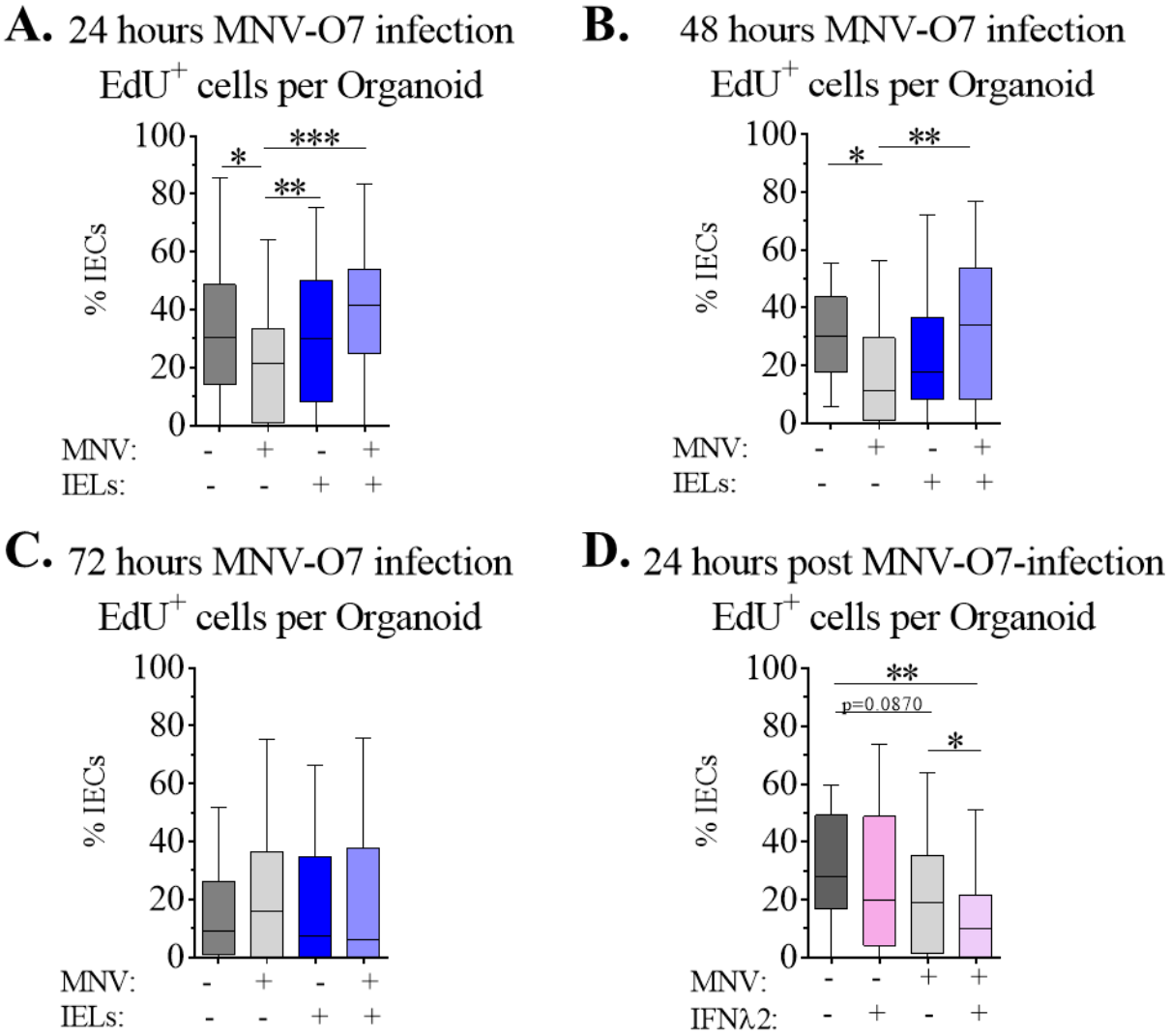

Figure 4.11. Addition of IELs prevents the MNV-O7-mediated decrease in IEC proliferation. A-C) WT organoids were infected with MNV-O7 in the medium, with or without IELs, for 24, 48 and 72 hours. The wells were stained for the proliferation marker EdU with indicated conditions at A) 24 hours, B) 48 hours and C) 72 hours post MNV infection. Data are pooled from two experiments. D) 25 ng/ml IFNλ was added to steady state and MNV-infected organoids for 24 hours and assessed for EdU proliferation. Statistically significant changes were identified by one-way ANOVA.*: $p<0.05$., **: $p<0.01$., ***: $p<0.001$.

4.11. Combining organoids with *E. coli* led to reduction of proliferation

After observing that organoids respond to MNV-O7 infection with decrease in proliferation, I wanted to test if organoids respond in similar manner to the presence of other microorganisms. For the test, I used *E. coli*, a facultative anaerobe bacteria that is present in the intestine (Da Re et al., 2013). The different kinds of *E.coli* range from harmless to pathogenic, for which I have used a harmless strain usually used for feeding of *Caenorhabditis elegans*: *E. coli* OP50 (Kwon et al., 2017). *E. coli* was quantified using optical density (OD)-measurements at 600 nm and added in ratio to the number of IECs present, which was estimated in same way as for determining MNV doses. I added three doses of *E. coli* OP50 to the culture medium or in Matrigel. I observed a dose-dependent decrease in EdU proliferation in the organoids when adding *E. coli* OP50 in the Matrigel, which was not observed when adding *E. coli* in the medium (Fig 4.12 A-B).

These data are opposite of what was observed with the MNV-O7 infected organoids, for which reduction in proliferation was observed when adding MNV-O7 in the medium only. Collectively, these data suggest two strategies for incorporating microorganisms/pathogens into the organoid system: either into the organoid culture medium or in the Matrigel droplets.

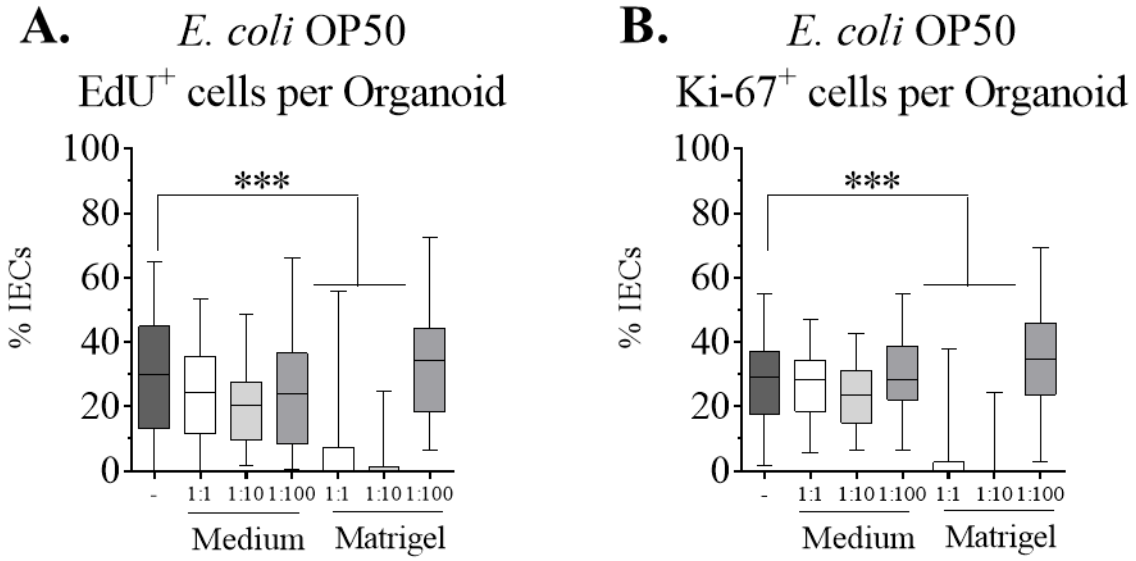

Figure 4.12. Addition of *E .coli* reduces the proliferation in organoids. Three concentrations of *E. coli* OP50 were added either in the organoid culture medium or in Matrigel for 24 hours before being analysed for the proliferation markers A) EdU and B) Ki-67. Statistically significant changes were identified by one-way ANOVA. ***: $p<0.001$.

4.12. Supplemental chapter figures

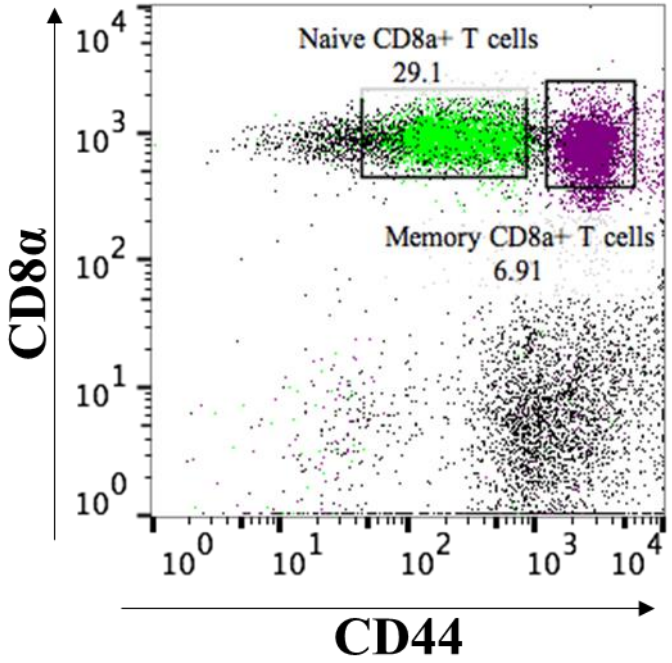

Supplemental Figure to 4.5: Naïve and Memory splenic CD8α$^+$ T cell sorting strategy. A representative flow cytometry plot illustrating the gating strategy used for sorting naïve (CD8α$^+$ CD44^{int}) and memory (CD8α$^+$ CD44^{Hi}) splenic T cells, after pre-gating on DAPI- lymphocytes. Other flow cytometry experiments including TCRαβ and TCRγδ antibodies confirmed that the gating above indeed sorted T cells. The sorted memory and naïve CD8α$^+$ cells were used for co-culture experiments and other experiments involving naïve and memory CD8α$^+$ T cells in this thesis.

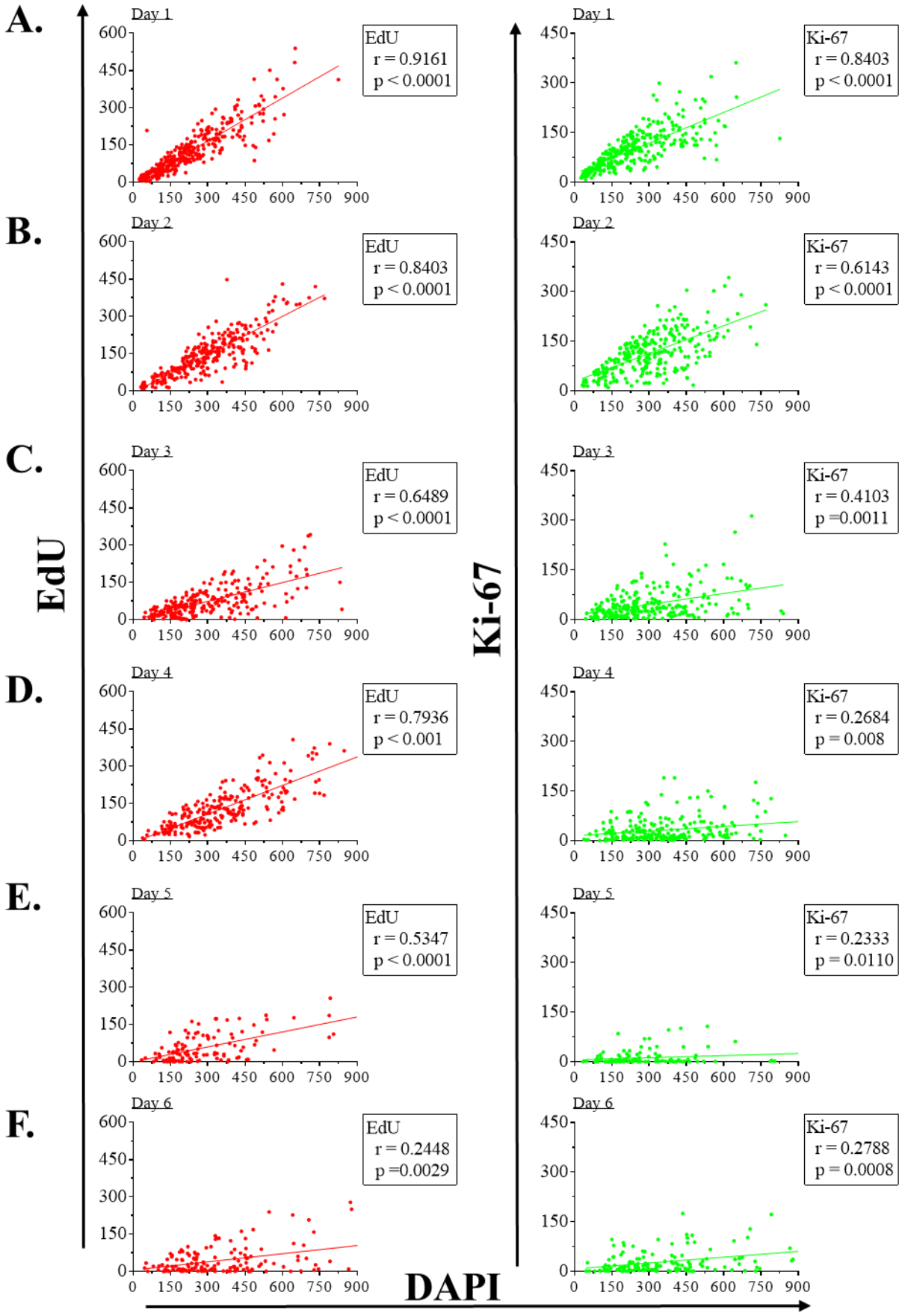

Supplemental Figure to 4.7-1: Organoid proliferation data. Spearman linear correlation analyses were performed on the number of EdU^+, $Ki\text{-}67^+$ and $DAPI^+$ IECs in the organoids at the indicated time points in culture. On the left side are the EdU graphs and on the right side the Ki-67 graphs for A) day one, B) day two, C) day three, D) day four, E) day five and F) day six after organoid passage, for three independent cultures performed in duplicate (one organoid culture) or triplicate (two organoid cultures).

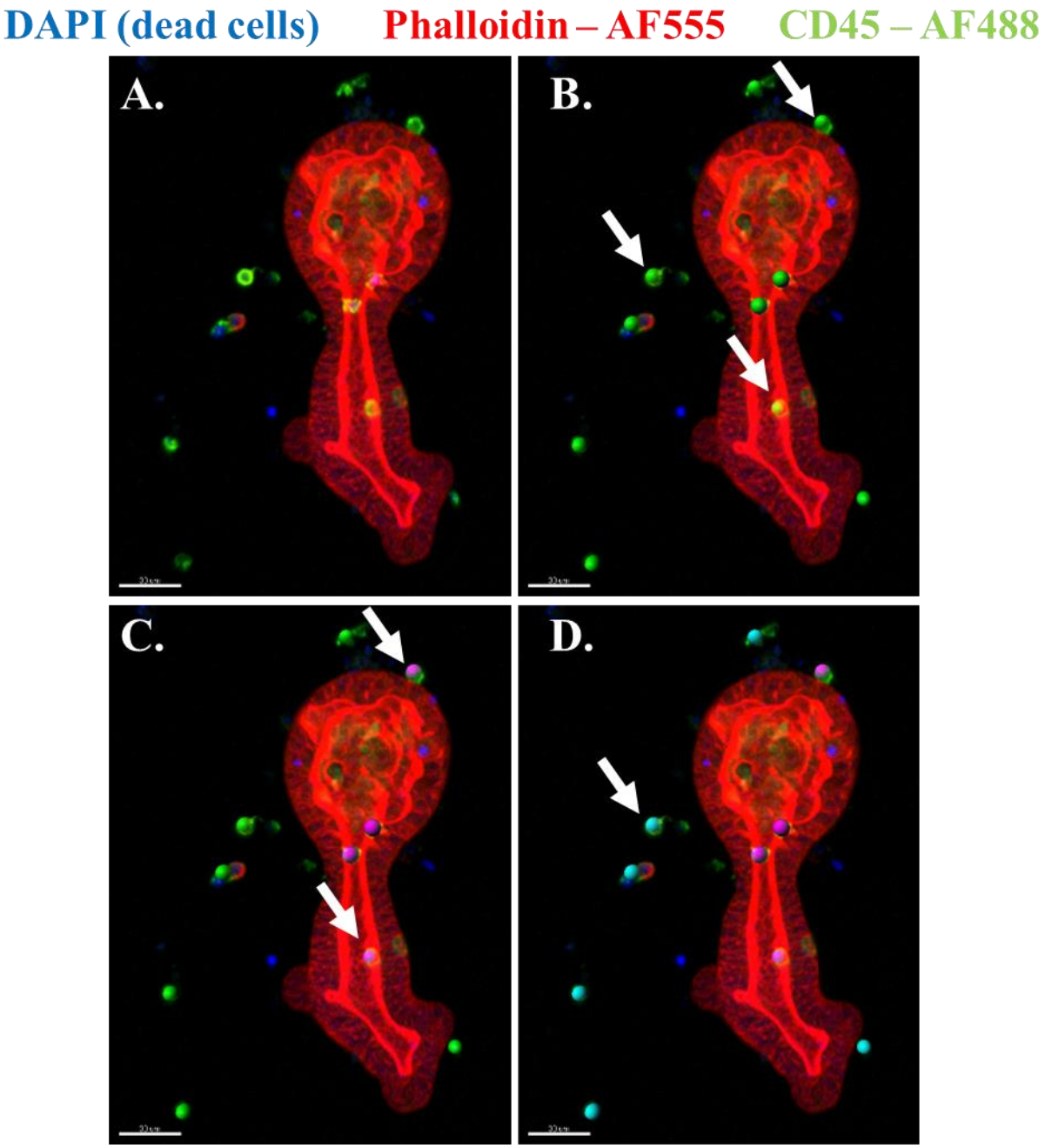

Supplemental Figure to 4.7-2: Image quantification of IEL-organoid cultures. A-D) IEL-organoid co-cultures were set up and stained as described previously. An image without quantification parameters is shown in Panel A). B-D) Same image as panel A, with addition of the quantification parameters: B) identifying all IELs with green spots (white arrows pointing at some examples), C) identifying the IELs associated with the organoid with pink spots (white arrows pointing at some examples) and D) identifying the IELs associated to the organoid with pink spots, while IELs not associated with the organoid are identified with blue spots (white arrows pointing at some examples).

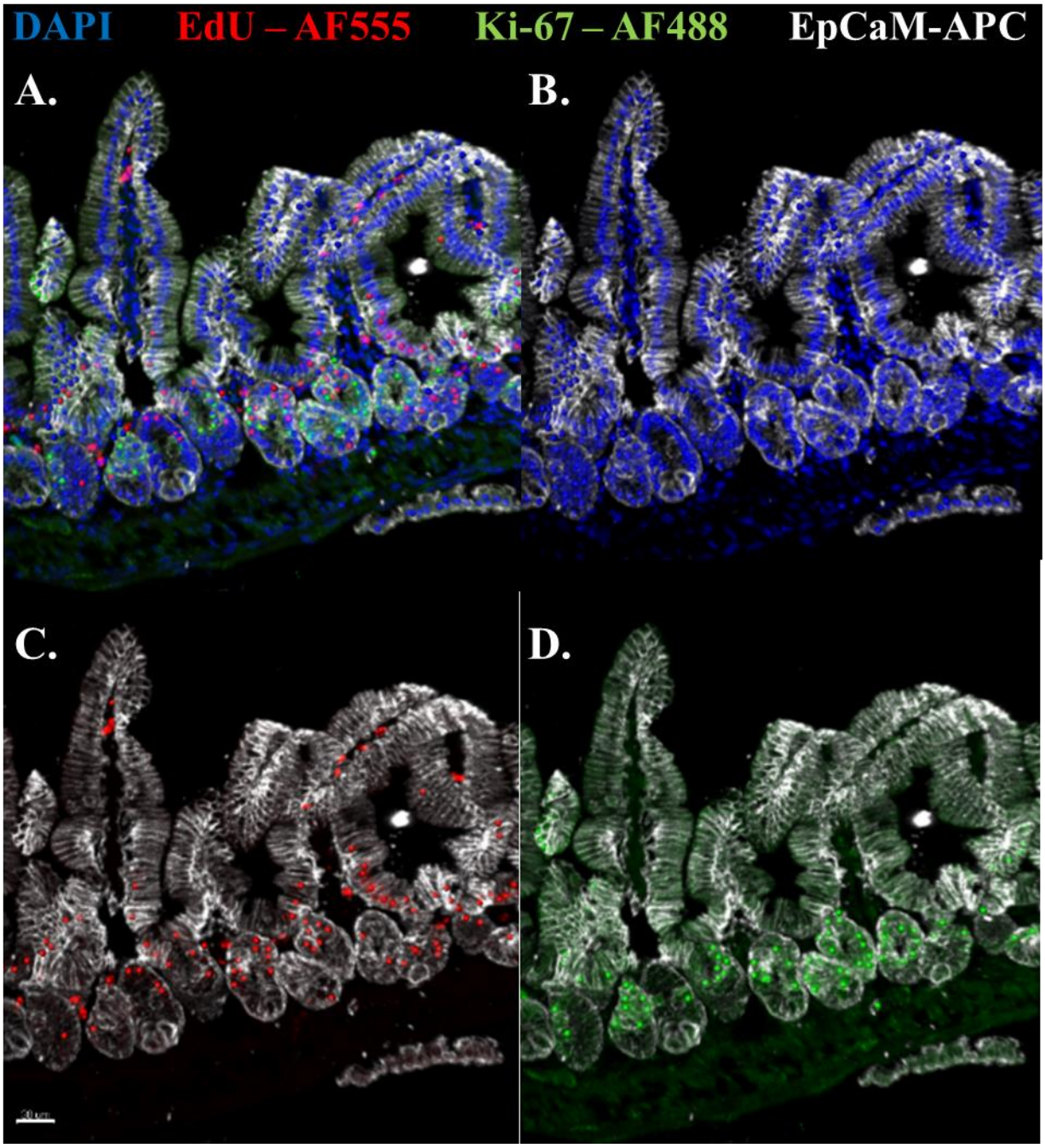

Supplemental Figure to 4.7-3: Image quantification of intestinal tissue-sections. A-D) Small intestinal tissues from WT mice were harvested and stained for DAPI, Ki-67, EdU and EpCAM in order to apply a similar quantification method to them. A) Shows an example image with all stainings and quantification colour-coded quantification spots, while panel B-D) focuses on the B) DAPI, C) EdU, D) Ki-67 staining and their respective quantification spots.

4.12. Chapter Discussion

To summarise the findings described within this chapter, an IEL-organoid co-culture system has been established and validated. The observations that IELs associated with organoids survive for at least 4 days, and are found after passaging the co-culture system, provide an *in vitro* opportunity to dissect further the molecular mechanisms behind IEL biology, such as maintenance and activation of these cells.

The mechanism behind the organoid-mediated IEL survival is still unknown. The mechanisms could involve contact interactions between IELs and IECs, secreted factor(s) from IECs or a combination of both. If the survival mechanisms rely on IEC secreted factors, then it could be possible to culture IELs in the presence of the IEC-secreted factors. Until the mechanisms are known, the organoids need to be taken into account for the molecular mechanisms discovery. This could be done by adding mediators such as drugs and cytokines to organoid and IEL-organoid cultures. Such treatments will provide insights into how IECs react on their own, and hence which responses may originate from IELs themselves and which may depend on IEL-IEC interactions. To dissect further the organoid-mediated IEL survival, one could test whether soluble factors released from the organoids would be sufficient to maintain IELs alive. This could be done by adding complete organoid medium from organoids cultured for 1-3 days. If no, or only a small effect on IEL survival is observed, then it may suggest a more important role of contact interactions between IELs and organoids for IEL survival.

One of the highlights from this chapter is the automatic image quantification as shown in Figure 4.7. This provides fast and rapid quantification at the cellular level without destroying the 3D organization of the organoids. It allows smooth transition from *in vitro* techniques that involve quantification of the number of cells, for example to determine infection doses. This technique

would also be beneficial for IEL quantification. The IEL quantification in this chapter has been performed manually. I have tried to establish parameters for automated quantification of IELs as shown in Supplemental Figure to 4.7-2, by taking advantage of the fact that they are smaller than IECs and by using the TCRδ-eGFP reporter mice to distinguish TCRαβ$^+$ from TCRγδ$^+$ IELs. My testing of this approach so far seems promising. However, at present the detection is not without flaws. Occasionally false positive or false negative cells were scored for both my IEL and IEC parameters, particularly when trying to distinguish intraepithelial localized IELs from associated IELs. Depending on which day post passage the organoids are harvested, the number of detected IEC (by DAPI quantification) varies from about 50-600 IECs. Hence, one falsely quantified IEC will have maximum impact of 2 % on the small organoids. IELs on the other hand, are much sparser on the organoids, ranging from one to 15 IELs per organoid. In that scenario, a falsely quantified IEL can have a much bigger impact on the data and its interpretation. To avoid that, the individual images still require manual inspections.

In addition, I have established similar quantification parameters for intestinal tissue sections (Supplemental Figure to 4.7-3). Having this would enable organoids to be the transition model between *in vitro* and *in vivo* studies, such as confirming organoid findings *in vivo.* An example of findings reported in this chapter that need *in vivo* confirmation is the difference in the properties of IECs between WT and IL-15Rα-/- organoids. As IL-15Rα-/- organoids have lower proliferative capacity and increased RegIIIγ and RegIIIβ mRNA production, it is tempting to draw parallels with the positive impact of IL-22 on IECs with respect to proliferation, and RegIIIγ and RegIIIβ production. To investigate this further, I need to have similar methods as used for the organoids to quantify these parameters from the mice. As tissue sectioning includes intestinal supporting cells, which are not present in the organoids, I needed to make use of EpCAM staining to distinguish IECs from other cells. As shown in

(Supplemental Figure to 4.7-3) the quantification seems to identify the right cells. This technical advance will work for further organoid studies and may apply for other organoid tissues as well.

The observation that IELs survive on a similar high level on IL-15Rα-/- organoids as WT organoids, suggests that IL-15 trans-presentation is not strictly required for IEL survival for the first 4 days in culture (Fig 4.9 B). My IEL transfer experiment illustrates that IELs can be found in the small intestinal compartment in IL-15Rα-/-Rag2-/- mice, suggesting that IL-15 trans-presentation is not strictly required *in vivo* either (Fig 4.9 D). There are fewer IELs recovered from these mice compared to Rag2-/- recipients, suggesting that IL-15 trans-presentation may be involved, instead, for the long-term maintenance of IELs. A previously proposed mechanism for IL-15-mediated survival has been via modulation of the anti-apoptotic factor Bcl-2. Induced expression of Bcl-2 in IL-15-/- mice increases the numbers of IELs, but not to the same level as found in WT mice. Similarly induced Bcl-2 expression in WT mice did not alter the number of IELs (Nakazato et al., 2007). This example demonstrates the complexity of the *in vivo* intestinal situation for which the organoid-based approaches can assist in addressing the mechanisms.

One of the outstanding questions from this chapter is which are the missing factor(s) required to increase the number of IELs per IEC to the level that is observed *in vivo.* Middendorp et al. have performed RNA sequencing on mouse crypt and villus structures isolated *ex vivo* and compared the gene expression profiles with organoids. This data-set suggests that organoids resemble the crypt structures better than the villus structures (Middendorp et al., 2014). Tissue sections of small intestine stained for CD3 as a marker of IELs show that IELs can be found in both crypts and villi domains (Kuo et al., 2001). Hence, there is a risk that IELs present in the

villi *in vivo* are not homing to the small intestinal organoids due to the organoids' closer resemblance to crypt structures. An important aspect is whether this reported gene expression profile translates into protein expression. This information could pinpoint differences between the IECs *in vivo* and *ex vivo* and thereby suggest potential targets for improving IEL numbers. The IELs used are isolated from the small intestine and transfer experiments show that IELs are subsequently found in the small intestine (Fig 4.9 D). Assessment of the spleens showed very few IELs (data not shown), suggesting that i.v. injected IELs home specifically to the small intestine. This suggests that the processing and sorting strategy employed for the IELs does not impair their homing capacity. A potential option why the homing seems to work *in vivo* could be the presence of intestinal supportive cells, which are missing in our co-culture system and which may provide factors important for IEL homing and maintenance.

Microbiota is not present in my system, but data from antibiotic-treated and germ-free mice suggest that these mice do not have a drastic decrease in the number of IELs compared to control mice. This suggests that the microbiota may not be the critical factor for this aspect. Undoubtedly, microbiota does have an impact the IEC barrier and the intestinal immune system, meaning that incorporation of microbiota into the system would be a beneficial for future research. There will be hurdles to incorporating microbiota into the organoid system, as there is clearly a risk of overgrowth and contamination. One could try to add heat-killed bacteria to the organoid system, bearing in mind that some microbial products will be altered by this processing. Another possibility would be to try to gene modify bacteria to reduce their proliferative capacity and add this to the organoids in low concentration.

Another important factor is the extracellular matrix: IELs may be affected by the extracellular matrix present in the Matrigel and may miss homing signals from the organoids. One could try

a similar co-culture method to that used here, but test other options instead of Matrigel, such as collagen gel and PEG gels, to see if that would affect the number of IELs per organoid. An alternative approach would be to perform a titration of the percentage of Matrigel present in the droplets. All reported experiments have been performed with 50 % Matrigel with the remaining 50 % containing basal organoid medium. If Matrigel affects the IEL homing, then I may be able to see an effect by altering the percentage of Matrigel. If increasing percentage of Matrigel decrease the IEL-incorporation rate then Matrigel may be a hindrance for IELs. If increasing percentage of Matrigel increase IEL-incorporation rate, then maybe IELs can use Matrigel for migration to the organoids.

All of these approaches will pin down which factor(s) are missing from the *in vivo* system. An increase in the numbers of IELs recoverable per organoid would also allow other methods to be used such as sequencing and flow cytometry.

There remains much need for method optimization for organoid co- and tri- culture systems, but it is apparent that these types of cultures could lead to an explosion of new and interesting mechanistic discoveries concerning intestinal immune tolerance and responses to infections.

Chapter 5: IELs have a different activation and metabolic status compared to other CD8α$^+$ T cells

In the previous chapter, my focus was on the requirements for IEL survival and to address whether organoids could provide the required conditions for long-term *in vitro* IEL survival. I demonstrated differences in the interactions between organoids co-cultured with IELs, naïve or memory CD8α$^+$ splenic T cells in terms of location of the cells on the organoids (Fig 4.5 E-F) as well as their survival (Fig 4.9 B). In this and the coming two chapters, I will investigate further the differences in terms of activation requirements between IELs and other T cells, such as splenic CD8α$^+$ T cells and T cells found in other epithelial barrier sites such as skin and lung.

5.1. BALT: bronchus-associated lymphoid tissues

There is a clear need for an organized immune system in the lungs, to be able to cope with exposure to potential pathogens and other danger accompanying oxygen inhalation. Similar to the intestinal immune system, the first line of defence in the lungs consists of a single-cell epithelial barrier. Like IECs, lung epithelial cells express pattern recognition receptors (PRRs) and can respond to stimuli by secreting damage-associated molecular patterns (DAMPs), cytokines and antimicrobial peptides (AMPs). There are two types of lung epithelia cells: type I and type II. The vast majority of lung epithelial cells are of type I. These cells are very thin and are responsible for the gas exchange (Leiva-Juárez et al., 2017). There are various immune cells in-between and beneath the lung epithelial cells such as DCs, MPs, ILCs, TCRαβ$^+$ and TCRγδ$^+$ T cells (Lloyd and Marsland, 2017). There are reported to be approximately similar number of CD4$^+$ and CD8$^+$ T cells in the lung (Zens et al., 2017). In a manner analogous to intestinal DCs, lung DCs scan the lung lumen for antigens and then

migrate to the mediastinal lymph nodes (MedLN) to induce T cell responses (Deckers et al., 2017). Beneath a specific set of lung epithelial cells, which have similarities to intestinal M cells, there are aggregates of T and B cells. These aggregates are called BALT. BALT-like structures can also be induced by inflammation and infection when they are also referred as inducible BALT (iBALT) (Foo and Phipps, 2010).

In the past, the lung compartment has been thought to be sterile. However, there is a population of microbiota in the lower part of the lung (Lloyd and Marsland, 2017). The lung microbiota affects the lung immune composition, as germ-free (GF) mice have altered composition compared to conventional mice (Belkaid and Naik, 2013).

5.2. SALT: skin-associated lymphoid tissues

In the 1980s, it was proposed that there is a specialised immunological organisation of immune cells and structures in the skin, based on the fact that there are skin-specific APCs and T cells, as well skin epithelial cells, keratinocytes, providing a distinct immunological environment (Streilein, 1983). As with iBALTs, it appear to be possible to induce SALT structures (Ono and Kabashima, 2015).

The skin is separated into two compartments, named epidermis and dermis, which have similarities to the intestinal IEC and LP compartments. In the epidermis, there are immune cells such as DCs called Langerhans cells (LCs) and dendritic epidermal T cells (DETCs), while in the dermis there are dermal DCs, MPs, ILCs and TCRαβ$^+$ and TCRγδ$^+$ T cells (Tay et al., 2014). As mentioned in the Introduction section 1.6.3, DETCs express Vγ5 (Allison and Havran, 1991). Live imaging footages illustrate how DETCs interact with skin epithelial cells (Zaid et al., 2014), in a similar manner as IELs interact with IECs (Edelblum et al.,

2012). As with IELs, there is a reduction in the number of DETCs in AhR-/- mice (Kadow et al., 2011), as well as unknown ligands for the TCR of DETCs (Tay et al., 2014). In the skin and thymus epithelial cells, there is an immunoglobulin-like protein called Skint1. Without expression of Skint1, the number of DETCs are reduced (Boyden et al., 2008). Equivalent proteins to Skint1 have been discovered in the intestinal compartment, namely butyrophilin-like (Btnl)1, Btnl4 and Btnl6 (Bas et al., 2011). Btnl1-/- mice have very few TCRγδ$^+$ IELs, while Btnl4-/- mice have similar number of IELs as control mice (Di Marco Barros et al., 2016).

5.3. GALT: gut-associated lymphoid tissues

As described in the Introduction section 1.6.1, there is a single-cell layer of IEC that acts as a first line of defence. The IEC barrier and the LP compartment are classified as intestinal effector sites. There are various immune cells in these compartments such as DCs, MPs, ILCs and T cells. IELs, consisting of mainly CD8α$^+$ TCRγδ$^+$ cells, reside between cells of the intestinal epithelial barrier, while LPLs, consisting of mainly CD4$^+$ TCRαβ$^+$ cells, are found in the LP compartment. In addition to the effector site, there are intestinal inductive sites, namely mesenteric lymph nodes (MLNs), cryptopatches (CPs), isolated lymphoid follicles (ILFs) and Peyer's patches (PPs).

MLNs are lymph nodes associated with the mesenteric fat in the intestines. They are connected to the intestine via lymphatic vessels. In MLNs, T cell can become activated by DCs that have migrated from the intestinal sites with antigens. Which MLN intestinal DCs are migrating to seems not to be random: a recent study suggest that DCs scan for antigens in specific intestinal segments, as well as migrating to specific MLNs (Houston et al., 2015).

Beneath follicle-associated epithelium (FAE), there are PPs. FAE consists of M cells, which enable transfer of lumenal antigens through the IEC barrier (Mabbott et al., 2013). PPs are an important source of IgA production. Lymphoid-tissue inducer (LTi) cells can induce PP formation and typically there are between six to 12 PPs per small intestine of a mouse (Reboldi and Cyster, 2016; MacDonald, 2003; Prinz et al., 2003).

In addition to MLNs and PPs, there are CPs and ILFs. These are aggregates important for activation and differentiation and mainly consist of T, B and LTi cells. CPs are random clusters found in the LP compartment (MacDonald, 2003). They are present in Rag2-/-mice, in the absence of microbiota, but not in the absence of the RORγt nuclear receptor. This dependence may be linked to LTi cells that are also dependent on RORγt expression. A lack of CPs does not affect the IEL population (Pabst et al., 2005). CPs can then form ILFs (Pabst et al., 2005). Unlike CPs, ILFs are dependent on the microbiota (Pearson et al., 2012). There are about 100-200 ILFs per mouse small intestine (Buettner and Lochner, 2016).

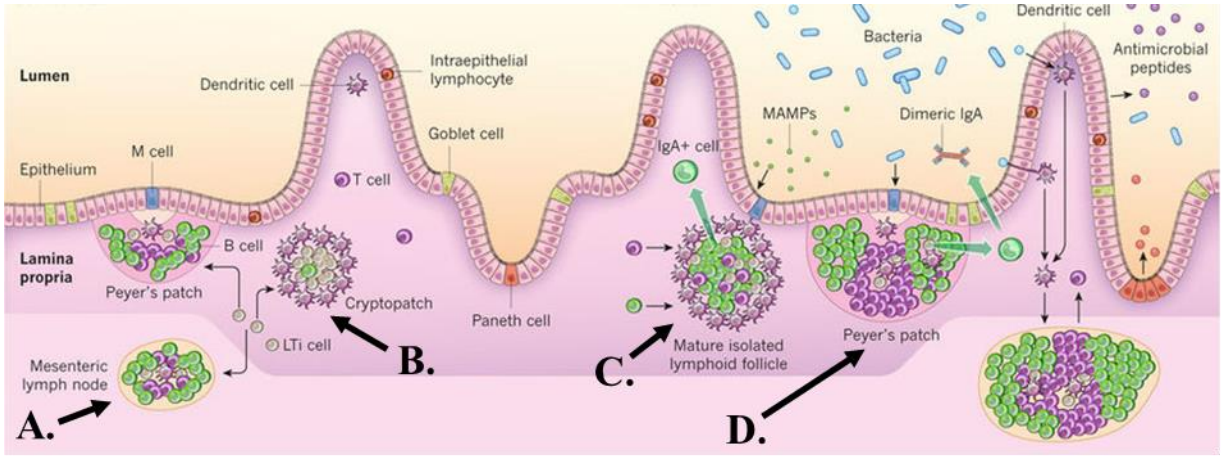

Figure 5.1 Schematic illustration of the gut-associated lymphoid tissue (GALT). Like other mucosal-associated lymphoid tissues (MALTs) such as BALT and SALT, GALT is lined by a barrier of epithelial cells. Underneath the epithelia barrier, there are a variety of lymphoid structures indicated by the black arrows: A) mesenteric lymph node (MLN), B) cryptopatches (CPs), C) isolated lymphoid follicle (ILF) and D) Peyer's patches (PPs). Modified from Maynard C. et al, Nature (2012).

5.4. Overview of mitochondrial structure and function

The mitochondrion was discovered in the 1890s (Ernster and Schatz, 1981). This organelle is the primary source of adenosine triphosphate (ATP) and of the production of reactive oxygen species (ROS), as well as important in the maintenance of ion homeostasis, such as Ca^{2+}, in the cell (Rourke et al., 2005). The number of mitochondria per cell varies between cell types, with mammalian erythrocytes having no mitochondria, while hepatocytes have thousands of mitochondria per cell (Cereghetti and Scorrano, 2006). The mitochondrion possesses of two membranes, an inner and an outer mitochondrial membrane, iMM and oMM. iMM have multiple of invaginations and the invaginated spaces have been named cristae. The space between iMM and oMM is called the inter-membrane space, while the space that iMM bounds is called the matrix (Fig 5.2 A). Unlike other organelles, mitochondria have their own DNA, (mtDNA), which encodes genes for the components of electron transport chain (ETC) complexes. Unlike nuclear DNA, mtDNA is not associated with histones. As a result, mtDNA is more fragile, and is susceptible to ROS damage (Batandier et al., 2002). Mitochondria are dependent on nuclear DNA to encode for proteins for remaining organelle functions (Goios et al., 2007).

Mitochondria are dynamic organelles that can undergo fragmentation (fission) or biogenesis, formation of networks, (fusion). Proteins that have been suggested to be involved in mitochondrial fusion are optic atrophy 1 (Opa1), mitofusin 1 and 2 (Mfn1 and Mfn2, respectively), while dynamin-related protein 1 (Drp1) has been linked to mitochondrial fission (Fig 5.2 A). These dynamics of mitochondrial fission and fusion are important for mitochondrial function (Westermann, 2010). In addition, the shape of the mitochondria has recently received attention for being important for immune functions. Using photo-activatable mitochondria (PhAM)-mice (Pham et al., 2012), it has been shown that Teff and

Tmem cells have distinct mitochondrial shapes. Teff cells have punctate mitochondria, while Tmem cells have tubular network-like mitochondria (Buck et al., 2016). These observations have been confirmed using MitoTracker Green (MTG) staining (van der Windt et al., 2012). Additional study has reported on remodeling of the cristae: from loose connected to tightly connected and associated these observations with immune functions (Klein Geltink et al., 2017). Teff and Tmem cells have distinct metabolic profiles, as will be described in section 5.4.3, linking mitochondrial structure to immunological function.

In the iMM, there are five enzyme complexes denoted complex I, II, III, IV and V (Kühlbrandt, 2015). These complexes are involved in the ETC for generation of adenosine tri-phosphate (ATP). In addition, a specific family of lipids called cardiolipins (CLs), are found in mammalian iMM and Gram-positive and Gram-negative bacteria membranes (Paradies et al., 2014; El Khoury et al., 2017).

5.4.1 Cardiolipins (CLs) – almost exclusively found in mitochondria

A CL consists of four acyl chains, most of which are highly unsaturated and are attached to a carbon-backbone structure (Yin and Zhu, 2012). The composition and the number of CL species varies with tissue. As an example, mouse heart tissue contain 39 identified CL species (Han et al., 2006). CLs are thought to be able to affect most mitochondrial proteins such as the complex I, III, IV, V and Opa1 and therefore the CL composition may also affect mitochondrial functions such as mitochondrial respiration and membrane potential (Kameoka et al., 2017; Chicco and Sparagna, 2007; Paradies et al., 2014; Acehan et al., 2011; Jiang et al., 2000). CLs have been analysed using biochemical and mass spectrometric techniques. In addition, a dye called 10-N-nonyl-acridine orange (NAO), which is reported to bind to CLs

reasonably specifically, has been used to quantify CLs via flow cytometry (Ferlini and Scambia, 2007; Rodriguez et al., 2008).

5.4.2. Electron transport chain (ETC) for generation of ATP and ROS

The ETC, also known as the respiratory chain, consists of the five mentioned complexes I, II, III, IV and V. These transport electrons for reactions that lead ultimately to ATP production. As by-product from the ETC, about 1-3 % of the oxygen consumption finds its way to become ROS (Batandier et al., 2002). ROS is also generated in a process called reverse electron transfer (RET). This process has been reported to be controlled by complex II and the concentration of succinate (Hosler et al., 2006). Mitochondrial ROS can function as a signaling molecule in redox pathways within the mitochondria, in the cytosol and nucleus (Murphy, 2009).

Factors that have been reported to be positively affected by mitochondrial ROS are nuclear factor of activated T-cells (NFAT) and NF-κB (Weinberg et al., 2015). Complex I (NADH dehydrogenase) is the major source of mitochondrial ROS production (Brandt, 2006). In addition to its role in the ETC, complex II (succinate dehydrogenase) is also taking part in the Krebs's cycle for generation of additional ATP (Cecchini, 2003). Complexes III and IV are responsible for proton uptake by cytochrome reduction and oxidation, respectively (Hosler et al., 2006). Complex V (ATP synthase) is responsible for ATP production by adding a phosphate to adenosine diphosphate (ADP) (Jonckheere et al., 2012).

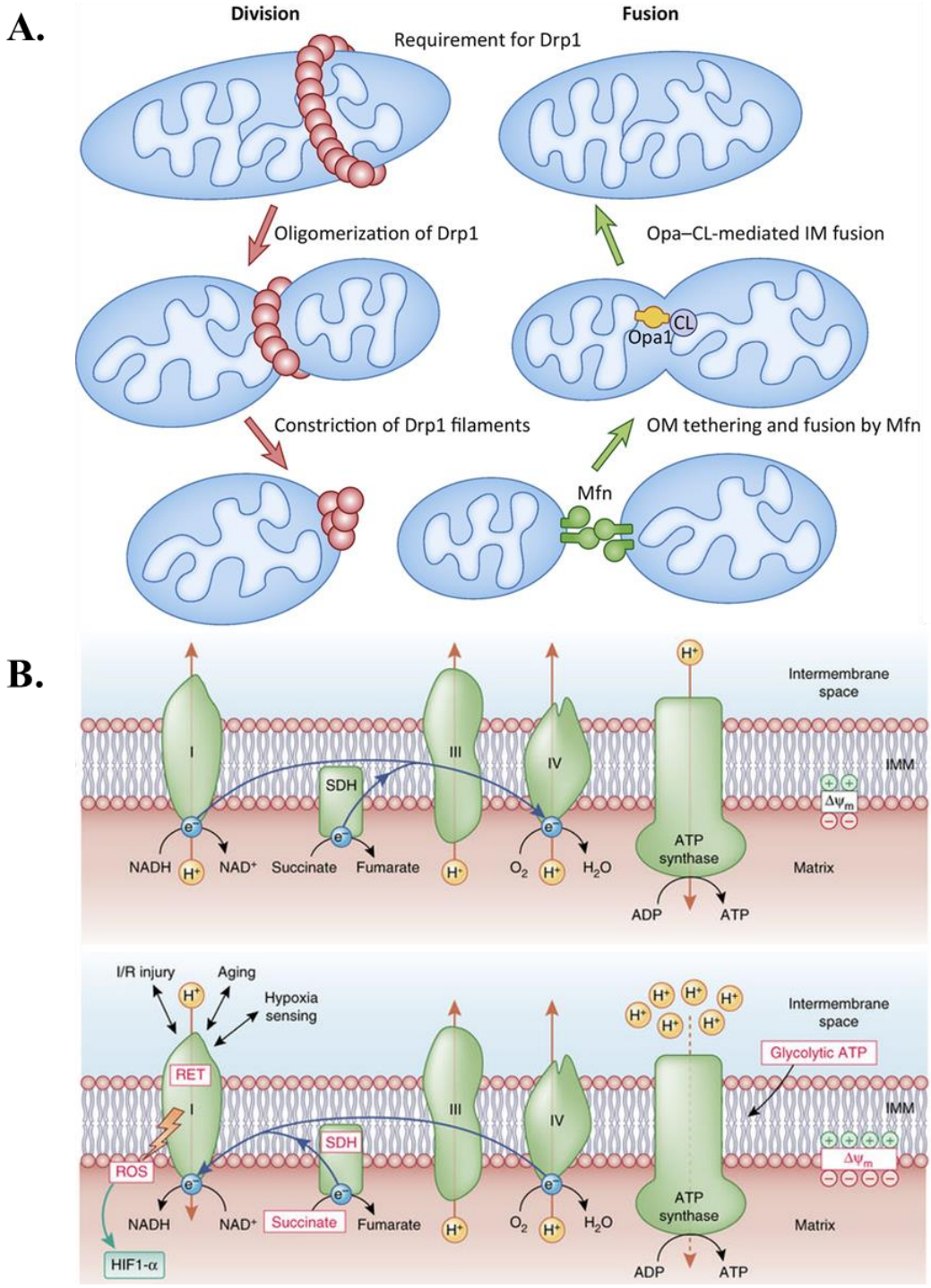

Figure 5.2 Schematic overview of the structure of mitochondria. A) Illustration of mitochondrial structure with inner and outer membrane, as well as some proteins involved in mitochondrial fission (left) and fusion (right). B) In the iMM, there are the five respiratory complexes with their typical chemical reaction indicated. The lower part of panel B shows the changes in ETC that can lead to RET and ROS production. Panel A is modified from *Trends in Cell Biology* DOI: (10.1016/j.tcb.2017.08.011), while panel B is modified from E. L. Mills, B. Kelly, L. A. J. O'Neill, *Nat. Immunol*. 18, 488–498 (2017).

5.4.3. Metabolic pathways: ATP, metabolite and signalling molecules generation

Glycolysis is ten-step reactions of glucose into pyruvate, which leads to ATP generation as well as generation of metabolites that can be used to fuel the tricarboxylic acid (TCA) cycle and amino acid synthesis. Glycolysis only generates two ATP per glucose molecule, making it a rather inefficient way to generate ATP. However, there are other advantages of glycolysis for the immune cells, which will be described later in this section. The TCA cycle, also known as Krebs cycle and the citric acid cycle, occur in the mitochondria and generates additional ATP, other metabolites that can be used for fatty acid synthesis (FAS) and fuel oxidative phosphorylation (OXPHOS). The TCA cycle can also be fuelled by glutamine that can be transformed into α-ketoglutarate, one of the metabolites in the TCA cycle (Fig 5.3). The TCA cycle and OXPHOS generates more ATP per molecule than glycolysis. OXPHOS can generate 36 ATPs per glucose molecule. In addition, OXPHOS generates mitochondrial ROS that subsequently affect cellular signalling pathways, but mitochondrial ROS can also lead to cell damage. Finally, fatty acid oxidation (FAO) can generate lots of ATP depending on the length of the fatty acid, while fatty acid synthesis (FAS) can be used to generate lipid-derived molecules required by the cells (Buck et al., 2015; O'Neill et al., 2016).

The metabolic pathways have several intersections with each other; substrates from one metabolic pathway can affect other pathways. As an example, FAO include the molecule acetyl-Coenzyme A (CoA), which also can enter the TCA cycle (Dimeloe et al., 2016). TCA cycle generates reduced electron carrier, which complex I and II make use of for ETC and OXPHOS (Dimeloe et al., 2016). Citrate and oxaloacetate, two TCA cycle metabolites, can instead be involved in lipid biosynthesis and amino acid biosynthesis, respectively (Dimeloe et al., 2016). The extracellular and intracellular environment has important role to whether

the TCA cycle is used to fuel OXPHOS or for lipid and amino acid biosynthesis, which will consequently have effects on the cell's energy supply and function. As examples of the extracellular environment effect on the cell's metabolism, addition of IL-7 increase T cells' glycolysis rate (Rathmell et al., 2001). Stimulation of CD8α$^+$ T cells with αCD3 and αCD28 lead to increased glycolysis but no significant changes on OXPHOS (van der Windt et al., 2013; Menk et al., 2018a). On the other hand, stimulation of 41BB, a marker expressed on activated CD4$^+$ and CD8α$^+$ T cells, leads to increased mitochondrial mass as well as increased OXPHOS rate (Menk et al., 2018b). Addition of exogenous lipids has been reported to increase OXPHOS in skin Trm cells (Pan et al., 2017).

Another factor that affect cell metabolism is the supply of oxygen in the tissue. There is a shortage of oxygen in the gastrointestinal tract. It has been showed that the level of oxygen in the murine intestinal lumen decreases along the longitudinal gut axis (Zheng et al., 2015). During hypoxic conditions, cells enhance their glycolysis rate over the OXPHOS rate. This is regulated on transcriptional level and two of the key factors in the hypoxia response are hypoxia-inducible factor (HIF) alpha and beta. HIFα and HIFβ form heterodimers, but these are stabilized during hypoxia and not normal oxygen levels. In fact, it has been reported that HIF is essential for cytokine production in Th17 (Shi et al., 2011) and Th1 (Shehade et al., 2015) cells. Hypoxia responses are also important for CD8 T cells. Cultured cells in shortage of oxygen leads to lower IL-2 and IFNγ production (Caldwell et al., 2001), while enhanced HIFα expression leads to increased production of cytokines (Doedens et al., 2013; Phan et al., 2016). OXPHOS plays a role in the hypoxia response as inhibition of mitochondrial respiration lead to de-stabilization of HIFα (Hagen et al., 2003), while mitochondrial ROS play a role to stabilize HIFα (Chandel et al., 1998). The importance of hypoxia response is

different in different cell types. Absence of hypoxia response lead to preferential differentiation to Treg cells over Th17 cells (Shi et al., 2011).

In addition, metabolic pathways also have effects on the cells' epigenetic signatures and mRNA translation. There is evidence that show that lipid-derived acetyl-CoA can induce histone acetylation (McDonnell et al., 2016). Another study has showed that the glycolysis-associated enzyme glyceraldehyde 3-phosphate dehydrogenase (GAPDH) can bind to IFNγ mRNA (Chang et al., 2013). Thus, GAPDH is not only involved in the generation of ATP and metabolites during glycolysis, but GAPDH also affect the IFNγ translation and production in e.g. Th1 cells and CTLs. Finally, a study has suggested that the position of mitochondria relative to immunological synapses affect the calcium influx in the cells (Schwindling et al., 2010). These data illustrate the impact metabolic pathways have on essential cellular functions which subsequently affect the cells' ability to generate immune responses.

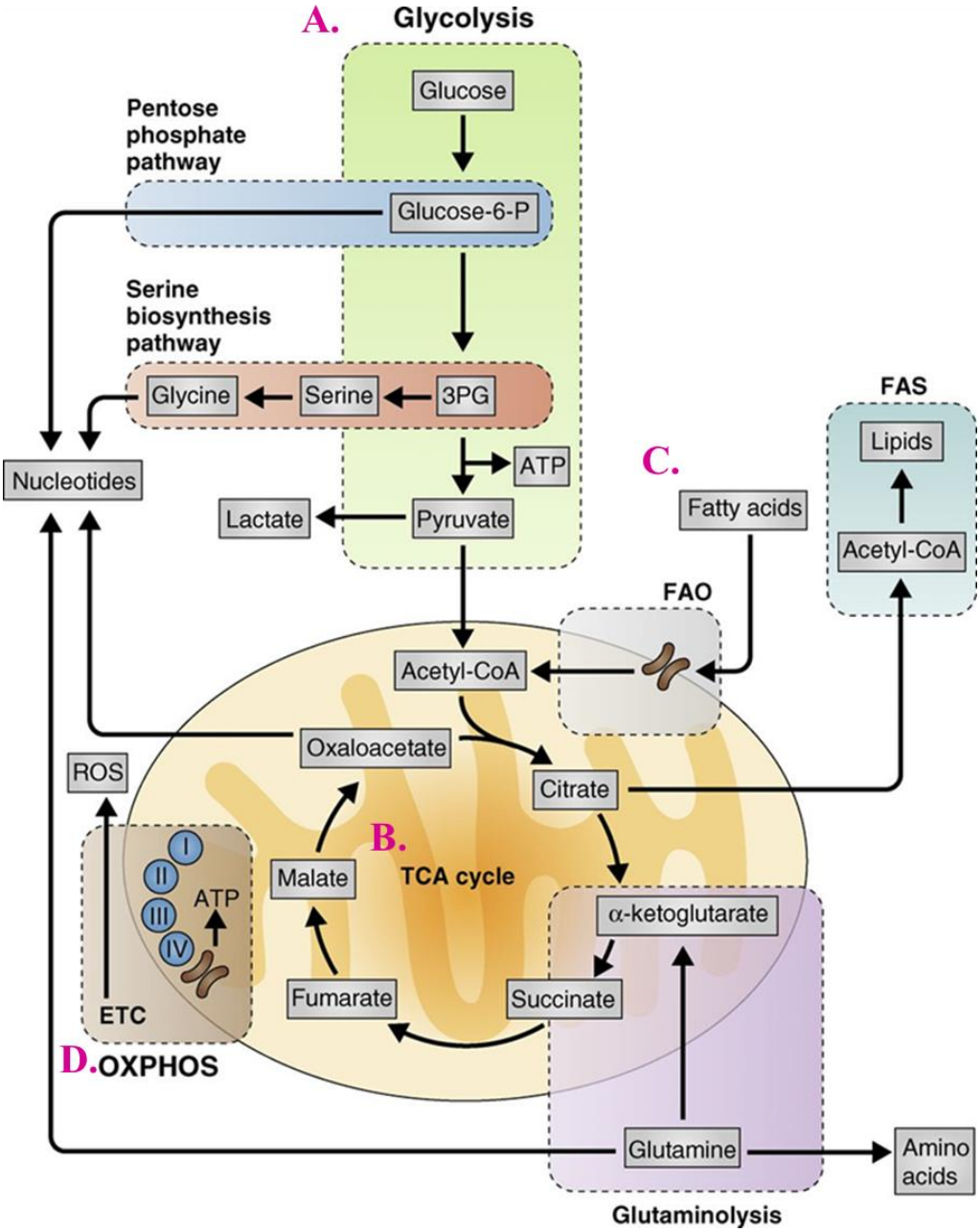

Figure 5.3 Schematic overview of the main metabolic pathways in cells. The figure illustrates the main cellular metabolic pathways such as A) glycolysis which results in ATP generation and the metabolite pyruvate that can enter B) tricarboxylic acid (TCA) cycle. The TCA cycle generates ATP. In addition, metabolites citrate and oxaloacetate can also be used for fatty acid synthesis (FAS) and nucleotide synthesis, respectively. Panel C) shows fatty acid oxidation (FAO) and FAS. FAS can generate lipids from acetyl-CoA, while FAO use fatty acids to fuel the TCA cycle with acetyl-CoA in the mitochondria. Panel D) shows oxidative phosphorylation (OXPHOS) that results in generation of ATP and reactive oxygen species (ROS), the later can act as secondary messenger in cell signalling. The figure is modified from Michael D. Buck et al. *J Exp Med* 2015.

5.4.4. The currently known role of mitochondria for innate and adaptive immunity

In recent years, the importance of the regulation of cell metabolism for the immune system has been recognized. This recognition has launched a field called immunometabolism. Naïve, effector and memory T cells have different energy demands. Naïve T cells require energy for their survival, while effector T cells additionally require energy for their effector functions. Therefore, the energy demand varies with the activation and differentiation state of T cells and the cell metabolism needs to adjust thereafter (O'Neill et al., 2016; Weinberg et al., 2015). To date, there are data supporting a role of mitochondrial functions in T cells and macrophages (MPs).

In MPs, it has been shown that M2 MPs have enhanced OXPHOS and FAO, while M1 MPs have enhanced glycolysis (O'Neill et al., 2016; Wang et al., 2018). It has also been shown that the protein Famin has an important role for MPs. Absence of Famin has been shown to lead to reduced mitochondrial ROS production and a shift of the metabolic programme towards glycolysis, with a subsequent decrease in production of the cytokines IL-1β and TNFα (Cader et al., 2016).

CD4$^+$ effector T cells are downregulating their use of fatty acid oxidation (FAO) in favor of fatty acid synthesis (FAS). In contrast, Treg cells use FAO more than fatty acid synthesis (O'Neill et al., 2016). Moreover, it has been demonstrated that CD4$^+$ T cells are dependent on glycolysis for Th1 and Th17 differentiation (Bantug et al., 2017). The expression of the glucose transporter (GLUT) has been reported to increase in TCR-activated CD4$^+$ and CD8α$^+$ T cells (Bantug et al., 2017). In addition, *in vitro* Th1 and CD8α$^+$ cells produce less IFNγ under glucose-depleted culture conditions (Cham and Gajewski, 2005). As previously

mentioned, GAPDH can affect IFNγ (Chang et al., 2013), providing one mechanistic explanation to why activated CD4$^+$ and CD8α$^+$ T cells depends on glycolysis. It has also showed that glutaminase (GLS) is essential for Th17 cell effector function as CD4-Cre-GLS$^{fl/fl}$ mice produce less IL-17 compared to controls. In contrast, Th1 cells from CD4-Cre-GLS$^{fl/fl}$ mice produce more IFNγ (Johnson et al., 2018), illustrating the different metabolic requirement for Th1 and Th17 cells.

The Erika Pearce laboratory has shown differences in metabolism between splenic naïve, effector and memory CD8α$^+$ T cells. One method they have used to assess the metabolic status of T cells is the Seahorse assay which can measure the respiratory consumption as an assessment of the level of OXPHOS. Splenic memory CD8α$^+$ T cells have higher mitochondrial spare respiratory capacity (SRC) than effector T cells (van der Windt et al., 2012). SRC is defined as the difference in oxygen consumption between basal and maximal OCR, as shown in Figure 5.5. SRC is the additional mitochondrial capacity cells can use during various stressed situations. In addition, it has been showed that memory CD8α$^+$ T cells contain more mtDNA and mitochondrial mass than effector T cells which correlates with increased OCR, ECAR, proliferation and IFNγ production (van der Windt et al., 2012, 2013). Another laboratory has shown that both CD8α$^+$ and CD4$^+$ T cells require mitochondrial ROS for IFNγ production (Sena et al., 2013).

In addition to above role in MPs and T cells, mitochondria are also involved in programmed cell death via apoptosis, via release of cytochrome c that subsequently can activate caspases to initiate apoptosis (Desagher and Martinou, 2000).

Initial immunometabolic studies have been performed on additional immune cells such as ILCs (Wilhelm et al., 2016). What applies for IELs remain to be elucidated. As metabolic pathways and metabolites have huge impact on many essential cellular functions and as mitochondria has a central role in metabolism (Fig 5.3), I will compare mitochondrial parameters between IELs and other T cells to understand further how the requirements for IEL activation may differ from other T cells.

5.5. IELs accumulate lipid droplets – a sign of their semi-activated status

As stated in the Introduction Chapter (1.6.3), IELs are a heterogeneous group of T cells, located to provide a second line of defence in the intestines. As IELs are at "the front" at the intestinal barrier site, it is thought that they are fast-acting effector T cells equipped to prevent and limit pathogen infection and tissue damage. Effector functions are metabolically costly. Therefore, I wanted to dissect further the differences between IELs and their equivalents, CD8α$^+$ T cells, in spleen. One way for cells to source energy is to store lipids in the cytoplasm. Using Nile Red staining for lipid droplet detection (Greenspan et al., 1985), I found that IELs have greater accumulation of lipids than CD8α$^+$ splenic T cells (Fig 5.4 A). As the majority of CD8α$^+$ splenic T cells in steady state mice are naïve and resting, I wanted to assess whether the low level of lipid accumulation in splenic CD8α$^+$ T cells remains during activation. To address this, I enriched CD8α$^+$ splenic T cells using magnetic cell separation

(MACS) and cultured them in the presence of plate-bound αCD3, αCD28 and soluble IL-2. Cells before and after activation were assessed for lipid droplet staining. One day after activation, an increase in Nile Red staining could already be observed (Fig 5.4 B). This increase in lipid storage remained stable for several days (Fig 5.4 B). A similar accumulation of lipids has been reported for skin Trm cells (Pan et al., 2017) as well as splenic Teff cells (O'Sullivan et al., 2014). These data, together with published data on the protein expression of lymphocyte activation markers on IELs (Wang et al., 2002), as well as gene expression data (Fahrer et al., 2001; Shires et al., 2001; Heng et al., 2008), support the model that IELs are in semi-activated state.

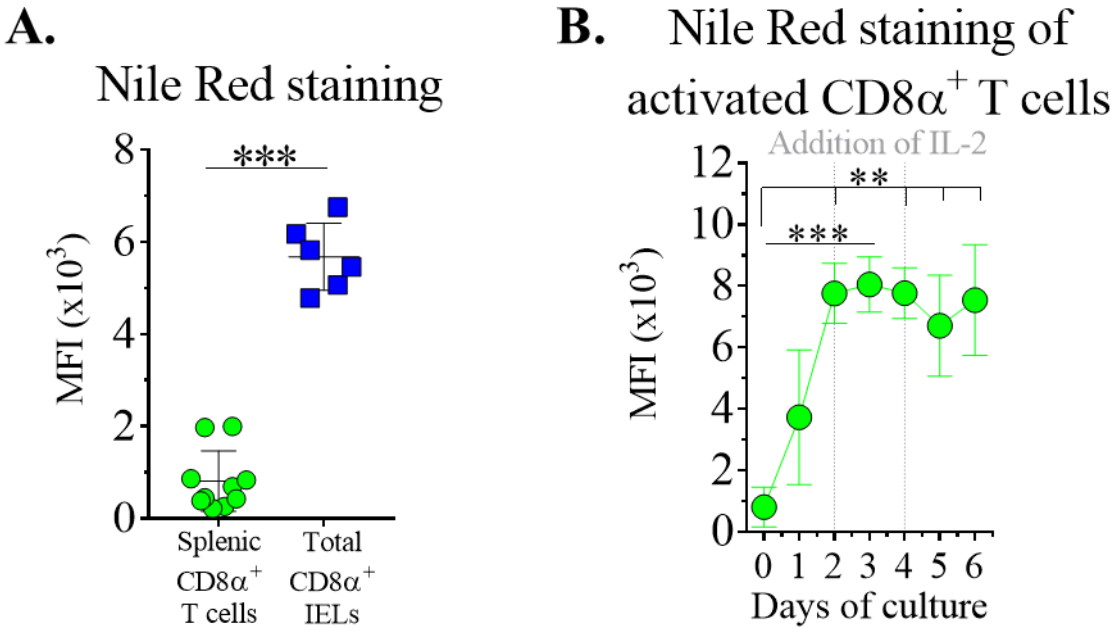

Figure 5.4. IELs have more accumulation of lipid droplets than splenic CD8α+ T cells.
A) Isolated total CD8α+ IELs and splenic CD8α+ T cells were stained for Nile Red and the mean fluorescent intensity (MFI) were quantified as mean ± SD from three independent experiments with two to four mice per experiment. B) MACS-enriched CD8α+ splenic T cells were cultured for 6 days with plate-bound αCD3 (1 µg/ml) and αCD28 (3µg/ml) and medium supplemented with 5 ng/ml IL-2. For each day post activation, Nile Red staining and quantification was performed from two independent experiments with three mice per experiment. Statistically significant changes were identified by A) the Mann-Whitney test and B) the Kruskal-Wallis test: **: p<0.01., ***: p<0.001.

5.6. IELs lack mitochondrial spare respiratory capacity (SRC)

Having observed that IELs exhibit an increased accumulation of stored lipids, I wanted to dissect further the metabolic differences between IELs and splenic CD8α$^+$ T cells. To do this, Spela Konjar tested the mitochondrial function of these cells by Seahorse mitochondrial stress assay. This assay measures the mitochondrial oxygen consumption rate (OCR) in cells deposited in tissue culture wells. At different time points, the compounds oligomycin, carbonylcyanide p-trifluoromethoxyphenylhydrazone (FCCP), antimycin A and rotenone were added to the cells. Addition of FCCP depolarizes the mitochondria membranes, which forces the cells into a state that generates the maximal possible OCR. The difference between basal and maximal OCR is defined as spare respiratory capacity (SRC) that the cells can use during challenging situations such as infections (van der Windt et al., 2016). In the present circumstances, I wanted to test if IELs had similar basal OCR and SRC to splenic CD8α$^+$ T cells. When plating the same number of IELs and splenic CD8α$^+$ T cells, I observed that IELs had a similar basal OCR as splenic CD8α$^+$ T cells (Fig 5.5). Surprisingly, it appeared that IELs had no SRC (Fig 5.4), suggesting that steady state IELs are not able to maximize their mitochondrial respiratory function, which both splenic naïve and memory CD8α$^+$ T cells can.

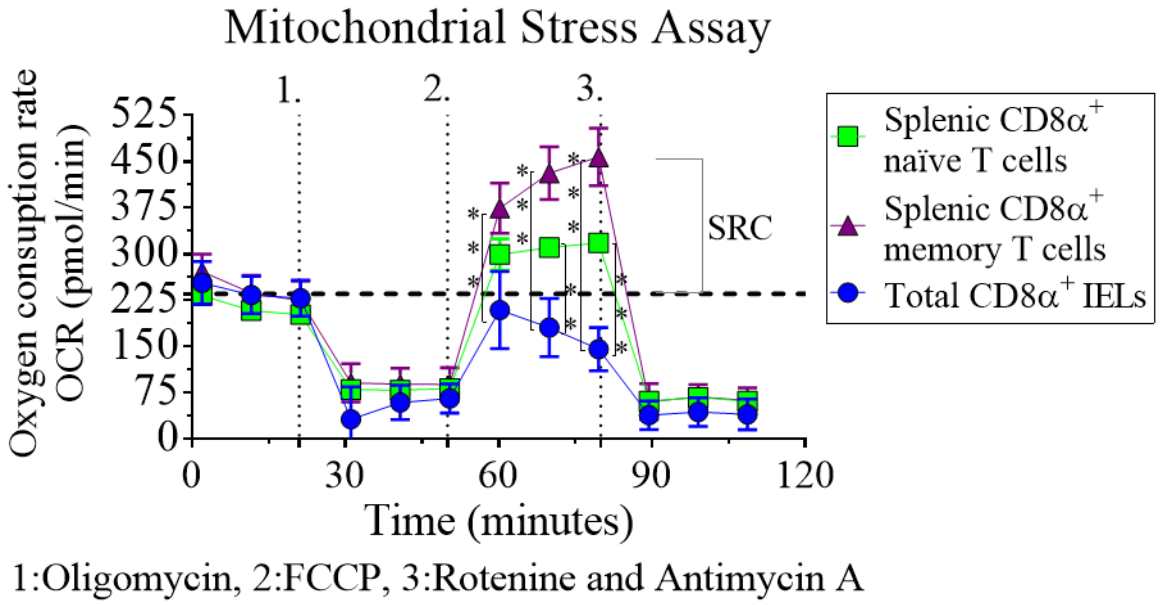

Figure 5.5. IELs have no spare respiratory capacity (SRC) while splenic CD8α$^+$ T cells do. 750 000 FACS-sorted total CD8α$^+$ IELs and splenic naïve and memory CD8α$^+$ T cells were plated on Seahorse plates and assessed using Seahorse mitochondrial stress assays. The data are representative of two independent experiments and are presented as mean ± SEM. Statistically significant changes were identified by two-way ANOVA: **: p<0.01., ***: p<0.001.

5.7. IELs have lower mitochondrial mass compared to splenic T cells

The lack of SRC in IELs suggested that their mitochondria may be in a different state in comparison to the mitochondria of splenic CD8α$^+$ T cells. To pinpoint further the cause of this difference, I used a mitochondrial probe called MitoTracker Green (MTG). MTG is a carbocyanine-based dye that binds to mitochondria independently of their membrane potential. Therefore, MTG has been used to estimate mitochondrial mass (Agnello et al., 2008). Performing this staining showed that both naïve and memory splenic CD8α$^+$ T cells have bright MTG staining, generating high mean fluorescent intensity (MFI) of MTG (Fig 5.6 A-B). However, IELs have significantly lower staining compared to splenic CD8α$^+$ T cells (Fig 5.6 A-B). The level of MTG staining in IELs is above the level of the MTG Fluorescent-Minus-One (FMO) control, suggesting that IELs have low mitochondrial mass

(Fig 5.6 A). The FMO control was treated the same way as the other samples but did not receive the MTG probe. Therefore, it can be used to aid to determine whether or not there is positive MTG staining in the samples. The use of FMO controls is common in flow cytometry (Tung et al., 2007). A similar level of MTG staining was observed in the four main IEL subsets (Fig 5.6 C). Interestingly, CD4$^+$ CD8αα$^+$ IELs exhibited significantly higher MTG staining than the other IEL subsets, but lower than memory and naïve splenic CD8α$^+$ T cells (Fig 5.6 C). These data suggest that all IEL subsets have lower mitochondrial mass than splenic CD8α$^+$ T cells.

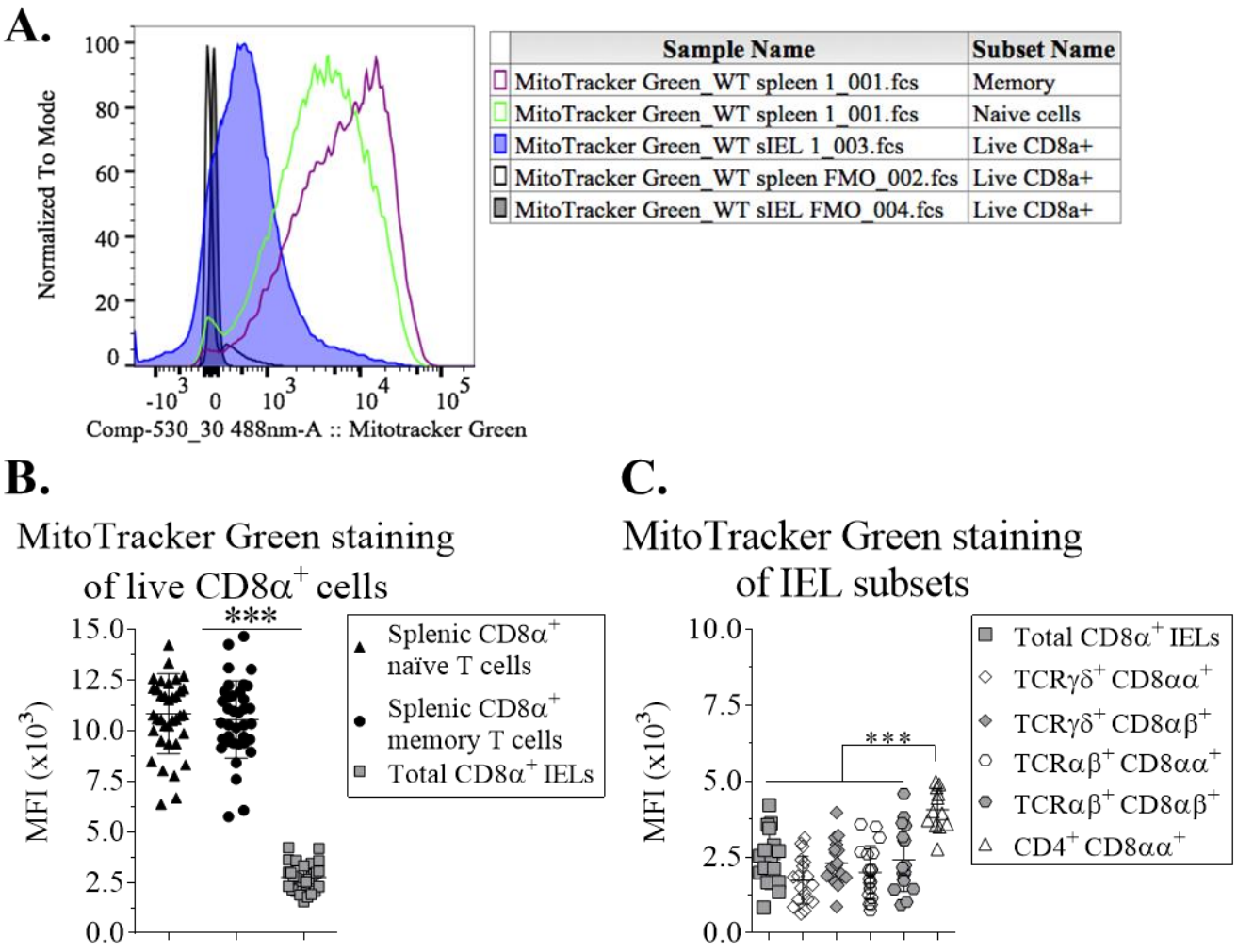

Figure 5.6. IELs have lower mitochondrial mass than splenic CD8α$^+$ T cells. WT IELs and splenic CD8α$^+$ T cells were isolated and stained for MTG according to the manufacturer's instructions. A) A representative histogram showing MTG staining of CD8α$^+$ IELs and splenic CD8α$^+$ T cells. B-C) Quantification of MTG MFI from B) CD8α$^+$ IELs, memory and naïve splenic CD8α$^+$ T cells and C) IEL subsets, as indicated. Data are quantified as mean ± SD from B) 10 and C) five independent experiments with two to five mice used per experiment. Statistically significant changes were identified by one-way ANOVA. ***: $p<0.001$.

5.8. Other epithelial-resident and TCRγδ$^+$ lymphocytes have more mitochondrial mass than IELs

As splenic CD8α$^+$ T cells can be classified as systemic T cells and IELs more closely resemble tissue-resident T cells, e.g. with the expression of CD103 and CD69, I next wanted to test if this MTG phenotype is shared with other TCRγδ$^+$ cells and epithelial-resident lymphocytes. As described in the introduction in this chapter, there are some similarities between IELs and epithelial-resident lymphocytes located in skin and lung, particularly DETCs. For the experiments, T cells from spleen, small intestine, liver, lung and skin were isolated and stained for MitoTracker Green. In addition to isolate IELs from the IEC compartment, lamina propria lymphocytes (LPLs) were isolated from the LP compartment. The long digestion protocol for LPLs is usually accompanied by a higher level of cell death than in the other isolation protocols used (data not shown). Therefore, the LPLs group has the fewest replicates presented (Fig 5.7 F-H). As the ratio of CD4$^+$ to CD8α$^+$ T cells varies in the different tissues and the majority of non-intestinal TCRγδ$^+$ cells do not express CD8α, the MTG MFIs were quantified from the live TCR$^+$ population in all tissues, followed by assessing TCRαβ and TCRγδ specifically. DETCs have a bespoke gating strategy, gated by Vγ3 staining (according to Garman's nomenclature; alternative name is Vγ5 from Heilig & Tonegawa's nomenclature) in combination with high TCRγδ staining (Sano and Park, 2014), and the results for these cells are therefore only plotted in the TCRγδ plot (Fig 5.6 G). This assessment revealed that it is only IELs and TCRγδ$^+$ LPLs that have low mitochondrial mass. All other tested populations have significantly higher MTG staining compared to IELs (Fig 5.7 F-H). Additional gating on CD103$^+$ TCR$^+$ cells, resembling Trm cells, led to similar results as Figure 5.6 F. Liver lymphocytes have similar MTG staining to splenic T cells. Interestingly, lung lymphocytes have even higher MTG staining than splenic T cells (Fig 5.7 F-H). TCRγδ$^+$ cells found in lung, liver and spleen have significantly higher MTG staining

compared to TCRγδ$^+$ IELs (Fig 5.7 G). These data suggest that the MTG phenotype in IELs is not linked to the preference of expressing TCRγδ over TCRαβ, with TCRγδ$^+$ LPLs being the only found exception. Collectively, these data suggest additional difference between IELs and other TCRγδ$^+$ cells and epithelial-resident lymphocytes, possibly linked to their different epithelial barrier requirements and challenges.

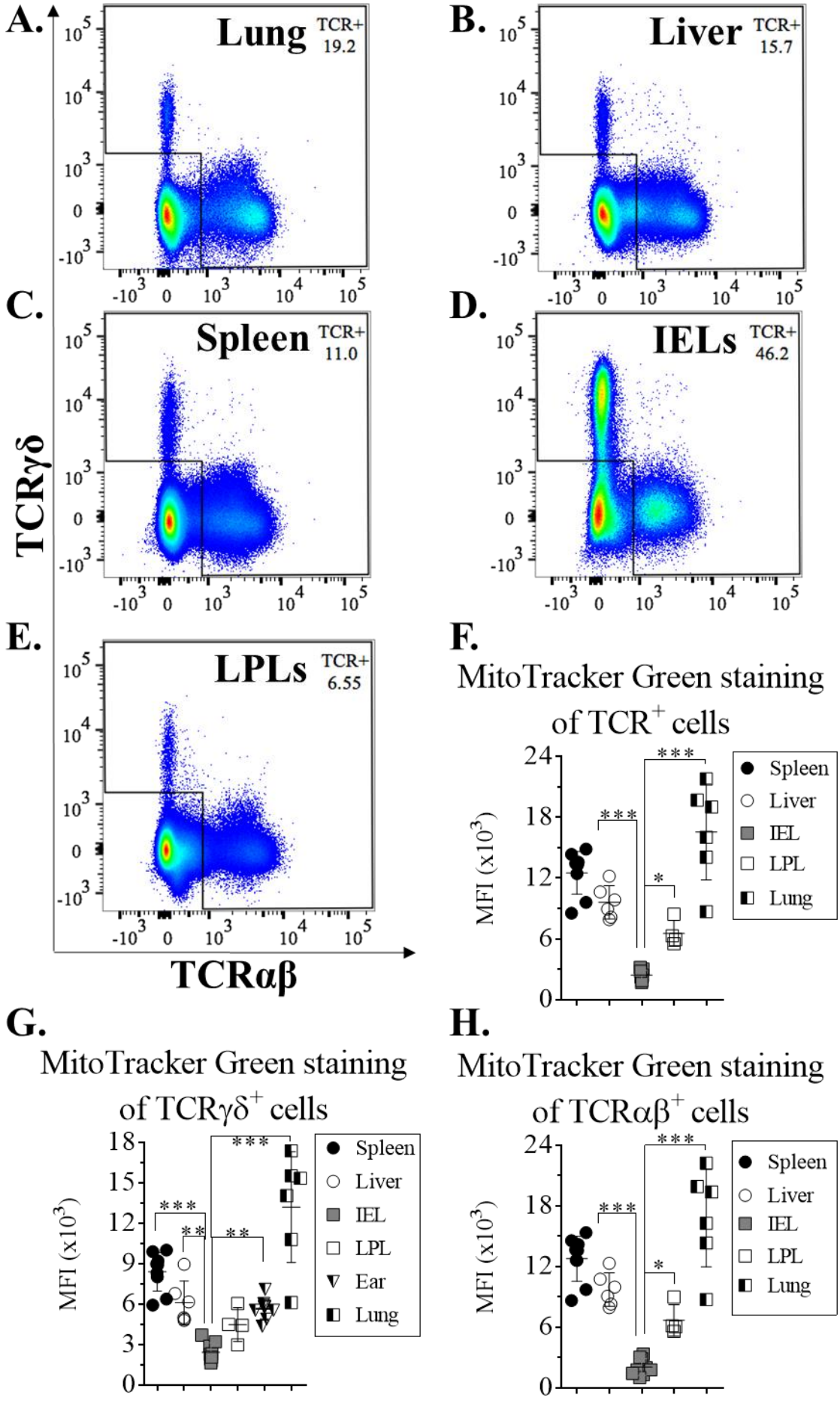

Figure 5.7. IELs are set apart from other TCRγδ$^+$ cells and epithelial-resident lymphocytes by their MTG staining. T cells from spleen, small intestine, lung, skin and liver were isolated and assessed for MTG staining by flow cytometry A-C) Example plots for TCR staining for A) lung, B) liver, C) spleen, D) IEL and E) LP lymphocytes. All panels were pre-gated on live single cells. F-H) MTG MFI quantification from F) total lymphocytes (TCR$^+$), G) TCRαβ$^+$ cells and H) TCRγδ$^+$ cells presented as mean ± SD from two to three independent experiments with three mice used per experiment. Statistically significant changes were identified by one-way ANOVA. *: p<0.05., **: p<0.01., ***: p<0.001.

5.9. Additional differences in IEL mitochondria: higher cardiolipin (CL) content and lower mitochondrial potential than splenic CD8α$^+$ T cells

As IELs seem to have restricted mitochondrial mass and SRC, I wanted to assess the amount of CLs in IELs, as it is known that CLs may have an effect on mitochondrial functions. As an initial step, I wanted to assess this question using flow cytometry with the CL-binding dye NAO. The fluorescence of NAO correlates, in an inverse linear manner, with the amount of CLs present (Mileykovskaya et al., 2001; Kaewsuya et al., 2007). Using NAO, I assessed total CD8α$^+$ IELs, naïve and memory splenic CD8α$^+$ T cells. Surprisingly, the NAO staining suggested that IELs contain more CLs than naïve and memory splenic CD8α$^+$ T cells (Fig 5.8 A-B). There was also a trend visible in the data suggesting that naïve splenic CD8α$^+$ T cells may contain more CLs than memory cells, although this did not reach statistical significance with used statistical method (Fig 5.7 B). Assessment of the different IEL subsets showed no differences in NAO staining, not even with CD4$^+$ CD8αα$^+$ IELs that had previously shown higher MTG and MTO staining (Fig 5.7 C).

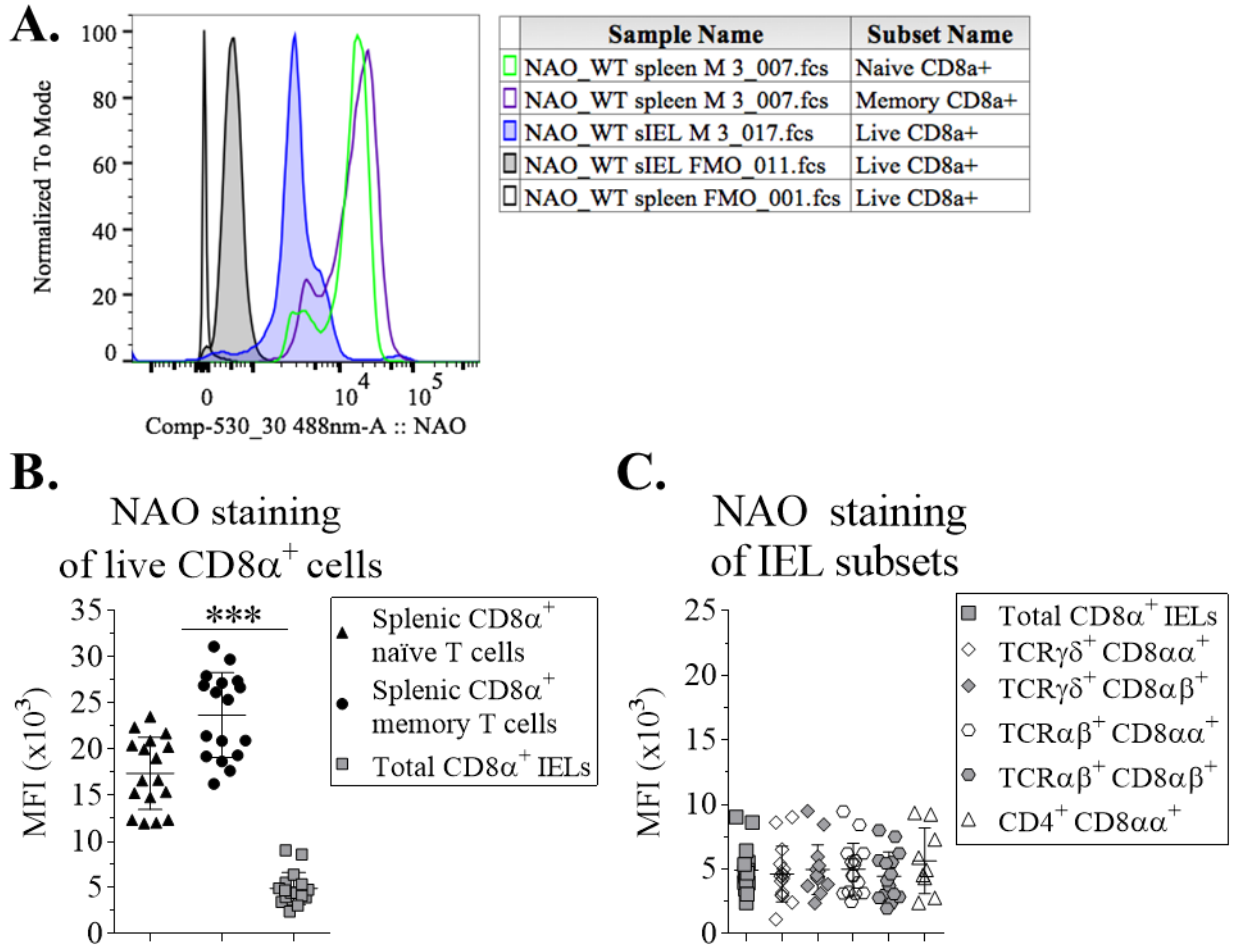

Figure 5.8. IELs have higher cardiolipin (CL) content than splenic CD8α$^+$ T cells. WT CD8α$^+$ IELs and splenic CD8α$^+$ T cells were isolated and stained for NAO according to the manufacturer's instructions. A) A representative histogram showing NAO staining of CD8α$^+$ IELs and splenic CD8α$^+$ T cells. B-C) Quantification of NAO MFI from B) CD8α$^+$ IELs, memory and naïve splenic CD8α$^+$ T cells and C) IEL subsets. Data are presented as mean ± SD from six independent experiments with two to three mice per experiment. Statistically significant changes were identified by the Kruskal-Wallis test. ***: $p<0.001$.

After observing that IELs have no SRC and lower MTG staining than other T cells, I next wanted to assess if there are more differences in IEL mitochondria, in order eventually to be able to discover the mechanism(s) behind the observed differences. An important factor for high mitochondrial OCR is mitochondrial membrane potential. There is a rosamine-based dye called MitoTracker Orange (MTO), that is in a reduced and non-fluorescent state until it

enters actively respiratory mitochondria (Agnello et al., 2008). Therefore, MTO is in use to assess mitochondrial membrane potential. Using this probe on IELs and splenic CD8α$^+$ T cells, I observed that IELs have lower MTO staining than naïve and memory splenic CD8α$^+$ T cells (Fig 5.9 A-B). These findings are in line with the lack of SRC in IELs. When assessing the different IEL subsets, I found that CD4$^+$ CD8αα$^+$ IELs have higher potential than the remaining IEL subsets (Fig 5.9 C). In addition, TCRγδ$^+$ CD8αβ$^+$ IELs have higher membrane potential than TCRαβ$^+$ CD8αα$^+$ and TCRγδ$^+$ CD8αα$^+$ IELs (Fig 5.9 C). Both CD4$^+$ CD8αα$^+$ and TCRγδ$^+$ CD8αβ$^+$ IELs have significantly lower membrane potential than splenic CD8α$^+$ T cells.

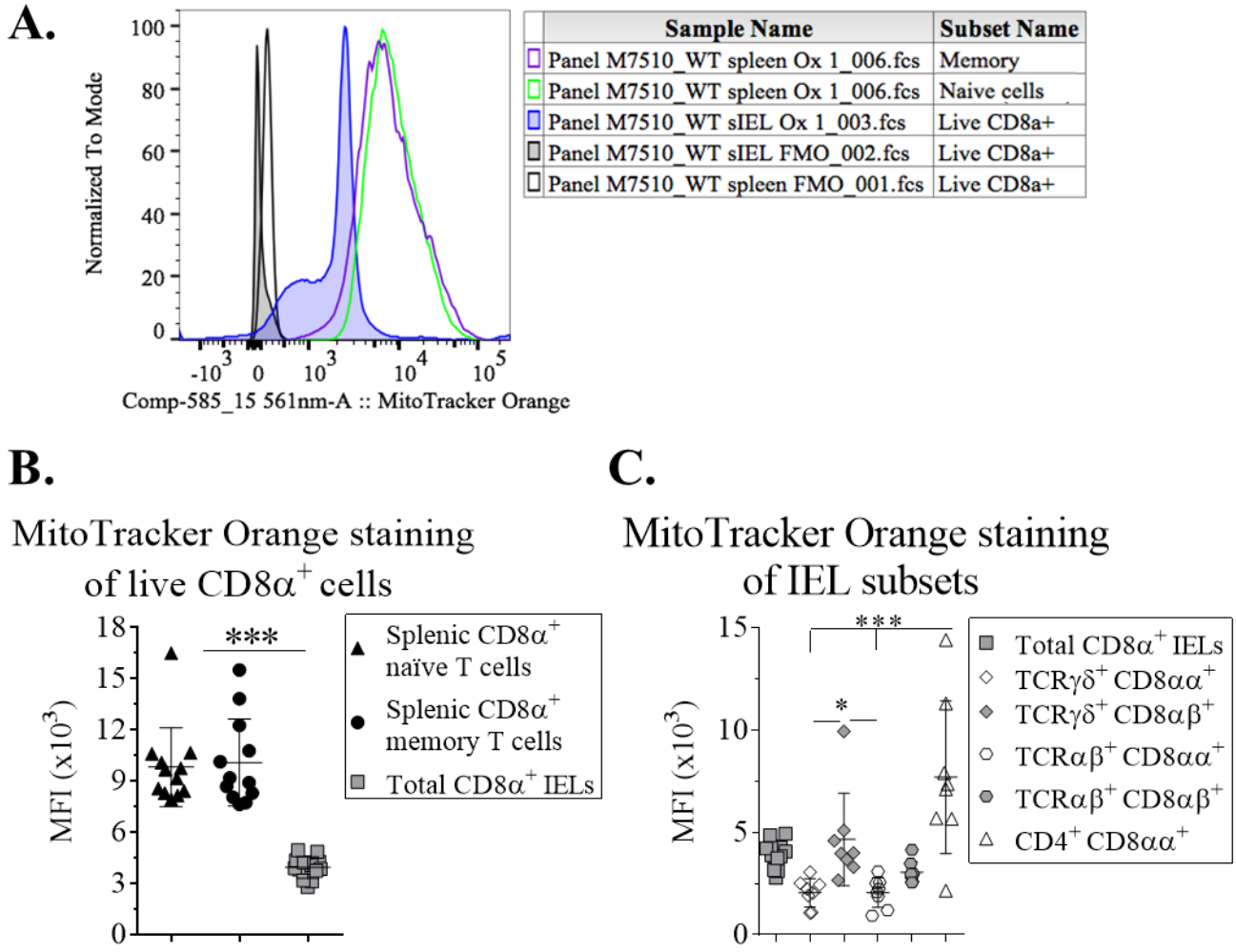

Figure 5.9. Mitochondrial membrane potential is lower in IELs than in splenic CD8α$^+$ T cells. WT CD8α$^+$ IELs and splenic CD8α$^+$ T cells were isolated and stained for MTO, according to the manufacturer's instructions. A) A representative histogram showing MTO staining of CD8α$^+$ IELs and splenic CD8α$^+$ T cells. B-C) Quantification of MTO MFI from B) CD8α$^+$ IELs, memory and naïve splenic CD8α$^+$ T cells and C) IEL subsets. Data are presented as mean ± SD from B) five and C) four independent experiments with two mice per experiment. Statistically significant changes were identified by the Kruskal-Wallis test. *: $p<0.05$, ***: $p<0.001$.

5.10. IELs have similar mitochondrial ROS production to splenic CD8α$^+$ T cells

Considering the fact that ROS production is a by-product from OXPHOS, then the previous data would suggest that IELs would have a lower level of ROS production than splenic CD8α$^+$ T cells To test this hypothesis, I used a probe that specifically detects mitochondrial ROS, namely MitoSOX (Batandier et al., 2002; Murphy, 2009). When assessing IELs, naïve and memory splenic CD8α$^+$ T cells, I surprisingly found similar level of ROS production from all three populations (Fig 5.9 B). The IEL histogram showed bimodal expression (Fig 5.10 A), indicating that the mitochondrial ROS production level may vary between the different IEL subsets. Interestingly, it seems that mitochondrial ROS is produced mainly by CD8αβ$^+$ IELs, regardless of which TCR that is expressed (Fig 5.10 C). These data may highlight functional differences between CD8αβ$^+$ and CD8αα$^+$ IELs. Previously published data have focussed mainly on the difference between TCRαβ$^+$ and TCRγδ$^+$ IELs.

Collectively, the mitochondrial probes MTO, MitoSOX and NAO suggest that IELs have lower mitochondrial membrane potential, higher content of CLs and similar production of mitochondrial ROS production when comparing to splenic CD8α$^+$ T cells.

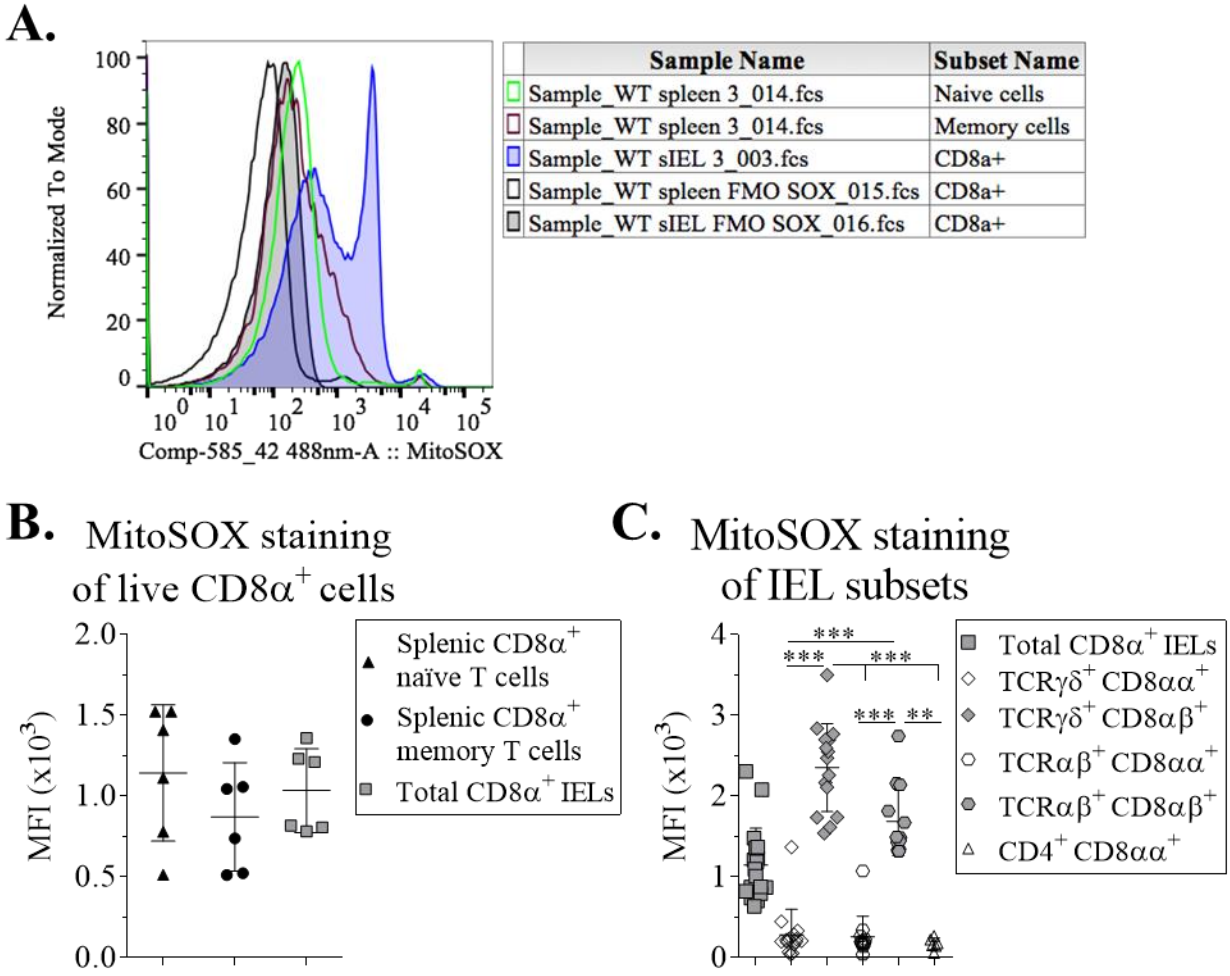

Figure 5.10. IELs have a similar level of mitochondrial ROS production to splenic CD8α+ T cells. WT CD8α+ IELs and splenic CD8α+ T cells were isolated and stained for MitoSOX according to the manufacturer's instructions. A) A representative histogram showing MitoSOX staining between CD8α+ IELs and splenic CD8α+ T cells. B-C) Quantification of MitoSOX MFI from B) CD8α+ IELs, memory and naïve splenic CD8α+ T cells and C) IEL subsets. Data are presented as mean ± SD from B) two and C) six independent experiments with two to three mice per experiment. Statistically significant changes were identified by one-way ANOVA. **: p<0.01., ***: p<0.001.

5.11. Low mitochondrial mass may not prevent cytolytic capacity in IELs

Next, I wanted to address whether the differences in IEL mitochondria reported in this chapter, could lead to differences in immune effector functions. To test this, I isolated IELs and splenic CD8α$^+$ T cells and re-stimulated them with PMA, ionomycin and brefeldin for two hours. Longer re-stimulation times, as regularly used for stimulation of other types of T cells, led to very poor IEL survival (data not shown), in line with the observation that IELs survive poorly *in vitro* without the support of intestinal organoids (see Chapter 4). After the re-stimulation, IELs and splenic CD8α$^+$ T cells were stained for IFNγ, TNFα, Ki-67 and granzyme B. I observed that splenic CD8α$^+$ T cells produced IFNγ and TNFα, while IELs produced very low levels of IFNγ and TNFα (Fig 5.10 A-C). Both IELs and CD8α$^+$ T cells have low levels of proliferation at steady state, as measured by Ki-67 staining (Fig 5.11 D). As expected from the literature, the IELs had high proportion of cells that expressed granzyme B compared to splenic CD8α$^+$ T cells (Fig 5.11 A and E). This applies to all five IEL subsets, with similar percentage of granzyme B, expect TCRαβ$^+$ CD8αβ$^+$ IELs that have significantly lower (Fig 5.11 E). These data are in line with previous publications (Fahrer et al., 2001) and suggest that the low mitochondrial mass may not prevent IELs to prepare themselves for cytotoxic activity.

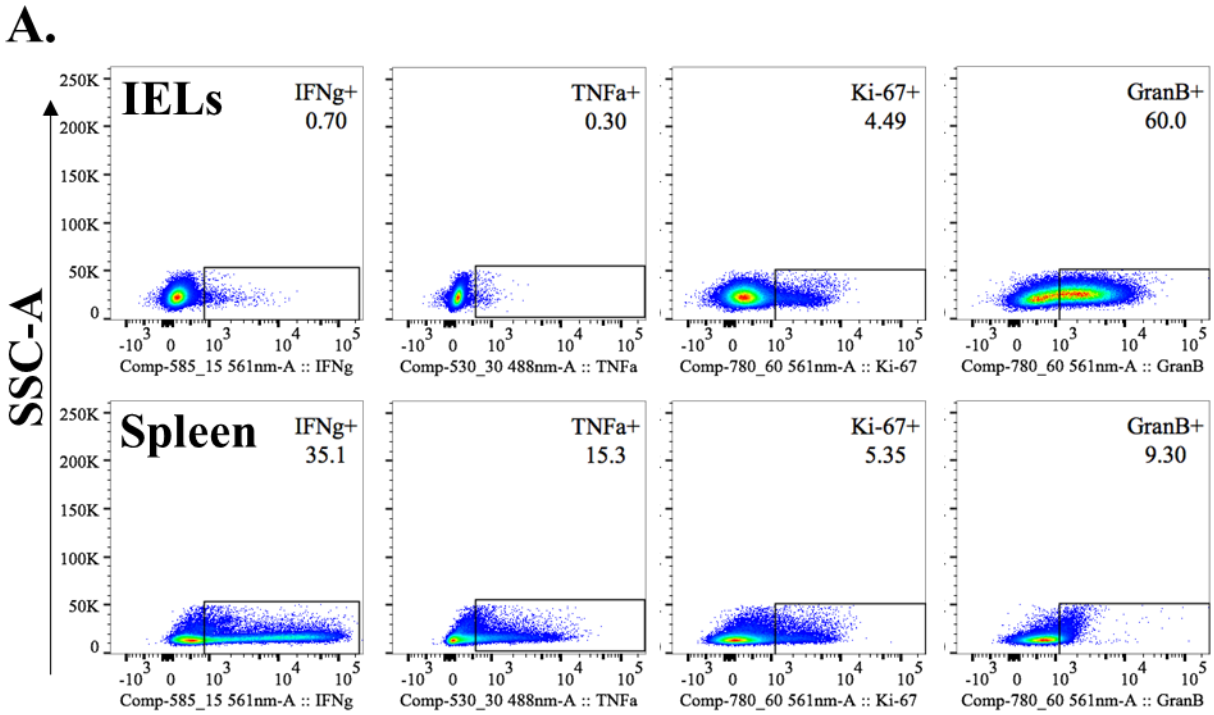

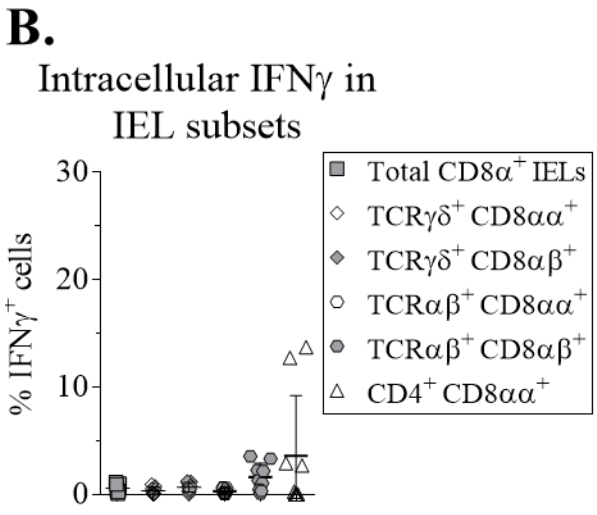

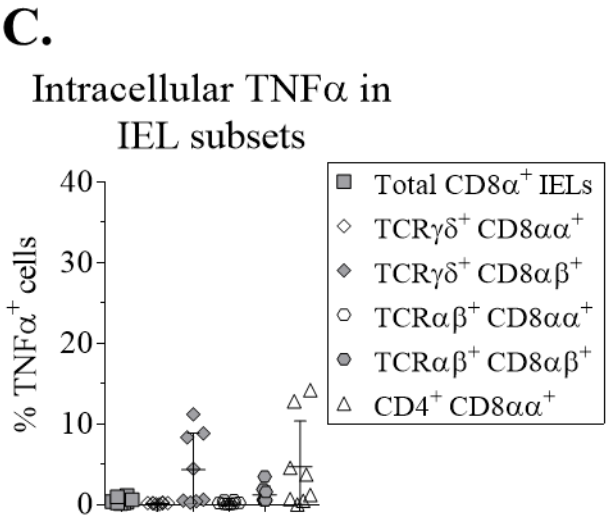

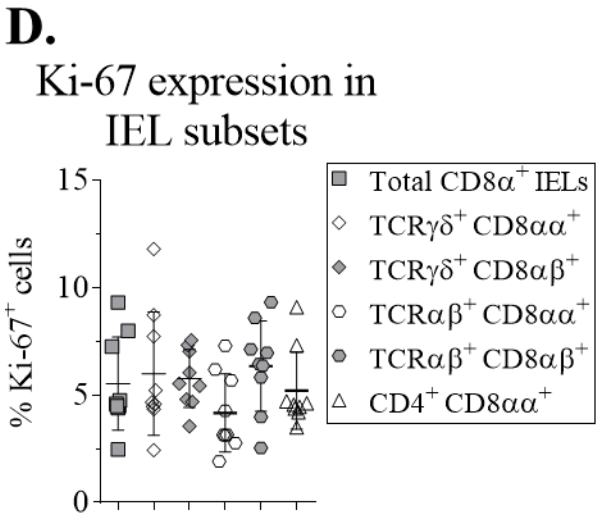

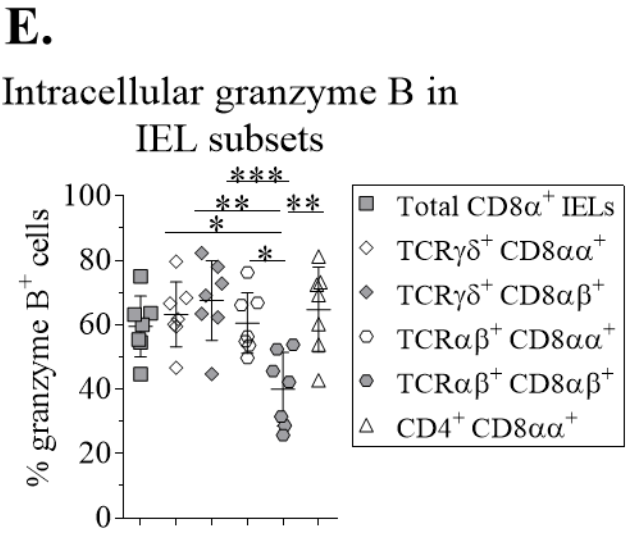

Figure 5.11. Despite low mitochondrial mass, IELs are equipped with granzyme B. WT CD8α$^+$ IELs and splenic CD8α$^+$ T cells were isolated, re-stimulated for two hours prior to intracellular staining for IFNγ, TNFα, Ki-67 and Granzyme B. A) Representative gating of IFNγ$^+$, TNFα$^+$, Ki-67$^+$ and Granzyme B$^+$ cells from CD8α$^+$ IELs and splenic CD8α$^+$ T cells. B-E) Quantification of the percentage of B) IFNγ$^+$, C) TNFα$^+$, D) Ki-67$^+$ and E) granzyme B$^+$ from IELs subsets. Data are presented as mean ± SD from six independent experiments with two to three mice used per experiment. Statistically significant changes were identified by one-way ANOVA. *: $p<0.05$., **: $p<0.01$., ***: $p<0.001$.

5.12. Supplemental chapter figures

A.

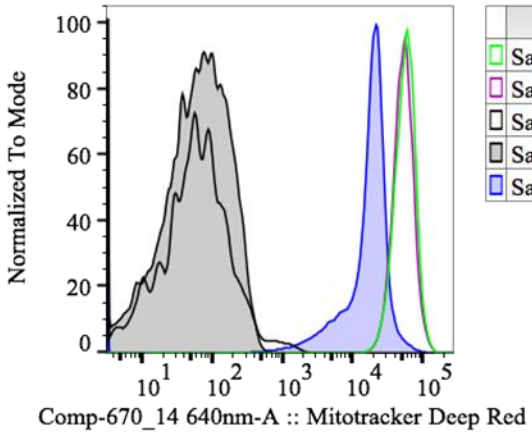

	Sample Name	Subset Name
	Sample_WT spleen 1_006.fcs	Naive T cells
	Sample_WT spleen 1_006.fcs	Memory T cells
	Sample_WT spleen FMO_001.fcs	Live CD8a+
	Sample_WT sIEL FMO_002.fcs	Live CD8a+
	Sample_WT sIEL 1_003.fcs	Live CD8a+

B.

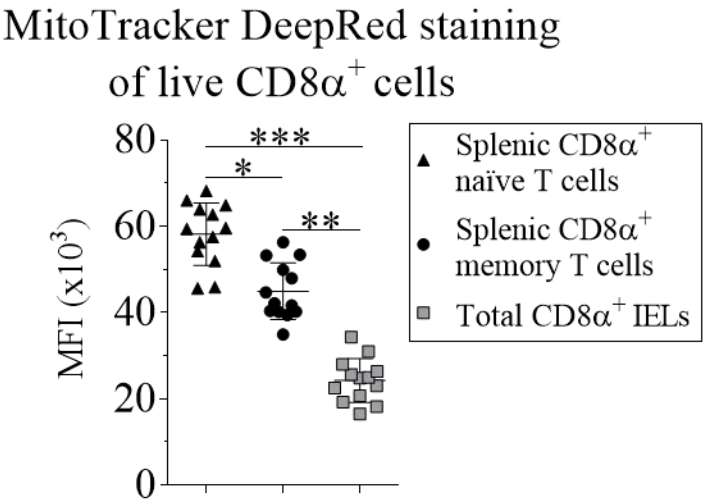

Supplemental Figure to 5.6: MitoTracker Deep Red (MTDR) staining show a similar difference as MTG staining between splenic CD8α$^+$ T cells and IELs. WT CD8α$^+$ IELs and splenic CD8α$^+$ T cells were isolated and stained for MTDR. A) A representative histogram showing MTDR staining between CD8α$^+$ IELs and splenic CD8α$^+$ T cells. B) Quantification of MTDR MFI from CD8α$^+$ IELs, memory and naïve splenic CD8α$^+$ T cells. Data are quantified as mean ± SD from four independent experiments with three to four mice used per experiment. Statistically significant changes were identified by one-way ANOVA. *: p<0.05., **: p<0.01,***: p<0.001.

5.13. Chapter Discussion

Summarising the findings reported in this chapter, I have shown that IELs have a different metabolic status compared to other T cells. IELs have more lipid droplets accumulated compared to splenic CD8α$^+$ T cells. Moreover, IELs have lower mitochondrial mass and membrane potential than splenic CD8α$^+$ T cells. Interestingly, IELs have higher CL content and surprisingly similar mitochondrial ROS production compared to splenic CD8α$^+$ T cells. Similar low mitochondrial mass is observed in TCRγδ$^+$ LPLs, but in no other TCRγδ$^+$ T cells and epithelial-resident T cells found in spleen, liver, skin and lung, setting IELs apart even further from non-intestinal T cells.

One outstanding question to address is how IELs are using their stored lipids. It has been reported that both skin Trm and splenic Teff cells also have higher accumulation of lipids (Pan et al., 2017; O'Sullivan et al., 2014). Interestingly, like IELs, skin Trm cells do not have any SRC. Addition of exogenous lipids, in the form of palmitate, increased the SRC in skin Trm. The uptake of exogenous lipids turned out to be important for *in vivo* survival of skin Trm cells (Pan et al., 2017), suggesting that IELs may be using their lipids for the same reason.

The observation that IELs have no SRC was surprising. The difference in SRC response between naïve and memory CD8α$^+$ T cells is expected from previous literature (van der Windt et al., 2012). However, a possibility is that IELs require even higher concentration of FCCP, than used for the experiment presented in Figure 5.5, to reach threshold to unleash maximal OCR. One could test different doses FCCP on the IELs, to be able to confirm or rule out this possibility. Recent data suggest that the amount of SRC might be linked to the co-stimulatory molecules expressed on the cells. This report used CD8α$^+$ chimeric antigen

receptor (CAR) T cells and engineered which costimulatory molecules that were expressed on them. The authors compared CD28 and 41-BB signalling domains. They discovered that after antigen stimulation, 41-BB$^+$ CAR T cells had a higher SRC response compared to CD28$^+$ CAR T cells. The CD28$^+$ CAR T cells had instead a higher extracellular acidification rate (ECAR) and higher expression of genes linked to glycolysis such as glucose transporter 1 (GLUT1). On the other hand, 41-BB$^+$ CAR cells had higher gene expression linked to fatty acid oxidation (FAO) such as fatty acid binding protein (FAB)5 (Kawalekar et al., 2016). These data put co-stimulatory molecules in the spotlight for further investigations. As mentioned previously in the Introduction section 1.6.2, most WT steady state IELs express CD8αα as co-receptor. CD8αα has been reported to be able to interact with thymus leukemia antigen (TL), which is expressed on IEC. It has also been hypothesised that the CD8αα homodimer may have repressive functions (Cheroutre and Lambolez, 2008). If CD8αα is having a role in the SRC response, then differences between CD8αα$^+$ TCRγδ$^+$/ TCRαβ$^+$ IELs and CD8αβ$^+$ TCRγδ$^+$/ TCRαβ$^+$ IELs should be observed. IEL subset data from MitoSOX assessment showed that CD8αβ$^+$ IELs have higher mitochondrial ROS production, despite all subsets having similar mitochondrial mass.

Next, I described the interesting observation that IELs are different in regard to MTG staining compared to other TCRγδ$^+$ and epithelial-resident lymphocytes. The only exception was TCRγδ$^+$ LPLs. These data suggest that IELs are unique in regards to mitochondrial mass compared to other lymphocytes. There is a report suggesting that IELs may migrate between IEC and LP compartments (Edelblum et al., 2012). When assessing the CD8 staining pattern of TCRγδ$^+$ LPLs, the majority of them do not express CD8αα or CD8αβ (data not shown), suggesting that the small TCRγδ$^+$ LPL population may not be merely migrated IELs.

Interestingly, CD4$^+$ CD8αα$^+$ IELs have higher mitochondrial mass than the other IEL subsets. This may be linked to the expression of CD4, as splenic CD4$^+$ T cells have even higher MTG staining than splenic CD8α$^+$ T cells (data not shown). This observation may be linked to different energy demands of CD4$^+$ and CD8α$^+$ T cells. As previously stated, the intestinal epithelial site is faced with the challenge to achieve a delicate balance of tolerance and protective responses. Hence, it was surprising that IELs seem to have low mitochondrial mass and no SRC to use to generate more energy for effector functions. Both skin and lung epithelial-resident lymphocytes also need to be immunologically controlled to prevent autoimmunity. However, lung and skin epithelial sites are less permeable than the intestinal barrier, allowing e.g. oxygen to pass through instead of large dietary compounds.

One outstanding question is when IELs obtain this altered mitochondrial state. Are these mitochondrial properties found in IEL precursors, or are they induced when IELs are homing to the intestinal epithelial compartment? A recent publication suggests that other TCRγδ$^+$ T cells have already established their commitment towards IFNγ or IL-17 production when they are in the thymus (Sumaria et al., 2017). Preliminary data from the same laboratory suggest that IFNγ- and IL-17-secreting TCRγδ$^+$ T cells have different SRC: IFNγ-committed TCRγδ$^+$ T lack SRC, while IL-17-committed TCRγδ$^+$ T cells have SRC. These data support the possibility that the mitochondrial state of IELs may be set prior to homing to the intestinal compartment. One could perform MTG staining on thymocytes to get insights into this. However, one would need to be able to distinguish IEL precursors from other T cells precursors. Having an answer to the question whether the IEL mitochondrial phenotype is intrinsic or extrinsic would give insights about the mechanisms behind it, and whether it may be possible to change the mitochondrial phenotype in IELs.

A possible explanation for the lower mitochondrial mass could relate to the balance between mitochondrial fission and fusion. The intrinsic environment in IELs may be favouring mitochondrial fission. Moreover, a process that can go hand in hand with mitochondrial fission is mitophagy – a form of autophagy of mitochondria (Van Der Bliek et al., 2017). Therefore, assessing the expression of mitophagy-associated factors may provide insights if this is occurring in IELs or not. If IELs have higher mitochondrial mass prior to homing to the intestinal compartment, then factor(s) in the intestinal environment may promote mitophagy in IELs. Despite low mitochondrial mass, all IEL subsets have accumulation of granzyme B. This means IELs should be capable of performing cytotoxic functions, which may be sufficient to fulfil their role in the maintenance of intestinal homeostasis. Further studies of IEL mitochondria, effector functions and activation, will be necessary to answer these questions.

The interesting observation that the CL content seems higher in IELs compared to splenic CD8α$^+$ T cells shows that this is a feature to look into further. As described, CLs may be able to affect mitochondrial function. Hence, it is tempting to speculate that the higher amount of CLs in IELs may spatially hinder some mitochondrial function(s), particularly considering the fact that IELs, in addition, have lower mitochondrial mass and therefore likely less volume. To the best of my knowledge, it is not possible to image into the details of CL distribution, but it is possible to assess the CL composition by mass spectrometry, which will be shown in Chapter 6.

Finally, these differences in IEL mitochondria, compared to those of splenic CD8α$^+$ T cells, could potentially be linked to the poor survival of IELs *in vitro*. A connection between mitochondria and apoptosis has long been established. It has been reported that mitochondria

can release pro-apoptotic factors, such cytochrome c, during mitochondrial structural change and mitochondria fragmentation (Cereghetti and Scorrano, 2006). The similar level of mitochondrial ROS in IELs compared to splenic CD8α$^+$ T cells (Fig 5.9 B), may also be a potential reason why IELs survive so poorly *in vitro*, when cultured on their own. The amount of mitochondrial ROS relative to the small mitochondrial mass may be damaging for the IELs e.g. via damage of mtDNA. If the mtDNA in IELs is damaged, then it may lead to defects in the genes encoding the ETC complexes, which is important for mitochondrial function. It is tempting to speculate that organoid-mediated IEL survival (see Chapter 4, Figure 4.9) might be linked to the mitochondria in IELs either by direct or indirect mechanisms. Therefore, a potential next step could be to assess mitochondrial staining in IEL-organoid co-cultures. Unfortunately, MTG is not a fixable stain so another MitoTracker dye would have to be used, such as MitoTracker Deep Red (MTDR) that is fixable and shows a similar difference between splenic CD8α$^+$ T cells and IELs. Interestingly, this probe showed a statistically significant difference between splenic naïve and memory CD8α$^+$ T cells (Supplemental Figure to Fig 5.6). These data suggest that MTDR is not identical to MTG. Even if organoids do not affect the mitochondria in IELs directly, they may compensate any pro-apoptotic effect the IEL mitochondria generate. Another link could be via the accommodation of lipids in IELs. IECs have been reported to have stored lipids (Jennemann et al., 2012). Perhaps IELs can obtain their lipid accumulation from the IEC and dietary residues and that may be linked to their survival. It has been shown in cell lines that lipids can be transported between cells in thin dendrites connecting the cells (Astanina et al., 2015). Further experiments need to be performed to address this. For that, the established IEL-organoids co-culture system will be useful.

Collectively, this chapter highlights metabolic differences between IELs and other T cells, which may be linked to IEL activation and maintenance.

Chapter 6: IELs show mitochondrial plasticity during activation

The data presented in Chapter 5 suggest that the mitochondria in IELs are different to the mitochondria in splenic CD8α$^+$ T cells in terms of mitochondrial mass (Fig 5.6 A-B), mitochondrial membrane potential (Fig 5.9 A-B) and CL content (Fig 5.8 A-B). At this stage, two important questions arise. Firstly, what are the determining conditions that set IELs into this altered mitochondrial state in regards of mitochondrial mass, membrane potential and cardiolipin content? Secondly, does this altered mitochondrial stage lead to changes in IELs effector capacity compared to splenic CD8α$^+$ T cells? To address the second question, I need to purposely activate IELs. In physiological settings, IELs become activated during infectious and inflammatory conditions. However, there is a risk that IELs do not become activated during all infectious and inflammatory conditions. Therefore, I first wanted to use a method that for sure would activate IELs. For this purpose, I tested if *in vivo* injection of anti-CD3 (αCD3) antibody, mimicking TCR activation, would be sufficient to activate IELs to the extend effector functions are observed and test whether the tested mitochondrial properties assessed in Chapter 5 remain at a similar level after IEL activation.

6.1. TCR stimulation is sufficient to activate IELs, resulting in increased mitochondrial mass and Ki-67 expression

Previous publications have used *in vivo* injections of αCD3 antibody in doses from 0.25-200 µg per mouse (Neumann et al., 1992; Ellenhorn et al., 1988; Waters et al., 2009; Swamy et al., 2015; Ogata et al., 2014). One of these publications showed that the percentage of CD3$^+$ cells in the lymph nodes was drastically reduced after injection with 25 ug αCD3 antibody (Neumann et al., 1992), indicating that most T cells in the lymph node have reacted to the antibody. The same αCD3 concentration has been showed to result in reduced viral load in the murine norovirus (MNV) infection model (Swamy et al., 2015). Therefore, I wanted to

test if the dose of 25 ug αCD3 antibody per mouse can activate IELs. To confirm that the dose of αCD3 used affected IELs, I assessed the TCR staining in IELs already four hours post injection. By that time point, I observed a decrease in the staining intensity of both TCR$\alpha\beta^+$ and TCR$\gamma\delta^+$ IELs (Fig 6.1 A), suggesting that αCD3 has reached and affected both TCR$\alpha\beta^+$ and TCR$\gamma\delta^+$ IELs. However, at this time point, I detected no significant difference in MitoTracker Green (MTG) staining compared to non-treated IELs (Fig 6.1 D). Interestingly, an increase in the expression of the lymphocyte activation marker CD44 was observed at this time point (Fig 6.1 B), suggesting that IELs may have become more activated by the treatment. Quantification of CD44^{High} cells showed that there is a statistically significant increase in αCD3-treated IELs compared to non-treated IELs (Fig 6.1 C), Therefore, later time points were assessed.

At 24 and 48 hours post αCD3 stimulation, I observed an increase of MTG staining in IELs to a level similar to that found in splenic CD8α^+ T cells (Fig 6.1 D). By 24 hours post αCD3 stimulation, only TCR$\gamma\delta^+$ CD8$\alpha\beta^+$ and TCR$\alpha\beta^+$ CD8$\alpha\beta^+$ IELs had significantly increased their mitochondrial mass (Fig 6.1 E). These data suggest that the variation in MTG staining observed at 24 hours post αCD3 stimulation is due to TCR$\alpha\beta^+$ CD8$\alpha\beta^+$ IELs. At 48 hours, TCR$\gamma\delta^+$ CD8$\alpha\alpha^+$ and TCR$\alpha\beta^+$ CD8$\alpha\alpha^+$ IELs had also statistically significantly increased their mitochondrial mass. However, TCR$\alpha\beta^+$ CD8$\alpha\beta^+$ IELs remained the IEL subset with the highest increase in MTG staining (Fig 6.1 F). The CD44 staining remained heightened 24 and 48 hours post αCD3 stimulation (Fig 6.1 B-C). Quantification of CD44^{High} cells at 24 and 48 hours post αCD3 stimulation showed statistically significant increase compared to non-treated IELs (Fig 6.1 C).

The TCR staining returned to normal levels by 48 hours (Fig 6.1 A). Another lymphocyte activation marker, CD69, also showed increased expression in IELs at 24 hours post αCD3 stimulation. Interestingly, the increased CD69 expression seemed to be transient as the expression was returned to a lower level in activated IELs at 48 hours post αCD3 stimulation (Fig 6.2). Importantly, all IEL subsets, showed statistically significant increase in their MTG staining, as well as increased CD44 expression, suggesting that the vast majority of IELs had become activated by TCR stimulation.

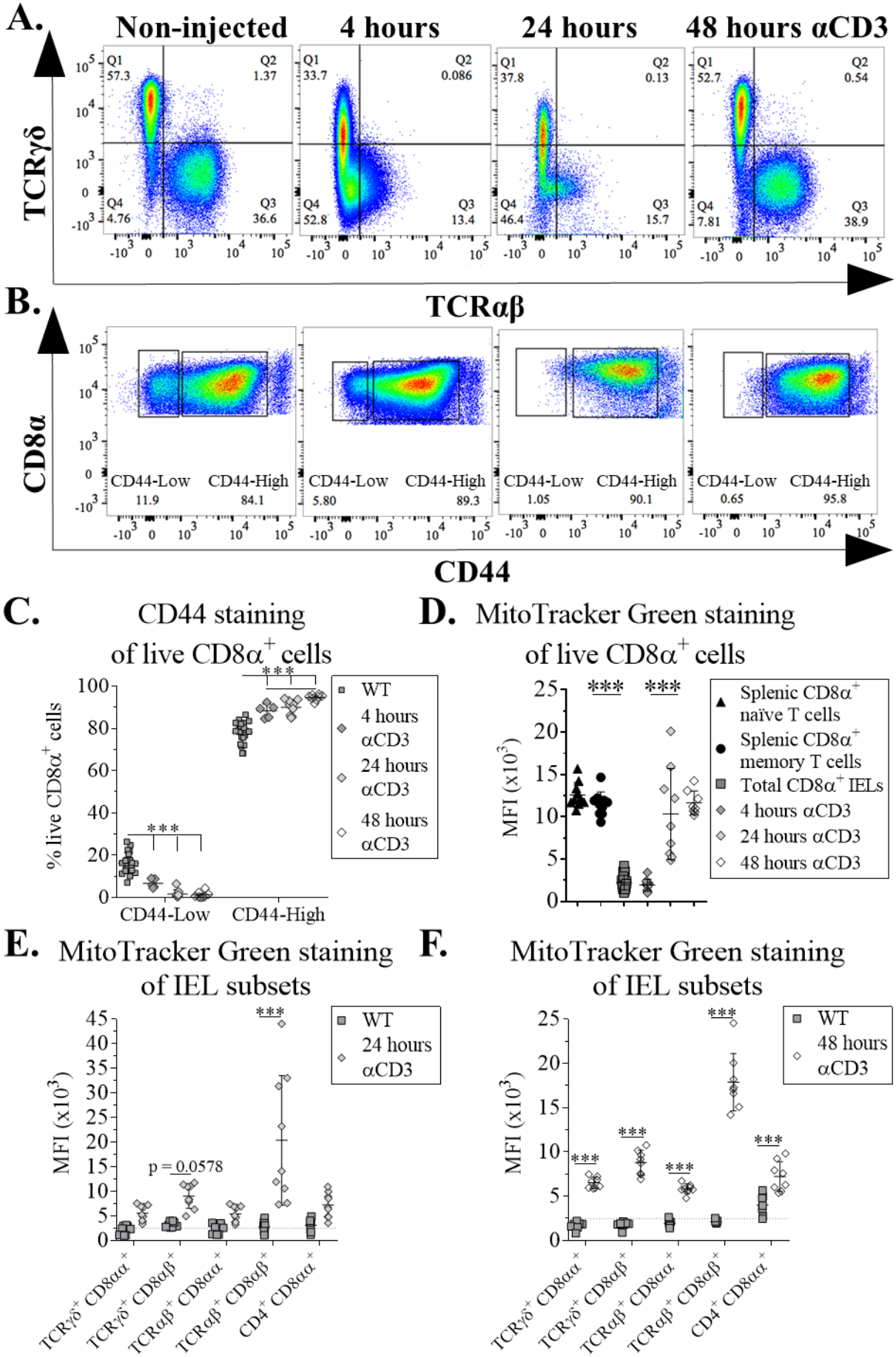

Figure 6.1. TCR stimulation increases mitochondrial mass and CD44 expression in IELs. WT mice were injected with 25 µg αCD3 antibody i.p. IELs and splenic CD8α$^+$ T cells were isolated from non-injected and αCD3-injected mice at the indicated time points. A-B) Representative FACS plots showing A) TCR and B) CD44 staining of live CD8α$^+$ IELs at indicated time points after αCD3 stimulation. C) Quantification of the proportion of CD44^{High} and CD44^{Low} cells in IELs from non-treated and αCD3-treated mice at indicated time points. D-F) Quantification of MTG MFI from D) memory and naïve splenic CD8α$^+$ T cells, non-injected IELs and IELs from αCD3-stimulated mice at indicated time points. E-F) MTG MFI from IEL subsets at indicated time points post αCD3-activation compared to non-injected IELs. Data are presented as mean ± SD from three independent experiments with two to five mice used per condition and experiment. Statistically significant changes were identified by D) one-way ANOVA or C, E, F) two-way ANOVA. ***: p<0.001.

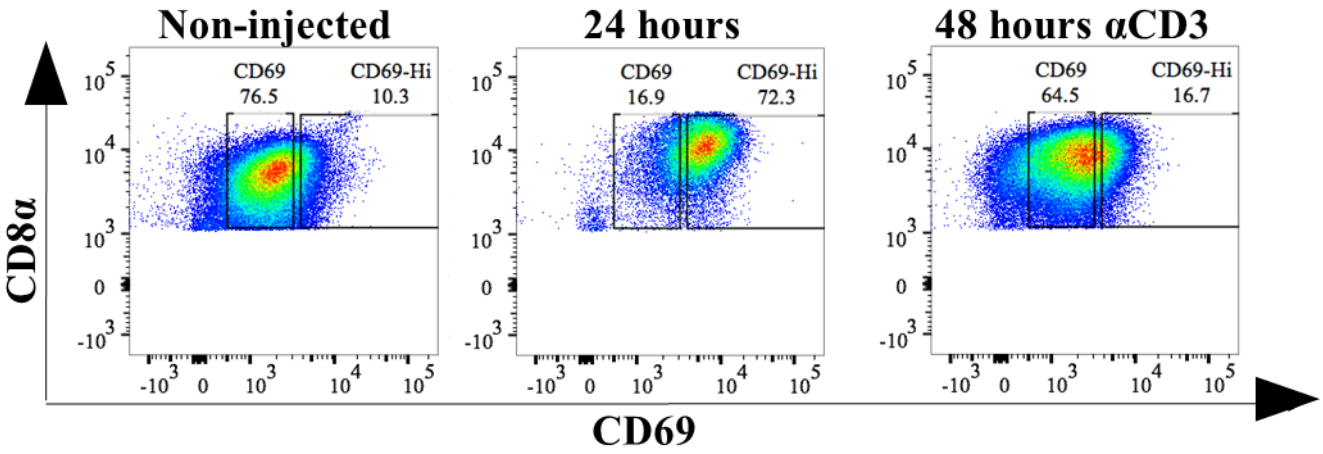

Figure 6.2. TCR stimulation led to transient increase of the activation marker CD69 Representative FACS plots of CD69 staining in total CD8α$^+$ IELs from non-treated and αCD3-treated mice for 24 and 48 hours. These plots are representative of two independent experiments.

In the previous chapter, I showed that non-treated IELs have low secretion of IFNγ and TNFα, as well as limited proliferation, measured by Ki-67 staining (Fig 5.11 B-D). As the mitochondrial mass in IELs increases after αCD3 stimulation, I next wanted to assess whether αCD3 stimulation also enables IELs to secrete IFNγ, TNFα and to proliferate. IELs and splenic CD8α$^+$ T cells were isolated and re-stimulated with PMA, ionomycin and

brefeldin, as previously described in the Material and Methods section. At 24 and 48 hours post αCD3 stimulation, I detected no increase in secretion of TNFα (Fig 6.3 B), but a slight increase in IFNγ secretion (Fig 6.3 A). However, I observed a significant increase in Ki-67 staining (Fig 6.3 C). At 24 hours αCD3 activation, $CD8\alpha\beta^+$ and $CD4^+CD8\alpha\alpha^+$ IELs responded the strongest (Fig 6.3 D), while all IEL subsets showed significant increases in Ki-67 expression at 48 hours post αCD3 stimulation (Fig 6.3 E).

This increase in Ki-67 was more noticeable in $TCR\alpha\beta^+$ $CD8\alpha\beta^+$ IELs, which have statistically significant higher Ki-67 expression than all other IEL subsets, expect $CD4^+CD8\alpha\alpha^+$ IELs (Fig 6.3 E). Next, I wanted to assess if these increases in MTG and Ki-67 could potentially be linked to each other. To do that, I performed Spearman correlation analysis of the proportion of $Ki\text{-}67^+$ IELs and MFI of MTG in total $CD8\alpha^+$ IELs at 48 hours post αCD3 stimulation. The Ki-67 increase correlates significantly with the increase in MTG staining (Fig 6.3 F). Interestingly, this increase in the proliferation marker has yet to show any effect on the numbers of IELs, as fewer IELs are found at 24 and 48 hours post αCD3-injection (Fig 6.3 G). This observation is in line with data obtained from BALB/c mice after αCD3 injection (Ogata et al., 2014). These observations link proliferation to increased mitochondrial mass in IELs. It is interesting to hypothesize that mitochondria may play a role in IEL activation. Whether mitochondrial mass increase is strictly required for IEL proliferation requires further investigations.

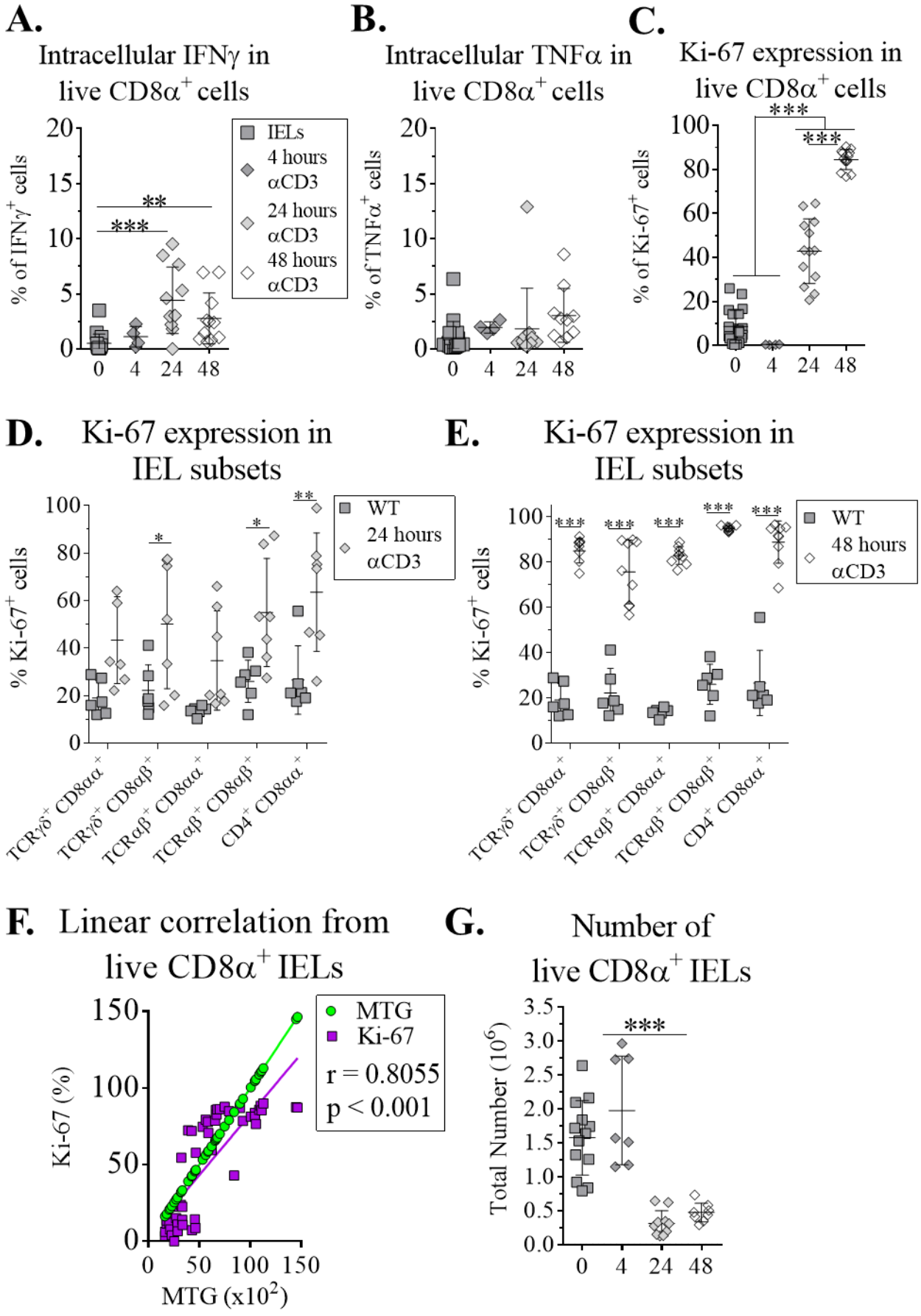

Figure 6.3. TCR stimulation led to increased IEL proliferation, but no cytokine production. WT mice were injected with 25 µg αCD3 antibody i.p. IELs were isolated from non-injected and αCD3-injected mice at the indicated time points. A-C) Quantification of the percentage of A) IFNγ$^+$, B) TNFα$^+$ and C) Ki-67$^+$ from CD8α$^+$ IELs at indicated time points D-E) Quantification of Ki-67$^+$ cells in IEL subsets at D) 24 and E) 48 hours post αCD3 injection. F) Spearman correlation for total CD8α$^+$ IEL in regards to MTG staining and Ki-67 staining. Data from panel F are presented from ten independent experiments with two to five mice used per condition and experiment. G) Quantification of total number of live CD8α$^+$ IELs at the indicated time points after αCD3 injection. Data are presented as mean ± SD from three independent experiments with two to five mice used per condition and experiment. Statistically significant changes were identified by one-way (Panel A-C and G) or two-way (Panel D-E) ANOVA. *: p<0.05., **: p<0.01., ***: p<0.001.

6.2. TCR-activated CD8αβ$^+$ IELs have higher production of mitochondrial ROS

The observed increase in MTG staining in IELs after αCD3-mediated activation invites one to hypothesise about mitochondrial plasticity during IEL activation. As shown in the previous chapter, non-treated IELs have lower mitochondrial membrane potential but higher CL content and similar mitochondrial ROS production to splenic naïve and memory CD8α$^+$ T cells (Fig 5.8-10). Therefore, it would be interesting to assess what potential additional effect(s) αCD3 stimulation may have on these mitochondrial properties. WT Mice were injected with 25 µg αCD3 antibody at indicated time points, IELs isolated and stained for MitoTracker Orange (MTO), MitoSOX and NAO, as previously described in the Materials and Methods section and shown in Figures 5.8-10. I observed that αCD3 activation of IELs also led to increased mitochondrial ROS production at 48 hours post αCD3 stimulation (Fig 6.4 A-C). Interestingly, TCRγδ$^+$ CD8αβ$^+$ IELs appeared to be the first IEL subset to respond (Fig 6.4 B). Moreover, it was only CD8αβ$^+$ IELs that increased mitochondrial ROS production, despite the vast majority of IELs showing an increase in their mitochondrial mass (Fig 6.1 D-F). These data highlight the heterogeneity in IEL activation responses.

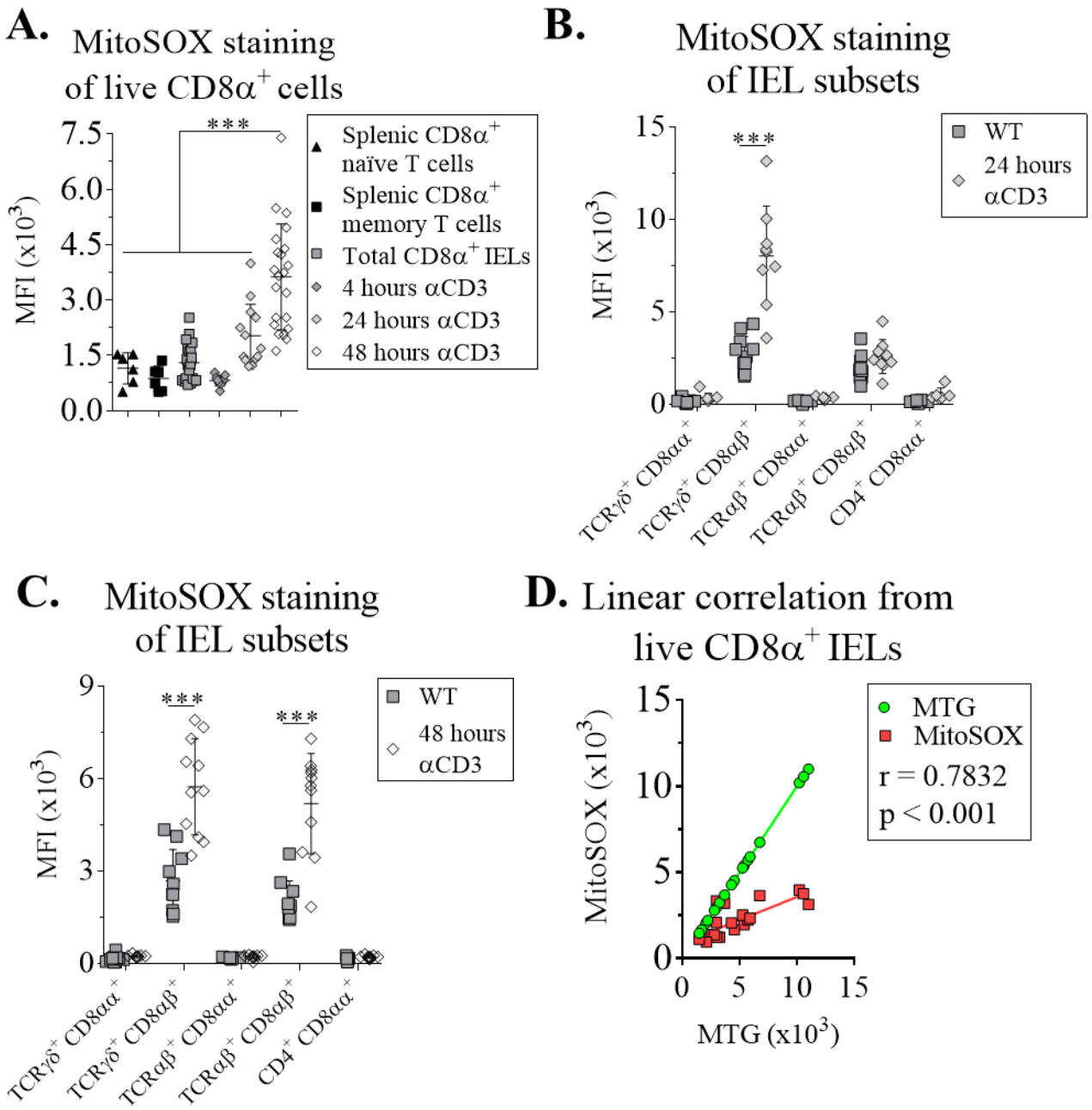

Figure 6.4. TCR-activated IELs have a higher level of mitochondrial ROS production. WT mice were injected with 25 µg αCD3 antibody i.p. IELs and splenic CD8α+ T cells were isolated from steady state and αCD3-stimulated mice, at indicated time points, and stained with MitoSOX. A-C) Quantification of MitoSOX MFI from A) memory and naïve splenic CD8α+ T cells, non-treated and αCD3-treated total CD8α+ IELs and B-C) IEL subsets from αCD3-stimulated mice at the indicated time points. D) Spearman correlation for total CD8α+ IEL in regard of MTG MFI and MitoSOX MFI. Data are presented as mean ± SD from three to five independent experiments with two to three mice per condition and experiment. Statistically significant changes were identified by A) one-way and B-C) two-way ANOVA. ***: p<0.001.

6.3. TCR-activated IELs have unchanged CL content and mitochondrial membrane potential

The increase in mitochondrial ROS production after IEL activation suggests that the mitochondria in CD8αβ$^+$ IELs may have increased OCR, which subsequently leads to increased ROS, or that OXPHOS is less efficient, resulting in increased ROS production. Surprisingly, I detected no statistically significant difference in terms of MTO staining, as a measure of mitochondrial membrane potential, between non-treated and αCD3-activated total CD8α$^+$ IELs (Fig 6.5 B). Interestingly, only TCRαβ$^+$ CD8αβ$^+$ IELs exhibited a statistically significant increase 48 hours after αCD3 activation (Fig 6.5 F). These data suggest that, although the mitochondrial mass in IELs increases (Fig 6.1 D-F), this does not seem to be subsequently lead to changes in mitochondrial membrane potential for the majority of IELs.

Another important feature is the amount of CLs in mitochondria. It has been showed that lack of CLs lead to decreased mitochondrial respiration (Acehan et al., 2011). Interestingly, when assessing the CL content in activated IELs, I observed that this does not change in αCD3-activated IELs (Fig 6.5 A, C and E). This trend applies to all IEL subsets. Data from CL mass spectrometry also support that IELs contain more CLs than splenic naïve CD8α$^+$ T cells, as well as IEL activation does not lead to significant changes in total CL content (Supplemental Figure to 6.5). These data indicate that the total content of CL is unchanged during the increase of mitochondrial mass, assessed by MTG staining. However, it still needs to be determined whether the same CL composition is maintained after αCD3-mediated activation.

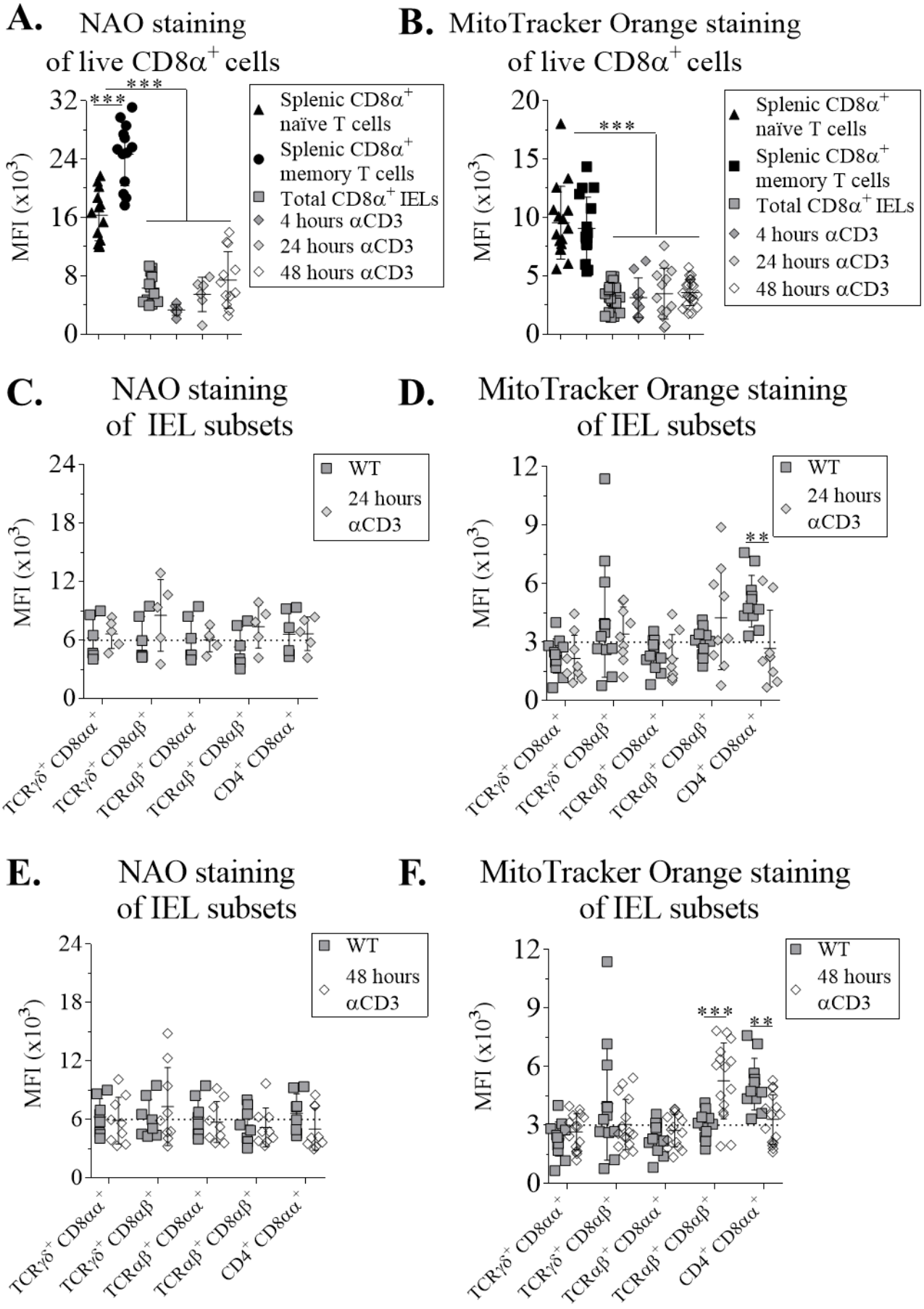

Figure 6.5. TCR-activated IELs have unchanged membrane potential and CL content. WT mice were injected i.p. with 25 µg αCD3 antibody i.p. IELs and splenic CD8α$^+$ T cells were isolated from steady state and αCD3 stimulated mice, at indicated time points, and stained for MTO and NAO. A, C, E) Quantification of NAO MFI from A) memory and naïve splenic CD8α$^+$ T cells and total CD8α$^+$ IELs or C, E) IEL subsets from non-treated and αCD3 stimulated mice at indicated time points. Data are presented as mean ± SD from two to three independent experiments with two to three mice per condition and experiment. B, D, F) Quantification of MTO MFI from B) memory and naïve splenic CD8α$^+$ T cells, steady state total CD8α$^+$ IELs or D, F) IEL subsets from non-treated and αCD3 stimulated mice at indicated time points. Data are presented as mean ± SD from three to six independent experiments with two to four mice per condition and experiment. Statistically significant changes were identified by A-B) one-way or C-F) two-way ANOVA. **: $p<0.01$., ***: $p<0.001$.

6.4. IELs become activated by αCD3 independently of other T cells

One important question to address is whether the response of IELs to αCD3 stimulation is influenced by other T cells, which will also become activated by this method. A hypothetical possibility is that IELs sense cytokines released from other αCD3-activated T cells, such as those found in MLNs and the LP compartment, and do not release cytokines themselves. To address this, I proposed to use IEL transfer into lymphocyte-deficient mice. In that context, IELs will be the only T cells that can respond to αCD3 antibody.

Before the activation assessment, I needed to check how well the different IEL subsets are reconstituted in the lymphocyte-deficient mice in order to have a representative IEL population to study. In addition to using Rag2-/- mice as hosts, there is a study that has used IL-2Rγ-/-Rag2-/- mice as hosts for IEL transfer (Klose et al. 2014). As mentioned in the Introduction (1.3), Rag enzymes are required for TCR and BCR arrangement. As a consequence, Rag2-/- mice lack T and B cells (Shinkai et al., 1992). IL-2Rγ is an essential part of the IL-2, -4, -7, -9, -15 and -21 receptors (Cao et al., 1995a; Asao et al., 2001). IL-

2Rγ-/-Rag2-/- mice are deficient in additional immune cells compared to Rag2-/- mice. As the signalling of previous mentioned cytokines cannot occur, in addition to lack T and B cells, IL-2Rγ-/-Rag2-/- mice have no NK cells (Cao et al., 1995b) and ILCs (Klose et al. 2014). In addition of being deficient in the immune cells, it has been reported that IL-2Rγ-/-Rag2-/- mice lack cryptopatches (Lambolez et al., 2006).

To test if the IEL reconstitution differs in these two host KO mouse lines, 100 000 FACS-sorted $CD8\alpha^+$ IELs per animal were injected into Rag2-/- and IL-2Rγ-/-Rag2-/- mice. The transferred IELs were in these host mice for three weeks prior to IEL isolation. Interestingly, I observed that IL-2Rγ-/-Rag2-/- mice had better IEL reconstitution than Rag2-/- mice in terms of IEL subset composition (Fig 6.6 A-F). When quantifying the distribution of the four main IEL subsets of the transferred IELs in Rag2-/- and IL-2Rγ-/-Rag2-/- mice and comparing them to the IEL subset distribution in WT mice (Fig 6.6 G), I observed that the IEL distribution in IL-2Rγ-/-Rag2-/- mice is more similar to WT mice compared to the IEL distribution in Rag2-/- mice (Fig 6.6 H). Of note, very few $CD4^+$ $CD8\alpha\alpha^+$ IELs were found in either type of recipient mice. Hence, data from this IEL subset are not reported in Figure 6.6 and 6.7.

As showed previously in Figure 4.9 D, the number of IELs reconstituted in IL-2Rγ-/-Rag2-/- mice is higher compared to Rag2-/- mice. In addition, it is only the transferred IELs in the IL-2Rγ-/-Rag2-/- hosts that showed increased number from the 100 000 IELs that were initially transferred (Fig 4.9 D). However, the number of IELs in the transferred Rag2-/- and IL-2Rγ-/-Rag2-/- mice is lower than the number of IELs found in WT mice. In WT mice, the lowest number of IELs that I have reported in this thesis is around $1x10^6$ cells (Fig 6.3 G and Fig 7.24 G), which is higher than the highest reported number of transferred IELs in IL-2Rγ-/-

Rag2-/- mice, that is around $0.5x10^6$ cells (Fig 4.9 D). Therefore, I decided to use IL-2Rγ-/-Rag2-/- mice as hosts for the IEL transfer activation experiment.

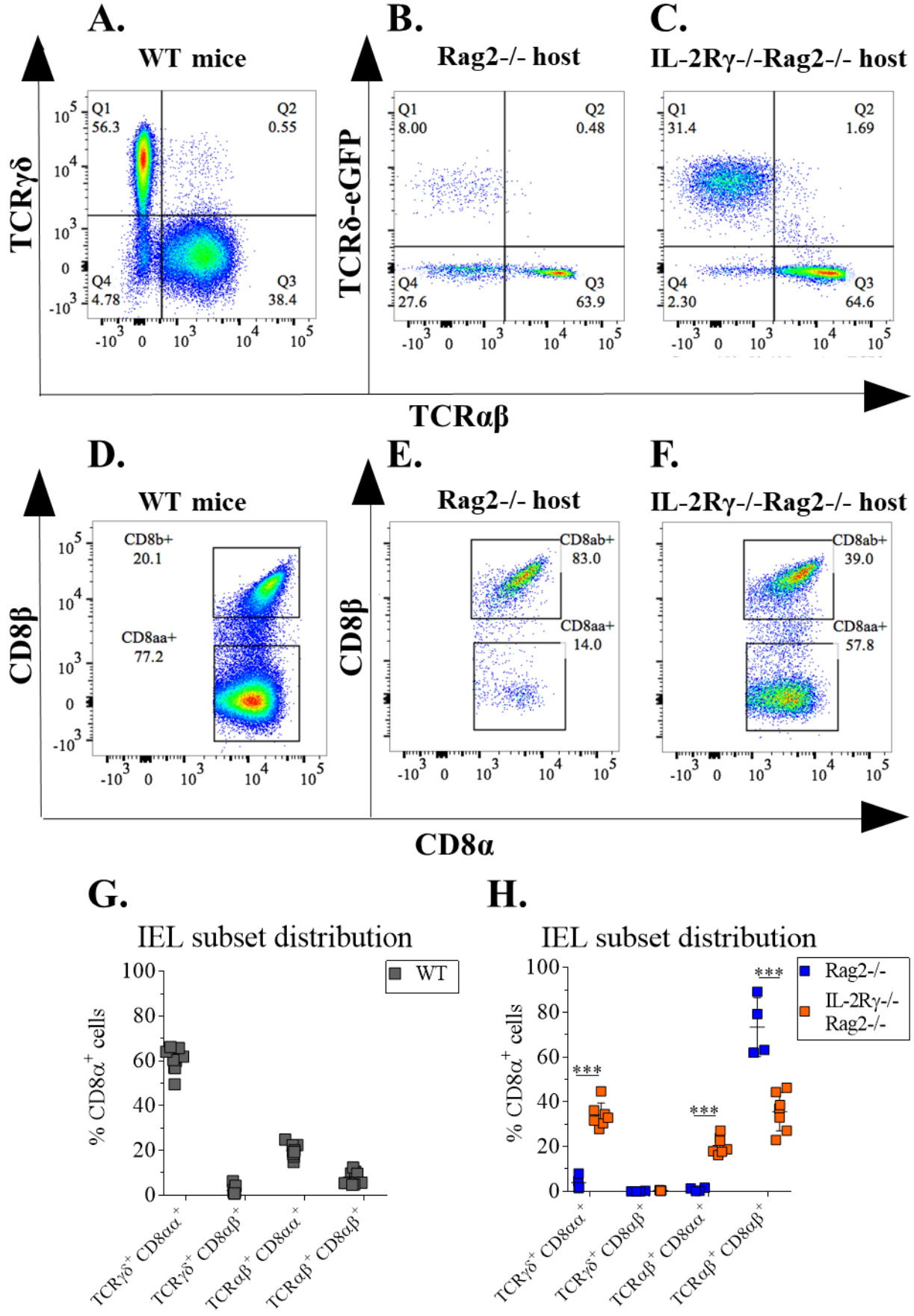

Figure 6.6. IEL transfer into IL-2Rγ-/-Rag2-/- mice generated a more representative IEL population compared to Rag2-/- mice. 100 000 FACS-sorted CD8α+ IELs were injected i.v. into Rag2-/- and IL-2Rγ-/-Rag2-/- mice. Three weeks post transfer, IELs were isolated from these mice. A-C) Representative FACS plots showing TCRαβ and TCRγδ staining. D-F) Representative FACS plots showing CD8β and CD8α staining to identify $CD8\alpha\beta^+$ and $CD8\alpha\alpha^+$ populations from indicate mouse line. For the WT IELs, pre-gating was made on live CD8α+ cells. As hosts were on a CD45.1 background, pre-gating was made on live $CD45.2^+$ $CD8\alpha^+$ cells for Panels B, C, E and F. These plots are representative of four independent experiments. G-H) Quantification of the four main IEL subsets in G) WT mice and H) IELs transferred into Rag2-/- and IL-2Rγ-/-Rag2-/- mice. Data are presented as mean ± SD from two independent experiments with two to five mice per condition and experiment. Statistically significant changes were identified by two-way ANOVA for panel H. ***: $p<0.001$.

IL-2Rγ-/-Rag2-/- mice cannot generate their own T cells, hence comparing IEL transfer with or without αCD3 stimulation will provide insights into the effects αCD3 antibody has directly on IELs, as well as give an indication of whether any effects seen in WT mice may be mediated by other T cells. 100 000 $CD8\alpha^+$ IELs per mouse were injected i.v. into IL-2Rγ-/-Rag2-/- mice. Three weeks post IEL transfer, one set of mice received αCD3 antibody i.p., while the other set of mice did not receive any injection. All mice were culled for analysis two days after αCD3 injection. I observed that the αCD3-activated IELs had a significant increase in Ki-67 expression (Fig 6.7 A), which applied to the four main IEL subsets as well (Fig 6.7 B). Interestingly, similar numbers of IELs were found in αCD3-treated and non-treated mice (Fig 6.7 C). This would suggest that the reduced number of IELs observed in WT mice that received αCD3 antibody is dependent on other T cells and not an intrinsic mechanism in IELs during the activation. Moreover, the Ki-67 response was lower compared to WT mice injected with the same dose of αCD3 and analysed at the same time point (Fig 6.3 C-E). WT mice injected with the same dose of αCD3 showed a reduction in the number of total $CD8\alpha^+$ IELs compared to non-injected controls (Fig 6.3 G). These data indicate that

the response of other T cells to αCD3 activation may influence the response of IELs, such as the number of IELs after activation.

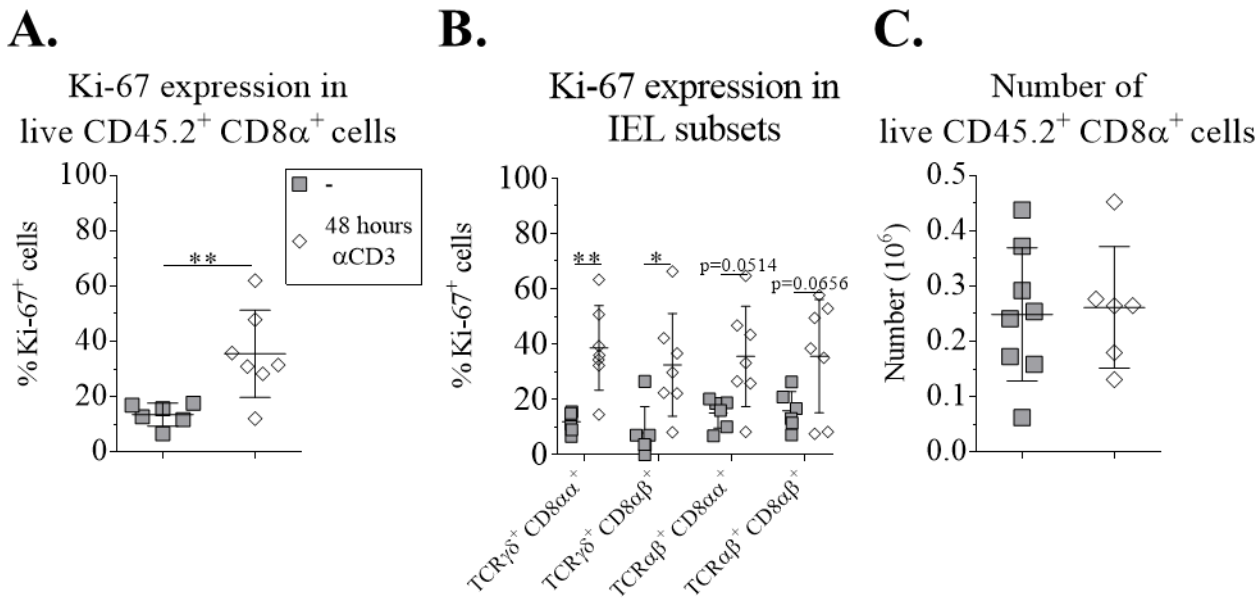

Figure 6.7. IELs respond directly to αCD3 activation. 100 000 sorted CD8α$^+$ IELs were transferred into IL-2Rγ-/-Rag2-/- mice. Three weeks after the IEL transfer, one set of mice were injected i.p. with 25 µg αCD3 antibody. Two days after αCD3 injection, IEL were isolated, quantified and stained for Ki-67. A-B) Percentage of Ki-67$^+$ IELs from A) total CD8α$^+$ IELs or B) the four main IEL subsets from non-treated and αCD3-treated mice. C) Quantification of total CD8α$^+$ IELs from non-treated and αCD3-treated mice. Data are presented as mean ± SD from two independent experiments with two to four mice per condition and experiment. Statistically significant changes were identified by unpaired t-test for Panel A and C and by two-way ANOVA for Panel B. *: p<0.05., **: p<0.01.

6.5. Co-stimulatory CD28 is not sufficient to trigger cytokine production in IELs

After observing that αCD3 activation led to an increase in MTG staining in IELs (Fig 6.1 D-F), but no cytokine production (Fig 6.3 A-B), I next asked what additional signal(s) are required for cytokine production from IELs. A co-stimulatory molecule for other T cells is CD28 engagement, of which can lead to increased cytokine production (Klein Geltink et al., 2017). CD28 is expressed on CD8αβ$^+$ IELs, but not on TCRγδ$^+$ IELs (Ohteki and

MacDonald, 1993). Therefore, I next tested whether αCD28 could be an additional signalling receptor for IELs, particularly for CD8αβ$^+$ IELs.

WT mice were injected i.p. with either αCD3 antibody or a combination of αCD3 and αCD28 antibodies and analysed 48 hours post injection. IELs were isolated and stained for MTG, MitoSOX and the cytokines IFNγ and TNFα. In the cytokine assessment, I observed no increase in either cytokine in IELs co-injected with αCD3 and αCD28 compared to αCD3 (Fig 6.8 A-B.) These data suggest that there are other factors missing in order to stimulate IELs to secrete cytokines. However, I observed statistically significant changes in terms of Ki-67 expression (Fig 6.8 C) for TCRγδ$^+$ CD8αβ$^+$ IELs only (Fig 6.8 D).

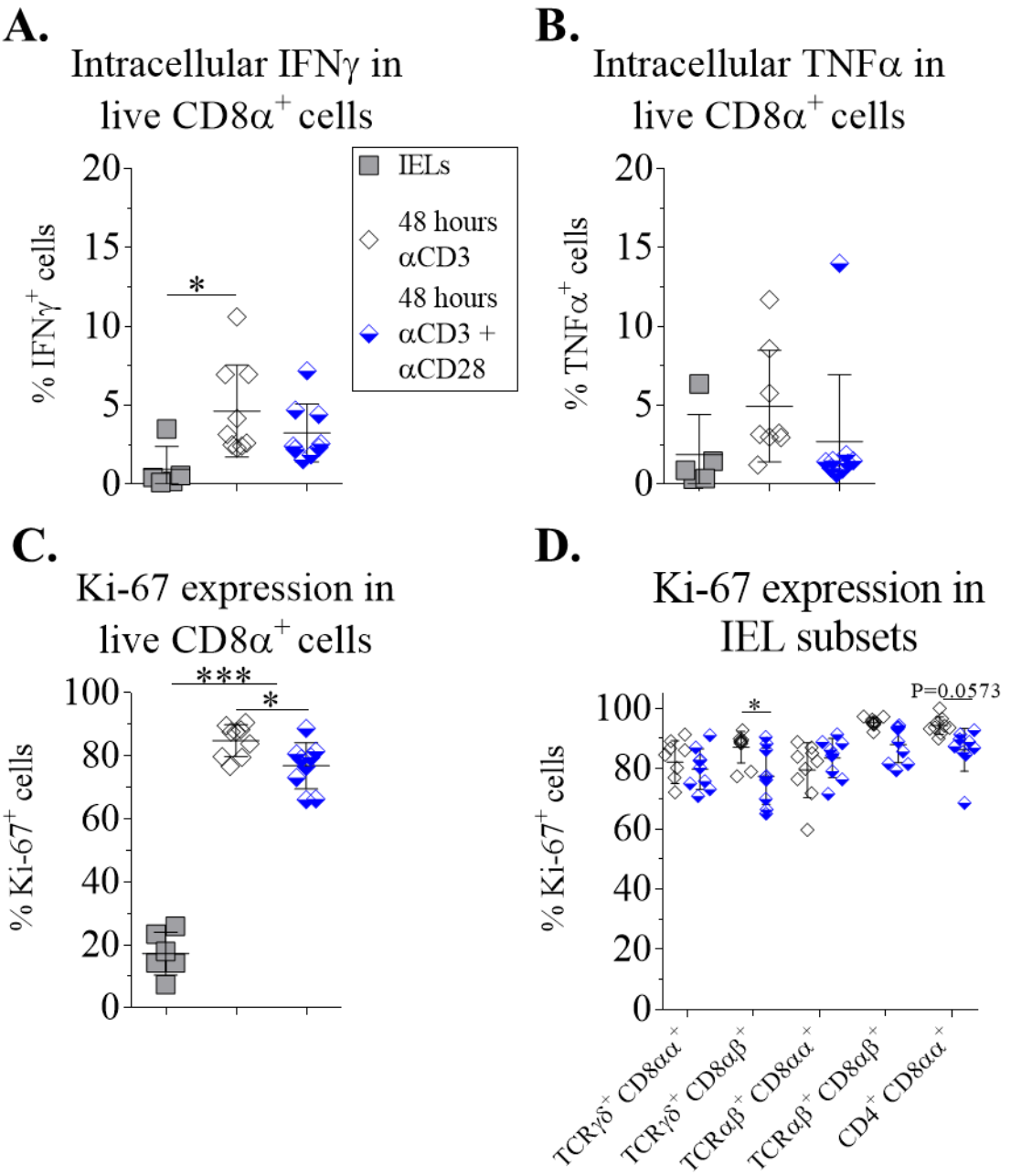

Figure 6.8. Co-stimulatory CD28 does not lead to cytokine production in IELs. WT mice were injected i.p. with 25 µg αCD3 antibody or a combination of 25 µg αCD3 and 25 µg αCD28 antibodies. IELs were isolated from non-injected and injected mice at 48 hours post injection and stained for intracellular cytokine staining. A-C) Quantification of the percentage of A) IFNγ$^+$, B) TNFα$^+$ and C) Ki-67$^+$ cells from total CD8α$^+$ IELs from indicated condition. D) Quantification of the percentage of Ki-67$^+$ cells from IEL subsets at 48 hours post injection. Data are quantified as mean ± SD from three independent experiments with two to three mice used per condition and experiment. Statistically significant changes were identified by one-way ANOVA (Panel A-C) and two-way ANOVA (Panel D). *: $p<0.05$., ***: $p<0.001$.

When assessing the MTG staining in αCD3 or αCD3 and αCD28 conditions, I observed no significant difference for total CD8α$^+$ IELs (Fig 6.9 A) and IEL subsets (Fig 6.9 C) at 48 hours post injection. The same trend applied to CD44 staining (Fig 6.9 E).

As I have previously observed that CD8αβ$^+$ IELs specifically produce mitochondrial ROS and CD8αβ$^+$ IELs are the subsets suggested to express CD28, I assessed MitoSOX levels for one of the CD28 experiments. These preliminary data suggest that at 48 hours post stimulation, there is a significant difference between αCD3- and αCD3+αCD28-stimulated IELs (Fig 6.9 D). Interestingly, these preliminary data suggest that TCRαβ $^+$ CD8αβ$^+$ IELs have significantly higher mitochondrial ROS production when stimulated with αCD3 and αCD28 antibodies (Fig 6.9 D). Collectively, these data indicate no essential role for CD28 for TCR-mediated IEL activation, despite data from Figure 6.7 indicating that other T cells may influence IEL activation responses.

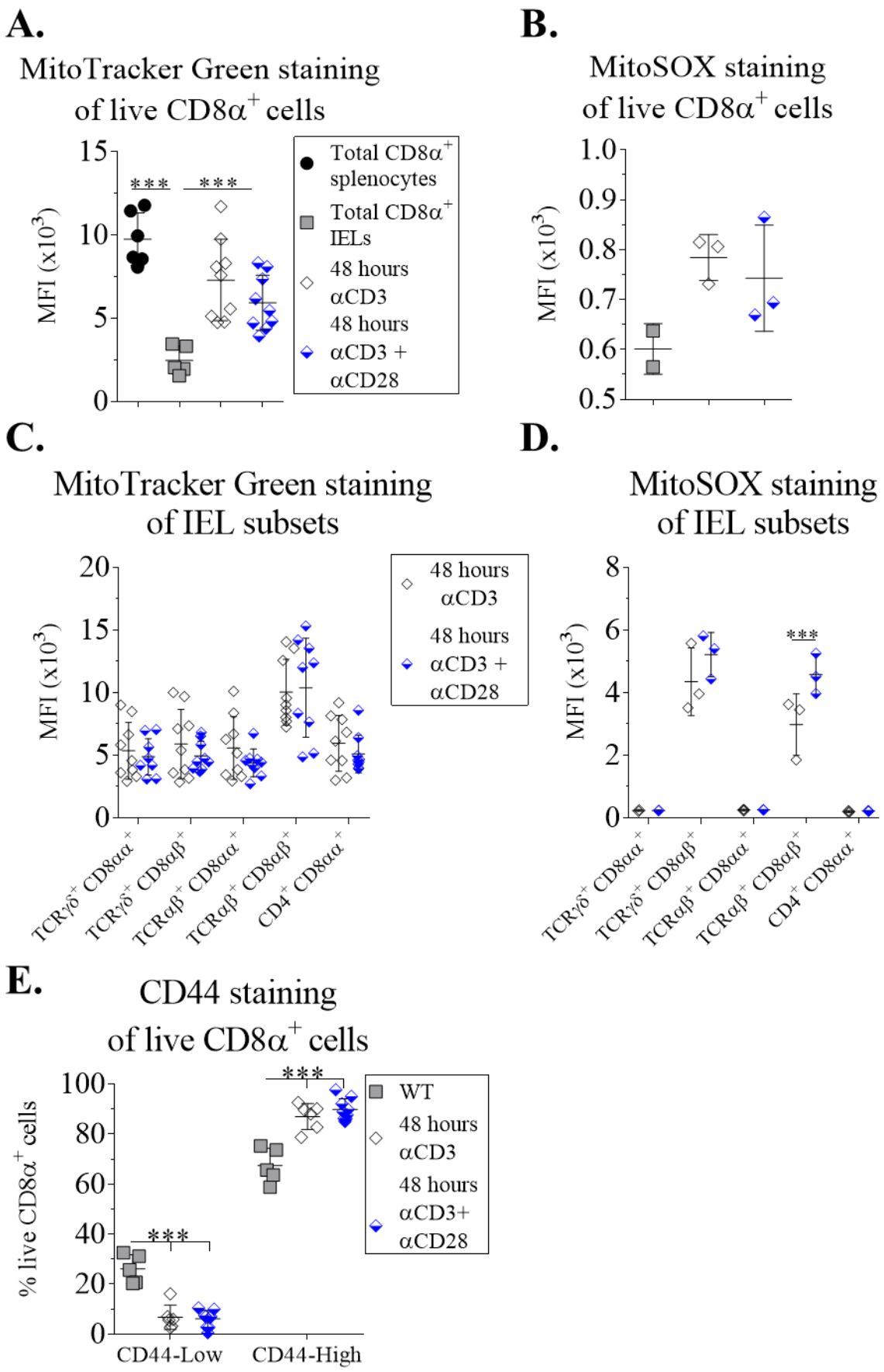

Figure 6.9. Co-stimulatory CD28 does not alter TCR-mediated IEL activation. WT mice were injected i.p. with 25 µg αCD3 antibody or a combination of 25 µg αCD3 and 25 µg αCD28 antibodies. IELs and splenic $CD8\alpha^+$ T cells were isolated from non-injected and injected mice, at the indicated time point, and stained for MTG and MitoSOX. A-B) Quantification of A) MTG or B) MitoSOX MFI for memory and naïve splenic $CD8\alpha^+$ T cells, steady state IELs. C-D) Quantification of C) MTG or D) MitoSOX MFI for IEL subsets. Data are presented as mean ± SD from one (Panel B+D) and three (Panel A+C) independent experiments with two to three mice used per condition and experiment. Statistically significant changes were identified by one-way (Panel A-B) or two-way ANOVA (Panel C-E). ***: $p<0.001$.

6.6. Mechanistic insights behind the mitochondrial changes in IELs during TCR-stimulated activation

After the observations from this chapter and Chapter 5, two important questions arise. Firstly, what are the determining conditions that set IELs into this mitochondrial compromised state in regards of mitochondrial mass, membrane potential and cardiolipin content? Secondly, which signalling pathways enable mitochondrial remodelling during IEL activation, resulting in an increase in mitochondrial mass?

There are numerous factors that have been suggested to be important for IEL maintenance, such as T-bet (Klose et al. 2014; Reis et al. 2014), Eomes (Klose et al. 2014) and AhR (Li et al., 2011). In the following sections, I will describe a series of experiments, the aim of which was to assess the steady state IELs in mice that have deficiency in these factors, as well as assessing if they are capable of remodelling their mitochondria after αCD3 stimulation, as observed with WT IELs. For the assessments, the time point of 48 hours post injection has been used.

6.7. T-bet-deficient IELs may have a higher threshold to enable increase in mitochondrial mass during activation

As mentioned in the introduction to IELs (see section 1.6.2), mice deficient in T-bet have altered IEL subset composition, with fewer TCR$\gamma\delta^+$ IELs (Klose et al. 2014; Reis et al. 2014). T-bet is a T-box factor encoded by the gene Tbx21. TCR activation and IL-12R stimulation are known to induce T-bet expression. IL-12R is expressed on IELs (Fahrer et al., 2001; Shires et al., 2001). T-bet is also expressed on a range of immune cells such as ILCs, B cells, Th1 cells, effector CD8α^+ T cells and TCR$\gamma\delta^+$ T cells (Lazarevic et al., 2013). Naïve splenic CD4$^+$ and TCR$\gamma\delta^+$ T cells lack T-bet expression (Yin et al., 2002), while all the four main IEL subsets express it (Klose et al. 2014). As T-bet can be induced by TCR activation, the question is whether T-bet may be involved in the activation response of IELs.

For the assessment, I used Rag1-Cre-Tbx21$^{fl/fl}$-RFP mice, which selectively deplete T-bet in Rag-dependent lymphocytes. I observed that control IELs from these mice had similar levels of MTG staining to WT IELs (Fig 6.10 A), except in TCR$\alpha\beta^+$ CD8$\alpha\beta^+$ IELs (Fig 6.10 C). These data suggest that T-bet-dependent pathways are not crucial to set IEL into a state with low mitochondrial mass. Interestingly, αCD3 injection of Rag1-Cre-Tbx21 mice generated intriguing results. In one experiment, I observed a decrease in the ability to increase MTG staining in IELs from these mice. This affected all IEL subsets (Fig 6.10 A and E, data points in red border colour). The same mice showed an increase in Ki-67 response, indicating that the mice had received their αCD3 antibody as expected (Fig 6.10 B and F). In addition, these data indicate that a Ki-67 increase is possible in the context of a lack of mitochondrial mass increase. However, in the repeat experiment I observed an increase in MTG staining in IELs from Rag1-Cre-Tbx21$^{fl/fl}$-RFP mice (Fig 6.10 A and E, data points in blue border colour). These data suggest that T-bet may not be strictly required for mitochondrial mass increase

during αCD3-medaited activation but may be involved in the threshold to enable this αCD3-mediated increase of MTG staining. This threshold may not have been reached in the first experiment but may have been in the second experiment.

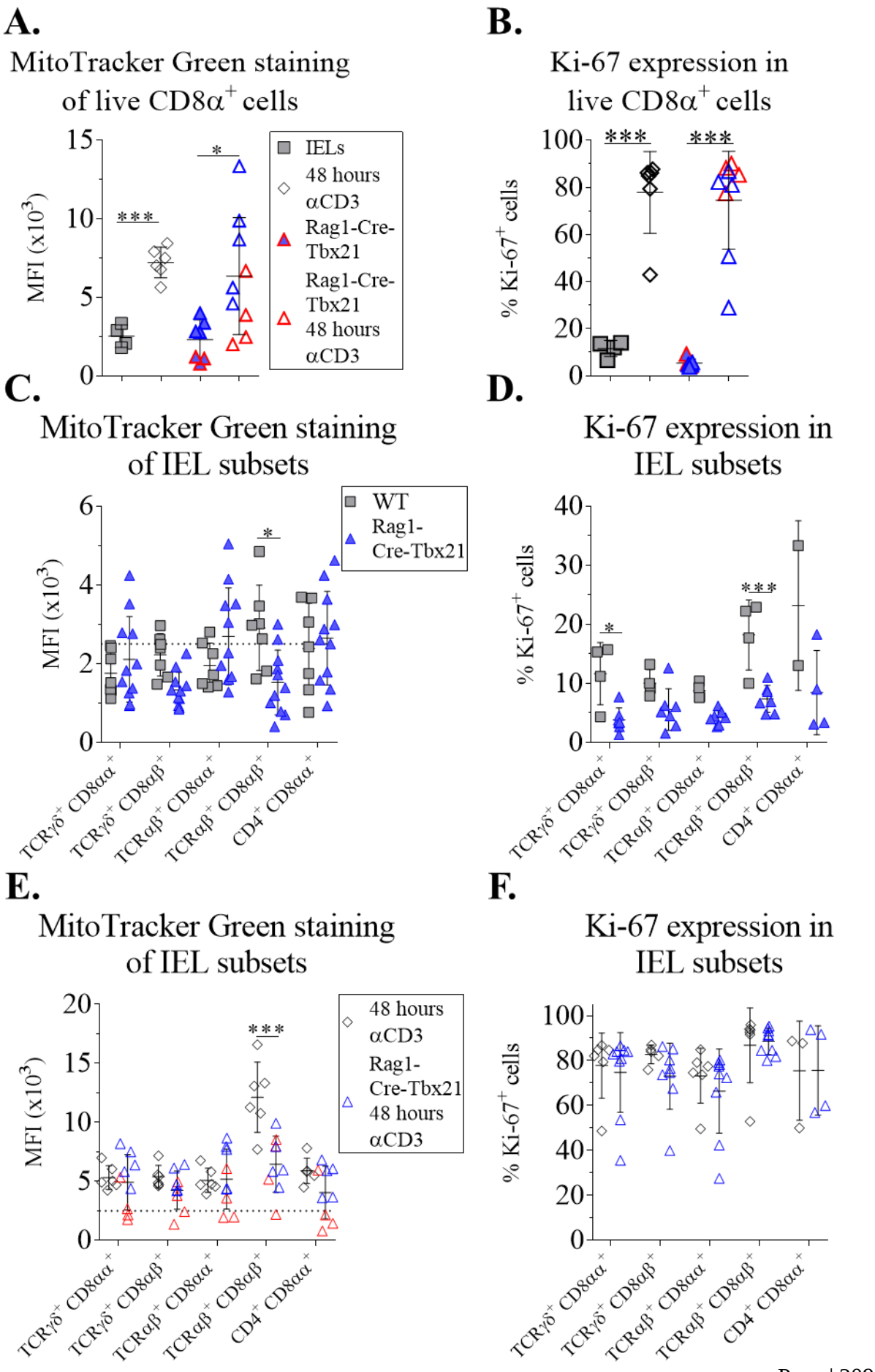

Figure 6.10. T-bet-deficient IELs may have a higher threshold to enable increase in mitochondrial mass during activation. WT and Rag1-Cre-Tbx21$^{fl/fl}$-RFP mice were injected i.p. with 25 µg αCD3 antibody. IELs were isolated from non-injected and αCD3-injected mice at 48 hours post injection and stained with MTG and Ki-67 antibody, as previously described. A, C, E) Quantification of MTG MFI from A) total CD8α$^+$ IELs from non-injected and αCD3-injected mice, C) non-treated IELs subsets and E) IEL subsets at 48 hours post injection. B, D, F) Ki-67 staining from B) total CD8α$^+$ IELs at steady state or 48 hours post αCD3 injection, D) non-treated IEL subsets and F) IEL subsets at 48 hours post injection. Data are presented as mean ± SD from two to three (Panel C) independent experiments with two to five mice per condition and experiment. Statistically significant changes were identified by one-way ANOVA (Panel A-B) or two-way ANOVA (Panel C-F). *: p<0.05., ***: p<0.001.

6.8. Eomes is dispensable to enable increase in mitochondrial mass and Ki-67 expression in IELs during activation

Another T-box factor is Eomesodermin (Eomes). Eomes is expressed in naïve CD8α$^+$ T cells (Yang et al., 2008; Pearce et al., 2003) as well as in IELs (Klose et al. 2014). It has been demonstrated that both T-bet and Eomes can induce IFNγ production (Pearce et al., 2003), suggesting that Eomes may complement T-bet-induced functions. As the experiments with T-bet showed conflicting results, I wanted to test if whether could gain any clarity by using Rag1-Cre-Eomes$^{fl/fl}$-RFP mice.

When assessing these mice, I observed that they have similar level of MTG staining as WT IELs (Fig 6.11 A), except for TCRαβ $^+$ CD8αβ$^+$ IELs (Fig 6.11 C). This is the same IEL subset that had a significantly lower MTG staining in Rag1-Cre-Tbx21$^{fl/fl}$-RFP mice (Fig 6.10 C). Overall, these data suggest that Eomes is not essential to set IELs into this mitochondrial state. When activating IELs in Rag1-Cre-Eomes$^{fl/fl}$-RFP mice with αCD3 antibody, I observed no differences compared to WT IELs in terms of MTG staining (Fig

6.11 A) except for TCRαβ^{+} CD8αβ^{+} IELs (Fig 6.11 E). In terms of Ki-67 response, there was not statistically significant difference (Fig 6.11 B), except for CD4^{+} CD8αα^{+} IELs (Fig 6.11 F). These data suggest that Eomes is dispensable for mitochondrial mass increase and the Ki-67 response, induced by αCD3 antibody injection. Together, these data suggest that, whether or not T-bet is involved in the increase of IEL mitochondrial mass, it is independent of Eomes.

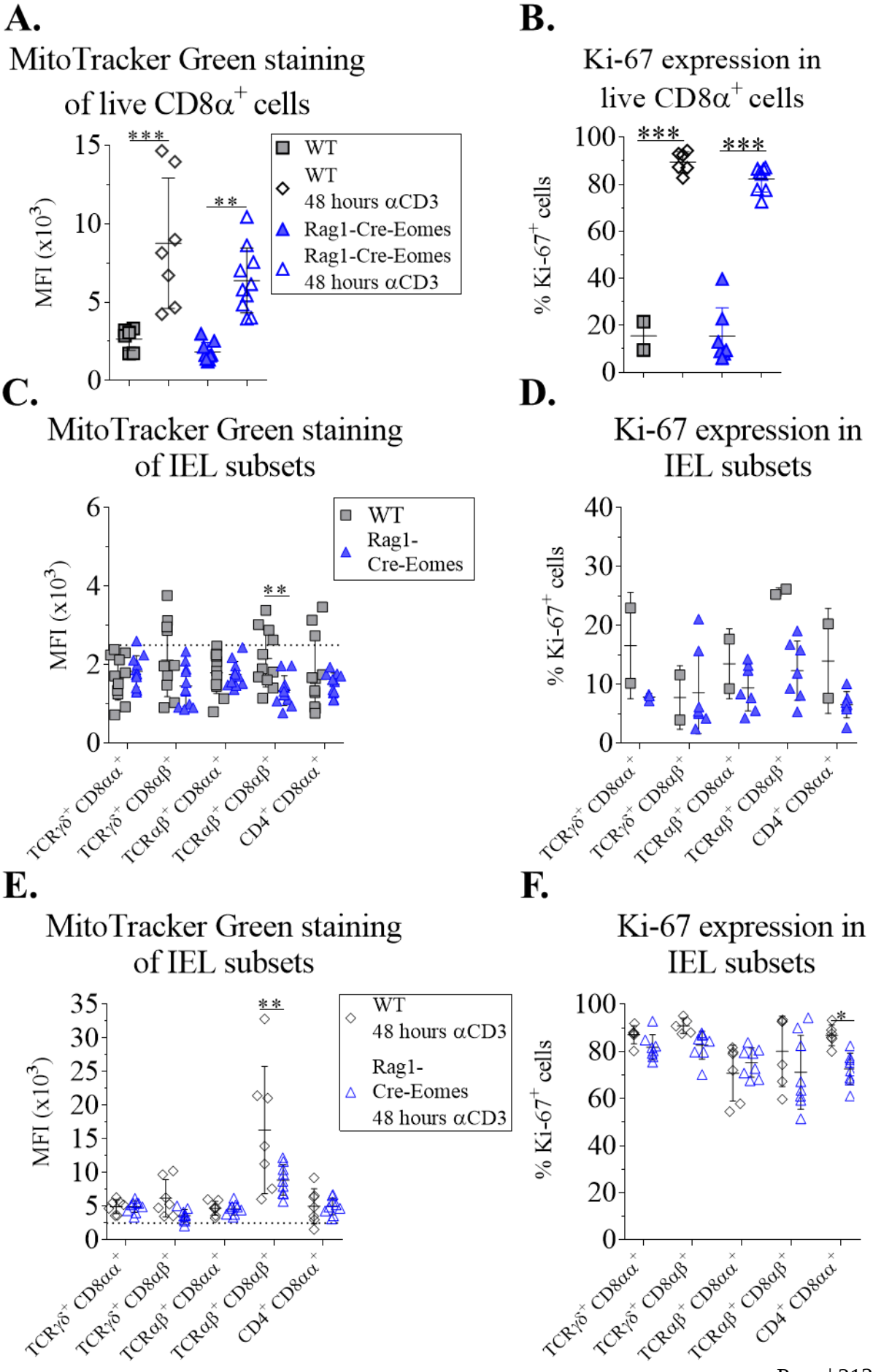

Figure 6.11. Eomes is dispensable to enable increase in mitochondrial mass and Ki-67 expression during activation. WT and Rag1-Cre-Eomes$^{fl/fl}$-RFP mice were injected i.p. with 25 µg αCD3 antibody. IELs were isolated from non-injected and αCD3-stimulated mice at 48 hours post injection and stained for MTG and Ki-67 staining, as previously described. A, C, E) Quantification of MTG MFI from A) total CD8α$^+$ IELs at 48 hours post αCD3 injection, C) non-treated IEL subsets and E) IEL subsets at 48 hours post αCD3 injection. B, D, F) Ki-67 staining from B) control total CD8α$^+$ IELs or at 48 hours post αCD3 injection, D) non-treated IEL subsets and F) IEL subsets at 48 hours post αCD3 injection. Data are presented as mean ± SD from two to three (Panel C) independent experiments with two to five mice per condition and experiment. Statistically significant changes were identified by one-way ANOVA (Panel A-B) or two-way ANOVA (Panel C-F). **: p<0.01., ***: p<0.001.

6.9. AhR may be involved in the threshold to enable MTG increase in IELs

AhR is a transcription factor that has been shown to be important for IEL maintenance, as AhR-/- mice have significantly fewer IELs (Li et al., 2011). The current AhR signalling model consists of AhR in the cytoplasm in a complex with AhR interacting protein (AIP), heat shock protein 90 (Hsp90) and p23. Upon ligand binding, the complex is released from AIP and transfers to the nucleus. In the nucleus, the complex associates with AhR nuclear translocator (Arnt). This complex binds to dioxin response element (DRE) elements leading to transcription of e.g. AhR repressor (AhRR) and Cyp1 enzymes. AhRR prevents complex formation with Arnt, while Cyp1 enzymes break down the AhR ligands (Stockinger et al., 2014). The role of AhR and its downstream targets in IEL activation is still unknown. Therefore, in the next sections, I will describe experiments to test the role of AhR, AhRR and Cyp1 enzymes in IEL activation.

For this assessment, I first used AhR-/- mice. For steady state IELs, similar levels of MTG staining were observed in WT and KO-mice (Fig 6.12 A and C). Interestingly, I obtained similar results regarding αCD3-induced activation as for Rag1-Cre-Tbx21-RFP mice (Fig

6.10 A and E): in one experiment, AhR-/- IELs failed to increase MTG staining (data point with red border line), but in the second experiment, they did (data points with blue border line) (Fig 6.12 A and E). The same trend was observed regarding Ki-67 response, which was increased in both cases (Fig 6.12 B and F). This again highlights that there appear to be ways for IELs to start proliferating extensively, independent of mitochondrial mass increase. An alternative is that the Ki-67 increase occurs prior to the increase in mitochondrial mass.

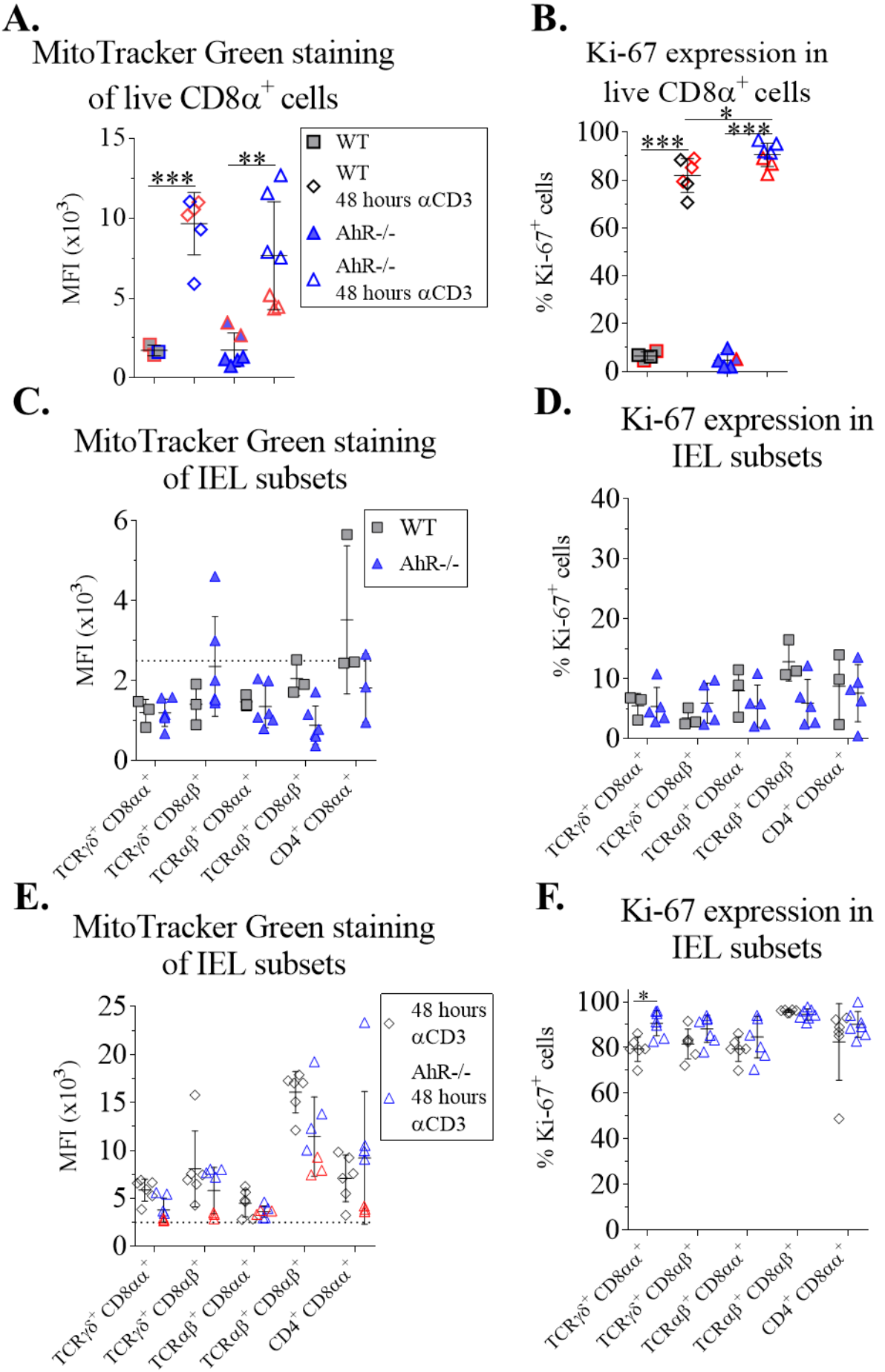

Figure 6.12. AhR may be involved in the threshold to enable MTG increase in IELs. WT and AhR-/- mice were injected i.p. with 25 µg αCD3 antibody. IELs were isolated from non-injected and αCD3-stimulated mice at 48 hours post αCD3 injection and stained for MTG and Ki-67 staining, as previously described. A, C, E) Quantification of MTG MFI from A) control total CD8α$^+$ T cells and total CD8α$^+$ IELs or indicated time point post αCD3 injection, C) non-treated IEL subsets and E) IEL subsets at 48 hours post αCD3 injection. B, D, F) Ki-67 staining from B) total CD8α$^+$ IELs at steady state or indicated time point post αCD3 injection, D) non-treated IEL subsets and F) IEL subsets at 48 hours post αCD3 injection. Data are presented as mean ± SD from two independent experiments with two to four mice per condition and experiment. Statistically significant changes were identified by one-way ANOVA (Panel A-B) or two-way ANOVA (Panel C-F). *: $p<0.05$., **: $p<0.01$., ***: $p<0.001$.

6.10. AhRR is dispensable in the TCR-mediated activation response in IELs

As mentioned above, AhRR is an important factor to reduce AhR signalling by preventing AhR-Arnt complex formation. Hence, I wanted to see if I could obtain clarifying evidence from Rag1-Cre-AhRR$^{fl/fl}$-RFP mice, to support the data obtained from AhR-/- mice. Control IELs from Rag1-Cre-AhRR$^{fl/fl}$-RFP mice had similar levels of MTG staining as WT IELs (Fig 6.13 A and C). Using αCD3 antibody injection to stimulate IELs from Rag1-Cre-AhRR$^{fl/fl}$-RFP mice, I observed that MTG increases in a similar manner to WT IELs (Fig 6.13 A and E). When assessing Ki-67 response, I observed no significant difference in the Ki-67 response (Fig 6.13 B and F). Collectively, these data indicate no essential role for AhRR in TCR-mediated IEL activation.

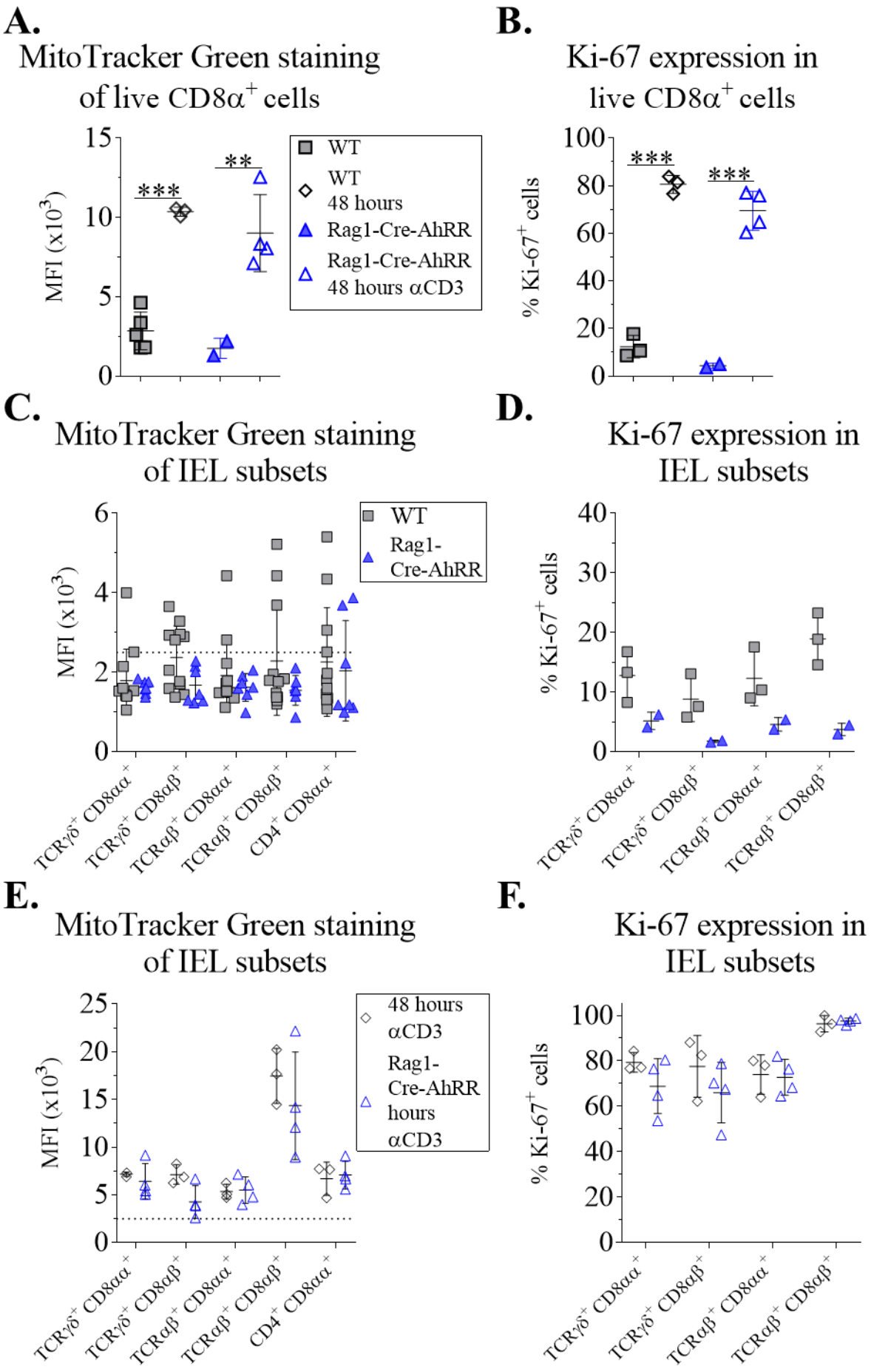

Figure 6.13. AhRR is dispensable for MTG increase and Ki-67 response. WT and Rag1-Cre-AhRR$^{fl/fl}$-RFP mice were injected i.p. with 25 µg αCD3 antibody. IELs were isolated from non-injected and αCD3-stimulated mice at 48 hours post αCD3 injection and stained for MTG and Ki-67 staining, as previously described. A, C, E) Quantification of MTG MFI from A) control total CD8α$^+$ T cells and total CD8α$^+$ IELs at 48 hours post αCD3 injection, C) non-treated IEL subsets and E) IEL subsets at 48 hours post αCD3 injection. B, D, F) Ki-67 staining from B) total CD8α$^+$ IELs at steady state or 48 hours post αCD3 injection, D) non-treated IEL subsets and F) IEL subsets at 48 hours post αCD3 injection. Data are presented as mean ± SD from one to three (Panel C) independent experiments with two to four mice per condition and experiment. Statistically significant changes were identified by one-way ANOVA (Panel A-B) or two-way ANOVA (Panel C-F). **: p<0.01., ***: p<0.001.

6.11. Cyp1a enzymes are involved in the αCD3-mediated Ki-67 response

AhR can affect the expression of Cytochrome P450 enzymes (Cyp) , Cyp1A1, 1A2 and 1B1 (Ciolino et al., 1999). These have been reported to be located in both mitochondria and the endoplasmic reticulum (ER) (Dong et al., 2013). Like AhRR, Cyp enzymes can reduce AhR signalling, in their case by breaking down AhR ligands.

For the assessment, I used Cyp1A1, 1A2 and 1B triple-/- mice (Cyp1aT-/-). Control IELs from Cyp1aT-/- mice show similar levels of MTG staining to WT IELs (Fig 6.14 A and C). Using αCD3 treatment of these mice, I observed that MTG staining increases in a similar manner to WT IELs, except in TCRαβ$^+$ CD8αβ$^+$ IELs (Fig 6.14 A and E). However, when assessing Ki-67 response, I observed a significant reduction in the Ki-67 response (Fig 6.14 B and F). This trend applies for all IEL subsets except TCRαβ$^+$ CD8αβ$^+$ IELs (Fig 6.14 F). As this trend was not observed in AhR-/- mice (Fig 6.12 B an F), it may be mediated in an AhR-independent manner.

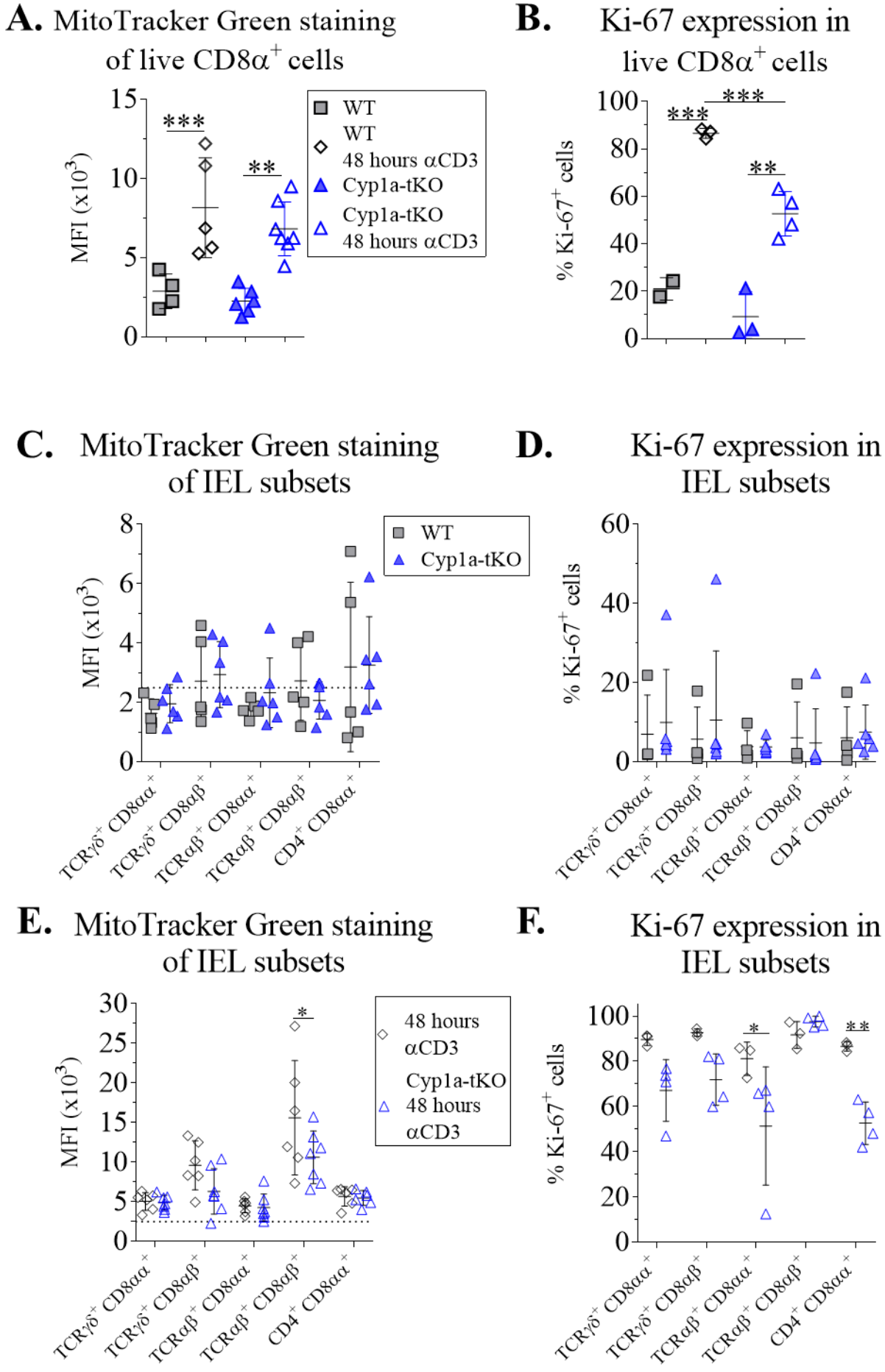

Figure 6.14. Cyp1a enzymes have a role in the αCD3-mediated Ki-67 response in IELs. WT and Cyp1aT-/- mice were injected i.p. with 25 µg αCD3 antibody. IELs were isolated from non-injected and αCD3-stimulated mice at 48 hours post αCD3 injection and stained for MTG and Ki-67 staining, as previously described. A, C, E) Quantification of MTG MFI from A) control total CD8α$^+$ IELs or 48 hours post αCD3 injection, C) non-treated IEL subsets and E) IEL subsets at 48 hours post αCD3 injection. B, D, F) Ki-67 staining from B) total CD8α$^+$ IELs at steady state or 48 hours post αCD3 injection, D) non-treated IEL subsets and F) IEL subsets at 48 hours post αCD3 injection. Data are presented as mean ± SD from one to two independent experiments with two to four mice per condition and experiment. Statistically significant changes were identified by one-way ANOVA (Panel A-B) or two-way ANOVA (Panel C-F). *: p<0.05., **: p<0.01., ***: p<0.001.

6.12. IEL activation leads to drastic CL composition alternations

Next, I wanted to assess in more detail whether the CL composition is altered in activated IELs. For that experiment, I FACS-sorted activated total CD8α$^+$ IELs from the *E. vermiformis* infected mice (see Chapter 7 for details about this model), non-infected total CD8α$^+$ IELs, naïve and memory splenic CD8α$^+$ T cells. Splenic CD8α$^+$ effector T cells were obtained by *in vitro* activation of CD8α$^+$ T splenocytes with plate-bound αCD3 and αCD28 antibodies for two days before cell quantification and pelleting. The cell pellets were then extracted for cardiolipin analysis by mass spectrometry undertaken by the Babraham Institute Lipidomics facility. I performed a principal component (PCA) analysis of all detected species of CLs.

PCA analysis is a dimension reduction method to visualize and analyze big set of data into principal components (PCs). PC1 can explain most of the variation in the data set, while PC2 is the second most important component to explain the variation in the data set (Ringnér, 2008). Part of the analysis is a list of data values, in this case CL species, that contribute the most to PC1 (Fig 6.15 B and Supplemental Fig 6.15 B). Supplemental Figure 6.15 illustrate the principle of PCA easier as the figure only plots the CL distribution between IELs and

activated IELs. In the list, there are three positive values for the three CL species CL 74_10, CL 74_9 and CL 72_9 (Supplemental Fig 6.15 B), which are all higher expressed in non-activated IELs. This is showed in the PCA plot by the horizontal lines (as PC1 is plotted on the x-axis) pointing towards non-activated IELs (Supplemental Fig 6.15 A). This can be confirmed by plotting the three CL species as done in Supplemental figure 6.15 C-E. Similar approach applies for the CL species with negative values that are pointing towards activated IELs and confirmed higher expression in Supplemental figure 6.15 F-O.

The analysis of non-activated IELs, activated IELs, naïve, memory and effector splenic CD8α$^+$ T cells showed that non-infected IELs are set apart from the other analysed lymphocyte populations by a specific lipid species designated CL-74_10 (Fig 6.15 A). From the PCA analysis, a list of the CLs that contributed to principal component one (PC1) can be obtained (Fig 6.15 B). Quantifications from this dataset showed that non-infected IELs contained significantly more CL 74_10 than the other assessed T cell populations. Importantly, the proportion of CL-74_10 is significantly reduced in activated IELs (Fig 6.15 C). When quantifying the CL species in relation to their lengths, I observed a shift in IELs from mainly CL-74 species to CL-72 species (Fig 6.15 G-H). CL 74 species are mainly expressed in naïve and memory splenic CD8α$^+$, while effector splenic CD8α$^+$ contain more CL 72, the same family of species that increases in activated IELs. I also performed PCA on steady state and activated IELs only from the same dataset, which highlighted that CL species CL 74_10, 74_9 and 72_9 are more abundant in non-activated IELs compared to activated IELs (Supplemental Figure to 6.15). These data support a model in which mitochondria remodelling is involved in the activation process of IELs.

A.

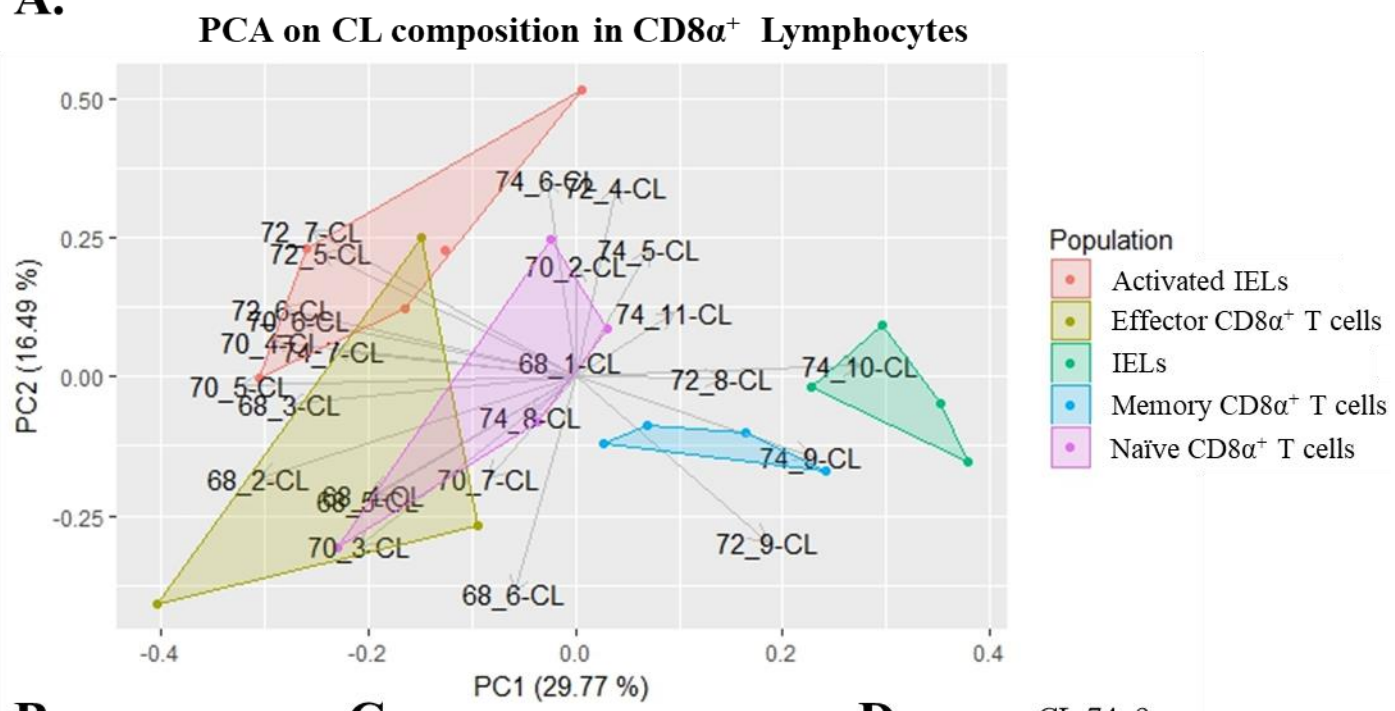

B.

CL Species	Contribution to PC1
74_10-CL	**0.271933257**
74_9-CL	**0.225081343**
70_3-CL	**-0.206809183**
74_7-CL	**-0.231273399**
72_5-CL	**-0.242378872**
72_7-CL	**-0.252176545**
70_6-CL	**-0.263353296**
68_3-CL	**-0.273067086**
72_6-CL	**-0.279660972**
70_4-CL	**-0.290252063**
68_2-CL	**-0.301827166**
70_5-CL	**-0.319392516**

C.

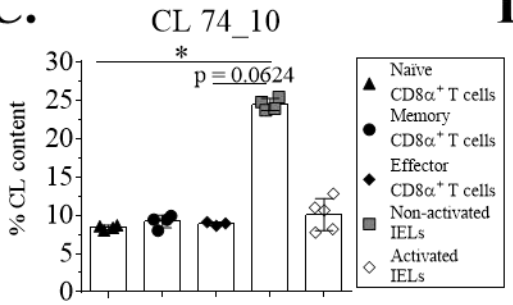

D.

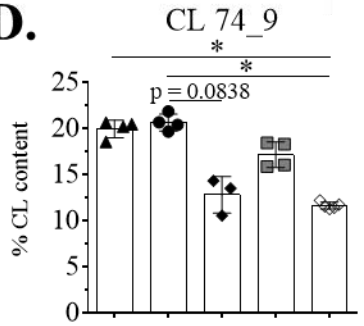

E.

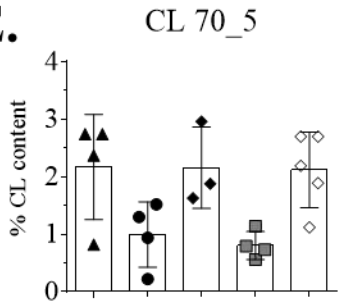

F.

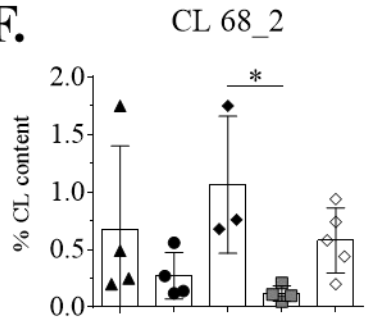

G.

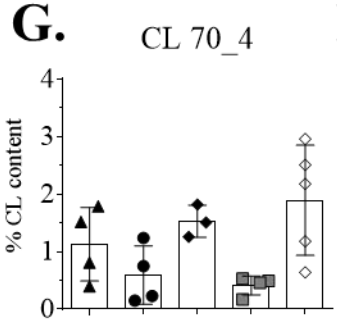

H.

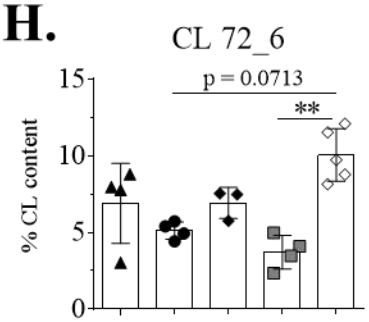

I.

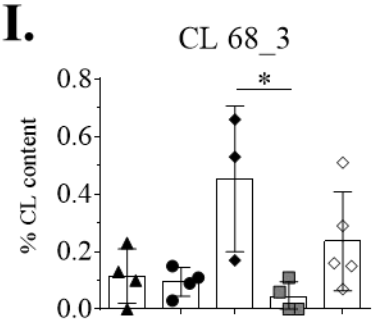

Figure 6.15. Activation of IELs leads to drastic changes in CL composition – Part 1. Infected and non-infected IELs and naïve and memory splenic $CD8a^+$ T cells were FACS-sorted, while effector $CD8\alpha^+$ T cells were obtained from *in vitro* culture. Lipids were extracted from these cell populations for analysis by mass spectrometry. A) PCA of the CL composition in the five tested T cell populations. Each coloured dot represents biological replicates of each cell population, while the coordinate system indicates how the CL species distributes on PC1, PC2 and cell populations. B) List of CL species that contribute the most to the principal components. C-I) Quantification of CL species C) 74_10, D) 74_9, E) 70_5, F) 68_2, G) 70_4, H) 72_6 and I) 68_3. Data are presented as mean ± SD from one experiment with cells sourced from three to five mice per condition. Statistically significant changes were identified by the Kruskal-Wallis test. *: $p<0.05$., **: $p<0.01$.

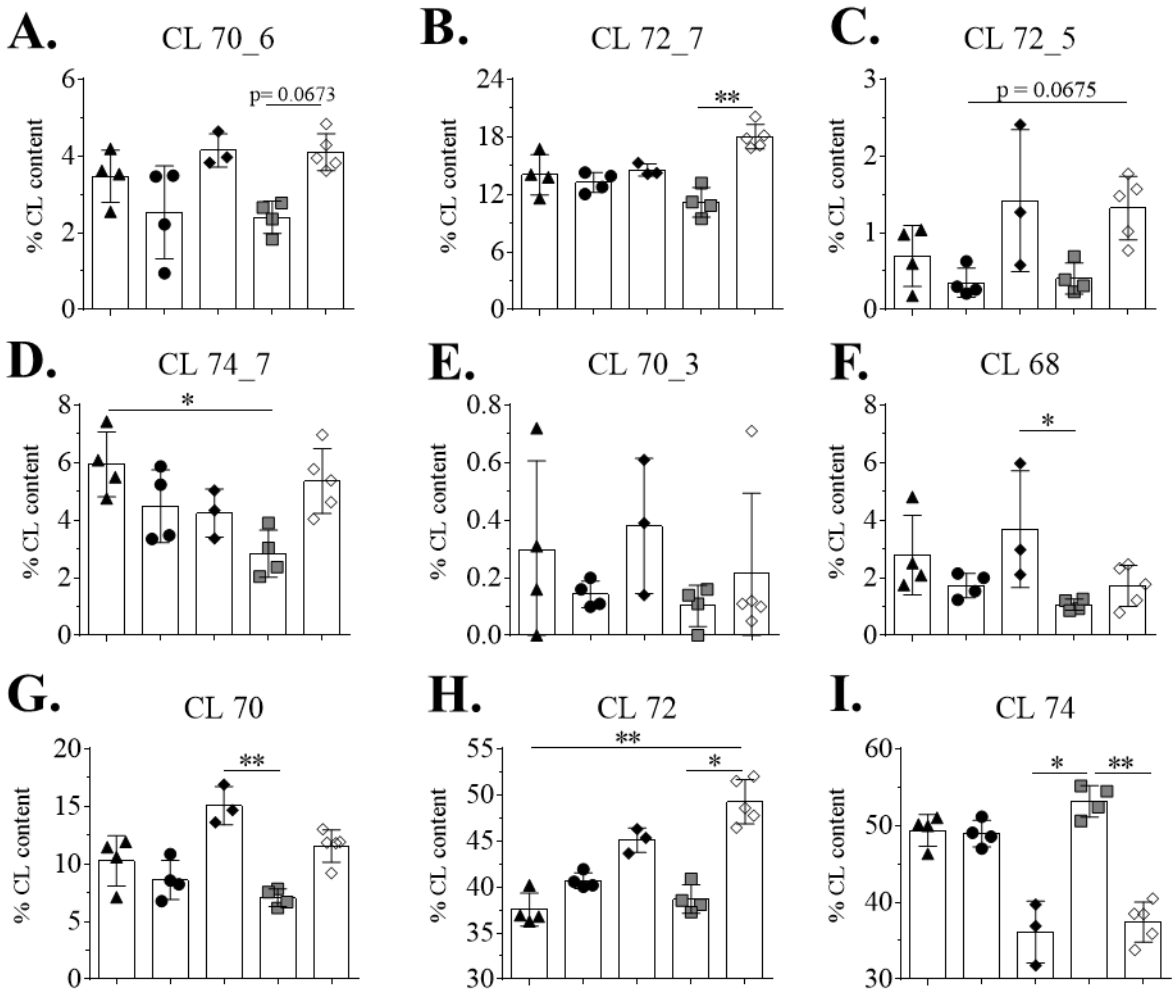

Figure 6.15. Activation of IELs leads to drastic changes in CL composition - Part 2. Same CL mass spectrometry data set as in Fig 6.15. A-H) Quantification of CL species A) 70_6, B) 72_7, C) 72_5, D) 74_7, E) 70_3 and total F) CL 68, G) CL 70, H) CL 72 and I) CL 74 species. Data are presented as mean ± SD from one experiment with cells sourced from three to five mice per condition. Statistically significant changes were identified by the Kruskal-Wallis test. *: $p<0.05$., **: $p<0.01$.

6.13. Supplemental chapter figures

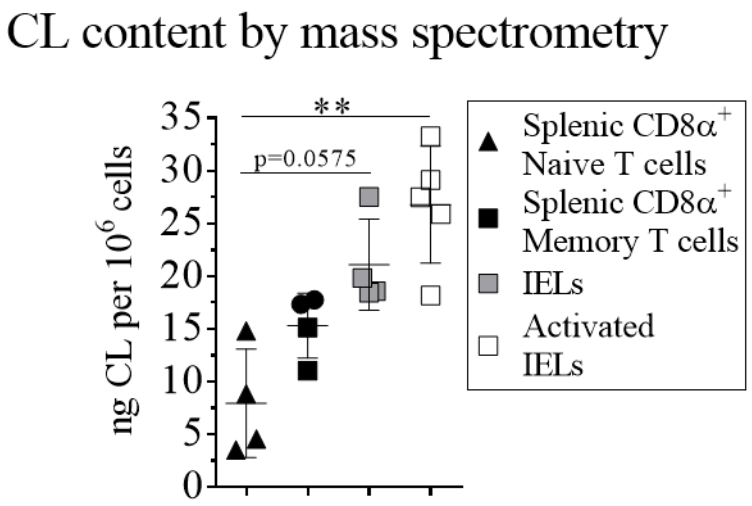

Supplemental Figure to 6.5. Quantification of the amount of CLs per 10^7 cells. Data are presented as mean ± SD from one experiment with cells sourced from four to five mice per group. Statistically significant changes were identified by the Kruskal-Wallis test: **: $p<0.01$.

Supplemental Table to 6.15. Table of CL species measured between non-infected IELs, infection-mediated activation of IELs, naïve, effector and effector splenic CD8α⁺ T cells.

Cardiolipin (CL) species			
68_1-CL	70_2-CL	72_4-CL	74_10-CL
68_2-CL	70_3-CL	72_5-CL	74_11-CL
68_3-CL	70_4-CL	72_6-CL	74_5-CL
68_4-CL	70_5-CL	72_7-CL	74_6-CL
68_5-CL	70_6-CL	72_8-CL	74_7-CL
68_6-CL	70_7-CL	72_9-CL	74_8-CL
			74_9-CL

A. **PCA on CL composition in non-infected and activated IELs**

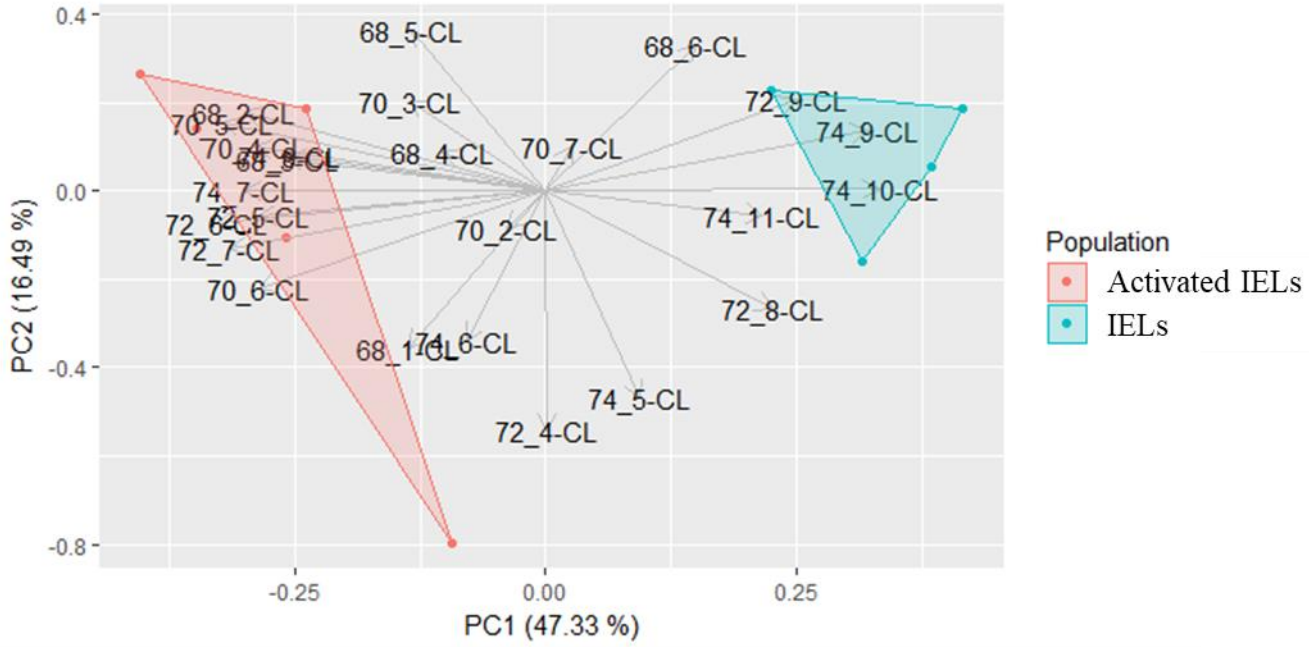

B.

CL Species	Contribution to PC1
74_10-CL	0.286808849
74_9-CL	0.27599384
72_9-CL	0.214990235
74_8-CL	-0.220018157
68_3-CL	-0.221669329
72_5-CL	-0.246480433
70_6-CL	-0.246706133
70_4-CL	-0.24902412
74_7-CL	-0.25844365
68_2-CL	-0.258646396
72_7-CL	-0.270809569
70_5-CL	-0.277208624
72_6-CL	-0.282786815

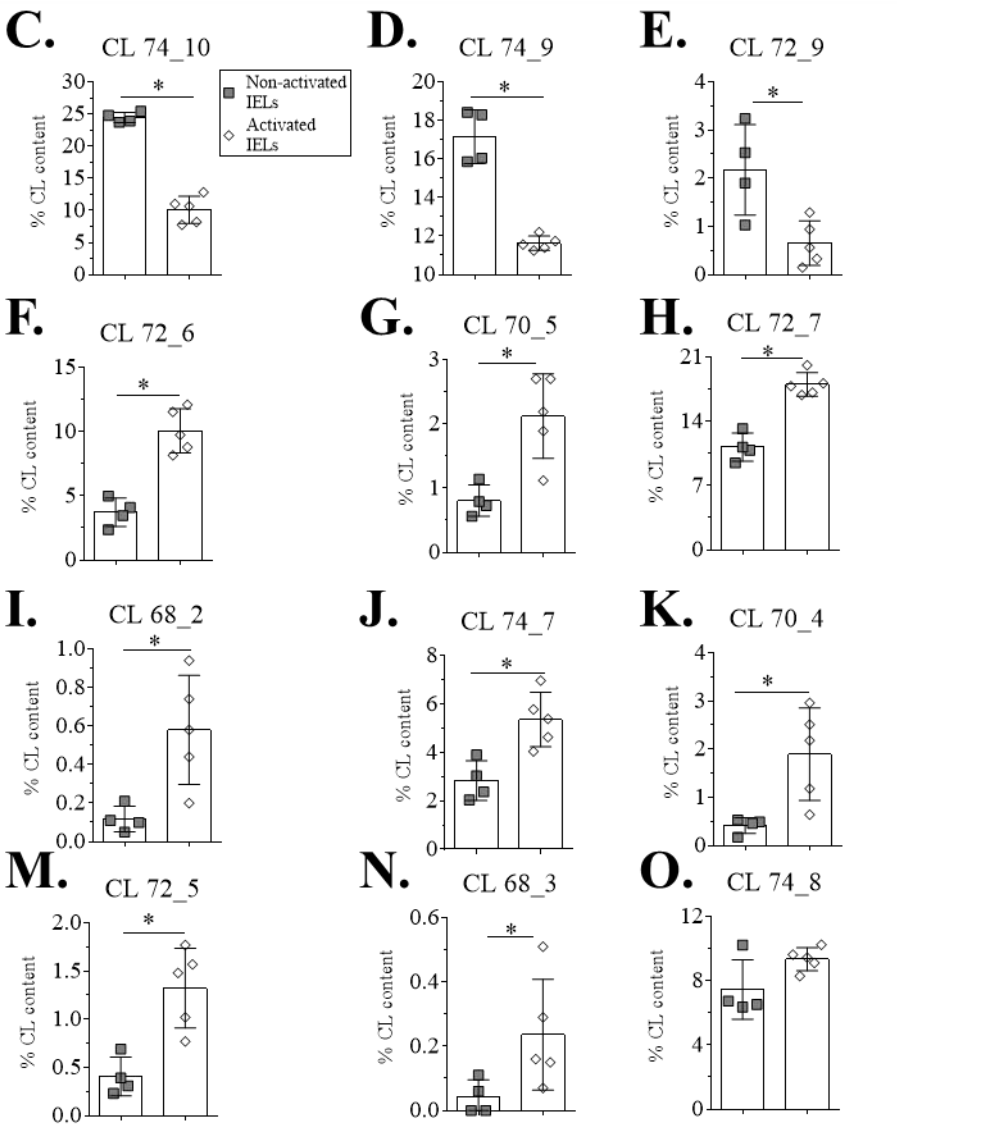

Supplemental Figure to 6.15. PCA analysis of CL species in activated and non-activated IELs. Non-infected and infected IELs, effector, naïve and memory splenic CD8a$^+$ T cells were FACS-sorted. Lipids were extracted from these cell populations for analysis by mass spectrometry, the same data set as used for 6.13 and 6.14, but this time focusing on IELs only. A) PCA analysis of the CL composition in steady state and activated IELs. Each coloured dot represents biological replicates of each cell population, while the coordinate system indicates how the CL species distributes on PC1, PC2 and cell populations. B) List of CL species that contribute the most to the principal components. C-O) Quantification of CL species C) 74_10, D) 74_9, E) 72_9, F) 72_6, G) 70_5, H) 72_7, I) 68_2, J) 74_7, K) 70_4, L) 70_6, M) 72_5, N) 68_3 and O) 74_8. Data are presented as mean ± SD from one experiment with cells sourced four to five mice per group. Statistically significant changes were identified by Mann-Whitney test. *: $p<0.05$.

6.14. Chapter Discussion

Summarising the findings in this Chapter, I showed that the mitochondrial mass in IELs increased after TCR activation *in vivo*. In addition, the mitochondrial ROS production and proliferation, measured by Ki-67 staining, also increased, while the mitochondrial membrane potential and CL content remained at similar levels to the non-activated IELs. I also showed a potential role of T-bet and AhR in the threshold for the TCR-mediated mitochondrial mass increase. The Cyp enzymes, that are located in mitochondria and ER, seem to play a role in the TCR-mediated proliferative response. Finally, I showed that the mitochondria in IELs are distinct from those in splenic naïve, memory and effector CD8α$^+$ T cells in respect of their CL composition. IELs have high level of CL 74 species, particularly CL 74_10. Upon activation using the *E. vermiformis* model, the CL composition in IELs alters drastically. Collectively, these data support a model of mitochondria-dependent activation mechanism for IELs.

One of my earliest observations of altered IEL activation was the increase in the level of the lymphocyte activation molecule CD44. In control mice, there are IELs that have high, intermediate and low expression of CD44 (Fig 6.1 B). CD8αβ^{+} IELs tend to have a higher proportion of cells that are CD44^{Hi} (data not shown). As early as 4 hours after αCD3 antibody stimulation *in vivo*, I observed that all IELs have an increased CD44 expression. CD44 is a glycoprotein that, in addition to being used as a marker of activated lymphocytes, is an adhesion molecule. It has been reported that CD44 can interact with ECM, particularly the compound hyaluronan. It has also been reported that CD44-/- mice have lower Th1 cell responses, highlighting a potential link between CD44 and effector functions (Baaten et al., 2012). In addition to the increase in CD44 expression, I observed a transient increase of CD69, another activation marker. Unlike the CD44 expression that remained high for at least 48 hours post injection, CD69 expression went down by 48 hours post injection. Whether the increase in CD44 and CD69 expressions in IELs are linked to the later increased mitochondrial mass or if these are two separate events, is yet to be determined.

In recent years, the recognition of the importance of cell metabolism for immune functions has emerged. Some of the recent insights have been published by the Pearce laboratory. They have shown metabolic differences between splenic CD8α^{+} naïve, memory and effector T cells. In addition to using CD44 as marker to distinguish naïve and memory cells, they have used CD62L to distinguish Tmem and Teff cells. They have reported that Tmem cells have higher SRC than naïve T cells (van der Windt et al., 2012), a finding that is reproduced in Chapter 5. In addition, they found that Tmem cells have more mtDNA than Teff cells (van der Windt et al., 2012). This laboratory has also reported that Teff cells store more lipids than the other CD8α^{+} T cell subsets (O'Sullivan et al., 2014). These findings go in line with what I have reported in Chapter 5. Of particular relevance to my findings, the Pearce laboratory has

reported two cases of an increase in the MTG staining. In the first case, they treated cells with M1 (a mitochondrial fusion promoter) and Mdivi-1 (a mitochondrial fission inhibitor) and could report an increase in MTG staining for Teff cells. In the second case, cells were transfected with Opa1, which resulted in an increase in mitochondrial mass (Buck et al., 2016). Although the reported increase in mitochondrial mass was not as drastic as the ones I demonstrate for αCD3-activated IELs, these reported findings highlight a potential role of mitochondrial fusion that could possibly be involved to explain the increase in MTG staining I observed in αCD3-activated IELs. The Erika Pearce laboratory have also recently reported mitochondrial changes in respect of the cristae. Cristae being spatially close to each other was correlated with effector functions such as IFNγ production, which was reduced in Tmem cells in which the cristae were spatially more distant to each other. The tightening of cristae may be induced by CD28 stimulation (Klein Geltink et al., 2017).

Sequencing data from the Immgen project suggest that TCRγδ$^+$ IELs express Mfn1, Mfn2, Opa1 and Drp1 (Heng et al., 2008; Shay and Kang, 2013). Unfortunately, IELs survive poorly *in vitro*, unless cultured with organoids, as shown in Chapter 4. Therefore, addition of M1 and Mdivi-1 (promoting mitochondrial fusion) to the IEL-organoid co-culture system could be an option to address the mechanism behind the increase in MTG staining in TCR-activated IELs. If mitochondrial fusion is involved in the explanation behind the increase in mitochondrial mass, then further studies of the signalling mechanisms from the TCR stimulation to the mitochondria need to be performed. This understanding would uncover factors involved in IEL activation and also potential targets for modulating IEL activation responses.

Another interesting aspect from this work is the different kinetics of the activation markers. Data from this chapter suggest that CD44 is the marker that increases first. Staining of CD69 at 4 hours post αCD3-injection need to be performed to determine whether the increase in CD44 and CD69 occur at the same time. Previous data suggest that αCD3 treatment lead to rapid TCR clustering and internalization. *In vitro* experiments have demonstrated that TCR are clustered as early as 30 min after αCD3 stimulation (Yokosuka et al., 2005). The earliest time point at which it has been demonstrated that αCD3 stimulation leads to internalisation of the TCRs on IELs *in vivo*, is one hour post αCD3 injection in BALB/c mice (Ogata et al., 2014). Therefore, a proposed sequence of events for TCR-mediated IEL activation would be that expression of CD44 and CD69 increases; then, mitochondrial mass as indicated by MTG increases; the increase in proliferation as detected by Ki-67 appears to happen with the same kinetics as the increase of MTG staining. As a significant increase in mitochondrial ROS production is first observed 48 hours after activation (Fig 6.4 A), this would suggest that this may be happening after the mitochondrial mass has increased.

An interesting observation from this chapter is that the different IEL subsets respond differently to αCD3 stimulation, despite the fact that all IEL subsets have the same low mitochondrial mass to start with. Moreover, while TCRγδ$^+$ CD8αα$^+$ IELs are the most numerous subset in non-treated mice, it is the third largest IEL subset, TCRαβ$^+$ CD8αβ$^+$ IELs (Fig 4.3 A-B), that responds most strongly, while TCRαβ$^+$ CD8αα$^+$ and CD4$^+$ CD8αα$^+$ IELs respond the least. Moreover, TCRγδ$^+$ CD8αβ$^+$ IELs respond better than TCRγδ$^+$ CD8αα$^+$ IELs which could possibly be linked to the fact that the CD8αα homodimer may have repressive functions (Cheroutre and Lambolez, 2008). This serves to illustrate the heterogeneity of the IEL response to antigen presentation. Hypothetical explanations for these differences in IEL subsets could involve different thresholds to initiate the MTG increase or differences in

intracellular downstream signaling proteins in the different IEL subsets. As αCD3 stimulation is an artificial way to mimic of antigen presentation, it could also be that the other IEL subsets require different additional signals for a stronger response.

Another question remaining to be addressed is what IELs are using as source to enable the increase in mitochondrial mass. Assessment of the lipid droplet content in activated IELs could provide some insights. However, an alternative dye to Nile Red would need to be used to be able to address this question for all IEL subsets. This is because Nile Red has a broad emission spectrum (Greenspan et al., 1985), making multi-colour flow cytometry very difficult. An alternative dye that has been used to assess lipid content is BODIPY (O'Sullivan et al., 2014).

Despite the differences in mitochondrial mass increase, all IEL subsets respond with similar increases in Ki-67 expression, with TCRαβ$^+$ CD8αβ$^+$ IELs having a slightly higher Ki-67 response compared to the other IEL subsets (Fig 6.3 E). It remains to be determined whether there is a strict link between the increase in mitochondrial mass and the increase of cell proliferation (Ki-67). Correlation analysis does not prove causation. In this chapter, I reported two experiments in which an increase of Ki-67 was observed despite the lack of mitochondrial mass increase (Fig 6.10 A-B, Fig 6.12 A-B). An alternative explanation could be that the increase in Ki-67 expression is initiated before the increase in MTG staining. Using the IEL-organoid model could potentially clarify this matter.

In addition to the increase in Ki-67$^+$ cells, I also observed an increase in mitochondrial ROS production in activated IELs. Again, CD8αβ$^+$ IELs responded the most strongly, but this time no significant increase was observed in any of the CD8αα$^+$ IEL subsets (Fig 6.4 B-C). ROS

has been reported to be able to affect intracellular signaling such as acting on phosphates in the mitogen-activated protein kinase (MAPK) signaling pathway (Kamata et al., 2005; McCubbery et al., 2006). These observations could indicate that CD8αα$^+$ IEL have distinct functions compared to CD8αβ$^+$ IELs, as it is possible that different signaling cascades occur in the different IEL subsets. One potential reason for IELs to respond differently to αCD3-mediated activation, could be linked to feedback from the intestinal compartment, to which different IEL subsets may respond differentially. It has been shown that IECs start to secrete IL-33 after *in vivo* αCD3 injection (Pascual-Reguant et al., 2017). Additional factors may be secreted from IECs, which may have an impact on the outcome of αCD3-mediated activation of IELs.

Surprisingly, I observed no significant increase in the mitochondrial membrane potential in αCD3-activated IELs, except in the case of TCRαβ$^+$ CD8αβ$^+$ IELs (Fig 6.5 B, D and F). Possible explanations could be that mitochondrial membrane potential does not increase during TCR-mediated activation, or that such an increase may be transient. It could also be that IELs require the input of additional signals for mitochondrial membrane potential increase. An alternative option could be that such responses occur at later time points. These observations raise the question whether or not mitochondrial functions, such as OXPHOS, increased in activated IELs. I have tried to assess the OCR, using the Seahorse mitochondrial capacity stress assay as used in Chapter 5, in activated IELs. However, I have so far been unsuccessful, as activated IELs seem not to survive for the full period of the stress assay (data not shown). This observation may suggest that activated IELs are too fragile for the mitochondrial stress assay. A potential way to overcome this hurdle could be to design a shorter version of the mitochondrial stress assay, hoping that activated IELs may survive that. The mitochondrial membrane potential has been suggested to distinguish two profiles of

splenic CD8α$^+$ T cells. Splenic CD8α$^+$ T cells with lower mitochondrial membrane potential have higher SRC but lower production of IFNγ compared to splenic CD8α$^+$ T cells with higher mitochondrial membrane potential (Sukumar et al., 2016).

It was interesting to find that IELs reconstitute better in Rag2-/- IL-2Rγ-/- mice compared to Rag2-/- mice. This observation would suggest that the Rag2-/- IL-2Rγ-/- IEC compartment is more favourable for IEL maintenance, maybe because IL-2Rγ signalling can be inhibitory for IELs. FACS data, both my own and that of other member of laboratory, suggest that there are more NK1.1$^+$ cells in the IEC compartment in Rag2-/- mice compared to Rag2-/- IL-2Rγ-/- mice (data not shown), suggesting more compartmental space in the latter mouse line. The role of IL-2Rγ signalling for IEL activation and maintenance will be discussed further in Chapter 7.

An additional question to address is which factors enable IELs to increase their mitochondrial mass. In this chapter, I have tested several factors. None of the tested factors led to significantly higher mitochondrial mass compared to non-treated WT IELs (Fig 6.10-14). These data suggest that none of the tested factors are strictly involved to set IELs into this state of low mitochondrial mass. However, some differences were observed in these mice. First, Eomes-deficient IELs have lower mitochondrial mass in untreated and αCD3-treated TCRαβ$^+$ CD8αβ$^+$ IELs (Fig 6.11 A and E). Second, T-bet-deficient IELs have lower MTG staining in TCRαβ$^+$ CD8αβ$^+$ IELs, both at steady state and after αCD3-mediated activation (Fig 6.10 A and E). These data indicate that T-bet and Eomes may be involved in determining the mitochondrial mass for TCRαβ$^+$ CD8αβ$^+$ IELs. In addition, I observed a reduced Ki-67 response in Cyp1aT-/- mice (Fig 6.14 B and F). The involvement of Cyp1a enzymes may in this case be independent of AhR signaling pathways, as both AhR and AhRR-deficient IELs

show no differences in Ki-67 expression compared to WT IELs (Fig 6.12-13 B and F) and the data from AhR-/- mice are not consistent in regards of MTG staining after αCD3-mediated activation (Fig 6.12 A). However, there may be a combination of factors behind setting and releasing IELs from this mitochondrial compromised state. It could potentially be that IELs receive downregulating signals from the intestinal compartment. Sequencing analysis comparing steady state and TCR-activated IELs may pinpoint candidates to assess further in this regard.

Data from this Chapter also put focus on the mitochondrial composition, especially the CL content. I reported a shift in activated IELs' CL composition from mainly CL 74 species to CL 72 species (Fig 6.15). The diversity of the CL-species increases in activated IELs, with mainly 74_10, 74_9 and 72_9 decreasing during activation, in favor of a higher proportion of other CL species such as 72_6 and 72_7 (Supplemental Figure to 6.15). Although the presented data would need a repeat experiment to strengthen these findings, they suggest that alternation of CLs may play a role for IEL activation. Even small changes in the CL length and the number of double bindings may have a big impact on mitochondrial function in IELs. CLs have been reported to have an impact on mitochondrial functions such as electron transport. Defects in CLs have been associated with some diseases such as diabetes and Barth syndrome (heart disease involving an enlarged and weakened heart) (Paradies et al., 2014). Therefore, it is likely that CL remodelling, that seems to have taken place in activated IELs, is tightly regulated to avoid generating defective or dangerous IELs. It would be interesting to obtain an insight into the spatial distribution of the CL in the mitochondria of steady state and activated IELs. This would be particularly interesting as recent data from Pearce laboratory show that the spatial distribution of mitochondrial cristae seems to be important for T cell functions, such as secretion of IFNγ (Klein Geltink et al., 2017). However, I am not aware of

a technique that would allow imaging of mitochondria with sufficient resolution to be able to distinguish the different CL species. Imaging of total CLs could give insights into whether CLs in steady state IELs are distributed differently compared to activated IELs, as well as in comparison with naïve, memory and effect splenic CD8α$^+$ T cells. Whether the changes in CL composition are required for the increase in mitochondrial mass or are a consequence of changes to IEL mitochondria during activation, remains to be determined.

Data obtained from NAO staining suggest that the same CL content in steady state and activated IELs (Fig 6.5 A, C and E). These observations suggest the possibility that CLs are causing potential spatial hindrance in steady state IELs. In addition, there is evidence suggesting interactions between CL and caspases, linking CLs to apoptosis (Schug and Gottlieb, 2009). Again, this may provide clues about why IELs survive so poorly *in vitro,* when cultured in the absence of intestinal organoids. It needs to be confirmed whether the IEL activation methods used lead to similar changes in CLs, as the activated IELs used for the CL mass spectrometry derived from the *E. vermiformis* infection model (7.3). TCR-activated IELs may have a different CL content profile.

Finally, the quest for discovering cytokine-promoting signals for IELs needs to continue. Addition of anti-CD28 antibody did not induce cytokine production in IELs nor alter the increase in MTG staining (Fig 6.8-9). Previous publications suggest differences in CD28 expression in IELs, which is mainly found in CD8αβ$^+$ IELs (Ohteki and MacDonald, 1993; Gelfanov et al., 1995). CD28 has recently received additional attention in relation to as metabolic priming of CD8$^+$ T cells (Klein Geltink et al., 2017). CD8α$^+$ T cells stimulated with αCD3 and αCD28 generated more SRC, ECAR and IFNγ production compared to αCD3

stimulated T cells. In addition, this increase was reduced in the presence of etomoxir (ETO), an agent that blocks fatty acid oxidation (FAO) (Klein Geltink et al., 2017).

Collectively, this chapter highlights that IELs can increase their mitochondrial mass and mitochondrial ROS production, indicating mitochondria plasticity in IELs during activation. This increase also correlates with increased proliferation, but not cytokine production.

Chapter 7: Full IEL activation depends on lumenal/bacterial compound(s)

In Chapter 6, I showed that IELs increase their mitochondrial mass and mitochondrial ROS production after TCR-stimulation. These data suggest that IELs undergo mitochondrial plasticity during IEL activation. In addition, I observed an increase in the proliferation marker Ki-67 which correlated with the increased mitochondrial mass. Collectively, these data suggest that mitochondrial markers can be used as activation markers for IELs. Therefore, I wanted to assess whether I can obsere similar changes to mitochondrial mass in IELs during more physiological relevant settings such as IEC stress and intestinal infections. Observing similar observations during intesintal infections would support the notion that IELs undergo mitochondrial plasticity during activation. In addition, I want to assess whether I can observe cytokine production from IELs. Data from Chapter 6 suggest that TCR stimulaton alone seem insufficient to induce cytokine production in IELs. Intestinal infections may proivde the required context for cytokine production in IELs. Below, I will introduce the intestinal microbiota and the intestinal pathogens that will be assessed in this chapter.

7. Enteric microbiota and pathogens

The mammalian host is colonized by a large population of commensal microbiota, particularly at the mucosal sites such as the skin and the intestinal tract. *In utero*, mice receive some microbiotal colonization from the mother. The abundance of microbiota increases rapidly after birth through the additional entry of opportunistic microbiota present in the environment (Gensollen et al., 2016).

In the 1870s, it was shown that specific bacteria can cause specific diseases. It was Robert Koch that formed the germ theory of disease. He demonstrated that bacteria isolated from sick animals could cause the exact same disease in healthy animals, when these were injected

with bacteria isolated from the sick mice. His criteria for demonstrating a link between a specific type of bacteria and disease would later be known as Koch's postulates (Gradmann, 2014).

In 1989, Charles Janeway formulated the concept of pattern recognition receptors (PRRs) (Janeway Jr., 1989), which have been mentioned in previous chapters. These are important for the recognition of microbial molecular patterns by the immune system. PRRs signal via the signaling domain of myeloid differentiation gene 88 (MyD88), TNF receptor associated factor (TRAF) and TIR domain-containing adapter inducing interferon β (TRIF) (Neish, 2006).

Further understanding of microbiota has been made possible thanks to technological development of animal facilities that can host germ-free (GF)-mice. GF mice have smaller MLNs and PPs (Macpherson and Harris, 2004), fewer $CD4^+$ and $CD8^+$ T cells, as well as fewer $TCR\alpha\beta^+$ $CD8\alpha\beta^+$ IELs (Kawaguchi et al., 1993; Klose et al., 2014; Di Marco Barros et al., 2016). Despite these deficiencies, it has been reported that GF mice are protected from obesity (Bäckhed et al., 2007), suffer less severe EAE symptoms (Lee et al., 2011), less intestinal inflammation (Roulis et al., 2015) and intestinal cancer (Bongers et al., 2014). On the other hand, it has been shown that mice living under natural (wild) conditions cope with viral infections better than mice living under specific pathogen-free (SPF) conditions (Rosshart et al., 2017).

7.1. Enteric viral pathogens: Murine Norovirus (MNV)

There are many enteric viruses that can infect IECs and cause gastroenteritis such as rotavirus and murine norovirus (MNV). Rotavirus is a double-stranded RNA virus that infects villous

domains of the small intestine (Hernández et al., 2015). MNVs were introduced briefly in Chapter 4, for the MNV-organoid culture experiment, and will be in focus for part of this Chapter.

As previously mentioned, MNV is a single-stranded RNA virus that belongs to the virus family *Caliciviridae*. Numerous different MNV strains have been identified that cause either acute or persistent viral infection (Hsu et al., 2007; Shortland et al., 2014). MNVs have been successfully cultured in the macrophage cell line RAW.264.7 (Newman and Leon, 2015). Other cells that MNVs have been reported to be able to infect are DCs, MPs and B cells, and recent reports also suggest that some IEC subsets may be targets for MNV infection (Lee et al., 2017). Here, I will focus on the *in vivo* role of IEL activation in MNV infection, for which I hoped that MNV-O7 might generate interesting results. The *in vitro* data obtained in Chapter 4 suggested that MNV-O7, but not MNV-CW3, is able to infect IECs. Therefore, it would be interesting to see if *in vivo* MNV-O7 infection will lead to mitochondrial changes and cytokine secretion from IELs.

7.2. Bacterial pathogens: *Salmonella*

There are various different enteric pathogenic bacteria. For the work reported in this Chapter, I have been provided with small intestines from mice infected with *Salmonella* by Prof. Jonathan Heeney's laboratory. *Salmonella* is a Gram-negative bacterium belonging to the family *Enterobacteriaceae* (Miki et al., 2012). There are two species of *Salmonella: enterica* and *bongori*. In this thesis, *Salmonella enterica* will be used. *Salmonella* can cause self-limiting gastroenteritis in immunocompetent individuals (Crowley et al., 2016). It has been reported to be able to infect M-cells and underlying PPs, containing T and B cells (Gonzales et al., 2017).

7.3. Eukaryotic Pathogens: *Eimeria vermiformis (E. vermiformis)*

There are a range of enteric parasites that can infect the intestinal tract, such as the nematodes *Trichuris muris* and *Nippostrongylus brasiliensis* (Sorobetea et al., 2018) and intracellular parasites such as *Toxoplasma gondii (T. gondii)* (Weight et al., 2015) and *Eimeria species*. In this section, I will mainly focus on *Eimeria species*.

Eimeria species are a group of intracellular protozoan parasites that specifically invade IECs. *Eimeria* belong to the phylum of *Apicomplexan* parasites. Examples of other parasites in this phylum are *T.gondii, Cryptosporidium species* and *Plasmodium malariae* (Smith and Hayday, 2000a; Blake, 2015). There are numerous *Eimeria species*, but the focus in this thesis will be on *Eimeria vermiformis (E. vermiformis)* that specifically infects IECs in the lower parts of the murine small intestine, the jejenum and ileum (Todd and Lepp, 1971; Linh et al., 2009). Once *E. vermiformis* organisms have infected IECs, they undergo numerous replications. Both sporulated and non-sporulated *E. vermiformis* organisms are generated in IECs, which are subsequently shed into the faeces. In C57BL/6 WT mice, *E. vermiformis* parasites can be detected in the faeces starting from day six post infection, with a peak of parasite shedding taking place around nine to ten days post infection (Inagaki-Ohara et al., 2006; Rose et al., 1984, 1986; Linh et al., 2009; Roberts et al., 1996). In WT mice, *E. vermiformis* infection is self-limiting. The number of days *E. vermiformis* is actively shedding, termed patency, is usually five to ten days depending on the infection dose (Guedes, 2017) and mouse strain (Rose et al., 1986). Using various knock-out (KO)-mice and neutralizing antibodies, the role of T cells in *E. vermiformis* infection has been established. Mice lacking TCR$\alpha\beta^+$ T cells develop more severe infection in terms of parasite shedding and patency (Roberts et al., 1996). TCRβ-/- mice are more susceptible than WT mice during both primary and secondary *E. vermiformis* infection. The involvement of TCR$\gamma\delta^+$ T cells seems

to depend on age, as young mice (up til four week of age) lacking TCRγδ$^+$ T cells have higher oocyst shedding compared to controls (Ramsburg et al., 2003). Using treatment of animals with neutralizing antibodies, it was shown that mice given anti-CD8 or anti-CD4 antibodies have higher oocyst shedding and length of patency, particularly αCD4-treated mice (Rose et al., 1992). In addition, a role for IFNγ in *E. vermiformis* infection has been established. IFNγR-/- mice have a very high parasite shedding (Smith and Hayday, 2000a), suggesting that IFNγ is essential to control *E. vermiformis* infection. TCRβ-/- mice treated with αIFNγ antibody suffer from a parasite load similar to what is found in TCR(βxδ)-/- mice (Smith and Hayday, 2000b). Anti-IFNγ treament led to worse infection in terms of numbers of parasites shed – even when anti-IFNγ antibody is injected into mice 6 days after infection (Rose et al., 1989).

As previously known, IELs can produce IFNγ. In addtion, it has been suggested that IELs have a role in *E. vermiformis* infection via cytokine production and that they aid IECs to preserve the barrier integrity (Inagaki-Ohara et al., 2006). Therefore, the *E. vermiformis* infection model seems to be a potentially good candidate as a physiological model for assessing IEL activation.

7.4. Gut microbiota

Bacteria have been organised in Bergey's manual based on their morphology, staining reactions and other characterized features (Breed et al., 1944). One of the first distinctions between types of bacteria was discovered to be the ability to retain crystal violet stain, better known as Gram staining, characteristic of some bacteria but not of others (Bartholomew and Mittwer, 1952). These two categories, Gram-negative and Gram-positive bacteria, will be described in the next two sections. For the past decade, classification of different families of

microbiota has been performed using sequencing of the 16S rRNA. This is present in all self-replicating cells and the sequence evolves slowly over time (Pace, 1997; Woese and Fox, 1977). Bacteria can be classified into different phyla, classes, orders, families, genera and species (Fig 7.1). There are five different murine intestinal microbiota phyla identified: *Actinobacteria, Bacteroidetes, Firmicutes, Proteobacteria* and *Verrucomicrobia*, which can be divided further into various classes as shown in the figure (Lagkouvardos et al., 2016). The focus here will be on the bacteria found at intestinal sites.

7.4.2 Gram-positive bacteria

As the name suggests, these bacteria stain positive for the famous Gram stain. For both Gram-negative and Gram-positive bacteria, their cell wall contains polysaccharides and peptidoglycans. Unlike those of Gram-negative bacteria, the cell walls of Gram-positive bacteria contain lipoteichoic acid (LTA) (Malanovic and Lohner, 2016). Gram-positive bacteria can be divided further on the basis of low and high content of guanine and cytosine (G+C) (Muto and Osawa, 1987). Phyla belonging to Gram-positive bacteria are *Firmicutes* and *Actinobacteria* (Lawley and Walker, 2013) (Fig 7.1).

There are various antibiotics available to treat various bacterial diseases. There are antibiotics that specifically target Gram-negative or Gram-positive bacteria. One of the antibiotics that targets Gram-positive bacteria specifically is vancomycin. Vancomycin targets Gram-positive bacteria by inhibiting peptidoglycan synthesis (Kohanski et al., 2010).

In addition to antibiotics that target Gram-positive bacteria specifically, there are broad-spectrum antibiotics that target both Gram-positive and Gram-negative bacteria. An example of a broad-spectrum antibiotic is ampicillin. Ampicillin is a β-lactam antibiotic that targets

the enzyme transpeptidase that is required for bacterial cell wall synthesis (Moore et al., 1979). Another broad-spectrum antibiotic is streptomycin. Streptomycin kills bacteria by preventing protein syntheis by interacting with the ribosomal 16S subunit (Springer et al., 2001).

7.4.2 Gram-negative bacteria

Unlike Gram-positive bacteria, Gram-negative bacteria contain two membranes: one outer and one cytoplasmic membrane. In the outer membrane, there are lipopolysaccharides (LPS) (Costerton et al., 1974). Just like Gram-positive bacteria, Gram-negative bacteria can be divided further by low and high content of guanine and cytosine (G+C) (Muto and Osawa, 1987). Phyla belonging to Gram-negative bacteria are *Bacteroidetes*, *Proteobacteria* (Lawley and Walker, 2013) and *Verrucomicrobia* (Schlesner, 2015; Lin et al., 2016) and (Fig 7.1).

One example of an antibiotic that is targeting Gram-negative bacteria is colistin, also known as polymyxin E. It has been shown that colistin is specifically targeting bacteria within the Gram-negative spectrum. Colistin binds to the LPS on the outer membrane of Gram-negative bacteria. This binding leads to changes in cell permeability, ultimately leading to the death of the bacteria (Falagas and Kasiakou, 2005).

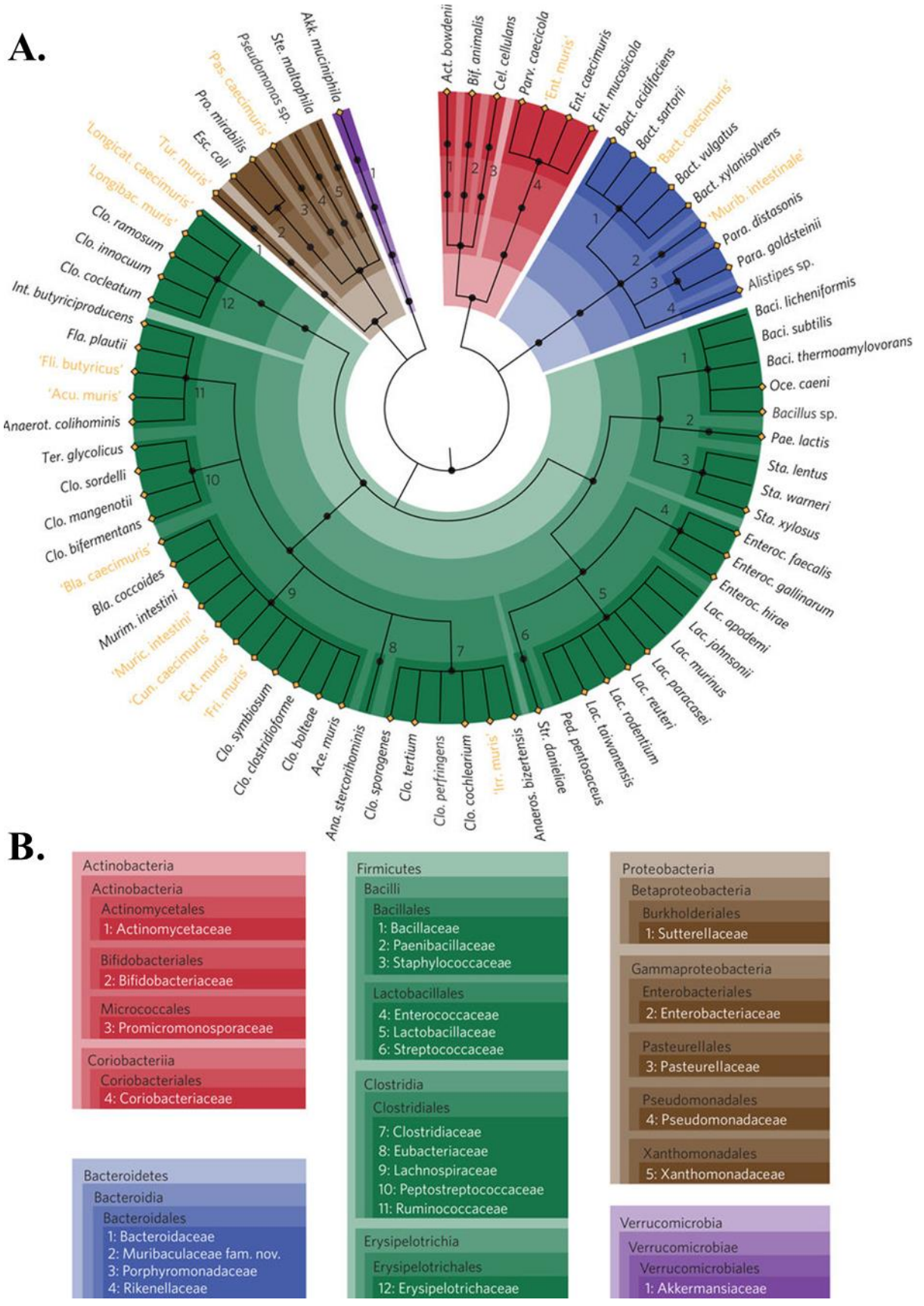

Figure 7.1. Overview of the taxonomic classification of murine microbiota. The relationship between different bacteria can be categorized into phylum, class, order, family, genus and species. A) Cladogram of identified bacteria from phylum to family level. The cladogram is colour-coded according to phylum. The names in yellow are newly identified in Lagkouvardos et al, Nat Microbiol (2016). B) Table of the colour-coded phylum. Within each box there are boxes representing class, order and family for respective phylum. Adapted from Lagkouvardos et al, Nat Microbiol (2016).

7.5. IEC stress in Villin-Cre- XBP1$^{fl/fl}$ mice is not sufficient to fully activate IELs

After observing that TCR stimulation via αCD3 injection can activate IELs (see Chapter 6), I next wanted to assess physiological conditions in which IEL activation could occur. As previously mentioned in the Introduction (1.6.1), IECs contain the antigen presenting machinery (Shao et al., 2005; Hershberg and Mayer, 2000). This feature makes IECs potential candidates for antigen presentation towards IELs. IECs may interact with IELs via other cell-cell interactions, particularly during stressful situations for IECs, which may subsequently activated IELs. Here, I used Villin-Cre-XBP1$^{fl/fl}$ mice as a model of IEC stress.

As mentioned in the Introduction, XPB1 is a component of the ER stress response to cope with unfolded proteins (the unfolded protein response, UPR). XBP1 has been reported to induce some UPR genes (Ron and Walter, 2007), as well as expansion of the ER (Shaffer et al., 2004). It is possible to deplete XBP1 specifically in the intestinal compartment, using the Cre-Loxp system employing the Villin gene promoter for Cre. Villin-Cre-XBP1$^{fl/fl}$ mice lack Paneth cells and have a significant reduction in the number of goblet cells. Sixty one percent of these mice develop spontaneous small intestinal inflammation. Yet, this inflammation does not lead to IEC barrier leakages, as demonstrated using the fluorescein isothiocyanate (FITC)-dextran assay. However, these mice are more susceptible to *Listeria monocytogenes*

infection, as well as suffering more severe weight loss than WT mice do during DSS-induced colitis (Kaser et al., 2008).

In order to address whether deficiency in XBP1 is involved in IEC-IEL interactions, or if XBP1 deficiency in IELs could be sufficient to activate IELs, I compared IELs from Villin-Cre-XBP1$^{fl/fl}$ and Rag1-Cre-XBP1$^{fl/fl}$ mice with WT controls. A recent report has suggested an important role of the contact sites between mitochondria and ER for Tmem re-call response (Bantug et al., 2018). It is possible that such interaction could have a role in IEL activation. IELs were isolated from the three mouse strains and stained for MitoTracker Green (MTG), as previously described. I observed heightened expression of the lymphocyte activation marker CD44 in IELs from Rag1-Cre-XBP1$^{fl/fl}$ mice and particularly in IELs from Villin-Cre-XBP1$^{fl/fl}$ mice (Fig 7.2 A-B). Heightened expression of CD44 was observed earlier in TCR-activated IELs (Fig 6.1 B), suggesting that depletion of XBP1 in IECs may be affecting the activation status of IELs.

However, I observed no statistically significant differences in MTG staining in total CD8α$^+$ IELs from WT, Rag1-Cre-XBP1$^{fl/fl}$ and Villin-Cre-XBP1$^{fl/fl}$ mice (Fig 7.2 C). When assessing the different IEL subsets, I found no significant differences in IEL subsets from Villin-Cre-XBP1$^{fl/fl}$ mice (Fig 7.2 D). Interestingly, I found statistically significant reductions in MTG staining in TCRαβ$^+$ CD8αβ$^+$ and CD4$^+$CD8αα$^+$ IELs from Rag1-Cre-XBP1 mice (Fig 7.2 E). These data suggest that the IEC stress induced in Villin-Cre-XBP1$^{fl/fl}$ mice is not sufficient to trigger changes in mitochondrial mass but is altering the level of CD44. As the CD44 observation was observed in Villin-Cre-XBP1$^{fl/fl}$ mice, this indicates that IEC-IEL interactions have occurred and subsequently altered the activation state of IELs.

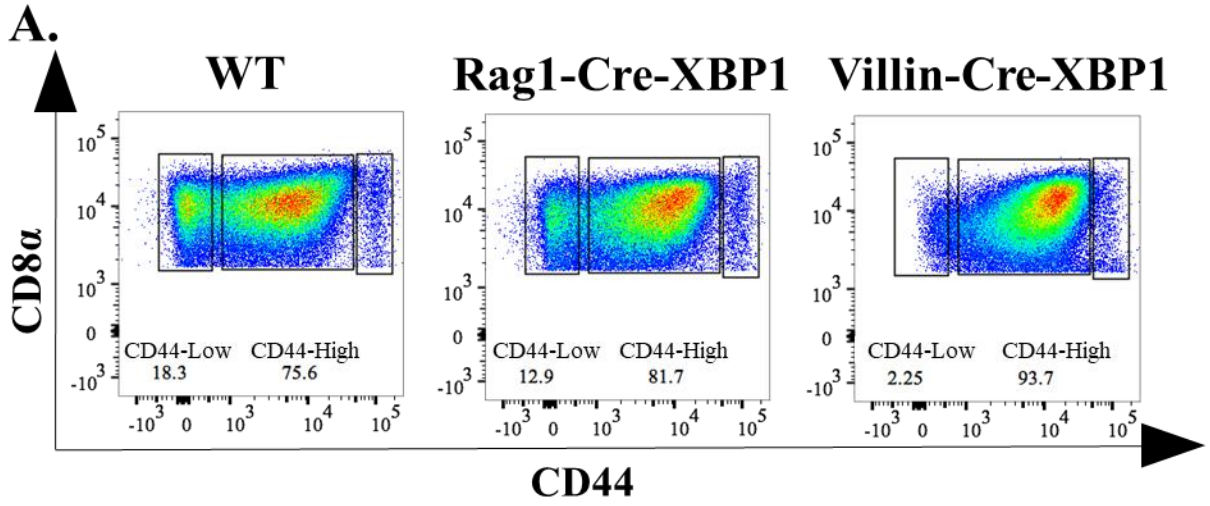

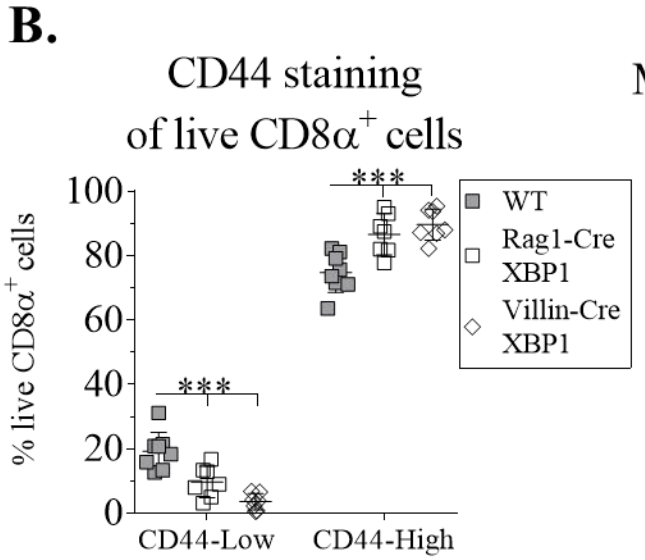

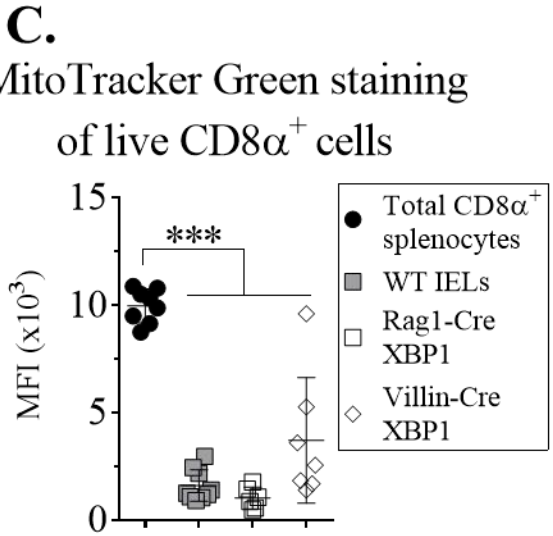

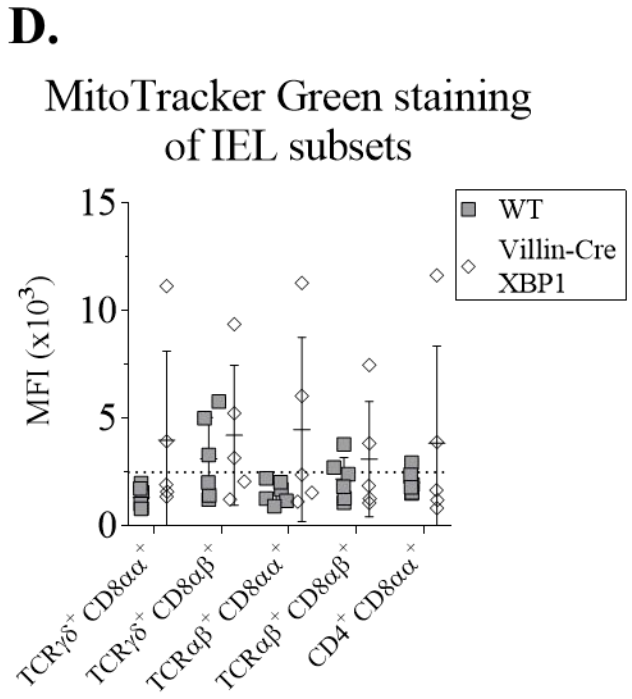

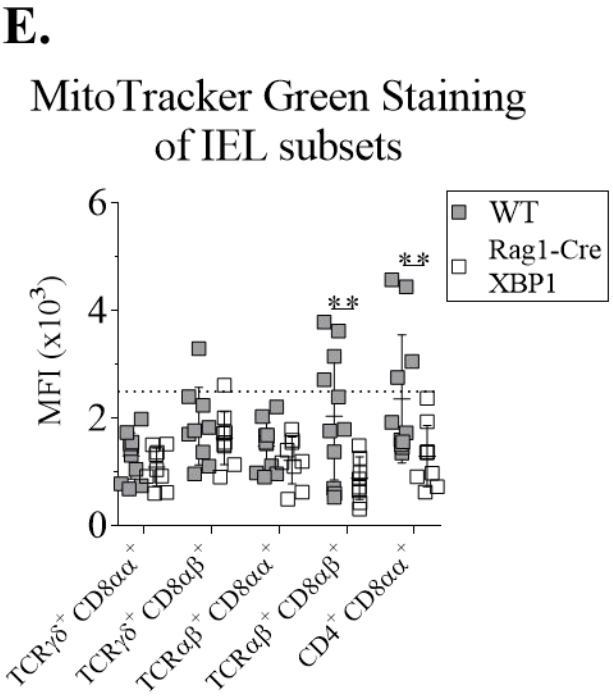

Figure 7.2 IEC stress in Villin-Cre-XBP1$^{fl/fl}$ mice is not sufficient to fully activate IELs. IELs were isolated from WT, Rag1-Cre-XBP1$^{fl/fl}$ and Villin-Cre-XBP1$^{fl/fl}$ mice and stained for MTG. A) Representative plots of CD44 staining in IELs from the different mouse lines. Pre-gating was made on live CD8α^{+} IELs. B) Quantification of the proportion of CD44^{Low} and CD44^{High} cells, according to gating in Panel A. C-E) Quantification of MTG MFI from C) total CD8α^{+} IELs, memory and naïve splenic CD8α^{+} T cells and D-E) IEL subsets from the indicated mouse lines. Data are quantified as mean ± SD from two independent experiments with two to four mice used per group and experiment. Statistically significant changes were identified by one-way ANOVA for Panel C and two-way ANOVA for Panel B, D and E. **: p<0.01., ***: p<0.001.

7.6. IELs become fully activated during *E. vermiformis* infection

As Villin-Cre-XBP1$^{fl/fl}$ mice failed to fully activate IELs, I wanted to test if IEC stress in the context of intestinal infection would be sufficient to activate IELs. I decided to use the *E. vermiformis* infection model. As described in the introduction to this chapter, *E. vermiformis* organisms infect specifically the lower part of the intestinal epithelium. If *E. vermiformis* infection is sufficient to activate IELs, then I would expect to observe the strongest response in ileum-sourced IELs. Previous work from this and other laboratories suggests that the first sign of parasite shedding occurs around six days post infection and that the peak of *E. vermiformis* infection, in terms of parasite load, occurs around ten days post infection (Inagaki-Ohara et al. 2006; Rose et al. 1984; Rose and Hesketh 1986; Linh et al. 2009; Roberts et al. 1996). Therefore, day five and ten post *E. vermiformis* infection seemed suitable days to assess IEL activation. My laboratory colleague Joana Guedes had performed dose titration experiments of *E. vermiformis* at the Babraham Institute, which suggested that a dose of 1000 oocysts per WT mouse generated an infection with clear parasite shedding, but without weight loss or other animal welfare concerns (Guedes, 2017). Therefore, Joana Guedes prepared *E. vermiformis* and infected WT mice with 1000 oocysts of *E. vermiformis* via oral gavage. I killed the infected mice and non-infected control mice at day five and ten

post infection. For the first experiments, I divided the small intestine into the three regions duodenum, jejunum and ileum and isolated IELs from them.

As an initial step of the analysis, I compared IELs from the three intestinal regions from non-infected mice to test whether these IELs are similar in terms of MTG and CD44 staining. When assessing CD44 staining, I observed that ileum-sourced IELs have higher expression of CD44 staining compared to those from the duodenum or the jejunum (Fig 7.3 A). When quantifying the percentage of $CD44^{Low}$ and $CD44^{High}$ cells, I observed that ileum-sourced IELs have statistically significantly higher proportion of $CD44^{High}$ cells compared to duodenum-sourced IELs (Fig 7.3 B). When assessing the MTG staining, I observed that ileum-sourced IELs have a statistically significantly higher MTG staining than duodenum- or jejunum-sourced IELs (Fig 7.3 C). This increase in MTG staining applied to all ileal IEL subsets (Fig 7.3 D). Collectively, these data indicate that ileum-sourced IELs are in a more activated state than other small intestinal IELs.

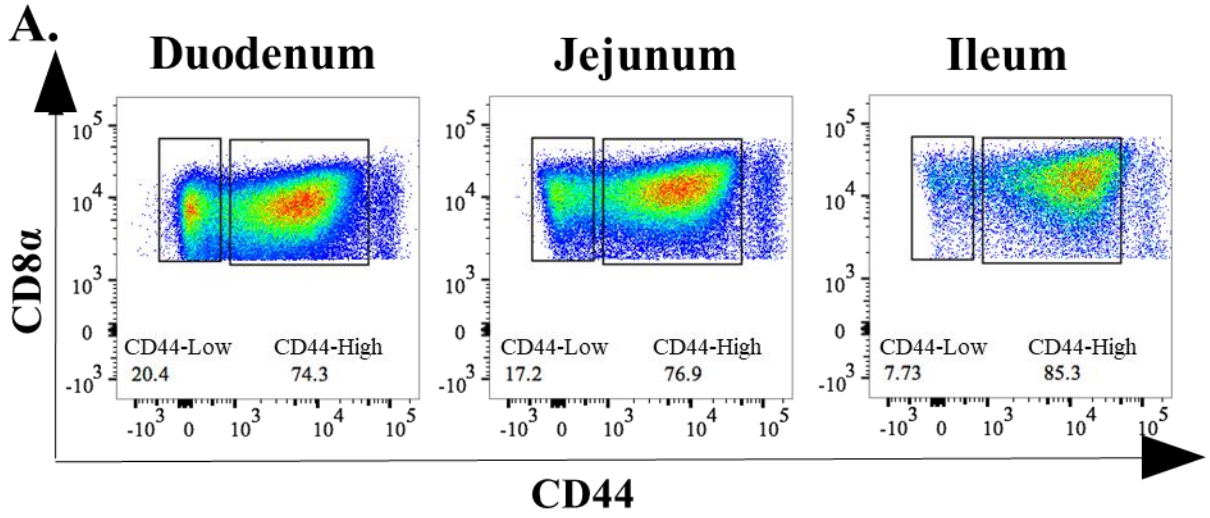

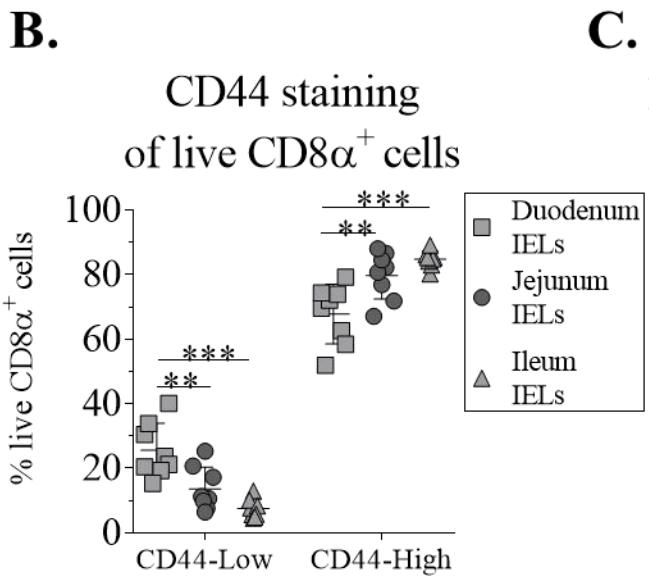

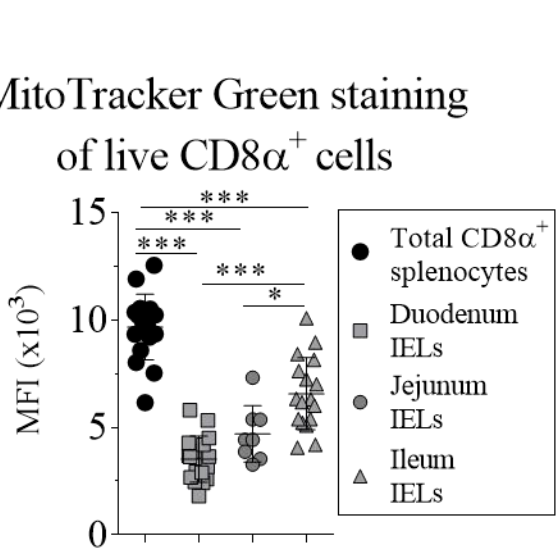

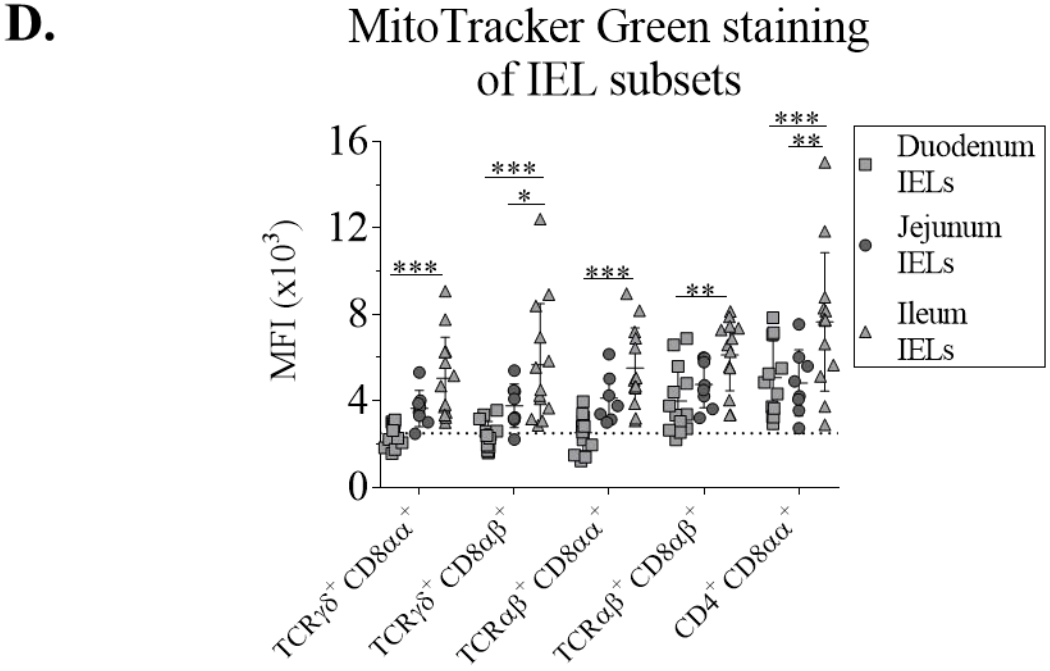

Figure 7.3 Ileum-sourced IELs are in a more activated state than other small intestinal IELs. WT small intestine was divided into three equal parts to isolate duodenum-sourced IELs, jejunum-sourced IELs and ileum-sourced IELs. These IELs were stained for MTG as previously described. A) Representative FACS plots showing CD44 staining of IELs from the three indicated intestinal sections. Pre-gating was made on live $CD8\alpha^+$ IELs. B) Quantification of the proportion of $CD44^{Low}$ and $CD44^{High}$ cells, according to gating as showed in Panel A. C-D) Quantification of MTG MFI from C) total $CD8\alpha^+$ splenocytes and total $CD8\alpha^+$ IELs from the three intestinal sections and D) IEL subsets from the indicated intestinal sections. Data are quantified as mean ± SD from two independent experiments with four to five mice used per experiment. Statistically significant changes were identified by one-way ANOVA for Panel C and two-way ANOVA for Panel B and D. *: $p<0.05$., **: $p<0.01$., ***: $p<0.001$.

When comparing *E. vermiformis*-infected IELs with non-infected IELs, I observed an increase in CD44 expression; both duodenum-and jejunum-sourced IELs showed a lower proportion of $CD44^{Low}$ cells at day five and day ten post infection (Fig 7.4 A-B). Ileum-sourced IELs, that already have a higher expression of CD44 at steady state (Fig 7.3 A-B), showed a significantly higher expression at day ten post infection only (Fig 7.4 C). These data indicate that all IELs in the small intestine become more activated during the *E. vermiformis* infection.

When assessing MTG staining, I observed that IELs from all three intestinal segments have a statistically significant increase in MTG staining at day five post infection (Fig 7.4 D). Interestingly, while duodenum-and jejunum-sourced IELs have MTG staining that is not significantly different compared to non-infected controls at day ten post infection, ileum-sourced IELs maintain significantly increased MTG staining compared to non-infected controls (Fig 7.4 D). These data fit with the fact that *E. vermiformis* organisms infect the lower part of the small intestine. When assessing the different IEL subsets, I found that ileal

CD8αβ$^+$ IELs responded first and most strongly (Fig 7.4 E and F). The same trend was observed in αCD3-activated IELs (Fig 6.1 E and F), CD4$^+$ CD8αα$^+$ IELs did no significantly alter their MTG staining, while the remaining subsets either trend to do or statistically significantly increase their MTG staining (Fig 7.4 F). An alternative statistical method, multiple t-test for each IEL subset individually, indicated that all IEL subsets except CD4$^+$ CD8αα$^+$ IELs have statistically increased MTG staining. Interestingly, the differences in response in the different IEL subsets are not as drastic as for αCD3-mediated IEL activation (Fig 6.1 D-F), suggesting that the activation mechanism(s) may be differ between αCD3-mediated and *E. vermiformis*-mediated IEL activation.

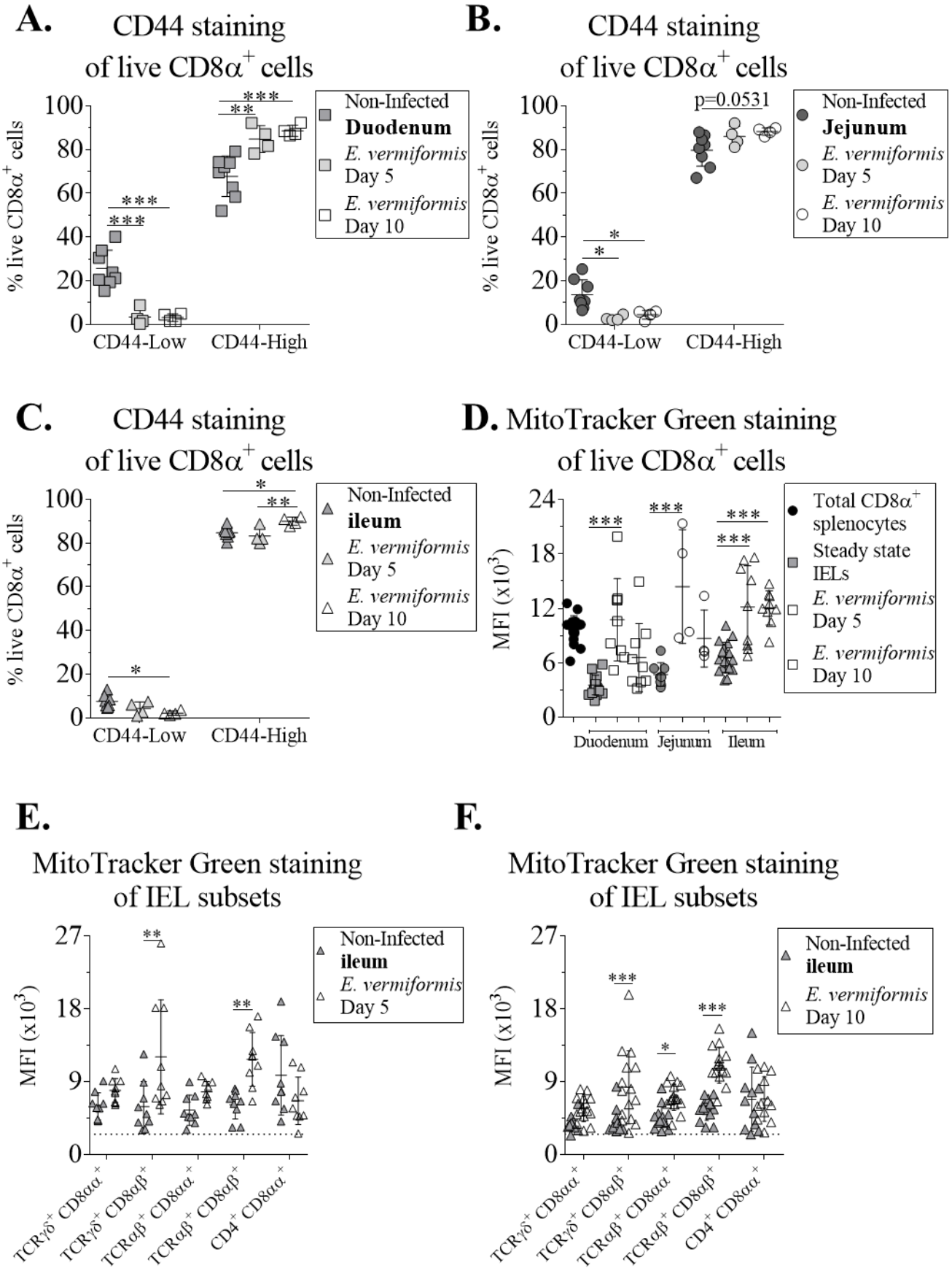

Figure 7.4 IELs increase their mitochondrial mass and CD44 staining during *E. vermiformis* infection. WT mice were infected with 1000 oocysts of *E. vermiformis* via oral gavage. Five and ten days post infection, infected and non-infected control mice were culled and small intestine was divided into three equal parts to isolate duodenum-sourced IELs, jejunum-sourced IELs and ileum-sourced IELs. These were stained for MTG as previously described. A-C) Quantification of the proportion of $CD44^{Low}$ and $CD44^{High}$ cells from infected and non-infected IELs sourced from A) duodenum, B) jejunum and C) ileum. D) Quantification of MTG MFI from total $CD8\alpha^{+}$ splenocytes and total $CD8\alpha^{+}$ IELs sourced from the three intestinal segments from infected and non-infected mice. E-F) MTG MFI in ileal IEL subsets comparing non-infected cells with E) five and F) ten days post *E. vermiformis* infection. Data are presented as mean ± SD from one (jejunum samples), two or four (Panel F) independent experiments with four to five mice per condition and experiment. Statistically significant changes were identified by one-way ANOVA for Panel D and two-way ANOVA for Panel A, B, C, E and F. *: $p<0.05$., **: $p<0.01$., ***: $p<0.001$.

The data above suggest that IELs from *E. vermiformis*-infected mice are activated. Next, I assessed whether *E vermiformis* infection would provide conditions that lead to cytokine production from the activated IELs. IELs from infected and non-infected mice were re-stimulated as previously described. Interestingly, control ileal IELs produced small amounts of both IFNγ and TNFα (Fig 7.5 E-F). At day five post infection, no statistically significant increase in IFNγ or TNFα production could be observed in any of the activated IELs (Fig 7.5 A-F). At the peak of infection, day ten, ileal IELs exhibit a statistically significant increase in both IFNγ and TNFα production (Fig 7.5 E-F). At this time point, duodenum-sourced IELs showed a similarly very low production of IFNγ and TNFα (Fig 7.5 A-B), while jejunum-sourced IELs showed a statistically significant increase in IFNγ and TNFα production (Fig 7.5 C-D). However, ileum-sourced IELs have a higher production of IFNγ and TNFα than those obtained from the jejunum. These increases in intracellular IFNγ and TNFα in activated ileal IELs correlated with the increase in MTG staining (Fig 7.5 G-H), supporting the notion that these IELs may become activated in a mitochondria-dependent manner.

In addition to producing cytokines, IELs from infected mice show increased expression of the proliferation marker Ki-67 compared to IELs from non-infected mice (Fig 7.6 A-C). Unlike the cytokine production in ileal IELs, Ki-67 expression is already significantly increased by day five post infection. As with the other assessed activation parameters, ileal IELs respond most strongly with regards of Ki-67 expression (Fig 7.6 C). The increase in Ki-67 expression in total $CD8\alpha^+$ IELs correlated with the increase in MTG staining (Fig 7.6 D), again supporting the notion of mitochondria-dependent IEL activation.

After observing that ileum-sourced IELs have specifically increased production of cytokines and Ki-67, I next wanted to find out which ileal IEL subsets are responsible for these

increases. Interestingly, TCRαβ$^+$ CD8αβ$^+$ IELs responded most strongly for all three intracellular parameters. In addition to TCRαβ$^+$ CD8αβ$^+$ IELs, TCRγδ$^+$ CD8αβ$^+$ and CD4$^+$ CD8αα$^+$ IELs also exhibited statistically significant increases in Ki-67 expression and production of IFNγ and TNFα (Fig 7.7 A-C).

Collectively, these data suggest that the whole small intestine is affected by *E. vermiformis* infection with regards to IEL activation. As *E. vermiformis* is specifically infecting IECs, crosstalk between IEC and IELs may be causing the increase in MTG staining. For subsequent *E. vermiformis* experiments, ileum-sourced IELs were isolated as these had the strongest response towards *E. vermiformis* infection.

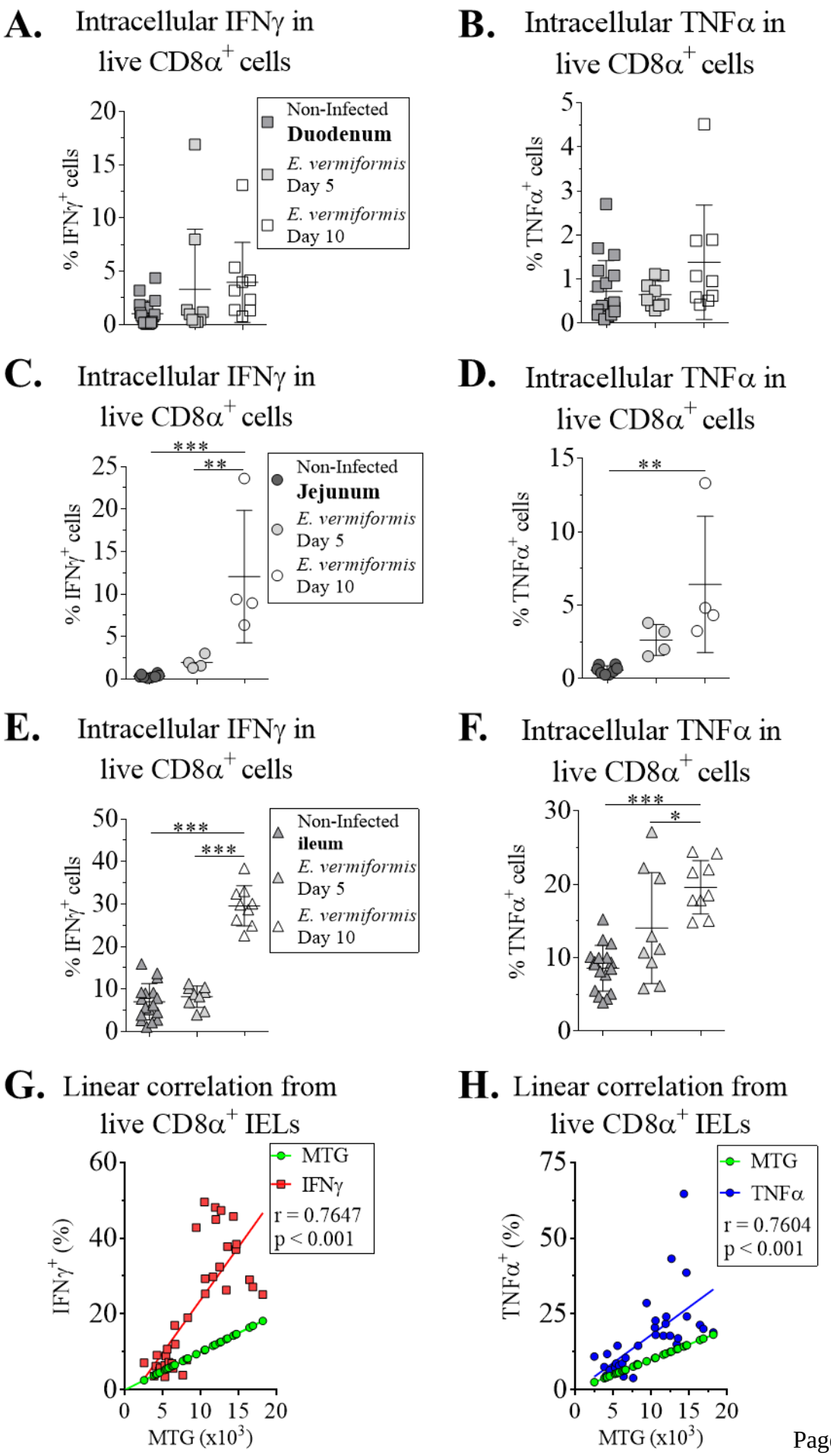

Figure 7.5 IELs produce cytokines during *E. vermiformis* infection. WT mice were infected with 1000 oocysts of *E. vermiformis* via oral gavage. Five and ten days post infection, infected and non-infected control mice were culled. The small intestine was divided into three equal parts to isolate duodenum-sourced, jejunum-sourced and ileum-sourced IELs. These IELs were re-stimulated and stained for IFNγ and TNFα. A-F) IFNγ (left) and TNFα (right) staining in total $CD8\alpha^+$ IELs sourced from A-B) duodenum**,** C-D) jejunum and E-F) ileum from non-infected and infected mice at day five and ten post infection. G-H) Spearman correlation between total ileal $CD8\alpha^+$ IELs from day 10 post infection between MTG staining and G) IFNγ or H) TNFα. Data are presented as mean ± SD from one (jejunum samples), two (duodenum samples) or five (ileum samples) independent experiments with two to five mice per condition and experiment. Statistically significant changes were identified by one-way ANOVA for panel A-F and Spearman correlation for Panel G and H.*: $p<0.05$., **: $p<0.01$., ***: $p<0.001$.

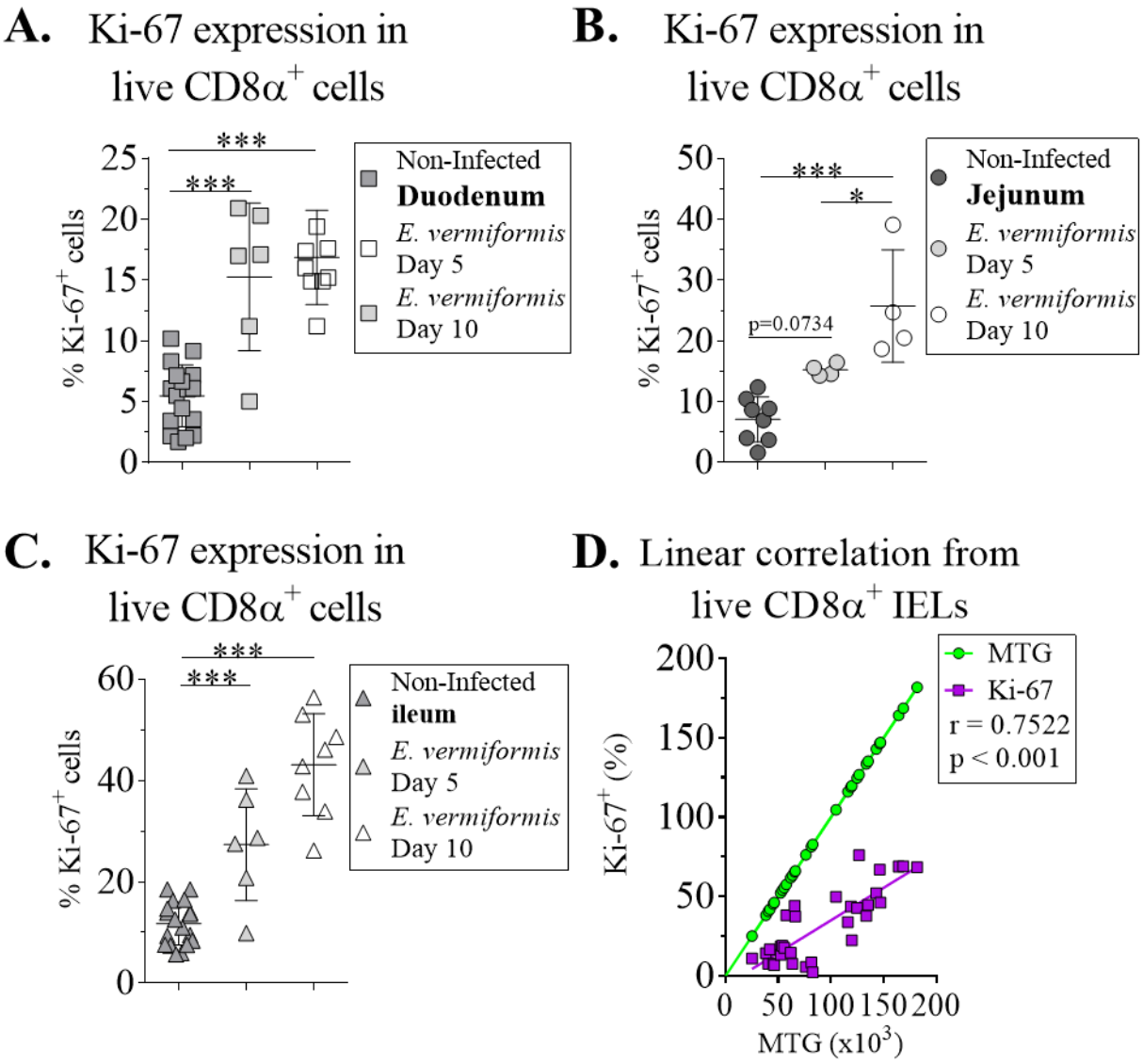

Figure 7.6. IELs increase their expression of Ki-67 during *E. vermiformis* infection. WT mice were infected with 1000 oocysts of *E. vermiformis* via oral gavage. Five and ten days post infection, infected and non-infected control mice were culled. The small intestine was divided into three equal parts to isolate duodenum-sourced IELs, jejunum-sourced IELs and ileum-sourced IELs. These were stained for Ki-67. A-C) Ki-67 staining in total CD8α$^+$ IELs sourced from A) duodenum**,** B) jejunum and C) ileum from non-infected and infected mice at day five and ten post infection. D) Spearman correlation between total ileal CD8α$^+$ IELs from day ten post infection between MTG staining and percentage of Ki-67. Data are presented as mean ± SD from one (jejunum samples), two (duodenum samples) or five (ileum samples) independent experiments with two to five mice per condition and experiment. Statistically significant changes were identified by one-way ANOVA for panel A-C and Spearman correlation for Panel D.*: p<0.05., ***: p<0.001.

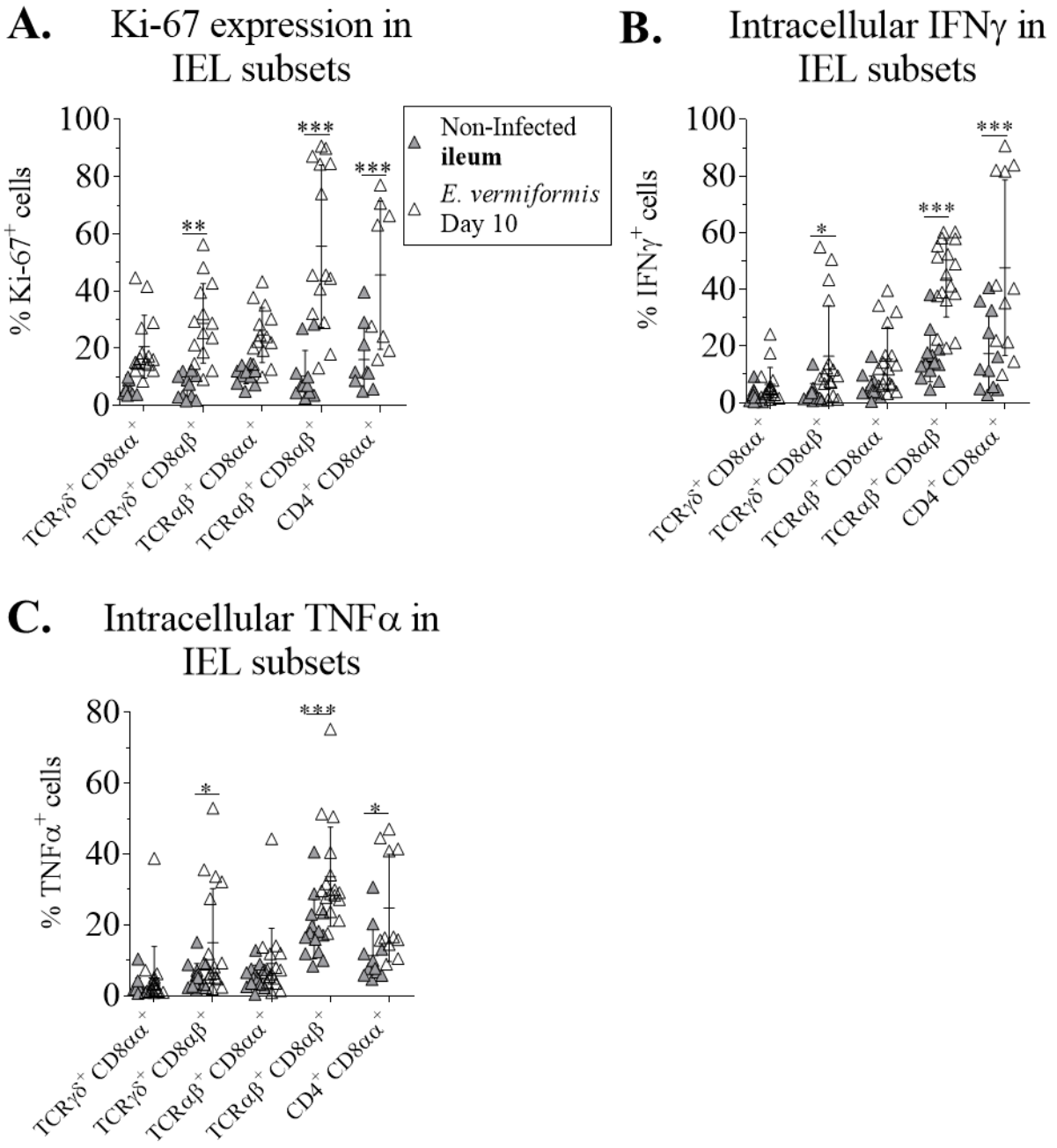

Figure 7.7. During *E. vermiformis* infection, TCRαβ⁺ CD8αβ⁺ IELs responded most strongly in regards to Ki-67 expression and cytokine production. WT mice were infected with 1000 oocysts of *E. vermiformis* via oral gavage. Ten days post infection, infected and non-infected control mice were culled and ileum-sourced IELs isolated and stained for A) Ki-67, B) IFNγ or C) TNFα. Data are presented as mean ± SD from four independent experiments with two to five mice per condition and experiment. Statistically significant changes were identified by two-way ANOVA. *: p<0.05., **: p<0.01., ***: p<0.001.

7.7. *E. vermiformis*-activated IELs have higher mitochondrial ROS production, but show no increase in mitochondrial membrane potential

As ileal IELs produce cytokines during *E. vermiformis* infection, they seem to be in a more activated state compared to αCD3-stimulated IELs. Therefore, I next wanted to address whether *E. vermiformis*-mediated activation of IELs bring about an increase in mitochondrial ROS production as well as an increase in mitochondrial membrane potential. The latter would enable IELs to generate SRC, which non-treated IELs lack (Fig 5.5). Data from *E. vermiformis*-infected mice showed that ileal $CD8\alpha^+$ IELs had an increased mitochondrial ROS production, measured by MitoSOX staining (Fig 7.8 A). This increase in mitochondrial ROS production correlates with the increase in MTG staining (Fig 7.8 C). As with αCD3-stimulated IELs (fig 6.4 C), only $CD8\alpha\beta^+$ IELs exhibited statistically significant increase in mitochondrial ROS production (Fig 7.8 B).

Interestingly, IELs activated via *E. vermiformis* infection showed no statistically significant increase in MTO staining (Fig 7.9 A). For this quantification only, the MTO MFI of $CD8\alpha^+$ TCR^+ cells were plotted because in this case the small proportion of $CD8\alpha^+$ TCR^- cells had very high MTO staining. This led to a very high MTO MFI, which could not be traced to any of the IEL subsets. When assessing IEL subsets, only $CD4^+$ $CD8\alpha\alpha^+$ IELs exhibited a statistically significant increase in MTO staining (Fig 7.9 B). Therefore, it is likely that IELs activated via *E. vermiformis* infection still lack SRC. In addition, as with αCD3-stimulated IELs, these IELs do not have significant changes in their CL content, measured by NAO staining (Fig 7.9 C). This applied to all IEL subsets (Fig 7.9 D). As shown in Figure 6.15, the composition of CLs alters in activated compared to non-activated IELs, suggesting that there are changes to CLs taking place, but not resulting in changed total amount of CLs.

These data, together with the data from the previous chapter, support a model in which IELs show mitochondrial plasticity during activation and this activation may proceed in a mitochondria-dependent manner.

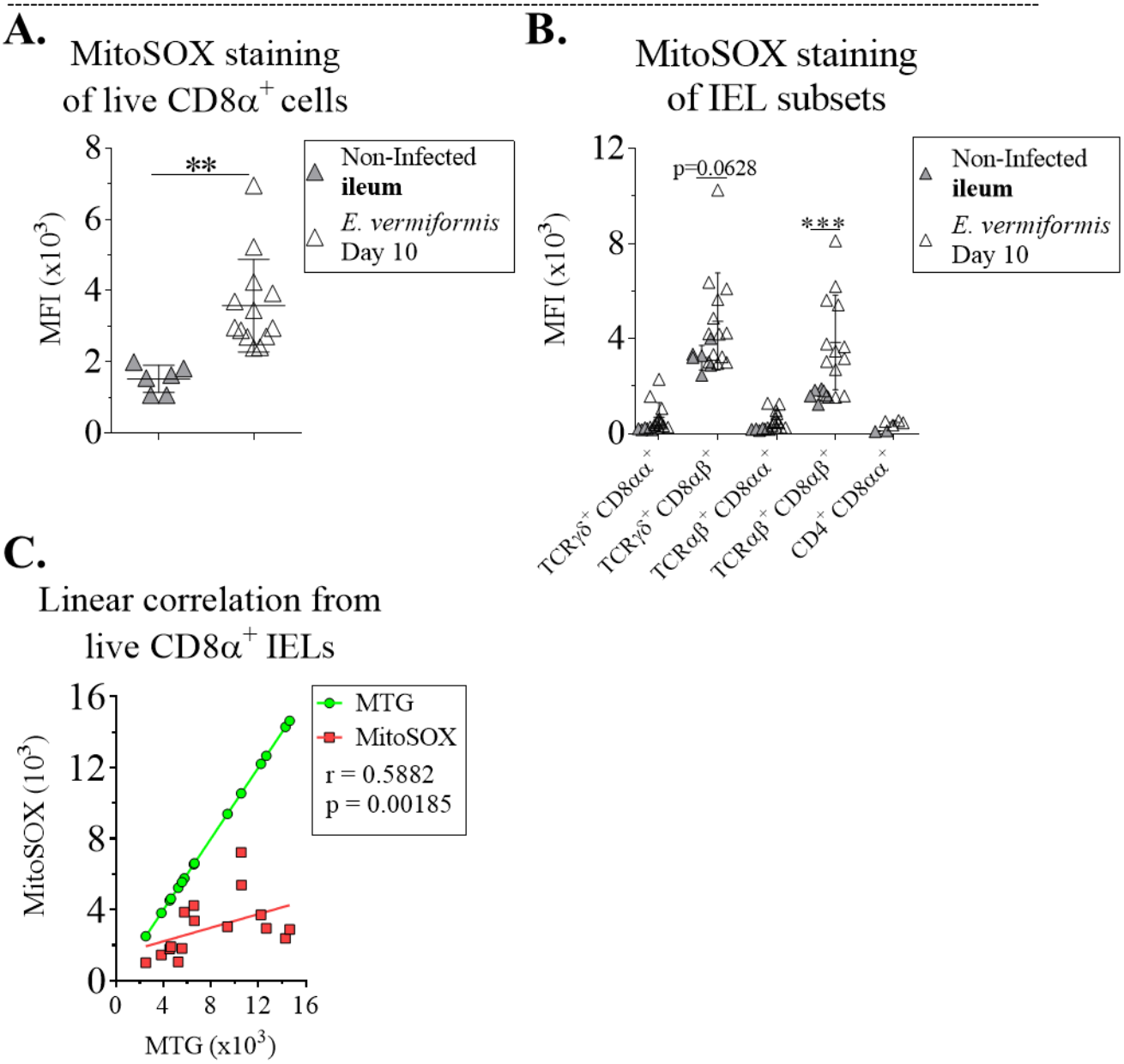

Figure 7.8 *E. vermiformis*-activated IELs have a higher level of mitochondrial ROS production. WT mice were infected with 1000 oocysts of *E. vermiformis* via oral gavage. Ten days post infection, infected and non-infected control mice were culled and ileum-sourced IELs isolated. These IELs were stained for MitoSOX, A-B) Quantification of MitoSOX MFI between non-infected and infected A) total CD8α$^+$ IELs or B) IEL subsets. C) Spearman correlation between total ileal CD8α$^+$ IELs from day ten post infection between MTG staining and MitoSOX staining. Data are presented as mean ± SD from four independent experiments with two to four mice per condition and experiment. Statistically significant changes were identified by t-test (Panel A) and two-way ANOVA (Panel B). **: p<0.01., ***: p<0.001.

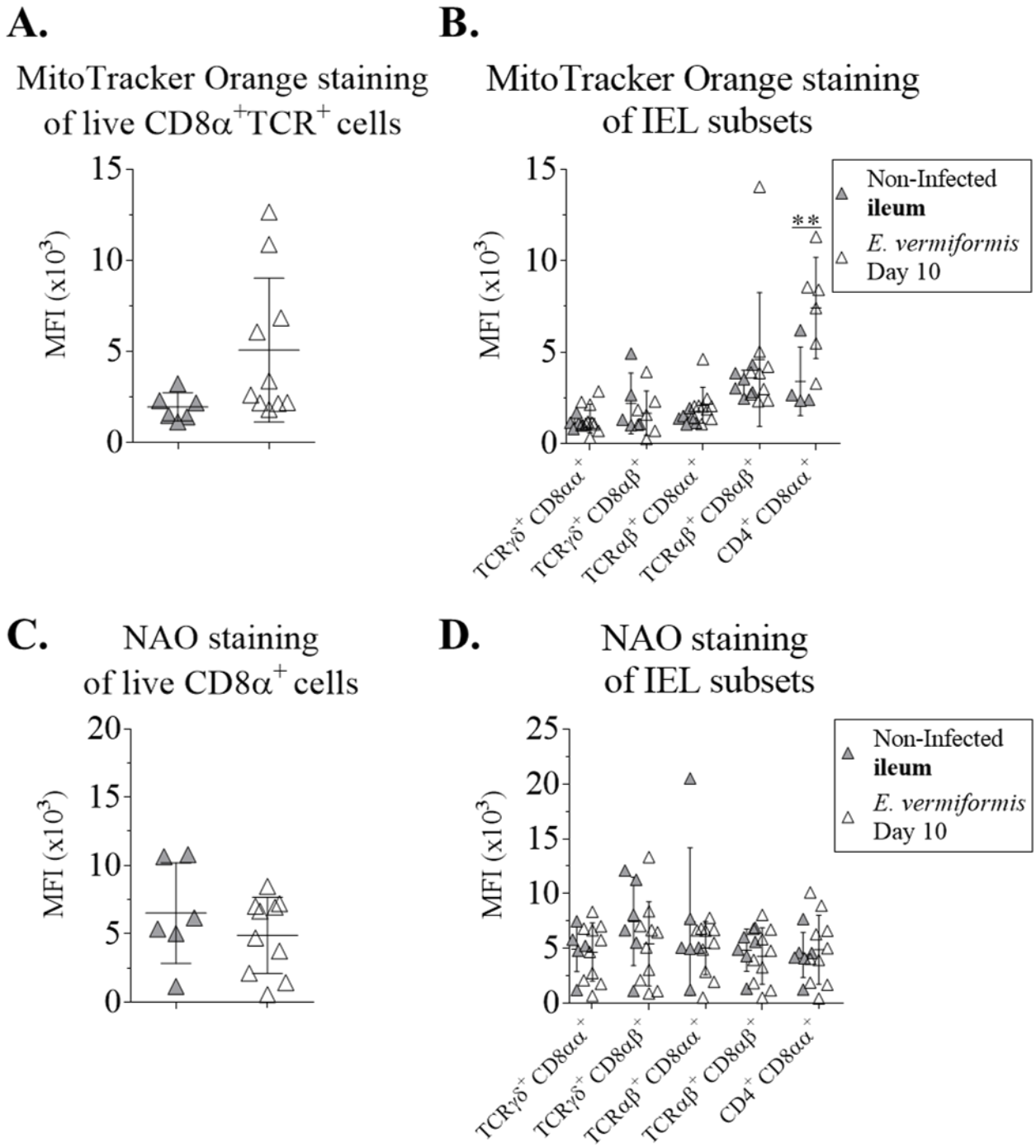

Figure 7.9 *E. vermiformis*-activated IELs show no increase in mitochondrial membrane potential. WT mice were infected with 1000 oocysts of *E. vermiformis* via oral gavage. Ten days post infection, infected and non-infected control mice were culled and ileum-sourced IELs isolated. These IELs were stained for MTO and NAO. A-B) MTO MFI between non-infected and infected A) total $CD8\alpha^{+}TCR^{+}$ IELs, or B) IEL subsets. C-D) NAO MFI between non-infected and infected C) total $CD8\alpha^{+}$ IELs, or D) IEL subsets. Data are presented as mean ± SD from three independent experiments with two to four mice per condition and experiment. Statistically significant changes were identified by Mann-Whitney test (Panel A and C) or two-way ANOVA (Panel B and D): **: $p<0.01$.

7.8. MNV-CW3 infection, but not MNV-O7, leads to IEL activation.

After observing that *E. vermiformis* infection can activate IELs, I next wanted to assess whether other intestinal pathogens are able to activate IELs. With kind support from Jonathan Heeney's laboratory at the Department of Veterinary Medicine at University of Cambridge and his Ph.D. student Osama Eisa, I was able to obtain MNV-infected small intestines for IEL activation assessment. For this work, two different MNV strains have been used, namely MNV-O7 and MNV-CW3. Previous data obtained from combining MNV and αCD3 models showed a reduction in the MNV viral load in mice that have been pre-treated with αCD3 8 hours prior to MNV-O7 infection (Swamy et al., 2015).

Knowing the distinct differences in pathology between these MNV strains, as mentioned in the introduction to this chapter, as well as observing that MNV-O7, but not MNV-CW3 seem to be able to infect IECs (Fig 4.10), I wanted to test whether IELs become activated during MNV-infection, and if so, whether they might play a role in the immune response towards MNV. WT mice from the Babraham Institute (the animal unit was known to be free of MNV) were transferred to the Pathology Unit at University of Cambridge (animal unit tested positive for MNV), to ensure that we are assessing IEL response towards primary MNV infection. These mice were oral gavaged with 5 x 10^6 TCID50 of MNV-O7 or MNV-CW3. Both MNV-O7 and MNV-CW3 infection reach their peak viral load already after one day of infection (data not shown), so we decided to cull the mice two, four and seven days post infection. After these time points, a small section from each ileum was taken for Osama Eisa to perform viral quantification assays. The rest of the small intestines were transferred to me to isolate IELs and assess their activation.

Surprisingly, despite the fact that MNV-O7 seems to infect IECs, and the existence of a paper suggesting the IELs may be capable of reducing of MNV viral levels (Swamy et al., 2015), I observed no statistically significant increase in MTG staining of IELs from MNV-O7-infected mice (Fig 7.10 B). In other models, such as Villin-Cre-XBP1$^{fl/fl}$ mice, I have detected increased expression of CD44, even though there is no significant difference in MTG staining (Fig 7.2 A-B). For IELs isolated from MNV-O7-infected mice, I observed a statistically significant increase in the proportion of CD44^{High} cells (Fig 7.10 A), suggesting that IELs from MNV-O7-infected mice have become more activated, but not as activated as observed in *E. vermiformis* and αCD3 models.

Even more surprisingly, IELs from MNV-CW3-infected mice had both increased CD44 staining (Fig 7.10 A), and MTG staining (Fig 7.10 C). This increase in MTG staining applies to TCRαβ$^+$ CD8αβ$^+$, TCRγδ$^+$ CD8αβ$^+$, TCRγδ$^+$ CD8αα$^+$ and TCRαβ$^+$ CD8αα$^+$ IELs (Fig 7.10 F). Interestingly, the activation appears to be of similar amplitude in these subsets compared to other activation models such as αCD3 and *E. vermiformis* infection. Viral quantification from MNV-O7- and MNV-CW3-infected mice showed that all mice were infected as expected from previous data obtained in the Heeney laboratory (Fig 7.10 D and E). Therefore, the lack of full activation of IEL in MNV-O7-infected mice is probably not due to poor infection levels. These data suggest that MNV-O7 and MNV-CW3 cause different infection in the small intestine, resulting in IEL activation in the case of MNV-CW3 infection, but not in MNV-O7 infection.

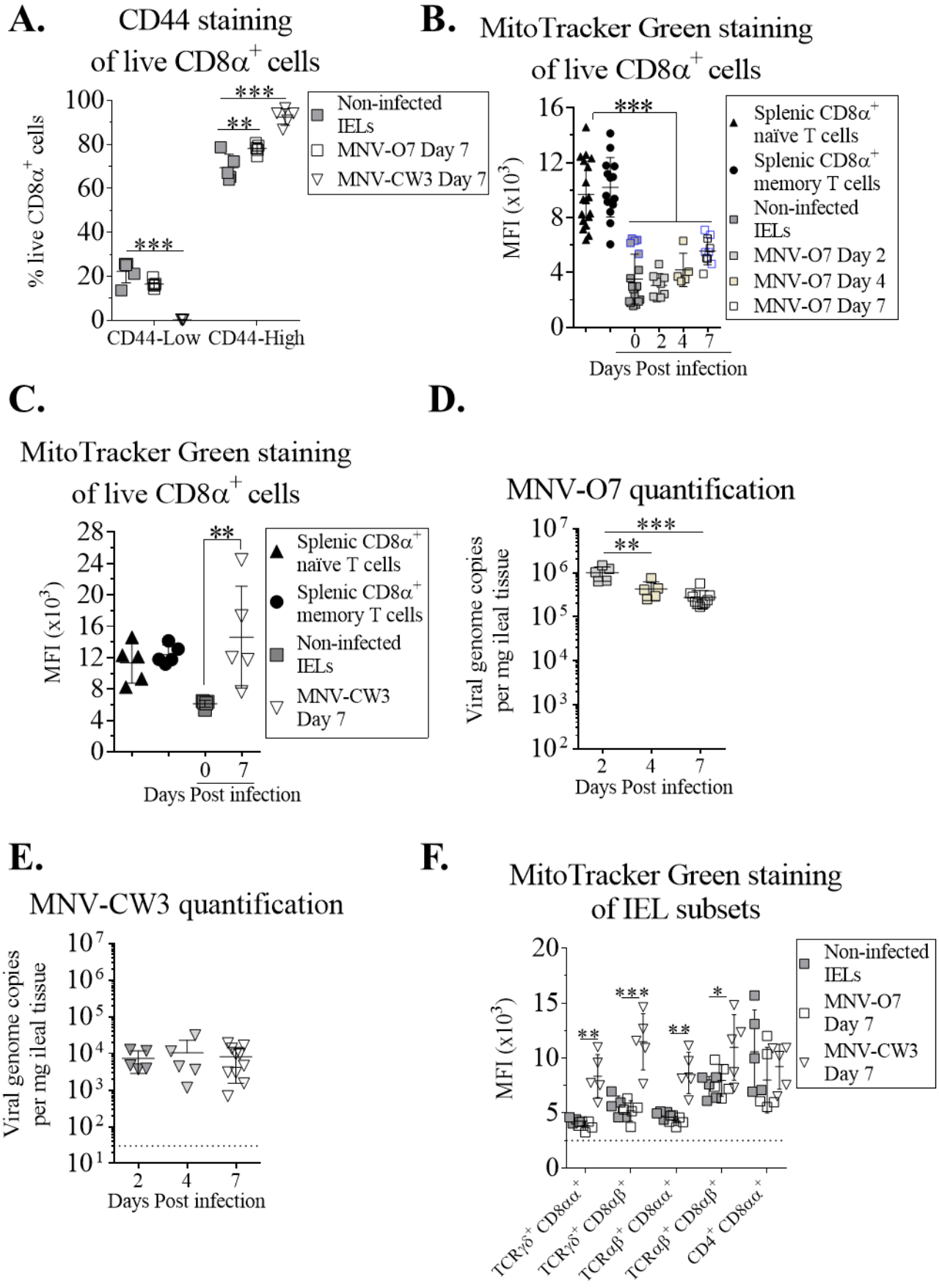

Figure 7.10. MNV infection-induced IEL activation is dependent on the MNV-strain. WT mice were infected with 5 x 10^6 TCID MNV-O7 or MNV-CW3 via oral gavage. Two, four and seven days post infection, infected and non-infected control mice were culled and IELs isolated. A) Quantification of $CD44^{Low}$ and $CD44^{High}$ cells from the non-infected and MNV-infected mice at day 7 post infection. B-C) Quantification of MTG MFI from total $CD8\alpha^+$ splenocytes and total $CD8\alpha^+$ IELs from non-infected mice and mice infected with B) MNV-O7 or C) MNV-CW3 at indicated time points post infection. D-E) Viral quantification of ileum from D) MNV-O7- or E) MNV-CW3-infected mice. F) Quantification of MTG MFI in IEL subsets from non-infected, MNV-O7- or MNV-CW3 infected at day 7 post infection. Data are presented as mean ± SD from one to two independent experiments with three to five mice per condition and experiment. Statistically significant changes were identified by one-way ANOVA for Panel B-E or two-way ANOVA for Panel A and F.*: $p<0.05$., **: $p<0.01$., ***: $p<0.001$.

7.9. *Salmonella* infection does not activate IELs

After observing that infections caused by an intestinal parasite and an enteric virus led to IEL activation, I wanted to test if enteric bacterial pathogen may be able to activate IELs as well. If so, then IELs may possess the capability to recognize bacterial, viral and eukaryotic pathogens. For this assessment, I obtained intestines from *Salmonella*-infected mice thanks to Jonathan Heeney and Osama Eisa. For the experiment, mice from the Babraham Institute were transferred to the Pathology Unit at University of Cambridge. There, the mice were infected with *Salmonella*. As the *Salmonella* infection level in the intestinal compartment lasts for a few hours only (Carter and Collins, 1974), infected mice were taken at two, four, twelve and 24 hours post infection. For these experiments, faecal samples were taken to quantify and confirm successful *Salmonella* infection, while the whole small intestine was used for MTG assessment. Despite successful infection (Fig 7.11 A), IELs were not statistically significantly activated during *Salmonella* infection as shown by MTG staining (Fig 7.11 B) and the proportion of $CD44^{Low}$ and $CD44^{High}$ cells (Fig 7.11 C).

These findings are surprising, considering a recent report suggesting that IELs respond to *Salmonella* infection. In addition to demonstrating that TCRγδ$^+$ IEL migrate differently between IECs in non-infected mice compared to *Salmonella*-infected mice, the authors also demonstrated that TCRγδ$^+$ IELs have increased SRC (Hoytema van Konijnenburg et al., 2017). These data indicate that TCRγδ$^+$ IELs have altered metabolically due to the infection. However, I could not detect an increase in mitochondrial mass.

Collectively, the data from the tested infection models suggest that not all intestinal pathogen infections lead to IEL activation. Therefore, further experiments are required to pinpoint what is the common feature of IEL activation in the *E. vermiformis* and MNV-CW3 infection models, which appear to be absent in the MNV-O7 and *Salmonella* infection models.

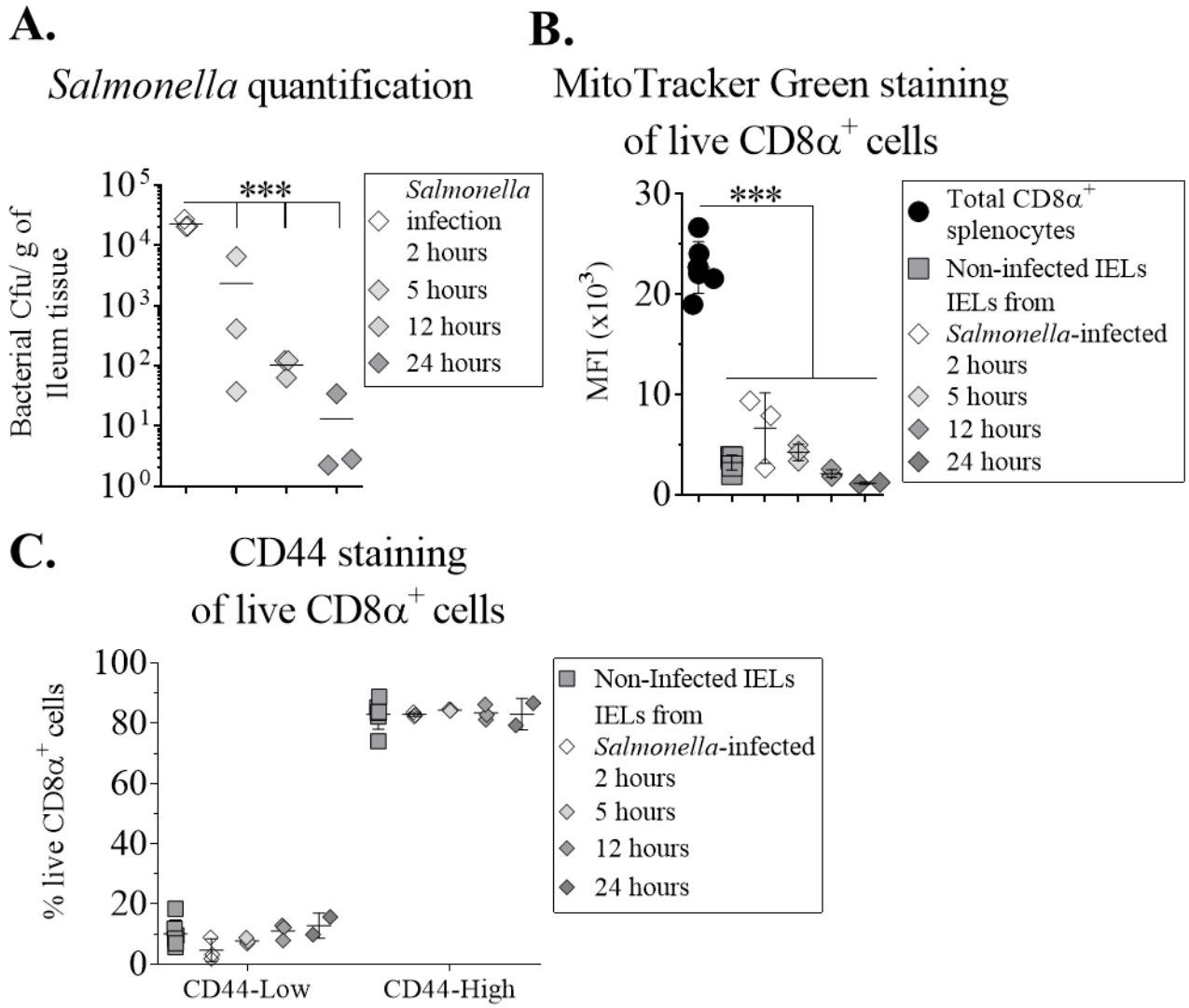

Figure 7.11. *Salmonella* infection fails to activate IELs. WT mice from the Babraham Institute were transferred to the University of Cambridge for *Salmonella* infection (4-6.2 x 10^8 colony-forming units, cfu) via oral gavage. A) Faecal quantification of *Salmonella* organisms at the tested time points. B) Quantification of MTG MFI of total CD8α$^+$ IELs and splenocytes at the indicated time points after infection. C) Quantification of the proportion of CD44^{Low} and CD44^{High} IELs, from non-infected and *Salmonella*-infected mice. Data are presented as mean ± SD (Panel B and C) or mean (Panel B) with two to three mice per time point. Statistically significant changes were identified by one-way ANOVA. ***: p<0.001.

7.10. IELs are activated in IL-22-/- mice in a microbiota-dependent manner

One potential aspect of intestinal pathology is that the IEC barrier becomes compromised or damaged. One factor that has been shown to be important for IEC proliferation and mucus production is the interleukin IL-22. Addition of IL-22 increased the production of Muc-1, -2 and -3 (Turner et al., 2013). Therefore, it is possible that IL-22-/- mice have a thinner mucus layer at the intestinal site compared to WT mice. Cells that have been reported to produce IL-22 are IELs (Ahlfors et al., 2014), ILCs (Sonnenberg et al., 2011), NK-like cells (Fuchs and Colonna, 2011), Th17 and Th22 cells (Liang et al., 2006; Zheng et al., 2007). It has been reported that IL-22-/- mice have different microbiota composition, containing more segmented filamentous bacteria (SFB), a Gram-positive commensal bacteria (Davis and Savage, 1974; Vaishnava et al., 2011) compared to WT mice (Shih et al., 2014). In addition, it has been reported that IL-22-/- mice have reduced production of antimicrobial peptides (AMPs) such as RegIIIβ and RegIIIγ (Zenewicz et al., 2013). IL-22-/- mice have been reported to be more susceptible to intestinal infections: they suffer from weight loss and succumb to the intestinal *Citrobacter rodentium* infection, while WT mice cope with the infection (Zheng et al., 2008). Mice on DSS-induced colitis had statistically significant slower weight recovery when receiving anti-IL-22 via i.p injection every other day (Neufert et al., 2010). These data suggest an important role for IL-22 in intestinal homeostasis.

Hence, I wanted to assess the activation status of IELs in IL-22-/- mice. I observed that IELs from these mice have higher MTG staining compared to WT controls (Fig 7.12 A). This applied to all IEL subsets except $CD4^+$ $CD8\alpha\alpha^+$ IELs (Fig 7.12 C). In addition to having increased MTG staining, IL-22-/- IELs have increased expression of CD44 (Fig 7.12 B), a marker that I have demonstrated to be increased in IELs from αCD3-treated mice (Fig 6.1 A),

Villin-Cre-XBP1$^{fl/fl}$ mice (Fig 7.2 A-B), *E. vermiformis*-infected mice (Fig 7.4 A-C) and MNV-CW3-infected mice (Fig 7.10 A).

As IL-22-/- mice are reported to have defects in their IEC barrier, I wanted to test whether the activation of IELs observed in IL-22-/- mice might be due to commensal microbiota that may be situated closer to the intestinal barrier and may even translocate through the IEC barrier. To address this, I used a broad-spectrum antibiotic depletion model on IL-22-/- mice. To deplete the majority of commensal microbiota, I used a cocktail of antibiotics (consisting of colistin, ampicillin and streptomycin), which has been successfully used by another laboratory (Sawa et al., 2011). This antibiotic cocktail was administered into drinking water of WT and IL-22-/- mice for 14 days *ab libitum*, with refill of the antibiotic cocktail every 5 days. After 14 days of antibiotic depletion, the mice were culled and IELs isolated from the small intestine. I observed significant enlargement of the caecum of antibiotic-treated mice compared to non-treated mice (data not shown). This phenotype of an enlarged caecum is observed in germ-free mice as well (Savage and Dubos, 1968; Reikvam et al., 2011), suggesting that the antibiotic cocktail used has depleted a considerable amount of commensal microbiota. Interestingly, I observed that IELs from antibiotic-treated IL-22-/- mice have significantly reduced MTG staining compared to IELs from non-treated IL-22-/- mice (Fig 7.12 A). This reduction in MTG staining is at a level that is not statistically significantly different compared to non-treated WT IELs (Fig 7.12 A). Antibiotic treatment of WT mice did not alter the MTG staining in their IELs (Fig 7.12 A). In addition to the reduction in MTG staining, antibiotic treatment also reduced the heightened CD44 staining of IELs in IL-22-/- mice (Fig 7.12 B). These observations suggest that IELs in IL-22-/- mice have entered a less activated state after the antibiotic treatment. Interestingly, non-treated IL-22-/- mice have very low production of IFNγ (Fig 7.12 D), TNFα (Fig 7.12 E) and expression of the

proliferation marker Ki-67 (Fig 7.12 F). These data suggest that the activation in IL-22-/- may be different compared to αCD3-activated and *E. vermiformis*-activated IELs, of which the former showed an increase in IEL Ki-67 expression (Fig 6.3) while the latter showed an increase in both IEL Ki-67 expression and production of TNFα and IFNγ (Fig 7.5). Importantly, these data suggest that commensal microbiota are activating IELs in IL-22-/- mice.

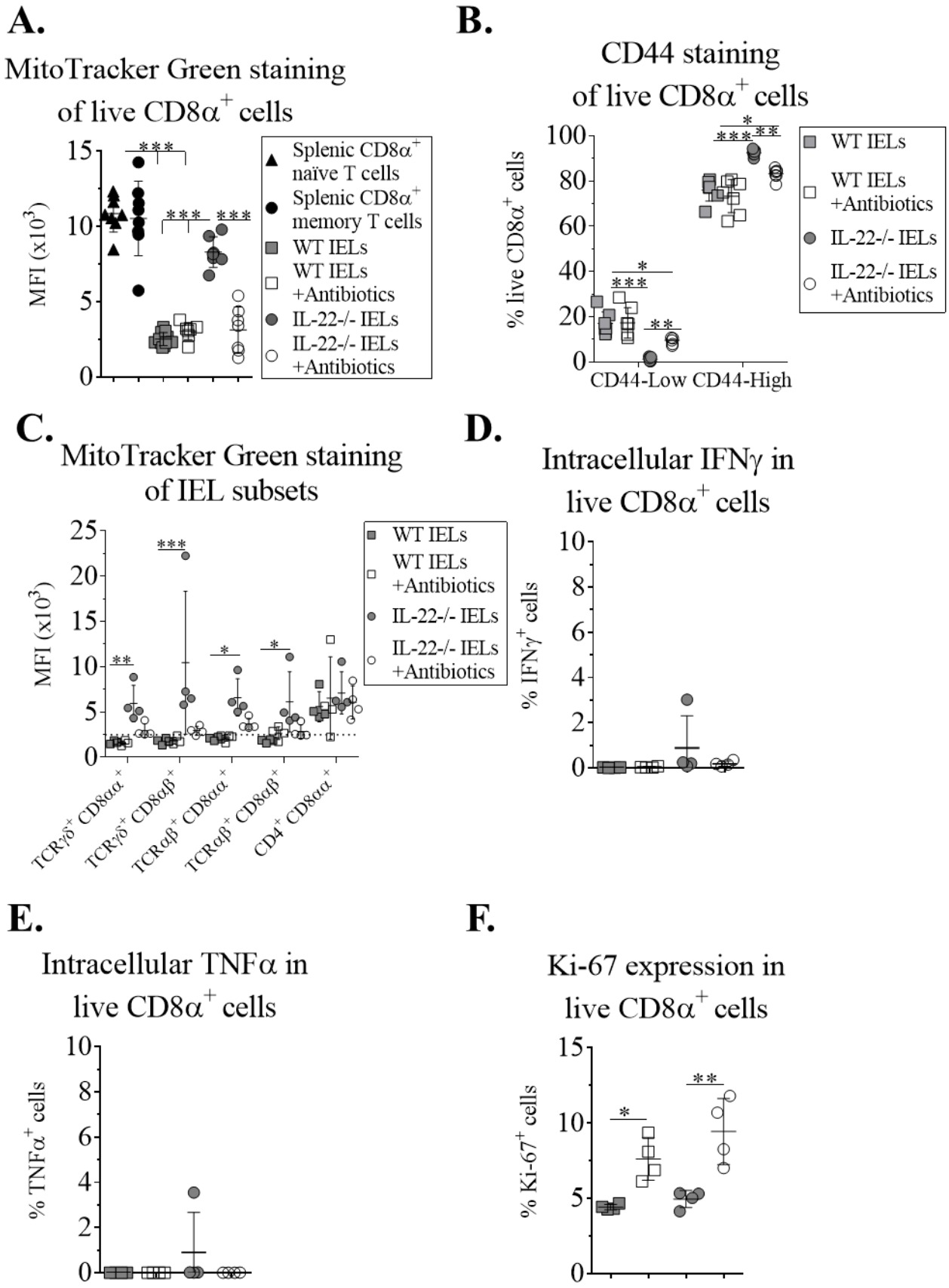

Figure 7.12. IELs in IL-22-/- mice are activated in a microbiota-dependent manner. WT and IL-22-/- mice were treated with broad-spectrum antibiotics (1 g/l ampicillin, 1 g/l colistin and 5 g/l streptomycin) in their drinking water *ad libitum* for 14 days. Afterwards, IELs were isolated and analysed by flow cytometry. A) Quantification of MFI of MTG staining of total $CD8\alpha^+$ IELs and splenocytes from non-treated and antibiotic-treated WT and IL-22-/- IELs**.** B) Quantification of $CD44^{Low}$ and $CD44^{High}$ cells from non-treated and antibiotic-treated WT and IL-22-/- IELs. C) Representative MTG MFI quantification from IEL subsets from non-treated and antibiotic-treated WT and IL-22-/- mice. D-F) Quantification of the percentage of D) $IFN\gamma^+$, E) $TNF\alpha^+$ and F) $Ki\text{-}67^+$ cells amongst $CD8\alpha^+$ IELs from non-treated and antibiotic-treated WT and IL-22-/- IELs. Data are presented as mean ± SD from one (Panel C-F) to two (Panel A and B) independent experiments with three to four mice per condition and experiment. Statistically significant changes were identified by one-way ANOVA for Panel A, D-F or two-way ANOVA Panel B and C. *: $p<0.05$., **: $p<0.01$., ***: $p<0.001$.

7.11. Commensal microbiota are activating IELs in MNV-CW3 infection

After observing that the IEL activation in IL-22-/- mice was mediated in a microbiota-dependent manner, I next wanted to address whether the microbiota may play a role in the other IEL activation models. It may be that the IEL activation observed in MNV-CW3 and *E. vermiformis* infection models are mediated by the pathogens, the fact that the pathogens may cause damage to the IEC barrier that subsequently lead to increase exposure of the microbiota to the intestinal immune system, or combination of the two scenarios. To address this, I combined the MNV-CW3 or *E. vermiformis* infection models with broad-spectrum antibiotic treatment.

For the MNV-CW3 experiment, WT mice were treated with broad-spectrum antibiotics for 10 days prior to infection at the Pathology Unit at University of Cambridge, as described in section 7.8. Interestingly, for MNV-CW3-infected mice, Osama's quantification of the MNV-CW3 viral load showed a statistically significant reduction in antibiotic-treated mice compared to non-treated infected mice at day seven post infection (Fig 7.13 F), suggesting a role of commensal microbiota for MNV-CW3 pathology. Even more interestingly, I detected a significant decrease in MTG staining between antibiotic-treated and non-treated mice, to a level similar to non-treated IELs (Fig 7.13 D). Antibiotic treatment of MNV-CW3-infected mice significantly reduced the MTG MFI in all IEL subsets, even in $CD4^+$ $CD8\alpha\alpha^+$ IELs (Fig 7.13 E). The same trend applies to CD44 staining, which is increased during MNV-CW3 infection, but this increase is prevented by antibiotic treatment. (Fig 7.13 A-C). Interestingly, the IEL activation at day 7 post MNV-CW3 infection, measured by MTG staining, was lower compared to the experiment presented in Figure 7.10 E. The viral quantification between the

two experiments were similar, indicating that the level of IEL activation is affected by other factors than only on MNV viral load.

When assessing intracellular staining of Ki-67, TNFα and IFNγ, I observed that MNV-CW3 infection leads to IEL activation that is not accompied by increase in Ki-67 expression or intracellular TNFα and IFNγ in IELs (Fig 7.14 A-C).

These data suggest that it is not MNV-CW3 *per se* that activates IELs, as MNV-CW3 is still present in the antibiotic-treated mice. In addition, lack of mitochondria-dependent IEL activation does not seem to be critical for controlling MNV-infection, as the viral load is lower compared to infected controls.

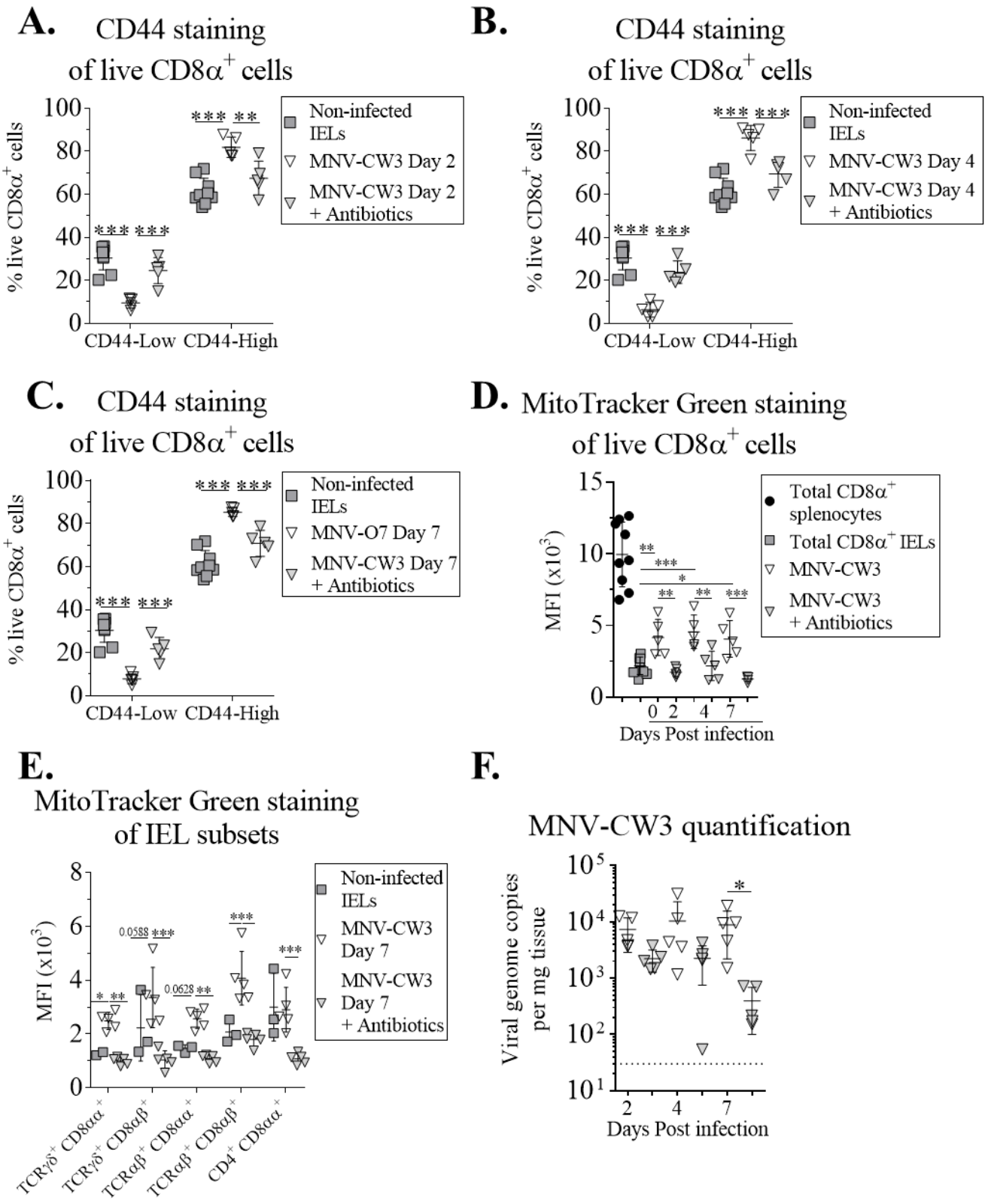

Figure 7.13. Commensal microbiota are activating IELs in MNV-CW3 infection. WT mice were treated with broad-spectrum antibiotics (1 g/l ampicillin, 1 g/l colistin and 5 g/l streptomycin) for ten days prior to infection with 5 x 10^6 TCID MNV-CW3 via oral gavage. Mice remained on antibiotic treatment after the infection and were culled at indicated days after MNV infection. A-C) Quantification of $CD44^{Low}$ and $CD44^{High}$ cells from non-treated and antibiotic-treated WT mice on MNV-CW3 infection at A) day two, B) day four and C) day seven post infection. D) Quantification of MFI of MTG staining of total $CD8\alpha^+$ IELs and splenocytes at indicated time points after MNV-CW3 infection. E) Quantification of MTG MFI in IEL subsets in indicated condition. F) Viral quantification of indicated time points and conditions. Data are presented as mean ± SD from one experiment with three to five mice per condition and experiment. Statistically significant changes were identified by one-way ANOVA (Panel D), two-way ANOVA (Panel A, B, C and E) and the Kruskal-Wallis test (Panel F). *: $p<0.05$., **: $p<0.01$., ***: $p<0.001$.

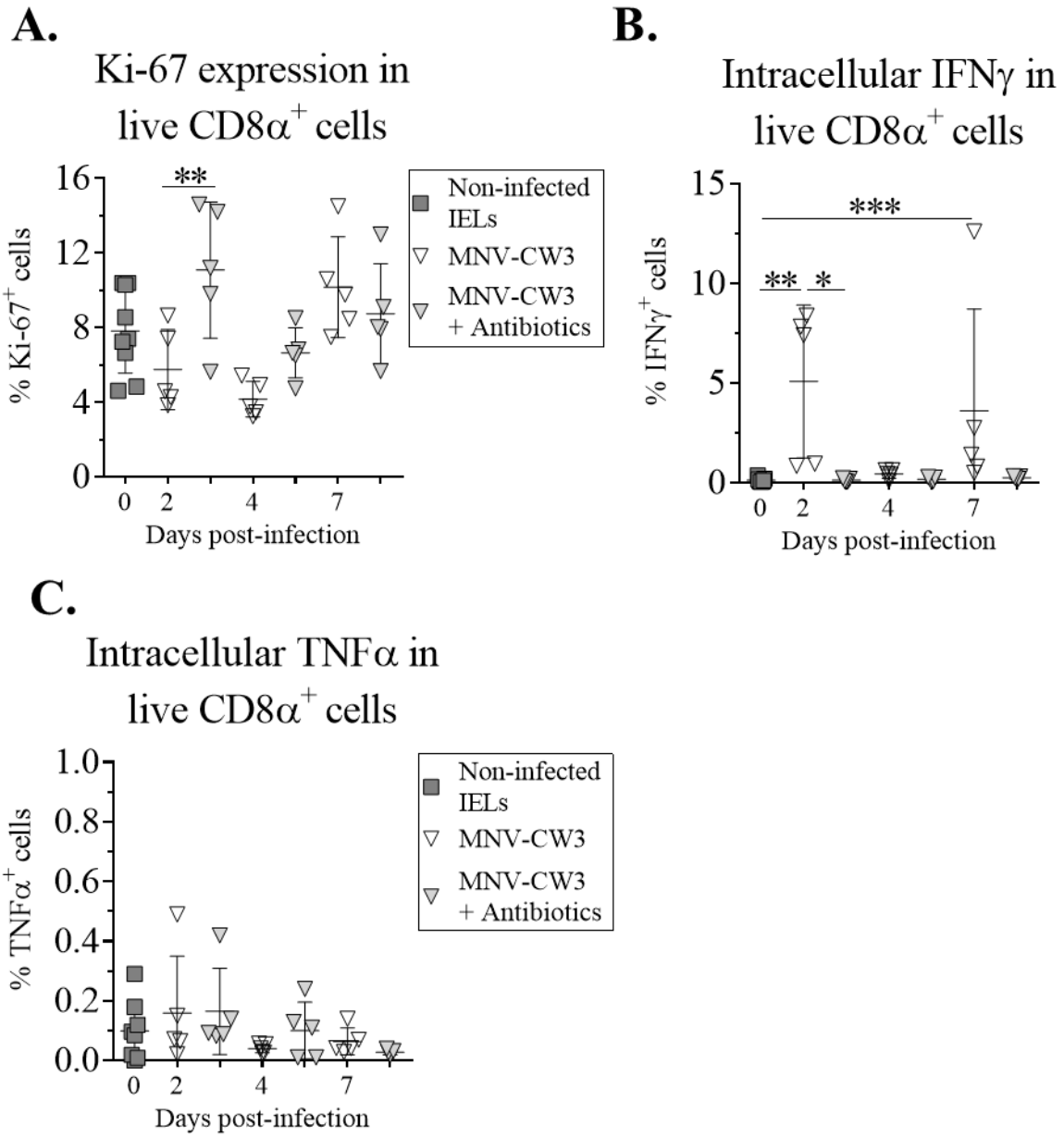

Figure 7.14. IEL activation by MNV-CW3 infection does not lead to cytokine production. WT mice were treated with broad-spectrum antibiotics (1 g/l ampicillin, 1 g/l colistin and 5 g/l streptomycin) for ten days prior to infection with 5 x 10^6 TCID MNV-CW3 via oral gavage. Mice remained on antibiotic treatment after the infection and were culled at indicated days after MNV infection. A-C) Total CD8α$^+$ IELs from indicated conditions quantified for A) Ki-67 expression, B) intracellular IFNγ and C) intracellular TNFα. Data are presented as mean ± SD from one experiment with three to five mice per condition and experiment. Statistically significant changes were identified by one-way ANOVA. *: $p<0.05$., **: $p<0.01$., ***: $p<0.001$.

7.12. Commensal microbiota are activating IELs in *E. vermiformis* infection

As IEL activation during MNV-CW3 infection seems to be mediated via commensal microbiota, I next wanted to assess whether this may be the case for the *E. vermiformis* infection model as well. WT mice were pre-treated with broad-spectrum antibiotic treatment (1 g/l ampicillin and 5 g/l streptomycin) for five days prior to infection with 1000 oocysts *E. vermiformis* via oral gavage. Mice remained on antibiotic treatment and were culled after 10 days of infection. Ileum-sourced IELs were isolated and analyzed by flow cytometry.

When I analyzed the CD44 staining, I observed that IELs from antibiotic-treated *E. vermiformis*-infected mice had similar proportion of $CD44^{High}$ and $CD44^{Low}$ cells as non-treated *E. vermiformis*-infected mice (Fig 7.15 A). These data suggest that *E. vermiformis*-infection *per se* can alter the activation status of IELs despite the depletion of microbiota. Interestingly also for this infection model, I observed a statistically significant decrease in MTG staining in IELs from *E. vermiformis*-infected mice on antibiotic treatment compared to non-treated infected controls (Fig 7.15 B). This reduction in MTG staining applied to all IEL subsets that have previously shown to increase their MTG staining during *E. vermiformis* infection without antibiotic treatment (Fig 7.15 C). These reductions in MTG staining by antibiotic treatment is likely not due to changed *E. vermiformis* infection because both groups of mice had similar level of total shed *E. vermiformis* oocysts (Fig 7.15 D). *E. vermiformis*-infected mice on antibiotic treatment had similar weight curve as non-treated infected mice (Fig 7.17 B). Excitingly, antibiotic treatment of *E. vermiformis* infected mice also showed reduction in MitoSOX staining for total $CD8\alpha^+$ IELs (Fig 7.15 E), as well $CD8\alpha\beta^+$ IELs (Fig 7.15 F). These data indicate that commensal microbiota is inducing the mitochondrial changes in IEL activation during intestinal infections. Therefore, it is interesting to assess

whether activated IELs still have increased expression of Ki-67 and intracellular TNFα and IFNγ even in the presence of antibiotics. I observed that antibiotic treatment of *E. vermiformis* infected mice lead to IELs that have lower intracellular staining of Ki-67 (Fig 7.16 A-B), IFNγ (Fig 7.16 C-D) and TNFα (Fig 7.16 E-F). These data are suggesting that commensal microbiota are activating IELs and not *E. vermiformis* organisms *per se*.

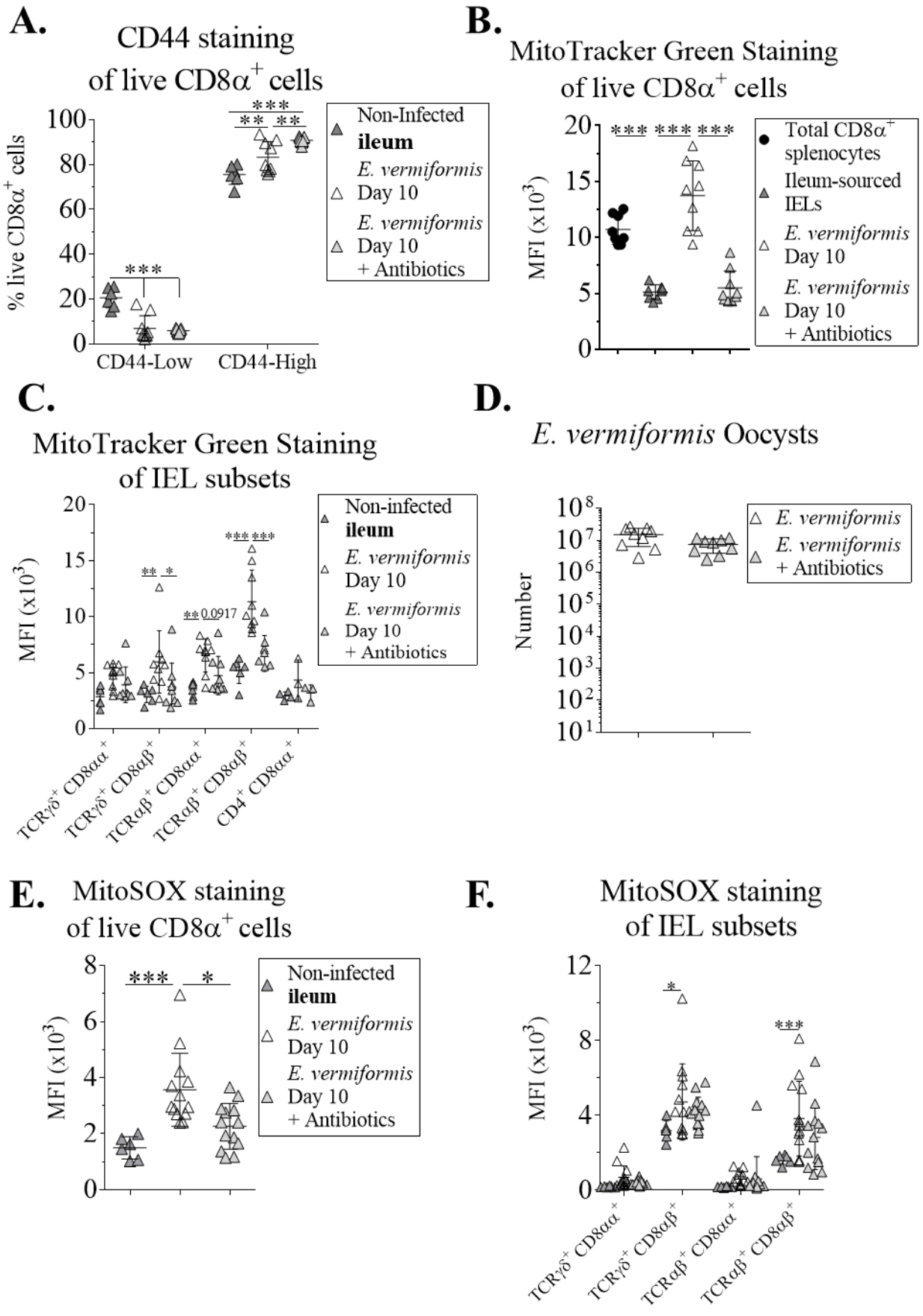

Figure 7.15. Commensal microbiota are activating IELs in *E. vermiformis* infection. WT mice were treated with broad-spectrum antibiotics (1 g/l ampicillin and 5 g/l streptomycin) for five days prior to infection with 1000 oocysts of *E. vermiformis*. Mice remained on antibiotic treatment until ten days post infection. Ileum-sourced IELs were isolated and analysed by flow cytometry. A) Quantification of $CD44^{Low}$ and $CD44^{High}$ cells from indicated conditions. B) Quantification of MFI of MTG staining in total ileal $CD8\alpha^+$ IELs and splenocytes from indicated condition of infection and antibiotic treatment. C) Quantification of MFI of MTG in IEL subsets from the same conditions as Panel B. D) Quantification of shed *E. vermiformis* oocysts between antibiotic-treated and non-treated mice. E) Quantification of MitoSOX MFI of total ileal $CD8\alpha^+$ IELs from non-infected and infected mice with or without antibiotic treatment. F) Quantification of MFI of MitoSOX of IEL subsets from the same conditions as Panel E. Data are presented as mean ± SD from four independent experiments with two to five mice per condition and experiment. Statistically significant changes were identified by one-way ANOVA (Panel B and E), Mann-Whitney test (Panel D) or two-way ANOVA (Panel A, C and E). *: $p<0.05$., **: $p<0.01$., ***: $p<0.001$.

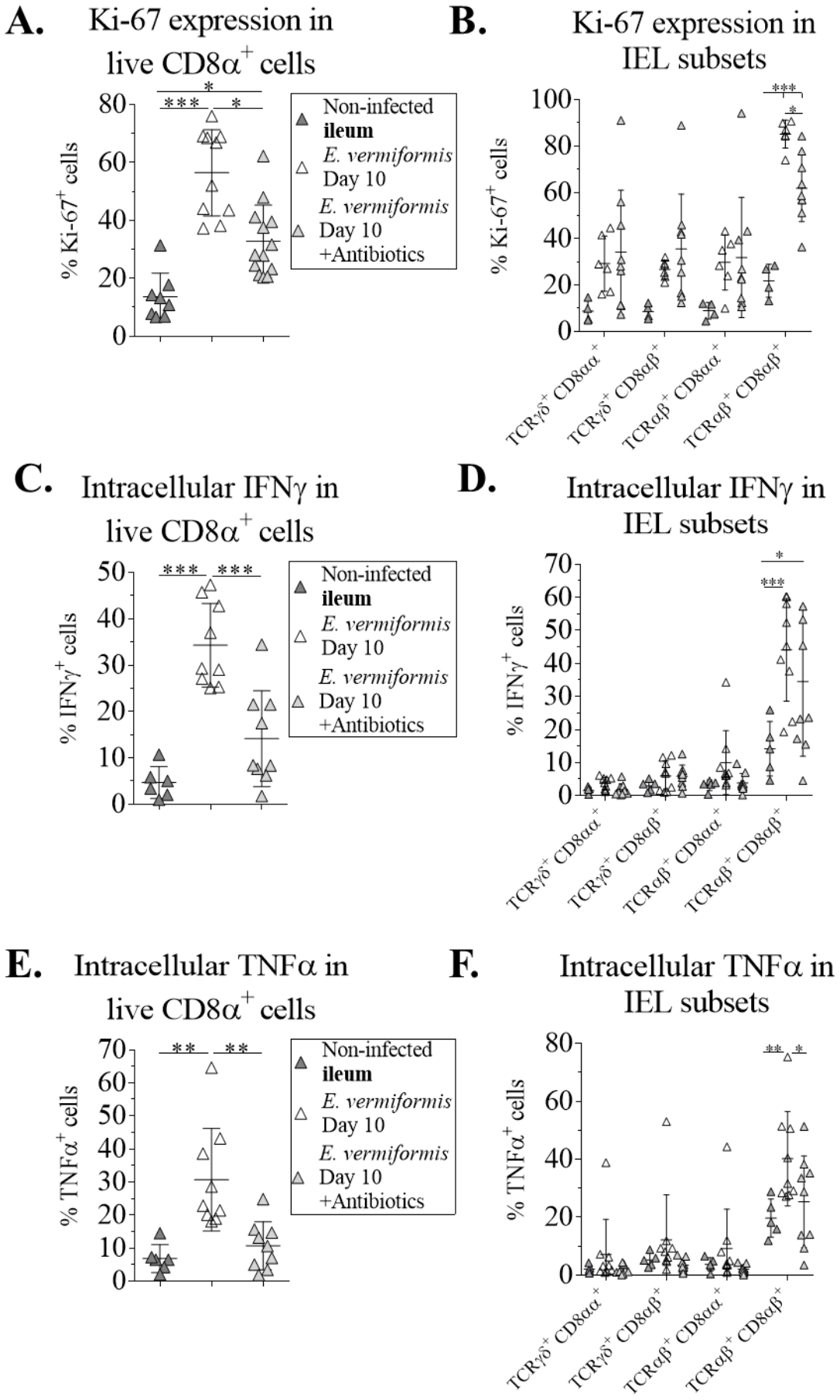

Figure 7.16. Commensal microbiota are mediating the cytokine production in activated IELs. WT mice were treated with broad-spectrum antibiotics (1 g/l ampicillin and 5 g/l streptomycin) for five days prior to infection with 1000 oocysts of *E. vermiformis*. Mice remained on antibiotic treatment until 10 days post infection. Ileum-sourced IELs were isolated and analysed by flow cytometry. A-B) Quantification of Ki-67$^+$ cells from A) total ileal CD8α$^+$ IELs or B) IEL subsets from non-infected and infected mice with or without antibiotic treatment. C-D) Quantification of IFNγ from C) total ileal CD8α$^+$ IELs or D) IEL subsets from non-infected and infected mice with or without antibiotic treatment. E-F) Quantification of TNFα from E) total ileal CD8α$^+$ IELs or F) IEL subsets from non-infected and infected mice with or without antibiotic treatment. Data are presented as mean ± SD from four independent experiments with two to five mice per condition and experiment. Statistically significant changes were identified by one-way ANOVA or two-way ANOVA. *: $p<0.05$., **: $p<0.01$., ***: $p<0.001$.

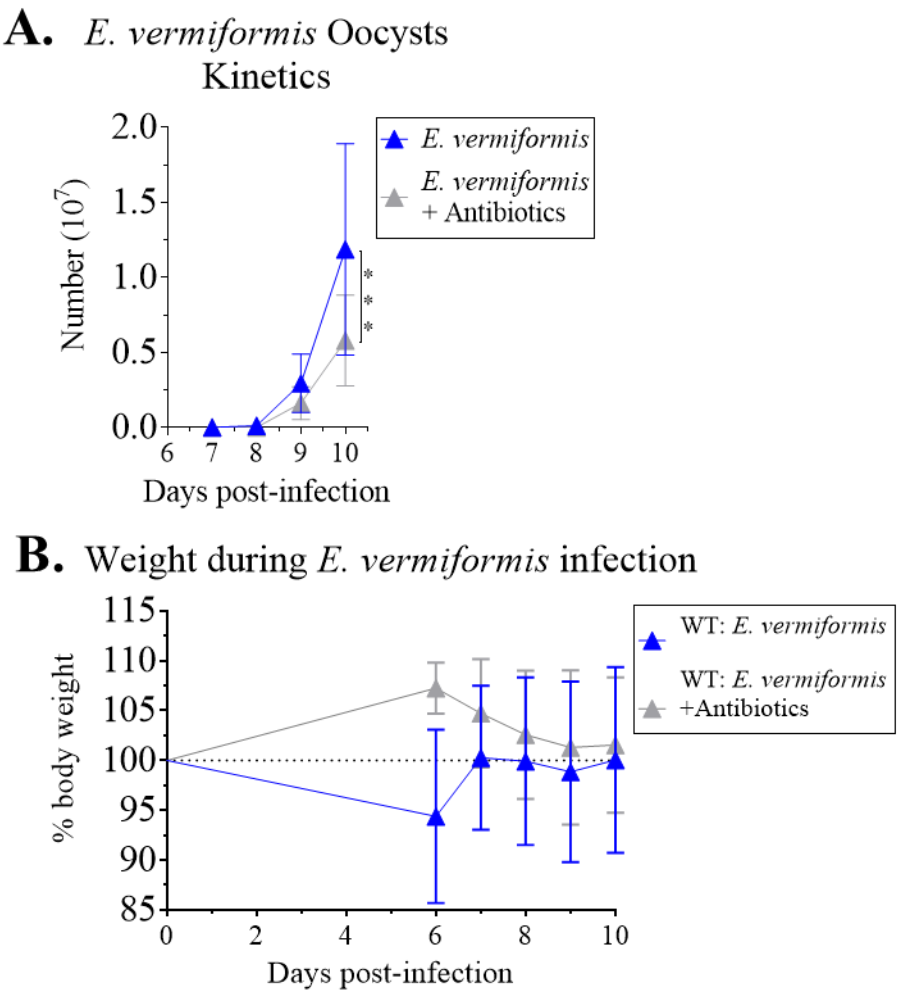

Figure 7.17. Broad-spectrum antibiotic treatment does not lead to a more severe *E. vermiformis* infection. WT mice were treated with broad-spectrum antibiotics (1 g/l ampicillin and 5 g/l streptomycin) for five days prior to infection with 1000 oocytes of *E. vermiformis*. Mice remained on antibiotic treatment until ten days post infection. A) Oocyst kinetics shed from indicated conditions. B) Mice's weight during the infection. The weight data are normalized to the weight on infection date. Data are presented as mean ± SD from three independent experiments with three to four mice per condition and experiment. Statistically significant changes were identified by two-way ANOVA. ***: $p<0.001$.

7.13. Gram-positive microbiota are activating IELs in *E. vermiformis*-infection

After these observations, I next asked whether the whole spectrum of the commensal microbiota are able to activate IELs. To address this, I used antibiotic mixtures that are targeting Gram–negative (colistin) or Gram-positive (vancomycin) bacteria for five days. Afterwards these and non-treated mice were infected with 1000 oocysts *E. vermiformis* via oral gavage for ten days prior to IEL analysis.

Non-, colistin- and vancomycin-treated *E. vermiformis* infected mice shed similar level of *E. vermiformis* (Fig 7.18 D). These data suggest that the antibiotic treatments are not affecting the infection level until day ten post infection. Of note, in one of the experiments, the level of shed oocysts is lower compared to the other experiment. Data from the experiment with lower shed oocysts is marked with red borderline in Figure 7.18 and 7.19. Interestingly, I observed that MTG staining is reduced specifically in IELs from vancomycin-treated *E. vermiformis*-infected mice, while colistin-treated *E. vermiformis*-infected mice showed similar level of MTG as non-treated infected mice (Fig 7.18 B). This trend applied to the IEL subsets (Fig 7.18 C). These data suggest that Gram-positive bacteria susceptible to vancomycin-treatment are activating IELs. This notion is supported by the observation that TCR$\gamma\delta^{+}$CD8$\alpha\beta^{+}$ and CD4^{+}CD8$\alpha\alpha^{+}$ IELs from colistin-treated mice have even higher MTG MFI compared to non-treated IELs (Fig 7.18 C). When depleting Gram-negative bacteria, there will be more space for Gram-positive bacteria to colonize the intestinal compartment.

Interestingly, vancomycin-treated IELs showed a trend of lower MitoSOX staining compared to non-treated IELs (Fig 7.18 E-F). However, when assessing the MitoSOX MFI in IEL

subsets, TCR$\alpha\beta^{+}$CD8$\alpha\beta^{+}$ IELs from vancomycin-treated mice have significantly higher MFI compared to non-treated and non-infected IELs (Fig 7.18 F).

Excitingly when assessing the level of Ki-67, TNFα and IFNγ, I observed that vancomycin-treatment reduces the intracellular level of these factors in IELs, while colistin-treatment leads to similar or tendency to higher levels compared to non-treated *E. vermiformis*-infected mice (Fig 7.19 A, C and E). This trend is clearer when assessing IEL subsets. Both intracellular IFNγ (Fig 7.19 C-D) and TNFα (Fig 7.19 E-F) were higher in colistin-treated condition. As with MitoSOX staining, vancomycin-treated mice had IELs with higher Ki-67 expression compared to non-treated *E. vermiformis*-infected (Fig 7.19 A-B). Collectively, these data support the notion that commensal microbiota are activating IELs, specifically the Gram-positive spectrum.

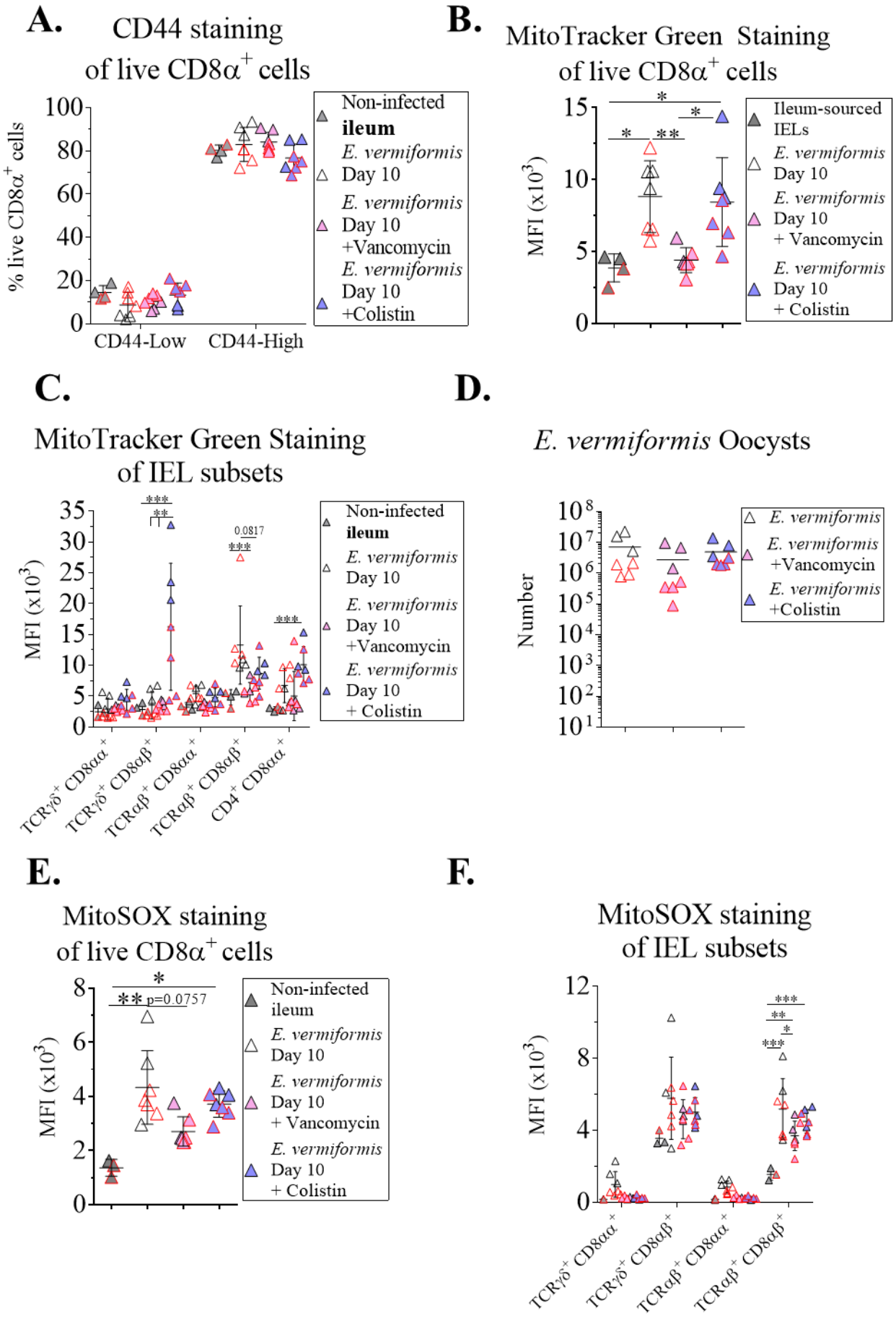

Figure 7.18. IELs are selectively activated by Gram-positive bacteria during intestinal parasite infection. WT mice were treated with 1 g/l colistin or 1 g/l vancomycin for five days prior to infection with 1000 oocytes of *E. vermiformis*. Mice remained on antibiotic treatment until ten days post infection. Ileum-sourced IELs were isolated and analysed by flow cytometry. A) Quantification of $CD44^{Low}$ and $CD44^{High}$ cells from indicated conditions. B) Quantification of MFI of MTG staining in total ileal $CD8\alpha^{+}$ IELs and splenocytes from indicated condition of infection and antibiotic treatment. C) Quantification of MFI of MTG of IEL subsets from same conditions as Panel B. D) Quantification of shed *E. vermiformis* oocysts between antibiotic-treated and non-treated mice. E) Quantification of MitoSOX MFI of total ileal $CD8\alpha^{+}$ IELs from non-infected and infected mice with or without antibiotic treatment. F) Quantification of MFI of MitoSOX staining in IEL subsets from same conditions as Panel E. Data are presented as mean ± SD from two independent experiments with two to five mice per group and experiment. Statistically significant changes were identified by one-way ANOVA (Panel B and E), Mann-Whitney test (Panel D) or two-way ANOVA (Panel A, C and E).*: $p<0.05$., **: $p<0.01$., ***: $p<0.001$.

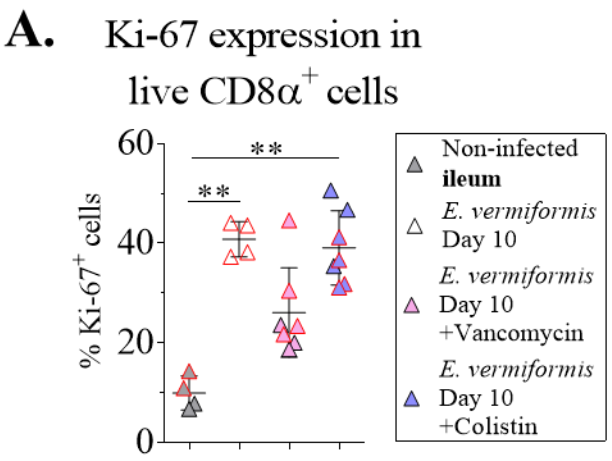

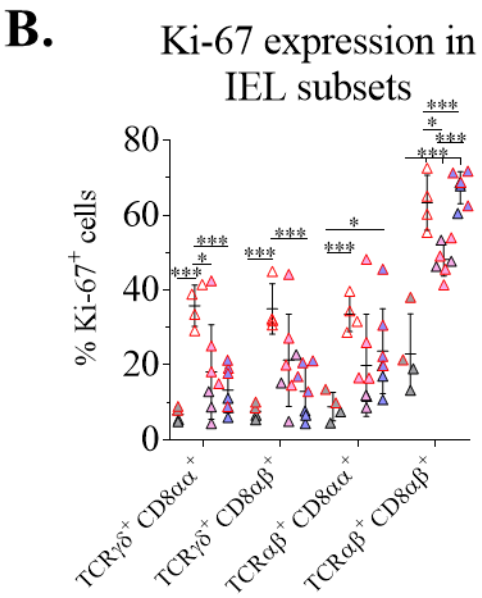

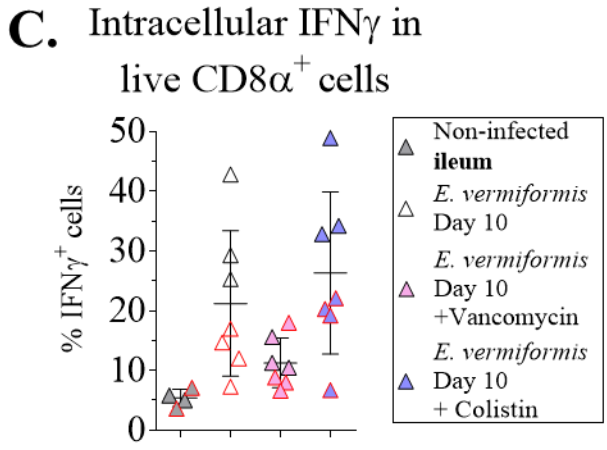

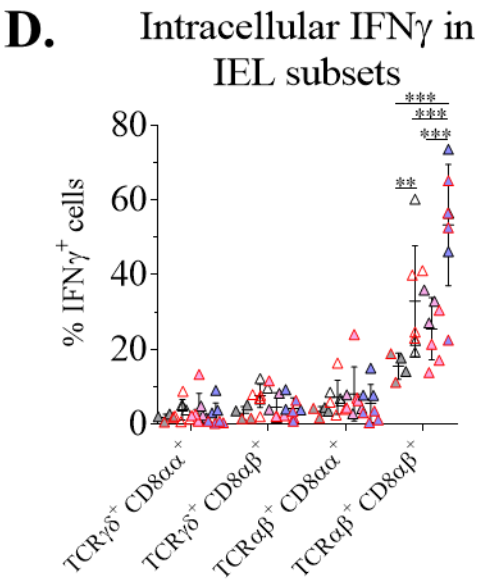

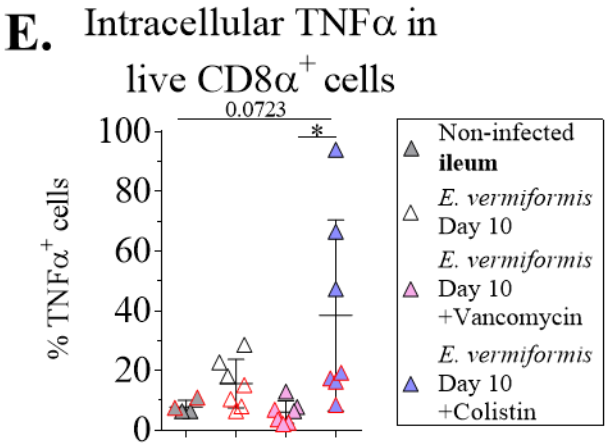

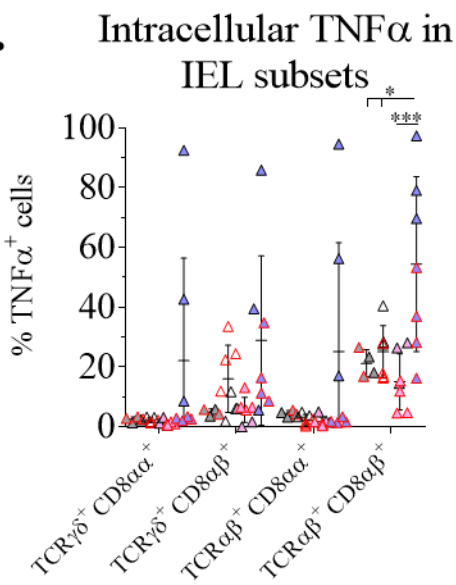

Figure 7.19. The cytokine production in activated IELs is mediated by Gram-positive bacteria. WT mice were treated with 1 g/l colistin or 1 g/l vancomycin for five days prior to infection with 1000 oocysts of *E. vermiformis* via oral gavage. Mice remained on antibiotic treatment til ten days post infection. Ileum-sourced IELs were isolated and analysed by flow cytometry. A-B) Quantification of Ki-67$^+$ cells from A) total ileal CD8α$^+$ IELs or B) IELs subsets from non-infected and infected mice with or without antibiotic treatment. C-D) Quantification of IFNγ from C) total ileal CD8α$^+$ IELs or D) IELs subsets from non-infected and infected mice with or without antibiotic treatment. E-F) Quantification of TNFα from E) total ileal CD8α$^+$ IELs or F) IELs subsets from non-infected and infected mice with or without antibiotic treatment. Data are presented as mean ± SD from two independent experiments with two to five mice per group and experiment. Statistically significant changes were identified by one-way ANOVA or two-way ANOVA.*: $p<0.05$., **: $p<0.01$., ***: $p<0.001$.

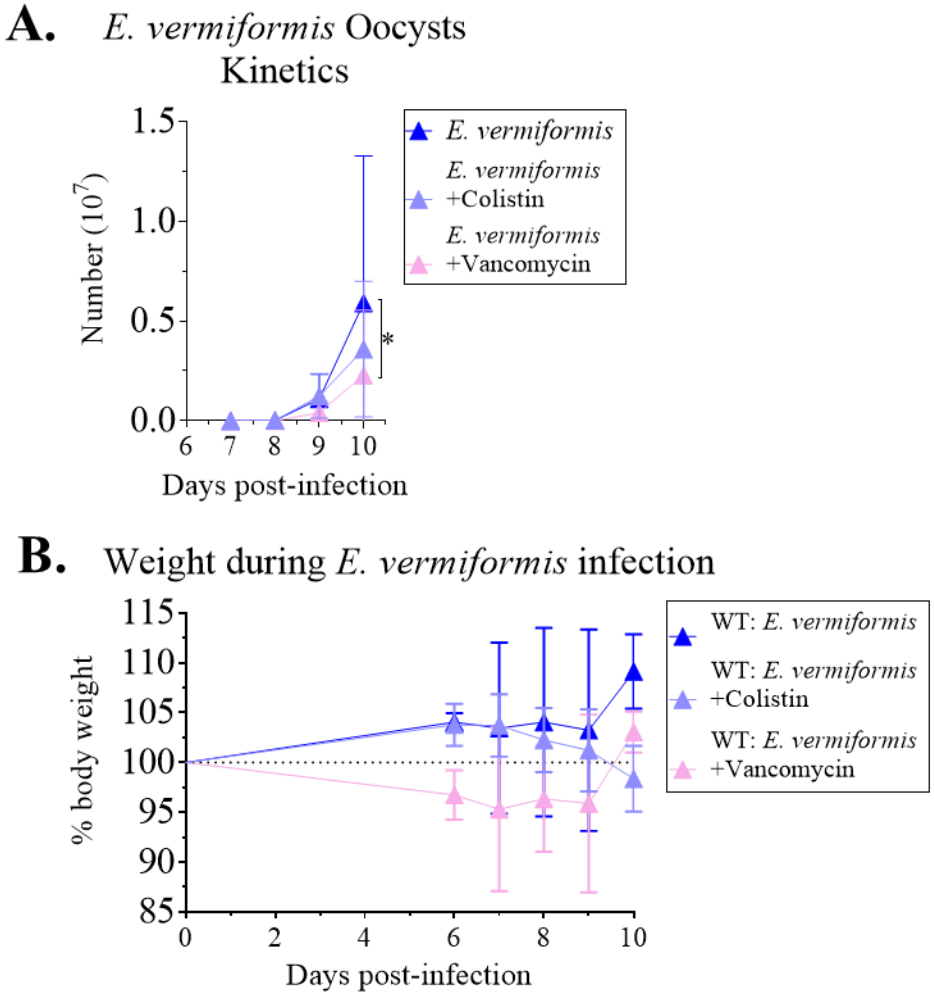

Figure 7.20. Gram-positive and Gram-negative antibiotic treatments do not lead to a more severe *E. vermiformis* infection. WT mice were treated with 1 g/l colistin or 1 g/l vancomycin for five days prior to infection with 1000 oocysts of *E. vermiformis* via oral gavage. Mice remained on antibiotic treatment until ten days post infection. A) Oocyst kinetics shed from indicated conditions. B) Mice weight during the infection. The weight data are normalized to the weight on infection date. Data are presented as mean ± SD from two independent experiments with three to four mice per condition and experiment. Statistically significant changes were identified by two-way ANOVA. *: $p<0.05$.

7.14. IELs are not essential for coping with the parasite load of *E. vermiformis*

After showing potential microbiota-dependent mechanism for IEL activation, I next wanted to address the physiological role of IEL activation during *E. vermiformis* infection. Data shown in Figure 7.15 D suggest that IEL activation may not be essential for controlling *E. vermiformis* parasite load because similar parasite load is detected in antibiotic-treated and non-treated infected mice. However, there is the possibility that other T cells in the LP compartment may compensate the lack of effector functions from IELs. Therefore, I wanted to assess whether IELs alone can help the host to cope with *E. vermiformis* infection.

To address this question, the idea would be to sort IELs into lymphocyte-deficient mice. Findings from the previous chapter suggest that IL-2Rγ-/-Rag2-/- mice would be the ideal IEL transfer hosts (Fig 6.6 A-F). However, these mice are more susceptible to *E. vermiformis* infection. Data from my lab colleague Joana Guedes showed that IL-2Rγ-/-Rag2-/- mice receiving 1000 oocysts of *E. vermiformis* succumb to the infection within 9 days of infection (Guedes, 2017). As illustrated in previous section, lower infection rate of *E. vermiformis* seems to lead to less IEL activation (Fig 7.18-19). These observations are in line with my hypothesis that it is commensal microbiota that activate IELs during *E. vermiformis* infection. Therefore, using a lower infection dose with IL-2Rγ-/-Rag2-/- mice may not detect IEL activation, and hence address my question. As shown in Figure 6.6 B and D, the IELs found in Rag2-/- mice after IEL transfer, are mainly TCRαβ$^+$ CD8αβ$^+$ IELs, the IEL subset that have been shown to respond the strongest in the tested activation and infection models (Fig 6.1, 7.4 and 7.13). Therefore, I decided to use Rag2-/- mice as hosts for this set of experiments.

For the experiment, I had six groups of mice: WT, Rag2-/- and Rag2-/- mice transferred with total CD8α$^+$ IELs, with or without broad-spectrum antibiotic treatment consisting of ampicillin and streptomycin. The three groups of antibiotic-treated mice received antibiotics for five days, before all six groups of mice were infected with 1000 oocysts of *E. vermiformis* via oral gavage. Six days post infection, the mice were single caged with sand bedding to enable faeces collection and parasite quantification. At day ten post infection, the mice were culled for IEL activation assessment. As expected from previous data, Rag2-/- mice had higher oocyst load compared WT mice (Fig 7.21 A-B). Surprisingly, this increase in parasite load observed in Rag2-/- mice was reduced by antibiotic treatment, to a level similar to *E. vermiformis*-infected WT mice (Fig 7.21 A-B). These data suggest that the parasite load in Rag2-/- mice, compared to WT mice, is induced in a microbiota-dependent manner. Addition of IELs to Rag2-/- mice did not significantly alter the parasite load (Fig 7.21 A-B), suggesting that IELs are not critical to control *E. vermiformis* infection. Although the weight data from these mice had large variation, there is a clear trend that Rag2-/- mice lose more weight compared to WT mice, which is not reduced by adding antibiotic treatment or IELs alone, but combination of antibiotic treatment and IELs tends to reduce the weight loss (Fig 7.21 C). These data could suggest that IELs may have a role in limiting pathology rather than directly affect the parasite load. Interestingly, the number of recovered IELs from Rag2-/- were fewer than expected from previous IEL transfer data, in which the mice received no additional treatment prior to analysis (Fig 7.21 D-E). These data would suggest that most of the transferred IELs die during the course of *E. vermiformis* infection. Interestingly, *E. vermiformis* infection of WT mice lead to increased number of ileal IELs (Fig 7.21 F). Further studies are required to determine the physiological role of mitochondria-dependent IEL activation.

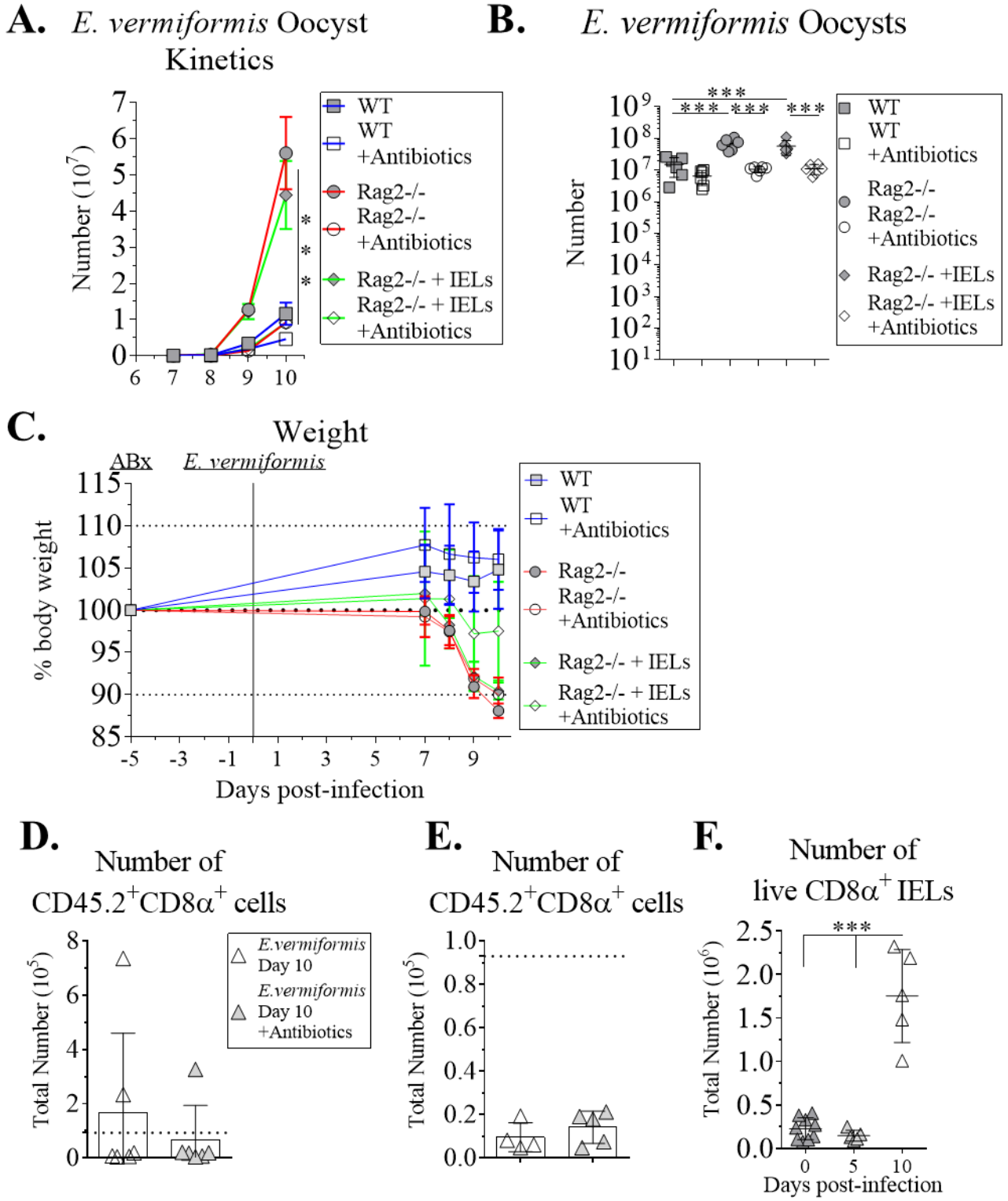

Figure 7.21. The increase of *E. vermiformis* parasite load in Rag2-/- mice is dependent on commensal microbiota. WT, Rag2-/- and Rag2-/- mice transferred with total CD8α$^+$ IELs with or without broad-spectrum antibiotics (1 g/l ampicillin and 5 g/l streptomycin) for five days prior to infection with 1000 oocysts of *E. vermiformis* via oral gavage.

Figure 7.21. The increase of *E. vermiformis* parasite load in Rag2-/- mice is dependent on commensal microbiota (cont.) A) Kinetics of shed *E. vermiformis* oocysts from the indicated mice and treatment. B) Total number of shed *E. vermiformis* oocysts until day ten post infection**.** C) Weight curve of indicated mice with weight prior to antibiotic treatment used as initial weight. D-E) The number of recovered IELs from Rag2-/- hosts from initial 100 000 IELs transferred. The dotted line indicates the average number of IELs recovered from Rag2-/- transferred with IELs but without additional treatments (see Figure 4.9 D). Panel D include all mice, while Panel E excludes the outliners (above dotted line) to illustrate the number of recovered IELs in remaining mice. F) Representative graph of the number of total ileal CD8α^+ IELs from non-infected and infected mice at indicated time points. Data are presented as mean ± SD from two independent experiments with three mice per condition and experiment. Statistically significant changes were identified by two-way ANOVA (Panel A), unpaired t-test (Panel D-E) and one-way ANOVA (Panel B and F). ***: $p<0.001$.

7.15. Anti-CD3-mediated IEL activation is not reduced by antibiotics

After observing that commensal microbiota seems to play a role in all tested infection models, I next wanted to address whether the same applies for the αCD3 model used in Chapter 6. One report is indeed suggesting that αCD3 injection can cause leakiness in the IEC barrier (Musch et al., 2002), suggesting that the IEL activation could potentially be of a similar character to IL-22-/- mice (Fig 7.12).

To address this, mice were split into two groups: one group receiving broad-spectrum antibiotic treatment (ampicillin and streptomycin) and one group not receiving antibiotics. After ten days of antibiotic treatment, both groups of mice received αCD3 antibody via i.p. injection and were culled for IEL analysis at 48 hours post injection. Interestingly, I observed no statistically significant difference between antibiotic-treated and non-treated αCD3-injected mice in regards to proportion of CD44^{High} and CD44^{Low} cells (Fig 7.22 A). IELs in antibiotic treated mice had not significant different CD44 staining compared to IELs in non-

treated mice, suggesting that antibiotic treatment *per se* is not affecting the activation status of IELs in regards to CD44 staining. Interestingly, the same trend was observed in regards to MTG staining (Fig 7.22 B-D) as well as Ki-67 expression (Fig 7.22 D-E). These data suggest that commensal microbiota is not essential for the activation response in the αCD3 model. In addition, these data suggest that there may be at least two different pathways for IELs to become activated: via microbiota leakiness into IEC barrier and via antigen presentation. What the potential antigen-presented ligands may be and which cell type(s) that present the antigens to IELs, remain to be determined.

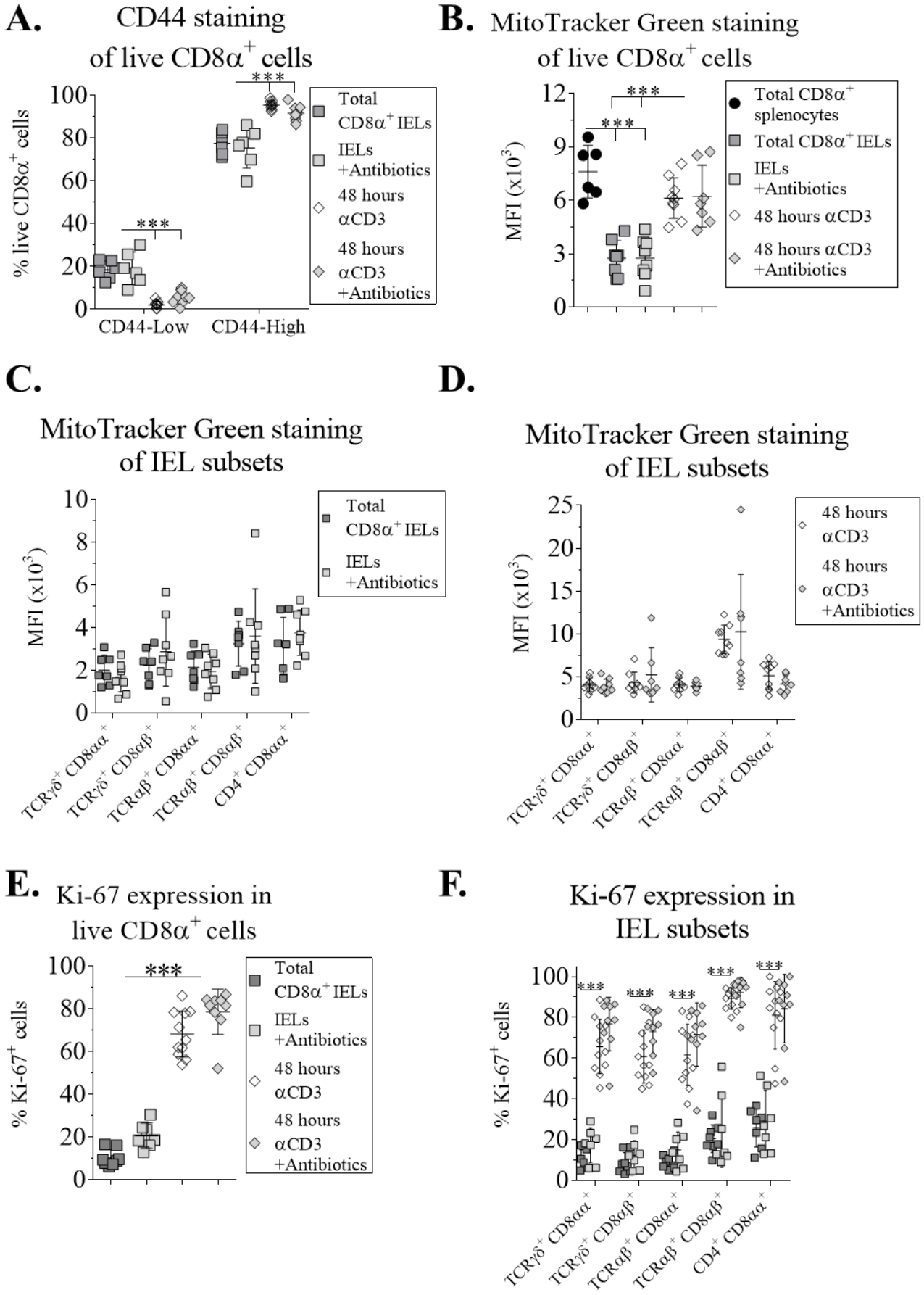

Figure 7.22. αCD3-mediated IEL activation is not reduced by antibiotic treatment. WT mice were treated with broad-spectrum antibiotics (1 g/l ampicillin and 5 g/l streptomycin) for ten days prior to injection with 25 µg αCD3 antibody i.p. Two days after injection, mice were culled, IELs isolated and analysed. A) Quantification of $CD44^{Low}$ and $CD44^{High}$ cells from indicated conditions. B) Quantification of MFI of MTG staining in total $CD8\alpha^+$ IELs and splenocytes from indicated conditions of infection and antibiotic treatment. C-D) Quantification of MFI of MTG of IEL subsets from same conditions as Panel B. E-F) Quantification of Ki-67^+ cells from E) total $CD8\alpha^+$ IELs or F) IEL subsets from indicated conditions. Data are presented as mean ± SD from three independent experiments with two to three mice per condition and experiment. Statistically significant changes were identified by one-way ANOVA or two-way ANOVA. ***: $p<0.001$.

7.16. DSS-induced colitis does not fully activate small intestinal IELs

As vancomycin- and broad-spectrum-antibiotic-treated *E. vermiformis*-infected mice had similar parasite load as non-treated *E. vermiformis*-infected mice (Fig 7.15 D and Fig 7.18 D), it suggests that IEL activation is not essential for controlling *E. vermiformis* parasite load. Data from Rag2-/- mice with transferred IELs suggest that IELs may instead play a role to limit pathology (Fig 7.21 A-C). Therefore, I next wanted to assess whether the role of IEL activation can be linked to IEC barrier healing. A model of IEC destruction and healing is DSS-induced colitis.

Previous data using DSS-induced colitis model suggest that mice deficient in IFNγ-/- have less severe DSS-induced disease course (Nava et al., 2010). Muc-2-/- mice showed a more severe disease outcome (Van der Sluis et al., 2006). Moreover, a link between the commensal microbiota and DSS-induced colitis symptoms has been demonstrated using IL-10-/- mice. These mice develop spontaneous colitis when housed in SPF conditions, but not when housed in GF conditions (Sellon et al., 1998). NOD2-/- mice have fewer IELs and exhibit more severe Trinitrobenzenesulfonic acid (TNBS)-induced colitis (Jiang et al., 2013). DSS-induced

colitis model has been linked to symptoms in the colon, but as DSS is administered in the drinking water, it will pass through the small intestine. Therefore, there is a possibility that DSS affect the small intestine as well. TCRγδ-/- mice showed a more severe DSS-induced colitis compared to controls (Ismail et al., 2009). TCRγδ$^+$ IELs are more numerous in the small intestine compared to the large intestine. Furthermore, a recent paper suggested that mice suffer from worse DSS-induced colitis when simultaneously on vancomycin-spiked drinking water (Huang et al., 2015). Hence, I wanted to test if the destruction of IEC barrier leads to IEL activation, and if so, whether that could explain the worsening of DSS-induced colitis in the presence of vancomycin.

To address this question, I need a dose of DSS that is causing colitis as expected but has a margin for potential worsening in colitis-symptoms when assessing what happens when IEL activation is blocked by vancomycin treatment. Doses of DSS used in previous literature varies from 1 % up to 5 % DSS (w/v) (Shon et al., 2015; Wirtz et al., 2007; Chassaing et al., 2015). I decided to use 2.5 % DSS which were given *ad libitum* to male WT mice for seven days, with drinking water exchange after three to four days. After the start of DSS administration, the mice were weighed daily as well as scored for colitis symptoms according to the table in Figure 7.23 A. I observed that the DSS-treated mice indeed lost weight (Fig 7.23 B-C), as well as observations of blood and diarrhea in the mice (Fig 7.23 D- E). Occasional mouse received general welfare concern from the animal technicians at day nine post DSS-administration (Fig 7.23 F). These data confirm successful DSS-induction of colitis as well as indicating that day five, seven and nine seem appropriate days to investigate whether IEL activation has occurred.

A.

Body weight loss		Occult/ Gross blood loss	
No weight loss	0	No blood	0
0-5 %	1	Dark faeces (suspicion of occult blood)	1
5-10 %	2	Clear evidence for blood on/ In faeces	2
10-20 %	3	Blood in rectum	3
>20 %	4	Blood in fur	4
Stool consistency		**General appearance**	
Well-formed/ normal	0	Normal	0
Pasty/ semi-formed	1	Piloerection only	1
Pasty/ some blood	2	Lethargy and piloerection	2
Diarrhoea that does not adhere to anus	3	Persistently hunched, lethargic and piloerection	3
Diarrhoea that adhere to anus	4	Motionless, sickly, sunken-eyed, ataxis	4

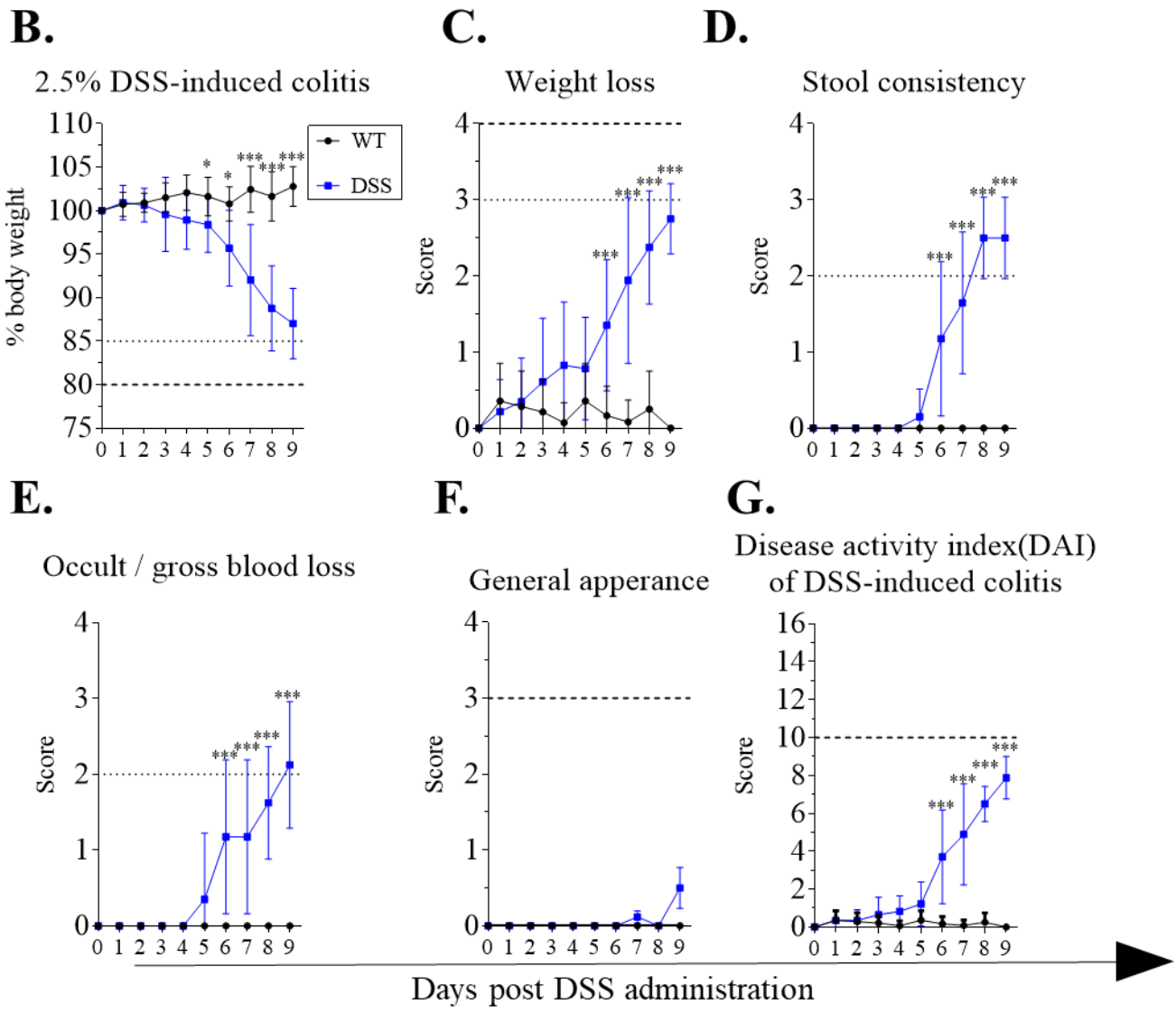

Figure 7.23. DSS-induced colitis model used for IEL activation assessment. Mice received 2.5 % DSS in their drinking water *ad libitum* for seven days. The DSS-treated mice were weighed and scored daily according to the table shown in panel A) for which grey areas highlight when mice are reaching moderate severity. B) Weight curve, C) weight score D) stool consistency, E) appearance of blood, F) general mice wellbeing and G) overall disease activity index (DAI) as a sum of scores from Panel C-F, for non-treated and DSS-treated mice. Data are presented as mean ± SD from three independent experiments with three to nine mice per condition and experiment. Statistically significant changes were identified by two-way ANOVA. *: $p<0.05$., ***: $p<0.001$.

Mice were taken day five, seven and nine post DSS-treatment and the small and large intestine and assessed for IEL activation. I first observed that the proportion of $CD44^{High}$ IELs is higher in DSS-treated mice at day seven and nine post DSS administration (Fig 7.24 A). Surprisingly, I observed no increase in MTG staining in small intestinal IELs, but instead I observed increase in MTG staining in large intestinal IELs at day nine post DSS administration (Fig 7.24 B-C). As I observed no significant increase in MTG staining, I expected to observe no significant increase in Ki-67, IFNγ and TNFα, which was the case for small intestinal IELs (Fig 7.24 D-F). Of note, I observed increased cytokine production from the large intestinal IELs at day seven and nine post DSS administration (data not shown), indicating that these IELs have become activated in a manner that have similarities to ileal-sourced IELs from *E. vermiformis*-infected mice.

I observed one difference between non-treated and DSS-treated small intestinal IELs: the number of IELs were significantly reduced at day five and seven post DSS administration (Fig 7.24 G). These data indicate that DSS affects the small intestine as well as the large intestine. Whether the missing IELs represent activated IELs that die, as observed in *E.*

vermiformis model using Rag2-/- mice transferred with IELs (Fig 7.21 E-F), or IELs that have migrated to other parts of the intestine, remains to be clarified.

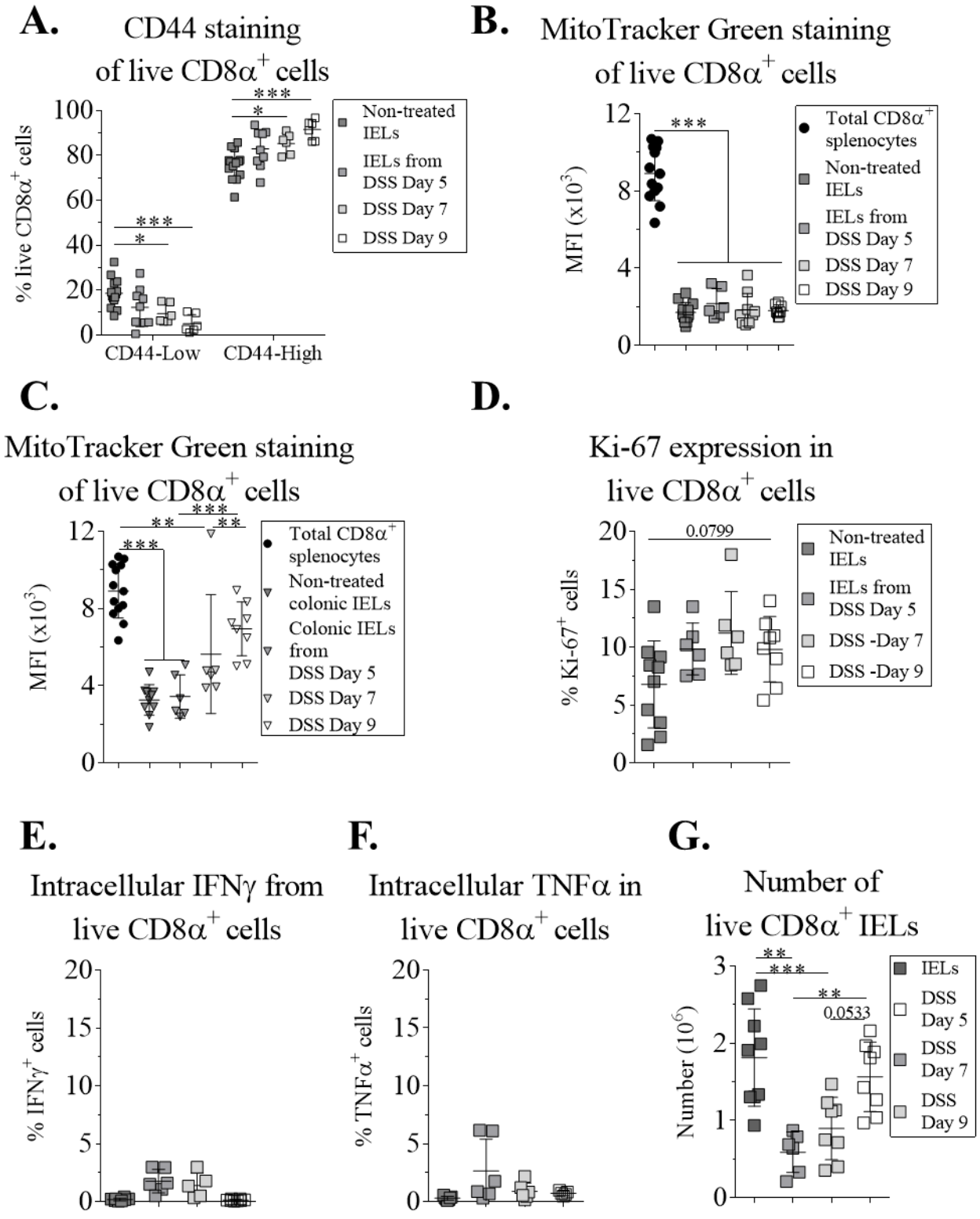

Figure 7.24. DSS-induced colitis model does not fully activate small intestinal IELs. Mice received 2.5 % DSS in their drinking water *ad libitum* for seven days. Mice were scored daily and culled at day five, seven and nine post DSS administration for IEL activation analysis. **A)** Quantification of $CD44^{Low}$ and $CD44^{High}$ cells from DSS-treated and control mice at indicated time point. B) Quantification of MTG MFI $CD8\alpha^+$ IELs from DSS-treated and control mice at indicated time points. C) Quantification of MTG MFI in $CD8\alpha^+$ IELs from DSS-treated and control mice at indicated time point. D-F) Quantification from total $CD8\alpha^+$ IELs for the intracellular markers D) Ki-67, E) IFNγ and F) TNFα. G) Number of total $CD8\alpha^+$ IELs DSS-treated and control mice at indicated time point. Data are presented as mean ± SD from two to three (day five samples) independent experiments with three mice per condition and experiment. Statistically significant changes were identified by one-way ANOVA (Panel B-G) or two-way ANOVA (Panel A). *: $p<0.05$., **: $p<0.01$., ***: $p<0.001$.

7.17. Common gamma chain signalling is involved in determining IEL activation state

After the exciting findings that commensal microbiota can activate IELs, there is a need to understand the mechanisms behind the microbiota-induced IEL activation. Some factors that have been reported to be involved in T cell activation and metabolism are the common gamma chain cytokines IL-2, -4, -9 -7, -15 and -21. For example, addition of IL-7 to memory $CD8\alpha^+$ T cell have been showed to increase their accumulation of lipids (Cui et al., 2015). I observed increased lipid accumulation in IELs from steady state mice (Fig 5.4 A). Exploring the effect of the other common gamma chain cytokines, it has been reported that addition of IL-15 to $CD8\alpha^+$ T cell cultures results in increased mitochondrial biogenesis (van der Windt et al., 2012). Addition of IL-15 to human IELs led to increased IFNγ production (Di Sabatino et al., 2006). Similar results were obtained from murine splenic T cells. In addition, it has been showed that the expression of IL-15 in IECs can increase in the presence of TLR2-ligand lipoteichoic acid (LTA) (Qiu et al., 2016). This finding is particularly interesting as I have demonstrated a role of Gram-positive bacteria in IEL activation during the *E.*

vermiformis infection. Whether Gram-positive microbiota induce IEL activation directly or indirectly remains to be determined. In addition, it was found the combination of IL-15 and IL-21 lead to even higher IFNγ production, while addition of IL-21 alone failed to induce IFNγ production (Zeng et al., 2005). Overall, these data suggest that common gamma chain cytokines have effect on mitochondrial biogenesis and cytokine production, two features that were observed in *E. vermiformis*-activated IELs. Therefore, there is a chance that the common gamma chain cytokine signaling may be involved in IEL activation.

Therefore, while performing the IEL transfer experiment to address the role of IL-15 trans-presentation for IEL survival (Fig 4.9 D), I also assessed the mitochondrial status of the IELs transferred into IL-2Rγ-/-Rag2-/- mice. As these mice were set up with IELs sourced from TCRδ-eGFP-reporter mice, I used MitoTracker Deep Red (MTDR) because MTG is not compatible with GFP staining. MTDR staining of steady state IELs, memory and naïve splenic CD8α$^+$ T cells generates similar results as MTG staining (Supplemental Figure to 5.6 in Chapter 5). However, the MTDR staining suggested a difference between memory and naïve splenic CD8α$^+$ T cells, which is not observed when using MTG staining, suggesting that MTDR and MTG are staining mitochondria in different manners.

Surprisingly, instead of observing that non-treated IELs transferred into IL-2Rγ-/-Rag2-/- mice had similar MTDR staining as WT mice, I observed heightened MTDR staining relative to WT IELs and IELs transferred into Rag2-/- mice (Fig 7.25 A). These data indicate that the intestinal compartment in IL-2Rγ-/-Rag2-/- mice enables heighten MTDR staining in IELs. This suggest that the presence common gamma chain in the intestinal epithelial compartment prevent IEL activation. Further analysis of these IELs in IL-2Rγ-/-Rag2-/- mice, I observed that there is no cytokine production from these IELs (Fig 7.25 C-D). However, there was a

statistically significant trend towards higher expression of the proliferation marker Ki-67 in IELs transferred into IL-2Rγ-/-Rag2-/- mice compared to control mice (Fig 7.25 B). These data suggest that IEL activation in IL-2Rγ-/-Rag2-/- hosts may be of similar to the activation observed in IL-22-/- mice.

As I have observed that commensal microbiota is the activating trigger in several infection models presented in this Chapter, I wanted to assess whether the commensal microbiota has a role for the increased activation status of IELs transferred into IL-2Rγ-/-Rag2-/- mice. Surprisingly, I observed that broad-spectrum antibiotics did not reduce the MTDR staining in these IELs (Fig 7.25 A), suggesting that the commensal microbiota is not involved in this IEL activation model. As observed with previous IEL activation assessment experiments including antibiotic treatment (Fig 7.12F, Fig 7.14 A, Fig 7.16 A and Fig 7.19 A), antibiotic treatment of IL-2Rγ-/-Rag2-/- mice that have received IELs showed higher expression of Ki-67 (Fig 7.25 B). These data suggest that this IEL activation maybe of a similar character to αCD3-mediated IEL activation to described in Chapter 6, which were not reduced by antibiotic treatment either (Fig 7.22).

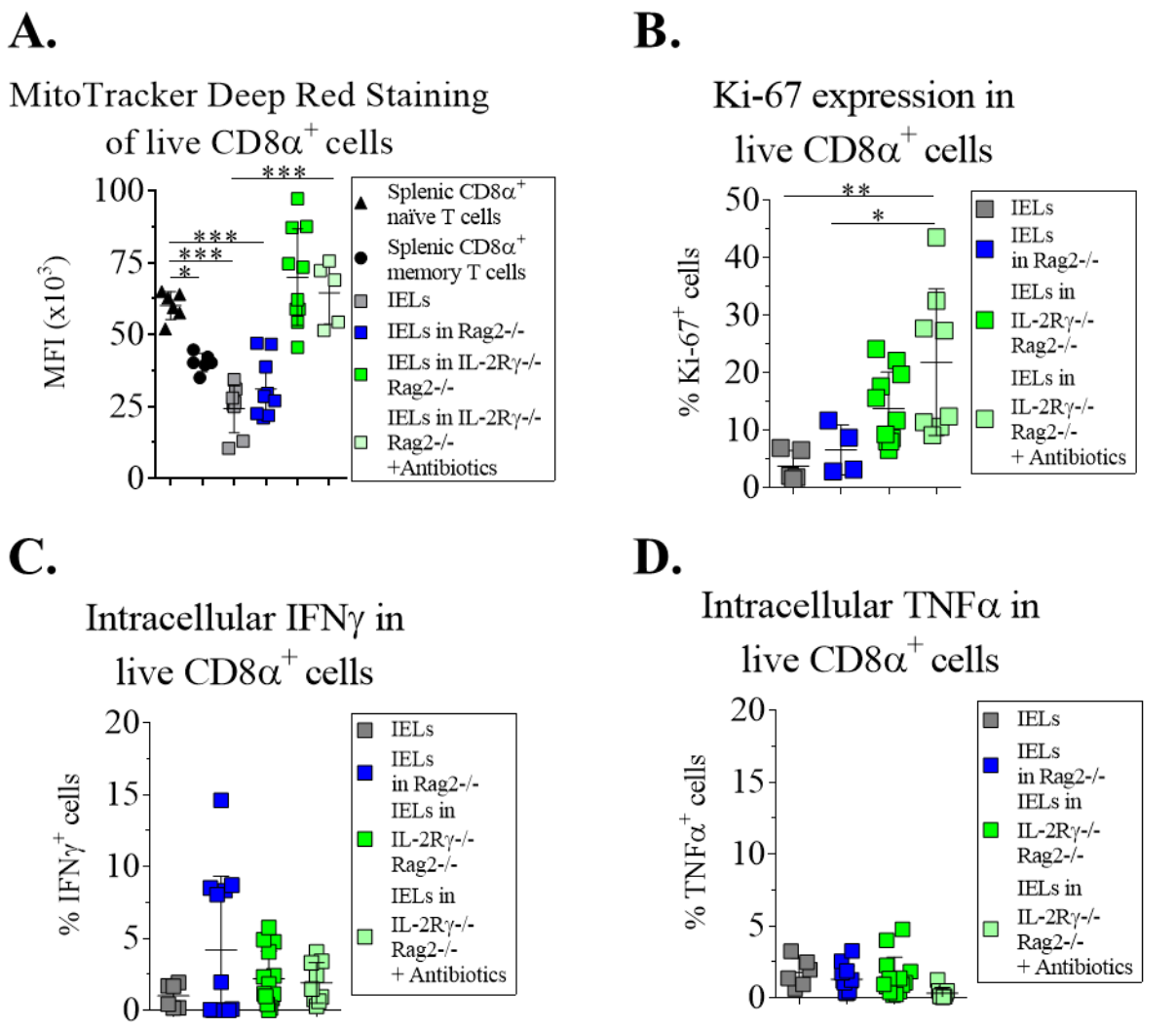

Figure 7.25. IELs transferred into IL-2Rγ-/-Rag2-/- mice have more mitochondrial mass in a microbiota-independent manner. Recipient mice were injected with 100 000 FACS-sorted CD8α$^+$ IELs. IELs were isolated from the mice 6 weeks post injection. A) Quantification of MTDR MFI from total CD8α$^+$ IELs from indicated condition**.** B) Percentage of Ki-67 in total CD8α$^+$ IELs from indicated hosts and conditions. C) Percentage of IFNγ in total CD8α$^+$ IELs from indicated hosts and conditions. D) Percentage of TNFα in total CD8α$^+$ IELs from indicated hosts and conditions. Data are presented as mean ± SD from two to three independent experiments with two to three mice per condition and experiment. Statistically significant changes were identified by one-way ANOVA. *: $p<0.05$., **: $p<0.01$., ***: $p<0.001$.

After these observations, I next asked what could be the cause of this phenotype. IL-2Rγ-/-Rag2-/- mice lack T and B cells, NK cells and ILCs (Almeida and Belz, 2016). Histology analysis has shown that the intestinal epithelium is altered in IL-2Rγ-/-Rag2-/- mice e.g. higher crypt heights compared to control mice (Cao et al., 1995). Lacking IL-2Rγ also have effects on DCs, mast cells, IECs and monocytes, and granulocytes (Reinecker and Podolsky, 1995), suggesting that there are potential cell-cell interactions that can affect the mitochondrial status in IELs.

As initial step, I wanted to assess whether the influence of IL-2Rγ signaling on IEL activation is due to the hematopoietic or non-hematopoietic cells, particularly whether IEC-IEL interactions may play a role. To address this, I transferred WT BM into Rag2-/- and IL-2Rγ-/-Rag2-/- mice. A study has showed that immune cell reconstitution is observed already two weeks after BM transfer (Auletta et al., 2004). Three weeks after the transfer, I analyzed the IELs in these BM chimeras. Interestingly, IELs in these mice show similar MTG staining as WT IELs (Fig 7.26 A). These data indicate that the IEL activation observed in IELs transferred into IL-2Rγ-/-Rag2-/- mice is linked to hematopoietic cells and not IEL-IEC interactions.

To pinpoint further which immune cells that could be involved, I set up bone marrow chimeras that in addition receive $CD8\alpha^+$ IEL transfer. By that, I could add back immune cell compartments that could be potentially involved in this IEL activation. Since transferred IELs into Rag2-/- mice do not show this increase in mitochondrial mass, measured by MTDR (Fig 7.25 A) and MTG (Fig 7.26 A), it suggests that T and B cells are not involved in this process. Therefore, it is more likely that either ILCs or NK cells may play a role, as both cells subsets are missing in IL-2Rγ-/-Rag2-/- mice. Previous reports have showed an important role for IL-

7 (Bostick and Zhou, 2015) and IL-15 signalling for ILC and NK cell (Kennedy et al., 2000) maintenance, respectively.

For the assessment IL-2Rγ-/-Rag2-/- mice were irradiated and received BM cells via transfer i.v from the following donor mice: Rag2-/-, IL-7R-/-Rag2-/-, IL-15R-/-Rag2-/- and IL-22-/-Rag2-/- mice. three weeks after initial transfer, IELs were FACS-sorted and transferred i.v. into these BM mice and plain IL-2Rγ-/-Rag2-/- mice that have also received irradiation treatment but no BM cells. Three weeks post the IEL transfer, mice were culled and IELs analysed. Supporting the observation from Fig 7.25 A, antibiotic treatment of IL-2Rγ-/-Rag2-/- mice did not significantly reduce the level of MTG compared to non-treated mice (Fig 7.26 B). However, the level of MTG staining is lower than usually found in splenic CD8α$^+$ T cells, which is not matching with findings in Fig 7.25 A showing similar mitochondrial staining compared to splenic CD8α$^+$ T cells. This could either be due to the different dyes used in the experiment or that the irradiation had side effects. Interestingly, IL-2Rγ-/-Rag2-/- mice receiving IL-22-/-Rag2-/- BM had higher MTG staining compared to controls receiving Rag2-/- BM. This increase was reversible by addition of broad-spectrum antibiotic treatment (Fig 7.26 B), suggesting that some IL-22-producing cells present in Rag2-/- BM may be involved in the activation process. Surprisingly, IL-2Rγ-/-Rag2-/- mice receiving IL-7R-/-Rag2-/- BM did not show these phenotype (Fig 7.26 B), suggesting that IL-7R-dependent ILCs may not be involved. However, IL-2Rγ-/-Rag2-/- mice receiving IL-15Rα-/-Rag2-/- BM showed similar results as IL-2Rγ-/-Rag2-/- mice receiving IL-7R-/-Rag2-/- BM (Fig 7.26 B). This data could suggest that NK cells may play a role. There is also a report suggesting a role of IL-15 for ILCs, particularly ILC1 (Gil-Cruz et al., 2016), which others have suggested support IL-7R-independent ILCs (Robinette et al., 2017).

Undoubtedly, there more research is required to fully understand the role of IL-2Rγ signaling in IEL activation, but these data indicate a role for other immune cells for IEL activation maintenance, potentially NK cells and/or IL-7-independent subsets of ILCs.

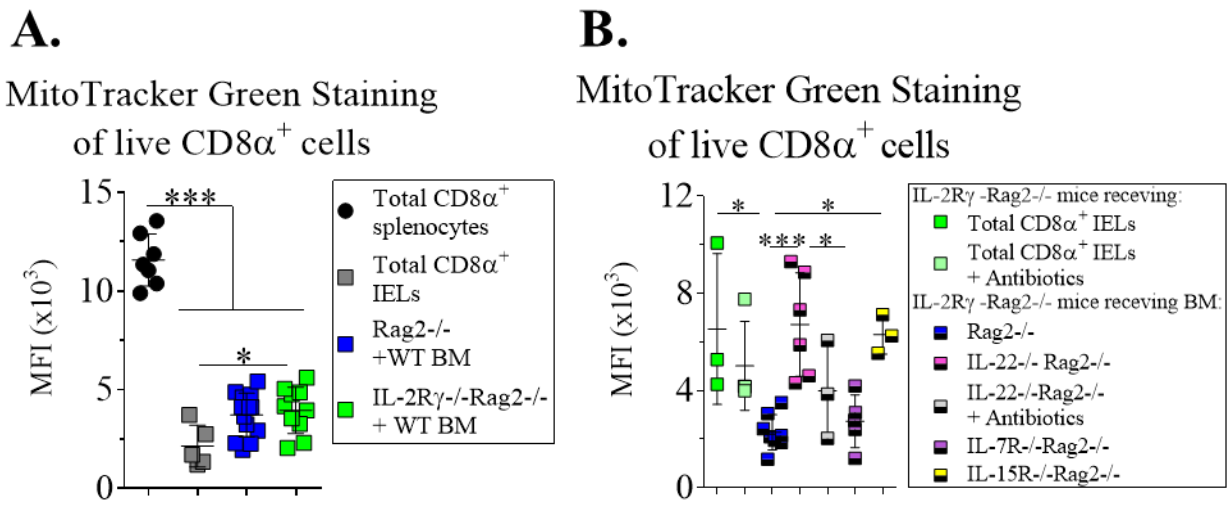

Figure 7.26. IELs transferred into IL-2Rγ-/-Rag2-/- mice are more activated due to IL-15R-dependent and/or IL-22 producing cells. A) IL-2Rγ-/-Rag2-/- mice and Rag2-/- mice were irradiated before receiving 2x10^6 WT BM via i.v. injection. 3 weeks post transfer, IELs were isolated and analysed. Panel A shows quantification of MTG MFI from WT total CD8α$^+$ splenocytes and total CD8α$^+$ IELs from the bone marrow chimeras. B) IL-2Rγ-/-Rag2-/- mice were irradiated prior to receiving indicated 2x10^6 Rag2-deficient bone marrow cells via i.v. injection. The bone marrow chimeras then received 100 000 total CD8α$^+$ IELs via i.v. injection. IELs were isolated from the mice 6 weeks post initial injection. Panel B shows quantification of MTG MFI from total CD8α$^+$ IELs from indicated condition. Data are presented as mean ± SD from three (Panel A) or two (Panel B) independent experiments with two to three mice per condition and experiment. Statistically significant changes were identified by one-way ANOVA. *: $p<0.05$., ***: $p<0.001$.

7.18. Supplemental figures

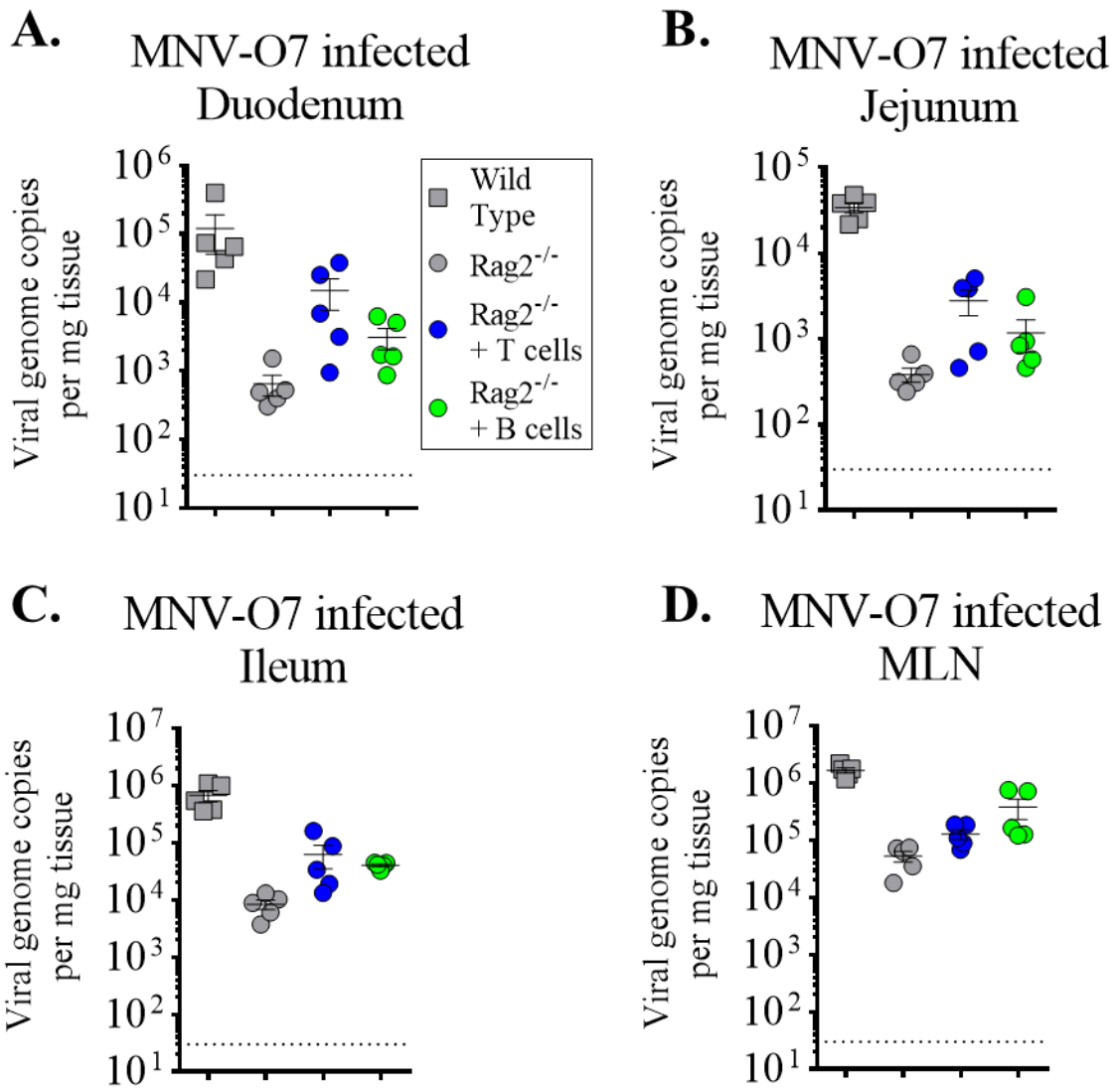

Supplemental Figure to 7.10. Adaptive immune system is used for MNV-O7 replication.
T and B cells sourced spleen and MLNs were FACS-sorted based on expression of CD19 and CD90.2. 1.0-2.5x10^6 of T cells, B cells or combination of T and B cells, were injected i.v. into Rag2-/- mice. After three weeks, the mice were transferred to the Pathology unit at University of Cambridge for MNV-O7 infection by Osama Eisa. The data are presented as mean ± SD from one experiment. Statistically significant changes were identified by one-way ANOVA.

7.19. Chapter Discussion

Summarising the findings in this chapter, IELs are activated in IL-22-/- mice and become activated during *E. vermiformis* and MNV-CW3 infections. Unlike TCR-mediated IEL activation, cytokine production was demonstrated in ileum-sourced IELs from *E. vermiformis* infected mice. Interestingly, the IEL activation observed in IL-22-/- mice, *E. vermiformis*- and MNV-CW3- infected mice were prevented in when depleting commensal microbiota, suggesting an essential role for commensal microbiota in IEL activation. Quantifications of the pathogen load in the infection model showed successful infection in the presence of antibiotics, suggesting that the pathogen themselves are not directly activating IELs. Surprisingly, IELs seem to become activated specifically by Gram-positive bacteria and/or its products. From the presented data, it is possible to hypothesize about a model in which IELs can become activated regardless of what is causing damage to the IEC barrier. As IELs' TCR antigen repertoire is more limited compared to other T cells, IELs could potentially utilize microbiota recognition as alternative way of becoming activated.

One remaining question to address is whether t microbiota-dependent IEL activation acts s in a direct or indirect manner. Preliminary data from the laboratory and Immgen project suggest that IELs express mRNA for PRRs that recognize Gram-positive bacteria such as TLR2, NOD1 and NOD2 (data not shown and (Shay and Kang, 2013). If these mRNA expressions translate into protein expression, then IELs may have the capacity to recognize the Gram-positive microbiota products. If IELs do not recognize the microbiota themselves, other possible pathways could involve antigen presentations from IECs, intestinal DCs or MPs. Any immune cell capable of recognizing the microbiota may be able to transfer activating signals to IELs that may lead to their activation. If IELs are activated by commensal microbiota in an indirect manner, then it may increase the time that IELs require to become

fully activated. However, data from the αCD3 activation model suggest that the MTG remodeling can be performed within 24 hours (Fig 6.1 D-E), which is rapid compared to other adaptive immune responses that takes days.

Another question that needs to be addressed is why IELs seems to become activated specifically by Gram-positive bacteria and not by both Gram-positive and Gram-negative bacteria. There are reports describing transgenic mice with designed TCRs that specifically respond to commensal antigens. One of these models, CBir1 transgenic mice, have TCRs that are specific to commensal-derived flagellin. Using these mice during *T. gondii* infection, IFNγ production was observed from splenic T cells (Hand et al., 2012). Flagellin has been reported to be able to originate from both Gram-positive and Gram-negative bacteria (Hayashi et al., 2001). Preliminary RNA sequencing data indicates that IELs do not express TLR5 mRNA (data not shown). Hence, the microbiota dependent activation in IELs is unlikely to be the same as described above, but a similar approach with gene-modified mice with transgenic TCRs for commensal may be an useful tool to dissect whether IELs' TCR is involved in the microbiota-dependent activation of IELs.

It seems that IELs are not activated by Gram-negative pathogen, as shown by the *Salmonella* experiment (Fig 7.11 B and C). Administration of DSS also failed to fully activate small intestinal IEL (Fig 7.24 A-B). However, increased IEL activation status was observed using CD44 staining. Moreover, the total number of $CD8\alpha^+$ IELs in the small intestine was reduced after DSS administration (Fig 7.24 G), suggesting that the small intestine is also affected by DSS administration. The notion that DSS-induced colitis is driven by commensal microbiota has been shown by using GF mice, which do not suffer from weight loss during DSS-induced colitis. However when GF mice receive either murine or human microbiota, these mice

exhibit colitis symptoms (Surana and Kasper, 2017). Data from Lora Hooper laboratory demonstrate that colonic TCRγδ$^+$ IELs have altered gene expression after DSS treatment. These changes were not observed when using GF mice (Ismail et al., 2009), suggesting that the commensal microbiota affected IELs after DSS treatment. Therefore, a potential explanation to why DSS-induced colitis do not fully activate small intestinal IELs could be that DSS affect the spectrum of microbiota that are capable of activating IELs. An alternative explanation could be that the used dose of DSS may not cause sufficient damage to the small intestinal epithelial barrier , hence IELs do not become activated by it..

There is a report suggesting that different antibiotic treatments affect the DSS-induced colitis outcome: vancomycin-treated mice showed worse DSS-induced colitis with increased weight loss, while streptomycin-treated mice had mitigated DSS response with lower weight loss compared to controls (Huang et al., 2015). The same report also showed differences in commensal microbiota composition by DSS-treatment. One of the main differences is the significant increased proportion of bacteria belonging to *Bacteroidaceae* family, which belongs to the Gram-negative spectrum (Huang et al., 2015). This could potentially be one of the explanations the IEL activation assessment results I obtained (Fig 7.24 B-C). Interestingly, colonic IELs increased their MTG staining 9 days post DSS administration (Fig 7.24 C). As expected, large intestinal IELs have similar low mitochondrial mass as small intestinal IELs (Fig 7.24 B-C). Further studies are required to determine whether the notion of mitochondria-mediated and microbiota-mediated IEL activation applies to colonic IELs as well as reported for small intestinal IELs in chapter 6 and 7.

Overall, this chapter highlights an important role of the commensal microbiota in IEL activation. In WT mice, goblet cells produce a mucus layer that spatially separates the IEC

barrier from the commensal microbiota. This spatial separation has been illustrated by intestinal tissue imaging using 16S rDNA probe to detect the microbiota. This distance has been estimated to be approximately 50 μm. However, mice that are deficient for MyD88 or RegIIIγ lack this spatial separation between the IEC barrier and microbiota (Vaishnava et al., 2011). In addition, RegIIIγ-/- mice had an increased proportion of bacteria belonging to the phylum *Firmicutes*, suggesting a role of RegIIIγ for keeping these bacteria under control. It has also been reported that old mice (18 months) have thinner intestinal mucus layer compared to young mice (3 months) mice (Elderman et al., 2017), suggesting that age is an important factor to monitor for further studies of the role of microbiota in IEL activation. As I have observed IEL activation in IL-22-/- mice (Fig 7.12 A-B), I would hypothesize that MyD88-/- and RegIIIγ-/- mice may also have IELs that have increased mitochondrial mass and/or increased CD44 staining, which may be prevented by antibiotic treatment just as showed for IL-22-/- mice (Fig 7.12 A and B). In the *E. vermiformis* model, it has been reported that the number of goblet cells decreases in the jejunum and ileum (Linh et al., 2009). As goblet cells are main producers of the mucus, it may suggest that the reduced number of goblet cells may lead to a decreased mucus layer and subsequently decreased spatial separation between the commensal microbiota, the IEC barrier and the IELs located between IECs. Another antimicrobial protein that has been suggested to be involved in the spatial separation between the IEC barrier and commensal microbiota is resistin-like molecule β (RELMβ). It has been shown that RELMβ specifically kills Gram-negative bacteria, with minor effects on Gram-positive bacteria. RELMβ is mainly produced by goblet cells in the colon for which an increase in the proportion of bacteria belonging to *Proteobacteria* was observed (Propheter et al., 2017).

After observing that there may be a preference for IELs to become activated by Gram-positive bacteria, I explore whether to see if previous literature could provide insights about common intestinal microbiota composition in C57BL/6 mice. Of note, there are reports that suggest that the intestinal microbiota is different in different mouse strains such as C57BL/6 and BALB/c mice (Krych et al., 2013), suggesting that there is the possibility that IELs sourced from other mouse strains may not respond to activation triggers in the same was as have been described in this thesis. Interestingly, it has recently been reported that the microbiota composition is undergoing diurnal oscillations (Thaiss et al., 2016). This report could also demonstrate that broad-spectrum antibiotic treatment with vancomycin, ampicillin, kanamycin and metronidazole could disrupt one set of genes (e.g. involved in DNA replication), while another set of genes were unaffected by the antibiotic treatment and a third set of genes actually gained diurnal oscillations by the treatment (Thaiss et al., 2016). The last two groups are not unexpected as antibiotic-treated mice have significantly reduced amount of microbiota, however some microbiota may remain present. Therefore, the time of the day samples are taken may play an important role for further studies on the role of the microbiota in IEL activation. Of the characterized bacteria phylum showed in Figure 7.1, it has been reported that both *Actinobacteria* and *Firmicutes* bacteria are Gram-positive, while *Bacteroidetes* and *Proteobacteria* bacteria are Gram-negative (Lawley and Walker, 2013). Therefore, the IEL activating triggers obtained from Gram-positive may belong to *Actinobacteria* and/or *Firmicutes* bacteria.

Publications including intestinal microbiota sequencing data vary in regards of which part of the microbiota taxonomy that is presented (phylum, class, order, family, genus or species, Fig 7.1 A-B). However, studying published data on intestinal microbiota composition in C57BL/6 mice from different animal facilities, there seem to be some common trends.

Several studies reported that the phylum *Bacterioidetes* is the most frequent phylum in C57BL/6 mice, followed by *Firmicutes* (Bongers et al., 2014; Pickard et al., 2014; Meisel et al., 2017; Langille et al., 2014). This finding is supported by other laboratories that have reported the intestinal microbiota composition in terms of class *Bacteroidia* (that belong to *Bacteroidetes*) (Thaiss et al., 2016; Meisel et al., 2017), as well as order *Bacteroidales* (that belong to *Bacteroidetes*) (Mu et al., 2017). However in one animal facility, the phylum *Firmicutes* was reported to be the most frequent bacteria(Huang et al., 2015). As these differences in intestinal microbiota composition exist in C57BL/6 mice housed at different animal facilities, it is important to be aware of which intestinal microbiota composition that is present in one's animal unit. Therefore, a next crucial experiment to dissect the mechanism of microbiota-induced IEL activation would be to characterize the intestinal microbiota composition in the C57BL/6 mice housed at the Babraham Institute. It is possible that there are several bacteria or bacterial products that may be able to activate the IELs. An initial step in the analysis of such studies would be to characterize the common intestinal microbiota composition from IL-22-/- mice, *E. vermiformis*-infected mice, *E. vermiformis*-infected mice on broad-spectrum, Gram-positive and Gram-negative antibiotic treatments would be helpful. In addition, if the common microbiota composition are absent or present in statistically significantly lower amount in *E. vermiformis* infected mice on vancomycin treatment and IL-22-/- mice on antibiotic treatment, then it will pinpoint which bacteria to screen for IEL activation assessment.

A next potential step to gain mechanistic insights could be to add TLR ligands to IEL-organoid co-cultures. For such experiments, I would need to adapt the co-culture system to be able to detect IEL activation by imaging. Of note, there are technical limitation to obtain similar amount of information as I have demonstrated with flow cytometric analysis in

Chapter 5, 6 and 7. Imaging is limited to 6 fluorescent parameters (Eissing et al., 2014), while flow cytometry that can detect up 18 fluorescent parameters per sample (Bendall et al., 2012). Therefore, another approach could be to optimize so that the number of IELs per organoid increases to the extent that flow cytometric analysis may be practically possible. The IEL-organoid-co-culture system would be a clean approach to address whether the microbiota-dependent activation of IELs is by a direct or an indirect mechanism since I can decide which cells that are present in the system. Sorting intestinal DCs or MPs would also be possible to add to IEL-organoid co-cultures and address the impact of other APCs in IEL activation.

The notion that Rag2-/- suffer from worse *E. vermiformis* infection compared to WT mice is expected from previous data (Guedes, 2017; Schito et al., 1996). However, it was surprising to observe that broad-spectrum antibiotic treatment reduced the oocyst output to a similar level to what is found in *E. vermiformis*-infected WT mice (Fig 7.21 A-B). Although IELs seemed not to play a significant role in controlling the *E. vermiformis* oocyst production, these data once again highlight the importance of commensal microbiota in health and disease. There is no statistically significant difference in parasite load between *E. vermiformis*-infected WT mice with or without antibiotic treatment, suggesting that broad-spectrum antibiotic treatment is not affecting *E. vermiformis* oocysts directly. . These data suggest that the increased parasite load in infected Rag2-/- mice is dependent on the microbiota. Intestinal microbiota sequencing in Rag2-/- mice showed that more than 60 % of the composition belong to the phylum *Firmicutes* (by *Lachospiracae* and *Ruminococcaceae* detection) (Shih et al., 2014). Whether the microbiota composition changes during *E. vermiformis* infection that promotes oocyst production needs to be determined, but it may indicate that the different microbiota composition in Rag2-/- mice may play a role. Another

feature likely involved in the observation is the lack of IgA, as there are no B cells present in these mice. The lack of B cells is likely to affect the microbiota that is no longer coated by IgA. It remains to be clarified whether it is the microbiota that directly affects the *E. vermiformis*-infected IECs in Rag2-/- mice, or if the microbiota affects immune cells that then affect the infected IECs and oocyst production. Flow cytometric analysis comparing innate immune cell composition in infected Rag2-/- mice, with or without antibiotic treatment, and non-infected controls mice, may provide insights. Additional follow-up experiments would include to have the same groups of mice as used for the experiments presented in Figure 7.21 but to monitor the mice until they eventually have cleared the infection. Although addition of IELs did not decrease the load, they may contribute to faster clearance of *E. vermiformis.*

In line with the observation that antibiotic treatment reduces the parasite load in *E. vermiformis* infected Rag2-/- mice, I observed a trend of reduced MNV-CW3 viral load in the presence of antibiotic treatment (Fig 7.13 F). Published data using MNV-CR6 infection showed that antibiotic treatment reduced the viral load to the detection limit as early as day 3 post infection (Baldridge et al., 2015), suggesting that commensal microbiota is essential for MNV-CR6 replication. Interestingly, MNV-O7 infection of Rag2-/- mice led to a lower viral load compared to WT mice (Supplemental to Figure to 7.10). These data suggest that T and B cells could be taken advantage of by MNV-O7. Transfer of T and B cells into Rag2-/- mice resulted in a tendency to have higher viral loads compared to Rag2-/- mice (Supplemental to Fig 7.10 A-C). A recent report suggested that acute MNV strains can infect T cells, B cells, macrophages, IECs as well as GALT structures (Grau et al., 2017). Transfer of IELs into Rag2-/- mice resulted in a similar viral load compared to Rag2-/- mice. Only when mice were injected with αCD3 antibody 8 hours post MNV-O7 and MNV-CW3 infection, Rag2-/-

mice with transferred IELs had significantly lower viral load compared to control mice (data not shown). These data indicate that IELs have the capacity to reduce MNV viral load-. A recent report has suggested that the capacity of $CD8\alpha^+$ T cells to respond to MNV infection is an important factor to determine whether MNV infection is going to result into an acute or chronic infection (Tomov et al., 2017).

Finally, I presented some data from IL-2Rγ-/-Rag2-/- mice receiving IELs that indicate that other immune cells may play a role in IEL activation, potentially IL-7R-independent and IL-15R-dependent ILCs. Although antibiotic treatment did not reduce IEL activation in IL-2Rγ-/-Rag2-/- mice,, publications have demonstrated differences in the microbiota between IL-2Rγ-/-Rag2-/- and Rag2-/- mice; particularly in regards to segmented filamentous bacteria (SFB) (Shih et al., 2014). As mention before, age seem to play a role for the microbiota (Langille et al., 2014). The transfer mice experiments involved the oldest mice used in my thesis. This is due to that mice cannot undergo procedures until they are at least 5 weeks old, and cells would need a minimum of 3 weeks post injection to reconstitute. However, the same age range applies for the control Rag2-/- mice, suggesting that aging microbiota may not be the only factor involved in the explanation of the differences in IL-2Rγ-/-Rag2-/- mice.

As IELs in IL-2Rγ-/-Rag2-/- mice showed no increase the in production of TNFα and IFNγ and Ki-67 expression, these data suggest that the activation observed in IELs transferred into IL-2Rγ-/-Rag2-/- mice could be of a similar character to IL-22-/- mice. The BM chimeras experiments aided to pinpoint further which cells that may be of importance for IEL activation. WT BM transferred into IL-2Rγ-/-Rag2-/- and Rag2-/- mice show a small increase in MTG staining compared to IELs in WT mice (Fig 7.26 A). These data suggest that the cells, that may affect IEL activation, may belong to the hematopoietic immune cells rather

than IECs. Similar results were obtained when transferring Rag2-/- bone marrow into IL-2Rγ-/-Rag2-/- mice that subsequently received IELs (Fig 7.26 B). These data suggest that T and B cells are not essential to modulate IEL activation inthis model. Interestingly, when transferring IL-22-/-Rag2-/- BM cells into IL-2Rγ-/-Rag2-/- mice that subsequently received IELs, I observed an increase in MTG staining. Surprisingly, this increase was reduced in the presence of antibiotics. As described previously, IL-22 is produced by lymphocytes, suggesting that ILCs may be involved. Surprisingly, I did not observe the same trend when using IL-7R-/-Rag2-/- BM cells into IL-2Rγ-/-Rag2-/- mice that subsequently received IELs (Fig 7.26 B). These data indicate that cells, that are independent of IL-7 signalling and produce IL-22, may be involved in IEL activation. There is a report suggesting that IL-15 maintain a subset of ILCs that are independent of IL-7 signalling (Robinette et al., 2017). These ILCs would be particularly interesting to include in future experiments to pinpoint the explanation why IELs in IL-2Rγ-/-Rag2-/- mice have higher mitochondrial mass compared to controls. Undoubtedly, more research would be required for full understanding of the role of IL-2Rγ signalling, and potentially ILCs, in IEL activation.

Collectively, the data presented in this chapter demonstrate an important role of microbiota in activation of IELs. Antibiotic treatment did not only reduce the increase in mitochondrial mass, but also reduced effector functions such as proliferation and cytokine production. These observations support a model of mitochondria-dependent IEL activation, for which commensal microbiota and TCR-stimulation are inducers of IEL activation.

Chapter 8: Discussion

The results chapters have investigated further into the requirements for IEL activation and maintenance. The findings from these chapters highlight an important role of IEC-IEL interactions for IEL survival, as intestinal organoids are sufficient to maintain the majority of organoid-associated IELs alive for at least four days (Fig 4.9 B). In addition, other findings from this thesis highlight that IELs undergo mitochondrial plasticity during activation. Non-treated IELs have lower mitochondrial mass and membrane potential than other CD8α^+ T cells, TCR$\gamma\delta^+$ T cells and epithelial-resident lymphocytes (Fig 5.6 F-H). This mitochondrial state was altered during activation, such as by αCD3 antibody injection and intestinal infections, demonstrating mitochondrial plasticity in IELs that seems linked to their activations state and effector functions.

8.1. IEL-organoid co-culture system provides an *in vitro* option for IELs

In Chapter 4, I established an IEL-organoid co-culture system (Fig 4.3 C). The usage of the co-culture systems was advanced further with the establishment of 3D imaging quantification algorithms for both IECs and IELs (Fig 4.7 B and Supplemental Figure to 4.7-2). These algorithms may be applicable to organoids sourced from other organs and other immune cells added to the organoids. In addition, I managed to initiate the start of adding additional complexity to the IEL-organoid system by establishing MNV- and *E. coli*-organoid cultures.

The exact mechanism behind the IEC-mediated IEL survival is currently unknown. TCR$\gamma\delta^+$ T cells sourced from other tissues, such as spleen and lymph nodes, are possible to culture *in vitro*, suggesting that the issues to culture IELs on their own is not strictly linked to the preference to express TCRγδ. The only known feature of the IEC-mediated IEL survival is that it is not strictly dependent on IL-15 trans-presentation (Fig 4.9 A-B). In addition to the

reports that IECs express classical antigen presenting machinery proteins, there are reports that IECs also express non-classical MHC molecules such as CD1d that may be involved in the interactions with IELs that result in IEL survival (Henderson et al., 2011; Luoma et al., 2014). A hypothesis may be that IECs are mediating the survival of IELs as one way to prevent autoimmunity. When an IEC is shed from the IEC barrier, it may take along IELs that subsequently die as well. Finally, it is possible to grow human intestinal organoids (In et al., 2016). This means that translational research based on the methods presented in Chapter 4 is a possibility. This could for example provide further insights about the mechanisms behind celiac disease, in which autoreactive IELs are thought to be involved in the pathology (Leon, 2011).

There is a huge interest in organoid co-cultures in the field. In recent years, different versions of organoid co-cultures have been reported. One group has co-cultured organoids with fibroblasts and shown that organoids co-cultured with fibroblast grow even in the absence of R-spondin in the culture medium. In these co-cultures, an increase in the mRNA expression of the lysozyme gene Lyz1, a gene associated with Paneth cells, has been reported (Lei et al., 2014). Innate lymphoid cells 3 (ILC3)-organoid co-cultures have also been reported and shown to have a positive impact on organoid growth in combination with the cytokine IL-23 (Lindemans et al., 2015). However, this study did not determine whether the ILC-mediated organoid growth was due to cytokine secretion from ILCs or due to contact interactions between ILCs and organoids. There have also been reports about T cell-organoid co-cultures. The Daniel Mucida laboratory reported a method of culturing splenic $CD8\alpha^+$ T cells with organoids. In addition to reporting this method, they also performed live-imaging of the co-cultures. The video footages capture some T cells associated with the organoids, but also show that there are plenty of splenic $CD8\alpha^+$ T not associated with organoids. (Rogoz et al.,

2015). Another group added culture medium from Th17 and Th22 T cell differentiation cultures to WT organoids and showed an increased in the gene expression of the AMPs RegIIIγ and RegIIIβ (Backert et al., 2014). These data highlight the impact of cytokines on organoids and hence the cytokine production from T cells need to be considered to be able to distinguish effects from cytokines production and contact interactions with T cells. There is also a report of lamina propria lymphocytes (LPLs)-organoid co-cultures (Hou et al., 2018). Finally, there has been a paper published describing an IEL-organoid co-culture system. This report illustrated IELs incorporated into organoids, quantified the number of IELs after culturing and showed that addition of IL-2, and particularly the combination of IL-2, IL-7 and IL-15, increased the number of IELs (Nozaki et al., 2016). These observations are in contrast to my findings reported in Chapter 4 (Fig 4.3 E-F). Of note, this report did not include a live-dead cell marker, making it unclear whether the reported IEL expansion represented live or dead IELs. In addition, they used GFP-reporter mice as donors for the cultured IELs. IECs are a cell type prone to autofluorescence (own data and (Prinz et al., 2006)). Autofluorescence can occur if cells contain proteins that have own fluorescence such as co-enzymes involved in redox reactions (Croce and Bottiroli, 2014). The IEL-organoid report did not include a strategy to avoid false-positive IEL quantification.

In addition to adding IELs to the organoids, I have also shown cultures of intestinal organoids with MNV-O7 and MNV-CW3 (Fig 4.10) and *E. coli* (Fig 4.12). The presence of MNV-O7, but not MNV-CW3, was confirmed by qPCR viral quantification analysis. I was able to observe a reduction in organoid proliferation in presence of either MNV-O7 or *E. coli*. I demonstrated that MNV-O7 reduced organoid proliferation only when added in the organoid culture medium. A potential explanation for this may be that MNV are virus particles, which do not have their own mobility capacity. Therefore, when adding MNV into the Matrigel,

they are likely to be trapped during the polymerization process. In contrast, *E. coli* seem to require to be present in the Matrigel to affect the organoids. Whether *E. coli* attach to organoids or secrete factors that affect organoid proliferation needs to be determined e.g. by staining for *E. coli*. These two examples of incorporation MNV and *E. coli* into the organoids show different strategies to successfully incorporate microorganisms/pathogens into organoids.

Overall, these advances in immune cell-organoid co-cultures, together with reports about various organoid infection models such as rotavirus (Saxena et al., 2016), norovirus (Ettayebi et al., 2016), *Salmonella enterica serovar Typhimurium* (Zhang et al., 2014) and *Listeria monocytogenes* (Nigro et al., 2016), will lead to very interesting experiments on how organoids themselves cope with infectious agents and how the coping mechanism(s) are potentially altered in the presence of one or more immune cells populations. For some of the infection models, the pathogens have been microinjected into the organoids. This has been done for pathogens such as *Helicobacter pylori* (Bartfeld et al., 2014) and *Salmonella enterica* (Wilson et al., 2014) to mimic better the natural infection route. However, it is a time-consuming approach to individually infect organoids. Modelling part of intestinal stress, inflammation or infection in organoids can also be mimicked by adding cytokines to the organoids. There have been studies exploring the mechanism of actions of the three types of interferon by adding them to intestinal organoids. One report demonstrated that IECs in the organoids respond to both IFN-λ and IFN-β, particularly in the organoid crypt domains (Bhushal et al., 2017). Addition of IFN-γ to organoids led to Paneth cell degranulation, increased level of active caspase-3 and ultimately fewer organoids compared to non-treated organoids (Farin et al., 2014).

Utilizing the organoid model, with tailored complexity of immune cell/pathogen/cytokine additions, will be a very valuable complement to the *in vivo* data for the further understanding of intestinal immunity.

8.2. IELs have altered mitochondrial status

In Chapter 5, I discovered additional differences between IELs and splenic CD8α$^+$ T cells in terms of lipid storage and mitochondrial properties. IELs have lower mitochondrial mass (Fig 5.6 A-B) and mitochondrial membrane potential (Fig 5.9 A-B) than splenic naïve and memory CD8α$^+$ T cells. In addition, IELs have higher content of CLs (Fig 5.8 A-B) and a similar level of mitochondrial ROS production (Fig 5.10 A-B) to splenic naïve and memory CD8α$^+$ T cells. Other TCRγδ and epithelial-resident T cells have significantly higher MTG staining (Fig 5.7 F-H), indicating that their mitochondrial mass is higher than IELs. These observations are putting IELs apart from other T cells.

Of note, there may be some differences between CD8α$^+$ and CD4$^+$ T cells, as splenic CD4$^+$ T cells have almost twice as high MTG MFI to CD8α$^+$ splenic T cells (data not shown). Therefore, further characterization of mitochondrial properties in other lymphocytes, such as CD4$^+$ T cells and ILCs, may provide further insights into the relationship between metabolic parameters and immune functions.

There is a possibility that the intestinal environment is involved in IELs' restricted mitochondria capacity, particularly interactions between IECs and IELs. The vast majority of LPLs do not share the low mitochondrial mass phenotype with IELs (Fig 5.7 F-H), despite that LPLs could be within reach for secreted factors from IECs. It is tempting to speculate that there may be some meaning behind the distinct differences between IELs and LPLs e.g.

in terms of TCR and co-receptor expressed, as well as mitochondrial mass. This may be to complement each other to maintain intestinal homeostasis. For some reason, it seems more important to maintain IELs under mitochondrial control compared to LPLs. It remains to be determined how this mitochondrial state is impacting the energy supply such as ATP production. It also remains to be determined at which time point during IEL development that this restricted mitochondrial state is imposed, and whether intrinsic or extrinsic signalling is involved.

8.3. IELs have mitochondrial plasticity induced by TCR-activation

After discovering that IELs have lower mitochondrial mass compared to other T cells, I discovered that there is mitochondrial plasticity in IELs. Activation of IELs, via TCR stimulation, led to significant increase in MTG staining (Fig 6.1 D-F). Interestingly, this increase was heterogeneous in the different IEL subsets with CD8αβ$^+$ IELs, particularly TCRαβ$^+$ CD8αβ$^+$ IELs, responding the strongest. The mechanisms behind the differences in response in the different IEL subsets need to be studied further.

In addition to the increase in MTG staining, I demonstrated that IELs gain increased mitochondrial ROS production (Fig 6.4 A-C) and Ki-67 expression (Fig 6.3 C-E). However, TCR stimulation was not sufficient to induce cytokine production in IELs (Fig 6.3 A-B). CD8α$^+$ splenic T cells from the same mice, showed increase cytokine production (data not shown). These observations are in line with the hypothesis that IELs are in poised state of activation and seem to require additional signaling for cytokine production compared to other T cells.

It remains to be determined whether the increase in MTG and Ki-67 are linked or separate events. As shown in the experiments in Chapter 6, there are cases in which Ki-67 response can be obtained without observing increase in mitochondrial mass (Fig 6.10 and Fig 6.12). These data suggest that the correlation between mitochondrial mass increase and proliferation may not mean they are strictly dependent on each other. An alternative explanation could be that increase in Ki-67 expression occurs before the increase in mitochondrial mass. The IEL-organoid co-culture model could be an option to investigate this further.

It also remains to be characterized the signalling cascade from TCR to mitochondria, and potentially from mitochondria to Ki-67 expression. Such characterization could provide targets to either boost or inhibit IEL activation responses. It would be interesting to test whether this mitochondrial plasticity is translating to human IELs. If so, this could have potential clinical implications in intestinal diseases in which a role of IELs have been implicated.

As shown in Chapter 6, the number of IELs after αCD3-mediated activation is reduced at24 and 48 hours post injection (Fig 6.3 G). These data suggest that activated IELs may die or migrate to other compartments. Using IEL transfer model combined with *E. vermiformis* infection, I also observe a reduction in the number of IELs (Fig 7.21 D-E), again suggesting that activated IELs may die. Interestingly in *E. vermiformis*-infected WT mice, there are more IELs recovered at the peak of infection compared to the controls (Fig 7.21 F), which could go against the notion that activated IELs may die. In addition, IELs transferred into IL-2Rγ-Rag2-/- mice showed similar number of IELs after αCD3-mediated activation (Fig 6.7 C). These data suggest that the reduction in the number of IELs, whether due to cell death or due to migration, is dependent on other cells. In the case of αCD3-mediated activation, it seems

that other activated T cells may be involved. In the case of the *E. vermiformis*-infection, IECs become infected and may produce signals that get interpreted differently depending on whether other adaptive immune cells are present. Ki-67 expression indicates that cells are in the cell cycle, however not at which stage of the cell cycle. Therefore, this increase in IELs could be explained by IELs coming from other part of the small intestine, LPLs or newly generated IELs that originate from proliferation. An alternative hypothesis would be that alternations in the IEC environment between WT and Rag2-/- mice may prevent proliferation from activating IELs.

In Chapter 6, I tested several factors to determine their role in steady state IELs as well as and αCD3-activated IELs (Fig 6.10-14). I discovered that there was some role of T-bet for specific IEL subsets, but no factor that seem in common with the different IEL subsets. To address this part more efficiently, one could sort steady state and TCR-activated IEL subsets to screen for differences between steady state and activated IELs, as well as common factors between the IEL subsets during steady state and activation. Another interesting aspect would be to study the same mice to see if they return to steady state at similar time. Prolonged or reduced activation time may have implications in disease models.

Changes in mitochondrial mass have been reported in other cell types. A report compared two different human endothelial cell lines: one healthy and one dystrophy cell line. There were differences in their basal MTG staining. When adding carbonyl cyanide m-chlorophenyl hydrazone (CCCP), an inducer of mitochondrial autophagy, to these cell lines, the healthy cell line responded by decreased MTG staining, while the dystrophy cell line did not respond (Benischke et al., 2017). Similar trend was observed in fibroblasts (Doménech et al., 2015). These data demonstrate mitochondrial remodeling in other cell types. In this case, the

mitochondrial remodeling was linked to disease. In addition, these data show a potential mechanism for IELs to return to steady state, if surviving the activation process, namely mitophagy.

An additional question to address is the biological benefit for IELs having to remodel their mitochondria for activation. The mitochondrial remodelling is probably a very costly process, particularly as it seems to be able to occur as rapid as 24 hours post activation. One hypothesis would be that IELs need to be strictly regulated to avoid autoimmune damages in the intestinal compartment. It may be less costly to have IELs forced to remodel their mitochondria for activation, than to cope with the damage hyper-active IELs may be able to cause.

8.4. Gram-positive commensal microbiota can activate IELs

In the last results chapter, I demonstrated mitochondria-dependent activation in models of intestinal inflammation. Using IEC-stressed mice, I showed that IELs were in a more heighten state of activation in terms of CD44 staining. However, these IELs lacked MTG increase, suggesting that IELs may require additional signals to increase MTG staining (Fig 7.2 A-C). In the *E. vermiformis* infection model, IELs did not only have increased MTG staining, mitochondrial ROS production and Ki-67 expression, they also produced IFNγ and TNFα (Fig 7.5 A-F). Just like the relationship between MTG and Ki-67 needs to be clarified, the potential link between MTG and cytokine secretion need to be determined. In Chapter 7, I showed that antibiotic treatment, targeting Gram-positive spectrum, prevented the increase in MTG staining (Fig 7.18 B). The same IELs also exhibited reduced cytokine production, suggesting that MTG increase may be required for cytokine production in IELs. Every time I

have observed cytokine production from activated IELs, the same IELs have also shown increase in MTG staining.

As mentioned in Chapter 7, these data support a model in which IEL can become activated when the IEC barrier integrity is compromised. However, one disadvantage of such a model is that IELs seem to become activated only by Gram-positive bacteria. The reasoning for such specificity needs to be determined. Does this mean that IELs are not involved in the response against Gram-negative pathogens or do IELs use other mechanisms, such as cytotoxicity, to respond against Gram-negative pathogens? The fact that mitochondria seem to have developed from Gram-negative bacteria (Morgun et al., 2015), may be involved in the lack of response to Gram-negative bacteria.

When continuing these studies, it is essential to control the mechanisms of action for used antibiotics, as some antibiotics have been suggested to be able to affect mitochondria (Watanabe et al., 2018; Langdon et al., 2016). Combination of ampicillin, vancomycin, neomycin and metronidazole decreased the MTG staining in IECs (Morgun et al., 2015). This is likely not the case for my experiments, as the three different antibiotics used are suggesting the same interpretation.

The diet is affecting the immune system as well as commensal microbiota. Examples of effects of the diet on the immune system are the role of RA for Th1 cells and AhR for IELs. Western diet, containing more fat than standard diet, negatively affect the IEC proliferation in TLR2-/-, TLR4-/- and NOD2-/- mice (Sardi et al., 2016; Chung et al., 2017). The western diet has also been shown to alter the microbiota composition in favor of the phylum *Firmicutes*, as well as reduced mucus layer and consequently reduced spatial separation

between the IEC barrier and commensal microbiota (Schroeder et al., 2017). In addition, the vitamin A derivate RA has shown role of RegIIIγ and RegIIIβ expression as mice feed on diet without vitamin A have lower expression of these AMPs (Goverse et al., 2016). As described earlier, RegIIIγ has an important role for microbiota segregation and composition, again linking diet to microbiota and immune responses. In addition, obesity is affecting the microbiota. Interestingly, some of these changes do not return to normal after the mice are no longer feed with high-fat diet (HFD). *Mogibacterium, Christensenlla* and *Lactobacillus reutri* are some reported microbiota that is still altered in mice that have previously received HFD diet (Thaiss et al., 2016).

In addition to the diet, a report used PCA to distinguish between young and old mice based on their intestinal microbiota (Langille et al., 2014). It has also been reported that the gender of the mice also affect their microbiota (Yurkovetskiy et al., 2013; Markle et al., 2013). Hence monitoring intestinal microbiota composition and age may be essential for future experiments. This view is shared by others, such as Stappenbeck and Virgin who wrote a review on the matter (Stappenbeck and Virgin, 2016). They did not only mention the importance of bacteria, but also other commensal organisms such as virus and fungi.

A recent study compared the intestinal microbiota in laboratory-housed mice to mice living in the wild. Using 16S rRNA sequencing, they showed a distinct clustering difference between mice from the wild and laboratory-housed C57BL/6 mice; regardless of the source of the lab mice (Rosshart et al., 2017). In addition, the wild mice coped better with DSS-induced colitis and tumor occurrence than lab mice (Rosshart et al., 2017), suggesting that intestinal microbiota composition has an important role in the disease outcome. In addition, there is a report suggesting that the T cell response towards *T. muris* infection varies depending on

mouse strain (Little et al., 2014). These data are suggesting important strain differences that is linked to different microbiota composition.

The differences in the microbiota composition in bought mice also showed different severity during *Salmonella enterica serovar Typhimurium* infection (Thiemann et al., 2017). *Salmonella* infection itself seems to be able to alter the microbiota. The more *Salmonella* organisms the more *Proteobacteria* (Gram-negative) and *Bacilli* (Gram-positive) are present, while a negative correlation applies for *Bacteriodia* (Gram-negative) bacteria classes (Borton et al., 2017). Another report suggests that the microbiota is required to limit the *Salmonella* infection (Edelblum et al., 2017). Collectively, these data demonstrate the importance of the microbiota composition. Therefore, one of the next steps to understand the microbiota-dependent activation mechanisms in IELs would be to be perform sequence analysis of the intestinal microbiota. Bearing in mind the differences between laboratory-bought mice and different laboratory results, it may be a good idea to include microbiota sequencing in intestinal immunity research as standard. This information may become crucial for proper interpretation and reproducibility between different laboratories.

In addition to address the question whether the microbiota-dependent pathway is affecting IELs directly or indirectly, it is important to determine the molecular mechanistic effects on IELs. Data from Assay for Transposase-Accessible Chromatin (ATAC) and enhancer sequencing demonstrate differences between IELs sourced from germ-free (GF) and conventional kept mice (Semenkovich et al., 2016). Enhancer sequencing data e.g. show that STAT3 enhancer is downregulated in conventional TCR$\gamma\delta^+$ and TCR$\alpha\beta^+$ IELs. (Semenkovich et al., 2016).

The microbiota has previously been shown to affect other immune cells. GF mice have no basal IL-17 production from Th17 cells sourced from the intestinal lamina propria, which SPF mice have (Atarashi et al., 2015). A recent report link changes in the diet, in that case higher salt concentration that affect the microbiota, which in turns affect Th17 cells. This study concluded that *Lactobacillius murinus* was affected by the salt concentration in the diet and therefore a link between diet, microbiota and Th17 cells (Wilck et al., 2017). In addition, Th1 cells seem also to be affected by commensal microbiota. Using RegIIIγ-/- mice, which lack the spatial separation of microbiota to the IEC barrier, it was shown that small intestinal LPLs have increased IFNγ production, which is reduced by antibiotic treatment (Vaishnava et al., 2011). MAIT cells have been shown to be able to become activated by riboflavin sourced from Gram-positive bacteria (Soudais et al., 2015). Metabolites from commensal microbiota, such as short-chain fatty acids (SCFAs), have been reported to induce generation of Treg cells in spleen and LNs (Arpaia et al., 2013). Other specific intestinal microbiota has been shown to increase the ratio of Treg cells (Sefik et al., 2015).

Commensal microbiota does not only affect T cells. Using germ-free mice, it was shown that intestinal B cell class switch to IgD to less extend compared to control mice (Choi et al., 2017). In addition, the innate immune system seems to be affected by commensal microbiota. One report has shown that macrophages could be activated by products from *Helicobacter hepaticus* via TLR2 and MyD88 signalling pathways (Danne et al., 2017). Another study demonstrated that the recruitment of macrophages, monocytes and neutrophils to the intestinal compartment after DSS-induced colitis is dependent on Gram-positive bacteria (Nakanishi et al., 2014). This observation could potentially be important to address whether IELs are activated by microbiota in a direct or indirect manner. If IELs are activated by microbiota indirectly by APCs, then less recruitment of APCs could lead to less or no IEL

activation. Whether Gram-positive bacteria affect intestinal DC migration would be interesting to address. Recently, is has been shown that LN-sourced T cells are actually de-activated, producing less IFNγ and TNFα, when exposed to bacterial supernatant from *Streptococcus pneumonia (S. pneumonia)* (Blevins et al., 2017). This is opposite response towards bacteria compared to what I have observed for IELs. Of note, in my case it is likely that commensal microbiota that is activating the IELs, which may differ from pathogenic bacteria such as *S. pneumonia*. Therefore, it will be interesting to study whether Gram-positive enteric pathogens are also capable of activating IELs in similar manner as Gram-positive commensal microbiota.

Finally, the role of the microbiota on immune responses goes beyond the intestinal compartment. The immune response against influenza is blunter in the absence of commensal microbiota (Ichinohe et al., 2011). Several studies have reported of various gut axis with other organs, such as gut-brain, gut-liver and gut-heart axis, for which the influencing factors sourced from the gut is originating from commensal metabolites. These studies highlight the importance of microbiota for overall health (Blacher et al., 2017).

Chapter 9. Conclusions

It is essential that the intestinal immune system is regulated properly to generate the appropriate response to dangers, such as pathogens, while simultaneously remaining tolerant towards commensal microbiota and dietary residues. There is a range of intestinal immune cells critical for providing effective, yet balanced immune responses. One particularly interesting class of intestinal immune cells are IELs. In defensive terms, they are located at "the front" between IECs in the IEC barrier, in an activated yet resting state. Most of the current knowledge of IELs is derived from *in vivo* experiments, because IELs survive poorly *in vitro.*

In Chapter 4, I investigated further the subject of IEL maintenance *in vitro*. Advancements into the cause of poor IEL survival would provide further insights into IELs' requirements for maintenance, as well as an *in vitro* option to study further aspects of IEL biology such as their activation. In this thesis, I have achieved advancements by combining IELs with intestinal organoid, "mini-gut", cultures. By establishing live/dead imaging staining for my co-culture system, I discovered that the majority of IELs associated with organoids remain alive for at least four days in cultures. I was also able to observe live IELs after organoid passage, indicating that IELs may be able to survive for even longer. These data suggest an important role of IEL-IEC interactions for IEL survival. In the same chapter, I also established quantification parameters to assess the numbers of the different subsets of IELs and IECs in my co-culture system (Fig 9.1 B-C). Using these parameters, I performed experiments with further complexity in the form of murine norovirus (MNV) addition. MNV-infection of organoids resulted in a decrease in the proliferation in organoids. Addition of IELs to MNV-organoid cultures prevented the MNV-mediated reduction in proliferation in organoids.

These experimental strategies may be applicable to other tissues, which can be cultured as organoids.

In Chapter 5, I discovered previously undescribed differences between IELs and other $CD8\alpha^+$ T cells, epithelial-resident lymphocytes and $TCR\gamma\delta^+$ cells. In recent years, the importance of cell metabolism for immune functions has gained attention. In this Chapter, I showed that IELs store more lipid droplets than splenic $CD8\alpha^+$ T cells. Moreover, IELs have surprisingly low mitochondrial mass compared to other $CD8\alpha^+$ T cells. I compared IELs with T cells isolated from the lung, liver and spleen, as well as with dendritic epidermal T cells (DETCs) and small intestinal lamina propria lymphocytes (LPLs). Only a small proportion of LPLs, the $TCR\gamma\delta^+$ LPLs, had a similarly low mitochondrial mass as IELs. Surprisingly, lung T cells had the highest measured mitochondrial mass. Although out of the scope of this thesis, the finding highlights the need for further investigations to understand the different demands of different T cells in the tissues. In addition, I discovered that IELs have lower mitochondrial membrane potential than splenic $CD8\alpha^+$ T cells. These data are in line with data obtained from Seahorse mitochondrial stress assays, demonstrating that IELs lack spare respiratory capacity (SRC), unlike naïve and memory splenic $CD8\alpha^+$ T cells. Surprisingly, IELs had similar levels of mitochondrial reactive oxygen species (ROS) production to splenic $CD8\alpha^+$ T cells. Mitochondria contain a specific lipid called cardiolipin (CL). In Chapter 5, I also made measurements of the content of CLs in cells and my results indicated that IELs have more CLs compared to splenic $CD8\alpha^+$ T cells. Overall, these data indicated that IELs have an altered mitochondrial state, which might contribute to explaining some of the many differences between IELs and other $CD8\alpha^+$ T cells.

In Chapter 6, I demonstrated that IELs exhibit mitochondrial plasticity: activation in the form of TCR stimulation led to increased mitochondrial mass. This applies to all IEL subsets. Interestingly, I observed a heterogeneous response among IEL subsets, with TCR$\alpha\beta^+$ CD8$\alpha\beta^+$ IELs manifesting the strongest response. I observed increased expression of the lymphocyte activation markers CD44 and CD69, of which the CD69 increase was only transient. In addition, I demonstrated that activated CD8$\alpha\beta^+$ IELs specifically have higher mitochondrial ROS production, while all IEL subsets showed increased Ki-67 expression. However, these activated IELs did not secrete effector cytokines such as IFNγ and TNFα. In addition, mitochondrial membrane potential did not alter, except in TCR$\alpha\beta^+$ CD8$\alpha\beta^+$ IELs. Moreover, the CL content did not alter in any of the IEL subsets, suggesting that the total amount of CLs remained at a similar level to that of non-activated IELs. Interestingly, the composition of CLs in IELs alters after IEL activation from mainly consisting of CL 74 species to CL 72 species. These data support a model in which mitochondria play a role in the IEL activation process.

Finally, in Chapter 7, I demonstrated IEL activation, measured by MTG and CD44 staining, during physiological circumstances such as intestinal infections using *Eimeria vermiformis (E. vermiformis)* and murine norovirus (MNV)-CW3. Surprisingly, infection with *Salmonella* and MNV-O7 did not lead to IEL activation. These observations suggest that triggers for IEL activation are present in some infection models but absent in others. This raised the question of what these IEL activation triggers might be. One key experiment in this regard was the assessment of IL-22-/- mice that had activated IELs despite a lack of on-going infection(s) or inflammation. IL-22 is an important cytokine for the IEC barrier. Administration of broad-spectrum antibiotics to IL-22-/- mice significantly lowered the level of IEL activation. Using an experimental approach combining antibiotic treatment with *E. vermiformis* and MNV-

CW3 infection models, I demonstrated that IEL activation is lowered to a level similar to that of non-infected animals in both infection models. These data highlight the commensal microbiota as one inducer of IEL activation and not the pathogens themselves. Another very interesting finding from this chapter is that the activation of IELs seems to be mediated specifically by Gram-positive bacteria. Mice, infected with *E. vermiformis* and on antibiotic treatment targeting Gram-positive bacteria, failed to show the same IEL activation as infected non-treated mice or infected mice treated with antibiotic targeting Gram-negative bacteria specifically. These observations are supported by DSS-induced colitis experiments. Previous literature has suggested that DSS-induced colitis alters the commensal microbiota in favor of more Gram-negative bacteria. This could explain why DSS-induced colitis did not lead to activation of IELs.

Interestingly, combining antibiotic treatment and αCD3-treatment did not show statistically significant differences, suggesting that TCR stimulation and microbiota activation of IELs may be two separate IEL activation pathways. Data from this chapter identify commensal microbiota as one essential component for mitochondria-mediated IEL activation. These data also invite the design of a model in which IEL can become activated regardless of the cause of leakiness of the IEC barrier.

Overall, the findings from this thesis provide evidence of IEC-mediated IEL survival, as well as a role for IELs to aid IEC proliferation during viral infection. In addition, findings from this thesis highlight an important role for mitochondria in IEL activation. These data are very exciting and should be pursued in further investigations into IEL biology.

IELs have been suggested to have roles in intestinal inflammatory diseases such as intestinal bowel disease (IBD) and celiac disease (CD). The new findings may aid in discovering and developing new targets for therapies for modulating IEL activation in intestinal disorders and diseases.

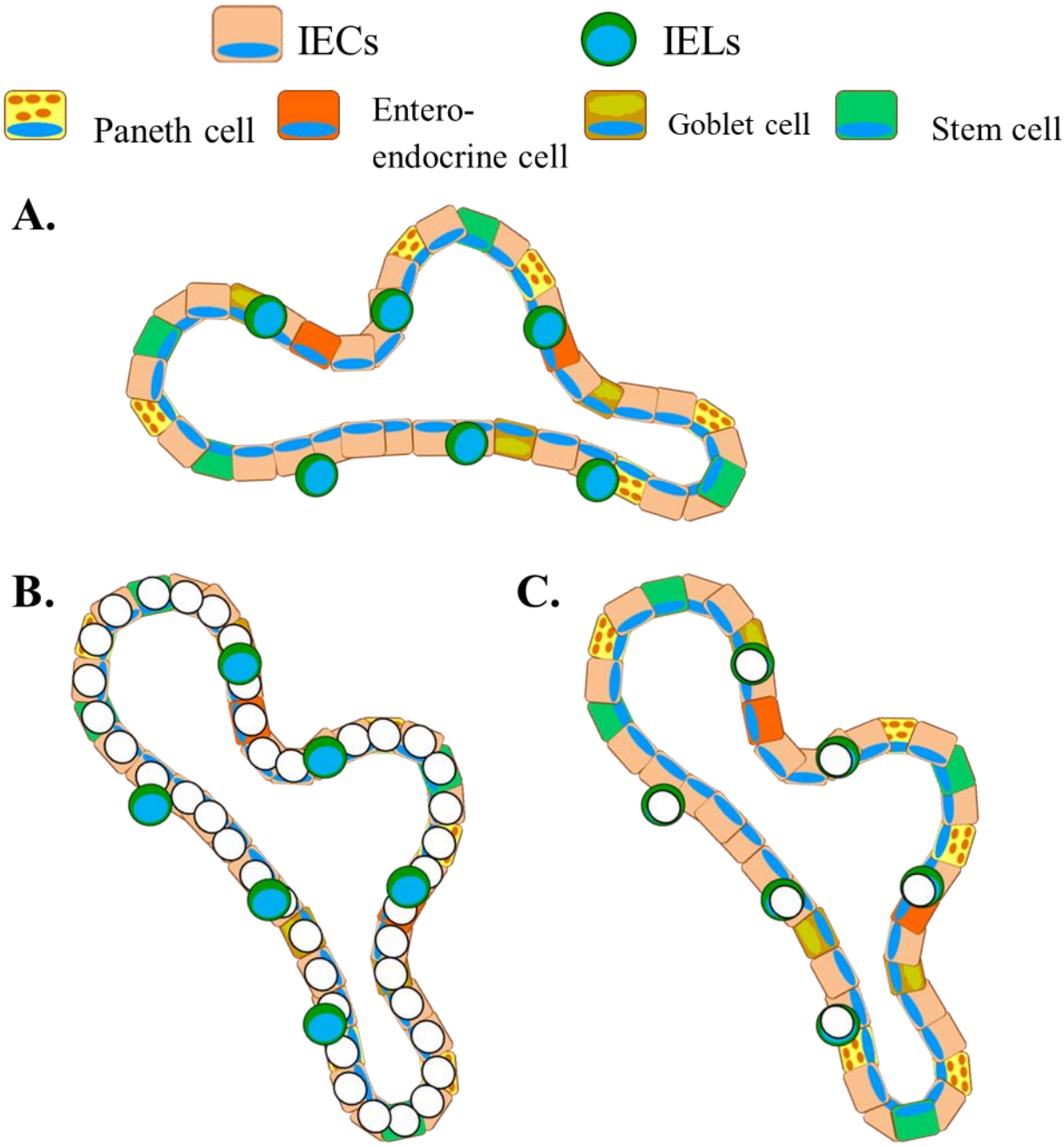

Figure 9.1 Summary of IEL maintenance. In this thesis, I have shown data suggesting that intestinal organoids can support IEL survival. A) shows an example of IELs and an organoid cultured together. I have established quantification parameters (white spots) for the IEL-organoid co-cultures for B) IECs and C) IELs. Using these parameters, I demonstrated differences in the proportion of proliferative IECs as well as goblet cell in IL-15Rα-/- organoids compared to WT organoids. I was also able to demonstrate that the proportion of proliferating IECs is reduced in the presence of MNV and *E. coli*. The IEL parameters require further optimization for full usage.

A. IELs have lower mitochondrial mass (MTG) compared to other T cells

	Small intestine				Spleen		Lung		Liver		Skin (ear)
	TCRγδ+ IELs	TCRαβ+ IELs	TCRγδ+ LPLs	TCRαβ+ LPLs	TCRγδ+	TCRαβ+	TCRγδ+	TCRαβ+	TCRγδ+	TCRαβ+	DECTs
MTG	Low	Low	Low	Medium	Medium	High	High	Very high	Medium	High	Medium

MTG-MitoTracker Green

B. TCR-stimulation is sufficient to activate IELs

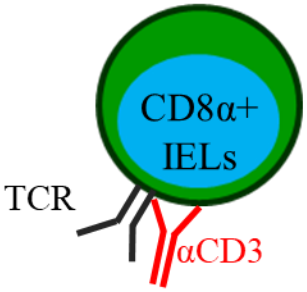

	TCRγδ+ CD8αα+	TCRγδ+ CD8αβ+	TCRαβ+ CD8αα+	TCRαβ+ CD8αβ+	CD4+ CD8αα+
MTG	+	++	+	+++	-
MTO	-	-	-	+	--
MitoSOX	-	+++	-	+++	-
NAO	-	-	-	-	-
Ki-67	+++	+++	+++	+++	+++
TNFα	-	-	-	-	-
IFNγ	-	-	-	-	-

Data from 48 hours post αCD3 injection

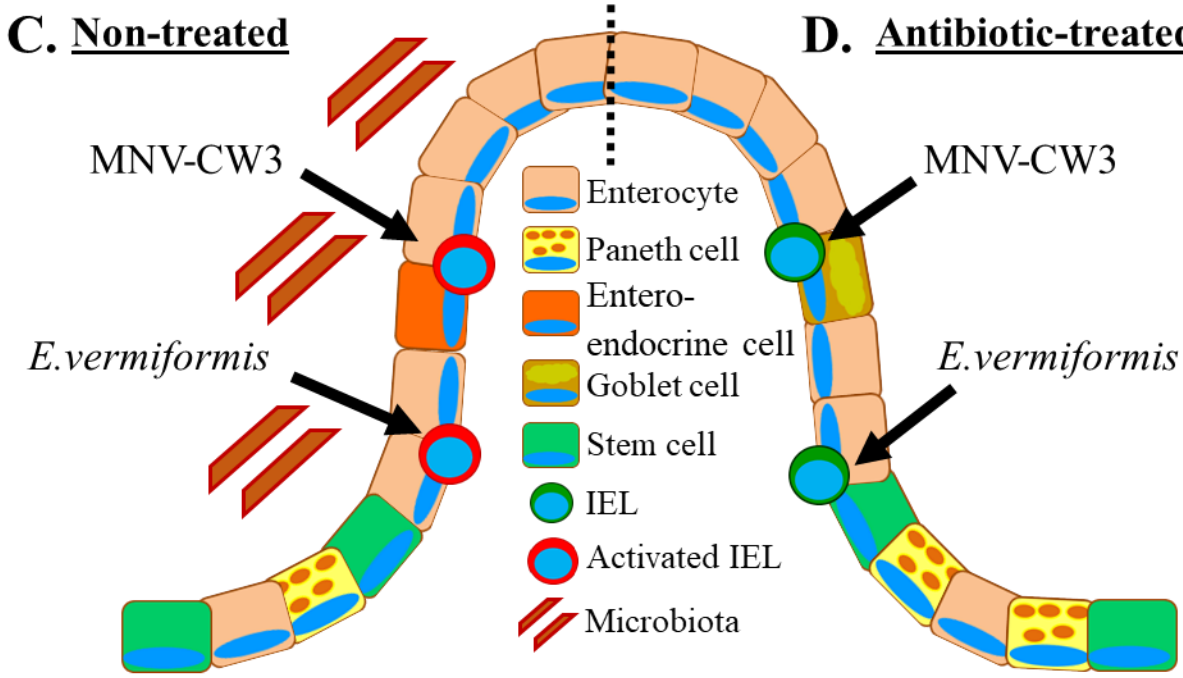

E.

	TCRγδ+ CD8αα+	TCRγδ+ CD8αβ+	TCRαβ+ CD8αα+	TCRαβ+ CD8αβ+	CD4+ CD8αα+
MTG	-	+++	+	+++	-
MTO	-	-	-	-	+
MitoSOX	-	+	-	+++	-
NAO	-	-	-	-	-
Ki-67	-	++	-	+++	+++
TNFα	-	+	-	+++	++
IFNγ	-	+	-	+++	+++

Data from 10 days post *E.vermiformis infection*

Figure 9.2 Graphical summary of findings related to IEL activation. In this thesis, I have shown that IELs have a different activation state compared to other T cells and that IELs can become activated via TCR- and microbiota stimulation Panel A) shows the different T cells tested that all have different mitochondrial masses compared to IELs, measured by MTG staining as shown in Chapter 5. Panel B) illustrates the observation from Chapter 6 that IELs can become activated by TCR-stimulation. The different IEL subsets respond differently to TCR stimulation as shown by the table. – indicates no difference, -- indicates reduction, + indicates increase, while ++ and +++ show greater increase by the measured parameter. Panel C) and D) shows a schematic illustration of the small intestine with the different IEC subsets, as well as findings from Chapter 7 suggesting that MNV-CW3 and *E. vermiformis* infection leads to IEL activation measured by MTG staining. Panel F) details the activation of the different IEL subsets at day 10 post infection. Interestingly, in antibiotic-treated conditions, the activation cause by MNV-CW3 and *E. vermiformis* did not occur. These observations indicate that it is the commensal microbiota that provides actual activation trigger(s) for IELs.

Chapter 10: References

Abraham, S.N., and A.L. St. John. 2010. Mast cell-orchestrated immunity to pathogens. *Nat. Rev. Immunol.* 10:440–452. doi:10.1038/nri2782.

Abreu, M.T. 2010. Toll-like receptor signalling in the intestinal epithelium: how bacterial recognition shapes intestinal function. *Nat. Rev. Immunol.* 10:131–144. doi:10.1038/nri2707.

Acehan, D., A. Malhotra, Y. Xu, M. Ren, D.L. Stokes, and M. Schlame. 2011. Cardiolipin affects the supramolecular organization of ATP synthase in mitochondria. *Biophys. J.* 100:2184–2192. doi:10.1016/j.bpj.2011.03.031.

Agnello, M., G. Morici, and A.M. Rinaldi. 2008. A method for measuring mitochondrial mass and activity. *Cytotechnology*. 56:145–149. doi:10.1007/s10616-008-9143-2.

Ahlfors, H., P.J. Morrison, J.H. Duarte, Y. Li, J. Biro, M. Tolaini, P. Di Meglio, A.J. Potocnik, and B. Stockinger. 2014. IL-22 Fate Reporter Reveals Origin and Control of IL-22 Production in Homeostasis and Infection. *J. Immunol.* 193:4602–4613. doi:10.4049/jimmunol.1401244.

Allison Bancroft, G.J., A.N. J McKenzie, A.J. Bancroft, and R.K. Grencis. 1998. Intestinal Nematode Infection A Critical Role for IL-13 in Resistance to A Critical Role for IL-13 in Resistance to Intestinal Nematode Infection. *J Immunol*. 160:3453–3461.

Allison, J.P., and W.L. Havran. 1991. The immunobiology of T cells with invariant γδ antigen receptors. *Annu. Rev. Immunol.* 9:679–705. doi:10.1146/annurev.iy.09.040191.003335.

Almeida, F.F., and G.T. Belz. 2016. Innate lymphoid cells : models of plasticity for immune homeostasis and rapid responsiveness in protection. *Mucosal Immunol.* 9:1103–1112. doi:10.1038/mi.2016.64.

De Andrés, A., C. Camarero, and G. Roy. 2015. Distal Duodenum Versus Duodenal Bulb: Intraepithelial Lymphocytes Have Something to Say in Celiac Disease Diagnosis. *Dig. Dis. Sci.* 60:1004–1009. doi:10.1007/s10620-014-3414-x.

Angelin-Duclos, C., G. Cattoretti, K.-I. Lin, and K. Calame. 2000. Commitment of B Lymphocytes to a Plasma Cell Fate Is Associated with Blimp-1 Expression In Vivo. *J. Immunol.* 165:5462–5471. doi:10.4049/jimmunol.165.10.5462.

Angelov, G.S., P. Guillaume, and I.F. Luescher. 2009. CD8β knockout mice mount normal anti-viral CD8+ T cell responses - but why? *Int. Immunol.* 21:123–135. doi:10.1093/intimm/dxn130.

Armaka, M., M. Apostolaki, P. Jacques, D.L. Kontoyiannis, D. Elewaut, and G. Kollias. 2008. Mesenchymal cell targeting by TNF as a common pathogenic principle in chronic inflammatory joint and intestinal diseases. *J. Exp. Med.* 205:331–337. doi:10.1084/jem.20070906.

Arpaia, N., C. Campbell, X. Fan, S. Dikiy, J. Van Der Veeken, P. Deroos, H. Liu, J.R. Cross, K. Pfeffer, P.J. Coffer, and A.Y. Rudensky. 2013. Metabolites produced by commensal bacteria promote peripheral regulatory T-cell generation. *Nature*. 504:451–455. doi:10.1038/nature12726.

Artis, D. 2008. Epithelial-cell recognition of commensal bacteria and maintenance of immune homeostasis in the gut. *Nat. Rev. Immunol.* 8:411–420. doi:10.1038/nri2316.

Artursson, P. 1990. Epithelial transport of drugs in cell culture. I: A model for studying the passive diffusion of drugs over intestinal absorbtive (Caco2) cells. *J. Pharm. Sci.* 79:476–482. doi:10.1002/jps.2600790604.

Asao, H., C. Okuyama, S. Kumaki, N. Ishii, S. Tsuchiya, D. Foster, and K. Sugamura. 2001. Common γ-Chain Is an Indispensable Subunit of the IL-21 Receptor Complex. *J. Immunol.* 167:1–5. doi:10.4049/jimmunol.167.1.1.

Askenase, M.H., S.-J. Han, A.L. Byrd, D. Morais da Fonseca, N. Bouladoux, C. Wilhelm, J.E. Konkel, T.W. Hand, N. Lacerda-Queiroz, X. Su, G. Trinchieri, J.R. Grainger, and Y. Belkaid. 2015. Bone-Marrow-Resident NK Cells Prime Monocytes for Regulatory Function during Infection. *Immunity*. 42:1130–1142. doi:10.1016/j.immuni.2015.05.011.

Astanina, K., M. Koch, C. Jüngst, A. Zumbusch, and A.K. Kiemer. 2015. Lipid droplets as a novel cargo of tunnelling nanotubes in endothelial cells. *Sci. Rep.* 5:11453. doi:10.1038/srep11453.

Astashkina, A., and D.W. Grainger. 2014. Critical analysis of 3-D organoid *in vitro* cell culture models for high-throughput drug candidate toxicity assessments. *Adv. Drug Deliv. Rev.* 69–70:1–18. doi:10.1016/j.addr.2014.02.008.

Atarashi, K., J. Nishimura, T. Shima, Y. Umesaki, M. Yamamoto, M. Onoue, H. Yagita, N. Ishii, R. Evans, K. Honda, and K. Takeda. 2008. ATP drives lamina propria Th17 cell differentiation. *Nature*. 455:808–812. doi:10.1038/nature07240.

Atarashi, K., T. Tanoue, M. Ando, N. Kamada, Y. Nagano, S. Narushima, W. Suda, A. Imaoka, H. Setoyama, T. Nagamori, E. Ishikawa, T. Shima, T. Hara, S. Kado, T. Jinnohara, H. Ohno, T. Kondo, K. Toyooka, E. Watanabe, S.I. Yokoyama, S. Tokoro, H. Mori, Y. Noguchi, H. Morita, I.I.I. Ivanov, T. Sugiyama, G. Nuñez, J.G. Camp, M. Hattori, Y. Umesaki, and K. Honda. 2015. Th17 Cell Induction by Adhesion of Microbes to Intestinal Epithelial Cells. *Cell*. 163:367–380. doi:10.1016/j.cell.2015.08.058.

Auletta, J.J., J.L. Devecchio, J.L.M. Ferrara, and F.P. Heinzel. 2004. Distinct phases in recovery of reconstituted innate cellular-mediated immunity after murine syngeneic bone marrow transplantation. *Biol. Blood Marrow Transplant.* 10:834–847. doi:10.1016/j.bbmt.2004.08.003.

Baaten, B.J.G., R. Tinoco, A.T. Chen, and L.M. Bradley. 2012. Regulation of antigen-experienced T cells: Lessons from the quintessential memory marker CD44. *Front. Immunol.* 3:1–12. doi:10.3389/fimmu.2012.00023.

Backert, I., S.B. Koralov, S. Wirtz, V. Kitowski, U. Billmeier, E. Martini, K. Hofmann, K. Hildner, N. Wittkopf, K. Brecht, M. Waldner, K. Rajewsky, M.F. Neurath, C. Becker, and C. Neufert. 2014. STAT3 Activation in Th17 and Th22 Cells Controls IL-22–Mediated Epithelial Host Defense during Infectious Colitis. *J. Immunol.* 193:3779–3791. doi:10.4049/jimmunol.1303076.

Bäckhed, F., J.K. Manchester, C.F. Semenkovich, and J.I. Gordon. 2007. Mechanisms underlying the resistance to diet-induced obesity in germ-free mice. *Proc. Natl. Acad. Sci. USA*. 104:979–984. doi:10.1073/pnas.0605374104.

Bain, C.C., C.L. Scott, H. Uronen-Hansson, S. Gudjonsson, O. Jansson, O. Grip, M. Guilliams, B. Malissen, W.W. Agace, and A.M. Mowat. 2013. Resident and pro-inflammatory macrophages in the colon represent alternative context-dependent fates of the same Ly6C^{hi} monocyte precursors. *Mucosal Immunol.* 6:498–510. doi:10.1038/mi.2012.89.

Bajénoff, M., E. Narni-Mancinelli, F. Brau, and G. Lauvau. 2010. Visualizing early splenic memory CD8$^+$ T cells reactivation against intracellular bacteria in the mouse. *PLoS One*. 5:1–14. doi:10.1371/journal.pone.0011524.

Baldridge, M.T., T.J. Nice, B.T. McCune, C.C. Yokoyama, A. Kambal, M. Wheadon, M.S. Diamond, Y. Ivanova, M. Artyomov, and H.W. Virgin. 2015. Commensal microbes and interferon- determine persistence of enteric murine norovirus infection. *Science.* 347:266–269. doi:10.1126/science.1258025.

Balmer, M.L., E.H. Ma, G.R. Bantug, J. Grählert, S. Pfister, T. Glatter, A. Jauch, S. Dimeloe, E. Slack, P. Dehio, M.A. Krzyzaniak, C.G. King, A.V. Burgener, M. Fischer, L. Develioglu, R. Belle, M. Recher, W. V. Bonilla, A.J. Macpherson, S. Hapfelmeier, R.G. Jones, and C. Hess. 2016. Memory CD8$^+$ T Cells Require Increased Concentrations of Acetate Induced by Stress for Optimal Function. *Immunity*. 44:1312–1324. doi:10.1016/j.immuni.2016.03.016.

Bantug, G.R., M. Fischer, J. Grählert, M.L. Balmer, G. Unterstab, L. Develioglu, R. Steiner, L. Zhang, A.S.H. Costa, P.M. Gubser, A.-V. Burgener, U. Sauder, J. Löliger, R. Belle, S. Dimeloe, J. Lötscher, A. Jauch, M. Recher, G. Hönger, M.N. Hall, P. Romero, C. Frezza, and C. Hess. 2018. Mitochondria-Endoplasmic Reticulum Contact Sites Function as Immunometabolic Hubs that Orchestrate the Rapid Recall Response of Memory CD8$^+$ T Cells. *Immunity*. 48:542–555. doi:10.1016/j.immuni.2018.02.012.

Bantug, G.R., L. Galluzzi, G. Kroemer, and C. Hess. 2017. The spectrum of T cell metabolism in health and disease. *Nat. Rev. Immunol.* 18:19–34. doi:10.1038/nri.2017.99.

Bao, S., K.W. Beagley, A.M. Murray, V. Caristo, K.I. Matthaei, I.G. Young, and A.J. Husband. 1998. Intestinal IgA plasma cells of the B1 lineage are IL-5 dependent. *Immunology*. 94:181–188. doi:10.1046/j.1365-2567.1998.00512.x.

Barkauskas, C.E., M.-I. Chung, B. Fioret, X. Gao, H. Katsura, and B.L.M. Hogan. 2017. Lung organoids: current uses and future promise. *Development*. 144:986–997. doi:10.1242/dev.140103.

Barker, N. 2014. Adult intestinal stem cells: critical drivers of epithelial homeostasis and regeneration. *Nat. Rev. Mol. Cell Biol.* 15:19–33. doi:10.1038/nrm3721.

Barker, N., J.H. van Es, J. Kuipers, P. Kujala, M. van den Born, M. Cozijnsen, A. Haegebarth, J. Korving, H. Begthel, P.J. Peters, and H. Clevers. 2007. Identification of stem cells in small intestine and colon by marker gene Lgr5. *Nature*. 449:1003–1007. doi:10.1038/nature06196.

Barker, N., M. Huch, P. Kujala, M. van de Wetering, H.J. Snippert, J.H. van Es, T. Sato, D.E. Stange, H. Begthel, M. van den Born, E. Danenberg, S. van den Brink, J. Korving, A. Abo, P.J. Peters, N. Wright, R. Poulsom, and H. Clevers. 2010. $Lgr5^{+}$ve Stem Cells Drive Self-Renewal in the Stomach and Build Long-Lived Gastric Units *In Vitro*. *Cell Stem Cell*. 6:25–36. doi:10.1016/j.stem.2009.11.013.

Bartfeld, S., T. Bayram, M. van de Wetering, M. Huch, H. Begthel, P. Kujala, R. Vries, P.J. Peters, and H. Clevers. 2014. In Vitro Expansion of Human Gastric Epithelial Stem Cells and Their Responses to Bacterial Infection. *Gastroenterology*. 148:126–136. doi:10.1053/j.gastro.2014.09.042.

Bartholomew, J.W., and T. Mittwer. 1952. The Gram Stain. *Bacteriol. Rev.* 16:1–29.

Bas, A., M. Swamy, L. Abeler-Dörner, G. Williams, D.J. Pang, S.D. Barbee, and A.C. Hayday. 2011. Butyrophilin-like 1 encodes an enterocyte protein that selectively regulates functional interactions with T lymphocytes. *Proc. Natl. Acad. Sci. USA*. 108:4376–4381. doi:10.1073/pnas.1010647108.

Basu, R., D.B. O'Quinn, D.J. Silberger, T.R. Schoeb, L. Fouser, W. Ouyang, R.D. Hatton, and C.T. Weaver. 2012. Th22 Cells Are an Important Source of IL-22 for Host Protection against Enteropathogenic Bacteria. *Immunity*. 37:1061–1075. doi:10.1016/j.immuni.2012.08.024.

Batandier, C., E. Fontaine, C. Kériel, and X.M. Leverve. 2002. Determination of mitochondrial reactive oxygen species: methodological aspects. *J. Cell. Mol. Med.* 6:175–187. doi:10.1111/j.1582-4934.2002.tb00185.x.

Beagley, K.W., K. Fujihashi, A.S. Lagoo, S. Lagoo-Deenadaylan, C.A. Black, A.M. Murray, A.T. Sharmanov, M. Yamamoto, J.R. McGhee, and C.O. Elson. 1995. Differences in intraepithelial lymphocyte T cell subsets isolated from murine small versus large intestine. *J. Immunol.* 154:5611–5619.

Belkaid, Y., and S. Naik. 2013. Compartmentalized and systemic control of tissue immunity by commensals. *Nat. Immunol.* 14:646–653. doi:10.1038/ni.2604.

Bendall, S.C., G.P. Nolan, M. Roederer, and P.K. Chattopadhyay. 2012. A deep profiler's guide to cytometry. *Trends Immunol.* 33:323–332. doi:10.1016/j.it.2012.02.010.

Benischke, A.S., S. Vasanth, T. Miyai, K.R. Katikireddy, T. White, Y. Chen, A. Halilovic, M. Price, F. Price, P.B. Liton, and U. V. Jurkunas. 2017. Activation of mitophagy leads to decline in Mfn2 and loss of mitochondrial mass in Fuchs endothelial corneal dystrophy. *Sci. Rep.* 7:1–11. doi:10.1038/s41598-017-06523-2.

Bergsbaken, T., M.J. Bevan, and P.J. Fink. 2017. Local Inflammatory Cues Regulate Differentiation and Persistence of $CD8^+$ Tissue-Resident Memory T Cells. *Cell Rep.* 19:114–124. doi:10.1016/j.celrep.2017.03.031.

Bhushal, S., M. Wolfsmüller, T.A. Selvakumar, L. Kemper, D. Wirth, M.W. Hornef, H. Hauser, and M. Köster. 2017. Cell polarization and epigenetic status shape the heterogeneous response to type III interferons in intestinal epithelial cells. *Front. Immunol.* 8:1–18. doi:10.3389/fimmu.2017.00671.

Bigby, M., J.S. Markowitz, P.A. Bleicher, M.J. Grusby, S. Simha, M. Siebrecht, M. Wagner, C. Nagler-Anderson, and L.H. Glimcher. 1993. Most γδ T cells develop normally in the absence of MHC class II molecules. *J. Immunol.* 151:4465–4475.

Bilate, A.M., D. Bousbaine, L. Mesin, M. Agudelo, J. Leube, A. Kratzert, S.K. Dougan, G.D. Victora, and H.L. Ploegh. 2016. Tissue-specific emergence of regulatory and intraepithelial T cells from a clonal T cell precursor. *Sci. Immunol.* 1:1–13. doi:10.1126/sciimmunol.aaf7471.

Blacher, E., M. Levy, E. Tatirovsky, and E. Elinav. 2017. Microbiome-Modulated Metabolites at the Interface of Host Immunity. *J. Immunol.* 198:572–580. doi:10.4049/jimmunol.1601247.

Blake, D.P. 2015. Eimeria genomics: Where are we now and where are we going? *Vet. Parasitol.* 212:68–74. doi:10.1016/j.vetpar.2015.05.007.

Blevins, L.K., D. Parsonage, M.B. Oliver, E. Domzalski, W.E. Swords, and M.A. Alexander-Miller. 2017. A novel function for the Streptococcus pneumoniae aminopeptidase N: Inhibition of T cell effector function through regulation of TCR signaling. *Front. Immunol.* 8:1–16. doi:10.3389/fimmu.2017.01610.

Van Der Bliek, A.M., M.M. Sedensky, and P.G. Morgan. 2017. Cell biology of the mitochondrion. *Genetics*. 207:843–871. doi:10.1534/genetics.117.300262.

Bohlson, S.S., D.A. Fraser, and A.J. Tenner. 2007. Complement proteins C1q and MBL are pattern recognition molecules that signal immediate and long-term protective immune functions. *Mol. Immunol.* 44:33–43. doi:10.1016/j.molimm.2006.06.021.

Bongers, G., M.E. Pacer, T.H. Geraldino, L. Chen, Z. He, D. Hashimoto, G.C. Furtado, J. Ochando, K.A. Kelley, J.C. Clemente, M. Merad, H. van Bakel, and S.A. Lira. 2014. Interplay of host microbiota, genetic perturbations, and inflammation promotes local development of intestinal neoplasms in mice. *J. Exp. Med.* 211:457–472. doi:10.1084/jem.20131587.

Boretto, M., B. Cox, M. Noben, N. Hendriks, A. Fassbender, H. Roose, F. Amant, D. Timmerman, C. Tomassetti, A. Vanhie, C. Meuleman, M. Ferrante, and H. Vankelecom. 2017. Development of organoids from mouse and human endometrium showing endometrial epithelium physiology and long-term expandability. *Development*. 144:1775–1786. doi:10.1242/dev.148478.

Boring, L., J. Gosling, S.W. Chensue, S.L. Kunkel, R. V Farese Jr., H.E. Broxmeyer, and I.F. Charo. 1997. Impaired monocyte migration and reduced type 1 (Th1) cytokine responses in C-C chemokine receptor 2 knockout mice. *J. Clin. Invest.* 100:2552–2561. doi:10.1172/jci119798.

Borton, M.A., A. Sabag-Daigle, J. Wu, L.M. Solden, B.S. O'Banion, R.A. Daly, R.A. Wolfe, J.F. Gonzalez, V.H. Wysocki, B.M.M. Ahmer, and K.C. Wrighton. 2017. Chemical and pathogen-induced inflammation disrupt the murine intestinal microbiome. *Microbiome*. 5:1–15. doi:10.1186/s40168-017-0264-8.

Bostick, J.W., and L. Zhou. 2015. Innate lymphoid cells in intestinal immunity and inflammation. *Cell. Mol. Life Sci.* 73:237–252. doi:10.1007/s00018-015-2055-3.

Boyden, L.M., J.M. Lewis, S.D. Barbee, A. Bas, M. Girardi, A.C. Hayday, R.E. Tigelaar, and R.P. Lifton. 2008. Skint1, the prototype of a newly identified immunoglobulin superfamily gene cluster, positively selects epidermal gammadelta T cells. *Nat. Genet.* 40:656–62. doi:10.1038/ng.108.

Brandl, K., G. Plitas, B. Schnabl, R.P. DeMatteo, and E.G. Pamer. 2007. MyD88-mediated signals induce the bactericidal lectin RegIIIγ and protect mice against intestinal Listeria monocytogenes infection. *J. Exp. Med.* 204:1891–1900. doi:10.1084/jem.20070563.

Brandt, U. 2006. Energy Converting NADH: Quinone Oxidoreductase (Complex I). *Annu. Rev. Biochem.* 75:69–92. doi:10.1146/annurev.biochem.75.103004.142539.

Brandtzaeg, P., and F.E. Johansen. 2005. Mucosal B cells: Phenotypic characteristics, transcriptional regulation, and homing properties. *Immunol. Rev.* 206:32–63. doi:10.1111/j.0105-2896.2005.00283.x.

Breed, R.S., E.G. Murray, and A.P. Hitchens. 1944. The Outline Classification Used in the Bergey Manual of Determinative Bacteriology. *Bacteriol. Rev.* 8:255–260.

Brown, C.C., D. Esterhazy, A. Sarde, M. London, V. Pullabhatla, I. Osma-Garcia, R. Al-Bader, C. Ortiz, R. Elgueta, M. Arno, E. de Rinaldis, D. Mucida, G.M. Lord, and R.J. Noelle. 2015. Retinoic Acid Is Essential for Th1 Cell Lineage Stability and Prevents Transition to a Th17 Cell Program. *Immunity*. 42:1–13. doi:10.1016/j.immuni.2015.02.003.

Bruce, D., and M.T. Cantorna. 2011. Intrinsic requirement for the vitamin D receptor in the development of CD8αα-expressing T cells. *J. Immunol.* 186:2819–2825. doi:10.4049/jimmunol.1003444.

Buck, M.D., D. O'Sullivan, R.I.K. Geltink, J.D. Curtis, C.-H. Chang, D.E. Sanin, J. Qiu, O. Kretz, D. Braas, G.J.W. van der Windt, Q. Chen, S.C.-C. Huang, C.M. O'Neill, B.T. Edelson, E.J. Pearce, H. Sesaki, T.B. Huber, A.S. Rambold, and E.L. Pearce. 2016. Mitochondrial Dynamics Controls T Cell Fate through Metabolic Programming. *Cell*. 30:1–14. doi:10.1016/j.cell.2016.05.035.

Buck, M.D., D. O'Sullivan, and E.L. Pearce. 2015. T cell metabolism drives immunity. *J. Exp. Med.* 212:1345–1360. doi:10.1084/jem.20151159.

Buettner, M., and M. Lochner. 2016. Development and function of secondary and tertiary lymphoid organs in the small intestine and the colon. *Front. Immunol.* 7:1–11. doi:10.3389/fimmu.2016.00342.

Bunker, J.J., S.A. Erickson, T.M. Flynn, C. Henry, J.C. Koval, M. Meisel, B. Jabri, D.A. Antonopoulos, P.C. Wilson, and A. Bendelac. 2017. Natural polyreactive IgA antibodies coat the intestinal microbiota. *Science.* 6619:1–20. doi:10.1126/science.aan6619.

Cader, M.Z., K. Boroviak, Q. Zhang, G. Assadi, S.L. Kempster, G.W. Sewell, S. Saveljeva, J.W. Ashcroft, S. Clare, S. Mukhopadhyay, K.P. Brown, M. Tschurtschenthaler, T. Raine, B. Doe, E.R. Chilvers, J.L. Griffin, N.C. Kaneider, R.A. Floto, M. D'amato, A. Bradley, M.J.O. Wakelam, G. Dougan, and A. Kaser. 2016. C13orf31 (FAMIN) is a central regulator of immunometabolic function. *Nat. Immunol.* 17:1046–1056. doi:10.1038/ni.3532.

Caldwell, C.C., H. Kojima, D. Lukashev, J. Armstrong, M. Farber, S.G. Apasov, and M. V. Sitkovsky. 2001. Differential Effects of Physiologically Relevant Hypoxic Conditions on T Lymphocyte Development and Effector Functions. *J. Immunol.* 167:6140–6149. doi:10.4049/jimmunol.167.11.6140.

Camarero, C., F. Leon, L. Sanchez, A. Asensio, and G. Roy. 2007. Age-related variation of intraepithelial lymphocytes subsets in normal human duodenal mucosa. *Dig. Dis. Sci.* 52:685–691. doi:10.1007/s10620-006-9176-3.

Cao, X., E.W. Shores, J. Hu-Li, M.R. Anver, B.L. Kelsall, S.M. Russell, J. Drago, M. Noguchi, A. Grinberg, E.T. Bloom, W.E. Paul, S.I. Katz, P.E. Love, and W.J. Leonard. 1995. Defective lymphoid development in mice lacking expression of the common cytokine receptor γ chain. *Immunity.* 2:223–238. doi:10.1016/1074-7613(95)90047-0.

Carter, P.B., and F.M. Collins. 1974. The route of enteric infection in normal mice. *J. Exp. Med.* 139:1189–1203. doi:10.1084/jem.139.5.1189.

Cash, H.L., C. V. Whitham, C.L. Behrendt, and L. V. Hooper. 2006. Symbiotic bacteria direct expression of an intestinal bactericidal lectin. *Science.* 313:1126–1130. doi:10.1126/science.1127119.

Cecchini, G. 2003. Function and Structure of Complex II of the Respiratory Chain. *Annu. Rev. Biochem.* 72:77–109. doi:10.1146/annurev.biochem.72.121801.161700.

Cereghetti, G.M., and L. Scorrano. 2006. The many shapes of mitochondrial death. *Oncogene*. 25:4717–4724. doi:10.1038/sj.onc.1209605.

Cerf-Bensussan, N., A. Jarry, N. Brousse, B. Lisowska-Grospierre, D. Guy-Grand, and C. Griscelli. 1987. A monoclonal antibody (HML-1) defining a novel membrane molecule present on human intestinal lymphocytes. *Eur. J. Immunol.* 17:1279–1285. doi:10.1002/eji.1830170910.

Cham, C.M., G. Driessens, J.P. O'Keefe, and T.F. Gajewski. 2008. Glucose Deprivation Inhibits Multiple Key Gene Expression Events and Effector Functions in $CD8^+$ T Cells. *Eur. J. Immunol.* 38:2438–2450. doi:10.1016/S1470-2045(10)70146-7.

Cham, C.M., and T.F. Gajewski. 2005. Glucose Availability Regulates IFN-gamma Production and p70S6 Kinase Activation in $CD8^+$ Effector T Cells. *J. Immunol.* 174:4670–4677. doi:10.4049/jimmunol.174.8.4670.

Chandel, N.S., E. Maltepe, E. Goldwasser, C.E. Mathieu, M.C. Simon, and P.T. Schumacker. 1998. Mitochondrial reactive oxygen species trigger hypoxia-induced transcription. *Proc. Natl. Acad. Sci.* 95:11715–11720. doi:10.1073/pnas.95.20.11715.

Chang, C.H., J.D. Curtis, L.B. Maggi, B. Faubert, A. V. Villarino, D. O'Sullivan, S.C.C. Huang, G.J.W. Van Der Windt, J. Blagih, J. Qiu, J.D. Weber, E.J. Pearce, R.G. Jones, and E.L. Pearce. 2013. Posttranscriptional control of T cell effector function by aerobic glycolysis. *Cell*. 153:1239–1251. doi:10.1016/j.cell.2013.05.016.

Chassaing, B., J.D. Aitken, M. Malleshappa, and M. Vijay-Kumar. 2015. Dextran Sulfate Sodium (DSS)-Induced Colitis in Mice. *Curr. Protoc. Immunol.* 18:1199–1216. doi:10.1002/0471142735.im1525s104.

Cheng, H. 1974. Origin , Differentiation and Renewal o f the Four Main Epithelial Cell Types in the Mouse Small Intestine IV. Paneth Cells. *Am. J. Anat.* 141:521–536. doi:10.1002/aja.1001410406.

Cheng, H., and C.P. Leblond. 1974. Origin, differentiation and renewal of the four main epithelial cell types in the mouse small intestine III. Entero-endocrine cells. *Am. J. Anat.* 141:503–520. doi:10.1002/aja.1001410403.

Chennupati, V., T. Worbs, X. Liu, F.H. Malinarich, S. Schmitz, J.D. Haas, B. Malissen, R. Förster, and I. Prinz. 2010. Intra- and intercompartmental movement of γδ T cells: intestinal intraepithelial and peripheral γδ T cells represent exclusive nonoverlapping populations with distinct migration characteristics. *J. Immunol.* 185:5160–5168. doi:10.4049/jimmunol.1001652.

Cheroutre, H., and M.M. Husain. 2013. CD4 CTL: living up to the challenge. *Semin. Immunol.* 25:273–81. doi:10.1016/j.smim.2013.10.022.

Cheroutre, H., and F. Lambolez. 2008a. The thymus chapter in the life of gut-specific intra epithelial lymphocytes. *Curr. Opin. Immunol.* 20:185–191. doi:10.1016/j.coi.2008.03.009.

Cheroutre, H., and F. Lambolez. 2008b. Doubting the TCR Coreceptor Function of CD8αα. *Immunity*. 28:149–159. doi:10.1016/j.immuni.2008.01.005.

Cheroutre, H., F. Lambolez, and D. Mucida. 2011. The light and dark sides of intestinal intraepithelial lymphocytes. *Nat. Rev. Immunol.* 11:445–456. doi:10.1038/nri3007.

Cherwinski, B.Y.H.M., J.H. Schumacher, K.D. Brown, and T.R. Mosmann. 1987. Two types of mouse helper T cell clone. III. Further differences in lymphokine synthesis between Th1 and Th2 clones revealed by RNA hybridization, functionally monospecific bioassays, and monoclonal antibodies. *J. Exp. Med.* 166:1229–1244. doi:10.1084/jem.166.5.1229.

Chicco, A.J., and G.C. Sparagna. 2007. Role of cardiolipin alterations in mitochondrial dysfunction and disease. *Am. J. Physiol. Cell Physiol.* 292:33–44. doi:10.1152/ajpcell.00243.2006.

Chieppa, M., M. Rescigno, A.Y.C. Huang, and R.N. Germain. 2006. Dynamic imaging of dendritic cell extension into the small bowel lumen in response to epithelial cell TLR engagement. *J. Exp. Med.* 203:2841–52. doi:10.1084/jem.20061884.

Choi, J.H., K.-W. Wang, D. Zhang, X.X. Zhan, T. Wang, C. Bu, C.L. Behrendt, M. Zeng, Y. Wang, T. Misawa, X. Li, M. Tang, X.X. Zhan, L. Scott, S. Hildebrand, A.R. Murray, E.M.Y. Moresco, L. V Hooper, and B. Beutler. 2017. IgD class switching is initiated by microbiota and limited to mucosa-associated lymphoid tissue in mice. *Proc. Natl. Acad. Sci. USA*. 114:1196–1204. doi:10.1073/pnas.1621258114.

Chung, E.J., E. ju Do, S.Y. Kim, E.A. Cho, D.H. Kim, S. Pak, S.W. Hwang, H.J. Lee, J.S. Byeon, B.D. Ye, D.H. Yang, S.H. Park, S.K. Yang, J.H. Kim, and S.J. Myung. 2017. Combination of metformin and VSL#3 additively suppresses western-style diet induced colon cancer in mice. *Eur. J. Pharmacol.* 794:1–7. doi:10.1016/j.ejphar.2016.11.012.

Ciolino, H.P., P.J. Daschner, and G.C. Yeh. 1999. Dietary flavonols quercetin and kaempferol are ligands of the aryl hydrocarbon receptor that affect CYP1A1 transcription differentially. *Biochem. J.* 340:715–22. doi:10.1042/0264-6021:3400715.

Clevers, H. 2013. The intestinal crypt, a prototype stem cell compartment. *Cell*. 154:274–84. doi:10.1016/j.cell.2013.07.004.

Clevers, H., and R. Nusse. 2012. Wnt/β-catenin signaling and disease. *Cell*. 149:1192–1205. doi:10.1016/j.cell.2012.05.012.

Coll, M.L., K. Rosen, V. Ladeda, and J. Filmus. 2002. Increased Bcl-xL expression mediates v-Src-induced resistance to anoikis in intestinal epithelial cells. *Oncogene*. 21:2908–2913. doi:10.1038/sj/onc/1205388.

Cooper, A.M., D.K. Dalton, T.A. Stewart, J.P. Griffin, D.G. Russell, and I.M. Orme. 1993. Disseminated Tuberculosis in Interferon gamma Gene-disrupted Mice. *J. Exp. Med.* 178:2243–2247. doi:10.1084/jem.178.6.2243.

Costerton, J.W., J.M. Ingram, and K.J. Cheng. 1974. Structure and function of the cell envelope of Gram-negative bacteria. *Bacteriol. Rev.* 38:87–110.

Croce, A.C., and G. Bottiroli. 2014. Autofluorescence spectroscopy and imaging : a tool for biomedical research and diagnosis. *Eur. J. Histochem.* 58. doi:10.4081/ejh.2014.2461.

Crowley, S.M., L.A. Knodler, and B.A. Vallance. 2016. Salmonella and the Inflammasome: Battle for Intracellular Dominance. *Curr. Top. Microbiol. Immunol.* 397:43–67. doi:10.1007/978-3-319-41171-2.

Cruz-Guilloty, F., M.E. Pipkin, I.M. Djuretic, D. Levanon, J. Lotem, M.G. Lichtenheld, Y. Groner, and A. Rao. 2009. Runx3 and T-box proteins cooperate to establish the transcriptional program of effector CTLs. *J. Exp. Med.* 206:51–59. doi:10.1084/jem.20081242.

Cui, G., M.M. Staron, S.M. Gray, P.C. Ho, R.A. Amezquita, J. Wu, and S.M. Kaech. 2015. IL-7-induced glycerol transport and TAG synthesis promotes memory $CD8^+$ T cell longevity. *Cell*. 161:750–761. doi:10.1016/j.cell.2015.03.021.

Cukrowska, B., A. Sowińska, J.B. Bierła, E. Czarnowska, A. Rybak, and U. Grzybowska-Chlebowczyk. 2017. Intestinal epithelium, intraepithelial lymphocytes and the gut microbiota - Key players in the pathogenesis of celiac disease. *World J. Gastroenterol.* 23:7505–7518. doi:10.3748/wjg.v23.i42.7505.

Cummings, R.J., G. Barbet, G. Bongers, B.M. Hartmann, K. Gettler, L. Muniz, G.C. Furtado, J. Cho, S.A. Lira, and J.M. Blander. 2016. Different tissue phagocytes sample apoptotic cells to direct distinct homeostasis programs. *Nature*. 539:565–569. doi:10.1038/nature20138.

Dalton, T.P., M.Z. Dieter, R.S. Matlib, N.L. Childs, H.G. Shertzer, M.B. Genter, and D.W. Nebert. 2000. Targeted Knockout of Cyp1a1 Gene Does Not Alter Hepatic Constitutive Expression of Other Genes in the Mouse [Ah] Battery. *Biochem. Biophys. Res. Commun.* 267:184–189. doi:10.1006/bbrc.1999.1913.

Danne, C., G. Ryzhakov, M. Martínez-López, N.E. Ilott, F. Franchini, F. Cuskin, E.C. Lowe, S.J. Bullers, J.S.C. Arthur, and F. Powrie. 2017. A Large Polysaccharide Produced by Helicobacter hepaticus Induces an Anti-inflammatory Gene Signature in Macrophages. *Cell Host Microbe*. 22:733–745. doi:10.1016/j.chom.2017.11.002.

Davis, C.P., and D.C. Savage. 1974. Habitat, Succession, Attachment, and Morphology of Segmented, Filamentous Microbes Indigenous to the Murine Gastrointestinal Tract. *Infect. Immun.* 10:948–956.

Deckers, J., K. De Bosscher, B.N. Lambrecht, and H. Hammad. 2017. Interplay between barrier epithelial cells and dendritic cells in allergic sensitization through the lung and the skin. *Immunol. Rev.* 278:131–144. doi:10.1111/imr.12542.

DeJonge, R.E., X.-P. Liu, C.R. Deig, S. Heller, K.R. Koehler, and E. Hashino. 2016. Modulation of Wnt Signaling Enhances Inner Ear Organoid Development in 3D Culture. *PLoS One*. 11:1–14. doi:10.1371/journal.pone.0162508.

Desagher, S., and J.-C. Martinou. 2000. Mitochondria as the central control point of apoptosis. *Trends Cell Biol.* 10:369–377. doi:10.1016/S0962-8924(00)01803-1.

Dimeloe, S., A.-V. Burgener, J. Graehlert, and C. Hess. 2016. T cell metabolism governing activation, proliferation and differentiation; a modular view. *Immunology*. 1–10. doi:10.1111/imm.12655.

Disanto, J.P., W. Mullert, D. Guy-grand, A. Fischer, and K. Rajewskyt. 1995. Lymphoid development in mice with a targeted deletion of the interleukin 2 receptor γ chain. *Proc. Natl. Acad. Sci. USA*. 92:377–381. doi:10.1073/pnas.92.2.377.

Djuretic, I.M., D. Levanon, V. Negreanu, Y. Groner, A. Rao, and K.M. Ansel. 2007. Transcription factors T-bet and Runx3 cooperate to activate Ifng and silence Il4 in T helper type 1 cells. *Nat. Immunol.* 8:145–53. doi:10.1038/ni1424.

Doedens, A.L., A.T. Phan, M.H. Stradner, J.K. Fujimoto, J. V. Nguyen, E. Yang, R.S. Johnson, and A.W. Goldrath. 2013. Hypoxia-inducible factors enhance the effector responses of $CD8^+$ T cells to persistent antigen. *Nat. Immunol.* 14:1173–1182. doi:10.1038/ni.2714.

Doménech, E., C. Maestre, L. Esteban-Martínez, D. Partida, R. Pascual, G. Fernández-Miranda, E. Seco, R. Campos-Olivas, M. Pérez, D. Megias, K. Allen, M. López, A.K. Saha, G. Velasco, E. Rial, R. Méndez, P. Boya, M. Salazar-Roa, and M. Malumbres. 2015. AMPK and PFKFB3 mediate glycolysis and survival in response to mitophagy during mitotic arrest. *Nat. Cell Biol.* 17:1304–1316. doi:10.1038/ncb3231.

Dong, H., H.G. Shertzer, M.B. Genter, F.J. Gonzalez, V. Vasiliou, C. Jefcoate, and D.W. Nebert. 2013. Mitochondrial targeting of mouse NQO1 and CYP1B1 proteins. *Biochem. Biophys. Res. Commun.* 14:727–732. doi:10.1161/CIRCRESAHA.112.280016.

Dotiwala, F., S. Sen Santara, A.A. Binker-Cosen, B. Li, S. Chandrasekaran, and J. Lieberman. 2017. Granzyme B Disrupts Central Metabolism and Protein Synthesis in Bacteria to Promote an Immune Cell Death Program. *Cell*. 1–13. doi:10.1016/j.cell.2017.10.004.

Driehuis, E., and H. Clevers. 2017. CRISPR/Cas 9 genome editing and its applications in organoids. *Am. J. Physiol. - Gastrointest. Liver Physiol.* 312:257–265. doi:10.1152/ajpgi.00410.2016.

Dye, B.R., D.R. Hill, M.A. Ferguson, Y.-H. Tsai, M.S. Nagy, R. Dyal, J.M. Wells, C.N. Mayhew, R. Nattiv, O.D. Klein, E.S. White, G.H. Deutsch, and J.R. Spence. 2015. In vitro generation of human pluripotent stem cell derived lung organoids. *Elife*. 4:1–25. doi:10.7554/eLife.05098.

Eberl, G., M. Colonna, J.P. Di Santo, and a. N.J. McKenzie. 2015. Innate lymphoid cells: A new paradigm in immunology. *Science.* 348:1–8. doi:10.1126/science.aaa6566.

Eberl, G., and D.R. Littman. 2004. Thymic Origin of Intestinal alphabeta T Cells Revealed by Fate Mapping of RORgammat^{+} Cells. *Science.* 305:248–251. doi:10.1126/science.1096472.

Edelblum, K.L., G. Sharon, G. Singh, M.A. Odenwald, A. Sailer, S. Cao, S. Ravens, I. Thomsen, K. El Bissati, R. McLeod, C. Dong, S. Gurbuxani, I. Prinz, S.K. Mazmanian, and J.R. Turner. 2017. The Microbiome Activates CD4 T-cell–mediated Immunity to Compensate for Increased Intestinal Permeability. *Cell. Mol. Gastroenterol. Hepatol.* 4:285–297. doi:10.1016/j.jcmgh.2017.06.001.

Edelblum, K.L., L. Shen, C.R. Weber, A.M. Marchiando, B.S. Clay, Y. Wang, I. Prinz, B. Malissen, A.I. Sperling, and J.R. Turner. 2012. Dynamic migration of γδ intraepithelial lymphocytes requires occludin. *Proc. Natl. Acad. Sci. USA.* 109:7097–7102. doi:10.1073/pnas.1112519109.

Edelblum, K.L., G. Singh, M.A. Odenwald, A. Lingaraju, K. El Bissati, R. Mcleod, A.I. Sperling, and J.R. Turner. 2015. γδ Intraepithelial Lymphocyte Migration Limits Transepithelial Pathogen Invasion and Systemic Disease in Mice. *Gastroenterology*. 148:1417–1426. doi:10.1053/j.gastro.2015.02.053.

Egan, C.E., K.J. Maurer, S.B. Cohen, M. Mack, K.W. Simpson, and E.Y. Denkers. 2011. Synergy between intraepithelial lymphocytes and lamina propria T cells drives intestinal inflammation during infection. *Mucosal Immunol.* 4:658–70. doi:10.1038/mi.2011.31.

Eissing, N., L. Heger, A. Baranska, R. Cesnjevar, M. Büttner-Herold, S. Söder, A. Hartmann, G.F. Heidkamp, and D. Dudziak. 2014. Easy performance of 6-color confocal immunofluorescence with 4-laser line microscopes. *Immunol. Lett.* 161:1–5. doi:10.1016/j.imlet.2014.04.003.

Elderman, M., B. Sovran, F. Hugenholtz, K. Graversen, M. Huijskes, E. Houtsma, C. Belzer, M. Boekschoten, P. De Vos, J. Dekker, J. Wells, and M. Faas. 2017. The effect of age on the intestinal mucus thickness, microbiota composition and immunity in relation to sex in mice. *PLoS One*. 12:1–22. doi:10.1371/journal.pone.0184274.

Ellenhorn, J.D.I., R. Hirsch, H. Schreiber, and J.A. Bluestone. 1988. *In Vivo* Administration of Anti-CD3 Prevents Malignant Progressor Tumor Growth. *Science.* 569–572.

Elliott, J.F., E.P. Rock, P.A. Patten, M.M. Davis, and Y. Chien. 1988. The adult T-cell receptor delta-chain is diverse and distinct from that of fetal thymocytes. *Nature*. 336:403–405. doi:10.1038/331627a0.

Emoto, Y., M. Emoto, M. Miyamoto, I. Yoshizawa, and S.H.E. Kaufman. 2004. Functionally active CD8αβ^{+} TCRγδ intestinal intraepithelial lymphocytes in athymic nu/nu mice. *Int. Immunol.* 16:111–117. doi:10.1093/intimm/dxh008.

Ermund, A., A. Schütte, M.E. V Johansson, J.K. Gustafsson, and G.C. Hansson. 2013. Studies of mucus in mouse stomach, small intestine, and colon. I. Gastrointestinal mucus layers have different properties depending on location as well as over the Peyer's patches. *Am. J. Physiol. Gastrointest. Liver Physiol.* 305:341–347. doi:10.1152/ajpgi.00046.2013.

Ernster, L., and G. Schatz. 1981. Mitochondria : A Historical Review. *J. Cell Biol.* 91:227–255. doi:0021-9525/81/12/0227s/29.

van Es, J.H., M.E. van Gijn, O. Riccio, M. van den Born, M. Vooijs, H. Begthel, M. Cozijnsen, S. Robine, D.J. Winton, F. Radtke, and H. Clevers. 2005. Notch/γ-secretase inhibition turns proliferative cells in intestinal crypts and adenomas into goblet cells. *Nature*. 435:959–63. doi:10.1038/nature03659.

Ettayebi, K., S.E. Crawford, K. Murakami, J.R. Broughman, U. Karandikar, V.R. Tenge, F.H. Neill, S.E. Blutt, X. Zeng, L. Qu, B. Kou, A.R. Opekun, D. Burrin, D.Y. Graham, S. Ramani, R. Atmar, and M.K. Estes. 2016. Replication of human noroviruses in stem cell – derived human enteroids. *Science.* 5211:1–13. doi:10.1126/science.aaf5211.

Fagarasan, S., M. Muramatsu, K. Suzuki, H. Nagaoka, H. Hiai, and T. Honjo. 2002. Critical Roles of Activation-Induced Cytidine Deaminase in the Homeostasis of Gut Flora. *Science.* 298:1424–1427. doi:10.1126/science.1077336.

Fahlén, L., S. Read, L. Gorelik, S.D. Hurst, R.L. Coffman, R.A. Flavell, and F. Powrie. 2005. T cells that cannot respond to TGF-β escape control by $CD4^+$ $CD25^+$ regulatory T cells. *J. Exp. Med.* 201:737–746. doi:10.1084/jem.20040685.

Fahrer, A.M., Y. Konigshofer, E.M. Kerr, G. Ghandour, D.H. Mack, M.M. Davis, and Y.H. Chien. 2001. Attributes of γδ intraepithelial lymphocytes as suggested by their transcriptional profile. *Proc. Natl. Acad. Sci. USA.* 98:10261–10266. doi:10.1073/pnas.171320798.

Falagas, M.E., and S.K. Kasiakou. 2005. Colistin: the revival of polymyxins for the management of multidrug-resistant gram-negative bacterial infections. *Clin. Infect. Dis.* 40:1333–1341. doi:10.1097/01.inf.0000174577.97635.7b.

Fallon, P.G., S.J. Ballantyne, N.E. Mangan, J.L. Barlow, A. Dasvarma, D.R. Hewett, A. McIlgorm, H.E. Jolin, and A.N.J. McKenzie. 2006. Identification of an interleukin (IL)-25–dependent cell population that provides IL-4, IL-5, and IL-13 at the onset of helminth expulsion. *J. Exp. Med.* 203:1105–1116. doi:10.1084/jem.20051615.

Farin, H.F., J.H. Van Es, and H. Clevers. 2012. Redundant sources of Wnt regulate intestinal stem cells and promote formation of paneth cells. *Gastroenterology.* 143:1518–1529. doi:10.1053/j.gastro.2012.08.031.

Farin, H.F., W.R. Karthaus, P. Kujala, M. Rakhshandehroo, G. Schwank, R.G.J. Vries, E. Kalkhoven, E.E.S. Nieuwenhuis, and H. Clevers. 2014. Paneth cell extrusion and release of antimicrobial products is directly controlled by immune cell-derived IFN-γ. *J. Exp. Med.* 211:1393–1405. doi:10.1084/jem.20130753.

Ferlini, C., and G. Scambia. 2007. Assay for apoptosis using the mitochondrial probes, Rhodamine123 and 10-N-nonyl acridine orange. *Nat. Protoc.* 2:3111–3114. doi:10.1038/nprot.2007.397.

Foo, S.Y., and S. Phipps. 2010. Regulation of inducible BALT formation and contribution to immunity and pathology. *Mucosal Immunol.* 3:537–544. doi:10.1038/mi.2010.52.

Forman, R., M. Bramhall, L. Logunova, M. Svensson-Frej, S.M. Cruickshank, and K.J. Else. 2016. Eosinophils may play regionally disparate roles in influencing IgA^+ plasma cell numbers during large and small intestinal inflammation. *BMC Immunol.* 17:1–12. doi:10.1186/s12865-016-0153-0.

French, J.D., C.L. Roark, W.K. Born, and R.L.O. Brien. 2005. γδ T cell homeostasis is established in competition with αβ T cells and NK cells. *Proc. Natl. Acad. Sci.* 102:14741–14726. doi:10.1073/pnas.0507520102.

Frey, M.R., A. Golovin, and D. Brent Polk. 2004. Epidermal growth factor-stimulated intestinal epithelial cell migration requires Src family kinase-dependent p38 MAPK signaling. *J. Biol. Chem.* 279:44513–44521. doi:10.1074/jbc.M406253200.

Frossi, B., C. Tripodo, C. Guarnotta, A. Carroccio, M. De Carli, S. De Carli, M. Marino, A. Calabrò, and C. Pucillo. 2016. Mast cells are associated with the onset and progression of celiac disease. *J. Allergy Clin. Immunol.* 139:1266–1275. doi:10.1016/j.jaci.2016.08.011.

Fuchs, A., and M. Colonna. 2011. Natural killer (NK) and NK-like cells at mucosal epithelia: Mediators of anti-microbial defense and maintenance of tissue integrity. *Eur. J. Microbiol. Immunol.* 1:257–266. doi:10.1556/EuJMI.1.2011.4.1.

Fung-Leung, W.-P., M.W. Schilham, A. Rahemtulla, T.M. Kündig, M. Vollenweider, J. Potter, W. van Ewijk, and T.W. Mak. 1991. CD8 is needed for development of cytotoxic T cells but not helper T cells. *Cell*. 65:443–449. doi:10.1016/0092-8674(91)90462-8.

Galli, S.J., and M. Tsai. 2013. IgE and mast cells in allergic disease. *Nat. Med.* 18:693–704. doi:10.1038/nm.2755.

Garman, R.D., P.J. Doherty, and D.H. Raulet. 1986. Diversity, rearrangement, and expression of murine T cell gamma genes. *Cell*. 45:733–742. doi:10.1016/0092-8674(86)90787-7.

Gelfanov, V., Y.G. Lai, V. Gelfanova, J.Y. Dong, J.P. Su, and N.S. Liao. 1995. Differential requirement of CD28 costimulation for activation of murine $CD8^+$ intestinal intraepithelial lymphocyte subsets and lymph node cells. *J. Immunol.* 155:76–82.

Gensollen, T., S.S. Iyer, D.L. Kasper, and R.S. Blumberg. 2016. How colonization by microbiota in early life shapes the immune system. *Science*. 352:539–544. doi:10.1126/science.aad9378.

Gerbe, F., C. Legraverend, and P. Jay. 2012. The intestinal epithelium tuft cells: specification and function. *Cell. Mol. life Sci.* 69:2907–17. doi:10.1007/s00018-012-0984-7.

Gerbe, F., E. Sidot, D.J. Smyth, M. Ohmoto, I. Matsumoto, V. Dardalhon, P. Cesses, L. Garnier, M. Pouzolles, B. Brulin, M. Bruschi, Y. Harcus, V.S. Zimmermann, N. Taylor, R.M. Maizels, and P. Jay. 2016. Intestinal epithelial tuft cells initiate type 2 mucosal immunity to helminth parasites. *Nature*. 529:226–230. doi:10.1038/nature16527.

Gerlach, K., Y. Hwang, A. Nikolaev, R. Atreya, H. Dornhoff, S. Steiner, H.-A. Lehr, S. Wirtz, M. Vieth, A. Waisman, F. Rosenbauer, A.N.J. McKenzie, B. Weigmann, and M.F. Neurath. 2014. Th9 cells that express the transcription factor PU.1 drive T cell-mediated colitis via IL-9 receptor signaling in intestinal epithelial cells. *Nat. Immunol.* 15:676–86. doi:10.1038/ni.2920.

Gerritsen, B., and A. Pandit. 2015. The memory of a killer T cell: Models of $CD8^+$ T cell differentiation. *Immunol. Cell Biol.* 94:236–241. doi:10.1038/icb.2015.118.

Gil-Cruz, C., C. Perez-Shibayama, L. Onder, Q. Chai, J. Cupovic, H.W. Cheng, M. Novkovic, P.A. Lang, M.B. Geuking, K.D. McCoy, S. Abe, G. Cui, K. Ikuta, E. Scandella, and B. Ludewig. 2016. Fibroblastic reticular cells regulate intestinal inflammation via IL-15-mediated control of group 1 ILCs. *Nat. Immunol.* 17:1388–1396. doi:10.1038/ni.3566.

Gjorevski, N., N. Sachs, A. Manfrin, S. Giger, M.E. Bragina, P. Ordóñez-Morán, H. Clevers, and M.P. Lutolf. 2016. Designer matrices for intestinal stem cell and organoid culture. *Nature*. 539:560–564. doi:10.1038/nature20168.

Goios, A., L. Pereira, M. Bogue, V. Macaulay, and A. Amorim. 2007. mtDNA phylogeny and evolution of laboratory mouse strains. *Cold Spring Harb. Lab. Press*. 17:293–298. doi:10.1101/gr.5941007.

Gonzales, A.M., S. Wilde, and K.L. Roland. 2017. New insights into the roles of Lpf and Stg fimbriae in Salmonella interactions with enterocytes and M cells. *Infect. Immun.* 85:1–12. doi:10.1128/IAI.00172-17.

Goverse, G., C. Labao-Almeida, M. Ferreira, R. Molenaar, S. Wahlen, T. Konijn, J. Koning, H. Veiga-Fernandes, and R.E. Mebius. 2016. Vitamin A Controls the Presence of $ROR\gamma^+$ Innate Lymphoid Cells and Lymphoid Tissue in the Small Intestine. *J. Immunol.* 196:5148–5155. doi:10.4049/jimmunol.1501106.

Gracz, A.D., and S.T. Magness. 2014. Defining hierarchies of stemness in the intestine: evidence from biomarkers and regulatory pathways. *Am. J. Physiol. Gastrointest. Liver Physiol.* 307:260–273. doi:10.1152/ajpgi.00066.2014.

Gradmann, C. 2014. A spirit of scientific rigour: Koch's postulates in twentieth-century medicine. *Microbes Infect.* 16:885–892. doi:10.1016/j.micinf.2014.08.012.

Grau, K.R., A.N. Roth, S. Zhu, A. Hernandez, N. Colliou, B.B. DiVita, D.T. Philip, C. Riffe, B. Giasson, S.M. Wallet, M. Mohamadzadeh, and S.M. Karst. 2017. The major targets of acute norovirus infection are immune cells in the gut-associated lymphoid tissue. *Nat. Microbiol.* 2:1–6. doi:10.1038/s41564-017-0057-7.

Greenspan, P., E.P. Mayer, and S.D. Fowler. 1985. Nile red: a selective fluorescent stain for intracellular lipid droplets. *J. Cell Biol.* 100:965–973. doi:10.1083/jcb.100.3.965.

Groh, V., A. Steinle, S. Bauer, and T. Spies. 1998. Recognition of stress-induced MHC molecules by intestinal epithelial γδ T cells. *Science.* 279:1737–1740. doi:10.1126/science.279.5357.1737.

Gu, Y.Z., J.B. Hogenesch, and C. a Bradfield. 2000. The PAS superfamily: sensors of environmental and developmental signals. *Annu. Rev. Pharmacol. Toxicol.* 40:519–561. doi:10.1146/annurev.pharmtox.40.1.519.

Gubser, P.M., G.R. Bantug, L. Razik, M. Fischer, S. Dimeloe, G. Hoenger, B. Durovic, A. Jauch, and C. Hess. 2013. Rapid effector function of memory $CD8^+$ T cells requires an immediate-early glycolytic switch. *Nat. Immunol.* 14:1064–1072. doi:10.1038/ni.2687.

Guedes, J.P.F.M. 2017. Host-Pathogen Interactions at the Intestinal Epithelial Barrier. *Univ. Cambridge Ph.D Thesis*. 1–182.

Guilliams, M., F. Ginhoux, C. Jakubzick, S.H. Naik, N. Onai, B.U. Schraml, E. Segura, R. Tussiwand, and S. Yona. 2014. Dendritic cells, monocytes and macrophages: a unified nomenclature based on ontogeny. *Nat. Rev. Immunol.* 14:571–578. doi:10.1038/nri3712.

Gury-BenAri, M., C.A. Thaiss, N. Serafini, D.R. Winter, A. Giladi, D. Lara-Astiaso, M. Levy, T.M. Salame, A. Weiner, E. David, H. Shapiro, M. Dori-Bachash, M. Pevsner-Fischer, E. Lorenzo-Vivas, H. Keren-Shaul, F. Paul, A. Harmelin, G. Eberl, S. Itzkovitz, A. Tanay, J.P. Di Santo, E. Elinav, and I. Amit. 2016. The Spectrum and Regulatory Landscape of Intestinal Innate Lymphoid Cells Are Shaped by the Microbiome. *Cell*. 166:1231–1246. doi:10.1016/j.cell.2016.07.043.

Guy-Grand, D., N. Cerf-Bensussan, B. Malissen, M. Malassis-Seris, C. Briottet, and P. Vassalli. 1991. Two gut intraepithelial $CD8^+$ lymphocyte populations with different T cell receptors: a role for the gut epithelium in T cell differentiation. *J. Exp. Med.* 173:471–81. doi:10.1084/jem.173.2.471.

Guy-Grand, D., P. Vassalli, G. Eberl, P. Pereira, O. Burlen-Defranoux, F. Lemaitre, J.P. Di Santo, A. a Freitas, A. Cumano, and A. Bandeira. 2013. Origin, trafficking, and intraepithelial fate of gut-tropic T cells. *J. Exp. Med.* 210:1839–1854. doi:10.1084/jem.20122588.

Haber, A.L., M. Biton, N. Rogel, R.H. Herbst, K. Shekhar, C. Smillie, G. Burgin, T.M. Delorey, M.R. Howitt, Y. Katz, I. Tirosh, S. Beyaz, D. Dionne, M. Zhang, R. Raychowdhury, W.S. Garrett, O. Rozenblatt-Rosen, H.N. Shi, O. Yilmaz, R.J. Xavier, and A. Regev. 2017. A single-cell survey of the small intestinal epithelium. *Nature*. doi:10.1038/nature24489.

Hagen, T., C.T. Taylor, F. Lam, and S. Moncada. 2003. Redistribution of Intracellular Oxygen in Hypoxia by Nitric Oxide: Effect on HIF1a. *Science.* 302:1975–1978. doi:10.1126/science.1088805.

Hall, J. a, J.R. Grainger, S.P. Spencer, and Y. Belkaid. 2011a. The role of retinoic acid in tolerance and immunity. *Immun. Rev.* 35:13–22. doi:10.1016/j.immuni.2011.07.002.

Hall, J.A., J.L. Cannons, J.R. Grainger, L.M. Dos Santos, W. Hand, S. Naik, E.A. Wohlfert, D.B. Chou, G. Oldenhove, M. Robinson, M.E. Grigg, R. Kastenmayer, P.L. Schwartzberg, and Y. Belkaid. 2011b. Essential Role for Retinoic Acid in the Promotion of CD4+ T Cell Effector Responses via Retinoic Acid Receptor Alpha. *Immunity*. 34: 435-47 doi: 10.1016/j.immuni.2011.03.003.

Han, X., K. Yang, J. Yang, H. Cheng, and R.W. Gross. 2006. Shotgun lipidomics of cardiolipin molecular species in lipid extracts of biological samples. *J. Lipid Res.* 47:864–879. doi:10.1194/jlr.D500044-JLR200.

Hand, T.W., L.M. Dos Santos, N. Bouladoux, J.M. Michael, A.J. Pagán, M. Pepper, C.L. Maynard, O. Charles, and Y. Belkaid. 2012. Acute Gastrointestinal Infection Induces Long-Lived Microbiota-Specific T Cell Responses. *Science.* 337:1553–1556. doi:10.1038/ni1112.

Hao, Z., and K. Rajewsky. 2001. Homeostasis of Peripheral B Cells in the Absence of B Cell Influx from the Bone Marrow. *J. Exp. Med.* 194:1151–1163. doi:10.1084/jem.194.8.1151.

Haramis, A.-P.G., H. Begthel, M. van den Born, J. van Es, S. Jonkheer, G.J.A. Offerhaus, and H. Clevers. 2004. De Novo Crypt Formation and Juvenile Polyposis on BMP Inhibition in Mouse Intestine. *Science.* 303:1684–1686. doi:10.1126/science.1093587.

Hayase, E., D. Hashimoto, K. Nakamura, C. Noizat, R. Ogasawara, S. Takahashi, H. Ohigashi, Y. Yokoi, R. Sugimoto, S. Matsuoka, T. Ara, E. Yokoyama, T. Yamakawa, K. Ebata, T. Kondo, R. Hiramine, T. Aizawa, Y. Ogura, T. Hayashi, H. Mori, K. Kurokawa, K. Tomizuka, T. Ayabe, and T. Teshima. 2017. R-Spondin1 expands Paneth cells and prevents dysbiosis induced by graft-versus-host disease. *J. Exp. Med.* 215:1–12. doi:10.1084/jem.20170418.

Hayashi, F., K.D. Smith, A. Ozinsky, T.R. Hawn, E.C. Yi, D.R. Goodlett, J.K. Eng, S. Akira, D.M. Underhill, and A. Aderem. 2001. The innate immune response to bacterial flagellin is mediated by Toll-like receptor 5. *Nature*. 410:1099–103. doi:10.1038/35074106.

Hayat, M., A. Cairns, M.F. Dixon, and S. O'Mahony. 2002. Quantitation of intraepithelial lymphocytes in human duodenum: what is normal? *J. Clin. Pathol.* 55:393–395.

Heiling, J.S., and S. Tonegawa. 1986. Diversity of murine gamma genes and expression in fetal and adult T lymphocytes. *Nature*. 322:836–839. doi:10.1038/322836a0.

Henderson, P., J.E. van Limbergen, J. Schwarze, and D.C. Wilson. 2011. Function of the intestinal epithelium and its dysregulation in inflammatory bowel disease. *Inflamm. Bowel Dis.* 17:382–395. doi:10.1002/ibd.21379.

Heng, T.S.P., M.W. Painter, T. Immunological, and G. Project. 2008. The Immunological genome project: networks of gene expression in immune cells. *Nat. Immunol.* 9:1091–1094. doi:10.1038/ni1008-1091.

Hernández, P.P., T. Mahlakõiv, I. Yang, V. Schwierzeck, N. Nguyen, F. Guendel, K. Gronke, B. Ryffel, C. Hölscher, L. Dumoutier, J.-C. Renauld, S. Suerbaum, P. Staeheli, and A. Diefenbach. 2015. Interferon-λ and interleukin 22 act synergistically for the induction of interferon-stimulated genes and control of rotavirus infection. *Nat. Immunol.* 16:698–707. doi:10.1038/ni.3180.

Hershberg, R.M., and L.F. Mayer. 2000. Antigen processing and presentation by intestinal epithelial cells - polarity and complexity. *Immunol. Today*. 21:123–128. doi:10.1016/S0167-5699(99)01575-3.

Horita, N., K. Tsuchiya, R. Hayashi, K. Fukushima, S. Hibiya, M. Fukuda, Y. Kano, T. Mizutani, Y. Nemoto, S. Yui, R. Okamoto, T. Nakamura, and M. Watanabe. 2014. Fluorescent labelling of intestinal epithelial cells reveals independent long-lived intestinal stem cells in a crypt. *Biochem. Biophys. Res. Commun.* 454:493–499. doi:10.1016/j.bbrc.2014.10.091.

Hosler, J.P., S. Ferguson-Miller, and D.A. Mills. 2006. Energy transduction: proton transfer through the respiratory complexes. *Annu. Rev. Biochem.* 75:165–187. doi:10.1146/annurev.biochem.75.062003.101730.

Hou, Q., L. Ye, H. Liu, L. Huang, Q. Yang, J. Turner, and Q. Yu. 2018. Lactobacillus accelerates ISCs regeneration to protect the integrity of intestinal mucosa through activation of STAT3 signaling pathway induced by LPLs secretion of IL-22. *Cell Death Differ.* 1–14. doi:10.1038/s41418-018-0070-2.

Houston, S. a, V. Cerovic, C. Thomson, J. Brewer, a M. Mowat, and S. Milling. 2015. The lymph nodes draining the small intestine and colon are anatomically separate and immunologically distinct. *Mucosal Immunol.* 9:1–11. doi:10.1038/mi.2015.77.

Howitt, M.R., S. Lavoie, M. Michaud, A.M. Blum, S. V Tran, J. V Weinstock, C.A. Gallini, K. Redding, R.F. Margolskee, L.C. Osborne, D. Artis, and W.S. Garrett. 2016. Tuft cells, taste-chemosensory cells, orchestrate parasite type 2 immunity in the gut. *Science.* 6279:1329–1333. doi:10.1126/science.aaf1648.

Hoytema van Konijnenburg, D.P., B.S. Reis, V.A. Pedicord, J. Farache, G.D. Victora, and D. Mucida. 2017. Intestinal Epithelial and Intraepithelial T Cell Crosstalk Mediates a Dynamic Response to Infection. *Cell*. 171:1–12. doi:10.1016/j.cell.2017.08.046.

Hsu, C.C., L.K. Riley, and R.S. Livingston. 2007. Molecular characterization of three novel murine noroviruses. *Virus Genes*. 34:147–155. doi:10.1007/s11262-006-0060-1.

Huang, S., W. Hendriks, A. Althage, S. Hemmi, H. Bluethmann, R. Kamijo, J. Vilcek, R. Zinkernagel, and M. Aguet. 1993. Immune response in mice that lack the interferon-gamma receptor. *Science.* 259:1742–1745. doi:10.1126/science.8456301.

Huang, W., L. Na, P.L. Fidel, and P. Schwarzenberger. 2004. Requirement of Interleukin-17A for Systemic Anti–*Candida albicans* Host Defense in Mice. *J. Infect. Dis.* 190:624–631. doi:10.1086/422329.

Huang, Y.-L., C. Chassard, M. Hausmann, M. von Itzstein, and T. Hennet. 2015. Sialic acid catabolism drives intestinal inflammation and microbial dysbiosis in mice. *Nat. Commun.* 6:8141. doi:10.1038/ncomms9141.

Huch, M., P. Bonfanti, S.F. Boj, T. Sato, C.J.M. Loomans, M. van de Wetering, M. Sojoodi, V.S.W. Li, J. Schuijers, A. Gracanin, F. Ringnalda, H. Begthel, K. Hamer, J. Mulder, J.H. van Es, E. de Koning, R.G.J. Vries, H. Heimberg, and H. Clevers. 2013a. Unlimited *in vitro* expansion of adult bi-potent pancreas progenitors through the Lgr5/R-spondin axis. *EMBO J.* 32:2708–2721. doi:10.1038/emboj.2013.204.

Huch, M., C. Dorrell, S.F. Boj, J.H. van Es, V.S.W. Li, M. van de Wetering, T. Sato, K. Hamer, N. Sasaki, M.J. Finegold, A. Haft, R.G. Vries, M. Grompe, and H. Clevers. 2013b. *In vitro* expansion of single $Lgr5^+$ liver stem cells induced by Wnt-driven regeneration. *Nature*. 494:247–50. doi:10.1038/nature11826.

Huch, M., H. Gehart, R. Van Boxtel, K. Hamer, F. Blokzijl, M.M.A. Verstegen, E. Ellis, M. Van Wenum, S.A. Fuchs, J. De Ligt, M. Van De Wetering, N. Sasaki, S.J. Boers, H. Kemperman, J. De Jonge, J.N.M. Ijzermans, E.E.S. Nieuwenhuis, R. Hoekstra, S. Strom, R.R.G. Vries, L.J.W. Van Der Laan, E. Cuppen, and H. Clevers. 2015. Long-term culture of genome-stable bipotent stem cells from adult human liver. *Cell*. 160:299–312. doi:10.1016/j.cell.2014.11.050.

Hughes, P., D. Marshall, Y. Reid, H. Parkes, and C. Gelber. 2007. The costs of using unauthenticated, over-passaged cell lines: How much more data do we need? *Biotechniques*. 43:575–586. doi:10.2144/000112598.

Hukelmann, J.L., K.E. Anderson, L. V Sinclair, K.M. Grzes, A.B. Murillo, P.T. Hawkins, L.R. Stephens, A.I. Lamond, and D.A. Cantrell. 2015. The cytotoxic T cell proteome and its shaping by the kinase mTOR. *Nat. Immunol.* 17:104–112. doi:10.1038/ni.3314.

Humblin, E., M. Thibaudin, F. Chalmin, V. Derangère, E. Limagne, C. Richard, R.A. Flavell, S. Chevrier, S. Ladoire, H. Berger, R. Boidot, L. Apetoh, F. Végran, and F. Ghiringhelli. 2017. IRF8-dependent molecular complexes control the Th9 transcriptional program. *Nat. Commun.* 8:1–13. doi:10.1038/s41467-017-01070-w.

Ichinohe, T., I.K. Pang, Y. Kumamoto, D.R. Peaper, J.H. Ho, T.S. Murray, and A. Iwasaki. 2011. Microbiota regulates immune defense against respiratory tract influenza A virus infection. *Proc. Natl. Acad. Sci. USA*. 108:5354–5359. doi:10.1073/pnas.1019378108/-/DCSupplemental.www.pnas.org/cgi/doi/10.1073/pnas.1019378108.

In, J.G., J. Foulke-Abel, M.K. Estes, N.C. Zachos, O. Kovbasnjuk, and M. Donowitz. 2016. Human mini-guts: new insights into intestinal physiology and host–pathogen interactions. *Nat. Rev. Gastroenterol. Hepatol.* 13:633–642. doi:10.1038/nrgastro.2016.142.

Inagaki-Ohara, K., F.N. Dewi, H. Hisaeda, A.L. Smith, F. Jimi, M. Miyahira, A.S.F. Abdel-Aleem, Y. Horii, and Y. Nawa. 2006. Intestinal intraepithelial lymphocytes sustain the epithelial barrier function against *Eimeria vermiformis* infection. *Infect. Immun.* 74:5292–5301. doi:10.1128/IAI.02024-05.

Intlekofer, A.M., A. Banerjee, N. Takemoto, S.M. Gordon, C.S. Dejong, H. Shin, C.A. Hunter, E.J. Wherry, T. Lindsten, and S.L. Reiner. 2008. Anomalous Type 17 Response to Viral Infection by $CD8^+$ T cells Lacking T-bet and Eomesdermin. *Science.* 321:408–411. doi:10.1126/science.1159806.

Ismail, A.S., C.L. Behrendt, and L. V Hooper. 2009. Reciprocal interactions between commensal bacteria and γδ intraepithelial lymphocytes during mucosal injury. *J. Immunol.* 182:3047–3054. doi:10.4049/jimmunol.0802705.

Ito, K., A. Nakajima, Y. Fukushima, K. Suzuki, K. Sakamoto, Y. Hamazaki, K. Ogasawara, N. Minato, and M. Hattori. 2017. The potential role of Osteopontin in the maintenance of commensal bacteria homeostasis in the intestine. *PLoS One*. 12:1–16. doi:10.1371/journal.pone.0173629.

Itohara, S., M. Peter, J. Lafaille, L. John, A. Nelson, A.F. Clarke, M.L. Hooper, A. Farr, and S. Tonegawa. 1993. T Cell Receptor δ Gene Mutant Mice : Independent Generation of αβ T cells and Programmed Rearrangements of γδ TCR genes. *Cell*. 72:337–348. doi:10.1016/0092-8674(93)90112-4.

Ivanov, I.I., K. Atarashi, N. Manel, E.L. Brodie, T. Shima, U. Karaoz, D. Wei, K.C. Goldfarb, C.A. Santee, S. V. Lynch, T. Tanoue, A. Imaoka, K. Itoh, K. Takeda, Y. Umesaki, K. Honda, and D.R. Littman. 2009. Induction of Intestinal Th17 Cells by Segmented Filamentous Bacteria. *Cell*. 139:485–498. doi:10.1016/j.cell.2009.09.033.

Jabaji, Z., C.M. Sears, G.J. Brinkley, N.Y. Lei, V.S. Joshi, J. Wang, M. Lewis, M. Stelzner, M.G. Martín, and J.C.Y. Dunn. 2013. Use of collagen gel as an alternative extracellular matrix for the in vitro and in vivo growth of murine small intestinal epithelium. *Tissue Eng. Part C. Methods*. 19:961–9. doi:10.1089/ten.TEC.2012.0710.

Jabri, B., and E. Ebert. 2007. Human $CD8^+$ intraepithelial lymphocytes: a unique model to study the regulation of effector cytotoxic T lymphocytes in tissue. *Immunol. Rev.* 215:202–214. doi:10.1111/j.1600-065X.2006.00481.x.

Janeway Jr., C.A. 1989. Approaching the Asymptote? Evolution and Revolution in Immunology. *Cold Spring Harb. Lab. Press*.

Jennemann, R., S. Kaden, R. Sandhoff, V. Nordström, S. Wang, M. Volz, S. Robine, N. Amen, U. Rothermel, H. Wiegandt, and H.J. Gröne. 2012. Glycosphingolipids are essential for intestinal endocytic function. *J. Biol. Chem.* 287:32598–32616. doi:10.1074/jbc.M112.371005.

Jiang, F., M.T. Ryan, M. Schlame, M. Zhao, Z. Gu, M. Klingenberg, N. Pfanner, and M.L. Greenberg. 2000. Absence of cardiolipin in the crd1 null mutant results in decreased mitochondrial membrane potential and reduced mitochondrial function. *J. Biol. Chem.* 275:22387–22394. doi:10.1074/jbc.M909868199.

Jiang, L., Y. Shen, D. Guo, D. Yang, J. Liu, X. Fei, Y. Yang, B. Zhang, Z. Lin, F. Yang, X. Wang, K. Wang, J. Wang, and Z. Cai. 2016. EpCAM-dependent extracellular vesicles from intestinal epithelial cells maintain intestinal tract immune balance. *Nat. Commun.* 7:1–15. doi:10.1038/ncomms13045.

Jiang, W., X. Wang, B. Zeng, L. Liu, A. Tardivel, H. Wei, J. Han, H.R. MacDonald, J. Tschopp, Z. Tian, and R. Zhou. 2013. Recognition of gut microbiota by NOD2 is essential for the homeostasis of intestinal intraepithelial lymphocytes. *J. Exp. Med.* 210:2465–2476. doi:10.1084/jem.20122490.

Johnson, M.O., M.M. Wolf, M.Z. Madden, G. Andrejeva, A. Sugiura, D.C. Contreras, D. Maseda, M. V. Liberti, K. Paz, R.J. Kishton, M.E. Johnson, A.A. de Cubas, P. Wu, G. Li, Y. Zhang, D.C. Newcomb, A.D. Wells, N.P. Restifo, W.K. Rathmell, J.W. Locasale, M.L. Davila, B.R. Blazar, and J.C. Rathmell. 2018. Distinct Regulation of Th17 and Th1 Cell Differentiation by Glutaminase-Dependent Metabolism. *Cell*. 1–16. doi:10.1016/j.cell.2018.10.001.

Jonckheere, A.I., J.A.M. Smeitink, and R.J.T. Rodenburg. 2012. Mitochondrial ATP synthase: architecture, function and pathology. *J. Inherit. Metab. Dis.* 35:211–225. doi:10.1007/s10545-011-9382-9.

K.Mackay, L., M. Minnich, N.A.M. Kragten, Y. Liao, B. Nota, C. Seillet, A. Zaid, K. Man, S. Preston, D. Freestone, A. Braun, E. Wynne-Jones, F.M. Behr, R. Stark, D.G. Pellicci, D.I. Godfrey, G.T. Belz, M. Pellegrini, T. Gebhardt, M. Busslinger, W. Shi, F.R. Carbone, R.A.W. van Lier, A. Kallies, and K.P.J.M. van Gisbergen. 2016. Hobit and Blimp1 instruct a universal transcriptional program of tissue residency in lymphocytes. *Science.* 352:459–463. doi:10.1126/science.aad2035.

Kadivar, M., J. Petersson, L. Svensson, and J. Marsal. 2016. CD8αβ^{+} γδ T Cells: A Novel T Cell Subset with a Potential Role in Inflammatory Bowel Disease. *J. Immunol.* 197:4584–4592. doi:10.4049/jimmunol.1601146.

Kadow, S., B. Jux, S.P. Zahner, B. Wingerath, S. Chmill, B.E. Clausen, J. Hengstler, and C. Esser. 2011. Aryl Hydrocarbon Receptor Is Critical for Homeostasis of Invariant γδ T Cells in the Murine Epidermis. *J. Immunol.* 187:3104–3110. doi:10.4049/jimmunol.1100912.

Kaewsuya, P., N.D. Danielson, and D. Ekhterae. 2007. Fluorescent determination of cardiolipin using 10-N-nonyl acridine orange. *Anal. Bioanal. Chem.* 387:2775–2782. doi:10.1007/s00216-007-1135-0.

Kamata, H., S.I. Honda, S. Maeda, L. Chang, H. Hirata, and M. Karin. 2005. Reactive oxygen species promote TNFα-induced death and sustained JNK activation by inhibiting MAP kinase phosphatases. *Cell*. 120:649–661. doi:10.1016/j.cell.2004.12.041.

Kameoka, S., Y. Adachi, K. Okamoto, M. Iijima, and H. Sesaki. 2017. Phosphatidic Acid and Cardiolipin Coordinate Mitochondrial Dynamics. *Trends Cell Biol.* 28:67–76. doi:10.1016/j.tcb.2017.08.011.

Kaser, A., A.H. Lee, A. Franke, J.N. Glickman, S. Zeissig, H. Tilg, E.E.S. Nieuwenhuis, D.E. Higgins, S. Schreiber, L.H. Glimcher, and R.S. Blumberg. 2008. XBP1 Links ER Stress to Intestinal Inflammation and Confers Genetic Risk for Human Inflammatory Bowel Disease. *Cell*. 134:743–756. doi:10.1016/j.cell.2008.07.021.

Kawaguchi, M., M. Nanno, Y. Umesaki, S. Matsumoto, Y. Okada, Z. Cai, T. Shimamura, Y. Matsuoka, M. Ohwaki, and H. Ishikawa. 1993. Cytolytic activity of intestinal intraepithelial lymphocytes in germ-free mice is strain dependent and determined by T cells expressing γδ T-cell antigen receptors. *Proc. Natl. Acad. Sci. USA*. 90:8591–8594. doi:10.1073/pnas.90.18.8591.

Kawalekar, O.U., R.S. O'Connor, J.A. Fraietta, L. Guo, S.E. McGettigan, A.D. Posey, P.R. Patel, S. Guedan, J. Scholler, B. Keith, N. Snyder, I. Blair, M.C. Milone, and C.H. June. 2016. Distinct Signaling of Coreceptors Regulates Specific Metabolism Pathways and Impacts Memory Development in CAR T Cells. *Immunity*. 44:380–390. doi:10.1016/j.immuni.2016.01.021.

Kennedy, M.K., M. Glaccum, S.N. Brown, E. a Butz, J.L. Viney, M. Embers, N. Matsuki, K. Charrier, L. Sedger, C.R. Willis, K. Brasel, P.J. Morrissey, K. Stocking, J.C. Schuh, S. Joyce, and J.J. Peschon. 2000. Reversible defects in natural killer and memory CD8 T cell lineages in interleukin 15-deficient mice. *J. Exp. Med.* 191:771–80. doi:10.1084/jem.191.5.771.

Van Kerckhove, C., G. Russell, K. Deusch, K. Reich, A. Bhan, H. DerSimonian, and M. Brenner. 1992. Oligoclonality of human intestinal intraepithelial T cells. *J. Exp. Med.* 175:57–63. doi:10.1084/jem.175.1.57.

El Khoury, M., J. Swain, G. Sautrey, L. Zimmermann, P. Van Der Smissen, J.L. Décout, and M.P. Mingeot-Leclercq. 2017. Targeting Bacterial Cardiolipin Enriched Microdomains: An Antimicrobial Strategy Used by Amphiphilic Aminoglycoside Antibiotics. *Sci. Rep.* 7:1–12. doi:10.1038/s41598-017-10543-3.

Kim, K.-A. 2005. Mitogenic Influence of Human R-Spondin1 on the Intestinal Epithelium. *Science.* 309:1256–1259. doi:10.1126/science.1112521.

Klein Geltink, R.I., D. O'Sullivan, M. Corrado, A. Bremser, M.D. Buck, J.M. Buescher, E. Firat, X. Zhu, G. Niedermann, G. Caputa, B. Kelly, U. Warthorst, A. Rensing-Ehl, R.L. Kyle, L. Vandersarren, J.D. Curtis, A.E. Patterson, S. Lawless, K. Grzes, J. Qiu, D.E. Sanin, O. Kretz, T.B. Huber, S. Janssens, B.N. Lambrecht, A.S. Rambold, E.J. Pearce, and E.L. Pearce. 2017. Mitochondrial Priming by CD28. *Cell*. 171:385–390. doi:10.1016/j.cell.2017.08.018.

Kleinman, H.K., and G.R. Martin. 2005. Matrigel: Basement membrane matrix with biological activity. *Semin. Cancer Biol.* 15:378–386. doi:10.1016/j.semcancer.2005.05.004.

Kleinman, H.K., M.L. McGarvey, L.A. Liotta, P.G. Robey, K. Tryggvason, and G.R. Martin. 1982. Isolation and Characterization of Type IV Procollagen, Laminin, and Heparan Sulfate Proteoglycan from the EHS Sarcoma. *Biochemistry*. 21:6188–6193. doi:10.1021/bi00267a025.

Klose, C.S.N., K. Blatz, Y. D'Hargues, P.P. Hernandez, M. Kofoed-Nielsen, J.F. Ripka, K. Ebert, S.J. Arnold, A. Diefenbach, E. Palmer, and Y. Tanriver. 2014a. The Transcription Factor T-bet Is Induced by IL-15 and Thymic Agonist Selection and Controls CD8αα^{+} Intraepithelial Lymphocyte Development. *Immunity*. 41:230–243. doi:10.1016/j.immuni.2014.06.018.

Klose, C.S.N., M. Flach, L. Möhle, L. Rogell, T. Hoyler, K. Ebert, C. Fabiunke, D. Pfeifer, V. Sexl, D. Fonseca-Pereira, R.G. Domingues, H. Veiga-Fernandes, S.J. Arnold, M. Busslinger, I.R. Dunay, Y. Tanriver, and A. Diefenbach. 2014b. Differentiation of type 1 ILCs from a common progenitor to all helper-like innate lymphoid cell lineages. *Cell*. 157:340–356. doi:10.1016/j.cell.2014.03.030.

Knoop, K.A., N. Kumar, B.R. Butler, S.K. Sakthivel, R.T. Taylor, T. Nochi, H. Akiba, H. Yagita, H. Kiyono, and I.R. Williams. 2009. RANKL is necessary and sufficient to initiate development of antigen-sampling M cells in the intestinal epithelium. *J. Immunol.* 183:5738–5747. doi:10.4049/jimmunol.0901563.

Kober, O.I., D. Ahl, C. Pin, L. Holm, S.R. Carding, and N. Juge. 2014. γδ T-cell-deficient mice show alterations in mucin expression, glycosylation, and goblet cells but maintain an intact mucus layer. *Am. J. Physiol. Gastrointest. Liver Physiol.* 306:582–593. doi:10.1152/ajpgi.00218.2013.

Koehler, K.R., J. Nie, E. Longworth-Mills, X.-P. Liu, J. Lee, J.R. Holt, and E. Hashino. 2017. Generation of inner ear organoids containing functional hair cells from human pluripotent stem cells. *Nat. Biotechnol.* 1–9. doi:10.1038/nbt.3840.

Kohanski, M.A., D.J. Dwyer, and J.J. Collins. 2010. How antibiotics kill bacteria: From targets to networks. *Nat. Rev. Microbiol.* 8:423–435. doi:10.1038/nrmicro2333.

Kolaczkowska, E., and P. Kubes. 2013. Neutrophil recruitment and function in health and inflammation. *Nat. Rev. Immunol.* 13:159–175. doi:10.1038/nri3399.

Konkel, J.E., T. Maruyama, A.C. Carpenter, Y. Xiong, B.F. Zamarron, B.E. Hall, A.B. Kulkarni, P. Zhang, R. Bosselut, and W. Chen. 2011. Control of the development of CD8αα^{+} intestinal intraepithelial lymphocytes by TGF-β. *Nat. Immunol.* 12:312–319. doi:10.1038/ni.1997.

Koo, B.-K., V. Sasselli, and H. Clevers. 2013. Retroviral gene expression control in primary organoid cultures. *Curr. Protoc. Stem Cell Biol.* 27:1–8. doi:10.1002/9780470151808.sc05a06s27.

Kopan, R., and M.X.G. Ilagan. 2009. The Canonical Notch Signaling Pathway: Unfolding the Activation Mechanism. *Cell*. 137:216–233. doi:10.1016/j.cell.2009.03.045.

Korinek, V., N. Barker, P. Moerer, E. Van Donselaar, G. Huls, P.J. Peters, and H. Clevers. 1998. Depletion of epithelial stem-cell compartments in the small intestine of mice lacking Tcf-4. *Nat. Genet.* 19:379–383. doi:10.1038/1270.

Kreymborg, K., R. Etzensperger, L. Dumoutier, S. Haak, A. Rebollo, T. Buch, F.L. Heppner, J.-C. Renauld, and B. Becher. 2007. IL-22 Is Expressed by Th17 Cells in an IL-23-Dependent Fashion, but Not Required for the Development of Autoimmune Encephalomyelitis. *J. Immunol.* 179:8098–8104. doi:10.4049/jimmunol.179.12.8098.

Kronenberg, M., and L. Gapin. 2002. The unconventional lifestyle of NKT cells. *Nat. Rev. Immunol.* 2:557–568. doi:10.1038/nri854.

Krych, L., C.H.F. Hansen, A.K. Hansen, F.W.J. van den Berg, and D.S. Nielsen. 2013. Quantitatively Different, yet Qualitatively Alike: A Meta-Analysis of the Mouse Core Gut Microbiome with a View towards the Human Gut Microbiome. *PLoS One*. 8:1–11. doi:10.1371/journal.pone.0062578.

Kühlbrandt, W. 2015. Structure and function of mitochondrial membrane protein complexes. *BMC Biol.* 13:1–11. doi:10.1186/s12915-015-0201-x.

Kunisawa, J., I. Takahashi, and H. Kiyono. 2007. Intraepithelial lymphocytes: Their shared and divergent immunological behaviors in the small and large intestine. *Immunol. Rev.* 215:136–153. doi:10.1111/j.1600-065X.2006.00475.x.

Kuo, S., A. El Guindy, C.M. Panwala, P.M. Hagan, and V. Camerini. 2001. Differential appearance of T cell subsets in the large and small intestine of neonatal mice. *Pediatr. Res.* 49:543–551. doi:10.1203/00006450-200104000-00017.

Kwon, G., J. Lee, J.-H. Koh, and Y.-H. Lim. 2017. Lifespan Extension of Caenorhabditis elegans by Butyricicoccus pullicaecorum and Megasphaera elsdenii with Probiotic Potential. *Curr. Microbiol.* 75:1–8. doi:10.1007/s00284-017-1416-6.

Van Laethem, F., A.N. Tikhonova, and A. Singer. 2012. MHC restriction is imposed on a diverse T cell receptor repertoire by CD4 and CD8 co-receptors during thymic selection. *Trends Immunol.* 33:437–441. doi:10.1016/j.it.2012.05.006.

Lagkouvardos, I., R. Pukall, B. Abt, B.U. Foesel, J.P. Meier-Kolthoff, N. Kumar, A. Bresciani, I. Martínez, S. Just, C. Ziegler, S. Brugiroux, D. Garzetti, M. Wenning, T.P.N. Bui, J. Wang, F. Hugenholtz, C.M. Plugge, D.A. Peterson, M.W. Hornef, J.F. Baines, H. Smidt, J. Walter, K. Kristiansen, H.B. Nielsen, D. Haller, J. Overmann, B. Stecher, and T. Clavel. 2016. The Mouse Intestinal Bacterial Collection (miBC) provides host-specific insight into cultured diversity and functional potential of the gut microbiota. *Nat. Microbiol.* 1:1–16. doi:10.1038/nmicrobiol.2016.131.

Lahvis, G.P., and C.A. Bradfield. 1998. Ahr null alleles: Distinctive or different? *Biochem. Pharmacol.* 56:781–787. doi:10.1016/S0006-2952(98)00134-8.

Lai, Y.-G., M.-S. Hou, A. Lo, S.-T. Huang, Y.-W. Huang, H.-F. Yang-Yen, and N.-S. Liao. 2013. IL-15 modulates the balance between Bcl-2 and Bim via a Jak3/1-PI3K-Akt-ERK pathway to promote CD8αα$^+$ intestinal intraepithelial lymphocyte survival. *Eur. J. Immunol.* 43:2305–2316. doi:10.1002/eji.201243026.

Lambolez, F., M.-L.L. Arcangeli, A.-M.M. Joret, V. Pasqualetto, C. Cordier, J.P. Di Santo, B. Rocha, and S. Ezine. 2006. The thymus exports long-lived fully committed T cell precursors that can colonize primary lymphoid organs. *Nat. Immunol.* 7:76–82. doi:10.1038/ni1293.

Lancaster, M.A., M. Renner, C.-A.A. Martin, D. Wenzel, L.S. Bicknell, M.E. Hurles, T. Homfray, J.M. Penninger, A.P. Jackson, and J.A. Knoblich. 2013. Cerebral organoids model human brain development and microcephaly. *Nature*. 501:373–379. doi:10.1038/nature12517.

Langdon, A., N. Crook, and G. Dantas. 2016. The effects of antibiotics on the microbiome throughout development and alternative approaches for therapeutic modulation. *Genome Med.* 8:1–16. doi:10.1186/s13073-016-0294-z.

Langille, M.G., C.J. Meehan, J.E. Koenig, A.S. Dhanani, R.A. Rose, S.E. Howlett, and R.G. Beiko. 2014. Microbial shifts in the aging mouse gut. *Microbiome*. 2:1–12. doi:10.1186/s40168-014-0050-9.

Lapointe, T.K., and a. G. Buret. 2012. Interleukin-18 facilitates neutrophil transmigration via myosin light chain kinase-dependent disruption of occludin, without altering epithelial permeability. *AJP Gastrointest. Liver Physiol.* 302:343–351. doi:10.1152/ajpgi.00202.2011.

Lavelle, E.C., C. Murphy, L.A.J. O'Neill, and E.M. Creagh. 2010. The role of TLRs, NLRs, and RLRs in mucosal innate immunity and homeostasis. *Mucosal Immunol.* 3:17–28. doi:10.1038/mi.2009.124.

Lawley, T.D., and A.W. Walker. 2013. Intestinal colonization resistance. *Immunology*. 138:1–11. doi:10.1111/j.1365-2567.2012.03616.x.

Lazarevic, V., X. Chen, J.-H. Shim, E.-S. Hwang, E. Jang, A.N. Bolm, M. Oukka, V.K. Kuchroo, and L.H. Glimcher. 2011. T-bet represses Th17 differentiation by preventing Runx1-mediated activation of the gene encoding RORγt. *Nat. Immunol.* 12:96–104. doi:10.1038/ni.1969.

Lazarevic, V., L.H. Glimcher, and G.M. Lord. 2013. T-bet: A bridge between innate and adaptive immunity. *Nat. Rev. Immunol.* 13:777–789. doi:10.1038/nri3536.

Lee, K.N., and O.Y. Lee. 2016. The Role of Mast Cells in Irritable Bowel Syndrome. *Gastroenterol. Res. Pract.* 2016:1–11. doi:10.1155/2016/2031480.

Lee, S., C.B. Wilen, A. Orvedahl, B.T. Mccune, K. Kim, R.C. Orchard, S.T. Peterson, T.J. Nice, M.T. Baldridge, and H.W. Virgin. 2017. Norovirus Cell Tropism Is Determined by Combinatorial Action of a Viral Non-structural Protein and Host Cytokine Article Norovirus Cell Tropism Is Determined by Combinatorial Action of a Viral Non-structural Protein and Host Cytokine. *Cell Host Microbe*. 22:449–459. doi:10.1016/j.chom.2017.08.021.

Lee, Y.J., K.L. Holzapfel, J. Zhu, S.C. Jameson, and K.A. Hogquist. 2013. Steady-state production of IL-4 modulates immunity in mouse strains and is determined by lineage diversity of iNKT cells. *Nat. Immunol.* 14:1146–1154. doi:10.1038/ni.2731.

Lee, Y.K., J.S. Menezes, Y. Umesaki, and S.K. Mazmanian. 2011. Proinflammatory T-cell responses to gut microbiota promote experimental autoimmune encephalomyelitis. *Proc. Natl. Acad. Sci.* 108:4615–4622. doi:10.1073/pnas.1000082107.

Lee, Y.K., H. Turner, C.L. Maynard, J.R. Oliver, D. Chen, C.O. Elson, and C.T. Weaver. 2009. Late developmental plasticity in the T helper 17 lineage. *Immunity*. 30:92–107. doi:10.1016/j.immuni.2008.11.005.

Lei, N.Y., Z. Jabaji, J. Wang, V.S. Joshi, G.J. Brinkley, H. Khalil, F. Wang, A. Jaroszewicz, M. Pellegrini, L. Li, M. Lewis, M. Stelzner, J.C.Y. Dunn, and M.G. Martín. 2014. Intestinal subepithelial myofibroblasts support the growth of intestinal epithelial stem cells. *PLoS One*. 9:1–11. doi:10.1371/journal.pone.0084651.

Leiva-Juárez, M.M., J.K. Kolls, and S.E. Evans. 2017. Lung epithelial cells: therapeutically inducible effectors of antimicrobial defense. *Mucosal Immunol.* 11:21–34. doi:10.1038/mi.2017.71.

Leon, F. 2011. Flow cytometry of intestinal intraepithelial lymphocytes in celiac disease. *J. Immunol. Methods*. 363:177–186. doi:10.1016/j.jim.2010.09.002.

Li, Y., S. Innocentin, D.R. Withers, N.A. Roberts, A.R. Gallagher, E.F. Grigorieva, C. Wilhelm, and M. Veldhoen. 2011. Exogenous stimuli maintain intraepithelial lymphocytes via aryl hydrocarbon receptor activation. *Cell*. 147:629–640. doi:10.1016/j.cell.2011.09.025.

Liang, S.C., X.-Y. Tan, D.P. Luxenberg, R. Karim, K. Dunussi-Joannopoulos, M. Collins, and L.A. Fouser. 2006. Interleukin (IL)-22 and IL-17 are coexpressed by Th17 cells and cooperatively enhance expression of antimicrobial peptides. *J. Exp. Med.* 203:2271–2279. doi:10.1084/jem.20061308.

Lickwar, C.R., J.G. Camp, M. Weiser, J.L. Cocchiaro, D.M. Kingsley, T.S. Furey, S.Z. Sheikh, and J.F. Rawls. 2017. Genomic dissection of conserved transcriptional regulation in intestinal epithelial cells. *PLoS Biol.* 15:1–40. doi:10.1371/journal.pbio.2002054.

Lin, J.Y., J.A. Russell, J.G. Sanders, and J.T. Wertz. 2016. Cephaloticoccus gen. Nov., a new genus of 'Verrucomicrobia' containing two novel species isolated from Cephalotes ant guts. *Int. J. Syst. Evol. Microbiol.* 66:3034–3040. doi:10.1099/ijsem.0.001141.

Lin, L., A.S. Ibrahim, X. Xu, J.M. Farber, V. Avanesian, B. Baquir, Y. Fu, S.W. French, J.E.J. Edwards, and B. Spellberg. 2009. Th1-Th17 cells mediate protective adaptive immunity against Staphylococcus aureus and Candida albicans infection in mice. *PLoS Pathog.* 5. doi:10.1371/journal.ppat.1000703.

Lindemans, C.A., M. Calafiore, A.M. Mertelsmann, M.H. O'Connor, J.A. Dudakov, R.R. Jenq, E. Velardi, L.F. Young, O.M. Smith, G. Lawrence, J.A. Ivanov, Y.-Y. Fu, S. Takashima, G. Hua, M.L. Martin, K.P. O'Rourke, Y.-H. Lo, M. Mokry, M. Romera-Hernandez, T. Cupedo, L.E. Dow, E.E. Nieuwenhuis, N.F. Shroyer, C. Liu, R. Kolesnick, M.R.M. van den Brink, and A.M. Hanash. 2015. Interleukin-22 promotes intestinal-stem-cell-mediated epithelial regeneration. *Nature*. 528:560–564. doi:10.1038/nature16460.

Linh, B.K., T. Hayashi, and Y. Horii. 2009. *Eimeria vermiformis* infection reduces goblet cells by multiplication in the crypt cells of the small intestine of C57BL/6 mice. *Parasitol. Res.* 104:789–794. doi:10.1007/s00436-008-1256-1.

Little, M.C., R.J.M. Hurst, and K.J. Else. 2014. Dynamic Changes in Macrophage Activation and Proliferation during the Development and Resolution of Intestinal Inflammation. *J. Immunol.* 193:4684–4695. doi:10.4049/jimmunol.1400502.

Liu, C.P., R. Ueda, J. She, J. Sancho, B. Wang, G. Weddell, J. Loring, C. Kurahara, E.C. Dudley, A. Hayday, C. Terhorst, and M. Huang. 1993. Abnormal T cell development in CD3-ζ-/- mutant mice and identification of a novel T cell population in the intestine. *EMBO J.* 12:4863–4875. doi:10.1002/j.1460-2075.1993.tb06176.x.

Lloyd, C.M., and B.J. Marsland. 2017. Lung Homeostasis: Influence of Age, Microbes, and the Immune System. *Immunity*. 46:549–561. doi:10.1016/j.immuni.2017.04.005.

Lodolce, J.P., D.L. Boone, S. Chai, R.E. Swain, T. Dassopoulos, S. Trettin, and A. Ma. 1998. IL-15 receptor maintains lymphoid homeostasis by supporting lymphocyte homing and proliferation. *Immunity*. 9:669–676. doi:10.1016/S1074-7613(00)80664-0.

Lood, C., L.P. Blanco, M.M. Purmalek, C. Carmona-Rivera, S.S. De Ravin, C.K. Smith, H.L. Malech, J.A. Ledbetter, K.B. Elkon, and M.J. Kaplan. 2016. Neutrophil extracellular traps enriched in oxidized mitochondrial DNA are interferogenic and contribute to lupus-like disease. *Nat. Med.* 22:146–153. doi:10.1038/nm.4027.

Luda, K.M., T. Joeris, E.K. Persson, A. Rivollier, M. Demiri, K.M. Sitnik, L. Pool, J.B. Holm, F. Melo-Gonzalez, L. Richter, B.N. Lambrecht, K. Kristiansen, M.A. Travis, M. Svensson-Frej, K. Kotarsky, and W.W. Agace. 2016. IRF8 Transcription-Factor-Dependent Classical Dendritic Cells Are Essential for Intestinal T Cell Homeostasis. *Immunity*. 44:860–874. doi:10.1016/j.immuni.2016.02.008.

Luoma, A.M., C.D. Castro, and E.J. Adams. 2014. γδ T cell surveillance via CD1 molecules. *Trends Immunol.* 35:613–621. doi:10.1016/j.it.2014.09.003.

Ma, L.J., L.F. Acero, T. Zal, and K.S. Schluns. 2009. Trans-presentation of IL-15 by intestinal epithelial cells drives development of CD8αα IELs. *J. Immunol.* 183:1044–1054. doi:10.4049/jimmunol.0900420.

Mabbott, N. a, D.S. Donaldson, H. Ohno, I.R. Williams, and A. Mahajan. 2013. Microfold (M) cells: important immunosurveillance posts in the intestinal epithelium. *Mucosal Immunol.* 6:666–677. doi:10.1038/mi.2013.30.

MacDonald, T.T. 2003. The mucosal immune system. *Parasite Immunol.* 25:235–246. doi:632.

Mackay, L.K., A. Rahimpour, J.Z. Ma, N. Collins, A.T. Stock, M.L. Hafon, J. Vega-Ramos, P. Lauzurica, S.N. Mueller, T. Stefanovic, D.C. Tscharke, W.R. Heath, M. Inouye, F.R. Carbone, and T. Gebhardt. 2013. The developmental pathway for $CD103^{+}CD8^{+}$ tissue-resident memory T cells of skin. *Nat. Immunol.* 14:1294–1301. doi:10.1038/ni.2744.

Mackay, L.K., E. Wynne-Jones, D. Freestone, D.G. Pellicci, L.A. Mielke, D.M. Newman, A. Braun, F. Masson, A. Kallies, G.T. Belz, and F.R. Carbone. 2015. T-box Transcription Factors Combine with the Cytokines TGF-β and IL-15 to Control Tissue-Resident Memory T Cell Fate. *Immunity*. 43:1101–1111. doi:10.1016/j.immuni.2015.11.008.

Macpherson, A.J., and N.L. Harris. 2004. Interactions between commensal intestinal bacteria and the immune system. *Nat. Rev. Immunol.* 4:478–485. doi:10.1038/nri1373.

Madison, B.B., L. Dunbar, X.T. Qiao, K. Braunstein, E. Braunstein, and D.L. Gumucio. 2002. cis Elements of the Villin Gene Control Expression in Restricted Domains of the Vertical (Crypt) and Horizontal (Duodenum, Cecum) Axes of the Intestine. *J. Biol. Chem.* 277:33275–33283. doi:10.1074/jbc.M204935200.

Magombedze, G., P.B.J. Reddy, S. Eda, and V. V Ganusov. 2013. Cellular and population plasticity of helper $CD4^{+}$ T cell responses. *Front. Physiol.* 4:206. doi:10.3389/fphys.2013.00206.

Maki, K., S. Sunaga, Y. Komagata, Y. Kodaira, A. Mabuchi, H. Karasuyama, K. Yokomuro, J. Miyazaki, and K. Ikuta. 1996. Interleukin 7 receptor-deficient mice lack γδ T cells. *Proc. Natl. Acad. Sci. USA*. 93:7172–7177. doi:10.1073/pnas.93.14.7172.

Malanovic, N., and K. Lohner. 2016. Gram-positive bacterial cell envelopes: The impact on the activity of antimicrobial peptides. *Biochim. Biophys. Acta Biomembr*. 1858:936–946. doi:10.1016/j.bbamem.2015.11.004.

Mangan, P.R., L.E. Harrington, D.B. O'Quinn, W.S. Helms, D.C. Bullard, C.O. Elson, R.D. Hatton, S.M. Wahl, T.R. Schoeb, and C.T. Weaver. 2006. Transforming growth factor-β induces development of the Th17 lineage. *Nature*. 441:231–234. doi:10.1038/nature04754.

Mantovani, A., A. Sica, and M. Locati. 2005. Macrophage polarization comes of age. *Immunity*. 23:344–346. doi:10.1016/j.immuni.2005.10.001.

Di Marco Barros, R., N.A. Roberts, R.J. Dart, P. Vantourout, A. Jandke, O. Nussbaumer, L. Deban, S. Cipolat, R. Hart, M.L. Iannitto, A. Laing, B. Spencer-Dene, P. East, D. Gibbons, P.M. Irving, P. Pereira, U. Steinhoff, and A. Hayday. 2016. Epithelia Use Butyrophilin-like Molecules to Shape Organ-Specific γδ T Cell Compartments. *Cell*. 167:203–218. doi:10.1016/j.cell.2016.08.030.

Markle, J.G.M., D.N. Frank, S. Mortin-toth, C.E. Robertson, L.M. Feazel, U. Rolle-kampczyk, M. Von Bergen, K.D. Mccoy, A.J. Macpherson, and J.S. Danska. 2013. Sex Differences in the Gut. *Science.* 339:1084–1088. doi:10.1126/science.1233521.

Mattner, J., K.L. DeBord, N. Ismail, R.D. Goff, C. Cantu, D. Zhou, P. Saint-Mezard, V. Wang, Y. Gao, N. Yin, K. Hoebe, O. Schneewind, D. Walker, B. Beutler, L. Teyton, P.B. Savage, and A. Bendelac. 2005. Exogenous and endogenous glycolipid antigens activate NKT cells during microbial infections. *Nature*. 434:525–529. doi:10.1038/nature03408.

Mayassi, T., and B. Jabri. 2018. Human intraepithelial lymphocytes. *Mucosal Immunol.* 1–9. doi:10.1038/s41385-018-0016-5.

Mayer, J.U., M. Demiri, W.W. Agace, A.S. MacDonald, M. Svensson-Frej, and S.W. Milling. 2017. Different populations of $CD11b^{+}$ dendritic cells drive Th2 responses in the small intestine and colon. *Nat. Commun.* 8:15820. doi:10.1038/ncomms15820.

McCormack, M.P., A. Forster, L. Drynan, R. Pannell, and T.H. Rabbitts. 2003. The LMO2 T-cell oncogene is activated via chromosomal translocations or retroviral insertion during gene therapy but has no mandatory role in normal T-cell development. *Mol. Cell. Biol.* 23:9003–13. doi:10.1128/MCB.23.24.9003.

McCubbery, J.A., M.M. Lahair, and R.A. Franklin. 2006. Reactive Oxygen Species-Induced Activation of the MAP Kinase Signaling Pathways. *Antioxid. Redox Signal.* 8:1775–1789. doi:10.1089/ars.2007.1811.

McDole, J.R., L.W. Wheeler, K.G. McDonald, B. Wang, V. Konjufca, K. a Knoop, R.D. Newberry, and M.J. Miller. 2012. Goblet cells deliver luminal antigen to $CD103^+$ dendritic cells in the small intestine. *Nature*. 483:345–9. doi:10.1038/nature10863.

McDonnell, E., S.B. Crown, D.B. Fox, B. Kitir, O.R. Ilkayeva, C.A. Olsen, P.A. Grimsrud, and M.D. Hirschey. 2016. Lipids Reprogram Metabolism to Become a Major Carbon Source for Histone Acetylation. *Cell Rep.* 17:1463–1472. doi:10.1016/j.celrep.2016.10.012.

Meisel, M., T. Mayassi, H. Fehlner-Peach, J.C. Koval, S.L. O'Brien, R. Hinterleitner, K. Lesko, S. Kim, R. Bouziat, L. Chen, C.R. Weber, S.K. Mazmanian, B. Jabri, and D.A. Antonopoulos. 2017. Interleukin-15 promotes intestinal dysbiosis with butyrate deficiency associated with increased susceptibility to colitis. *ISME J.* 11:15–30. doi:10.1038/ismej.2016.114.

Menk, A. V., N.E. Scharping, R.S. Moreci, X. Zeng, C. Guy, S. Salvatore, H. Bae, J. Xie, H.A. Young, S.G. Wendell, and G.M. Delgoffe. 2018a. Early TCR Signaling Induces Rapid Aerobic Glycolysis Enabling Distinct Acute T Cell Effector Functions. *Cell Rep.* 22:1509–1521. doi:10.1016/j.celrep.2018.01.040.

Menk, A. V., N.E. Scharping, D.B. Rivadeneira, M.J. Calderon, M.J. Watson, D. Dunstane, S.C. Watkins, and G.M. Delgoffe. 2018b. 4-1BB costimulation induces T cell mitochondrial function and biogenesis enabling cancer immunotherapeutic responses. *J. Exp. Med.* 215:jem.20171068. doi:10.1084/jem.20171068.

Middendorp, S., K. Schneeberger, C.L. Wiegerinck, M. Mokry, R.D.L. Akkerman, S. van Wijngaarden, H. Clevers, and E.E.S. Nieuwenhuis. 2014. Adult stem cells in the small intestine are intrinsically programmed with their location-specific function. *Stem Cells*. 32:1–7. doi:10.1002/stem.1655.

Miki, T., O. Holsts, and W.-D. Hardt. 2012. The bactericidal activity of the C-type lectin regIIIβ against gram-negative bacteria involves binding to lipid A. *J. Biol. Chem.* 287:34844–34855. doi:10.1074/jbc.M112.399998.

Mileykovskaya, E., W. Dowhan, R.L. Birke, D. Zheng, L. Lutterodt, and T.H. Haines. 2001. Cardiolipin binds nonyl acridine orange by aggregating the dye at exposed hydrophobic domains on bilayer surfaces. *FEBS Lett.* 507:187–190. doi:10.1016/S0014-5793(01)02948-9.

Min, B., A. Thornton, S.M. Caucheteux, S.A. Younes, K. Oh, J. Hu-Li, and W.E. Paul. 2007. Gut flora antigens are not important in the maintenance of regulatory T cell heterogeneity and homeostasis. *Eur. J. Immunol.* 37:1916–1923. doi:10.1002/eji.200737236.

Mombaerts, P., E. Mizoguchi, M.J. Grusby, L.H. Glimcher, A.K. Bhan, and S. Tonegawa. 1993. Spontaneous development of inflammatory bowel disease in T cell receptor mutant mice. *Cell*. 75:275–282. doi:10.1016/0092-8674(93)80069-Q.

Moolenbeek, C., and E.J. Ruitenberg. 1981. The "Swiss roll": a simple technique for histological studies of the rodent intestine. *Lab. Anim.* 15:57–59. doi:10.1258/002367781780958577.

Moore, B.A., S. Jevons, and K.W. Brammer. 1979. Inhibition of transpeptidase activity in Escherichia coli by thienamycin. *Antimicrob. Agents Chemother.* 15:831–833. doi:10.1128/AAC.15.6.831.

Morgun, A., A. Dzutsev, X. Dong, R.L. Greer, D.J. Sexton, J. Ravel, M. Schuster, W. Hsiao, P. Matzinger, and N. Shulzhenko. 2015. Uncovering effects of antibiotics on the host and microbiota using Transkingdom Gene Networks. *Gut.* 64:1732–1743. doi:10.1136/gutjnl-2014-308820.

Mori-Akiyama, Y., M. van den Born, J.H. van Es, S.R. Hamilton, H.P. Adams, J. Zhang, H. Clevers, and B. de Crombrugghe. 2007. SOX9 is required for the differentiation of paneth cells in the intestinal epithelium. *Gastroenterology.* 133:539–546. doi:10.1053/j.gastro.2007.05.020.

Mortier, E., R. Advincula, L. Kim, S. Chmura, J. Barrera, B. Reizis, B. a. Malynn, and A. Ma. 2009. Macrophage- and Dendritic-Cell-Derived Interleukin-15 Receptor Alpha Supports Homeostasis of Distinct $CD8^+$ T Cell Subsets. *Immunity*. 31:811–822. doi:10.1016/j.immuni.2009.09.017.

Mosmann, T.R., H. Cherwinski, M.W. Bond, M.A. Giedlin, and R.L. Coffman. 1986. Two types of murine helper T cell clone. I. Definition according to profiles of lymphokine activities and secreted proteins. *J. Immunol.* 136:2348–2357. doi:10.1111/j.1442-9071.2011.02672.x.

Mu, Q., V.J. Tavella, J.L. Kirby, T.E. Cecere, M. Chung, J. Lee, S. Li, S.A. Ahmed, K. Eden, I.C. Allen, C.M. Reilly, and X.M. Luo. 2017. Antibiotics ameliorate lupus-like symptoms in mice. *Sci. Rep.* 7:1–14. doi:10.1038/s41598-017-14223-0.

Mucida, D., Y. Park, G. Kim, O. Turovskaya, I. Scott, M. Kronenberg, and H. Cheroutre. 2007. Reciprocal Th17 and regulatory T cell differentiation mediated by retinoic acid. *Science.* 317:256–260. doi:10.1126/science.1145697.

Mukherjee, S., S. Vaishnava, and L. V. Hooper. 2008. Multi-layered regulation of intestinal antimicrobial defense. *Cell. Mol. Life Sci.* 65:3019–3027. doi:10.1007/s00018-008-8182-3.

Muñoz-Ruiz, M., N. Sumaria, D.J. Pennington, and B. Silva-Santos. 2017. Thymic Determinants of γδ T Cell Differentiation. *Trends Immunol.* 38:336–344. doi:10.1016/j.it.2017.01.007.

Muranski, P., and N.P. Restifo. 2013. Essentials of Th17 cell commitment and plasticity. *Blood*. 121:2402–2414. doi:10.1182/blood-2012-09-378653.

Murphy, M.P. 2009. How mitochondria produce reactive oxygen species. *Biochem. J.* 417:1–13. doi:10.1042/BJ20081386.

Musch, M.W., L.L. Clarke, D. Mamah, L.R. Gawenis, Z. Zhang, W. Ellsworth, D. Shalowitz, N. Mittal, P. Efthimiou, Z. Alnadjim, S.D. Hurst, E.B. Chang, and T.A. Barrett. 2002. T cell activation causes diarrhea by increasing intestinal permeability and inhibiting epithelial Na^+/K^+-ATPase. *J. Clin. Invest.* 110:1739–1747. doi:10.1172/JCI200215695.Introduction.

Muto, A., and S. Osawa. 1987. The guanine and cytosine content of genomic DNA and bacterial evolution. *Proc. Natl. Acad. Sci. USA*. 84:166–169. doi:10.1073/pnas.84.1.166.

Nakajima, K., Y. Maekawa, K. Kataoka, C. Ishifune, J. Nishida, H. Arimochi, A. Kitamura, T. Yoshimoto, S. Tomita, S. Nagahiro, and K. Yasutomo. 2013. The ARNT-STAT3 axis regulates the differentiation of intestinal intraepithelial TCRαβ^{+}CD8αα^{+} cells. *Nat. Commun.* 4:1–11. doi:10.1038/ncomms3112.

Nakanishi, Y., T. Sato, and T. Ohteki. 2014. Commensal Gram-positive bacteria initiates colitis by inducing monocyte/macrophage mobilization. *Mucosal Immunol.* 8:153–160. doi:10.1038/mi.2014.53.

Nakazato, K., H. Yamada, T. Yajima, Y. Kagimoto, H. Kuwano, and Y. Yoshikai. 2007. Enforced expression of Bcl-2 partially restores cell numbers but not functions of TCRγδ intestinal intraepithelial T lymphocytes in IL-15-deficient mice. *J. Immunol.* 178:757–764. doi:178/2/757.

Nalapareddy, K., K.J. Nattamai, R.S. Kumar, R. Karns, K.A. Wikenheiser-Brokamp, L.L. Sampson, M.M. Mahe, N. Sundaram, M.-B. Yacyshyn, B. Yacyshyn, M.A. Helmrath, Y. Zheng, and H. Geiger. 2017. Canonical Wnt Signaling Ameliorates Aging of Intestinal Stem Cells. *Cell Rep.* 18:2608–2621. doi:10.1016/j.celrep.2017.02.056.

Nava, P., S. Koch, M.G. Laukoetter, W.Y. Lee, K. Kolegraff, C.T. Capaldo, N. Beeman, C. Addis, K. Gerner-Smidt, I. Neumaier, A. Skerra, L. Li, C.A. Parkos, and A. Nusrat. 2010. Interferon-γ Regulates Intestinal Epithelial Homeostasis through Converging β-Catenin Signaling Pathways. *Immunity*. 32:392–402. doi:10.1016/j.immuni.2010.03.001.

Neish, A. 2006. TLRS in the gut. II. Flagellin-induced inflammation and antiapoptosis. *Am. J. Physiol.* 292:462–466. doi:10.1152/ajpgi.00274.2006.

Neufert, C., G. Pickert, Y. Zheng, N. Wittkopf, M. Warntjen, A. Nikolaev, W. Ouyang, M.F. Neurath, and C. Becker. 2010. Activation of epithelial STAT3 regulates intestinal homeostasis. *Cell Cycle*. 9:652–655. doi:10.4161/cc.9.4.10615.

Neumann, C.M., J.A. Oughton, and N.I. Kerkvliet. 1992. Anti-CD3-induced T-cell activation in vivo -- I. flow cytometric analysis of dose-responsive, time-dependent, and cyclosporin A-sensitive paramaters of $CD4^+$ and $CD8^+$ cells from the draining lymph nodes of C57B1/6 mice. *Int. J. Immunopharmacol.* 14:1295–1304. doi:10.1016/0192-0561(92)90066-T.

Newman, K.L., and J.S. Leon. 2015. Norovirus immunology: Of mice and mechanisms. *Eur. J. Immunol.* 45:2742–2757. doi:10.1002/eji.201545512.

Nice, T.J., M.T. Baldridge, B.T. McCune, J.M. Norman, H.M. Lazear, M. Artyomov, M.S. Diamond, and H.W. Virgin. 2015. Interferon-λ cures persistent murine norovirus infection in the absence of adaptive immunity. *Science.* 347:269–273. doi:10.1126/science.1258100.

Niehrs, C. 2012. The complex world of WNT receptor signalling. *Nat. Rev. Mol. Cell Biol.* 13:767–779. doi:10.1038/nrm3470.

Nigro, G., M. Hanson, C. Fevre, M. Lecuit, and P.J. Sansonetti. 2016. Intestinal Organoids as a Novel Tool to Study Microbes – Epithelium Interactions. *Methods Mol. Biol.* doi:10.1007/7651.

Nikolić, M.Z., and E.L. Rawlins. 2017. Lung Organoids and Their Use To Study Cell-Cell Interaction. *Curr. Pathobiol. Rep.* 5:223–231. doi:10.1007/s40139-017-0137-7.

Nozaki, K., W. Mochizuki, Y. Matsumoto, T. Matsumoto, M. Fukuda, T. Mizutani, M. Watanabe, and T. Nakamura. 2016. Co-culture with intestinal epithelial organoids allows efficient expansion and motility analysis of intraepithelial lymphocytes. *J. Gastroenterol.* 1–5. doi:10.1007/s00535-016-1170-8.

O'Neill, L.A.J.J., R.J. Kishton, and J. Rathmell. 2016. A guide to immunometabolism for immunologists. *Nat. Rev. Immunol.* 16:553–565. doi:10.1038/nri.2016.70.

O'Sullivan, D., G.J.W. van der Windt, S.C.-C. Huang, J.D. Curtis, C.-H. Chang, M.D. Buck, J. Qiu, A.M. Smith, W.Y. Lam, L.M. DiPlato, F.-F. Hsu, M.J. Birnbaum, E.J. Pearce, and E.L. Pearce. 2014. Memory $CD8^+$ T Cells Use Cell-Intrinsic Lipolysis to Support the Metabolic Programming Necessary for Development. *Immunity.* 41:75–88. doi:10.1016/j.immuni.2014.06.005.

Ogata, M., Y. Ota, M. Nanno, R. Suzuki, and T. Itoh. 2014. Activation of intra-epithelial lymphocytes; Their morphology, marker expression and ultimate fate. *Cell Tissue Res.* 356:217–230. doi:10.1007/s00441-013-1786-4.

Ohteki, T., and H.R. MacDonald. 1993. Expression of the CD28 costimulatory molecule on subsets of murine intestinal intraepithelial lymphocytes correlates with lineage and responsiveness. *Eur. J. Immunol.* 23:1251–1255. doi:10.1002/eji.1830230609.

Omilusik, K.D., J.A. Best, B. Yu, S. Goossens, A. Weidemann, J. V Nguyen, E. Seuntjens, A. Stryjewska, C. Zweier, R. Roychoudhuri, L. Gattinoni, L.M. Bird, Y. Higashi, H. Kondoh, D. Huylebroeck, J. Haigh, and A.W. Goldrath. 2015. Transcriptional repressor ZEB2 promotes terminal differentiation of $CD8^+$ effector and memory T cell populations during infection. *J. Exp. Med.* 212:2027–2039. doi:10.1084/jem.20150194.

Ono, S., and K. Kabashima. 2015. Proposal of inducible skin-associated lymphoid tissue (iSALT). *Exp. Dermatol.* 24:630–631. doi:10.1111/exd.12716.

Ootani, A., X. Li, E. Sangiorgi, Q.T. Ho, H. Ueno, S. Toda, H. Sugihara, K. Fujimoto, I.L. Weissman, M.R. Capecchi, and C.J. Kuo. 2009. Sustained *in vitro* intestinal epithelial culture within a Wnt-dependent stem cell niche. *Nat. Med.* 15:701–706. doi:10.1038/nm.1951.Sustained.

Orkin, R.W., P. Gehron, E.B. McGoodwin, G.R. Martin, T. Valentine, and R. Swarm. 1977. A murine tumor producing a matrix of basement membrane. *J. Exp. Med.* 145:204–20. doi:10.1084/jem.145.1.204.

Owens, B.M.J., and A. Simmons. 2013. Intestinal stromal cells in mucosal immunity and homeostasis. *Mucosal Immunol.* 6:224–34. doi:10.1038/mi.2012.125.

Pabst, O., H. Herbrand, T. Worbs, M. Friedrichsen, S. Yan, M.W. Hoffmann, H. Körner, G. Bernhardt, R. Pabst, and R. Förster. 2005. Cryptopatches and isolated lymphoid follicles: Dynamic lymphoid tissues dispensable for the generation of intraepithelial lymphocytes. *Eur. J. Immunol.* 35:98–107. doi:10.1002/eji.200425432.

Pace, N.R. 1997. A Molecular View of Microbial Diversity and the Biosphere. *Science (80-.).* 276:734–740. doi:10.1126/science.276.5313.734.

Pan, Y., T. Tian, C.O. Park, S.Y. Lofftus, S. Mei, X. Liu, C. Luo, J.T. O'Malley, A. Gehad, J.E. Teague, S.J. Divito, R. Fuhlbrigge, P. Puigserver, J.G. Krueger, G.S. Hotamisligil, R.A. Clark, and T.S. Kupper. 2017. Survival of tissue-resident memory T cells requires exogenous lipid uptake and metabolism. *Nature*. 543:252–256. doi:10.1038/nature21379.

Paradies, G., V. Paradies, V. De Benedictis, F.M. Ruggiero, and G. Petrosillo. 2014. Functional role of cardiolipin in mitochondrial bioenergetics. *Biochim. Biophys. Acta Bioenerg.* 1837:408–417. doi:10.1016/j.bbabio.2013.10.006.

Pascual-Reguant, A., J.B. Sarmadi, C. Baumann, R. Noster, D. Cirera-Salinas, C. Curato, P. Pelczar, S. Huber, C. Zielinski, M. Löhning, A. Hauser, and E. Esplugues. 2017. TH17 cells express ST2 and are controlled by the alarmin IL-33 in the small intestine. *Mucosal Immunol.* 10:1431–1442. doi:10.1038/mi.2017.5.

Paul, W.E., and J. Zhu. 2010. How are TH2-type immune responses initiated and amplified? *Nat. Rev. Immunol.* 10:225–235. doi:10.1038/nri2735.

Pearce, E.L., A.C. Mullen, G.A. Martins, C.M. Krawczyk, A.S. Hutchins, V.P. Zediak, M. Banica, C.B. DiCioccio, D.A. Gross, C. Mao, H. Shen, N. Cereb, S.Y. Yang, T. Lindsten, J. Rossant, C.A. Hunter, and S.L. Reiner. 2003. Control of Effector $CD8^+$ T Cell Function by the Transcription Factor Eomesodermin. *Science.* 302:1041–1043. doi:10.1126/science.1090148.

Pearson, C., H.H. Uhlig, and F. Powrie. 2012. Lymphoid microenvironments and innate lymphoid cells in the gut. *Trends Immunol.* 33:289–296. doi:10.1016/j.it.2012.04.004.

Pellegrinet, L., V. Rodilla, Z. Liu, S. Chen, U. Koch, L. Espinosa, K.H. Kaestner, R. Kopan, J. Lewis, and F. Radtke. 2011. Dll1- and Dll4-mediated notch signaling are required for homeostasis of intestinal stem cells. *Gastroenterology*. 140:1230–1240. doi:10.1053/j.gastro.2011.01.005.

Pereira, C., F. Araújo, C.C. Barrias, P.L. Granja, and B. Sarmento. 2015. Dissecting stromal-epithelial interactions in a 3D in vitro cellularized intestinal model for permeability studies. *Biomaterials*. 56:36–45. doi:10.1016/j.biomaterials.2015.03.054.

Perrigoue, J.G., S.A. Saenz, M.C. Siracusa, E.J. Allenspach, B.C. Taylor, P.R. Giacomin, M.G. Nair, Y. Du, C. Zaph, N. van Rooijen, M.R. Comeau, E.J. Pearce, T.M. Laufer, and D. Artis. 2009. MHC class II-dependent basophil-CD4$^+$ T cell interactions promote Th2 cytokine-dependent immunity. *Nat. Immunol.* 10:697–705. doi:10.1038/ni.1740.

Persson, E.K., E. Jaensson, and W.W. Agace. 2010. The diverse ontogeny and function of murine small intestinal dendritic cell/macrophage subsets. *Immunobiology*. 215:692–697. doi:10.1016/j.imbio.2010.05.013.

Persson, E.K., H. Uronen-Hansson, M. Semmrich, A. Rivollier, K. Hägerbrand, J. Marsal, S. Gudjonsson, U. Håkansson, B. Reizis, K. Kotarsky, and W.W. Agace. 2013. IRF4 Transcription-Factor-Dependent CD103$^+$CD11b$^+$ Dendritic Cells Drive Mucosal T Helper 17 Cell Differentiation. *Immunity*. 38:958–969. doi:10.1016/j.immuni.2013.03.009.

Peterson, L.W., and D. Artis. 2014. Intestinal epithelial cells: regulators of barrier function and immune homeostasis. *Nat. Rev. Immunol.* 14:141–153. doi:10.1038/nri3608.

Pham, A.H., J.M. McCaffery, and D.C. Chan. 2012. Mouse lines with photo-activatable mitochondria (PhAM) to study mitochondrial dynamics. *Genesis*. 50:833–843. doi:10.1007/s10955-011-0269-9.

Phan, A.T., A.L. Doedens, A. Palazon, P.A. Tyrakis, K.P. Cheung, R.S. Johnson, and A.W. Goldrath. 2016. Constitutive Glycolytic Metabolism Supports CD8$^+$ T Cell Effector Memory Differentiation during Viral Infection. *Immunity*. 45:1024–1037. doi:10.1016/j.immuni.2016.10.017.

Pickard, J.M., C.F. Maurice, M. a. Kinnebrew, M.C. Abt, D. Schenten, T. V. Golovkina, S.R. Bogatyrev, R.F. Ismagilov, E.G. Pamer, P.J. Turnbaugh, and A. V. Chervonsky. 2014. Rapid fucosylation of intestinal epithelium sustains host–commensal symbiosis in sickness. *Nature*. 514:638–641. doi:10.1038/nature13823.

Pinchuk, I. V., R.C. Mifflin, J.I. Saada, and D.W. Powell. 2010. Intestinal Mesenchymal Cells. *Curr. Gastrointest. Rep.* 12:310–318. doi:10.1007/s11894-010-0135-y.

Pott, J., T. Mahlakoiv, M. Mordstein, C.U. Duerr, T. Michiels, S. Stockinger, P. Staeheli, and M.W. Hornef. 2011. IFN-λ determines the intestinal epithelial antiviral host defense. *Proc. Natl. Acad. Sci. USA*. 108:7944–7949. doi:10.1073/pnas.1100552108.

Pott, J., and S. Stockinger. 2017. Type I and III interferon in the gut: Tight balance between host protection and immunopathology. *Front. Immunol.* 8:1–15. doi:10.3389/fimmu.2017.00258.

Powrie, F., R. Correa-Oliveira, S. Mauze, and R.L. Coffman. 1994a. Regulatory interactions between CD45RB^{high} and CD45RB^{low} CD4^{+} T cells are important for the balance between protective and pathogenic cell-mediated immunity. *J. Exp. Med.* 179:589–600. doi:10.1084/jem.179.2.589.

Powrie, F., M.W. Leach, S. Mauze, S. Menon, L.B. Caddle, and R.L. Coffman. 1994b. Inhibition of Th1 responses prevents inflammatory bowel disease in scid mice reconstituted with CD45RB^{hi} CD4^{+} T cells. *Immunity*. 1:553–562. doi:10.1016/1074-7613(94)90045-0.

Prinz, I., A. Sansoni, A. Kissenpfennig, L. Ardouin, M. Malissen, and B. Malissen. 2006. Visualization of the earliest steps of γδ T cell development in the adult thymus. *Nat. Immunol.* 7:995–1003. doi:10.1038/ni1371.

Prinz, M., G. Huber, A.J.S. Macpherson, F.L. Heppner, M. Glatzel, H. Pietro Eugster, N. Wagner, and A. Aguzzi. 2003. Oral prion infection requires normal numbers of Peyer's patches but not of enteric lymphocytes. *Am. J. Pathol.* 162:1103–1111. doi:10.1016/S0002-9440(10)63907-7.

Propheter, D.C., A.L. Chara, T.A. Harris, K.A. Ruhn, and L. V Hooper. 2017. Resistin-like molecule β is a bactericidal protein that promotes spatial segregation of the microbiota and the colonic epithelium. *Proc. Natl. Acad. Sci. USA.* 114:11027–11033. doi:10.1073/pnas.1711395114.

Purwar, R., C. Schlapbach, S. Xiao, H.S. Kang, W. Elyaman, X. Jiang, A.M. Jetten, S.J. Khoury, R.C. Fuhlbrigge, V.K. Kuchroo, R.A. Clark, and T.S. Kupper. 2012. Robust tumor immunity to melanoma mediated by interleukin-9-producing T cells. *Nat. Med.* 18:1248–1253. doi:10.1038/nm.2856.

Qi, Z., Y. Li, B. Zhao, C. Xu, Y. Liu, H. Li, B. Zhang, X. Wang, X. Yang, W. Xie, B. Li, J.D.J. Han, and Y.G. Chen. 2017. BMP restricts stemness of intestinal Lgr5^{+} stem cells by directly suppressing their signature genes. *Nat. Commun.* 8:1–14. doi:10.1038/ncomms13824.

Qiu, Y., A. Pu, H. Zheng, M. Liu, W. Chen, W. Wang, W. Xiao, and H. Yang. 2016. TLR2-Dependent Signaling for IL-15 Production Is Essential for the Homeostasis of Intestinal Intraepithelial Lymphocytes. *Mediators Inflamm.* 2016:1–12. doi:10.1155/2016/4281865.

Rahimpour, A., H.F. Koay, A. Enders, R. Clanchy, S.B.G. Eckle, B. Meehan, Z. Chen, B. Whittle, L. Liu, D.P. Fairlie, C.C. Goodnow, J. McCluskey, J. Rossjohn, a. P. Uldrich, D.G. Pellicci, and D.I. Godfrey. 2015. Identification of phenotypically and functionally heterogeneous mouse mucosal-associated invariant T cells using MR1 tetramers. *J. Exp. Med.* 212:1–14. doi:10.1084/jem.20142110.

Ramanan, D., and K. Cadwell. 2016. Review Intrinsic Defense Mechanisms of the Intestinal Epithelium. *Cell Host Microbe*. 19:1–8. doi:10.1016/j.chom.2016.03.003.

Ramsburg, E., R. Tigelaar, J. Craft, and A. Hayday. 2003. Age-dependent Requirement for γδ T Cells in the Primary but Not Secondary Protective Immune Response against an Intestinal Parasite. *J. Exp. Med.* 198:1403–1414. doi:10.1084/jem.20030050.

Rathmell, J.C., E.A. Farkash, W. Gao, and C.B. Thompson. 2001. IL-7 Enhances the Survival and Maintains the Size of Naive T Cells. *J. Immunol.* 167:6869–6876. doi:10.4049/jimmunol.167.12.6869.

Da Re, S., J. Valle, N. Charbonnel, C. Beloin, P. Latour-Lambert, P. Faure, E. Turlin, C. Le Bouguenec, G. Renauld-Mongenie, C. Forestier, and J.-M.M. Ghigo. 2013. Identification of commensal Escherichia coli genes involved in biofilm resistance to pathogen colonization. *PLoS One*. 8:1–12. doi:10.1371/journal.pone.0061628.

Reboldi, A., and J.G. Cyster. 2016. Peyer's patches: Organizing B-cell responses at the intestinal frontier. *Immunol. Rev.* 271:230–245. doi:10.1111/imr.12400.

Reikvam, D.H., A. Erofeev, A. Sandvik, V. Grcic, F.L. Jahnsen, P. Gaustad, K.D. McCoy, A.J. Macpherson, L.A. Meza-Zepeda, and F.E. Johansen. 2011. Depletion of murine intestinal microbiota: Effects on gut mucosa and epithelial gene expression. *PLoS One*. 6:1–13. doi:10.1371/journal.pone.0017996.

Reinecker, H.C., and D.K. Podolsky. 1995. Human intestinal epithelial cells express functional cytokine receptors sharing the common gamma γc chain of the interleukin 2 receptor. *Proc. Natl. Acad. Sci. U. S. A.* 92:8353–8357. doi:10.1073/pnas.92.18.8353.

Reiner, S., and R. Locksley. 1995. The Regulation of Immunity to *Leishmania Major*. *Annu. Rev. Immunol.* 13:151–177. doi:10.1146/annurev.iy.13.040195.001055.

Reis, B.S., D.P. Hoytema van Konijnenburg, S.I. Grivennikov, and D. Mucida. 2014. Transcription factor T-bet regulates intraepithelial lymphocyte functional maturation. *Immunity*. 41:244–256. doi:10.1016/j.immuni.2014.06.017.

Reis, B.S., K. Lee, M.H. Fanok, C. Mascaraque, M. Amoury, L.B. Cohn, A. Rogoz, O.S. Dallner, P.M. Moraes-Vieira, A.I. Domingos, and D. Mucida. 2015. Leptin Receptor Signaling in T Cells Is Required for Th17 Differentiation. *J. Immunol.* 25:1–8. doi:10.4049/jimmunol.1402996.

Ribot, J.C., A. DeBarros, D.J. Pang, J.F. Neves, V. Peperzak, S.J. Roberts, M. Girardi, J. Borst, A.C. Hayday, D.J. Pennington, and B. Silva-Santos. 2009. CD27 is a thymic determinant of the balance between interferon-gamma- and interleukin 17-producing gammadelta T cell subsets. *Nat. Immunol.* 10:427–436. doi:10.1038/ni.1717.

Ricklin, D., G. Hajishengallis, K. Yang, and J.D. Lambris. 2010. Complement: A key system for immune surveillance and homeostasis. *Nat. Immunol.* 11:785–797. doi:10.1038/ni.1923.

Ringnér, M. 2008. What is principal component analysis? *Nat. Biotechnol.* 26:303–304. doi:http://dx.doi.org/10.1016/j.clml.2011.09.099.

Ritsma, L., E.J.A. Steller, S.I.J. Ellenbroek, O. Kranenburg, I.H.M. Borel Rinkes, and J. van Rheenen. 2013. Surgical implantation of an abdominal imaging window for intravital microscopy. *Nat. Protoc.* 8:583–594. doi:10.1038/nprot.2013.026.

Rivollier, A., J. He, A. Kole, V. Valatas, and B.L. Kelsall. 2012. Inflammation switches the differentiation program of Ly6C^{hi} monocytes from antiinflammatory macrophages to inflammatory dendritic cells in the colon. *J. Exp. Med.* 209:139–155. doi:10.1084/jem.20101387.

Roberts, S.J., A.L. Smith, A.B. West, L. Wen, R.C. Findly, M.J. Owen, and A.C. Hayday. 1996. T-cell $\alpha\beta^+$ and $\gamma\delta^+$ deficient mice display abnormal but distinct phenotypes toward a natural, widespread infection of the intestinal epithelium. *Proc. Natl. Acad. Sci. USA*. 93:11774–11779. doi:10.1073/pnas.93.21.11774.

Robinette, M.L., J.K. Bando, W. Song, T.K. Ulland, S. Gilfillan, and M. Colonna. 2017. IL-15 sustains IL-7R-independent ILC2 and ILC3 development. *Nat. Commun.* 8:1–13. doi:10.1038/ncomms14601.

Rocha, B., P. Vassalli, and D. Guy-Grand. 1994. Thymic and extrathymic origins of gut intraepithelial lymphocyte populations in mice. *J. Exp. Med.* 180:681–6. doi:10.1084/jem.180.2.681.

Rodriguez, M.E., K. Azizuddin, P. Zhang, S. mao Chiu, M. Lam, M.E. Kenney, C. Burda, and N.L. Oleinick. 2008. Targeting of mitochondria by 10-N-alkyl acridine orange analogues: Role of alkyl chain length in determining cellular uptake and localization. *Mitochondrion*. 8:237–246. doi:10.1016/j.mito.2008.04.003.

Rogoz, A., B.S. Reis, R.A. Karssemeijer, and D. Mucida. 2015. A 3-D enteroid-based model to study T-cell and epithelial cell interaction. *J. Immunol. Methods*. 421:89–95. doi:10.1016/j.jim.2015.03.014.

Romagnani, A., V. Vettore, T. Rezzonico-Jost, S. Hampe, E. Rottoli, W. Nadolni, M. Perotti, M.A. Meier, C. Hermanns, S. Geiger, G. Wennemuth, C. Recordati, M. Matsushita, S. Muehlich, M. Proietti, V. Chubanov, T. Gudermann, F. Grassi, and S. Zierler. 2017. TRPM7 kinase activity is essential for T cell colonization and alloreactivity in the gut. *Nat. Commun.* 8:1–14. doi:10.1038/s41467-017-01960-z.

Romagnoli, P., H. Fu, Z. Qiu, C. Khairallah, Q. Pham, L. Puddington, K. Khanna, L. Lefrançois, and B. Sheridan. 2016. Differentiation of distinct long-lived memory CD4 T cells in intestinal tissues after oral *Listeria monocytogenes* infection. *Mucosal Immunol.* 10:520–530. doi:10.1038/mi.2016.66.

Ron, D., and P. Walter. 2007. Signal integration in the endoplasmic reticulum unfolded protein response. *Nat. Rev. Mol. Cell Biol.* 8:519–529. doi:10.1038/nrm2199.

Rosato, P.C., L.K. Beura, and D. Masopust. 2017. Tissue resident memory T cells and viral immunity. *Curr. Opin. Virol.* 22:44–50. doi:10.1016/j.coviro.2016.11.011.

Rose, M.E., P. Hesketh, M . Elaine Rose, and P. Hesketh. 1986. Eimerian Life Cycles: The Patency of Eimeria vermiformis, but Not Eimeria pragensis, is Subject to Host (Mus musculus) Influence. *J. Parasitol.* 72:949–954.

Rose, M.E., P. Hesketh, and D. Wakelin. 1992. Immune control of murine coccidiosis: $CD4^+$ and $CD8^+$ T lymphocytes contribute differentially in resistance to primary and secondary infections. *Parasitology*. 105:349–354. doi:10.1017/S0031182000074515.

Rose, M.E., D.G. Owen, and P. Hesketh. 1984. Susceptibility to coccidiosis: effect of strain of mouse on reproduction of Eimeria vermiformis. *Parasitology*. 88:45–54. doi:10.1017/S0031182000054330.

Rose, M.E., D. Wakelin, and P. Hesketh. 1989. Gamma interferon controls Eimeria vermiformis primary infection in BALB/c mice. *Infect. Immun.* 57:1599–1603. doi:10.1016/0014-4894(90)90032-8.

Ross, S.H., C. Rollings, K.E. Anderson, P.T. Hawkins, L.R. Stephens, and D.A. Cantrell. 2016. Phosphoproteomic Analyses of Interleukin 2 Signaling Reveal Integrated JAK Kinase-Dependent and -Independent Networks in $CD8^+$ T Cells. *Immunity*. 45:685–700. doi:10.1016/j.immuni.2016.07.022.

Rosshart, S.P., B.G. Vassallo, D. Angeletti, D.S. Hutchinson, A.P. Morgan, K. Takeda, H.D. Hickman, J.A. McCulloch, J.H. Badger, N.J. Ajami, G. Trinchieri, F. Pardo-Manuel de Villena, J.W. Yewdell, and B. Rehermann. 2017. Wild Mouse Gut Microbiota Promotes Host Fitness and Improves Disease Resistance. *Cell*. 171:1–14. doi:10.1016/j.cell.2017.09.016.

Roulis, M., G. Bongers, M. Armaka, T. Salviano, Z. He, A. Singh, U. Seidler, C. Becker, J. Demengeot, G.C. Furtado, S.A. Lira, and G. Kollias. 2015. Host and microbiota interactions are critical for development of murine Crohn's-like ileitis. *Mucosal Immunol.* 9:1–11. doi:10.1038/mi.2015.102.

Rourke, B.O., S. Cortassa, and M.A. Aon. 2005. Mitochondrial Ion Channels: Gatekeepers of Life and Death. *Physiology*. 20:303–315. doi:10.1152/physiol.00020.2005.

Roy, B., S. Agarwal, A.M. Brennecke, M. Krey, O. Pabst, S. Düber, and S. Weiss. 2013. B-1-cell subpopulations contribute differently to gut immunity. *Eur. J. Immunol.* 43:2023–2032. doi:10.1002/eji.201243070.

Ruscher, R., R.L. Kummer, Y.J. Lee, S.C. Jameson, and K.A. Hogquist. 2017. CD8αα intraepithelial lymphocytes arise from two main thymic precursors. *Nat. Immunol.* 18:771–780. doi:10.1038/ni.3751.

Di Sabatino, A., R. Ciccocioppo, F. Cupelli, B. Cinque, D. Millimaggi, M.M. Clarkson, M. Paulli, M.G. Cifone, and G.R. Corazza. 2006. Epithelium derived interleukin 15 regulates intraepithelial lymphocyte Th1 cytokine production, cytotoxicity, and survival in coeliac disease. *Gut*. 55:469–477. doi:10.1136/gut.2005.068684.

Sano, Y., and J.M. Park. 2014. Loss of epidermal p38α signaling prevents UVR-induced inflammation via acute and chronic mechanisms. *J. Invest. Dermatol.* 134:2231–2240. doi:10.1038/jid.2014.153.

Sardi, C., P. Luchini, A. Emanuelli, A. Giannoni, E. Martini, L.M. Manara, L. Sfondrini, M. Kallikourdis, M. Sommariva, and C. Rumio. 2016. Three months of western diet induces small intestinal mucosa alteration in TLR KO mice. *Microsc Res Tech*. 80:1–7. doi:10.1002/jemt.22831.

Sato, T., and H. Clevers. 2012. Primary Mouse Small Intestinal Epithelial Cell Cultures. *Methods Mol. Biol.* 945:319–328. doi:10.1007/978-1-62703-125-7_19.

Sato, T., and H. Clevers. 2013. Growing self-organizing mini-guts from a single intestinal stem cell: mechanism and applications. *Science.* 340:1190–1194. doi:10.1126/science.1234852.

Sato, T., J.H. van Es, H.J. Snippert, D.E. Stange, R.G. Vries, M. van den Born, N. Barker, N.F. Shroyer, M. van de Wetering, and H. Clevers. 2011. Paneth cells constitute the niche for Lgr5 stem cells in intestinal crypts. *Nature*. 469:415–418. doi:10.1038/nature09637.

Sato, T., R.G. Vries, H.J. Snippert, M. van de Wetering, N. Barker, D.E. Stange, J.H. van Es, A. Abo, P. Kujala, P.J. Peters, and H. Clevers. 2009. Single Lgr5 stem cells build crypt-villus structures in vitro without a mesenchymal niche. *Nature*. 459:262–5. doi:10.1038/nature07935.

Savage, D.C., and R. Dubos. 1968. Alterations in the mouse cecum and its flora produced by antibacterial drugs. *J. Exp. Med. Med.* 128:97–110. doi:10.1084/jem.128.1.97.

Sawa, S., M. Lochner, N. Satoh-Takayama, S. Dulauroy, M. Bérard, M. Kleinschek, D. Cua, J.P. Di Santo, and G. Eberl. 2011. RORγt^{+} innate lymphoid cells regulate intestinal homeostasis by integrating negative signals from the symbiotic microbiota. *Nat. Immunol.* 12:320–6. doi:10.1038/ni.2002.

Saxena, K., S.E. Blutt, K. Ettayebi, X. Zeng, J.R. Broughman, S.E. Crawford, U.C. Karandikar, N.P. Sastri, M.E. Conner, A.R. Opekun, D.Y. Graham, W. Qureshi, V. Sherman, J. Foulke-abel, J. In, O. Kovbasnjuk, N.C. Zachos, M. Donowitz, and M.K. Estes. 2016. Human Intestinal Enteroids: a New Model To Study Human Rotavirus Infection, Host Restriction, and Pathophysiology. *J. Virol*. 90:43–56. doi:10.1128/JVI.01930-15.Editor.

Schito, M.L.., J.R.. Barta, and B. Chobotar. 1996. Comparison of Four Murine Eimeria Species in Immunocompetent and Immunodeficient Mice. *J. Parasitol.* 82:255–262.

Schlesner, H. 2015. Verrucomicrobium. *Bergey's Man.* 6. doi:10.1002/9781118960608.gbm01285.

Schmidt, J. V, G.H. Sutt, J.K. Reddy, M.C. Simont, and C.A. Bradfield. 1996. Characterization of a murine Ahr null allele: involvement of the Ah receptor in hepatic growth and development. *Proc. Natl. Acad. Sci. USA*. 93:6731–6736. doi:10.1073/pnas.93.13.6731.

Schmitt, E., and T. Bopp. 2017. Discovery and initial characterization of Th9 cells: the early years. *Semin. Immunopathol.* 39:5–10. doi:10.1007/s00281-016-0610-0.

Schön, M.P., A. Arya, E.A. Murphy, C.M. Adams, U.G. Strauch, W.W. Agace, J. Marsal, J.P. Donohue, H. Her, D.R. Beier, S. Olson, L. Lefrancois, M.B. Brenner, M.J. Grusby, and C.M. Parker. 1999. Mucosal T Lymphocyte Numbers Are Selectively Reduced in Integrin ae (CD103)-Deficient Mice. *J. Immunol.* 1:6641–6649.

Schonhoff, S.E., M. Giel-Moloney, and A.B. Leiter. 2004. Minireview: Development and differentiation of gut endocrine cells. *Endocrinology*. 145:2639–2644. doi:10.1210/en.2004-0051.

Schroeder, B.O., G.M.H. Birchenough, M. Ståhlman, L. Arike, M.E.V. Johansson, G.C. Hansson, and F. Bäckhed. 2017. Bifidobacteria or Fiber Protects against Diet-Induced Microbiota-Mediated Colonic Mucus Deterioration. *Cell Host Microbe*. 23:1–14. doi:10.1016/j.chom.2017.11.004.

Schug, Z.T., and E. Gottlieb. 2009. Cardiolipin acts as a mitochondrial signalling platform to launch apoptosis. *Biochim. Biophys. Acta Biomembr.* 1788:2022–2031. doi:10.1016/j.bbamem.2009.05.004.

Schwank, G., A. Andersson-Rolf, B.-K. Koo, N. Sasaki, and H. Clevers. 2013. Generation of BAC transgenic epithelial organoids. *PLoS One*. 8:1–6. doi:10.1371/journal.pone.0076871.

Schwindling, C., A. Quintana, E. Krause, and M. Hoth. 2010. Mitochondria Positioning Controls Local Calcium Influx in T Cells. *J. Immunol.* 184:184–190. doi:10.4049/jimmunol.0902872.

Scott-Browne, J.P., I.F. López-Moyado, S. Trifari, V. Wong, L. Chavez, A. Rao, and R.M. Pereira. 2016. Dynamic Changes in Chromatin Accessibility Occur in $CD8^+$ T Cells Responding to Viral Infection. *Immunity*. 45:1327–1340. doi:10.1016/j.immuni.2016.10.028.

Sefik, E., N. Geva-Zatorsky, S. Oh, L. Konnikova, D. Zemmour, A.M. McGuire, D. Burzyn, A. Ortiz-Lopez, M. Lobera, J. Yang, S. Ghosh, A. Earl, S.B. Snapper, R. Jupp, D. Kasper, D. Mathis, and C. Benoist. 2015. Individual intestinal symbionts induce a distinct population of $ROR\gamma^+$ regulatory T cells. *Science.* 349:993–997. doi:10.1126/science.aaa9420.

Seita, J., and I.L. Weissman. 2010. Hematopoietic Stem Cell: Self-renewal versus Differentiation. *Wiley Interdiscip Rev Syst Biol Med*. 2:640–653. doi:10.1002/wsbm.86.Hematopoietic.

Sellon, R.K., S. Tonkonogy, M. Schultz, L.A. Dieleman, W. Grenther, E. Balish, D.M. Rennick, and R.B. Sartor. 1998. Resident enteric bacteria are necessary for development of spontaneous colitis and immune system activation in interleukin-10-deficient mice. *Infect. Immun.* 66:5224–5231.

Semenkovich, N.P., J.D. Planer, P.P. Ahern, N.W. Griffin, C.Y. Lin, and J.I. Gordon. 2016. Impact of the gut microbiota on enhancer accessibility in gut intraepithelial lymphocytes. *Proc. Natl. Acad. Sci. USA.* 113:14805–14810. doi:10.1073/pnas.1617793113.

Sena, L.A., S. Li, A. Jairaman, M. Prakriya, T. Ezponda, D.A. Hildeman, C.R. Wang, P.T. Schumacker, J.D. Licht, H. Perlman, P.J. Bryce, and N.S. Chandel. 2013. Mitochondria Are Required for Antigen-Specific T Cell Activation through Reactive Oxygen Species Signaling. *Immunity*. 38:225–236. doi:10.1016/j.immuni.2012.10.020.

Shaffer, A.L., M. Shapiro-Shelef, N.N. Iwakoshi, A.H. Lee, S.B. Qian, H. Zhao, X. Yu, L. Yang, B.K. Tan, A. Rosenwald, E.M. Hurt, E. Petroulakis, N. Sonenberg, J.W. Yewdell, K. Calame, L.H. Glimcher, and L.M. Staudt. 2004. XBP1, downstream of Blimp-1, expands the secretory apparatus and other organelles, and increases protein synthesis in plasma cell differentiation. *Immunity*. 21:81–93. doi:10.1016/j.immuni.2004.06.010.

Shao, L., O. Kamalu, and L. Mayer. 2005. Non-classical MHC class I molecules on intestinal epithelial cells: Mediators of mucosal crosstalk. *Immunol. Rev.* 206:160–176. doi:10.1111/j.0105-2896.2005.00295.x.

Shaw, S.K., A. Hermanowski-Vosatka, T. Shibahara, B.A. McCormick, C.A. Parkos, S.L. Carlson, E.C. Ebert, M.B. Brenner, and J.L. Madara. 1998. Migration of intestinal intraepithelial lymphocytes into a polarized epithelial monolayer. *Am. J. Physiol.* 275:584–591. doi:10.1152/ajpgi.1998.275.3.G584.

Shay, T., and J. Kang. 2013. Immunological Genome project and systems immunology. *Trends Immunol.* 34:602–609. doi:10.1016/j.it.2013.03.004.Immunological.

Shehade, H., V. Acolty, M. Moser, and G. Oldenhove. 2015. Cutting Edge: Hypoxia-Inducible Factor 1 Negatively Regulates Th1 Function. *J. Immunol.* 195:1372–1376. doi:10.4049/jimmunol.1402552.

Shen, Z.-J., and J.S. Malter. 2015. XBP1, a determinant of the eosinophil lineage. *Nat. Immunol.* 16:793–794. doi:10.1038/ni.3214.

Shi, L.Z., R. Wang, G. Huang, P. Vogel, G. Neale, D.R. Green, and H. Chi. 2011. HIF1α–dependent glycolytic pathway orchestrates a metabolic checkpoint for the differentiation of TH17 and Treg cells. *J. Exp. Med.* 208:1367–1376. doi:10.1084/jem.20110278.

Shibahara, T., K. Miyazaki, D. Sato, H. Matsui, A. Yanaka, A. Nakahara, and N. Tanaka. 2005. Alteration of intestinal epithelial function by intraepithelial lymphocyte homing. *J. Gastroenterol.* 40:878–86. doi:10.1007/s00535-005-1631-y.

Shih, V.F.-S., J. Cox, N.M. Kljavin, H.S. Dengler, M. Reichelt, P. Kumar, L. Rangell, J.K. Kolls, L. Diehl, W. Ouyang, and N. Ghilardi. 2014. Homeostatic IL-23 receptor signaling limits Th17 response through IL-22-mediated containment of commensal microbiota. *Proc. Natl. Acad. Sci.* 111:13942–13947. doi:10.1073/pnas.1323852111.]

Shinkai, Y., G. Rathbun, K.-P. Lam, E.M. Oltz, V. Stewart, M. Mendelsohn, J. Charron, M. Datta, F. Young, A.M. Stall, and F.W. Alt. 1992. RAG-2-deficient mice lack mature lymphocytes owing to inability to initiate V(D)J rearrangement. *Cell*. 68:855–867. doi:10.1016/0092-8674(92)90029-C.

Shires, J., E. Theodoridis, and A.C. Hayday. 2001. Biological insights into TCR$\gamma\delta^+$ and TCR$\alpha\beta^+$ intraepithelial lymphocytes provided by serial analysis of gene expression (SAGE). *Immunity*. 15:419–434. doi:S1074-7613(01)00192-3.

Shon, W.-J., Y.-K. Lee, J.H. Shin, E.Y. Choi, and D.-M. Shin. 2015. Severity of DSS-induced colitis is reduced in Ido1-deficient mice with down-regulation of TLR-MyD88-NF-kB transcriptional networks. *Sci. Rep.* 5:17305. doi:10.1038/srep17305.

Shortland, A., J. Chettle, J. Archer, K. Wood, D. Bailey, B.A. Blacklaws, and J.L. Heeney. 2014. Pathology caused by persistent murine norovirus infection. *J. Gen. Virol.* 95:413–422. doi:10.1099/vir.0.059188-0.Pathology.

Sinclair, C., I. Bains, A.J. Yates, and B. Seddon. 2013. Asymmetric thymocyte death underlies the CD4:CD8 T-cell ratio in the adaptive immune system. *Proc. Natl. Acad. Sci. USA*. 110:2905–2914. doi:10.1073/pnas.1304859110.

Skoczek, D. a, P. Walczysko, N. Horn, A. Parris, S. Clare, M.R. Williams, and A. Sobolewski. 2014. Luminal microbes promote monocyte-stem cell interactions across a healthy colonic epithelium. *J. Immunol.* 193:439–451. doi:10.4049/jimmunol.1301497.

Van der Sluis, M., B.A.E. De Koning, A.C.J.M. De Bruijn, A. Velcich, J.P.P. Meijerink, J.B. Van Goudoever, H.A. Büller, J. Dekker, I. Van Seuningen, I.B. Renes, and A.W.C. Einerhand. 2006. Muc2-Deficient Mice Spontaneously Develop Colitis, Indicating That MUC2 Is Critical for Colonic Protection. *Gastroenterology*. 131:117–129. doi:10.1053/j.gastro.2006.04.020.

Smith, A.L., and A.C. Hayday. 2000a. Genetic dissection of primary and secondary responses to a widespread natural pathogen of the gut, Eimeria vermiformis. *Infect. Immun.* 68:6273–6280. doi:10.1128/IAI.68.11.6273-6280.2000.

Smith, A.L., and A.C. Hayday. 2000b. An αβ T-cell-independent immunoprotective response towards gut coccidia is supported by γδ cells. *Immunology*. 101:325–332. doi:10.1046/j.1365-2567.2000.00122.x.

Smith, P.D., C. Ochsenbauer-Jambor, and L.E. Smythies. 2005. Intestinal macrophages: unique effector cells of the innate immune system. *Immunol. Rev.* 206:149–159. doi:10.1111/j.0105-2896.2005.00288.x.

Snippert, H.J., L.G. van der Flier, T. Sato, J.H. van Es, M. van den Born, C. Kroon-Veenboer, N. Barker, A.M. Klein, J. van Rheenen, B.D. Simons, and H. Clevers. 2010. Intestinal crypt homeostasis results from neutral competition between symmetrically dividing Lgr5 stem cells. *Cell*. 143:134–144. doi:10.1016/j.cell.2010.09.016.

Sonnenberg, G.F., L.A. Fouser, and D. Artis. 2011. Border patrol: Regulation of immunity, inflammation and tissue homeostasis at barrier surfaces by IL-22. *Nat. Immunol.* 12:383–390. doi:10.1038/ni.2025.

Sorobetea, D., M. Svensson-Frej, and R. Grencis. 2018. Immunity to gastrointestinal nematode infections. *Mucosal Immunol.* 11:304–315. doi:10.1038/mi.2017.113.

Soudais, C., F. Samassa, M. Sarkis, L. Le Bourhis, S. Bessoles, D. Blanot, M. Herve, F. Schmidt, D. Mengin-Lecreulx, and O. Lantz. 2015. *In Vitro* and *In Vivo* Analysis of the Gram-Negative Bacteria-Derived Riboflavin Precursor Derivatives Activating Mouse MAIT Cells. *J. Immunol.* 15:4641–4649. doi:10.4049/jimmunol.1403224.

Springer, B., Y.G. Kidan, T. Prammananan, K. Ellrott, E.C. Böttger, and P. Sander. 2001. Mechanisms of Streptomycin Resistance : Selection of Mutations in the 16S rRNA Gene Conferring Resistance. *Antimicrob. Agents Chemother.* 45:2877–2884. doi:10.1128/AAC.45.10.2877.

Stappenbeck, T.S., and H.W. Virgin. 2016. Accounting for reciprocal host-microbiome interactions in experimental science. *Nature*. 534:191–199. doi:10.1038/nature18285.

Staton, T.L., A. Habtezion, M.M. Winslow, T. Sato, P.E. Love, and E.C. Butcher. 2006. $CD8^+$ recent thymic emigrants home to and efficiently repopulate the small intestine epithelium. *Nat. Immunol.* 2006:1–8. doi:10.1038/ni1319.

Steinman, R.M., and Z.A. Cohn. 1973. Identification of a novel cell type in the peripheral lymphoid organs of mice. *J. Exp. Med.* 137:1142–1162. doi:10.1084/jem.137.5.1142.

Steinman, R.M., and J. Idoyaga. 2010. Features of the dendritic cell lineage. *Immunol. Rev.* 234:5–17. doi:10.1111/j.0105-2896.2009.00888.x.

Steinman, R.M., and M.D. Witmer. 1978. Lymphoid dendritic cells are potent stimulators of the primary mixed leukocyte reaction in mice. *Proc. Natl. Acad. Sci. USA*. 75:5132–5136. doi:10.1084/jem.157.2.613.

Stockinger, B., P. Di Meglio, M. Gialitakis, and J.H. Duarte. 2014. The Aryl Hydrocarbon Receptor: Multitasking in the Immune System. *Annu. Rev. Immunol.* 32:403–432. doi:10.1146/annurev-immunol-032713-120245.

Strandmark, J., S. Steinfelder, C. Berek, A.A. Kühl, S. Rausch, and S. Hartmann. 2016. Eosinophils are required to suppress Th2 responses in Peyer's patches during intestinal infection by nematodes. *Mucosal Immunol.* 10:1–12. doi:10.1038/mi.2016.93.

Streilein, J.W. 1983. Skin-associated lymphoid tissues (SALT): origins and functions. *J. Invest. Dermatol.* 80:12–16. doi:10.1111/1523-1747.ep12536743.

Sukumar, M., J. Liu, G.U. Mehta, S.J. Patel, R. Roychoudhuri, J.G. Crompton, C.A. Klebanoff, Y. Ji, P. Li, Z. Yu, G.D. Whitehill, D. Clever, R.L. Eil, D.C. Palmer, S. Mitra, M. Rao, K. Keyvanfar, D.S. Schrump, E. Wang, F.M. Marincola, L. Gattinoni, W.J. Leonard, P. Muranski, T. Finkel, and N.P. Restifo. 2016. Mitochondrial Membrane Potential Identifies Cells with Enhanced Stemness for Cellular Therapy. *Cell Metab.* 23:63–76. doi:10.1016/j.cmet.2015.11.002.

Sullivan, B.M., and R.M. Locksley. 2009. Basophils: A Nonredundant Contributor to Host Immunity. *Immunity*. 30:12–20. doi:10.1016/j.immuni.2008.12.006.

Sumagin, R., J.C. Brazil, P. Nava, H. Nishio, A. Alam, A.C. Luissint, D.A. Weber, A.S. Neish, A. Nusrat, and C.A. Parkos. 2016. Neutrophil interactions with epithelial-expressed ICAM-1 enhances intestinal mucosal wound healing. *Mucosal Immunol.* 9:1151–1162. doi:10.1038/mi.2015.135.

Sumaria, N., C.L. Grandjean, B. Silva-santos, and D.J. Pennington. 2017. Strong TCRγδ Signaling Prohibits Thymic Development of IL-17A-Secreting γδ T Cells. *Cell Rep.* 19:2469–2476. doi:10.1016/j.celrep.2017.05.071.

Sun, D., H. Lennernas, L.S. Welage, J.L. Barnett, C.P. Landowski, D. Foster, D. Fleisher, K.D. Lee, and G.L. Amidon. 2002. Comparison of human duodenum and Caco-2 gene expression profiles for 12,000 gene sequences tags and correlation with permeability of 26 drugs. *Pharm. Res.* 19:1400–1416. doi:10.1023/A:1020483911355.

Surana, N.K., and D.L. Kasper. 2017. Moving beyond microbiome-wide associations to causal microbe identification. *Nature*. 552:244–247. doi:10.1038/nature25019.

Suzuki, A., S. Sekiya, E. Gunshima, S. Fujii, and H. Taniguchi. 2010. EGF signaling activates proliferation and blocks apoptosis of mouse and human intestinal stem/progenitor cells in long-term monolayer cell culture. *Lab. Investig.* 90:1425–1436. doi:10.1038/labinvest.2010.150.

Suzuki, H., K.I. Jeong, T. Okutani, and K. Doi. 2000. Regional variations in the distribution of small intestinal intraepithelial lymphocytes in three inbred strains of mice. *J. Vet. Med. Sci.* 62:881–887. doi:10.1292/jvms.62.881.

Swamy, M., L. Abeler-Dörner, J. Chettle, T. Mahlakõiv, D. Goubau, P. Chakravarty, G. Ramsay, C. Reis e Sousa, P. Staeheli, B.A. Blacklaws, J.L. Heeney, and A.C. Hayday. 2015. Intestinal intraepithelial lymphocyte activation promotes innate antiviral resistance. *Nat. Commun.* 6:1–12. doi:10.1038/ncomms8090.

Taguchi, A., Y. Kaku, T. Ohmori, S. Sharmin, M. Ogawa, H. Sasaki, and R. Nishinakamura. 2014. Redefining the *in vivo* origin of metanephric nephron progenitors enables generation of complex kidney structures from pluripotent stem cells. *Cell Stem Cell*. 14:53–67. doi:10.1016/j.stem.2013.11.010.

Takasato, M., P.X. Er, H.S. Chiu, B. Maier, G.J. Baillie, C. Ferguson, R.G. Parton, E.J. Wolvetang, M.S. Roost, S.M. Chuva de Sousa Lopes, and M.H. Little. 2015. Kidney organoids from human iPS cells contain multiple lineages and model human nephrogenesis. *Nature*. 526:564–568. doi:10.1038/nature15695.

Tamoutounour, S., S. Henri, H. Lelouard, B. de Bovis, C. de Haar, C.J. van der Woude, A.M. Woltman, Y. Reyal, D. Bonnet, D. Sichien, C.C. Bain, A.M. Mowat, C. Reis e Sousa, L.F. Poulin, B. Malissen, and M. Guilliams. 2012. CD64 distinguishes macrophages from dendritic cells in the gut and reveals the Th1-inducing role of mesenteric lymph node macrophages during colitis. *Eur. J. Immunol.* 42:3150–3166. doi:10.1002/eji.201242847.

Tay, S.S., B. Roediger, P.L. Tong, S. Tikoo, and W. Weninger. 2014. The Skin-Resident Immune Network. *Curr. Dermatol. Rep.* 3:13–22. doi:10.1007/s13671-013-0063-9.

Thaiss, C.A., S. Itav, D. Rothschild, M.T. Meijer, M. Levy, C. Moresi, L. Dohnalová, S. Braverman, S. Rozin, S. Malitsky, M. Dori-Bachash, Y. Kuperman, I. Biton, A. Gertler, A. Harmelin, H. Shapiro, Z. Halpern, A. Aharoni, E. Segal, and E. Elinav. 2016a. Persistent microbiome alterations modulate the rate of post-dieting weight regain. *Nature*. 540:544–551. doi:10.1038/nature20796.

Thaiss, C.A., M. Levy, T. Korem, L. Dohnalová, H. Shapiro, D.A. Jaitin, E. David, D.R. Winter, M. Gury-BenAri, E. Tatirovsky, T. Tuganbaev, S. Federici, N. Zmora, D. Zeevi, M. Dori-Bachash, M. Pevsner-Fischer, E. Kartvelishvily, A. Brandis, A. Harmelin, O. Shibolet, Z. Halpern, K. Honda, I. Amit, E. Segal, and E. Elinav. 2016b. Microbiota Diurnal Rhythmicity Programs Host Transcriptome Oscillations. *Cell*. 167:1495–1510. doi:10.1016/j.cell.2016.11.003.

Thiemann, S., N. Smit, U. Roy, T.R. Lesker, E.J.C. Gálvez, J. Helmecke, M. Basic, A. Bleich, A.L. Goodman, U. Kalinke, R.A. Flavell, M. Erhardt, and T. Strowig. 2017. Enhancement of IFNγ Production by Distinct Commensals Ameliorates Salmonella-Induced Disease. *Cell Host Microbe*. 21:682–694. doi:10.1016/j.chom.2017.05.005.

Todd, K.S., and D.L. Lepp. 1971. The Life Cycle of *Eimeria vermiformis* Ernst, Chobotar and Hammond, 1971 in the Mouse *Mus musculus*. *J. Protozool.* 18:332–337. doi:10.1111/j.1550-7408.1971.tb03327.x.

Tomov, V.T., L.C. Osborne, D. V. Dolfi, G.F. Sonnenberg, L.A. Monticelli, K. Mansfield, H.W. Virgin, D. Artis, and E.J. Wherry. 2013. Persistent Enteric Murine Norovirus Infection Is Associated with Functionally Suboptimal Virus-Specific CD8 T Cell Responses. *J. Virol.* 87:7015–7031. doi:10.1128/JVI.03389-12.

Tomov, V.T., O. Palko, C.W. Lau, A. Pattekar, Y. Sun, R. Tacheva, B. Bengsch, S. Manne, G.L. Cosma, L.C. Eisenlohr, T.J. Nice, H.W. Virgin, and E.J. Wherry. 2017. Differentiation and Protective Capacity of Virus-Specific $CD8^+$ T Cells Suggest Murine Norovirus Persistence in an Immune-Privileged Enteric Niche. *Immunity*. 47:1–16. doi:10.1016/j.immuni.2017.09.017.

Tung, J.W., K. Heydari, R. Tirouvanziam, B. Sahaf, D.R. Parks, L.A. Herzenberg, and L.A. Herzenberg. 2007. Modern Flow Cytometry: A Practical Approach. *Clin. Lab. Med.* 27:453–468. doi:10.1016/j.cll.2007.05.001.

Tupin, E., and M. Kronenberg. 2006. Activation of Natural Killer T Cells by Glycolipids. *Methods Enzymol.* 417:185–201. doi:10.1016/S0076-6879(06)17014-7.

Turner, J.E., B. Stockinger, and H. Helmby. 2013. IL-22 Mediates Goblet Cell Hyperplasia and Worm Expulsion in Intestinal Helminth Infection. *PLoS Pathog.* 9:1–7. doi:10.1371/journal.ppat.1003698.

Urban, J., I. Katona, W. Paul, and F. Finkelman. 1991. Interleukin 4 is important in protective immunity to a gastrointestinal nematode infection in mice. *Proc. Natl. Acad. Sci. U. S. A.* 88:5513–7. doi:10.1073/pnas.88.13.5513.

Ussher, J.E., P. Klenerman, and C.B. Willberg. 2014. Mucosal-Associated Invariant T-Cells: New Players in Anti-Bacterial Immunity. *Front. Immunol.* 5:1–9. doi:10.3389/fimmu.2014.00450.

Vaishnava, S., C.L. Behrendt, A.S. Ismail, L. Eckmann, and L. V Hooper. 2008. Paneth cells directly sense gut commensals and maintain homeostasis at the intestinal host-microbial interface. *Proc. Natl. Acad. Sci. USA.* 105:20858–20863. doi:10.1073/pnas.0808723105.

Vaishnava, S., M. Yamamoto, K.M. Severson, K. a Ruhn, X. Yu, O. Koren, R. Ley, E.K. Wakeland, and L. V Hooper. 2011. The Antibacterial Lectin RegIIIγ Promotes the Spatial Segregation of Microbiota and Host in the Intestine. *Science.* 334:255–258.

VanDussen, K.L., A.J. Carulli, T.M. Keeley, S.R. Patel, B.J. Puthoff, S.T. Magness, I.T. Tran, I. Maillard, C. Siebel, A. Kolterud, A.S. Grosse, D.L. Gumucio, S.A. Ernst, Y.-H. Tsai, P.J. Dempsey, and L.C. Samuelson. 2012. Notch signaling modulates proliferation and differentiation of intestinal crypt base columnar stem cells. *Development.* 139:488–497. doi:10.1242/dev.070763.

Vivier, E., E. Tomasello, M. Baratin, T. Walzer, and S. Ugolini. 2008. Functions of natural killer cells. *Nat. Immunol.* 9:503–510. doi:10.1038/ni1582.

Walker, J. a, J.L. Barlow, and A.N.J. McKenzie. 2013. Innate lymphoid cells--how did we miss them? *Nat. Rev. Immunol.* 13:75–87. doi:10.1038/nri3349.

Wang, F., D. Scoville, X.C. He, M.M. Mahe, A. Box, J.M. Perry, N.R. Smith, N.Y. Lei, P.S. Davies, M.K. Fuller, J.S. Haug, M. McClain, A.D. Gracz, S. Ding, M. Stelzner, J.C.Y. Dunn, S.T. Magness, M.H. Wong, M.G. Martin, M. Helmrath, and L. Li. 2013. Isolation and characterization of intestinal stem cells based on surface marker combinations and colony-formation assay. *Gastroenterology*. 145:383–395. doi:10.1053/j.gastro.2013.04.050.

Wang, F., S. Zhang, I. Vuckovic, R. Jeon, A. Lerman, C.D. Folmes, P.P. Dzeja, and J. Herrmann. 2018. Glycolytic Stimulation Is Not a Requirement for M2 Macrophage Differentiation. *Cell Metab.* 28:463–475.e4. doi:10.1016/j.cmet.2018.08.012.

Wang, H.-C., Q. Zhou, J. Dragoo, and J.R. Klein. 2002. Most Murine $CD8^+$ Intestinal Intraepithelial Lymphocytes Are Partially But Not Fully Activated T Cells. *J. Immunol.* 169:4717–4722. doi:10.4049/jimmunol.169.9.4717.

Wang, N., H. Zhang, B.-Q. Zhang, W. Liu, Z. Zhang, M. Qiao, H. Zhang, F. Deng, N. Wu, X. Chen, S. Wen, J. Zhang, Z. Liao, Q. Zhang, Z. Yan, L. Yin, J. Ye, Y. Deng, H.H. Luu, R.C. Haydon, H. Liang, and T.-C. He. 2014a. Adenovirus-mediated efficient gene transfer into cultured three-dimensional organoids. *PLoS One*. 9:1–8. doi:10.1371/journal.pone.0093608.

Wang, X., H. Sumida, and J.G. Cyster. 2014b. GPR18 is required for a normal CD8αα intestinal intraepithelial lymphocyte compartment. *J. Exp. Med.* 211:2351–2359. doi:10.1084/jem.20140646.

Watanabe, K., M. Sugai, Y. Nambu, M. Osato, T. Hayashi, M. Kawaguchi, T. Komori, Y. Ito, and A. Shimizu. 2010. Requirement for Runx proteins in IgA class switching acting downstream of TGF-β1 and retinoic acid signaling. *J. Immunol.* 184:2785–2792. doi:10.4049/jimmunol.0901823.

Watanabe, Y., Y. Asami, S. Narusawa, S. Hashimoto, M. Iwatsuki, K. Nonaka, Y. Shinohara, T. Shiotsuki, N. Ichimaru, H. Miyoshi, S. Ōmura, and K. Shiomi. 2018. Ascosteroside C, a new mitochondrial respiration inhibitor discovered by pesticidal screening using recombinant Saccharomyces cerevisiae. *J. Antibiot. (Tokyo).* 71:146–148. doi:10.1038/ja.2015.43.

Waters, B., M. Qadura, E. Burnett, R. Chegeni, A. Labelle, P. Thompson, C. Hough, and D. Lillicrap. 2009. Anti-CD3 prevents factor VIII inhibitor development in hemophiliaAmice by a regulatory $CD4^{+}CD25^{+}$ dependent mechanism and by shifting cytokine production. *Blood*. 113:1. doi:10.1182/blood-2008-04-151597.The.

Wei, M., R. Shinkura, Y. Doi, M. Maruya, S. Fagarasan, and T. Honjo. 2011. Mice carrying a knock-in mutation of Aicda resulting in a defect in somatic hypermutation have impaired gut homeostasis and compromised mucosal defense. *Nat. Immunol.* 12:264–70. doi:10.1038/ni.1991.

Weight, C.M., E.J. Jones, N. Horn, N. Wellner, and S.R. Carding. 2015. Elucidating pathways of Toxoplasma gondii invasion in the gastrointestinal tract: Involvement of the tight junction protein occludin. *Microbes Infect.* 17:698–709. doi:10.1016/j.micinf.2015.07.001.

Weinberg, S.E., L.A. Sena, and N.S. Chandel. 2015. Mitochondria in the regulation of innate and adaptive immunity. *Immunity*. 42:406–417. doi:10.1016/j.immuni.2015.02.002.

West, A.P., I.E. Brodsky, C. Rahner, D.K. Woo, H. Erdjument-bromage, P. Tempst, M.C. Walsh, Y. Choi, G.S. Shadel, S. Ghosh, P.T. Hediye Erdjument-Bromage, M.C. Walsh, Y. Choi, G.S. Shadel, and S. Ghosh. 2011. TLR signalling augments macrophage bactericidal activity through mitochondrial ROS. *Nature*. 472:476–480. doi:10.1038/nature09973.

West, N.R., A.N. Hegazy, B.M.J. Owens, S.J. Bullers, B. Linggi, S. Buonocore, M. Coccia, D. Görtz, S. This, K. Stockenhuber, J. Pott, M. Friedrich, G. Ryzhakov, F. Baribaud, C. Brodmerkel, C. Cieluch, N. Rahman, G. Müller-Newen, R.J. Owens, A.A. Kühl, K.J. Maloy, S.E. Plevy, S. Keshav, S.P.L. Travis, and F. Powrie. 2017. Oncostatin M drives intestinal inflammation and predicts response to tumor necrosis factor – neutralizing therapy in patients with inflammatory bowel disease. *Nat. Med.* 23. doi:10.1038/nm.4307.

Westermann, B. 2010. Mitochondrial fusion and fission in cell life and death. *Nat. Rev. Mol. Cell Biol.* 11:872–884. doi:10.1038/nrm3013.

van Wijk, F., and H. Cheroutre. 2009. Intestinal T cells: Facing the mucosal immune dilemma with synergy and diversity. *Semin. Immunol.* 21:130–138. doi:10.1016/j.smim.2009.03.003.

Wilck, N., M.G. Matus, S.M. Kearney, S.W. Olesen, K. Forslund, H. Bartolomaeus, S. Haase, A. Mähler, A. Balogh, L. Markó, O. Vvedenskaya, F.H. Kleiner, D. Tsvetkov, L. Klug, P.I. Costea, S. Sunagawa, L. Maier, N. Rakova, V. Schatz, P. Neubert, C. Frätzer, A. Krannich, M. Gollasch, D.A. Grohme, B.F. Côrte-Real, R.G. Gerlach, M. Basic, A. Typas, C. Wu, J.M. Titze, J. Jantsch, M. Boschmann, R. Dechend, M. Kleinewietfeld, S. Kempa, P. Bork, R.A. Linker, E.J. Alm, and D.N. Müller. 2017. Salt-responsive gut commensal modulates TH17 axis and disease. *Nat. Publ. Gr.* 551:585–589. doi:10.1038/nature24628.

Wilhelm, C., O.J. Harrison, V. Schmitt, M. Pelletier, S.P. Spencer, J.F.U. Jr, M. Ploch, T.R. Ramalingam, R.M. Siegel, J.F. Urban, M. Ploch, T.R. Ramalingam, R.M. Siegel, and Y. Belkaid. 2016. Critical role of fatty acid metabolism in ILC2-mediated barrier protection during malnutrition and helminth infection. *J. Exp. Med.* 1409–1418. doi:10.1084/jem.20151448.

Wilson, S., A. Tocchi, M. Holly, W. Parks, and J. Smith. 2014. A small intestinal organoid model of non-invasive enteric pathogen-epithelial cell interactions. *Mucosal Immunol.* 8:352–361. doi:10.1038/mi.2014.72.

van der Windt, G.J.W., C.H. Chang, and E.L. Pearce. 2016. Measuring Bioenergetics in T Cells Using a Seahorse Extracellular Flux Analyzer. *Curr. Protoc. Immunol.* 113:1–3. doi:10.1002/0471142735.im0316bs113.

van der Windt, G.J.W., B. Everts, C.-H.H. Chang, J.D. Curtis, T.C. Freitas, E. Amiel, E.J.L. Pearce, and E.L. Pearce. 2012. Mitochondrial respiratory capacity is a critical regulator of $CD8^+$ T cell memory development. *Immunity*. 36:68–78. doi:10.1016/j.immuni.2011.12.007.

van der Windt, G.J.W., D. O'Sullivan, B. Everts, S.C.-C. Huang, M.D. Buck, J.D. Curtis, C.-H. Chang, A.M. Smith, T. Ai, B. Faubert, R.G. Jones, E.J. Pearce, and E.L. Pearce. 2013. CD8 memory T cells have a bioenergetic advantage that underlies their rapid recall ability. *Proc. Natl. Acad. Sci.* 110:14336–14341. doi:10.1073/pnas.1221740110.

Wirtz, S., C. Neufert, B. Weigmann, and M.F. Neurath. 2007. Chemically induced mouse models of intestinal inflammation. *Nat. Protoc.* 2:541–546. doi:10.1038/nprot.2007.41.

Woese, C.R., and G.E. Fox. 1977. Phylogenetic structure of the prokaryotic domain: The primary kingdoms. *Proc. Natl. Acad. Sci.* 74:5088–5090. doi:10.1073/pnas.74.11.5088.

Woolf, E., C. Xiao, O. Fainaru, J. Lotem, D. Rosen, V. Negreanu, Y. Bernstein, D. Goldenberg, O. Brenner, G. Berke, D. Levanon, and Y. Groner. 2003. Runx3 and Runx1 are required for CD8 T cell development during thymopoiesis. *Proc. Natl. Acad. Sci. U. S. A.* 100:7731–7736. doi:10.1073/pnas.1232420100.

Worthington, J.J., F. Reimann, and F.M. Gribble. 2017. Enteroendocrine cells-sensory sentinels of the intestinal environment and orchestrators of mucosal immunity. *Mucosal Immunol.* 11:3–20. doi:10.1038/mi.2017.73.

Wu, W., M. Sun, F. Chen, A.T. Cao, H. Liu, Y. Zhao, X. Huang, Y. Xiao, S. Yao, Q. Zhao, Z. Liu, and Y. Cong. 2016. Microbiota metabolite short-chain fatty acid acetate promotes intestinal IgA response to microbiota which is mediated by GPR43. *Mucosal Immunol.* 10:1–11. doi:10.1038/mi.2016.114.

Wurbel, M.-A., M. Malissen, D. Guy-Grand, B. Malissen, and J.J. Campbell. 2007. Impaired accumulation of antigen-specific CD8 lymphocytes in chemokine CCL25-deficient intestinal epithelium and lamina propria. *J. Immunol.* 178:7598–7606. doi:178/12/7598.

Yang, Y., J. Xu, Y. Niu, J.S. Bromberg, and Y. Ding. 2008. T-bet and Eomesodermin Play Critical Roles in Directing T Cell Differentiation to Th1 versus Th17. *J. Immunol.* 181:8700–8710. doi:10.4049/jimmunol.181.12.8700.

Yang, Y.P., H. Ma, A. Starchenko, W.J. Huh, W. Li, F.E. Hickman, Q. Zhang, J.L. Franklin, D.P. Mortlock, S. Fuhrmann, B.D. Carter, R.A. Ihrie, and R.J. Coffey. 2017. A Chimeric Egfr Protein Reporter Mouse Reveals Egfr Localization and Trafficking In Vivo. *Cell Rep.* 19:1257–1267. doi:10.1016/j.celrep.2017.04.048.

Yin, H., and M. Zhu. 2012. Free radical oxidation of cardiolipin: chemical mechanisms, detection and implication in apoptosis, mitochondrial dysfunction and human diseases. *Free Radic. Res.* 46:959–974. doi:10.3109/10715762.2012.676642.

Yin, X., H.F. Farin, J.H. van Es, H. Clevers, R. Langer, and J.M. Karp. 2014. Niche-independent high-purity cultures of Lgr5^{+} intestinal stem cells and their progeny. *Nat. Methods*. 11:106–112. doi:10.1038/nmeth.2737.

Yin, Z., C. Chen, S.J. Szabo, L.H. Glimcher, A. Ray, and J. Craft. 2002. T-Bet expression and failure of GATA-3 cross-regulation lead to default production of IFN-γ by γδ T cells. *J. Immunol.* 168:1566–1571. doi:10.4049/jimmunol.168.4.1566.

Yokosuka, T., K. Sakata-Sogawa, W. Kobayashi, M. Hiroshima, A. Hashimoto-Tane, M. Tokunaga, M.L. Dustin, and T. Saito. 2005. Newly generated T cell receptor microclusters initiate and sustain T cell activation by recruitment of Zap70 and SLP-76. *Nat. Immunol.* 6:1253–1262. doi:10.1038/ni1272.

Yokoyama, W.M., S. Kim, and A.R. French. 2004. The Dynamic Life of Natural Killer Cells. *Annu. Rev. Immunol.* 22:405–429. doi:10.1146/annurev.immunol.22.012703.104711.

Yu, Q., C. Tang, S. Xun, T. Yajima, and Y. Yoshikai. 2006. MyD88-Dependent Signaling for IL-15 Production Plays an Important Role in Maintenance of CD8αα TCRαβ and TCRγδ Intestinal Intraepithelial Lymphocytes. *J. Immunol.* 176:6180–6185. doi:10.4049/jimmunol.176.10.6180.

Yui, S., T. Nakamura, T. Sato, Y. Nemoto, T. Mizutani, X. Zheng, S. Ichinose, T. Nagaishi, R. Okamoto, K. Tsuchiya, H. Clevers, and M. Watanabe. 2012. Functional engraftment of colon epithelium expanded in vitro from a single adult $Lgr5^+$ stem cell. *Nat. Med.* 18:618–623. doi:10.1038/nm.2695.

Yurkovetskiy, L., M. Burrows, A.A. Khan, L. Graham, P. Volchkov, L. Becker, D. Antonopoulos, Y. Umesaki, and A. V. Chervonsky. 2013. Gender bias in autoimmunity is influenced by microbiota. *Immunity*. 39:400–412. doi:10.1016/j.immuni.2013.08.013.

Zaid, A., L.K. Mackay, A. Rahimpour, A. Braun, M. Veldhoen, F.R. Carbone, J.H. Manton, W.R. Heath, and S.N. Mueller. 2014. Persistence of skin-resident memory T cells within an epidermal niche. *Proc. Natl. Acad. Sci. USA*. 111:5307–5312. doi:10.1073/pnas.1322292111.

Zenewicz, L.A., X. Yin, G. Wang, E. Elinav, L. Hao, L. Zhao, and R.A. Flavell. 2013. IL-22 Deficiency Alters Colonic Microbiota To Be Transmissible and Colitogenic. *J. Immunol.* 190:5306–5312. doi:10.4049/jimmunol.1300016.

Zeng, R., R. Spolski, S.E. Finkelstein, S. Oh, P.E. Kovanen, C.S. Hinrichs, C.A. Pise-Masison, M.F. Radonovich, J.N. Brady, N.P. Restifo, J.A. Berzofsky, and W.J. Leonard. 2005. Synergy of IL-21 and IL-15 in regulating $CD8^+$ T cell expansion and function. *J. Exp. Med.* 201:139–148. doi:10.1084/jem.20041057.

Zens, K.D., J.K. Chen, R.S. Guyer, F.L. Wu, F. Cvetkovski, M. Miron, and D.L. Farber. 2017. Reduced generation of lung tissue-resident memory T cells during infancy. *J. Exp. Med.* 214:2915–2932. doi:10.1084/jem.20170521.

Zhang, J., and L. Li. 2005. BMP signaling and stem cell regulation. *Dev. Biol.* 284:1–11. doi:10.1016/j.ydbio.2005.05.009.

Zhang, L., M. Adileh, M.L. Martin, S. Klingler, J. White, X. Ma, L.R. Howe, A.M.C. Brown, and R. Kolesnick. 2017. Establishing estrogen-responsive mouse mammary organoids from single Lgr5$^+$ cells. *Cell. Signal.* 29:41–51. doi:10.1016/j.cellsig.2016.08.001.

Zhang, Y.-G., S. Wu, Y. Xia, and J. Sun. 2014. Salmonella-infected crypt-derived intestinal organoid culture system for host-bacterial interactions. *Physiol. Rep.* 2:1–11. doi:10.14814/phy2.12147.

Zheng, L., C.J. Kelly, and S.P. Colgan. 2015. Physiologic hypoxia and oxygen homeostasis in the healthy intestine. A Review in the Theme: Cellular Responses to Hypoxia. *Am. J. Physiol. - Cell Physiol.* 309:C350–C360. doi:10.1152/ajpcell.00191.2015.

Zheng, Y., D.M. Danilenko, P. Valdez, I. Kasman, J. Eastham-Anderson, J. Wu, and W. Ouyang. 2007. Interleukin-22, a TH17 cytokine, mediates IL-23-induced dermal inflammation and acanthosis. *Nature*. 445:648–651. doi:10.1038/nature05505.

Zheng, Y., P.A. Valdez, D.M. Danilenko, Y. Hu, S.M. Sa, Q. Gong, A.R. Abbas, Z. Modrusan, N. Ghilardi, F.J. De Sauvage, and W. Ouyang. 2008. Interleukin-22 mediates early host defense against attaching and effacing bacterial pathogens. *Nat. Med.* 14:282–289. doi:10.1038/nm1720.

Zhou, L., I.I. Ivanov, R. Spolski, R. Min, K. Shenderov, T. Egawa, D.E. Levy, W.J. Leonard, and D.R. Littman. 2007. IL-6 programs TH-17 cell differentiation by promoting sequential engagement of the IL-21 and IL-23 pathways. *Nat. Immunol.* 8:967–974. doi:10.1038/ni1488.

Zhu, J., and W.E. Paul. 2010. Peripheral CD4$^+$ T-cell differentiation regulated by networks of cytokines and transcription factors. *Immunol. Rev.* 238:247–262. doi:10.1111/j.1600-065X.2010.00951.x.

Ziegler, S.F. 2016. Division of labour by CD4$^+$ T helper cells. *Nat. Rev. Immunol.* 16:403–403. doi:10.1038/nri.2016.53.